50%

82-10

A Short Course on the Sediment Stability of Canadian Shelves

March 9-10, 1982

edited by: J.Vaughn Barrie

A SHORT COURSE
ON THE
SEDIMENT STABILITY OF CANADIAN SHELVES

March 9-10, 1982

edited by:

J. VAUGHN BARRIE

Technical Report
C-CORE Publication No. 82-10

C-CORE

CENTRE FOR COLD OCEAN RESOURCES ENGINEERING
MEMORIAL UNIVERSITY OF NEWFOUNDLAND
ST. JOHN'S, NEWFOUNDLAND, CANADA, A1B 3X5
TELEX 016 4794 TELEPHONE (709) 737-8354

The Centre for Cold Ocean Resources Engineering (C-CORE) was established at Memorial University of Newfoundland in St. John's in 1975. Its initial funding was provided by the Devonian Group of Charitable Foundations of Calgary. Ongoing funding now comes from government and industry.

The Centre's mandate is to undertake research that will assist the safe and orderly development of Canada's resources in cold and ice frequented oceans.

J. Vaughn Barrie (Editor)
Leader, Seabed Group
C-CORE

Published by C-CORE February 1984

ISBN 0-88901-106-0

ACKNOWLEDGEMENTS

The presentation, compilation and reduction of these short course notes into one manuscript were the result of the dedicated effort of many people. of whom only a few are mentioned here. Dr. C. Amos was the initial inspiration of the project and hopefully will be instrumental in its further development. Our gratitude to Drs. N. Morgenstern, M. Lewis, T. Chari and Mr. S. Blasco for their time and effort in presenting ongoing research from different areas of the Canadian continental shelf and leading discussions based on their work.

Susan Trim organized the logistics for the short course and related activities. We express our gratitude for her hard work. The many hours of manuscript organization, grammatical editing and compilation were generously undertaken by Susan Waterhouse and Eleanor Nesbitt-Friis. Appreciation is warmly expressed to M. Booton and L. Davis for their assistance. Support for this publication has been received from the National Research Council of Canada through a contribution arrangement.

TABLE OF CONTENTS

Page

Acknowledgements i

Table of Contents ii

List of Figures vii

List of Tables xix

Preface xxi

Chapter 1. **Overview of Continental Shelves**

A.W. Niederoda

1. Introduction - 1

   1.1 Definition of Zones 1

2. Sealevel History - 4

3. Oceanographic Zones of the Continental Shelves - - - - - 5

Chapter 2. **Review of Surficial Geology of the Eastern Canadian Continental Shelf**

J. V. Barrie

1. Introduction - 7

2. Eastern Canadian Shelf - - - - - - - - - - - - - - - - - - 9

   2.1 Area 1 The Scotian Shelf Region 9
   2.2 Area 2 The Grand Banks Region 15
   2.3 Sediment Stability 19
   2.4 Area 3 The Labrador Shelf 22

3. Summary - 35

Chapter 3. **The Continental Shelves off Baffin Island, the Arctic and the West Coast of Canada - Summary Review**

C.P.G. Pereira

1. Introduction - 37

2. Marine Geology of the Continental Shelves - - - - - - - - 41

   2.1 The Baffin Island Continental Shelf 41
   2.2 The Canadian Arctic Archipelago and Shelf Area 57
   2.3 The Beaufort Sea Continental Shelf 65
   2.4 The British Columbia Continental Shelf Margin 75

3. Summary - 81

Chapter 4. **Ice Scour: Methods of Analysis**

J.V. Barrie and C.M.T. Woodworth-Lynas

1. Introduction - 83

2. Methods of Iceberg Scour Analysis - - - - - - - - - - - - 87

   2.1 Repetitive Seabed Mapping 87
   2.2 Dating Scour Populations from Quaternary Evidence 87
   2.3 Direct Dating of Sediments in Scours 88
   2.4 Scour Equilibrium Analysis 88
   2.5 Statistical Analysis of Regional Ice 91
   2.6 Ice Scour Morphology 91
   2.7 Ice Keel Statistics 93
   2.8 Iceberg Grounding Analysis from Wellsite Observations 93
   2.9 Interrelationship with Other Features 94
   2.10 Scour Cross-cutting Analysis 95
   2.11 Dating of a Scoured Surface 96

3. Summary - 96

Chapter 5. **Boundary Layer Flow and the Physics of Sediment Transport**

D.A. Huntley

1. Preface - 99

2. Boundary Layer Flow - - - - - - - - - - - - - - - - - - - 101

   2.1 Introduction 101
   2.2 Types of boundary layer: the basic theoretical background 105

2.3 The Form Drag Problem 119
2.4 Combined Wave and Current Effects 125
2.5 Other complications 130
  2.5.1 Stratification due to sediment load
  2.5.2 Bedload effects on apparent roughness length
  2.5.3 Flow acceleration
  2.5.4 Stress intermittency
2.6 The Practical Estimation of Bed Stress 138
  2.6.1 Quadratic stress law 139
  2.6.2 The velocity profile method 142
  2.6.3 The eddy correlation method 144
  2.6.4 The viscous sublayer method 146

3. Non-cohesive Sediment Dynamics - - - - - - - - - - - - - 149

3.1 Introduction 149
3.2 Threshold of sediment motion 151
3.3 Bedload transport 159
  3.3.1 The Bagnold formula 160
  3.3.2 Einstein's bedload function 163
  3.3.3 Yalin's bedload equation 164
  3.3.4 Bedload transport in oscillatory flows 165
3.4 Suspended load transport 167

Chapter 6. **Sediment Transport in the Marine Environment**

A.W. Niederoda

1. Introduction - 173

2. Basics of Marine Sediments - - - - - - - - - - - - - - - 175

2.1 Sediment Types 175
2.2 Sediment Sizes 178
2.3 Sediment Shapes 182

3. Characteristics of Marine Flows and Sediment Transport - 185

3.1 Modes of Marine Sediment Transport 185
3.2 Benthic Boundary Layer Components 191
3.3 Cohesive and Non-Cohesive Sediment Erosion 193

4. Principles of Marine Bedload Dynamics - - - - - - - - - 195

4.1 Introduction 195
4.2 Description of Bedload Transport 196
4.3 Dynamics of Bedload Transport in Steady Uniform Flow 202
  4.3.1 Settling velocity of sediments 203
  4.3.2 Fluid forces acting on individual grains 209
  4.3.3 Initiation of bedload transport 213
  4.3.4 Bedload transport in steady uniform flow 220

4.4 Dynamics of Bedload Transport in Oscillating Flow 234
  4.4.1 Initiation of particle movement by oscillating flows 235
  4.4.2 Bedload transport in oscillating flows 241
  4.4.3 Dynamics of bedload transport due to the combined effects of waves and currents 245
  4.4.4 Erosion and deposition of bedload in the marine environment 249

5. Suspended Sediment Dynamics - - - - - - - - - - - - - - - - 253

5.1 Dynamics of Suspended Sediment Transport 254
5.2 Suspended Sediment Deposition 260
5.3 Erosion of Suspended Sediments 264

Chapter 7. **Bedforms on Continental Shelves - Their Genesis and Mobility**

C.L. Amos

1. Introduction - 279

2. The Genesis of Bedforms - - - - - - - - - - - - - - - - - - 285

2.1 Non-Cohesive bedforms 285
2.2 Cohesive bedforms 311
  2.2.1 Gravity flows 321
  2.2.2 Slides and slumps 322

3. The Morphology and Distribution of Shelf Bedforms - - - 333

3.1 Non-Cohesive Bedforms 333
  3.1.1 Current Formed Ripples 333
  3.1.2 Wave Formed Ripples 343
  3.1.3 Sand Waves 349
  3.1.4 Megaripples 356
  3.1.5 Sand Ribbons 363
  3.1.6 Sand Ridges 364
  3.1.7 Grain Flows 367
3.2 Cohesive Bedforms 371
  3.2.1 Sediment Gravity Flows 371
    A Turbidity Currents
    B Slumps and Slides
  3.2.2 Flute Marks and Megaflutes 374
  3.2.3 Transverse Scour Marks 375
  3.2.4 Longitudinal Furrows 376
  3.2.5 Pockmarks 376
  3.2.6 Pingos 378

Chapter 8. **Seabed Scour About Discrete Structures**

A.W. Niederoda and C. Dalton

1. Introduction - 381
2. Fluid Mechanics of the Scour Problem - - - - - - - - - - 381

   2.1 Secondary Flow 383
   2.2 Convective Accelerations of the Flow 385
   2.3 Flow in the Obstruction's Wake 386
   2.4 Flow Disturbances in Oscillating Flows 387
   2.5 Flow Disturbances in Due to the Combined Effect of Waves and Currents 388

3. Sediment Mechanics of the Scour Problem - - - - - - - - - 390

   3.1 Sediment Types 390
   3.2 Entrainment Criteria 390
   3.3 Transport, Erosion and Deposition 392

4. The Mechanics of Scour in Steady Currents - - - - - - - - 395

5. The Mechanics of Scour in Oscillating Flow - - - - - - - 399

6. Mechanics of Scour Due to Waves and Currents - - - - - - 404

7. Conclusions - 409

Chapter 9. **Discussion Sessions**

1. Beaufort Sea Experiences
   - chaired by S.M. Blasco - - - - - - - - - - - - - - - - 411

2. Eastern Canadian Shelf Experiences
   - chaired by C.F.M. Lewis - - - - - - - - - - - - - - - 415

3. Geotechnical Perspective
   - chaired by T.R. Chari - - - - - - - - - - - - - - - - 425

4. Open Discussion
   - chaired by J.V. Barrie - - - - - - - - - - - - - - - - 429

List of Authors 435

List of Discussion Leaders 436

List of Participants 437

REFERENCES 439

LIST OF FIGURES

Chapter 2

Figure		Page
2-01	Index map of eastern Canadian Continental Shelf.	10
2-02	Surficial geology of the Scotian Shelf and adjacent areas.	11
2-03	Diagrammatic cross-section of the Scotian Shelf showing the surficial geology across Emerald Bank and Emerald Basin over the overlying bedrock.	11
2-04	Distribution of geological, morphological and sedimentological feature of the Scotian Shelf and adjacent areas.	13
2-05	Regional bedrock geology of the northeastern Grand Banks of Newfoundland.	14
2-06	Geological cross-section of the northeastern edge of the Grand Bank in the Hibernia area.	18
2-07	Wave-induced bifurcating ripples at 80 metres water depth near the Hibernia discovery area.	19
2-08	Klein sidescan sonogram from the northeastern Grand Banks.	20
2-09	Arcuate sand waves on Grand Banks at 80 metres water depth.	22
2-10	The morphology and general bathymetry of the Labrador Continental Shelf.	23
2-11	Surficial sedimentary units on Hamilton Bank.	26
2-12	Glacial drift thickness along the Labrador coast.	27
2-13	Bathymetry of southern Saglek Bank.	29
2-14	Geological cross-section across southern Saglek Bank showing the surficial geological units and bedrock in relation to bathymetry.	31
2-15	Example of a Huntec DTS seismic profiling record from southern Saglek Bank.	32
2-16	Sidescan mosaic from a portion of southern Saglek Bank.	33

Chapter 3

Figure Page

3-01 Index map illustrating the extent of systematic coverage and type of marine geological survey undertaken by industry and government on the continental shelf areas that surround the coastal regions of Canada. 39

3-02 Structural types of continental margins as applied to the Canadian Continental Shelf. 40

3-03 The physiographic relief of the continental margins of Canada illustrating the principal characteristics of the shelf and slope area. 42

3-04 Map indicating marginal channels along the east coast of Canada. 44

3-05 A buried erosional depression feature in Tertiary bedrock as seen along an E-W geophysical transect at latitude 62°N. 46

3-06 Sediment textural distribution of the Baffin Bay area. 48

3-07 Surface oceanic circulation of the Baffin Bay area. 49

3-08 Sediment textural distribution off Exeter Bay, Davis Strait. 50

3-09 Observed apparent thickness of surficial deposits east and southeast of Baffin Island. 52

3-10 Areal distributional map of seismic activity greater than magnitude 3 in the Canadian Arctic. 56

3-11 Index map for the Canadian Arctic archipelago. 58

3-12 Map of northwestern approaches to the Arctic ocean. showing drowned physiographic features. Deep troughs are divided by median ridges and U shaped valleys. 59

3-13 Schematic northwest-southeast structural cross-section across the Beaufort Sea. 64

3-14 Physiographic provinces of the Beaufort Sea area. 66

3-15 Bathymetric map of the Beaufort Sea area. 67

3-16 Sediment distribution patterns for the Beaufort Sea area. 69

Figure Page

3-17 Hydrodynamic environments for the Beaufort Sea area. 71

3-18 Continental plate configuration off the British Columbia coast. 74

3-19 Bathymetric and physiographic map of the west coast of Canada. 74

3-20 Distribution of surficial sediments on the continental shelf, west central Vancouver Island. 78

Chapter 4

4-01 Diagrammatic presentation of iceberg scour mark, with representative bottom photographs from a submersible. 84

4-02 A sidescan mosaic of an area of south-central Saglek Bank showing the distinctive iceberg scours in plan and cross section. 86

4-03 Method for dating absolute age of a scour. 89

4-04 Underwater photograph of a small grounded ice island (iceberg) showing the formation of an ice scour in unconsolidated sediment. 90

4-05 Diagrammatic representation of a 'relict' iceberg scour mark with photographic examples. 92

4-06 Megaripples obliterating an iceberg scour on the northeastern Grand Banks in 80 m water depth as seen on a sidescan sonogram. 94

4-07 Morphological criteria for determining cross-cutting relationships. Each diagram is accompanied by a photograph of an example of the type of cross-cut, from original sonograms. 97

Chapter 5

5-01 Hydrodynamic zones of the Continental Shelf 102

5-02 Schematic of the relative size of molecular and turbulent (eddy) stresses close to a hydrodynamically smooth boundary. 107

5-03 Relationship between z_f/k_s and u_*k_s/v for hydraulically transitional flow. 109

5-04 Frictional effects on a geostrophic current near the bottom of the ocean (northern hemisphere). 111

Figure Page

5-05 Subdivisions of the benthic boundary layer. 113

5-06 Characteristic velocity profiles in the oscillatory boundary layer for a wave cycle. 115

5-07 Typical velocity field of the oscillatory turbulent boundary layer under a wind wave. 115

5-08 The "amplitude function" F vs. ζ_o 116

5-09 Plot of K_o/U_o vs. WZ_o/u_o, where u_o is the orbital velocity above the boundary layer. 117

5-10 Einstein's 1964 plot of u_*''/u vs. ψ_{35}. 122

5-11 Ratio of apparent bed roughness, k_{bc}, to true bed roughness, k_b, for waves and currents in the same direction. 129

5-12 Wave current friction factors for codirectional and transdirectional flow. 129

5-13 Schematic comparison of velocity profiles in stably stratified and neutral boundary layers. 133

5-14 Velocity and sediment concentration profiles for four cases of stratified flow. 133

5-15 Drag coefficient (C_{100}) as related to the Reynolds number. 140

5-16 Drag coefficient (C_{100}) as related to the Reynolds number for all data combined. 141

5-17 Determination of the friction velocity u_* and the roughness length z_o from a logarithmic velocity profile. 143

5-18 Schematic diagram showing the motion of horizontal turbulent momentum $\rho u'$ through a horizontal plane by vertical turbulent velocity ω'. 145

5-19 A linear -velocity profile in the laminar sublayer within 1 cm of the bed. 148

5-20 Non-dimensional boundary shear stress required to initiate sediment transport. as a function of the non-dimensional number representing fluid and sediment properties. 153

5-21 The Shield's curve for quartz grains in water. 155

Figure Page

5-22 The modified Shield's curve for a rippled bed. 155

5-23 Threshold orbital velocity required to initiate motion of grains of quartz, as a function of grain diameter and wave period. 157

5-24 Relationships between the coefficient K, the excess shear stress and the sediment diameter. 162

5-25 Nomogram relating U_*, j and K. 162

5-26 Variation in relative concentration of suspended sediment with relative depth above a datum. 168

5-27 Typical shapes of suspended sediment concentration in an oscillatory boundary layer. 170

Chapter 6

6-01 Qualitative roundness and sphericity illustrations for sand grains. 183

6-02 Schematic illustration of particle settling in isotropic turbulence. 187

6-03 Schematic diagram of upward and downward advection of suspended particles. 189

6-04 Schematic diagram of bedload transport. 190

6-05 Schematic diagram of forces causing bedload transport. 190

6-06 Representation of the rolling, sliding and saltating modes of bedload transport. 197

6-07 Trajectory of saltating bedload grain. 197

6-08 Schematic representation of ripple mark migration. 199

6-09 Schematic representation of the settling of a small sphere at low Reynolds number. 204

6-10 Definition sketch for force equilibrium of a settling sphere. 205

6-11 Definition sketch for forces acting on a discrete grain in the bedload. 210

6-12 Schematic representation of resultant forces acting on a saltating grain. 211

Figure Page

6-13 Schematic representation of the changes in resultant fluid forces acting on a saltating grain. 211

6-14 Schematic representation of forces considered in developing the Shield's parameter. 215

6-15 The Shield's diagram. 219

6-16 The modified Shield's diagram. 219

6-17 Definition sketch for Bagnold's sediment transport theory. 221

6-18 Definition sketch for Einstein's bedload transport theory. 227

6-19 Comparison of Einstein's bedload relationship with experimental data. 232

6-20 Comparison of the Einstein-Brown bedload transport relationship with measured data. 233

6-21 The Jonsson wave friction coefficient diagram. 239

6-22 The Kamphius wave friction coefficient diagram. 239

6-23 Comparison of measured values of sediment entrainment with that predicted by Madsen and Grant's application of the Shield's parameter to oscillating flow. 242

6-24 Comparison of measured data from Manohar's 1955 data on sediment transport due to waves with that predicted by Madsen and Grant through the application of the Einstein-Brown bedload transport formula to oscillating flows. 244

6-25 Figure showing the vertical distribution of relative concentration of suspended sediment against depth for different values of the parameter beta. 258

6-26 Weight loss per one minute versus deflection. 266

6-27 Shear vane strength versus critical shear stress for the Taylor Marl. 268

6-28 Critical shear stress versus moisture content. 269

6-29 Vane shear strength versus critical shear strength. 270

6-30 Critical tractive force determined from velocity profile versus plasticity index. 272

Figure Page

6-31 Critical tractive force determined from velocity profile versus dispersion ratio. 272

6-32 Specimen erosion rate versus shear stress. 274

6-33 Relationship between erosion and shear stress for differential SAR for the Yolo loam, concentration 0.005 N-w/c = 23%. 274

6-34 Variation of suspended sediment concentration with time and temperature. 274

Chapter 7

7-01 A summary of the main physical processes influencing continental shelf sediments. 280

7-02 The distribution of processes on the continental shelf. 281

7-03 A hypothetical reconstruction of a sandy shelf. 283

7-04 (A) The relationship of grain size to boundary layer flow close to the bed. 286

7-04 (B) The pattern of flow streamlines over ripple bedforms. 287

7-05 (A & B) The terminology used to define the morphology of rhythmic bedforms in non-cohesive material. 289

7-05 (C) The progression of bedforms resulting from an increase in unidirectional flow over silt and very fine sand, medium sand and coarse sand. 289

7-06 (A) The phase relationship between bedform type, mean flow velocity (over a flow depth of 40 cm) and grain size (mm). 290

7-06 (B) The succession of bedforms which develop on a sandy shelf in a diminishing current field (from 2.5 kts - 1.5 kts, i.e. 1.2 - 0.7 m/s). 292

7-07 (A and B) The phase relationship between mean flow depth, mean flow velocity and bedform type for medium sand substrates (A) and coarse sand substrates (B). 298

7-07 (C) The extrapolation of flume tank data to field conditions for medium sand substrates. 298

Figure Page

7-08 (A) The phase relationship between Reynolds number (Re), Froude number (Fr) and bedform types. 299

7-08 (B) The phase relationship between flow velocity, flow depth. Reynolds number and Froude number. 299

7-09 (A) The phase relationship between stream power (τ_o U) grain diameter (D) and bedform type for non-cohesive, sand-sized sediments. 302

7-09 (B) The phase relationship between shear velocity (U_*), grain diameter (D) and bedform type. 302

7-10 (A) The phase relationship between maximum orbital velocity under waves (U_{max}) and grain diameter. 307

7-10 (B) The relationship between the combined ratio of the maximum wave oscillatory velocity (U_w) and the unidirectional friction velocity (U_*), based on results from The Wash, E. England. 307

7-11 (A) A schematic of the sediment transport phases for non-cohesive material as a function of bottom stress. 312

7-11 (B) A schematic of the sediment transport phases for cohesive material as a function of bottom stress. 312

7-12 (A) The correlation between plasticity index and critical shear stress for erosion for a number of terrestrial soils. 315

7-12 (B) The correlation between critical shear stress and percentage clay. based on the analysis of a number of terrestrial samples. 315

7-13 The relationship between average flow velocity ($\bar{\mu}$) grain diameter (d) and sedimentation phase. 318

7-14 (A) Spiral vortices on the shelf inferred to create sand ridges. 319

7-14 (B) A schematic representation of spiral vortices originally used to explain linear features in deserts. 320

7-15 (A) The classification of sediment gravity flows of Middleton and Ludwick, (1975). 322

7-15 (B) An hypothetical evolution of a single flow. 323

7-15 (C) The internal structures of sediment gravity flows. 324

Figure Page

7.15 (D) Slumping generated at the edge of a grounded ice floe, or at the margin of scouring iceberg. 325

7-16 (A) A fine-grained depositional model for continental margins under well stratified water masses. 326

7-16 (B) A fine-grained, depositional model for continental margins under minimally stratified water masses. 326

7-17 (A) A proposed mechanism for transporting cohesive material across the continental shelf, based on observation on the North Puerto Rico Shelf. 328

7-17 (B) A proposed model for the transport of suspended sediment across the continental shelf, based on measurements made on the Oregon shelf. 329

7-18 A summary of sedimentation patterns on the Nova Scotian continental shelf leading to slumping at the shelf edge and the development of turbidity currents. {330 331

7-19 (A) A classification of ripple train crest patterns based on observation and flume tank experimentation. 337

7-19 (B) The sequence of ripple train crest patterns which will develop under varying unidirectional flows. 338

7-20 (A) A block diagram showing the internal structure and morphology of straight crested, current formed ripples. 339

7-20 (B) A block diagram showing the internal structure and morphology of undulatory, current formed ripples. 340

7-21 (A) A block diagram showing the internal structure and morphology of linguoid ripples. 341

7-21 (B) A block diagram showing the internal structure and morphology of lunate (3-D) megaripples. 342

7-22 (A) The frequency of occurrence of asymmetric ripples versus current ripples as a function of wave ripple symmetry index. 344

7-22 (B) The frequency of occurrence of asymmetric wave ripples versus current ripples as a function of ripple index. 344

Figure Page

7-22 (C) The values of various ripple indices at which waves or currents predominate in the generation of bedforms, and the intermediate zones where interpretation is difficult. 345

7-22 (D) A plan view of two sets of ripple train crests. 345

7-22 (E) The definition of the various ripple indices used to define ripple types. 345

7-23 (A) Wave ripple cross-lamination and morphology of symmetric wave ripples. 346

7-23 (B) A common sequence of bedforms generated on continental shelves showing the modification of current ripples (either sinuous or linguoid types) into wave formed ripples. 347

7-24 A composite diagram of ripple spacing ( ) versus orbital diameter (d_o) compiled by Miller and Komar (1980) from data by others. 348

7-25 (A) The relationship between water depth and sand wave height for selected Atlantic shelf sand wave fields. 351

7-25 (B) The relationship between sand wave height and sand wave wavelength for selected Atlantic shelf sand wave fields. 352

7-26 (A) An echogram through a sand wave field in the North Sea. 353

7-26 (B) Various profiles of sand waves from the southern bight of the North Sea. 354

7-26 (C) The migration rate of various types of bedforms as a function of current velocity, taken from a variety of locations worldwide. 354

7-27 Sand waves from the North Sea
(A) Photographs of the sand waves exposed during low tide in the Jade estuary.
(B) The internal structure of a sand wave showing the composite structure of cross-laminae.
(C) The internal structure of a spring tide sand wave showing composite cross-laminated bundles interpreted to have developed during successive spring tides. 355

Figure Page

7-28 A sidescan sonar record of sand waves with superimposed 2-D megaripples, from the Atlantic shelf near Cape Hatteras. 357

7-29 A sidescan sonar record of low amplitude sand waves with superimposed 3-D megaripples from the Long Island inner shelf. 358

7-30 (A) A phase diagram relating current speed (depth averaged), grain size (in phi units) and bedform types for the Minas Basin, Bay of Fundy. 359

7-30(B) A phase chart relating water depth. current speed and bedform type for the Minas Basin. 359

7-30 (C) The flow characteristics and sediment type for the generation of bedforms in Minas Basin. 359

7-31 A sidescan sonar and echo sounding record of planar 2-D megaripples from the Miramichi estuary, Gulf of St. Lawrence. 361

7-32 A sidescan sonar mosaic of the Hibernia region, Grand Banks of Newfoundland. 362

7-33(A) The distribution of tidal sand ridges in the southern North Sea. 365

7-33(B) The process of formation and modification of tidal sand ridges. 365

7-33 (C) Interpretation of three sparker profiles through tidal sand ridges of the southern North Sea. 366

7-34 The evolution of the surficial sediments on the Sable Island Bank and Scotian slope. Figures A-D show the development through time of the various recognized deposits. 369

7-35 (A) The location and nature of the famous Grand Banks slump and turbidity current which took place during 1929. 370

7-35 (B) The velocity of the 1929 turbidity current and the profile of its path. 372

7-36 A "bottle-neck" slump structure. typical of regions of high sedimentation rates and low shear strengths. 373

7-37 The development of pockmarks on the Scotian Shelf. the effect of degassing (or dewatering) of the seabed. 377

Figure Page

7-38 (A) The distribution of pingos on the MacKenzie delta. 379

7-38 (B) The formation of pingos in the Beaufort Sea. 380

7-38 (C) The stratigraphy on a specific pingo in the Beaufort Sea. 380

Chapter 8

8-01 Sketch of flow around a cylindrical obstruction. 382

8-02 Top (above) and upstream (below) views of the horseshoe vortex. 394

8-03 Flow and scour produced by a steady boundary layer flow. 397

8-04 Instantaneous flow and scour due to oscillating flow. 401

8-05 Stages of wave-induced scour hole formation. 402

LIST OF TABLES

Page

Chapter 3

Tables 3-I to 3-IV: Some possible engineering geo-hazards

Table 3-I Baffin Island Shelf 54
Table 3-II Arctic Shelf Area 63
Table 3-III Beaufort Sea 73
Table 3-IV British Columbia 80

Chapter 5

Table 5-I Physical processes and their scales 104
Table 5-II Typical values of boundary layer parameters 113
Table 5-III Mean C_{100} and 95% confidence limits for all boundary-layer data, regardless of bed configuration 141
Table 5-IV Various size grade scales in common use 154
Table 5-V Fall velocities for quartz grains in water 158
Table 5-VI Bagnold's bedload transport model 160

Chapter 6

Table 6-I Grain size scale for sediments 180
Table 6-II Properties of sediment aggregates 276
Table 6-III Parameters potentially related to the critical fluid shear stress to erode cohesive sediments 277

Chapter 7

Table 7-I The approximate mean current velocities (40 cm above the bed) bounding to the various types of constructional, non-cohesive bedforms for fine, medium, coarse and very coarse sand 294
Table 7-II The approximate entrainment stresses and velocities for the initiation of grain motion and for grain dispersion of sand size sediment 295
Table 7-III The range in threshold velocities for the generation of wave formed ripples and flat (plane) beds 308
Table 7-IV The critical stress for erosion of cohesive sediments, based on flume tank and in-situ measurements 313
Table 7-V Data on critical shear stress of sediments 316
Table 7-VI A review of terminology used to describe constructive non-cohesive bedforms by various authors 332
Table 7-VII Size parameters used to identify bedform types {334, 335}

PREFACE

Recent developments in research on the Canadian Continental Shelves have indicated that the nature and mechanics of surficial sediment distribution, transport and stability are central to a number of key problems related to the offshore oil and gas industry, as well as to the non-petroleum related resources. Early in 1981 Dr. Carl Amos conceived the idea of a course that would be an initial step in addressing this need. Through discussions with C-CORE the following short course was organized. The intention was to bring together experts in this field from both Canada and the United States to present the state of contemporary scientific and engineering thinking and apply this knowledge to Canadian shelf problems. The resultant course was held on the 9th and 10th of March, 1982; the edited notes are presented here.

Our hope is that these papers will form an initial base for a future more complete book on 'Sediment Stability of Canadian Continental Shelves' which will highlight some of the ongoing research. As this is an advancing science and offshore development off Canada's coast is accelerating, many concepts presented here will develop and change as our knowledge increases. Indeed, since these papers were written, edited and compiled for publication, advances in some of the ideas presented here have already been made. My hope is that this will serve as a useful working document that will form the base of future research.

J. Vaughn Barrie, Editor

Number/
Numéro

2

Chapter 1. OVERVIEW OF CONTINENTAL SHELVES

Alan W. Niederoda

1. INTRODUCTION

The purpose of this section is to establish an overall context for a short course on continental shelf sediment movement. Therefore, the major emphasis is to give a general overview of continental shelves and modern processes which influence them.

The shallow portion of the world's oceans which adjoins most land masses and is called the continental shelf, has different meanings to different people. To geologists, the continental shelves are merely a drowned extension of the continent. To oceanographers, the continental shelf environment represents a transition in the types and movements of water masses from the relatively steady conditions of the open ocean to the rapidly varying conditions of the coastal boundary layer. To an engineer. the continental shelf represents an area where he must fit his knowledge of a unique set of forces and processes to society's needs for placing structures and facilities in this area.

1.1 Definition of Zones

The initial definition of continental shelves was based primarily on their relatively shallow depth and gentle slopes. The basic concept is that continental shelves extend from just beyond the shore zone to the point where there is a relatively sharp change in the slope of the seafloor. Seaward of this point, the continental slope begins. The contrast in slopes is not necessarily major. Most continental shelf areas slope very gently, in the order of 1° or less, whereas most continental slopes range in steepness between 3 and 6°. Nevertheless, the vertical exaggeration which is generally incorporated into bathymetric maps make the diference in slope between these two areas appear to be dramatic. The intersection of the continental shelf with the continental slope is defined as the continental shelf break.

Continental shelves vary in width from almost nothing to more than 200 miles. The average depth of the continental shelf break is 130 metres (450 ft), but this ranges from as little as 50 metres to as much as 350 metres. On the average, continental shelves are approximately 65 km wide. The continental shelf is often divided into three regions. These are called the inner, middle and outer portions. The inner portion of the continental shelf generally abuts the shoreface. The shoreface is a transition zone between the continental shelf and the beach system on the shore. Actually, the beach and shoreface are separated by a zone of commonly breaking waves known as the surf zone. The shoreface generally has a much steeper slope than that of the inner continental shelf, although there is no marked interface between the two regions.

Offshore, beyond the outer continental shelf, the continental slope begins. The shelf break is punctuated in places by deep submarine canyons which are incised into the continental slope. The physiography of continental shelves is highly variable. In subtropical regions, extensive reefs develop on the shelf. Off major rivers, extensions of delta systems, cross the shelf. These submerged extensions of the delta systems are often characterized by numerous collapse holes, slump blocks, and mudflow channels. Other portions of the continental shelves contain large areas of shoals or banks. In extreme cases, such as George's Bank off the coast of Massachusetts, depths of less than 3 metres can be found many tens of miles offshore. Many areas of the continental shelves are covered with an assortment of large-scale sand waves which are often arranged in nearly regular geometric patterns. Deep channels also exist on the surface of continental shelves. These appear to have been former river drainages which were flooded during a recent rise in sea level.

The surficial sediments of continental shelves are also quite varied. Sand and gravel deposits are common. These may result from recent deposition of these sediments or from the reworking of previous deposits by the winnowing action of waves and currents. Extensive areas of mud deposits and areas of carbonate sands also exist on continental shelves.

2. SEA LEVEL HISTORY

In order to put the problem of modern sediment motion into an appropriate time frame, it is necessary to look back in earth history. Only as little as 10,000 years ago, worldwide sea levels were much lower. At this time, the great continental glaciers which covered most of North America, as well as large areas of Europe, Greenland and Antarctica, were at their maximum extent. The water which went into making up these great ice sheets came from evaporation of seawater. As these glaciers spread out across North America, their weight caused the level of the underlying land to subside. There is a growing body of evidence which suggests that the subsidence of land beneath the glaciers was offset by a general rise of the land in areas surrounding the glacier. This means that in many areas, the continental shelf was uplifted somewhat at the same time as the sea level was lowered. In other areas, closer to the location of maximum glacial loading, the level of both the land and the sea were lowered. In many areas, this history is further complicated by the action of deepseated earth movements which have changed the relative level of coastal lands locally. The history of the relative level of the sea compared to the adjoining land is complex and must be resolved area-by-area. A common pattern is for most or all of the continental shelf to have been exposed above sea level during the time of maximum glaciation. Therefore, many of the morphologic features and sediments presently characterizing the continental shelves originated from terrestrial processes at that time.

3. OCEANOGRAPHIC ZONES OF THE CONTINENTAL SHELVES

The inner. mid and outer portions of the continental shelves frequently constitute distinct zones where particular time and length scales are significant in characterizing the flow. The inner portion of the continental shelves are intimately coupled with the shorefaces. This region is referred to as the coastal boundary layer. Because of the proximity of the shoreline and relativity shallow depths, the circulation of this portion of the ocean responds rapidly to changing meteorological events. In temperate latitudes, these meteorological events tend to follow one another at intervals from 2 to 6 days. The coastal boundary layer is primarily affected by wind-driven circulation. The respose of the water mass to changing wind stresses is rapid. Onshore wind stresses tend to pile water against the shoreline and cause down-welling to occur over the shoreface. The major portion of these flows is constrained to a zone of about 3 to 5 miles in width. Offshore-directed flows tend to lower the mean water level along the shoreline. Thus, there is an intimate connection between the general slope of the sea surface in this area. current circulations, and wind stresses. During summertime conditions, the water masses of the inner continental shelf are often stratified. Warm water of relatively low density overlies cooler and saltier water. The interface between these water masses can be rather sharp. At times, when the coastal ocean is stratified, the circulation produced by changing wind stresses can become quite complex. Upwelling and downwelling currents along the shoreface develop a compensating flow near the level of the density interface between the surface and bottom water masses. In the presence of onshore or offshore-directed flows, both the slope of the sea surface and the slope of the density interface between water masses can change. This represents a change in the potential energy of the system which can convert to pressure-driven flow components in the coastal ocean.

The mid-shelf region is an area sufficiently removed from the coastal boundary, that its response to wind stress events is that of a relatiely shallow and relatively unconstrained ocean. Large-scale wave motions, often generated by processes occurring at the shelf break, can propagate across the mid-shelf region and cause local distortions in the sea surface slope. These changes in the slope of the sea surface are capable of driving currents in the mid-shelf region.

The outer continental shelf represents a transition zone between the deep ocean and the water masses of the continental shelf. The water masses of the continental shelf generally respond rapidly to seasonal changes in temperature due to the relatively shallow depths and high level of turbulent mixing. The adjacent ocean waters are often characterized by relatively strong ocean boundary currents (e.g., the Gulf Stream or the Alaska Current). A complex interaction develops between the water masses on either side of the outer continental shelf which can result in intrusions of ocean water over the shelf, or the generation of long-period wave motions which locally influence outer shelf currents and circulation.

Chapter 2. REVIEW OF SURFICIAL GEOLOGY OF THE EASTERN CANADIAN CONTINENTAL SHELF

J. Vaughn Barrie

1. INTRODUCTION

Seabed investigations of the Canadian Continental Shelves have been given a fresh impetus by new discoveries of hydrocarbons in the Beaufort Sea. on the Grand Banks of Newfoundland and the potential reserves on the Baffin, Labrador and Scotian Shelves. Economical exploitation of these natural resources, however, through a variety of seabed installations will depend on overcoming seabed geological and oceanographical problems.

Both industry and academic studies of the eastern Canadian offshore have been underway for the past 15 years, mainly independent of each other. The academic research surveys generally have been coordinated through Canadian research organizations from the Bedford Institute of Oceanography, and to a lesser degree through University research in Maritime regions. The primary objective of these studies is to determine the stratigraphy, sedimentary character and geological history of specific areas from which models may be constructed and extrapolated to other areas. These studies, however, have not looked at the sediment dynamics of the shelf until recently. Virtually, no consideration has been given to the geotechnical properties of shelf sediments outside of specific studies by the oil industry. On the other hand, industry has undertaken detailed site surveys of drilling locations primarily to satisfy government regulations (see; Offshore Exploratory Drilling, Procedures and Guidelines, 1980). Data collected generally includes bathymetric, high resolution seismic profiling, CDP seismics and side scan surveys with a few bottom samples as well as bottom photographs of the seabed. The minimum area covered is approximately 2 km^2 around the proposed wellsite. Many times operators extend this information base mainly to examine the ice scour density and distribution patterns. Rarely have these two individualistic approaches been assimilated to gain maximum information since the objectives of both sources of data collection are, initially, too diverse (Barrie and Snyder, 1981).

A knowledge of the stability of the seabed is critical to engineering studies. An initial broad geological appreciation of the surficial sediments and their geological history is necessary to understand the environment and the processes, both past and present, which affect sediment stability. The following review will outline briefly the surficial geology of these areas of the eastern Canadian Continental Shelves which are likely to be the focus for hydrocarbon exploration and ultimate extraction in the immediate and near future.

2. EASTERN CANADIAN SHELF

Nearly the whole of the eastern Canadian Continental Shelf was formerly glaciated. The typical shelf is characterized by a surficially 'rough' inner shelf which is an offshore continuation of the land, bordered by a relatively deep marginal channel and in many areas transverse depressions. This is followed offshore by elongated, flat-topped banks with intervening saddles to the continental slope (Fig. 2-01). The morphology of such shelves had been considered glacial in origin (by processes of glacial scour, (Holtedahl, 1956)) but recent evidence on the Scotian Shelf indicates the shelf is bedrock controlled (King, 1980) representing cuestas and mesas with adjacent lowland areas. Upon this basic bedrock morphology, glaciation and glaciomarine activity have since modified the banks and deposited glacially derived sediments over the entire shelf.

2.1 Area 1 The Scotian Shelf Region

The Scotian Shelf is divisible into five successive formations: Scotian Shelf Drift, Emerald Silt, Sambro Sand, Le Have Clay, and Sable Island Sand and Gravel (King, 1980; Parrott et al., 1980). The areal distributions of these units are shown in Figure 2-02 and a cross section is shown from an area south of Halifax across Emerald Basin and Emerald Bank in Figure 2-03

The Scotian Shelf Drift is the lowermost unit. It is a dark greyish brown, cohesive, poorly sorted sediment containing angular gravel which is sometimes in the boulder size range. The Emerald Silt, a proglacial formation, was formed under brackish

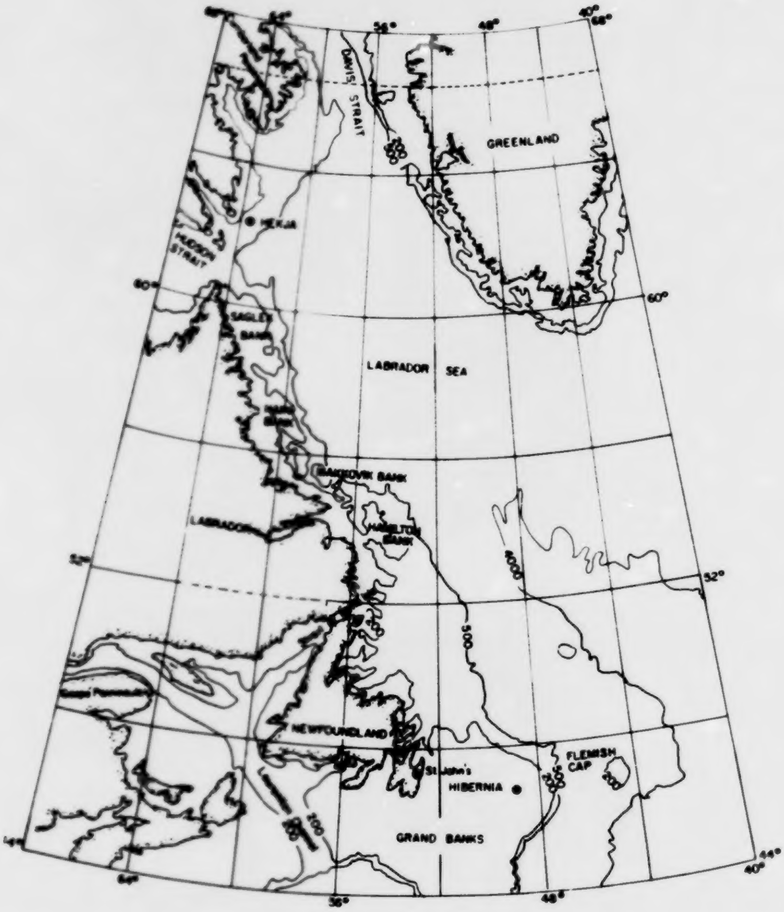

64°
56°
48°
40°
68°
DAVIS STRAIT
500
GREENLAND
HEKJA
HUDSON STRAIT
60°
60°
SAGLEK BANK
LABRADOR SEA
BANK
MAKKOVIK BANK
LABRADOR
HAMILTON BANK
4000
52°
52°
500
NEWFOUNDLAND
St John's
HIBERNIA
FLEMISH CAP
500
200
200
500
GRAND BANKS
44°
64°
56°
48°
40°
44°

Figure 2-01 Index map of eastern Canadian Continental Shelf.

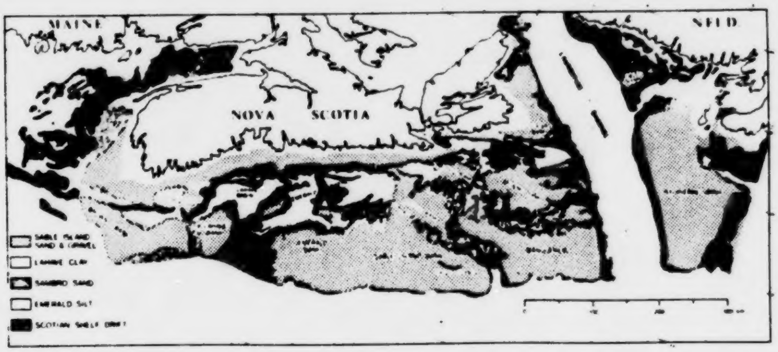
MAINE
NFLD
NOVA SCOTIA
SABLE ISLAND SAND & GRAVEL
LAHAVE CLAY
SAMBRO SAND
EMERALD SILT
SCOTIAN SHELF DRIFT

Figure 2-02 Surficial geology of the Scotian Shelf and adjacent areas (from King, 1980).

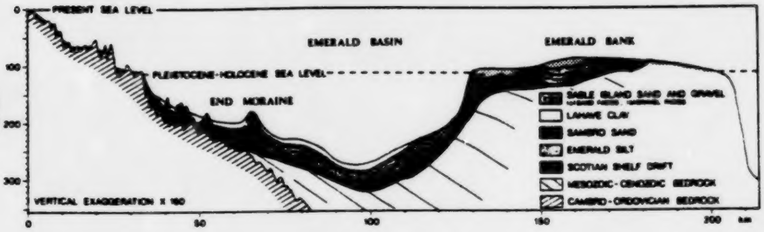
PRESENT SEA LEVEL
EMERALD BASIN
EMERALD BANK
PLEISTOCENE-HOLOCENE SEA LEVEL
END MORAINE
METRES
0
100
200
300
VERTICAL EXAGGERATION X 100
SABLE ISLAND SAND AND GRAVEL
LAHAVE CLAY
SAMBRO SAND
EMERALD SILT
SCOTIAN SHELF DRIFT
MESOZOIC-CENOZOIC BEDROCK
CAMBRO-ORDOVICIAN BEDROCK
0
50
100
150
200 km

Figure 2-03 Diagrammatic cross-section of the Scotian Shelf showing the surficial geology across Emerald Bank and Emerald Basin over the overlying bedrock (from King, 1980).

to marine conditions from floating ice. In some areas it is interbedded with till. The Scotian Shelf Drift and Emerald Silt were reworked by bottom currents resulting in the deposition of Sambro Sand. It was deposited sublitorally with respect to a late Pleistocene-Holocene shoreline which occurred 115 m below the present sealevel. Upon the Scotian Shelf Drift and Emerald Silt a marine silty clay (Le Have Clay) was laid during transgression in the basins and depressions of the shelf. Above 115 m water depth the Sable Island Sand and Gravel was deposited as a basal transgressive deposit overlying eroded remnants of Scotian Shelf Dirft and Emerald Silt. It is comprised of clean, medium to coarse-grained, very well sorted sand grading laterally into lag deposits of very coarse, well rounded gravel with boulders.

These deposits formed on a bedrock surface (Fig. 2-03) which to a large degree was inherited from a former coastal plain environment. Upon this, the continental ice sheet advanced and retreated. King (1980) states that the last major ice advance was fully developed at about 26,000 B.P. By the end of the Pleistocene, approximately 15,000 years B.P. (Milliman and Emery, 1968), sealevel stood at its lowest point, 115 m below present sealevel (King, 1970). During this low stand, Emerald Silt and glacial till in the peripheral areas of the basins were reworked and modified to form the sublitteral Sambro Sand, while the bank areas were subjected to subaerial erosion. As sealevel rose, the bank areas were transgressed and well sorted beach sands and lag deposits of well rounded gravel (Sable Island Sand and Gravel) were formed. The winnowed fines were deposited in the various basins to form Le Have Clay.

At the end of the Pleistocene. during a low sealevel stand, drainage systems were developed which drained to the shelf edge (Fig. 2-04). Many of these were deepened by glacial erosion (King, 1980). These have since been filled and can clearly be seen in the bathymetric and seismic profiles. Similarly, fiord-like features (Shepard, 1931; King, 1980) along the Laurentian Channel and in areas immediately offshore from Newfoundland (Fig.

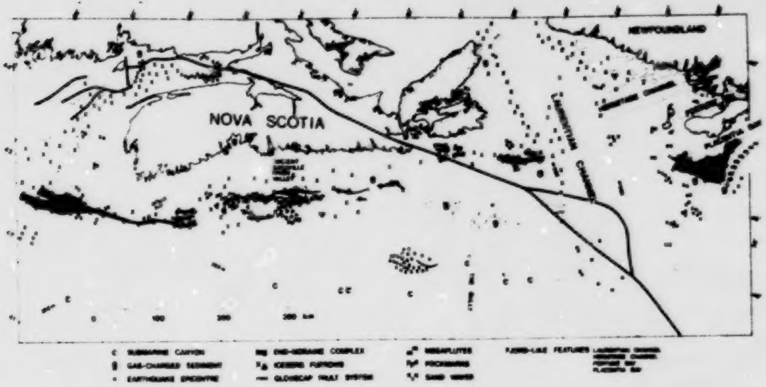
NEWFOUNDLAND
NOVA SCOTIA
100
200
300 km
SUBMARINE CANYON
GAS-CHARGED SEDIMENT
EARTHQUAKE EPICENTRE
END-MORAINE COMPLEX
ICEBERG FURROWS
GLOOSCAP FAULT SYSTEM
MEGAFLUTES
POCKMARKS
SAND WAVES
FJORD-LIKE FEATURES

Figure 2-04 Distribution of geological, morphological and sedimentological feature of the Scotian Shelf and adjacent areas (from King, 1980), which are important to engineering studies.

2-04) were created during the same period and are now fully submarine.

Many major depressions were incised along the shelf edge of the Scotian Shelf and Grand Banks by turbidity currents during this same period of low sealevel stand; these are the submarine canyons. Some of these canyons may well still be active as in the case of the Gully on the Scotian Shelf (Marlowe, 1967). Material derived from the Pleistocene glaciers and subsequent ice-rafting, that lies at the edge of the shelf above the submarine canyons is periodically suspended and moved downslope by the benthic currents (Stow, 1978). This process may be accompanied or enhanced by slumping on the upper slope and the generation of turbidity flows to the sediment fans at the base of the slope and on the continental rise.

Other geological features found on the Scotian Shelf that are physical evidence of hazards to seabed engineering are iceberg furrows and pochmarks (King and MacLean, 1970). Iceberg furrows found here are relict (King 1976). Pockmarks are cone

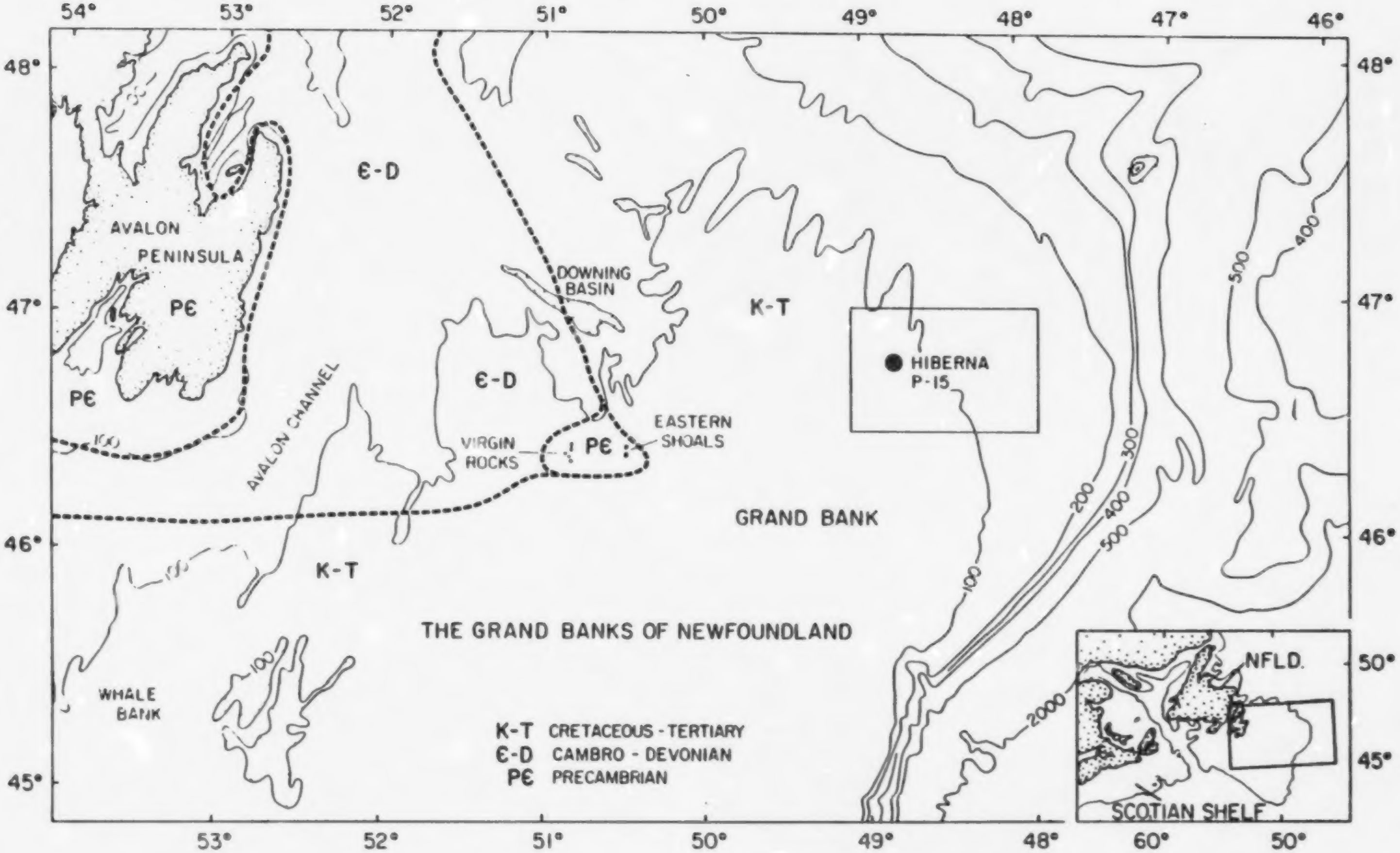
54°
53°
52°
51°
50°
49°
48°
47°
46°
48°
47°
46°
45°
AVALON
PENINSULA
PЄ
PЄ
Є-D
Є-D
DOWNING
BASIN
K-T
K-T
HIBERNA
P-15
VIRGIN
ROCKS
PЄ
EASTERN
SHOALS
AVALON CHANNEL
GRAND BANK
THE GRAND BANKS OF NEWFOUNDLAND
WHALE
BANK
100
200
300
400
500
2000
K-T CRETACEOUS - TERTIARY
Є-D CAMBRO - DEVONIAN
PЄ PRECAMBRIAN
NFLD.
SCOTIAN SHELF
60°
50°

Figure 2-05 Regional bedrock geology of the northeastern Grand Banks of Newfoundland (from King and Fader, 1980). The bathymetry is shown in metres.

shaped depressions occurring in unconsolidated fine sediment. commonly on the Scotian Shelf. They are thought to be formed by gas escaping from underlying sediments (Josenhans et al., 1979).

Bottom currents on the shelf have generated a large field of sand waves on the Scotian Shelf since the marine transgression (Ruffman et al., 1978; King, 1980). The formation of enhanced tidal currents in the Bay of Fundy has resulted in a complex environment of erosion and deposition of sediment and the formation and migration of two and three dimensional megaripples and sand waves. Specific studies have been undertaken in the headward portion of the Bay in Minas Basin (Amos, 1978) to determine the Holocene evolution.

2.2 Area 2 The Grand Banks Region

King and Fader (1980) divide the bedrock geology of the Grand Banks into three units. The stratigraphic base consists of a sequence of undifferentiated late Precambrian, metamorphic rocks (Unit 1) which are an extension of the rocks on the Avalon Peninsula. The Precambrian is either exposed or near the surface and basically inshore from the centre of the Avalon Channel (Fig. 2-05). Further offshore a succession of well indurated Palaeozoic sedimentary rocks (Unit 2) ranging in age from Cambrian to mid-Silurian overlie the Precambrian. Both Unit 1 and 2 are overlain by sedimentary rocks of Cretaceous and Tertiary age (Unit 3). These are found on the eastern portion of the Grand Banks (Fig. 2-05) and extend to the edge of the continental shelf.

Glacial or glaciomarine related sediments and transgressive sand and gravel surficially overlie Units 2 and 3 (King and Fader, 1980). Over most of the region the surficial sedimentary thickness is less than 2 m. The surficial sediment cover thickens in the Downing Basin, off the mouth of Conception Bay, and in the southern areas of the Avalon Channel.

Fader and King (1981) have proposed a preliminary geological history for the formation of the surficial units in the northern Grand Banks area. At the time of the last glaciation most of the Shelf in the northeastern Grand Banks area was covered by glacial till and glacio-marine sediments. These sediments rest unconformably on Tertiary "bedrock". In the Hibernia research area (Fig. 2-05) the beds underlying the surficial cover have been assigned a Tertiary age on the basis of identification of marine dinoflagellate fossils (Bujak, personal communication, 1981) found in samples collected from boreholes. They consist of semi-consolidated siltstones, mudstones and sandstones dipping 1 - 2° to the east (Fader and King, 1981). An angular unconformity which defines the top of the Tertiary which formed during a period of subaerial exposure, is probably a partially cemented hard surface as suggested from the borehole information. This surface probably was formed prior to transgression during the period of late Pleistocene low sea level stand.

Unlike areas of the Scotian Shelf and west of the Grand Banks, where Pleistocene buried channels are highly developed, there is a complete absence of channel development in the northeastern region of the Grand Banks. At the end of the

Pleistocene a large portion of the Grand Banks were subaerially exposed. Slatt (1974) shows evidence of this from analysis of sediment texture, $CaCO_3$ content and radiocarbon dates. The late Wisconsin-Holocene transgression commenced at about 15,000 years B.P. (Fader and King, 1981) causing a rapid redistribution of the Quaternary deposits into something approaching the present day pattern of sediment distribution. As previously noted on the Scotian Shelf to the south and the western Grand Banks of Newfoundland, the Pre-Holocene low sea stand has been estimated to lie between 110 to 120 m below present sea level (King 1970; Fader et al., 1983). Fader and King (1981) indicate that a low sealevel stand in the Hibernia may have occurred at the same water depth (110 to 120 m). A terrace with an upper elevation of 100 m water depth (Fig. 2-06) occurs along the northeastern edge of Grand Bank and may be an erosional feature representing the late Wisconsin low stand of sea level (Lewis and Barrie, 1981). This would mean that the terrace feature represents the nearshore zone of the early Holocene Atlantic. Above the terrace slope lies an upper terrace with sand ridges and alternating lag gravels in the troughs at approximately 80 m water depth (Lewis and Barrie, (1981) (Fig. 2-06). This is the location of the Hibernia discovery.

The present Holocene sediments are essentially compact medium to fine grained clean sands with varying amounts of pebbles, shells and gravels comparable to the Sable Island Sand and Gravel.

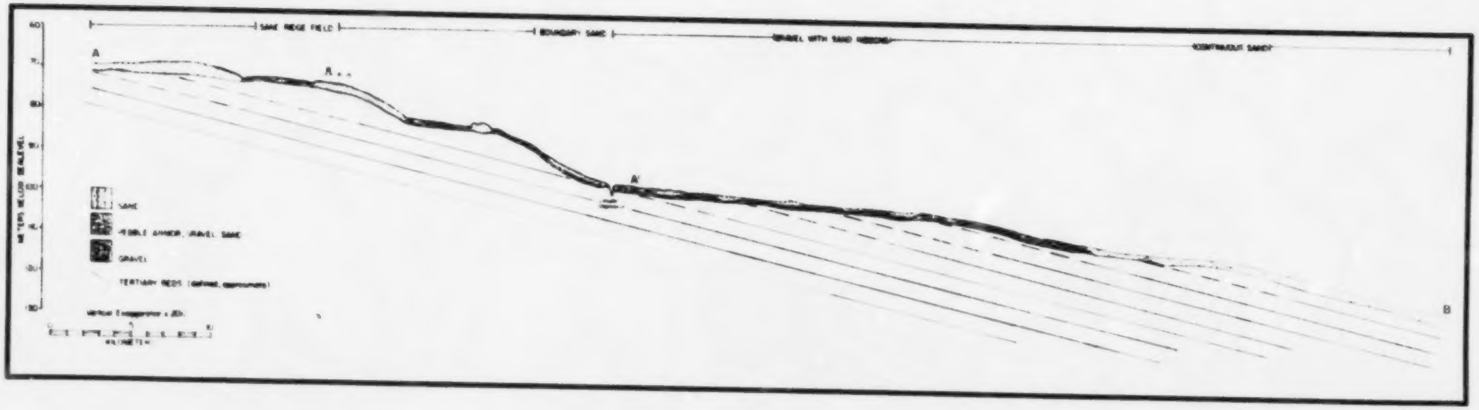
SAND RIDGE FIELD
BOUNDARY SAND
GRAVEL WITH SAND RIBBONS
CONTINUOUS SAND
A
A'
B
SAND
PEBBLE ARMOR, GRAVEL SAND
GRAVEL
TERTIARY BEDS (defined, approximate)
METERS BELOW SEALEVEL
KILOMETERS

The inflection (increased seabed slope) at about 100 metre water depth marks the position of the late Wisconsinan low sea stand that trends NNW through the area.

Figure 2-06 Geological cross-section of the northeastern edge of the Grand Bank in the Hibernia area.

2.3 Sediment Stability

In water depths greater than 110 to 120 m the seabed environment is relatively stable as seen from geophysical survey records and bottom photographs. Sediment transport is probably negligible. Above 110 to 120 m predicting the stability of the seabed depends on the interpretation of whether features on the seabed are relict (formed during the Holocene transgression) or modern. Small scale wave-formed ripples (Fig. 2-07) found on the thin surficial sands which overlie the lag gravels certainly indicate modern sediment transport and instability of surficial sands.

Figure 2-07 Wave-induced bifurcating ripples at 80 metres water depth near the Hibernia discovery area.

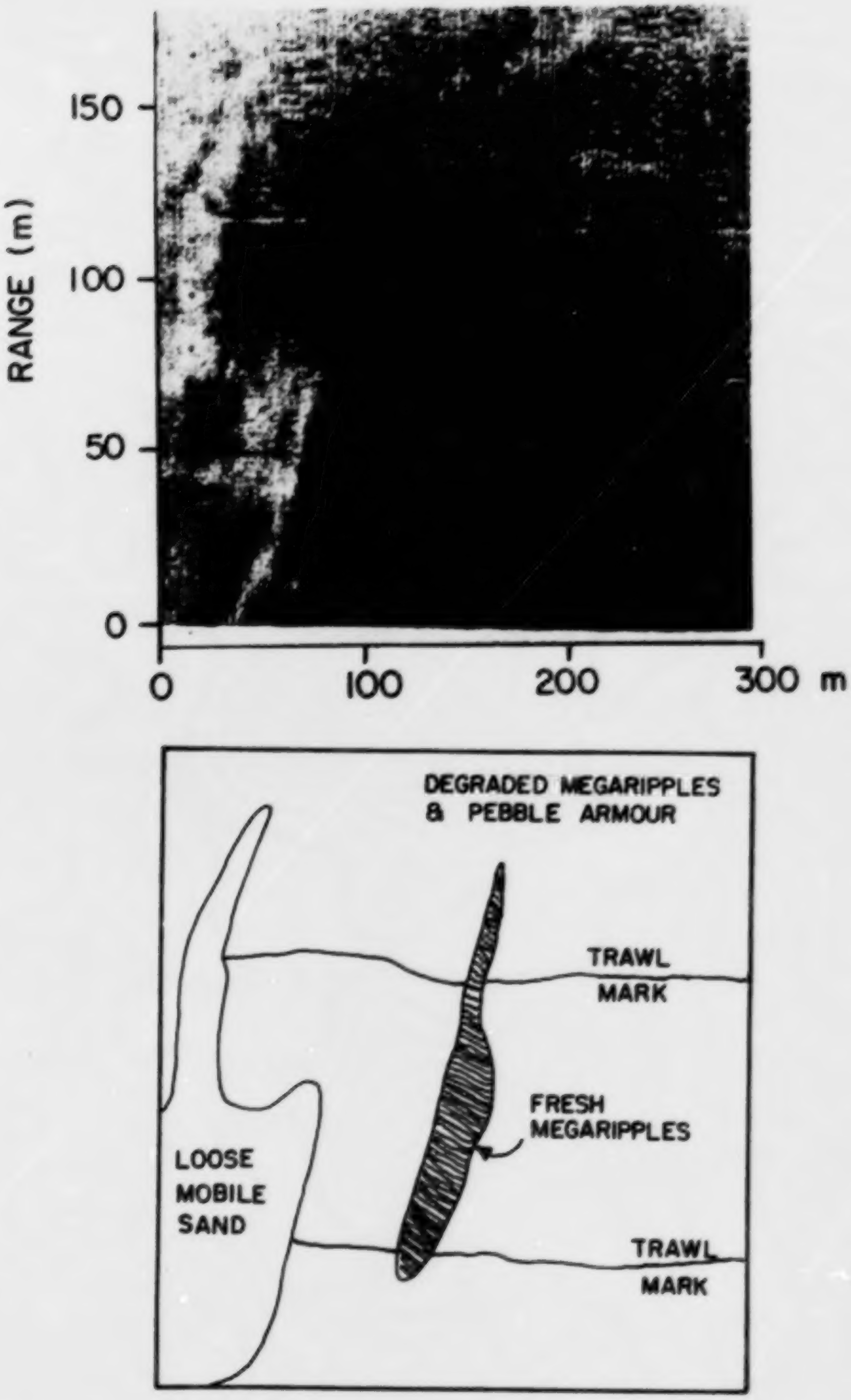
150
100
50
0
RANGE (m)
0
100
200
300 m
DEGRADED MEGARIPPLES & PEBBLE ARMOUR
TRAWL MARK
FRESH MEGARIPPLES
LOOSE MOBILE SAND
TRAWL MARK

Figure 2-08 Klein sidescan sonogram from the northeastern Grand Banks.

Fresh megaripples that appear to be migrating over otter board trawl marks from recent fishing operations are shown.

Sidescan sonar data from the Hibernia area (Fig. 2-08) shows evidence of megaripple migration across otter board trawl marks of recent offshore fishing operations. This demonstrates that modern sediment transport and sedimentary bedform migration occurs on the Grand Banks. Figure 2-09 shows another area of Hibernia with arcuate sand waves and megaripples superimposed on the stoss side.

From work undertaken in the Middle Atlantic Bight region of North America it was concluded that current velocities which are sufficient to form annual megaripples (short term response elements) and to move the sand waves (long term response elements) were generated only four to five times a year on an average, by storm surges (Swift and Freeland, 1978; Gadd et al., 1978). The megaripples in this area of the American Atlantic Shelf are short term response features tending to be erased in the quiet summer months by browsing organisms (Swift et al., 1979). Sand waves on the other hand are long term response features lasting a period of years (Swift et al., 1979). On the Grand Banks a similar hypothesis may explain the bedform morphologies though the frequency of unidirectional storm generated or oceanic currents is probably less. The existence of large fields of megaripples indicate that currents capable of transporting sediment occur at least once every few years. The larger sedimentary bedforms (sand ribbons and sand ridges) could well be relict features dating back to times of lower sealevels and higher paleo-current energies.

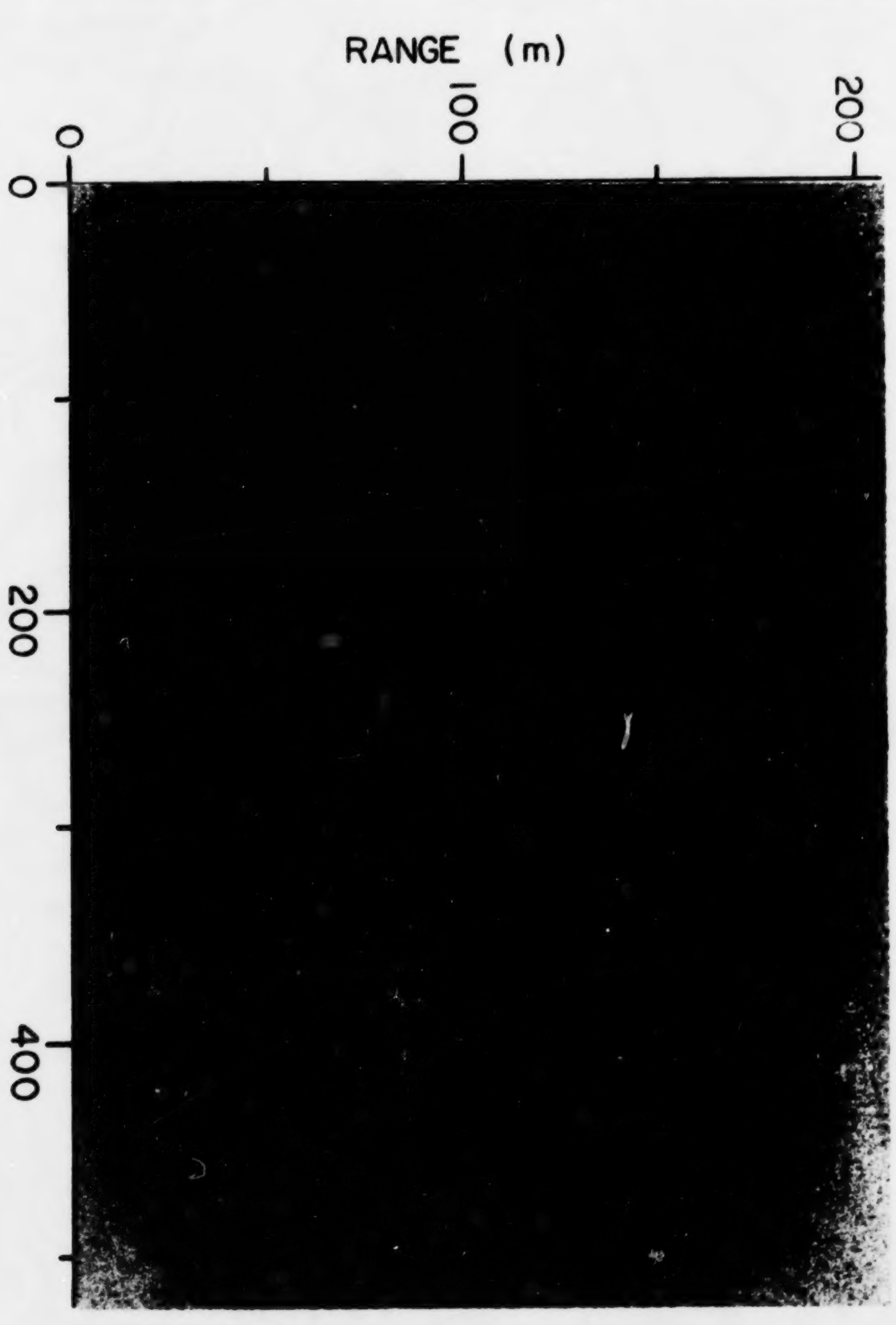
RANGE (m)
0
100
200
0
200
400
(m)

PHOTO ON
PRECEEDING
PAGE

Notice the superimposed megaripples on the stoss side of the sand waves, a common feature.

Figure 2-09 Arcuate sand waves on Grand Banks at 80 metres water depth.

2.4 Area 3 The Labrador Shelf

The Labrador Shelf, covering some 200.000 km^2, is a typical example of a glaciated shelf (Fig. 2-10). The irregular inshore region is separated by a discontinuous marginal channel from the seaward shelf, characterized by relatively flat topped banks. Transverse depressions known as saddles separate the banks. The Labrador marginal trough is a unique depressional feature which parallels the present coastline and separates Precambrian crystalline rocks, to the west, from the Mesozoic/Cenozoic coastal plain strata, to the east.

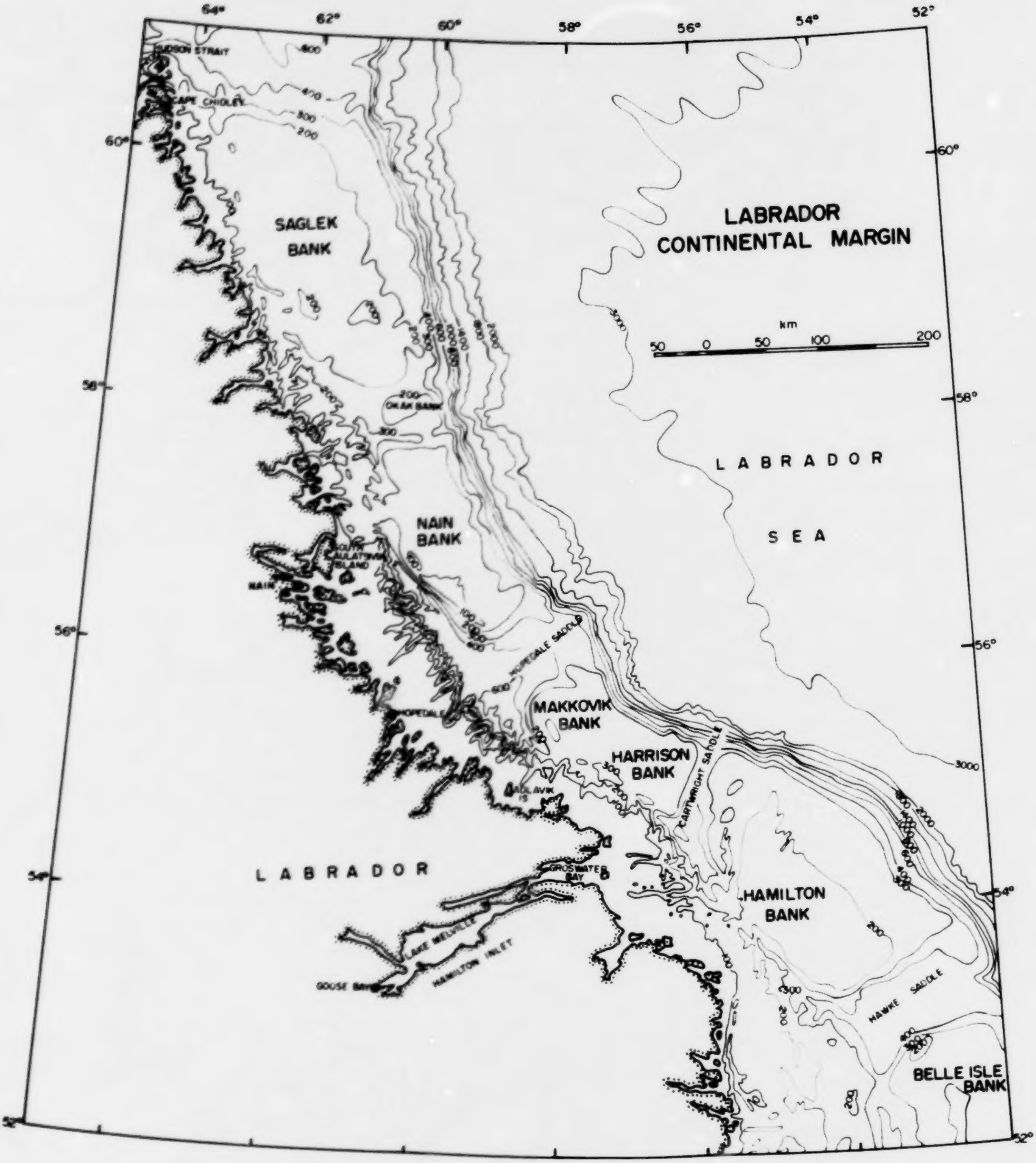

64°
62°
60°
58°
56°
54°
52°
HUDSON STRAIT
CAPE CHIDLEY
SAGLEK BANK
LABRADOR CONTINENTAL MARGIN
km
50 0 50 100 200
OKAK BANK
LABRADOR SEA
NAIN BANK
SOUTH AULATSIVIK ISLAND
NAIN
HOPEDALE SADDLE
MAKKOVIK BANK
HOPEDALE
HARRISON BANK
CARTWRIGHT SADDLE
ADLAVIK IS
GROSWATER BAY
LABRADOR
HAMILTON BANK
LAKE MELVILLE
HAMILTON INLET
GOOSE BAY
HAWKE SADDLE
BELLE ISLE BANK
200
300
400
600
2000
3000

Figure 2-10 The morphology and general bathymetry of the Labrador Continental Shelf.

At least three episodes of Pleistocene glaciations have been recognized in northern Labrador (Greene, 1974). The most recent event, correlated with the classical Wisconsinan (Prest, 1970), was the least extensive of the three ice sheets known to have covered Labrador. The exact extent and chronology of Pleistocene glaciations offshore is as yet poorly understood.

Three major glacial advances have been identified from glacial till deposits in Cartwright Saddle (Josenhans, 1983) which pre-date the late Wisconsinan glacial advance. Vilks and Mudie (1978), from palaeontological evidence, also suggest that sea ice cover during the late Wisconsinan (20.000 years B.P.) was similar to present day Cartwright Saddle. This further implies that the late Wisconsinan ice sheet never extended to the shelf edge. They further suggested that the Labrador Current had developed as early as 15.000 years B.P. in this southern Labrador Shelf region. On the other hand, earlier work based on physiographic and sedimentary evidence suggested that late Wisconsinan continental ice covered the entire southern Labrador Shelf during the last glacial event (e.g. Grant. 1972; Fillon, 1975; van der Linden et al., 1976; Denton and Hughs, 1981). On Hamilton Bank van der Linden, et al., (1976) interpret the bank morphology in terms of Wisconsinan glacial landforms. Features include end moraines, kames, subglacial meltwater channels, subaqueous kames and kettle fields, subaqueous outwash plain and ground moraine. Deglaciation was complete by about 9,000 B.P. according to Fillon (1975).

Recent work from northern Labrador, specifically on Saglek Bank, demonstrates that glacial ice remained as late as 6050 years B.P. (Fillon and Harmes, 1982). Saglek Bank is covered with a thick layer (100 to 300m) of compacted glacial and postglacial material (Grant. 1972; Fillon et al., 1978). Other workers (eg. Andrews, 1963; Prest, 1970; Ives, 1978) suggest from work on northern Labrador that an ice advance did not extend beyond the present coastline during the late Wisconsin. Clearly there is inadequate glacial stratigraphic evidence from Labrador shelf sediments to establish the glacial history and so these two divergent schools of thought, based on work from local areas, persist.

In summary, three glacial tills reflecting the glacial advances of variable lateral extent can be postulated for most of the Labrador Shelf (Josenhans, personal communication, 1983) none of which corresponds to the late Wisconsinan. The tills are thin over the Precambrian crystalline basement of the inner shelf and thicken in the bottom of the saddles (Grant, 1972). One top of the banks, other than Saglek Bank, the existence of till and its thickness is not known.

Postglacial sedimentation has taken place mostly in the saddles, marginal trough and on the continental slope. Here well stratified silt and clay occurs, such as seen in Cartwright Saddle (Vilks, 1980). In certain areas such as Hawke Saddle, sedimentation is dominated by periods of slumping and non-deposition (Vilks, 1980). This unit has been defined by van der Linden et al. (1976) as the Goose Clay (Fig. 2-11). In shallower

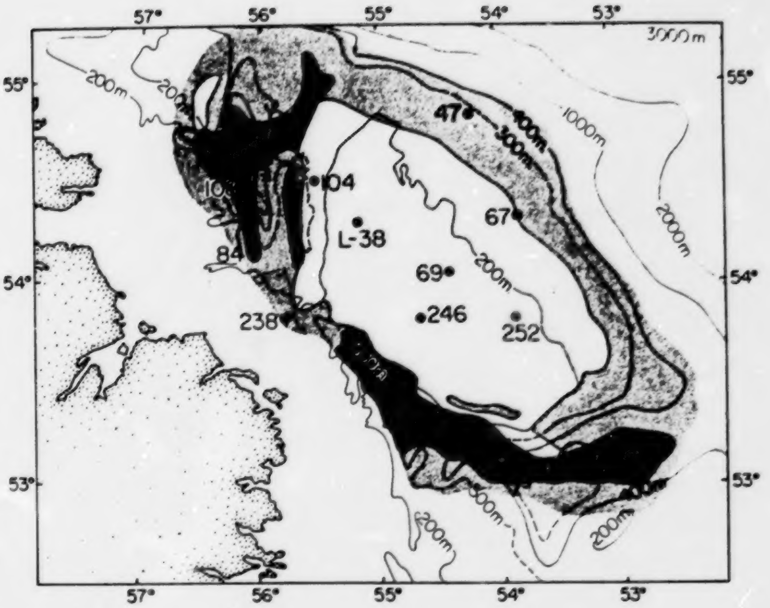

Dark pattern - Goose Clay; medium pattern - Cartwright (coarse) sand and gravel; central enclosed area - Groswater unit (largely fine sand).

Figure 2-11 Glacial drift thickness along the Labrador coast (Fillon et al., 1978).

water, on the Banks, postglacial sediments are very thin with a trend to have reworked sands and gravel mostly around the seaward perimeter of the Banks with finer silt, sand and gravel deposition on the inner surface of the Banks. This has only been well described on Hamilton Bank (van der Linden et al., 1976) where the peripheral unit was called the Cartwright Sand and Gravel and the central bank unit, the Groswater unit (Fig. 2-11). The strong reworking of sediment by bottom currents associated with storm waves noticed in the Cartwright Sand and Gravel unit (Fillon, 1976) can also be seen in Holocene cores from the Groswater Bay area (Vilks and Wang, 1981) by analysis of surface texture of quartz grains.

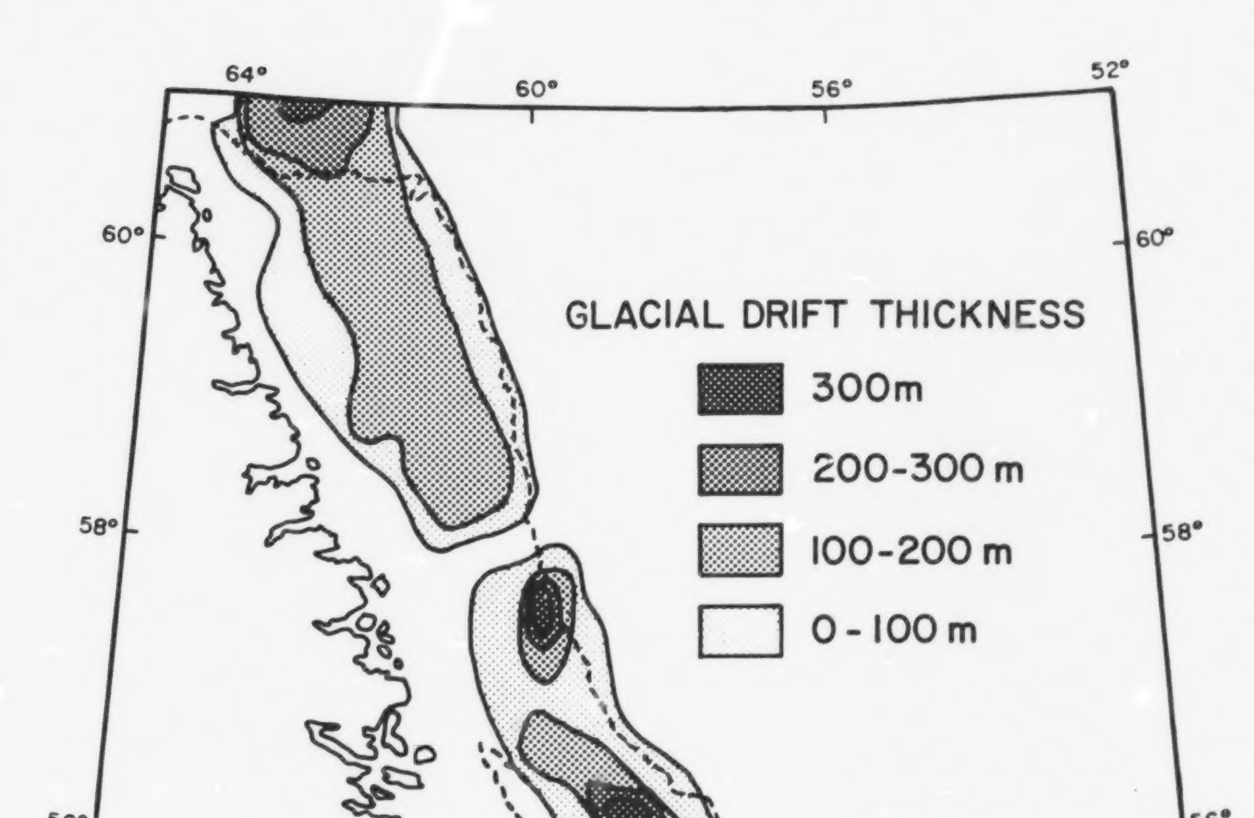
64°
60°
56°
52°
60°
58°
56°
54°
52°
GLACIAL DRIFT THICKNESS
300m
200-300 m
100-200 m
0 - 100 m

Figure 2-12 Glacial drift thickness along the Labrador coast (modified from Grant, 1972). The 500 metre isobath is shown.

Though evidence of the extent of the last glacial advance is still inconclusive, all evidence available indicates that sealevel stood much lower at the beginning of the Holocene and a rapid increase in sea level occurred subsequently. This caused a marine transgression in the present nearshore area.

The mid-Labrador Banks (Harrison, Makkovik, Nain) are presently under study (Lewis and Barrie. 1980; Josenhans, personal communication, 1982). Early indications show that the surficial sediment cover over most of the banks is much thinner than predicted by Grant (1972) (Fig. 2-12). No evidence of a marine transgression can be seen on Makkovik Bank and present day sedimentation is predominantly by ice rafting (Josenhans and Barrie, 1982). The surficial cover is mobile and in equilibrium with the modern hydrodynamic regime as seen by sediment origin and textures, heavy mineral analysis of hydraulic equivalence, the occurrence of biogenic microfauna and examination of side scan sonar surveys (Gilbert and Barrie. 1983). Iceberg interaction with the seabed is intense over these banks but the hard sub-surface limits deep iceberg keel penetration.

Saglek Bank is the largest and the most northerly of the Labrador Banks. It is covered with an extremely thick layer (100 to 300 m) of compacted glacial debris and glaciomarine sediment (Fillon, et al., 1978; Grant, 1972). On the southern portion of the bank, four sedimentological units have been identified (Fillon, 1980). The dominant unit, defined by a rough undulating boundary is Unit 3 dating from 26,000 years B.P. (Fillon, 1980).

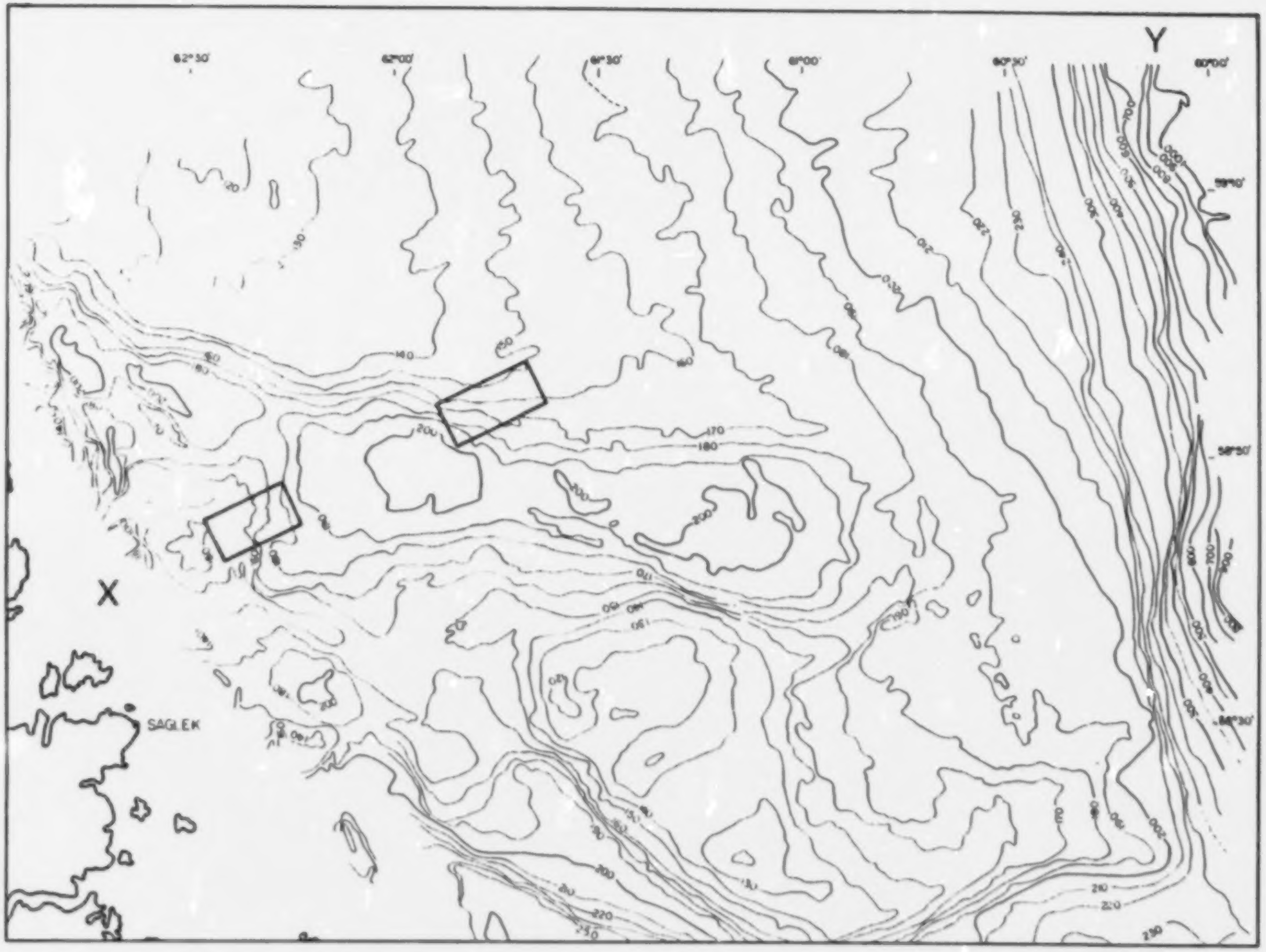
62°30'
62°00'
61°30'
61°00'
60°30'
60°00'
Y
X
SAGLEK
58°50'
58°30'
140
150
160
170
180
200
210
220
230
250
300
400
500
600
700
800
900
1000

The right hand box indicates the location of the mosaic in Figure 2-18. Line x-y represents the geological cross-section in Figure 2-14.

Figure 2-13 Bathymetry of southern Saglek Bank.

Unit 2 (21,000 to 26,000 years B.P.) which onlaps onto Unit 3 is the characteristic depositional unit in Karlsefini Basin between the east and west interbank regions (Fig. 2-13) and pinches out at about 170 m water depth. In small areas Unit 2 is overlain by the more recent Unit 1. The underlying unit, Unit 4, consists of an overcompacted fine sediment that is exposed on the eastern edge of the bank. Upon this geologic sequence lies the sand-silt Holocene surficial layer. In the central regions of the bank little reworking of the surficial sediment has taken place except for the seaward bank edge (Gilbert and Barrie, 1983). Figure 2-14 shows this sequence for an east-west cross section of Saglek Bank with an example of a Huntec DTS high resolution seismic profile for a portion of this section (Figure 2-15). This same sequence can be extrapolated for the rest of the bank (Fillon and Harmes, 1982) though there are morphological and sedimentological variations in the units.

Gustajtis (1979) implies that sealevel under both effects of isostatic recovery (following the melting of the ice sheets) and postglacial austatic rise has been declining slightly since the beginning of the Holocene over Saglek Bank. Evidence from deep shelf and slope terraces off Saglek Bank (Fillon et al. 1978) suggest that late Wisconsin sealevel was relatively close to the present levels in northern Labrador and no subaerial exposure occurred. This same inference of present declining sealevel has been made by Barrie (1980) in looking at the geological record of iceberg scouring on Saglek Bank.

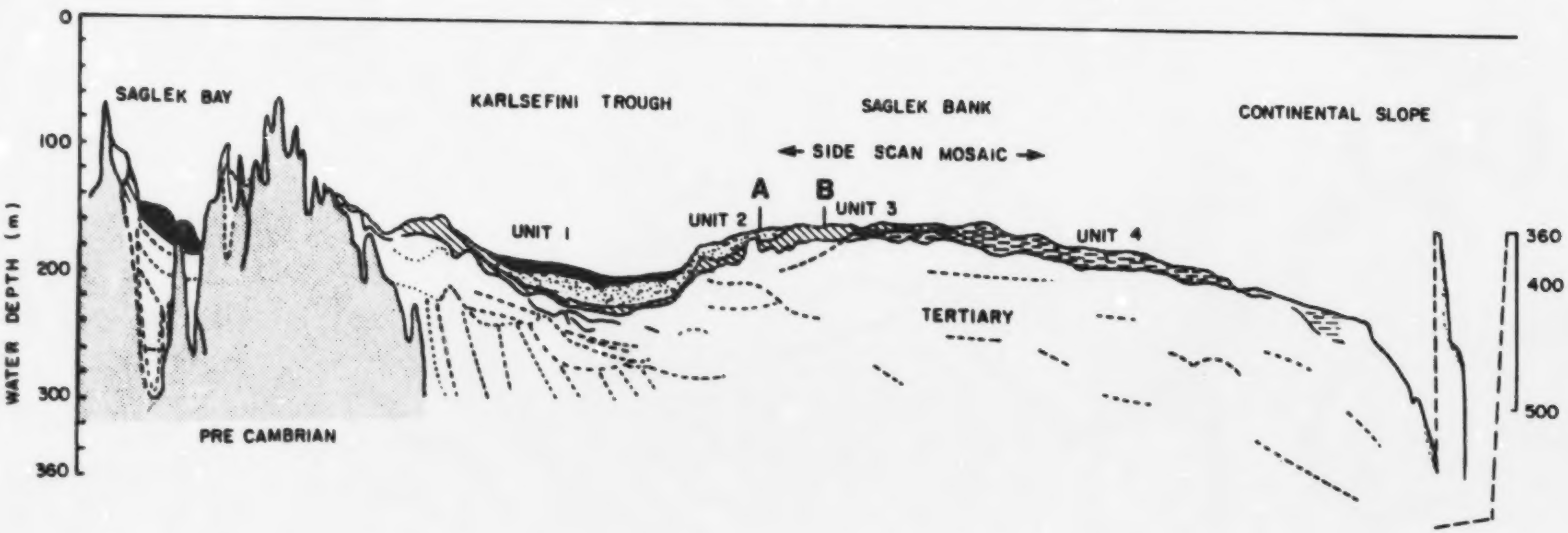

0
100
200
300
360
WATER DEPTH (m)
SAGLEK BAY
KARLSEFINI TROUGH
SAGLEK BANK
CONTINENTAL SLOPE
◄ SIDE SCAN MOSAIC ►
A
B
UNIT 1
UNIT 2
UNIT 3
UNIT 4
TERTIARY
PRE CAMBRIAN
360
400
500

Figure 2-14 Geological cross-section across southern Saglek Bank showing the surficial geological units and bedrock in relation to bathymetry (from Fillon and Harmes, 1982).

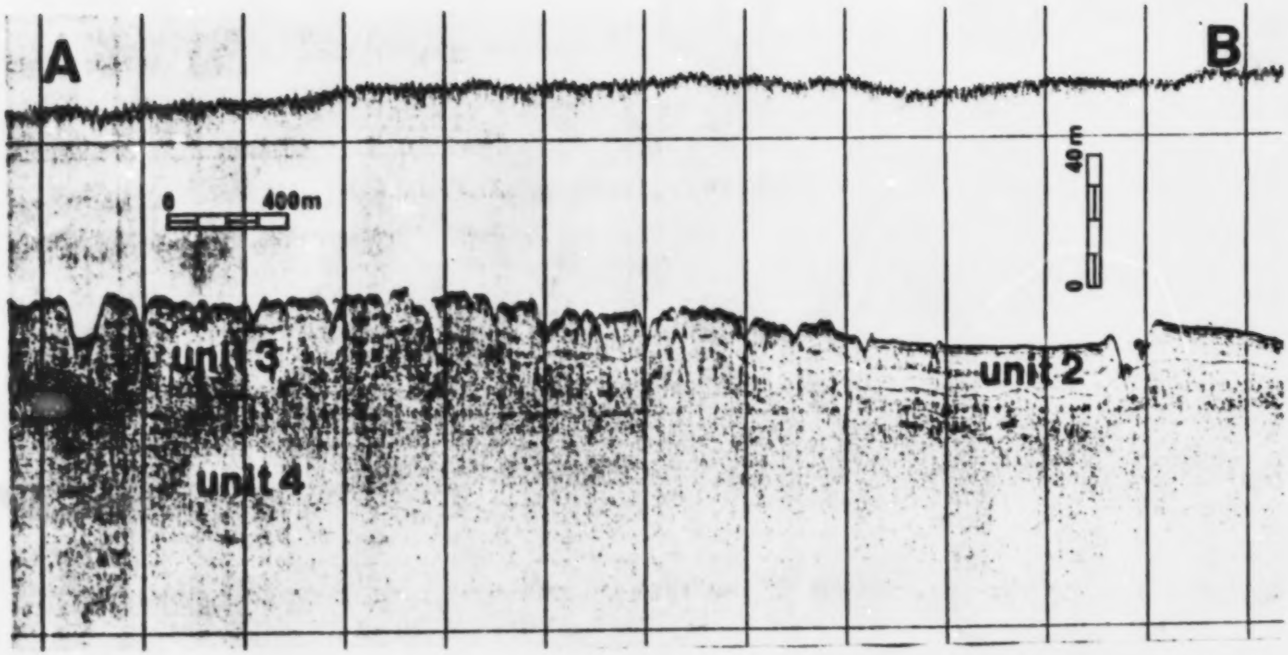

Figure 2-15 Example of a Huntec DTS seismic profiling record from southern Saglek Bank. The section falls between A and B on the cross-section in Figure 2-14.

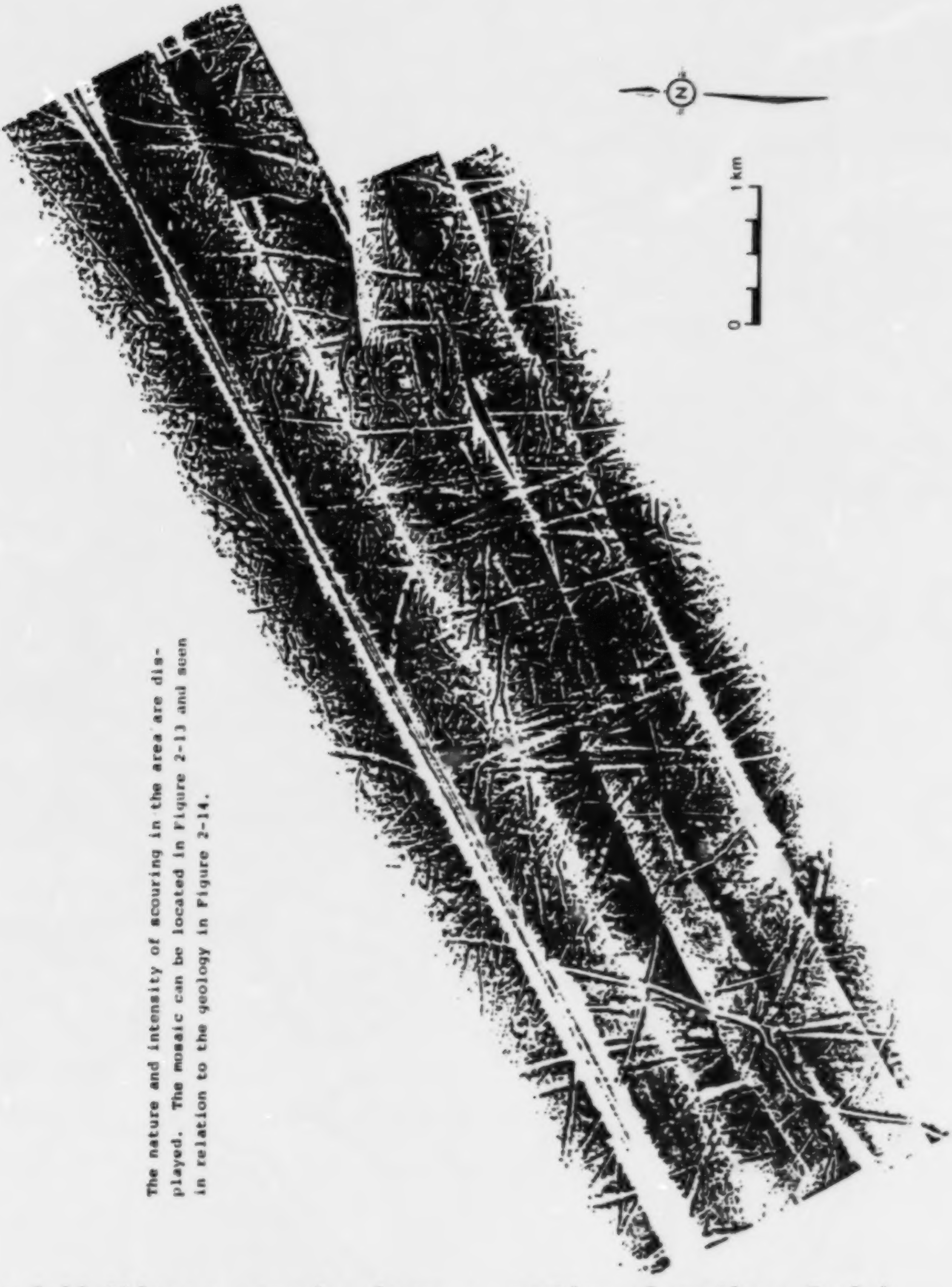

SIDE SCAN MOSAIC, SAGLEK BANK
CSS HUDSON 79·019

The nature and intensity of scouring in the area are displayed. The mosaic can be located in Figure 2-13 and seen in relation to the geology in Figure 2-14.

Figure 2-16 Sidescan mosaic from a portion of southern Saglek Bank.

Iceberg scouring is a dominant feature on Saglek Bank (Fig. 2-16). Both relict ice bottom scouring and modern scouring have taken place at water depths above 180 m and more recent scouring seems apparent below the 180 m water depth (Barrie, 1980). The scours are linear to curvilinear to crater-like in form, with average widths of 30 m at a mean scour depth of 5 m and lengths in excess of 3 km and trending north-south, reflecting the Labrador Current (Barrie, 1980). Two episodes of scouring can be seen for some areas of the Bank.

Terraces off the shelf edge represent old shorelines, or eroded morraines, and have associated steep scarps up to several metres high (Fillon et al., 1978). At the foot of the Continental slope, reflection profiles of the seabed show steep scarps about 150 m in height (Pelletier, 1979). The scarps face the continental slope which suggests that huge blocks of surficial material have been dislocated from an upper segment of the slope or outer shelf, and slid basinwards to depths of 2000m.

3. SUMMARY

Initial research demonstrates that in the south towards the Grand Banks and Scotian Shelf there was an intensifying marine transgression concurrent with possible glacial retreat in the northern Labrador Sea resulting in a gradational surficial geological development from a purely stagnet environment in the northern Labrador Sea to the dynamic Grand Banks and Scotian Shelf areas. The Labrador current was subsequently fully developed and seabed deformation by iceberg scouring and sediment reworking has modified the eastern Canadian Shelf to the present sedimentary environment.

Chapter 3. THE CONTINENTAL SHELVES OFF BAFFIN ISLAND, THE ARCTIC AND THE WEST COAST OF CANADA - SUMMARY REVIEW

Christopher P.G. Pereira

1. INTRODUCTION

Prior to the previous two decades little was known about the marine geology of the continental shelves off Baffin Island, the Canadian Arctic archipelago and along the British Columbia coast, because marine geological surveys in these areas had been few and far between (e.g. Johnston, 1921; Holtedahl, 1929; Trask, 1932; Fortier and Morley, 1956). In addition, the inhospitable climate and the seasonally restricted work periods, along with the very limited availability of experienced manpower (still a current problem) and logistical support, dictated that research in these areas had to be in the nature of regional reconnaissance surveys rather than site specific surveys. Furthermore, at the time, it was difficult to justify the financial expenditures involved, since there were anticipated to be negligible commercial returns from these multidisciplinary regional surveys. Nevertheless, scientifically the returns were valuable indeed.

During the 60's and ensuing years the Geological Survey of Canada increased its research activities in these areas. This came about for a number of reasons (including for reasons of goepolitics), but perhaps primarily because of the need to establish the natural energy resources available to Canada - a further impetus was provided by the oil crisis in the early 70's. Bearing in mind pertinent economic factors, initial geophysical studies indicated that prospects for substantial financial rewards were immense, and this led to an increase in exploration and multidisciplinary research activities in these areas both by government and industry, which in turn led to detailed site specific studies (eg. Buckley, 1971; Marlowe, 1965 and 1965a; Pelletier, 1964; 1966 and 1975; MacLean et al., 1977; Lewis, et al., 1977, McLaren, 1982). However, as indicated by Pelletier (1979), the east (south of Baffin Island) and west coast have been the benefactors of the most systematic coverage to date, and the Arctic, with the possible exception of the Beaufort Sea area, comes a poor second (Figure 3-01).

The continental margins that surround Canada have their genesis in different geotectonic mechanisms that manifest themselves over tens of millions of years. The type of continental shelf formed along each of the three coastal zones that encompass Canada are unique in their formation (see NRC 1979, page 37), but subsequent localized geological processes e.g. sedimentation, volcanic activity and eustasy superficially mask this uniqueness. The width of the continental shelves around the Canadian coastline vary from a few tens of kilometres off Baffin Island and British Columbia to a few hundred kilometres wide, as for instance off the island of Newfoundland and in the Arctic.

The continental margin along Baffin Island is now a passive margin, resulting from continental divergence (Figure 3-02), due to rifting between Greenland and Baffin Island moving the two landmasses apart (Emery, 1977). In contrast, the Canadian west

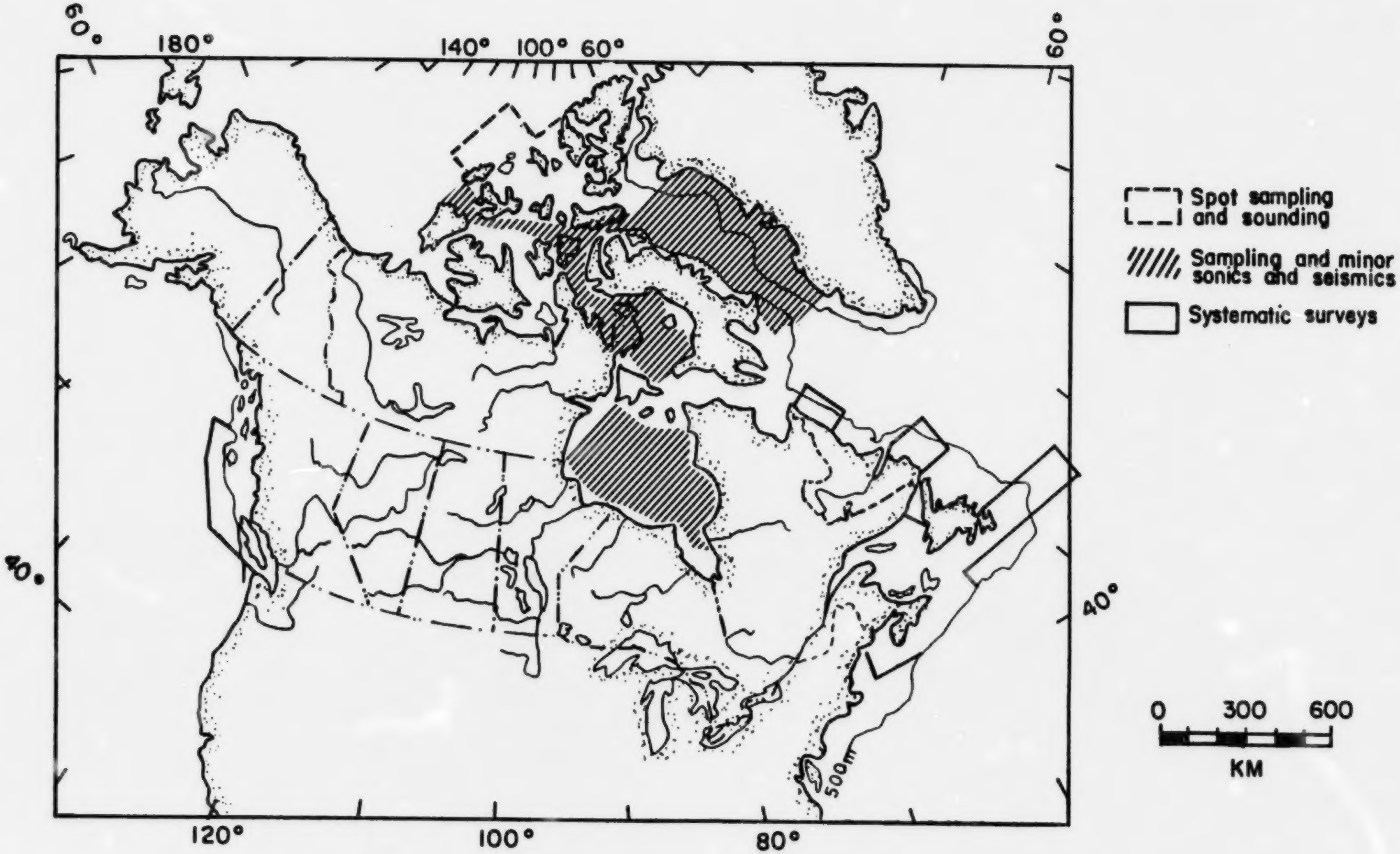
60°
180°
140° 100° 60°
60°
40°
40°
120°
100°
80°
500m
Spot sampling and sounding
Sampling and minor sonics and seismics
Systematic surveys
0
300
600
KM

Figure 3-01 Index map illustrating the extent of systematic coverage and type of marine geological survey undertaken by industry and government on the continental shelf areas that surround the coastal regions of Canada.

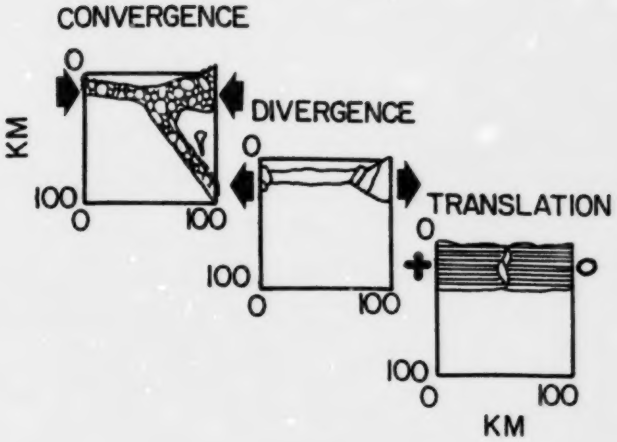

Figure 3-02 Structural types of continental margins as applied to the Canadian Continental Shelf.

coast continental margin is an active margin and a result of the convergent/translation type (Figure 3-02). Here, the Juan de Fuca Plate is the convergent plate and the Pacific Plate the tanslation plate, both of which are juxtaposed along with the remnants of the Explorer plate and the North American Plate (Figure 3-18). The Arctic continental archipelago area is a passive continental margin and was formed partly as a consequence of vertical tectonic movement (Pelletier, 1966).

Synthesis of recent regional marine geological surveys of the continental shelves that surround Canada have produced nearshore surficial geological maps (eg. off Baffin Island by Praeg, (1982); the Beaufort Sea by Pelletier, (pers. comm. 1982) and Blasco, (pers. comm. 1982), and off British Columbia by Bornhold, (1982). Further detailed regional geological and subsurface geological maps are being currently synthesized at the Regional Reconnaissance Section, Bedford Institute of Oceanography. Nova Scotia (MacLean, 1982, pers. comm.).

2. MARINE GEOLOGY OF THE CONTINENTAL SHELVES

A brief literature summary of the continental shelves, their subsurface geology and the associated geohazards are high-lighted and described in this chapter. The continental shelf area south of Baffin Island is described by Barrie (1983, this volume). Other detailed sedimentological, oceanographical and geotechnical processes and mechanics pertinent to the continental shelves (in many cases with illustrated examples from Canada) are discussed by other authors in this volume.

2.1 The Baffin Island Continental Shelf

Geophysical and magnetic studies of the Baffin Island and Davis Strait areas suggest that the separation of Baffin Island from Greenland was well underway in the Early Tertiary (Keen et al., 1974; Grandstein and Srivastava, 1980; and Srivastava, 1981;) and continued until the Middle Tertiary, when it lost its momentum and active spreading ceased. There has been no subsequent spreading activity in the area, although low to moderate levels of seismic activity does occur (vide, Wetmiller and Forsyth, 1978.) The continental margin is considered to be a passive margin (NRC, 1979). The East Baffin Island continental shelf is fairly narrow and can be divided for convenience into an inner and outer zone. The inner shelf is incised by fjords (Figure 3-03) and has a maximum width of about 70 km at a depth of 300 m. The outer shelf zone extends outwards for up to 200 km at a water depth of about 600 m. The continental shelf broadens and has very shallow slope gradients southeast of Baffin Island

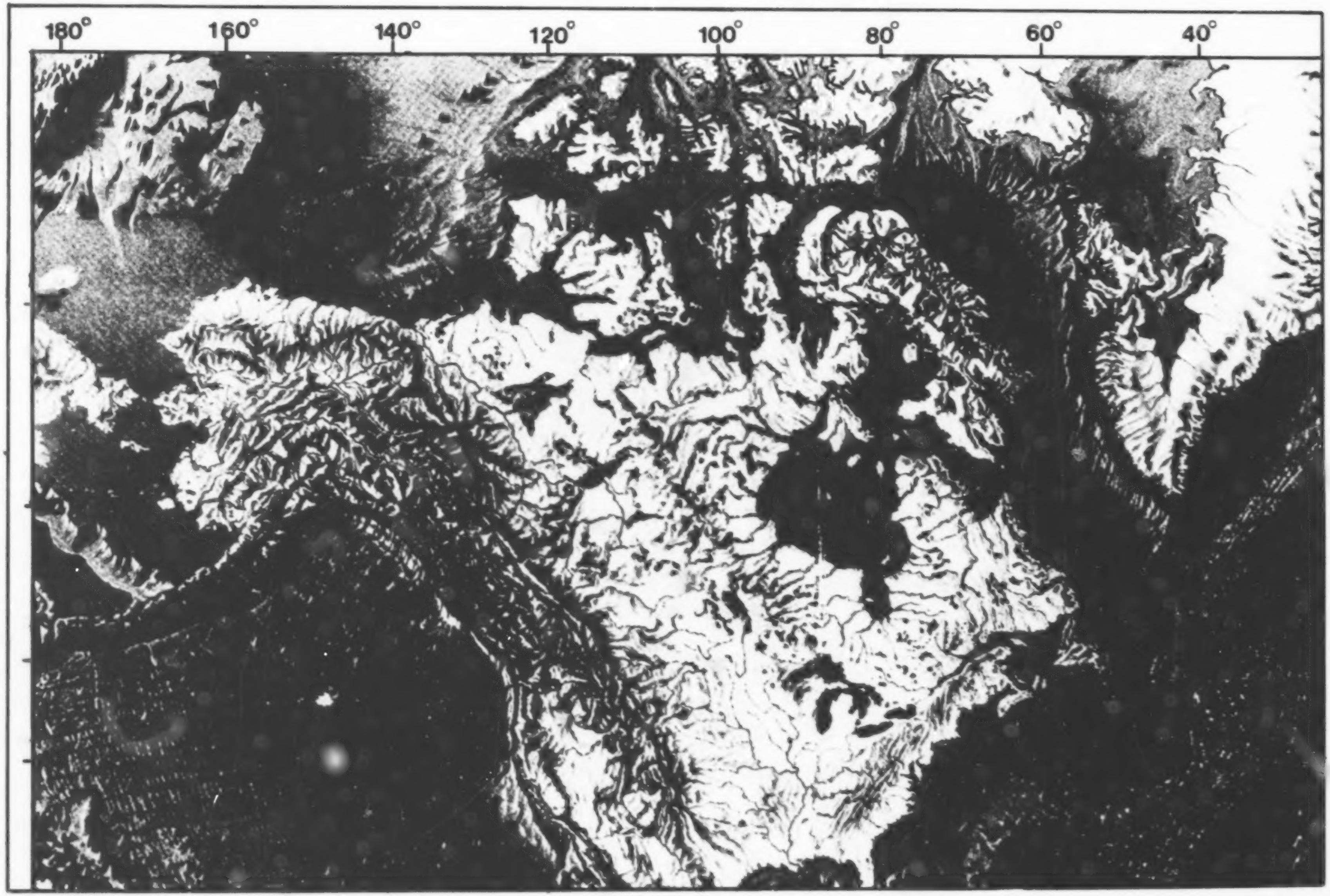
180°
160°
140°
120°
100°
80°
60°
40°

Figure 3-03 The physiographic relief of the continental margins of Canada illustrating the principal characteristics of the shelf and slope area.

and east of Lancaster Sound (Figures 3-03 and 3-11). In the latter instance the shallowing is due to the deposition of large quantities of sediment derived from the Arctic archipelago and transported to the area through the sounds and the channels. The shelf is transected by several linear troughs/submerged channels that are normal to the coast, e.g. off Scott Inlet, Buchan Gulf, Broughton Island, etc., which extended from the adjacent fjords on land, and by submerged headlands which sometimes extend out to the upper part of the continental slope. The channels are fringed by broad apron-shaped areas that are presumed to be of glacial origin and are presumably moraines (Pelletier, 1979; see also MacLean and Falconer, 1979; MacLean, 1982; Gilbert, 1982a and b). In marked contrast, off the west coast of Greenland the shelf is much broader, having prominent convexities formed by prograded deltas and attached fans where large quantities of sediments were discharged by the glaciers (Henderson et al., 1981). The subsurface geology of the east Baffin Island Shelf has been based mainly on regional geological considerations and long range correlation of geophysical characteristics (Grant, 1975), and hence must be regarded as tentative.

A discontinuous 'marginal channel' runs parallel to and off the east coast of Baffin Island (Figure 3-04). Bedrock to the east of this channel is Tertiary, that to the west is Precambrian and Palaeozoic (Figure 3-05). Holtedahl (1950 and 1970) suggests that the discontinuous marginal channel off the east coast of Baffin Island is of tectonic origin. A buried erosional depression in Tertiary bedrock, parallel to the southeast Baffin

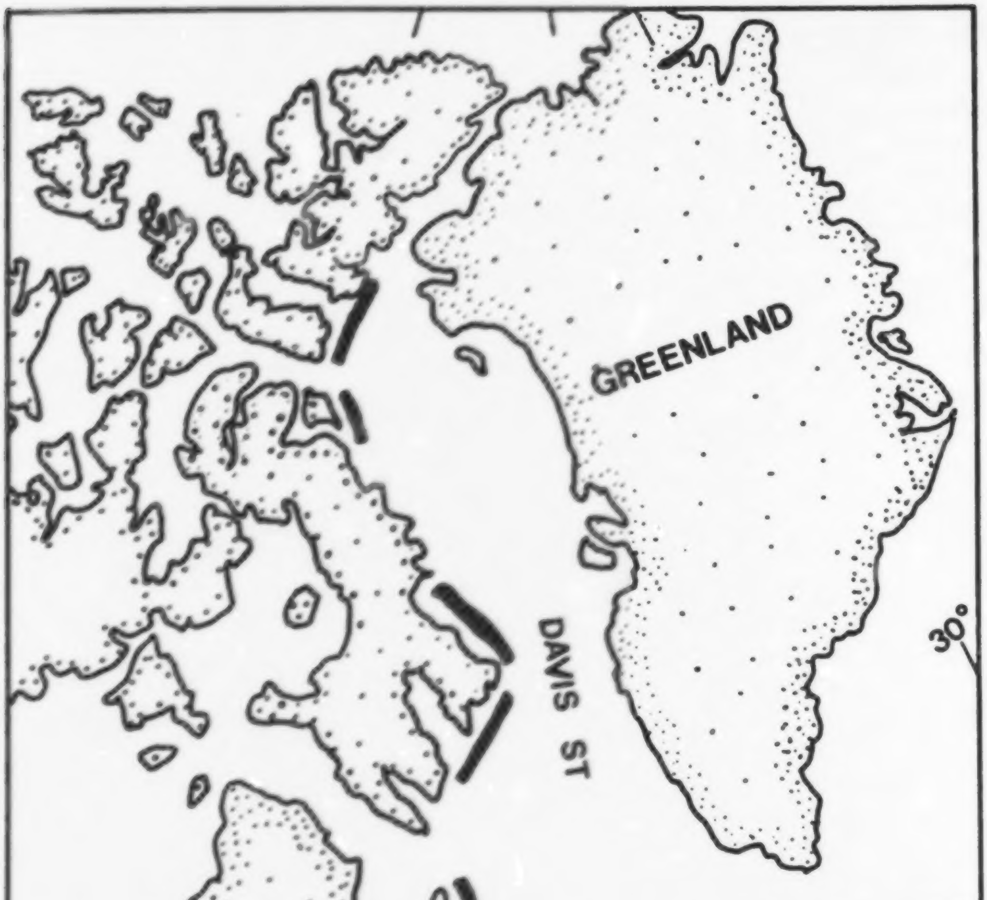
GREENLAND
DAVIS ST
Marginal Ch.
QUEBEC
80°
30°
50°
0 300
Km

Figure 3-04 Map indicating marginal channels along the east coast of Canada (from MacMillan, 1973).

Island coast. is also located almost immediately south of Resolution Island. The length of this depression is not known but it has a width of about 60 km (Figure 3-05) (vide Grant, 1975; Pereira et al., 1983). It has generally been accepted that this fragmented marginal channel (= small longitudinal depressions of Srivastava et al., 1981) is not correlatable with the marginal channel off Labrador; McMillan (1973), however, regards it as a continuation. Further south off Labrador, Grant (1966, 1970 and 1972) is of the opinion that the marginal channel is not primarily of tectonic origin, but rather has been predominantly formed by continental glaciers, eroding the bedrock while moving eastward from the mainland (see also Johnson, et al., 1975).

Studies of the sediment distribution patterns for the Eastern Baffin Island continental shelf have been few and, until recently, have only been undertaken as adjunct projects to primarily geophysical and hydrographical surveys. Present knowledge of the shelf sedimentology and/or shelf sediment dynamics of the region is restricted to a few localities (vide, Grant, 1971; Marlowe, 1968; Baker and Friedman, 1973; Kranck, 1964; Pereira et al., 1983), with extrapolations made for the unsampled area.

To the north, in the area east of Bylot Island and between Devon Island and Greenland, Grant (1971) undertook a sampling program, the results of which indicated that coarse and mostly ice-rafted material dominated the shallow shelf areas with progressively finer sediments offshore in deeper water. Later,

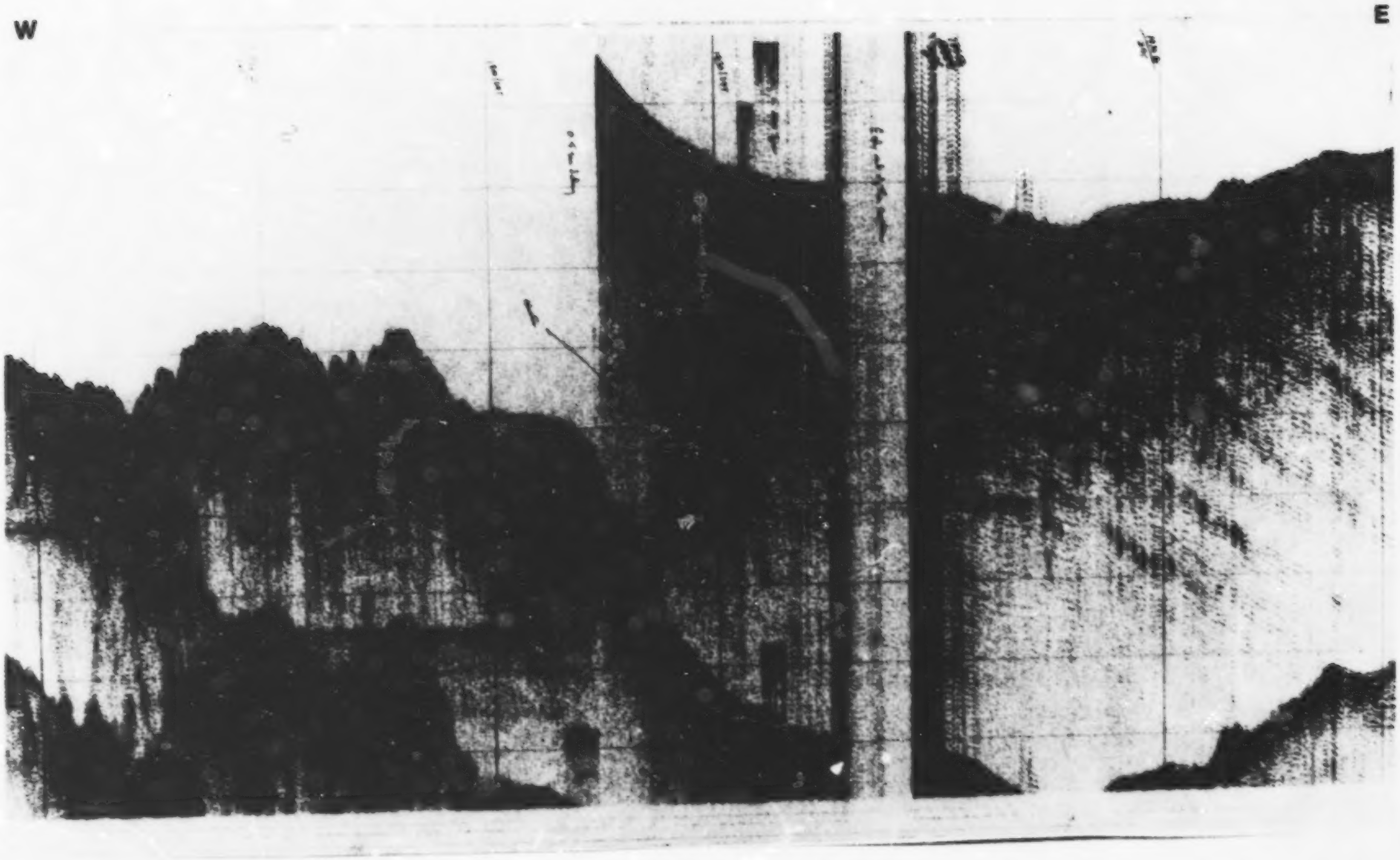

Figure 3-05 A buried erosional depression feature in Tertiary bedrock as seen along an E-W geophysical transect at latitude 62°N.

Number/
Numéro

3

Baker and Friedman, (1973), recorded similar results for the area, and described the shelf sediments as being constituted of sands and gravels intermixed with mud which were randomly distributed. This random distribution of sediment probably reflects its origin as ice-rafted debris, the occurrences of which Baker and Friedman (op. cit.) correlated to the surface sea currents in Baffin Bay. Where large depressions occurred on the shelf the sediments were predominantly fine grained, similar to those that floor the deep bathyal basin in the central part of Baffin Bay. In addition, on parts of the shelf, the dark colour of the surface sediments suggest reducing conditions, but the lighter colours of the sub-bottom sediment samples indicated oxidizing conditions, possibly indicative of Holocene (or older) changing current patterns. East of Lancaster Sound, the shelf broadens and fans out considerably (and has its slope gradients decrease measurably, Pelletier et al., 1975), no doubt as a result of the sediment input from the Arctic archipelago to the west.

Further south on the inner shelf zone from between Nova Zembla Island and off Scott Inlet, sediment overburden is of variable thickness (vide MacLean et al., 1981). In a recent survey in the area (MacLean, 1982b), sub-bottom profiler records indicated that sediment overburden is rarely less than 7 m deep. Sediment distribution for this area has not been examined although the sediment has been sampled.

Sediment distribution south of the Heckla and Griper banks down to the Cumberland peninsula follow a classical pattern

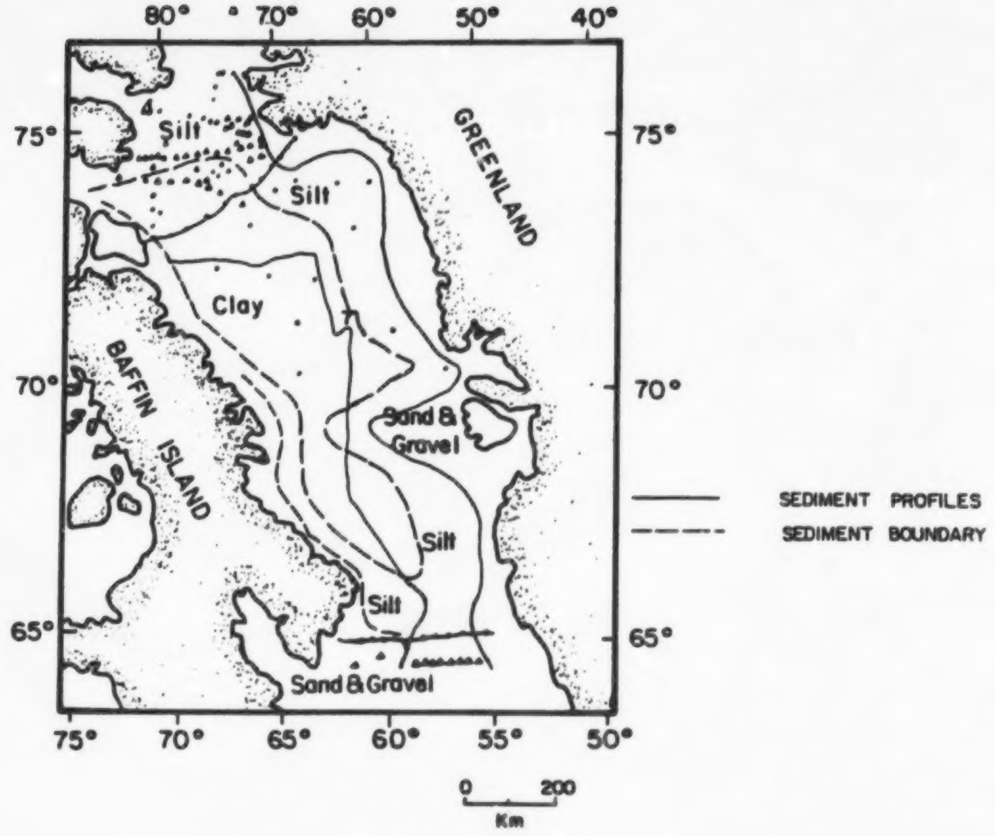
80°
70°
60°
50°
40°
75°
70°
65°
75°
70°
65°
60°
55°
50°
Silt
Silt
Clay
Sand & Gravel
Silt
Silt
Sand & Gravel
GREENLAND
BAFFIN ISLAND
SEDIMENT PROFILES
SEDIMENT BOUNDARY
0
200
Km

Figure 3-06 Sediment textural distribution of the Baffin Bay area.

(Figure 3-06). Gravels and sands are common along the inner and upper shelf area with silt dominating the outer shelf area - these sediments are thought to be locally derived. Superimposed upon this pattern of sediment distribution are the sediments deposited by icebergs, drifting over the area with the south flowing Canadian current that parallels the coastline (Figure 3-07). This contribution sometimes apparently inverts the

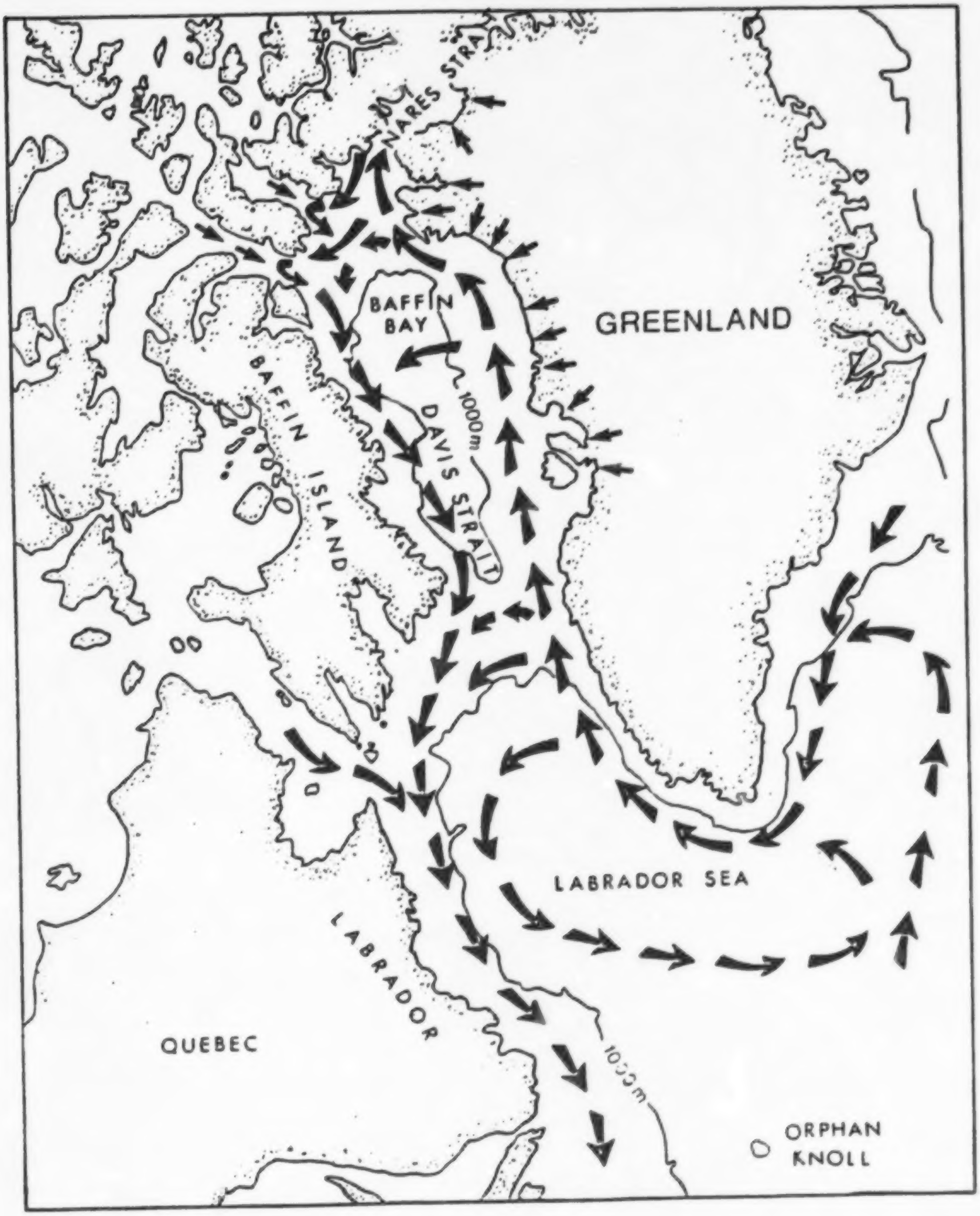
NARES STRAIT
BAFFIN BAY
GREENLAND
BAFFIN ISLAND
1000m
DAVIS STRAIT
LABRADOR SEA
LABRADOR
QUEBEC
1000m
ORPHAN KNOLL

Figure 3-07 Surface oceanic circulation of the Baffin Bay area.

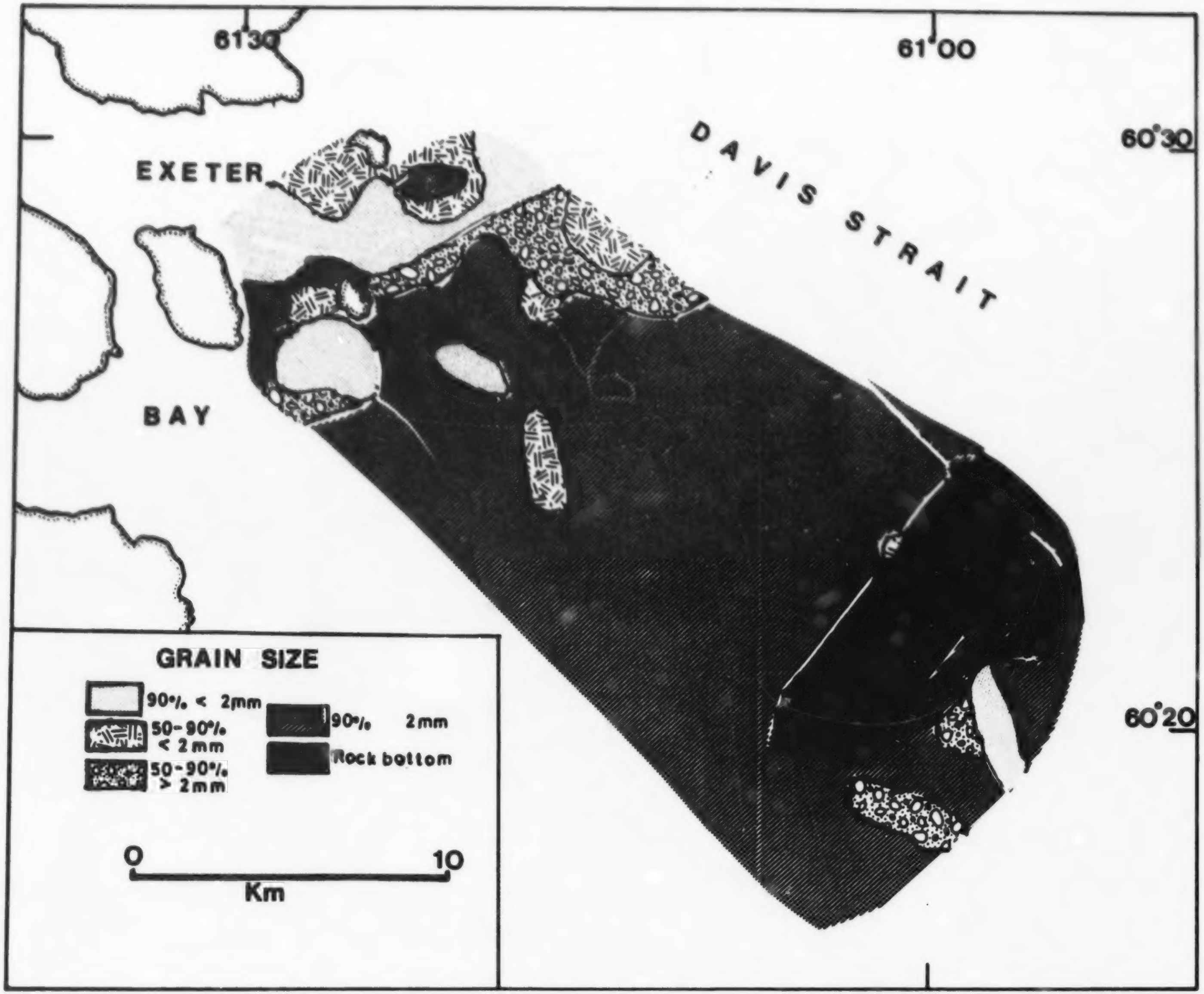
61°30
61°00
60°30
60°20
EXETER
BAY
DAVIS STRAIT
GRAIN SIZE
90% < 2mm
50-90% < 2mm
50-90% > 2mm
90% 2mm
Rock bottom
0
10
Km

Figure 3-08 Sediment textural distribution off Exeter Bay, Davis Strait (from Kranck, 1964).

'typical' pattern of sediment deposition along the shelf; e.g. Kranck (1964) in sediment studies in Exeter Bay, Baffin Island, (Figure 3-08), observed widespread deposits of coarse gravel and sand in the offshore area. Further inshore the sediment is fine to medium grained, homogeneous, well sorted and locally derived. The coarse gravel in the offshore zone is either glacial till or ice rafted material or a mixed combination of the two. Sediment cores taken from the deep basin have coarse sands at their base which become increasingly finer towards the top, indicative of a rising sea level since the Pleistocene.

The shelf off southern Baffin Island is blanketed by surficial deposits which are considered to be mainly drift material dating from the Quaternary glaciation. These sediment deposits are sandy gravels with silts in deeper water (Pereira and Gillespie. 1983). Throughout much of this area these deposits overlie a smooth erosional surface. The thickest accumulations of surficial deposits in the inshore areas lie opposite the mouths of the Hudson Strait, Frobisher Bay and Cumberland Sound (Figure 3-09). Off Hudson Strait there is deep erosion of the coastal plain strata and subsequent infilling by at least two major depositional units, presumably related to the Quaternary glacial period (Grant, 1975). The zero-edge of unconsolidated deposits off Hudson Strait and north-east from Frobisher Bay (Figure 3-09) lies on basement rocks just west of the coastal plain wedge. The rapid thickening of unconsolidated deposits seaward reflects depositional gradation of the escarpment marking this contact zone. Buried contacts are

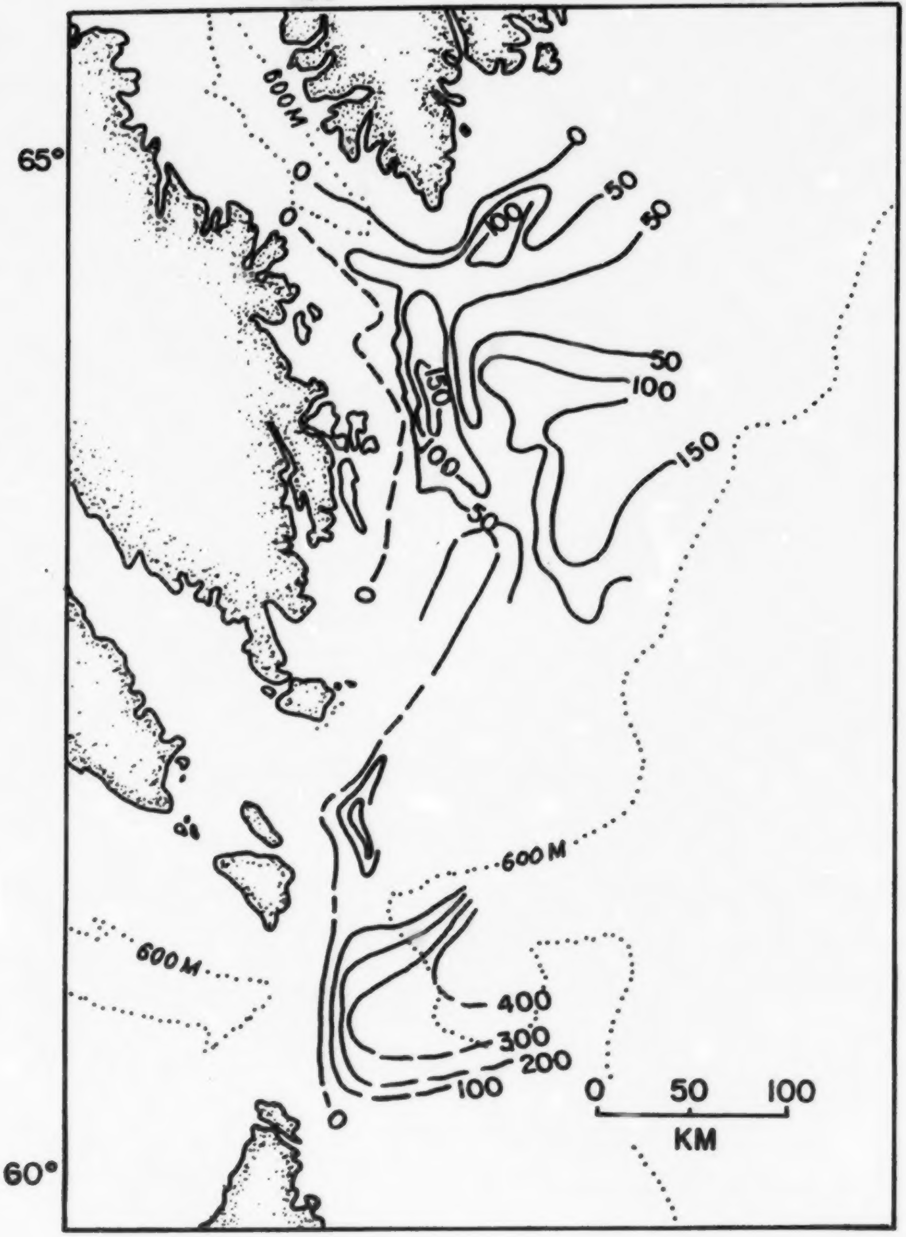
65°
60°
65°
60°
600M
0
0
100
50
50
50
100
150
150
100
50
0
600 M
600 M
400
300
200
100
0
0 50 100
KM

Figure 3-09 Observed apparent thickness of surficial deposits east and southeast of Baffin Island (from Grant, 1975).

likewise expressed by locally thick accumulations north and south of the entrance to Cumberland Sound (Grant, op. cit.). Sediment overburden thickens towards the shelf edge where it is about 50m thick. However, the distribution of sediment overburden is not even, and in places on the midshelf area bedrock is exposed. At the Hekja and Ralegh wellsite area, the overburden is about 7 m thick.

Along the southeastern coast of Baffin Island two dominant mineralogical facies persist: (1) an inner shelf type with heavy mineral assemblages, indicative of derivation from the Precambrian metamorphic and igneous rocks onshore and (2) an outer-shelf assemblage of limestone and dolomite pebbles which mainly appear to be ice-rafted from islands to the north. Ice-rafting has generally been accepted to be the dominant sediment contributor however studies in progress indicate that this may not be the case. Trask (1932) reports the occurrence of frosted quartz grains from sediment samples collected in this area, which he attributes to an aeolian origin. Similar frosted grains have also been recorded in moderate amounts from cores and sediment samples collected from the deeper inshore area down to the Hekja wellsite (Pereira, et al., 1983). Johnson (1967) suggests that the frosted grains originated from presently submerged Pleistocene aeolian sand dunes found in Ungava Bay which have been redistributed by the prevailing currents (vide McMillan, 1973).

From the very little that is known of the Baffin Island Shelf area, Pelletier (1979) suggests that the area could be a

TABLE 3-I

SOME POSSIBLE ENGINEERING GEOHAZARDS
BAFFIN ISLAND SHELF

1 LOOSE COARSE SEDIMENTS
(Ice rafted or Insitu)

2 ABSENCE OF FINES SUGGEST SCOURING BY CURRENTS (STRONG CURRENTS)

3 ICEBERGS SCOURS DOWN TO CA. 500 m?

4 VARIABLE SEDIMENT OVERBURDEN

5 SLUMPING OF SEDIMENTS IN FJORDS

6 TECTONIC AND SEISMIC EFFECTS

7 BURIED BOULDER BEDS

8 TURBIDITY FLOWS

minefield of major engineering geohazards (see Table 3-I). The inshore areas have deposits of loose coarse sediments that were either torn locally from the bedrock or were ice-rafted, and the absence of fine sediments suggest scouring and winnowing by strong, intense bottom currents. Pelletier (op. cit) developed a textural model for sedimentation which suggested that this is indeed an area of sufficient hydrodynamic strength to cause sediment scouring, and thus could be a significant engineering hazard. Pelletier's model gets support from current meter data from 1 m above the seabed from the Hekja/Palegh vicinity, which indicates peak currents as high as 35 cm s^{-1}.

The inner shelf is dissected by numerous fjords as deep as 800 m, and although these fjords could afford protection to bottom installations from the threat of drifting icebergs that continually scour the area (Lewis et al., 1977; Loken and Hodgson, 1971; Barrie, et al., 1982), they are themselves prone to sediment and associated slumps along with current scouring. Also tectonic and seismic behaviour may be intense, since Baffin Bay is the locus of many earthquake epicentres (Figure 3-10). As a consequence of this activity, together with excessive sedimentation on the shelf. slumping and turbidity flow can be expected and has taken place in the past (Marlowe, 1968, Piper, 1974).

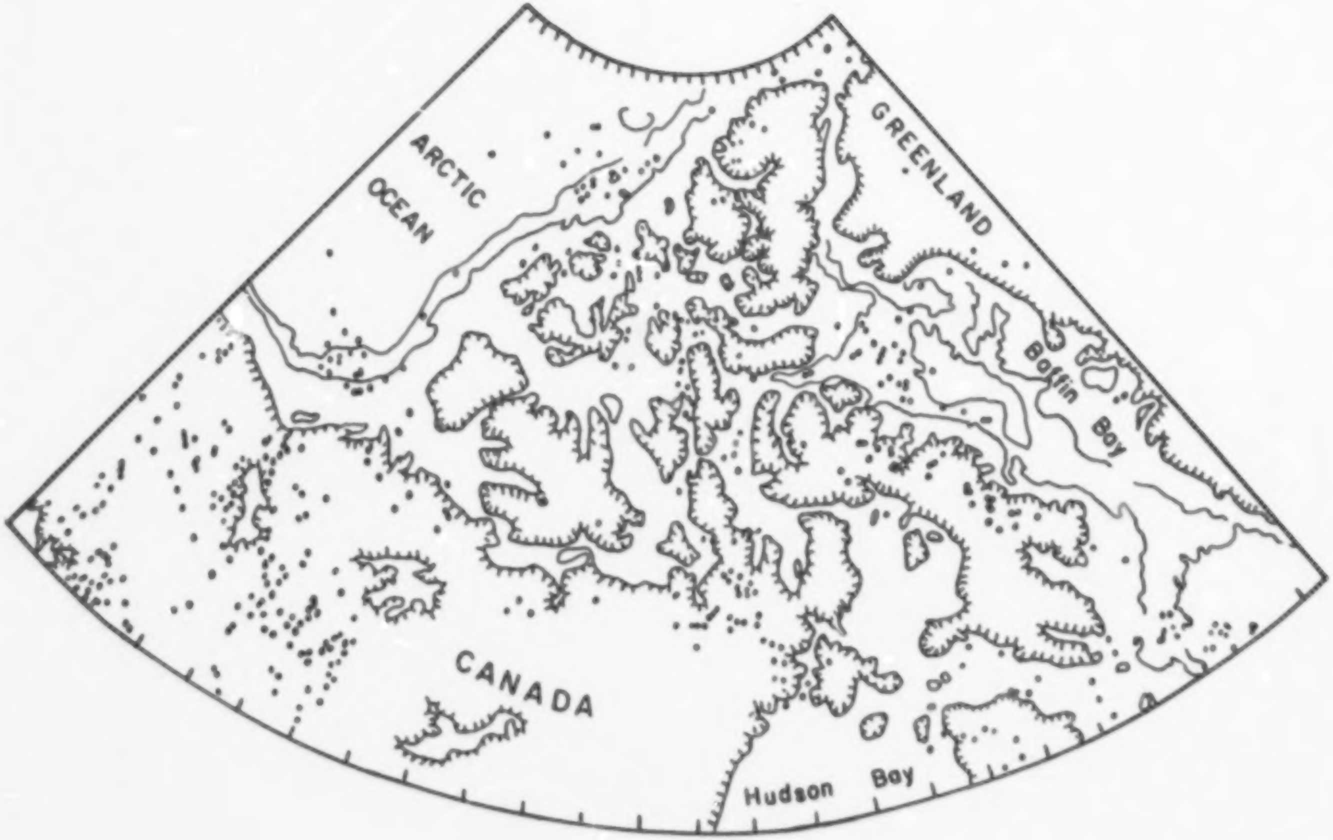
ARCTIC
OCEAN
GREENLAND
Baffin Bay
CANADA
Hudson Bay

Figure 3-10 Areal distributional map of seismic activity greater than magnitude 3 in the Canadian Arctic.

2.2 The Canadian Arctic Archipelago and Shelf Area

Survey work in the Archipelago and shelf area is at present limited to a maximum of about 5 months in the year, because the waters of the Archipelago are covered by sea-ice for the remaining period. Initial freeze-up occurs as early as mid-September, with the final break-up in the east occurring as late as July.

The region consists of a network of shallow channels connecting the Arctic Ocean in the west and Baffin Bay and the Labrador Sea in the east through the Hudson Strait and Lancaster Sound. The archipelago contains a number of seasonally navigable passages that are up to 120 km wide and with maximum depth of 700 m (Figure 3-11). Fortier and Morley (1956) postulated that most of these inter-island channels represent a submerged pre-existing drainage system possibly of Tertiary origin, initiated by geological processes such as faulting and folding. Later work by Bornhold et al. (1976) in Barrow Strait provided fresh evidence for this idea. Pelletier (1966) had earlier indicated that this drainage system had been modified by valley glaciers. Raised beaches, submerged cirques, hanging tributaries, U-shaped submarine valleys and cores taken at 400 m depth containing an ancient soil were all cited as evidence of terrestrial erosion, glaciation, submergence and subsequent emergence (Pelletier op. cit.).

The Canadian Arctic shelf area (Figure 3-12) west of the Archipelago but excluding the Beaufort Sea shelf can be split into two physiographic zones: an inner zone of submerged headlands and low-lying coastal and fluvial features and an outer

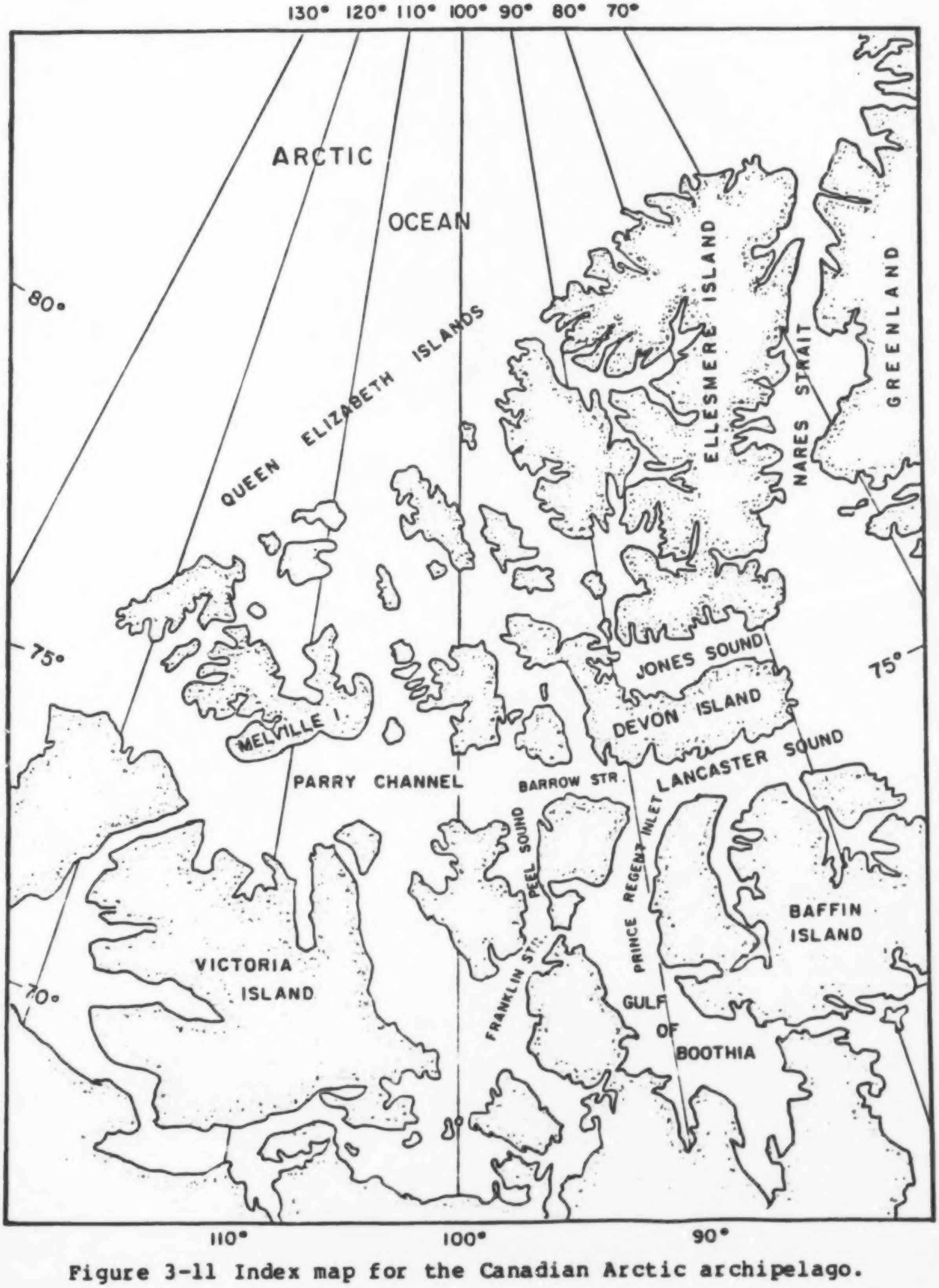
130° 120° 110° 100° 90° 80° 70°
ARCTIC
OCEAN
80°
QUEEN ELIZABETH ISLANDS
ELLESMERE ISLAND
NARES STRAIT
GREENLAND
75°
75°
JONES SOUND
DEVON ISLAND
MELVILLE I.
PARRY CHANNEL
BARROW STR.
LANCASTER SOUND
PEEL SOUND
PRINCE REGENT INLET
BAFFIN ISLAND
VICTORIA ISLAND
FRANKLIN STR.
GULF OF BOOTHIA
70°
110°
100°
90°

Figure 3-11 Index map for the Canadian Arctic archipelago.

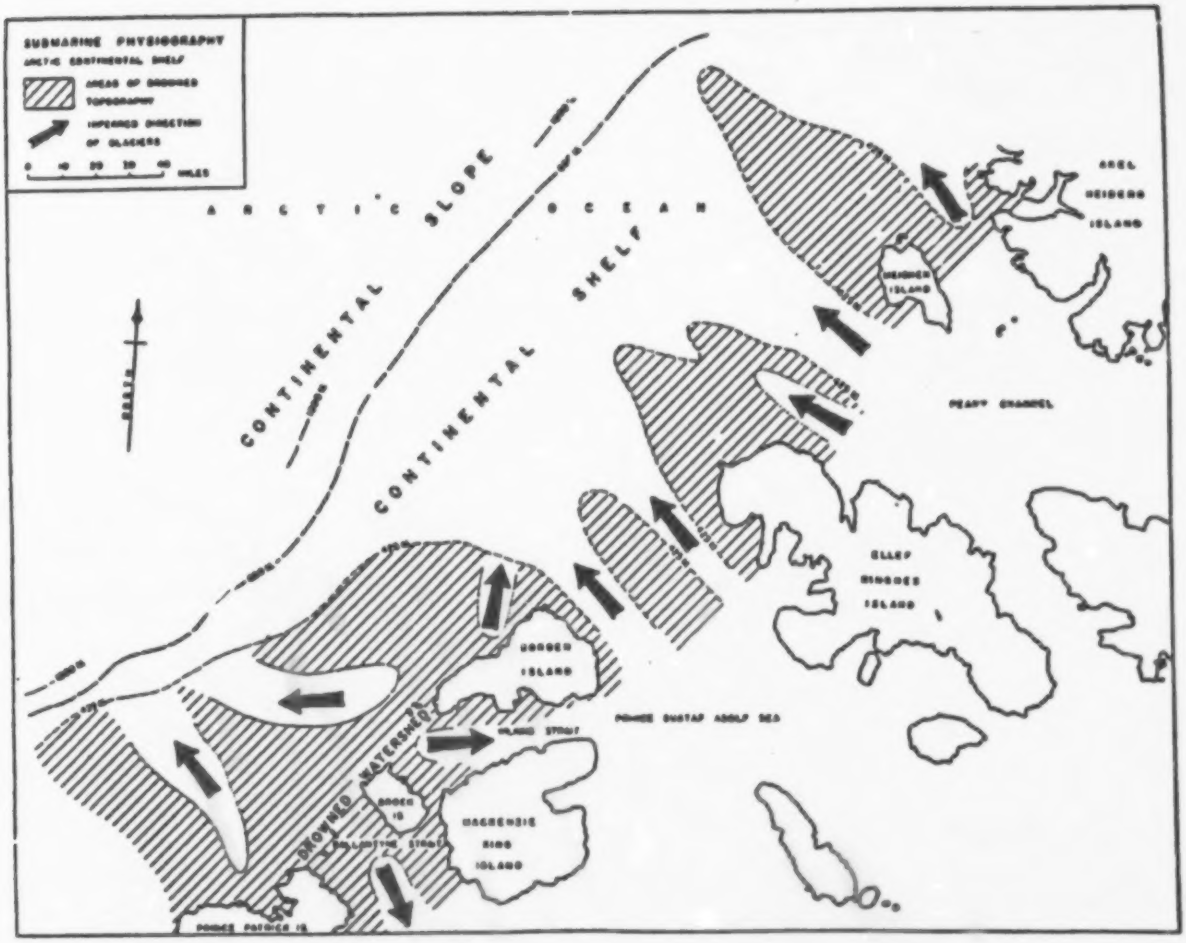
SUBMARINE PHYSIOGRAPHY
ARCTIC CONTINENTAL SHELF
AREAS OF DROWNED TOPOGRAPHY
INFERRED DIRECTION OF GLACIERS
0 10 20 30 40 MILES
ARCTIC OCEAN
CONTINENTAL SLOPE
CONTINENTAL SHELF
CONTINENTAL
NORTH
AXEL HEIBERG ISLAND
MEIGHEN ISLAND
PEARY CHANNEL
ELLEF RINGNES ISLAND
BORDEN ISLAND
PRINCE GUSTAF ADOLF SEA
WILKINS STRAIT
DROWNED WATERSHED
BROCK IS
MACKENZIE KING ISLAND
BALLANTYNE STRAIT
PRINCE PATRICK IS

Figure 3-12 Map of northwestern approaches to the Arctic ocean, showing drowned physiographic features. Deep troughs are divided by median ridges and U shaped valleys (from Pelletier, 1979.

zone of a broad featureless area with areal relief rarely in excess of 25 m.

The floors of the main channels of the western Arctic Archipelago are slightly hummocky with small disconnected basins along their length, sometimes having configurations not dissimilar to cirques or a system of paternoster lakes. Seabed elevation increases towards the open sea in the west, ending in transverse hummocky ridges that form submerged sills 25 to 50 m in height and between 65 and 80 km seaward of the western entrance of the channels. Pelletier (1966) suggests that these submerged sills may be relict terminal moraines of valley glaciers. Two southern channels, Ballantyne and Wilkins Straits off Mackenzie King and Borden islands differ in some respects from those described above. On the seaward side of these straits at a depth of 175 m black anaerobic mud occurs. This has been taken to suggest that a lack of circulation and non-passage of water through these western channels have occurred, due to the high sills that occur at the mouths of the channel. Relict rivers to the west of this sill drained directly into the Arctic ocean, whereas those to the east indirectly drained into the Arctic ocean via the main westward flowing channels. (Figure 3-12).

The eastern Arctic channels have a similar topographic development to those in the west. Submarine valleys enter from both Greenland and Ellesmere Island and drop to the main valley floor of northern Nares Strait as hanging tributaries. Sills are common at the mouths of submerged valleys, and a series of basins occur along the northern section of Nares channel between Ellesmere Island and Greenland.

On the Arctic continental shelf surficial sediments consist predominantly of mud and silt, but sand may be present in areas in amounts up to 100%; this is particularly the case in those areas that are underlain by late Mesozoic and Tertiary sandstones. Over topographic highs, drowned headlands and off headlands up to a distance of 65 km the sand content is high (>50%), and sorting is fair to good. In areas of topographic lows, fine material has settled and accumulated, and sorting is poor. Over the entire area of the continental shelf coarse material has been deposited from ice, and this processs is continuing.

Surficial sediment distribution patterns within the many channels and sounds of the Archipelago differ markedly between each other. and each is controlled by the local seabed topography, the sediment source and local physical environmental conditions.

In bodies of water such as Lancaster Sound and Prince Regent Inlet, there is commonly a zone of sediments of up to 25 km offshore which contain granules and larger material. The central areas of these waters are predominantly populated with silt and clay. The sediments of Barrow Strait, Prince Regent Inlet (Figure. 3-11) and Wellington Channel are a dark olive-grey, whereas those from Franklin Strait. Gulf of Boothia are a pale yellowish-brown. The dividing line is between Prince Regent Inlet and the eastern side of Somerset Island; the colour for these sediments is possibly determined by source area, however some of the depositional environments are anoxic, reducing environments. Marine sedimentation is quite rapid in certain areas (Perry, 1961). Sediments in the Eastern Arctic Archipelago are poorly sorted. Where the currents are vigorous, bedrock is exposed (Perry, op. cit).

The central part of Parry Channel (Figure 3-11), the surrounding coastal area and the inshore areas of the adjacent bays all contain coarse sand and gravel sediments, whereas the deeper parts are characterised by fine silts and clays. In Peel Sound (Figure 3-11) current scouring is most prominent in shallow areas. This is further supported by Blake and Lewis (1975), who took bottom photographs that reveal deposits of clean gravels, as well as plant stems and crinoid stalks, tilted in response to the bottom currents. Additional evidence of current scours were also observed on the records of the seismic reflection profiles in 350 m of water (Lewis et al., 1977).

To the northwest along the western approaches to the Arctic Archipelago sediments, seabed sampling has been undertaken (Pelletier 1979). The area around Ellef Ringnes Island and the Sverdrup channel (Figure 3-12) have sediments which are generally fine except near deltas and the central parts of the channel. McLaren (1982), who examined the sediments of Byam Channel, suggests that during the past deglaciation, glacio-marine sediments predominantly of silt with equal amounts of clay and sand and smaller amounts of gravel with cobbles were deposited; the sediments were derived locally. He further states that while present sedimentation rates are quite low, a considerable amount of sediment is reworked due to ice scouring of the seabed. In areas with little or no sediment cover the ice has torn boulders from the underlying bedrock.

The predominant engineering geohazards that occur in these areas are a result of the varying bedrock topography, the scouring of surficial sediments by current action, and by iceberg and pressure ridge scouring. In western Lancaster Sound, current scouring is evident in the form of the westward thinning of unconsolidated sediment deposits (Pelletier, 1979). Another deep seabed geological hazard to drilling is the occurrence of frozen gas hydrates in eastern Lancaster Sound.

TABLE 3-II

SOME POSSIBLE ENGINEERING GEOHAZARDS

ARCTIC SHELF AREA

VARYING BEDROCK TOPOGRAPHY

SCOURING BY CURRENTS

SCOURING BY ICEBERGS AND PRESSURE RIDGES

THINNING OF SEDIMENTS IN WESTERN LANCASTER SOUND

GAS HYDRATES IN EASTERN LANCASTER SOUND

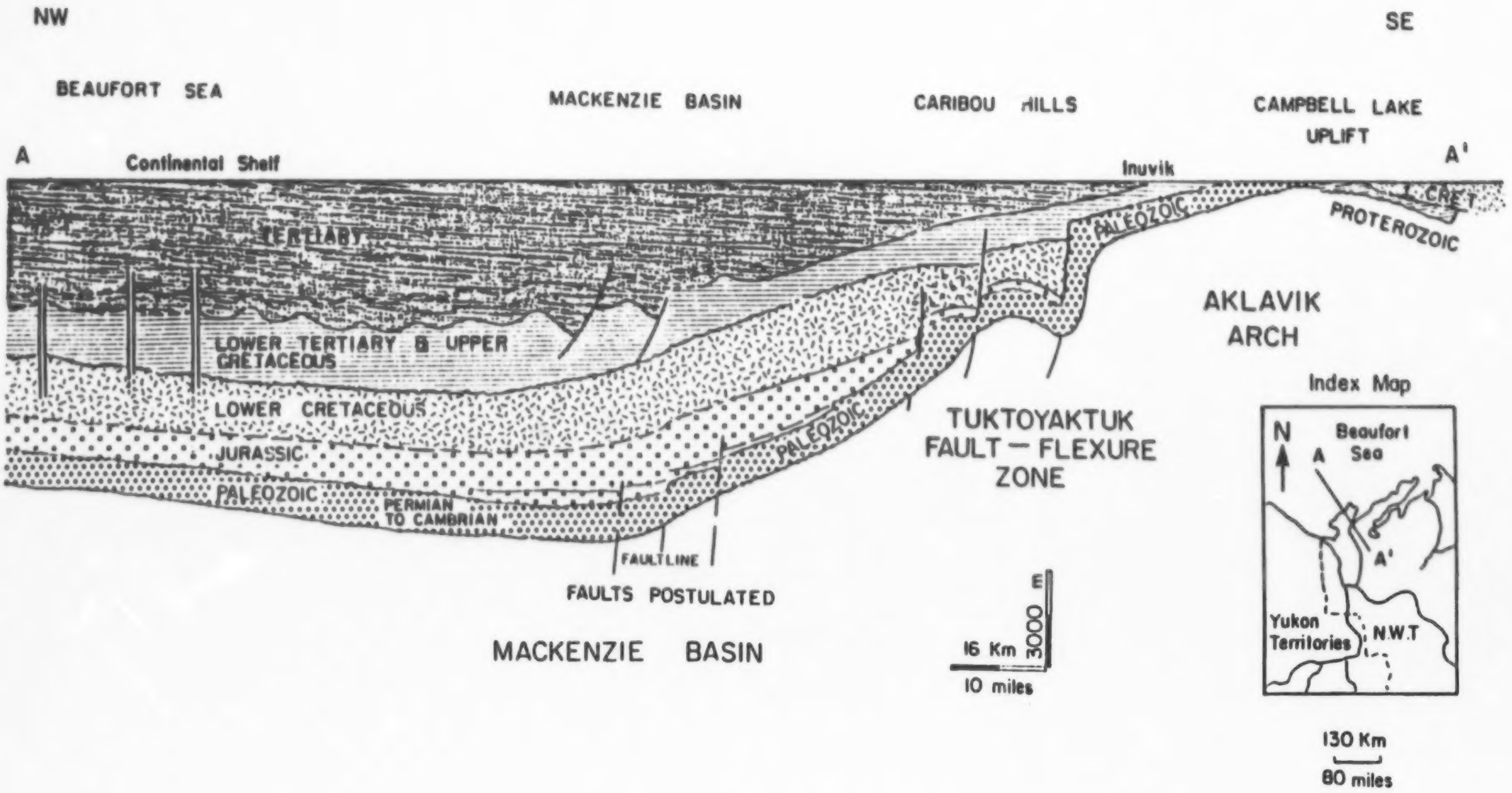
NW
SE
BEAUFORT SEA
MACKENZIE BASIN
CARIBOU HILLS
CAMPBELL LAKE UPLIFT
A
A'
Continental Shelf
Inuvik
TERTIARY
LOWER TERTIARY & UPPER CRETACEOUS
LOWER CRETACEOUS
JURASSIC
PALEOZOIC
PERMIAN TO CAMBRIAN
PALEOZOIC
PALEOZOIC
L. CRET.
PROTEROZOIC
AKLAVIK ARCH
TUKTOYAKTUK FAULT — FLEXURE ZONE
FAULTLINE
FAULTS POSTULATED
MACKENZIE BASIN
16 Km
10 miles
3000 m
Index Map
N
Beaufort Sea
A
A'
Yukon Territories
N.W.T
130 Km
80 miles

Figure 3-13 Schematic northwest-southeast structural cross-section across the Beaufort Sea (from Lerand, 1973).

2.3 The Beaufort Sea Continental Shelf

Seismic reflection and gravity data suggest that the structural and stratigraphic framework of the northern Canadian Cordillera and the adjacent Interior platform continue seaward onto the continental shelf (Yorath and Norris, 1975) (Figure 3-13). The Beaufort Sea is one of several marginal embayments with wide continental shelves that occur as indentations along the coastline of the Arctic Ocean. It is located at the junction of four physiographic provinces which have strongly influenced its palaeogeographic evolution (Figure 3-14). The Beaufort Sea area has almost certainly received sediments since the Jurassic or Early Cretaceous and quite possibly as early as the late Palaeozoic (Lerand, 1973).

The Beaufort Sea continental shelf gently slopes to the 100 m isobath which is approximately 100 km northwest of the Tuktoyaktuk Peninsula; the same 100 m isobath is about 70 km off the coast near the Yukon-Alaska border (Figures 3-14 and 3-15). The Mackenzie canyon bisects the continental shelf from the mouth of Mackenzie Bay at the northwest edge of the delta to the 500 m isobath near the shelf edge. The modern delta is an estuary delta of about 12,200 sq. km. Other than this prominent bathymetric feature, other smaller sedimentary features are to be found, which include: sand bars in the nearshore zone, fresh ice scours and pingoes down to 50 m. Further down the shelf to a depth of 80 m diapirs, mud lumps (which may possibly be mud volcanoes) and further out at the junction of the shelf and slope considerable slumping, faulting and dislocation of surficial beds

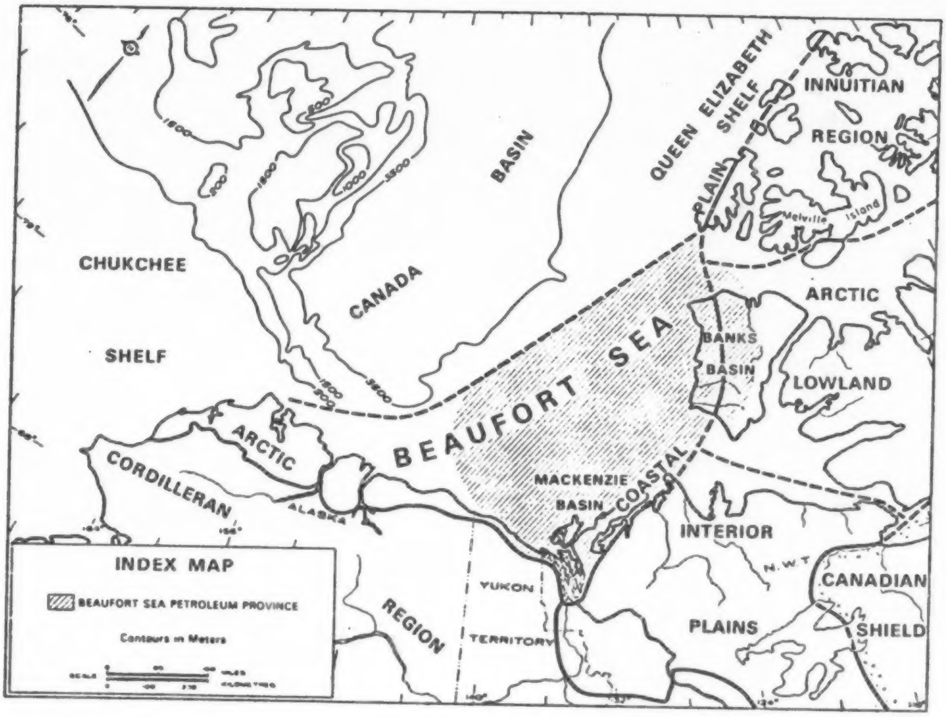

INNUITIAN
REGION
QUEEN ELIZABETH SHELF
PLAIN
Melville Island
BASIN
CANADA
CHUKCHEE
SHELF
ARCTIC
BANKS
BASIN
LOWLAND
BEAUFORT SEA
ARCTIC
CORDILLERAN
ALASKA
REGION
MACKENZIE
BASIN
COASTAL
INTERIOR
N.W.T.
CANADIAN
SHIELD
PLAINS
YUKON
TERRITORY
1500
500
1000
3500
200
INDEX MAP
▨ BEAUFORT SEA PETROLEUM PROVINCE
Contours in Meters

Figure 3-14 Physiographic provinces of the Beaufort Sea area.

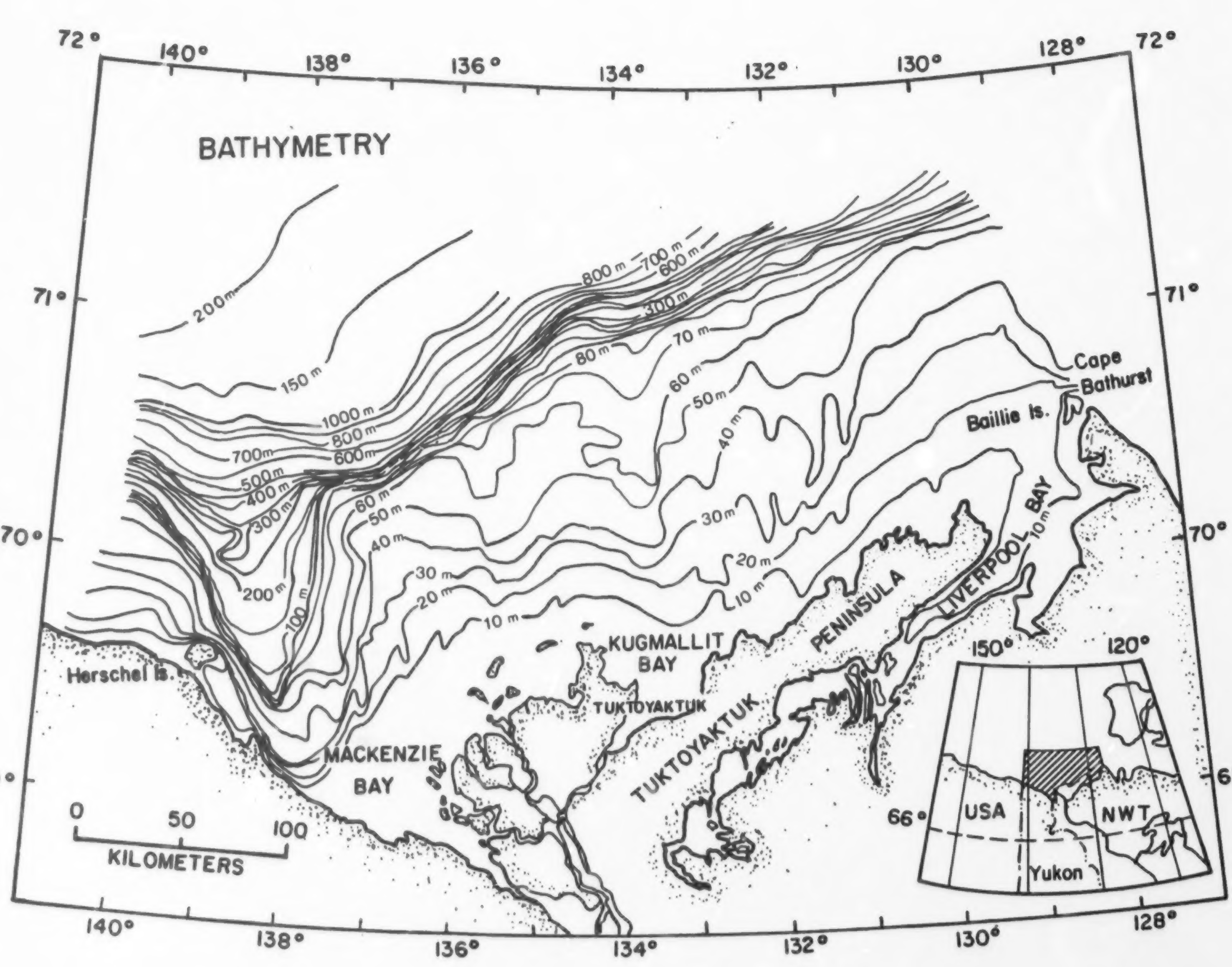
BATHYMETRY
72°
140°
138°
136°
134°
132°
130°
128°
71°
70°
69°
200m
150 m
1000 m
800 m
700m
600m
500m
400 m
300 m
200m
100 m
800 m
700 m
600 m
300 m
80 m
70 m
60 m
50 m
40 m
30m
20 m
10 m
Cape
Bathurst
Baillie Is.
LIVERPOOL BAY
PENINSULA
TUKTOYAKTUK
KUGMALLIT BAY
TUKTOYAKTUK
MACKENZIE BAY
Herschel Is.
0
50
100
KILOMETERS
150°
120°
66°
USA
NWT
Yukon

Figure 3-15 Bathymetric map of the Beaufort Sea area.

is a not uncommon occurrence (Pelletier, 1979). The present surficial sediments of the shelf area of the Mackenzie delta lie on top of 9150 m of Cenozoic and Mesozoic sediments (Figure 3-13). The shelf has been relatively stable during the Late Quaternary, but it has been subject to wide swings in shoreline positions accompanying worldwide eustatic changes in sea level which at about 14.000 BP was down to about the 70 m isobath (pers. comm. Lewis, 1982). Cores taken from the shelf suggest a rising sea level, in that the sands and deltaic complex retreat shoreward contemporaneously with the retreating shoreline and transgressing sea. Cores from the slope show evidence of slumping or turbidity currents, indicating an unstable seabed (Pelletier. 1979).

Pelletier (1975) and Vilks et al., (1979) analysed the surficial sediment distribution of the Beaufort Shelf area (Figure 3-16). The results indicated that very coarse sediments were predominant, both in the western part of the Beaufort Shelf and in the extreme east. The former are ice-rafted sediments which are now overconsolidated due to possible excessive ice-loading northwest of Herschel Island, and the latter sediments from the eastern extreme of the shelf are probably lag deposits resulting from bottom current scouring. Sands dominate the nearshore zone, along the coastal islands and along the eastern portion of the shelf. Mackenzie Bay is the deposition site of silt, whereas clays are found in the Mackenzie Canyon.

The bulk of the sediments that discharge from the Mackenzie river drift eastwards along the coast, while a little dispersion

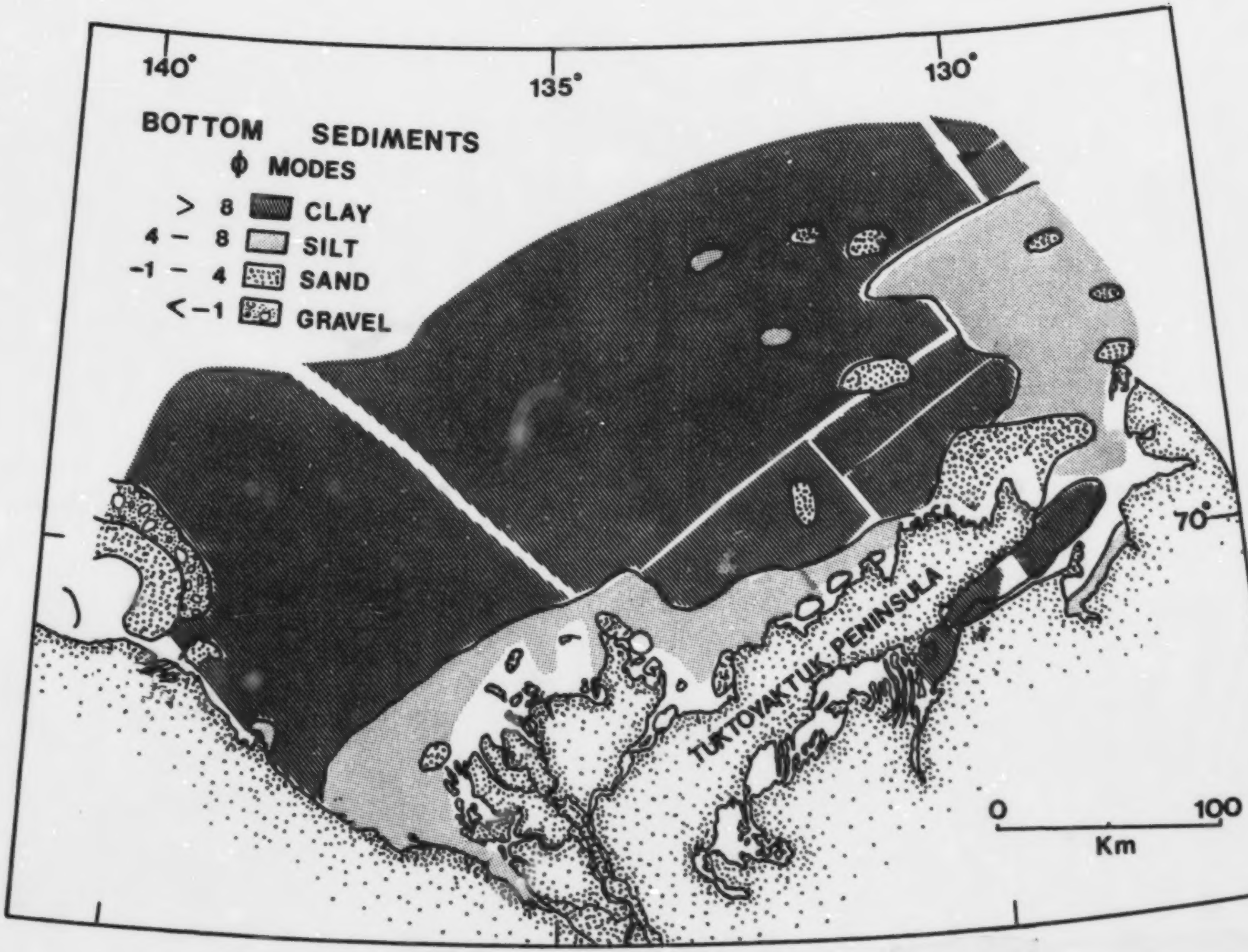
140°
135°
130°
70°
BOTTOM SEDIMENTS
ϕ MODES
> 8 CLAY
4 – 8 SILT
-1 – 4 SAND
<–1 GRAVEL
TUKTOYAKTUK PENINSULA
0
100
Km

Figure 3-16 Sediment distribution patterns for the Beaufort Sea area.

is a not uncommon occurrence (Pelletier, 1979). The present surficial sediments of the shelf area of the Mackenzie delta lie on top of 9150 m of Cenozoic and Mesozoic sediments (Figure 3-13). The shelf has been relatively stable during the Late Quaternary, but it has been subject to wide swings in shoreline positions accompanying worldwide eustatic changes in sea level which at about 14.000 BP was down to about the 70 m isobath (pers. comm. Lewis, 1982). Cores taken from the shelf suggest a rising sea level, in that the sands and deltaic complex retreat shoreward contemporaneously with the retreating shoreline and transgressing sea. Cores from the slope show evidence of slumping or turbidity currents, indicating an unstable seabed (Pelletier. 1979).

Pelletier (1975) and Vilks et al., (1979) analysed the surficial sediment distribution of the Beaufort Shelf area (Figure 3-16). The results indicated that very coarse sediments were predominant, both in the western part of the Beaufort Shelf and in the extreme east. The former are ice-rafted sediments which are now overconsolidated due to possible excessive ice-loading northwest of Herschel Island, and the latter sediments from the eastern extreme of the shelf are probably lag deposits resulting from bottom current scouring. Sands dominate the nearshore zone, along the coastal islands and along the eastern portion of the shelf. Mackenzie Bay is the deposition site of silt, whereas clays are found in the Mackenzie Canyon.

The bulk of the sediments that discharge from the Mackenzie river drift eastwards along the coast, while a little dispersion

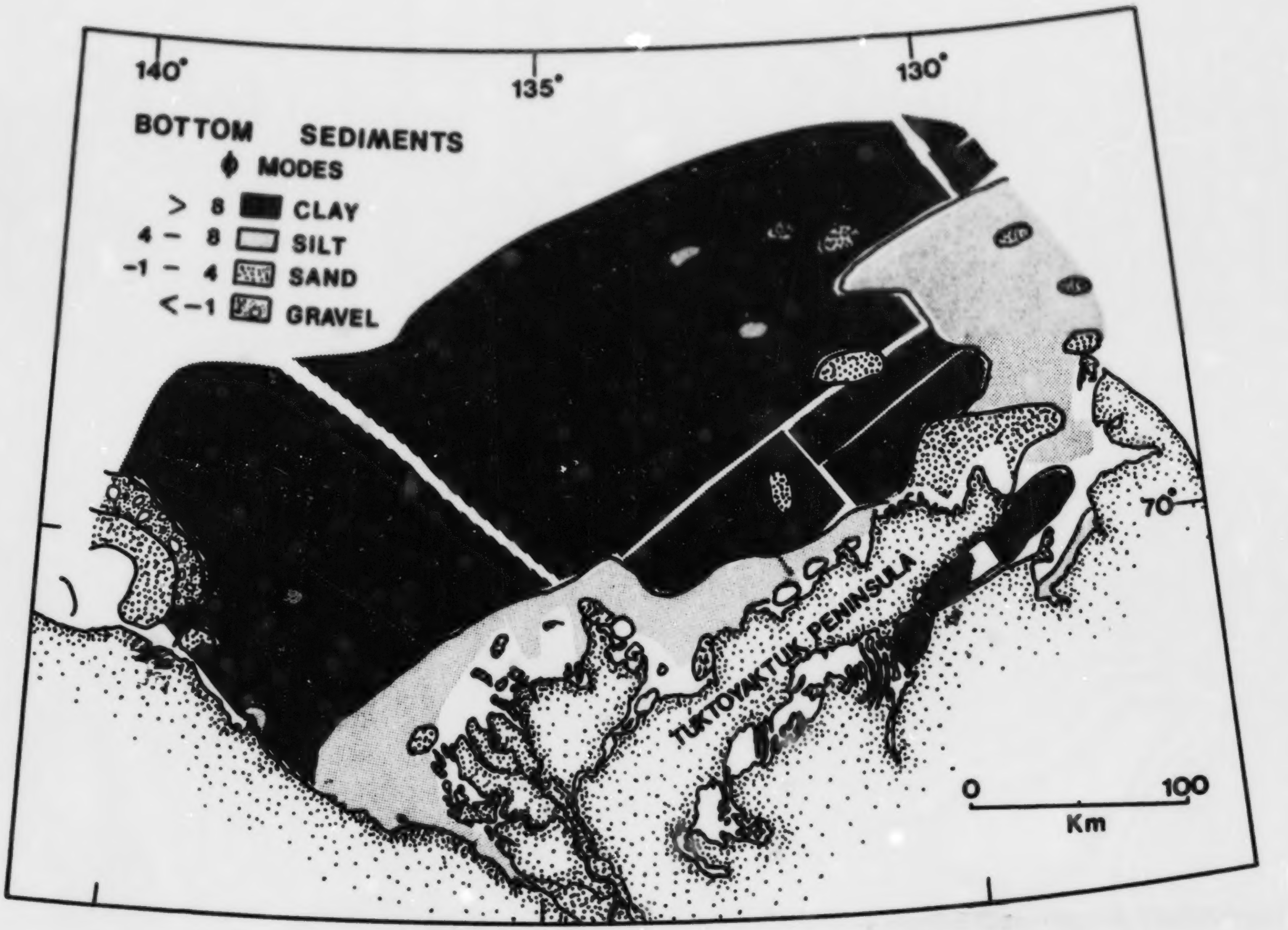
140°
135°
130°
70°
BOTTOM SEDIMENTS
ϕ MODES
> 8 CLAY
4 – 8 SILT
-1 – 4 SAND
<-1 GRAVEL
TUKTOYAKTUK PENINSULA
0
100
Km

Figure 3-16 Sediment distribution patterns for the Beaufort Sea area.

takes place towards the north for about 30 to 40 km over the Mackenzie Canyon. The eastward movement of the sediment is a consequence of the Coriolis force. An insignificant amount of sediment moves westward, possibly under the influence of the Pacific gyre (Pelletier 1979). Pelletier (op. cit.) determined three major hydrodynamic environments for this area with the possibility of one more immediately offshore. The hydrodynamic environments are indicated in Figure 3-17, and are as follows:

1) a very low energy regime represented by the depositional site of clay;
2) a low energy regime indicated by the silt deposits;
3) an intermediate energy regime nearshore where the sands were deposited;
4) the probable existence of a high energy regime existing immediately offshore, could not be determined due to the inability to collect the requisite sediment samples.

The first three environmental zones were confirmed by using a ternary textural model (Pelletier. 1975), but generally the Beaufort Sea is one of low energy due to the ice cover for much of the year (Pelletier. 1979). This interpretation of the three major hydrodynamic environments has been questioned by Blasco (Blasco, pers. comm., 1982), who suggests that the three zones in reality reflect beaches, corresponding to changes in sea-levels due to a combination of isostatic and eustatic changes in sea level. Sediment accumulation is at an average rate of 0.5 mm/yr east of the Mackenzie Canyon.

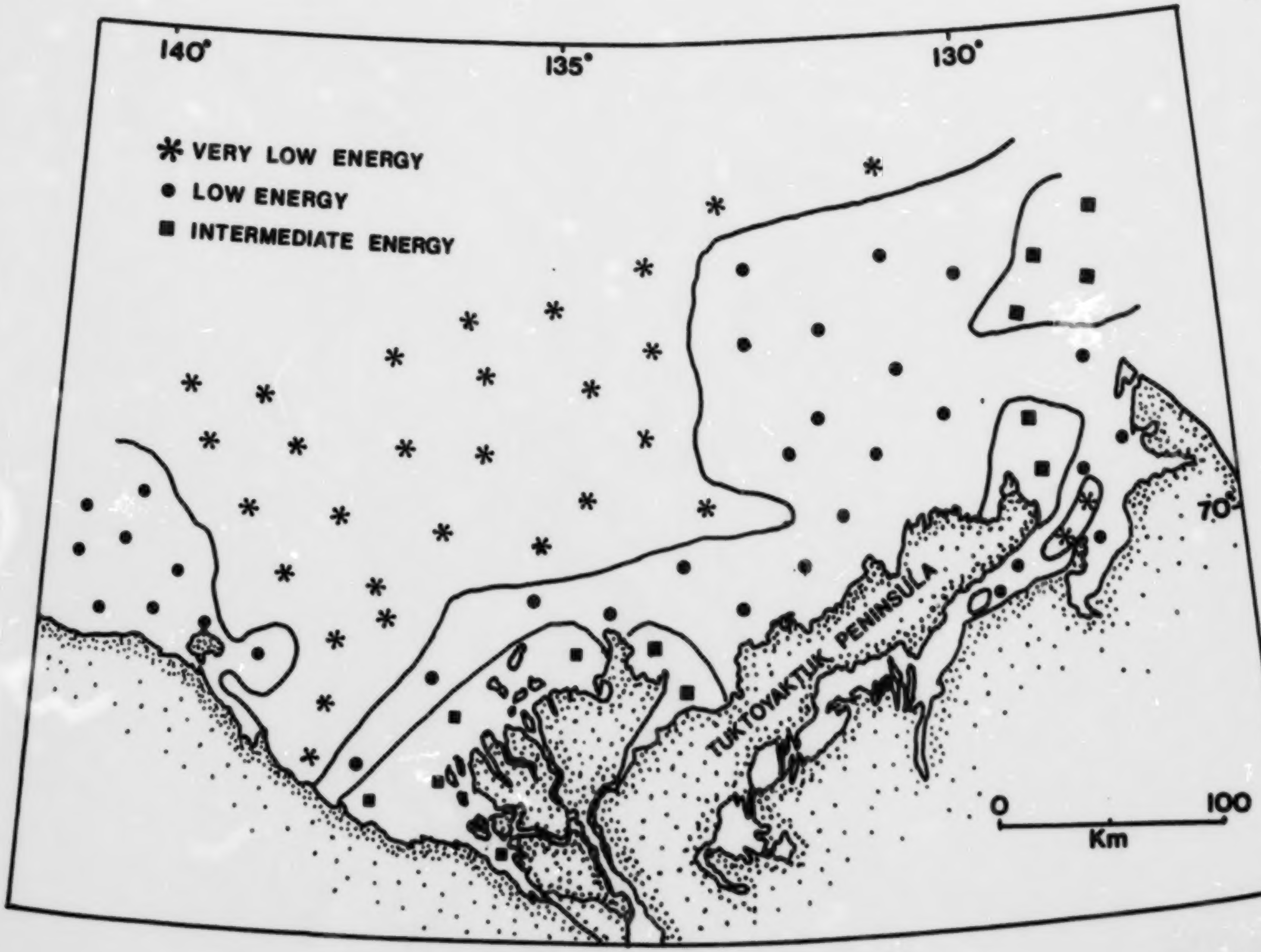
140°
135°
130°
70°
VERY LOW ENERGY
LOW ENERGY
INTERMEDIATE ENERGY
TUKTOYAKTUK PENINSULA
0
100
Km

Figure 3-17 Hydrodynamic environments for the Beaufort Sea area (Pelletier, 1979).

An unusual mixture of engineering geohazards exist in this area which is compounded by the freezing Arctic climate; a list of these geohazards are given in Table 3-III. Sea ice ridge scouring is a distinctive hazard in the shallow offshore water, but this can be overcome by dredging or burying installations in pits or trenches for protection. However, ice lenses and ice-bounded sediments will be a hindrance. Other not dissimilar features to consider are unstable and mobile shoals and coastal zone sand bars, as well as submarine ridges (Pelletier 1979). Submerged and buried river beds (Shearer, 1971) such as the Kugmallit Channel must be examined with respect to engineering hazards. The fact that these relict drainage channels are infilled with soft fine sediment means less loading ability will be available than that for the sandy beds of the old beaches.

TABLE 3-III

SOME POSSIBLE ENGINEERING GEOHAZARDS
BEAUFORT SEA

ICE SCOURING (ICE RIDGES, ICEBERGS)

ICE LENSES & ICE-BOUNDED SEDIMENTS

UNSTABLE AND MOBILE SAND SHOALS

SUBMARINE RIDGES

RELICT DRAINAGE CHANNELS INFILLED WITH SOFT SEDIMENTS

STRUDEL SCOURS - OVER-CONSOLIDATED SILTS OVERLAIN BY GRAVEL/SAND

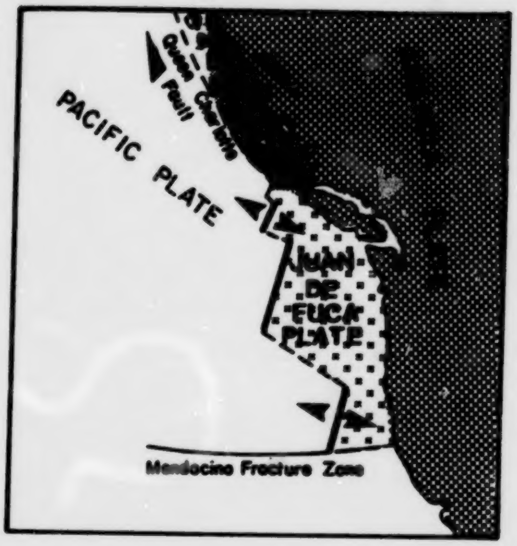
Queen Charlotte Fault
PACIFIC PLATE
JUAN DE FUCA PLATE
Mendocino Fracture Zone

Figure 3-18

Continental plate configuration off the British Columbia coast. (Arrows indicate movement of plates in relation to each other. See figure 3-02).

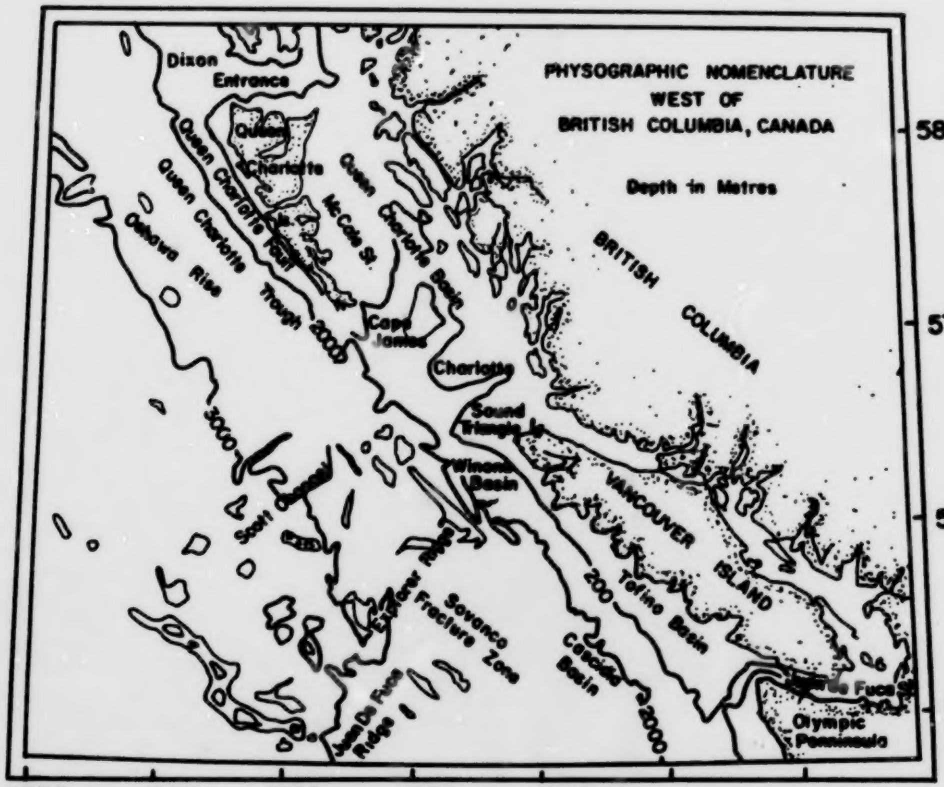
PHYSOGRAPHIC NOMENCLATURE
WEST OF
BRITISH COLUMBIA, CANADA
Depth in Metres
Dixon Entrance
Queen Charlotte
Queen Charlotte Fault
Queen Charlotte Trough
Oshawa Rise
McCole St.
Queen Charlotte Basin
Cape James
Charlotte
Sound
Triangle Is.
Winona Basin
BRITISH COLUMBIA
VANCOUVER ISLAND
Tofino Basin
Cascadia Basin
Scott Seamount
Explorer Ridge
Sovanco Fracture Zone
Juan De Fuca Ridge
Juan de Fuca St.
Olympic Penninsula
2000
3000
200
2000
58°
57°
56°
55°
130°
129°
128°
127°
126°
125°
124°

Figure 3-19 Bathymetric and physiographic map of the west coast of Canada.

2.4 The British Columbia Continental Shelf Margin

The continental shelf of the British Columbia coast lies within a tectonically active section of the earth's crust which includes the junction of the Pacific, the North American, the remnant Explorer plate and the Juan de Fuca plates (Figure 3-18) (Srivastava et al., 1971). The resultant palaeogeographical evolution of the margin, and in particular the shelf zone, is complex, and during the Cenozoic period two major periods of deformation resulted in faulting, folding and diapirism on the continental shelf. This deformation was not homogeneous throughout the length of the shelf zone, there being marked changes from north to south (vide, Chase et al., 1975; Tiffen et al., 1972). The surface morphology of the bedrock was probably further modified by the advancing glaciers of the Pleistocene age (which on their retreat left behind a legacy of dangers!). In certain areas some of these glaciers extended about 30 km out onto the shelf.

The width of the continental shelf off British Columbia varies considerably, west of Queen Charlotte Islands it is almost non-existant, but to the north of Vancouver Island it is about 120 km wide, at a water depth of about 200m (Figure 3-19), thereafter there is a steep slope that descends to 2500 m over a few kilometres of horizontal distance. Five major reentrants cut the continental shelf (Figure 3-19).

Notwithstanding the different surficial sediment distribution patterns that have been surveyed across the length of the shelf (Young and Chase, 1977; Tiffen, 1969; Claque, 1976;

Carter, 1972), a pattern emerged indicating that coarse to fine sand sedimentation occurred in the inshore areas, succeeded by silt further seaward and finally by clay deposition in the outer fringes of the deltas and bottoms of the basins (Pelletier 1979). Also, cores from the Fraser River delta (Figure 3-19), examined by Luternauer (1977), clearly showed rapid gradational changes in deltaic formations, progressing from sand to mudflats.

In the southwestern Hecate Strait (Figure 3-19), seismic reflection profiles suggest very complex geological structures due to tectonism; further south in the northwestern portion of Queen Charlotte Sound, these geological structures are modified by canyon-forming processes, and sand and gravel commonly overlie the complex bedrock structure (Young and Chase, 1977). Similar complex geological structures are seen in the seismic reflection profiles in the southern Strait of Georgia, and here heavy sedimentation from the Fraser River (Tiffen, 1969) has lent the area a very subdued topography. In contrast to this, the northern portion of the strait of Georgia has steep walled canyons which are infilled with soft sediments (Claque, 1976; see also Pelletier, 1979). In the central portion, coarse sediments are found at the head of the basin with fine deposits in the lower parts (Pharo and Barnes, 1976). An extensive surficial sedimentological study in Barkely Sound by Carter (1972) revealed a relict sand and gravel cover for most of the shelf, except within the basins and drowned river valleys where mud is prevalent. This relict cover, initially dispersed by glaciers and meltwater, was later inundated during the Holocene; it is now being partly reworked by the modern hydraulic regime. Later studies by Milliman (1976) found angular gravels on the outer shelf. which he related to erosion from nearby exposed bedrock; gravels inshore were more rounded, winnowed and presumably are a glacial lag deposit (Pelletier, op. cit.). Similar phenomena have been observed off the west coast of Vancouver Island (Yorath et al., 1978) and off Queen Charlotte Island (Tiffen et al., 1980. Sediment distribution patterns for the shelf area of west and central Vancouver Island has been summarized recently by Bornhold (1982) (Figure 3-20). In contrast to these relict sediments of the British Columbia coast, the adjacent shelf to the south off Washington State is mantled with modern sediments reflecting the large volume of sediment supplied by the Columbia River (Carter, 1972).

On the British Columbia Shelf most of the engineering geohazards are related to three major causes: (1) seismicity (2) bedrock topography and (3) the hydrodynamic environment (see Table 3-IV). Seismic shocks can easily trigger off submarine landslides, and in areas with steep slopes associated with unconsolidated sediments this could cause a slope failure and a sudden mass movement of the sediments (vide Luternauer and Swan, 1978). Also, thick moraines, a legacy of Pleistocene glaciers, are still present over the inshore shelves and where valleys have been overdeepened. Seismic activity can result in the glacial debris sliding suddenly into these valleys. The presence of this as yet uncharted glacial debris can render drilling and excavation difficult. Many submarine canyons which are no longer

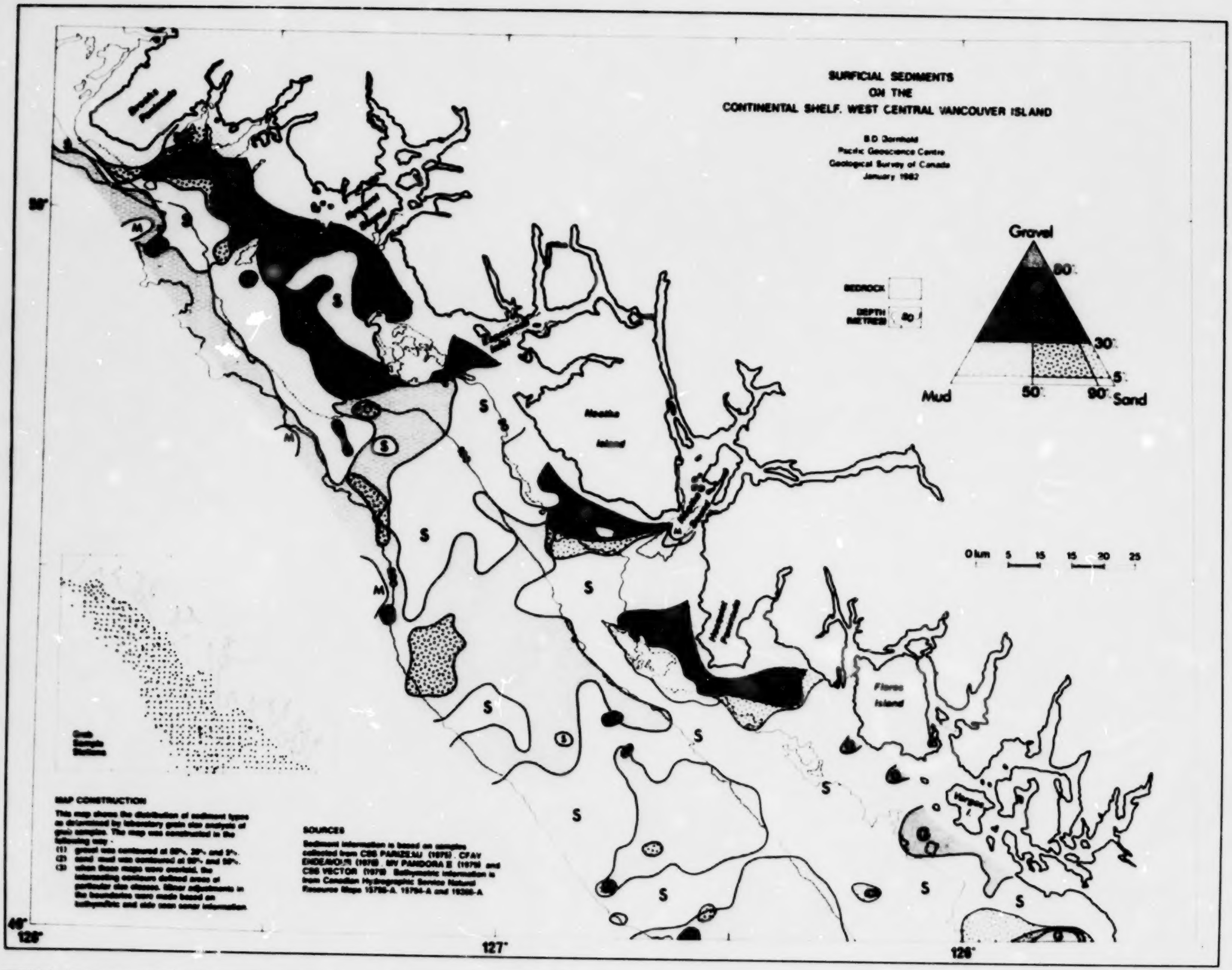

SURFICIAL SEDIMENTS
ON THE
CONTINENTAL SHELF, WEST CENTRAL VANCOUVER ISLAND

B.D. Bornhold
Pacific Geoscience Centre
Geological Survey of Canada
January 1982

BEDROCK
DEPTH METRES
80
Gravel
80
30
5
Mud
50
90
Sand
0 km 5 15 15 20 25
Nootka Island
Flores Island
Vargas I.
S
M
G
Grab Sample Stations
50°
49°
128°
127°
126°

MAP CONSTRUCTION

This map shows the distribution of sediment types as determined by laboratory grain size analysis of grab samples. The map was constructed in the following way:

(1) gravel was contoured at 80%, 30%, and 5%.
(2) sand: mud was contoured at 90% and 50%.
(3) when these maps were overlaid, the intersecting contours defined areas of particular size classes. Minor adjustments in the boundaries were made based on bathymetric and side scan sonar information.

SOURCES

Sediment information is based on samples collected from CSS PARIZEAU (1975), CFAV ENDEAVOUR (1978), MV PANDORA II (1979) and CSS VECTOR (1979). Bathymetric information is from Canadian Hydrographic Service Natural Resource Maps 15788-A, 15794-A and 15288-A

PHOTO
ON
PRECEEDING
PAGE

Figure 3-20 Distribution of surficial sediments on the continental shelf, west central Vancouver Island (from Bornhold, 1982).

active can be used as routes for seafloor crossings, however these canyons are still susceptible to catastrophic transport of consolidated sediments (Herzer. 1978; Pelletier. 1979). Across sections of the continental shelf, topography is extremely rough in areas of bedrock exposure. this may inhibit seafloor crossings of pipelines and cables. Seafloor topography is actually bedrock topography in approximately 10% of the shelves, and thus engineering difficulties may arise in traversing from bedrock to unconsolidated sediments (Pelletier. op. cit.).

The very substantial hydraulic environment in these waters is another grave potential hazard to engineering constructions. The exceedingly large ocean swell, coming in from the Pacific, produces oscillatory sand and gravel waves on the seabed in water depths down to 104 m off the west coast of Vancouver Island. Similar sand waves were also recorded at depths of 285 m in Johnstone Strait (Luternauer et al., 1978). This dimension of wave energy can easily scour and bury seabed installations in this area. In certain areas of the shelf bottom, currents scour the seabed vigorously so that bedrock is often exposed; this also causes significant sediment transport.

Inshore in the passages such as Georges Strait and Seymour Passage, tidal currents may induce similar effects as wave-generated or oceanic currents. Velocities of currents in these areas may exceed 400 cm s^{-1}. Closer inshore, coastal erosion may be accelerated by tsunamis, wave action and longshore currents. Both alongshore and offshore, marine erosion and sedimentation present sequential and separate problems of under-cutting by means of scour, and burial by means of sediment transport. (Pelletier, 1979).

TABLE 3-IV

SOME POSSIBLE ENGINEERING GEOHAZARDS
BRITISH COLUMBIA

SEISMIC SHOCKS	Landslides and areas of unconsolidated sediments, slope failure
BURIED MORAINES	Hindrance to drilling
SUBMARINE CANYONS	Failure of Slopes
INTERDIGIT HUMMOCKY BEDROCK AND SEDIMENTS	Difficulties when transversing from one to the other.
PHYSICAL ENVIRONMENT	Large ocean swell from Pacific. Sand waves down to 285 m.
BOTTOM SCOUR	

3. SUMMARY

This brief review summarizes some of the salient characteristics of the continental shelves north of Labrador and on the west coast of Canada, and highlights some of the geohazard problems that must be overcome to ensure a safe and well regulated usage of the petroleum resources found in these inhospitable areas. Some sterling initial work has been undertaken, as this brief review indicates, but these only highlight the problems. Solving them will require innovative methodologies and the will of concerted action.

Chapter 4. ICE SCOUR; METHODS OF ANALYSIS

J. Vaughn Barrie

and

Christopher M.T. Woodworth-Lynas

1.0 INTRODUCTION

When an ice keel loads and disturbs the seafloor it either becomes grounded and ceases to move on, or if it has sufficient kinetic energy under influence of swell, currents, wind or pressure from other ice, the keel penetrates the seafloor sediment and excavates a trough that is commonly referred to as a scour. Two kinds of ice are significant in seabed disturbance, icebergs and sea ice pressure ridges.

Ridges originate from the rafting of sheets of sea ice under pressure which produce keels of a few metres to a few tens of metres deep. These rarely exceed 40 m depth even in Arctic Ocean waters. Thus they are mainly significant in seabed disturbance on shallow shelves and in nearshore waters (Pelletier and Shearer, 1972; Reimnitz and Barnes, 1974; Kovacs and Mellor, 1974; Wadhams, 1975; Shearer and Blasco, 1975; Wahlgren, 1979; Lewis, 1980. On the other hand, thick glaciers and ice shelves which calve in deep water produce large icebergs with drafts commonly in the range of 100 to 200 m (Dinsmore, 1972) or larger (Murray, 1969). These keels are the principal agents for ice-related disturbance of sediments on the offshore banks of eastern Canada.

Linear excavations in the sediment (scours, scour marks,

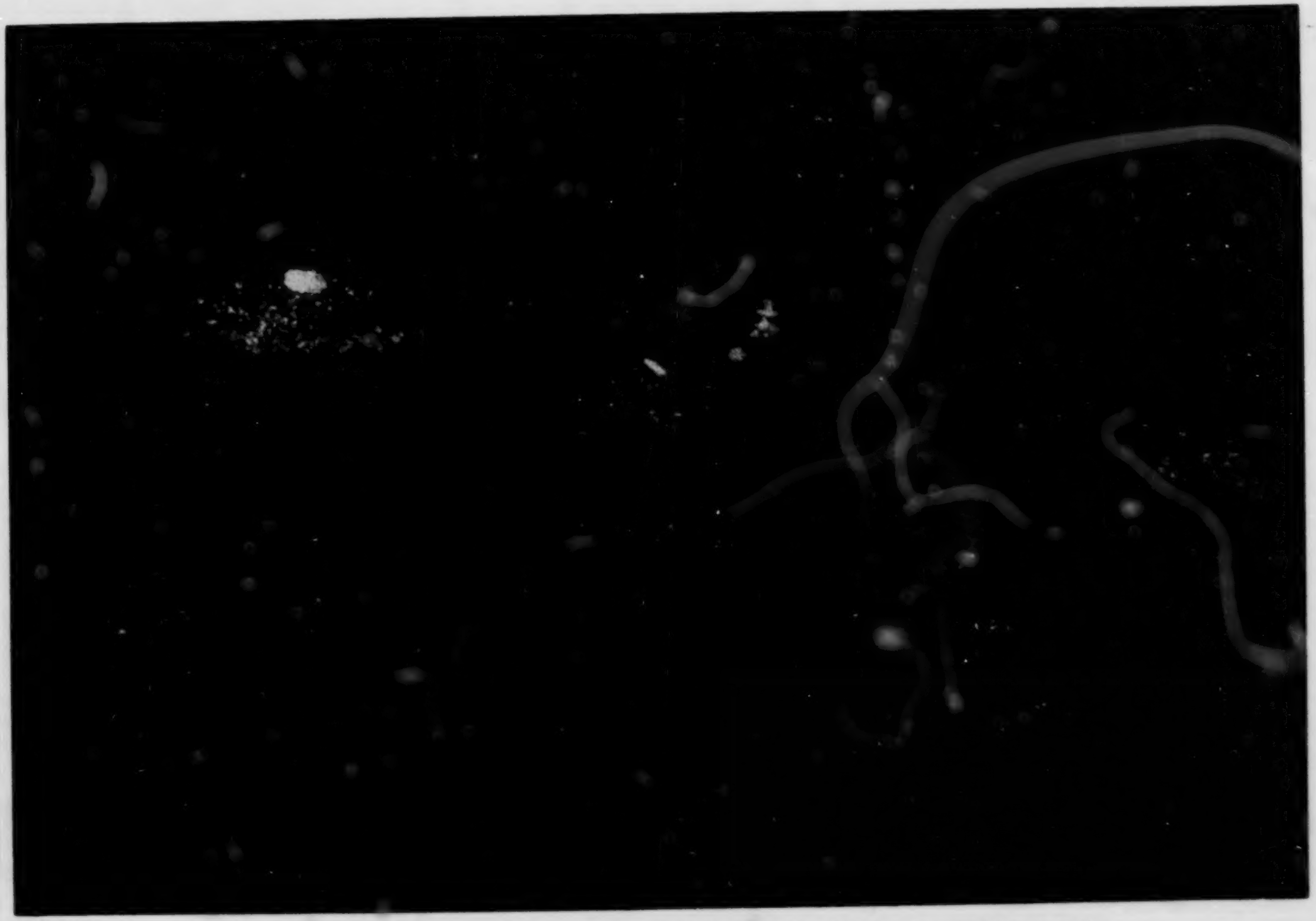

Figure 4-01 Diagrammatic presentation of iceberg scour mark, with representative bottom photographs from a submersible (from Josenhans and Barrie, 1982).

Number/
Numéro

4

gouges, scores, furrows, etc.) mark the passing of an ice keel. Embankments of displaced sediment are heaved up on either side of the scour trough (Fig. 4-01), possibly by shear failure and by lateral displacement and extrusion of material from beneath the keel. Similar embankments encircle the front edge of ice keels when they come to rest, delineating circular depressions called craters or pit marks. These iceberg-related features have been defined from sidescan sonar records on the shelves of the western Grand Banks (King, 1976), Belle Isle and the Labrador Shelf (Harris and Jollymore, 1974; Harris, 1974; Barrie, 1980; Josenhans and Barrie. 1982) and from Baffin Bay (Lewis et al., 1979). Iceberg scour marks and craters have also been described from the Grand Banks by Fader and King (1981) and Lewis and Barrie (1981). Figure 4-02 shows a composite record in plan and section of a wide variety of ice scour forms that occur on the Labrador Shelf.

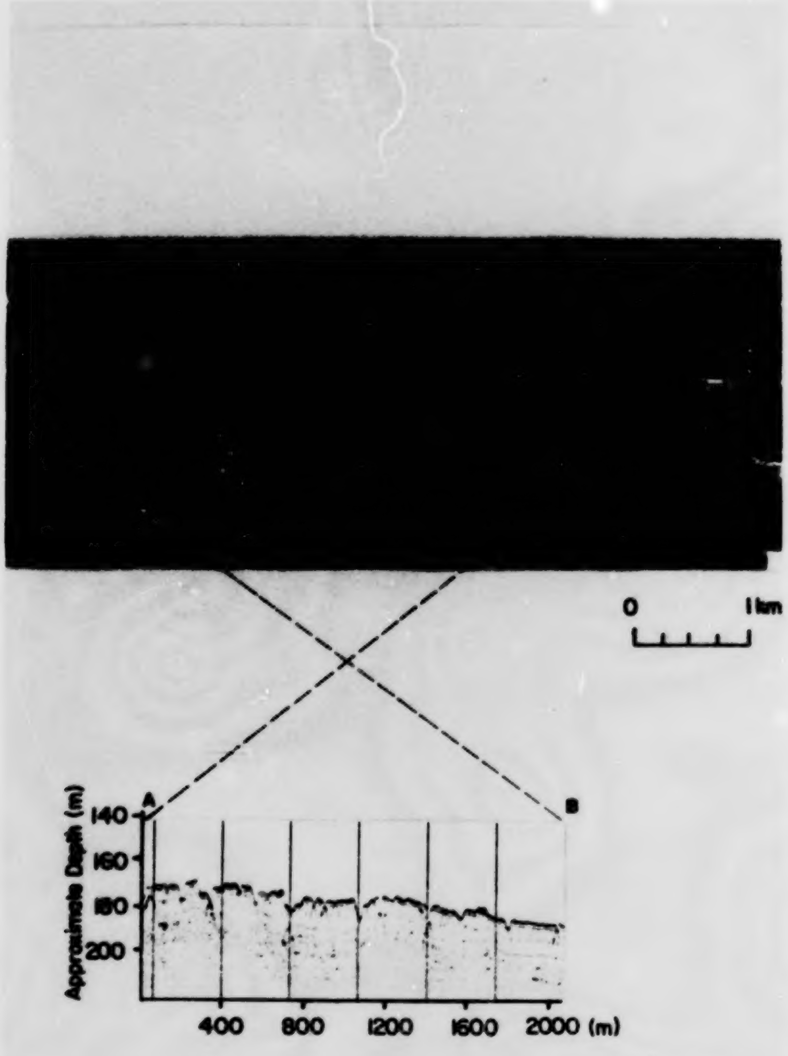

Figure 4-02 A sidescan mosaic of an area of south-central Saglek Bank showing the distinctive iceberg scours in plan and cross section.

2. METHODS OF ICEBERG SCOUR ANALYSIS

The understanding of scour frequency and the mechanism of the ice/seabed interaction is critical to design criteria for seabed installations. Much work has been directed towards the study of iceberg movement and flux along the Canadian east coast and sea ice movement in the Beaufort Sea. Also theoretical geotechnical models of iceberg scouring have been formulated (eg. Chari, 1978; Chari and Peters, 1981). In this paper various methods of analysing ice scour frequency are briefly described.

2.1 Repetitive Seabed Mapping

This method has been used successfully in the Beaufort Sea (e.g. Reimnitz and Barnes, 1974; Reimnitz et al., 1977; Lewis, 1978; Barnes et al., 1978) and on the Labrador Shelf (Lewis and Barrie, 1980). The method involves resurveying (usually on an annual basis) a specific area of the scoured seabed using sidescan sonar mosaicing techniques. By comparing the annual mosaics, newly formed scours are identified and counted, and a return rate can be computed (e.g. Lewis, 1978; Weeks et al., 1980, Pilkington and Marcellus, 1981).

2.2 Dating Scour Populations from Quaternary Evidence

This is a method for obtaining general ages for ancient scour populations using such evidence as;

a) the position of submerged strandlines (the ages of which are known) with respect to scour populations (King, 1976),

b) the location and duration of calving glacier margins which produced icebergs in areas that are now free of icebergs (King, 1976),

c) location of areas that are known to have been free from the effects of iceberg scouring at specific times during deglaciation (Fillon and Harmes, 1982).

2.3 Direct Dating of Sediments in Scours

This method involves the retrieval of datable material from sediments in a scour trough. Datable biogenic material from the infilling sediment at the scour bottom should yield the absolute age of the scour by the method outlined in Figure 4-03. Dating techniques include such methods as isotope dating, (C^{14} - 20,000 years; Pb^{210} - 200 years), amino acid racemization, electron spin resonance, biological growth and foraminiferal dating. However, in order to date a scour population a large number of samples are required from individual scour troughs. This requires highly accurate navigation, exact location of individual scours and precise remote coring techniques or, in shallower water, the use of divers.

2.4 Scour Equilibrium Analysis

Several workers have used the rate of infilling by sedimentation to estimate the absolute age of ice scours in the Beaufort Sea. However. too little is known about sedimentation rates and the processes of infilling in this region to obtain meaningful results (e.g. Hunting, 1971; Pelletier & Shearer, 1972; Lewis, 1978; Barnes & Reimnitz, 1979; Pilkington & Marcellus, 1981).

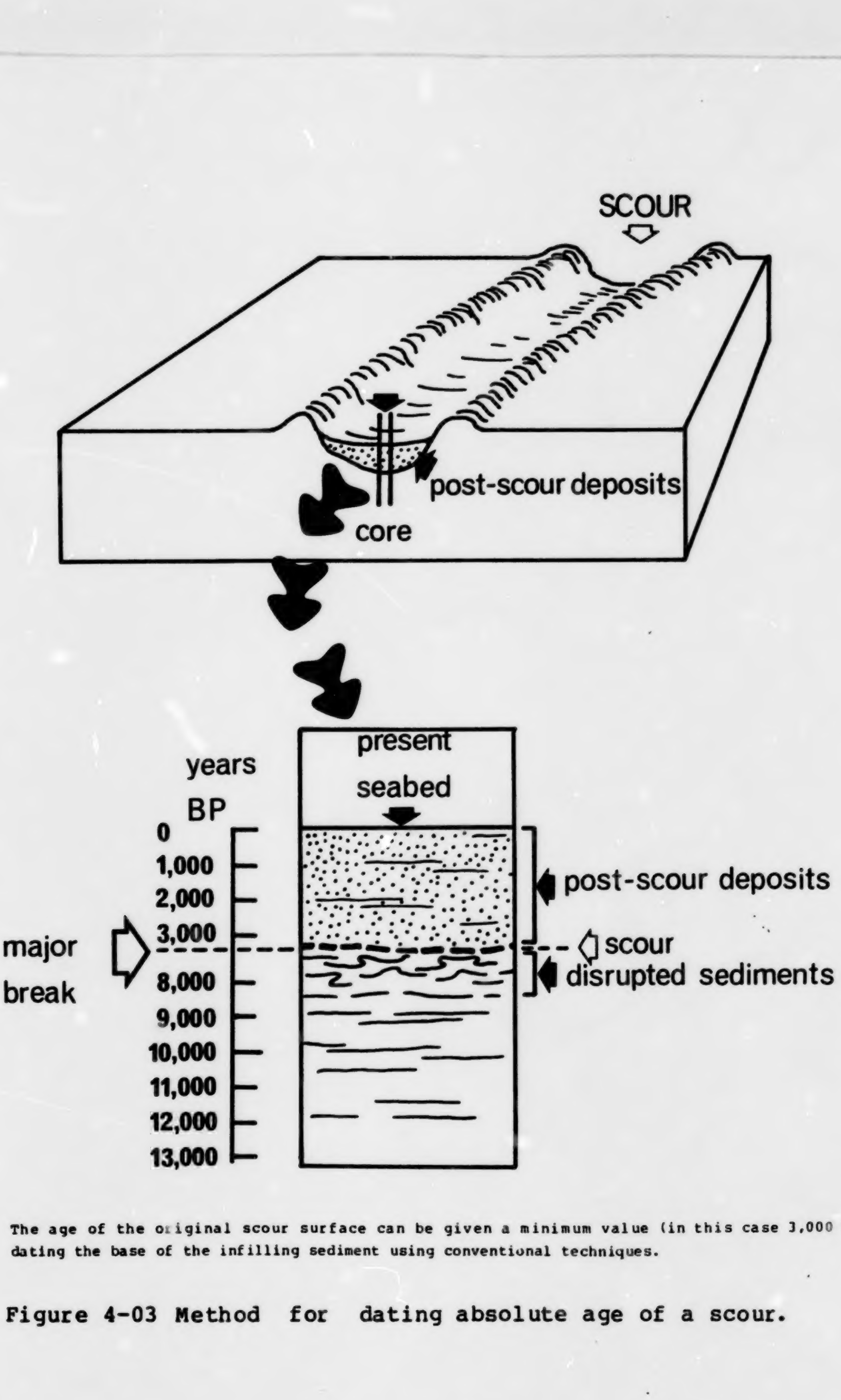
SCOUR
post-scour deposits
core
present seabed
years BP
0
1,000
2,000
3,000
8,000
9,000
10,000
11,000
12,000
13,000
major break
post-scour deposits
scour
disrupted sediments

The age of the original scour surface can be given a minimum value (in this case 3,000 B.P.) by dating the base of the infilling sediment using conventional techniques.

Figure 4-03 Method for dating absolute age of a scour.

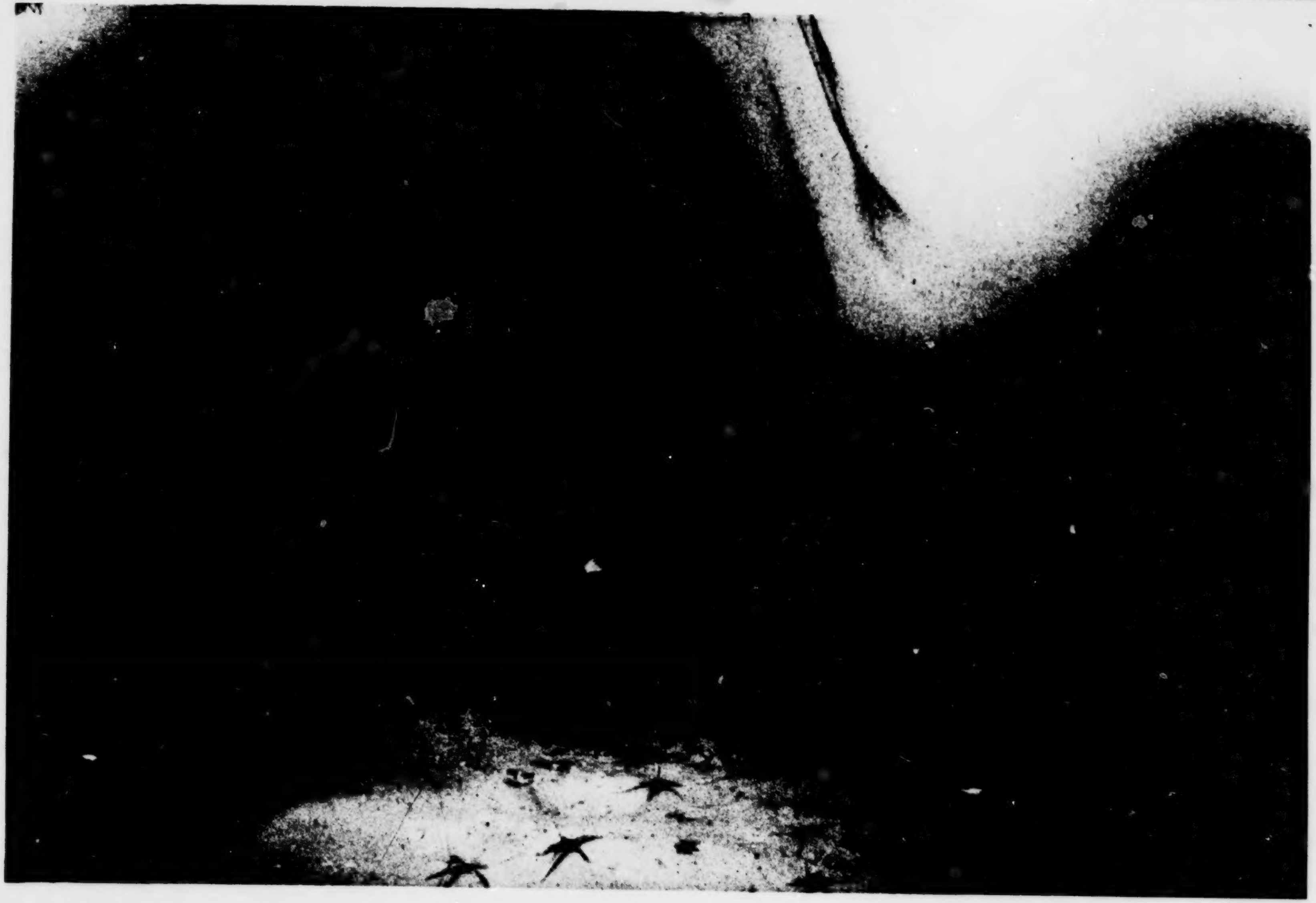

This ice island had drifted aground in the nearshore zone of Byam Martin Island in the Central Artic archipelago.

Figure 4-04 Underwater photograph of a small grounded ice island (iceberg) showing the formation of an ice scour in unconsolidated sediment (courtesy Dr. P. McLaren, GSC 202 842-Q).

2.5 Statistical Analysis of Regional Ice Scour Distribution

Compilation of the limits and variability of ice scours for the Beaufort Sea and Labrador Shelf can be described and analysed in a statistical sense. For example, scour depth frequency conforms to a negative exponential distribution which varies systematically with water depth (Lewis, 1978; Wahlgren, 1979; Weeks et al., 1980; Barrie, 1980). At the Bedford Institute of Oceanography a data bank of statistical scour parameters in various seabed environments is being compiled for the eastern Canadian continental shelf (d'Apollonia and Lewis, 1981). From these data sets, evidence of relative changes in scour frequency over time and probability of extreme soil penetration can be resolved. For example in the Hibernia region Lewis and Barrie (1981) formulated an extreme value distribution which estimates the statistical probability of encountering large scours along transects of specified lengths.

2.6 Ice Scour Morphology

The effects of small ice keels disrupting unconsolidated sediment in the central Arctic archipelago have been observed (Fig. 4-04) using SCUBA gear (McLaren, 1977). Josenhans and Barrie (1982) inferred relative ages of iceberg scours on Makkovik Bank in the Labrador Sea by examining scoured terrain from the manned submersible - **Pisces IV.** In this area relict iceberg scour features can be differentiated from fresher ones by the lack of fine material which has been winnowed away by current action in the scour ridges (Fig. 4-05) and by the extent of ice-

Figure 4-05 Diagrammatic representation of a 'relict' iceberg scour mark with photographic examples.

The lack of fine matrix is the result of gradual winnowing by bottom currents.

rafted deposits and biological colonization that have overtaken the scour trough.

2.7 Ice Keel Statistics

This method uses the distribution of estimated or measured keels that pass over a point on the sea floor and the measured scour penetration depth observed on the seafloor. It also draws on a knowledge of ice drift (Wadhams, 1975) and is therefore best suited to the dynamic polar pack ice beyond the fast ice zone. Keel depth distribution is inferred from ridge height data and from upward-looking profiling data obtained by submersible traverses or by upward-looking sonars fixed to the seabed (Pilkington and Marcellus, 1981). Using iceberg drift flux and estimated draft this method is also applicable to the eastern Canadian shelf areas.

2.8 Iceberg Grounding Analysis from Wellsite Observations

By recording iceberg drift observations from radar sitings during offshore drilling operations the behaviour of grounding bergs can be analysed. From this the frequency of scouring for a given area over a specific time can be established. Analysis of iceberg observations from Labrador is underway presently at C-CORE.

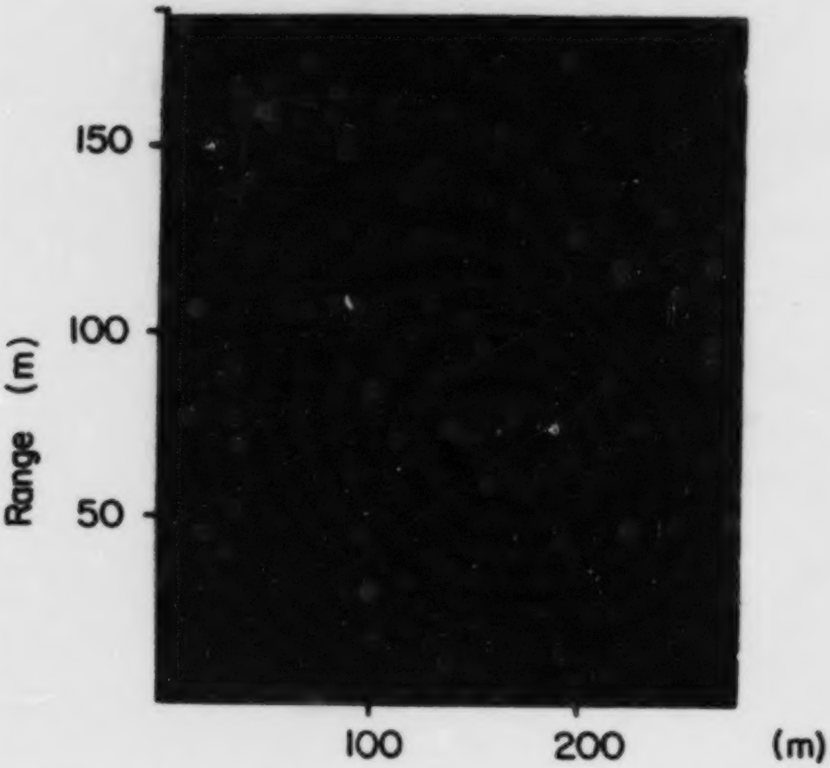

Figure 4-06 Megaripples obliterating an iceberg scour on the northeastern Grand Banks in 80 m water depth as seen on a sidescan sonogram.

2.9 Interrelationships with other Features

Barrie (1983) has shown that ice scour frequency can be determined by examining the effects of megaripples that migrate over and obliterate scour marks in the Hibernia discovery area on the Grand Banks (Fig. 4-06). Modern sedimentary bedform migration rates can be determined by comparing sidescan and other geophysical data collected in the same area at different times and by analysing the hydrodynamic data. Ice scours can be dated by analysing the degree of ice scour obliteration by bedform migration relative to the amount of ice scour disruption of fields of sedimentary bedforms. From this ratio a scour production rate can be formulated. This technique may also be useful in looking at the interrelationships between ice scours and trawl marks. These are generated by otter boards used in modern fishing operations in areas such as the Grand Banks.

2.10 Scour Cross-cutting Analysis

Weber (1958) was the first to note the cross-cutting relationships of scour marks in Great Slave Lake. Here, floe ice grooves that formed during the winter by grounding wind-blown ice cut the tops of furrows that were generated at the bed of a glacier during glacial times. The principle of cross-cutting with respect to scours in the Beaufort Sea was first mentioned by Pelletier and Shearer (1972). They observed "numerous occurrences of cross-cutting relationships ... indicating that several periods of ice-scouring have occurred". Berkson and Clay (1973) in their work on iceberg scours in western Lake Superior also noted cross-cutting relationships of late glacial iceberg scours. They constructed a map from sidescan records to show scour distribution and further interpreted scour cross-cuttings. However, they did not use this as a method for obtaining relative scour ages. Hnatiuk and Brown (1977) working in the Beaufort Sea correlated scour crossings with scour azimuth but found no significant relationship.

Although accurate absolute age dating of scours is not practically feasible by this method it is possible to determine the relative ages of scours using the cross-cutting relationships. Essentially, the oldest scours will be cut by younger scours but do not cut any others themselves. The youngest scours will be those that cut older scours but which are not cut by others. An example of the criteria for the scour cross-cutting technique is shown (Fig. 4-07) from an analysis of iceberg scouring on Saglek Bank and in the Davis Strait (Woodworth-Lynas, 1983).

2.11 Dating of a Scoured Surface

Another dating technique is to gauge the relative age of a scoured surface using methods similar to those of Dodd et al., (1963) in their study of size distribution of lunar impact craters. They plot graphs of crater diameter against number of craters per unit area. For each area on the moon the positions on the graphs and slopes of the lines with respect to each other correspond to the relative age of the cratered surface (vide Dodd et al., 1963; Hartmann, 1977a & b; Strom, 1977 and Moore et al., 1980). In the present work, undertaken at C-CORE for the Saglek Bank region, scour width was substituted for crater diameter.

3. SUMMARY

None of the above techniques are adequate in themselves for a comprehensive scour analysis but a combination of techniques used in relation to the surficial geology can give scientists and engineers a useful tool to analyse ice scour marks.

i

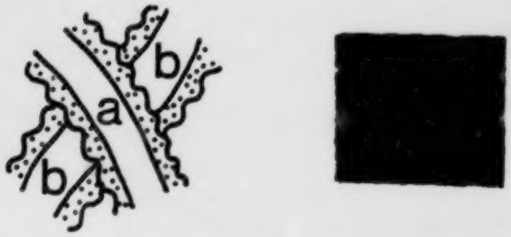

i) scour a. cuts scour b. Berm material of a. is thrown up into the trough of b.

ii

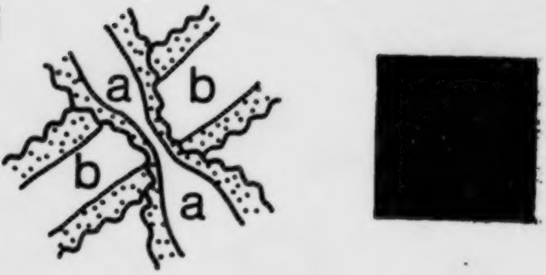

ii) as in i. but scour a. has an hour glass shape, indicating that scour b. has a pronounced trough.

iii

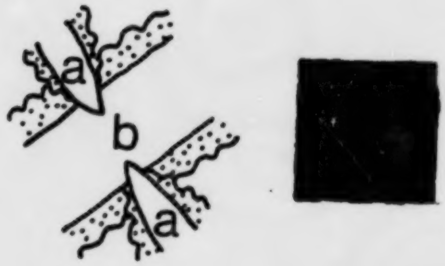

iii) as in ii. but trough of b. is deeper than keel of berg that cross-cut scour b., so that only the berms of scour b are cut.

iv

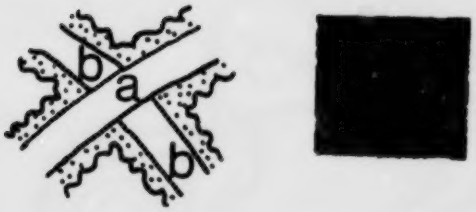

iv) scour a. is deeper than scour b., but berm material is not present across either scour trough so cross-cut is not known.

v

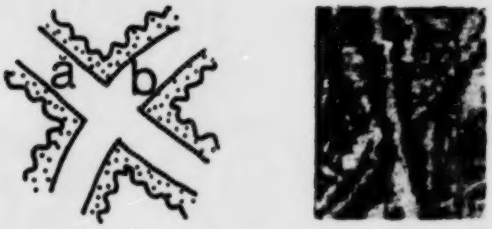

v) scours a. and b. are the same depth but absence of berm material in either trough means cross-cut is not known.

Figure 4-07 Morphological criteria for determining cross-cutting relationships. Each diagram is accompanied by a photograph of an example of the type of cross-cut, from original sonograms.

Number/
Numéro

5

Chapter 5. BOUNDARY LAYER FLOW AND THE PHYSICS OF SEDIMENT TRANSPORT

D.A. Huntley

1. PREFACE

This chapter deals with the physical ideas behind the description of the benthic boundary layer and the motion of sediment within it. In writing it, I have assumed that the important questions are the practical ones of estimating boundary layer conditions in the field, rather than the academic ones dealing with details. I have therefore tried to include equations, tables and diagrams which can be used for prediction as often as possible. In cases where explanations would be too involved for this review, reference is made to relevant publications.

Despite this approach, however, the complexity of the benthic boundary layer, and the current state of the art in understanding it are such that predictive formulae cannot be applied blindly. It is important to understand something of the physics behind such formulae. and to have a realistic attitude to their limitations. I have therefore included quite a bit of discussion of the problems associated with boundary layer prediction, and outlined some of the attempts being made to overcome them.

There does not appear to be any single book suitable to this part of the course. Graf's book, "Hydraulics of Sediment Transport" is widely quoted, but does not deal directly with the marine environment, and includes little of the physics of boundary layers. Middleton and Southard (1977) do discuss at some length the physics of sediment motion, but are not concerned with the practical prediction of boundary layer parameters. The most recent review of the physical problems of the benthic boundary layer is given by Bowden (1978).

The chapter is divided into two sections. The first deals with the water motion in the boundary layer, and the second deals with the response of the sediment to that motion. Of course, in practice the water/sediment system is coupled, so that this separation is somewhat artificial. We shall be forced to consider some aspects of this coupling in section 2.5.

2. BOUNDARY LAYER FLOW

2.1 Introduction

The most general definition of the **benthic boundary layer**, given by Bowden, (1978) is: the layer adjacent to the sea bed in which the flow is affected by processes occurring at the boundary and in which strong gradients of physical, chemical and biological properties may occur. In thickness it extends a few metres or tens of metres above the seabed and, in this general definition, may also be considered to extend into the seabed to include the depth of sediment movement and pore water exchanges. Of particular interest to physical oceanography and sediment dynamics is the influence the seabed has on the movement of water above it. At the stationary seabed the velocity of the flow must be zero, whereas above the boundary layer the velocity will be some bulk flow which is independent of the boundary. From a dynamical point of view, the boundary layer is the region of velocity gradient or **shear** between these end points.

In studying boundary layers on the continental shelf there are two main questions of relevance to sediment stability:

i) How does the velocity vary with distance from the seabed, i.e. what is the velocity profile?

ii) What force does the flow impose on the seabed? (the sediment response to this force is discussed in section 3 of this chapter). This fluid force is usually defined as a force per unit area of seabed, known as **stress**. The stress acting parallel to the boundary, tending to drag particles along the bed, is

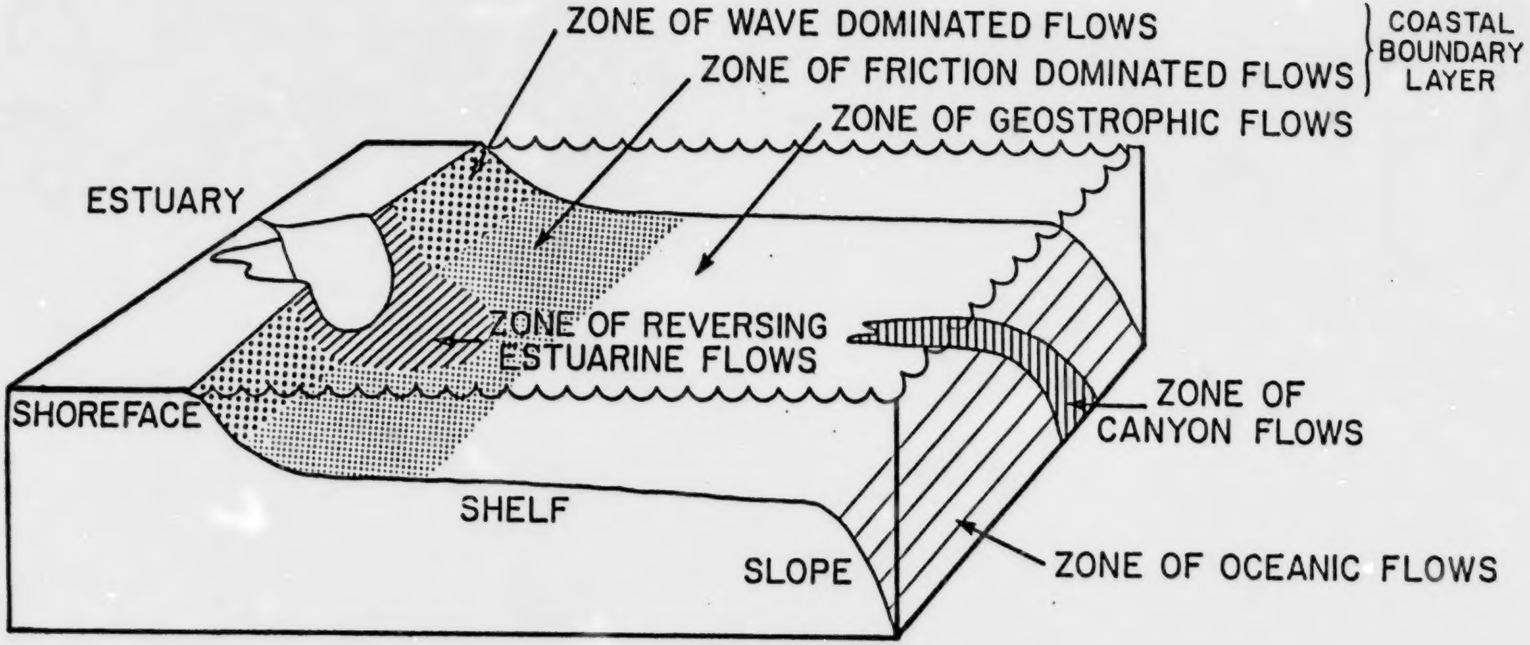
ZONE OF WAVE DOMINATED FLOWS
ZONE OF FRICTION DOMINATED FLOWS
COASTAL BOUNDARY LAYER
ZONE OF GEOSTROPHIC FLOWS
ESTUARY
ZONE OF REVERSING ESTUARINE FLOWS
SHOREFACE
ZONE OF CANYON FLOWS
SHELF
SLOPE
ZONE OF OCEANIC FLOWS

Figure 5-01 Hydrodynamic zones of the Continental Shelf

known as the **shear stress** (as opposed to the stress acting at right angles to the seabed, which is a pressure).

The velocity profile is important for determining forces on structures, for example, and is also vital for determining the transport of sediment in suspension. The shear stress is the parameter most commonly used to determine bedload transport and the quantity of sediment suspended in the water column.

One of the most difficult problems in attempting to estimate sediment transport on the continental shelf is the wide range of flow conditions which can occur. Figure 5.01 is one possible schematic of the different hydrodynamic zones on the shelf. The many spatial and time scales present are outlined in Table 5-I (from Mooers 1976). These time scales of motion interact with the seabed in different ways, some of which are discussed below. Unfortunately, while there is some understanding of the boundary layers for each time scale separately, work is only just beginning on the situation, perhaps most common on the shelf, in which several time scales of motion are present simultaneously. The problem here is that boundary layers are intrinsically non-linear, which is to say that the effect of combinations of different time scales cannot adequately be treated by simply summing their individual contributions.

In what follows it will be assumed that the form of the velocity field above the boundary layer is known. Discussion of the nature of shelf circulation is beyond the scope of this review. Articles by Mooers and others in Stanley and Swift (1976), and Csanady (1976) form good starting points for further

Table 5-I

Physical processes and their scales

Process	Time Scale	Horizontal Velocity Scale (cm/sec)	Alongshore* Scale (km)	Transshore Scale (km)	Vertical Structure†
Long-term mean (climatic variability)	Decade	~ 1	$\sim 10^2$–10^4	~Margin width	Barotropic and perhaps one baroclinic mode
Seasonal (year-to-year variability)	Annual and its harmonics	~ 10	$\sim 10^3$	~Shelf width	Barotropic and at least one baroclinic mode
Wind event (season-to-season and year-to-year variability)	Several days to several weeks	~ 100	$\sim 10^2$–10^3	A few horizontal modes, ~shelf width	Mainly barotropic and perhaps one or two baroclinic modes
Tidal (seasonal variability)	Diurnal and semidiurnal	~ 10	$\sim 10^2$–10^4	Entire margin ~ 1–10^3	Barotropic and a few baroclinic modes
Inertial (wind event-to-wind event variability)	Depends on latitude >diurnal, equatorward of 30° latitude; <lunar semidiurnal poleward of 72° latitude	~ 10	(?) 10	~(?) 10	~10 baroclinic modes
Edge wave (day-to-day variability)	Minutes	~ 10	~ 1	$\sim 10^{-1}$–10	Uniform (barotropic)
Surface gravity wave (sea and swell) (day-to-day variability)	Seconds	~ 10	$\sim 10^{-1}$	$10^{-3} - 10^{-1}$	Uniform (barotropic)

* Alongshore scale is an ambiguous quantity; here it has been defined to mean the scale of organized motions, i.e., the scale of coherent motion.

† The comments on vertical structure are appropriate to a density-stratified continental margin; for unstratified margins, the vertical structure is dominated by effects of surface and bottom (frictional) boundary layers.

reading in this area.

The next section deals with the basic theoretical ideas concerning boundary layers of various kinds. Section 2.3 then deals with the vital, yet often neglected, problem of form drag over bed forms. In section 2.4 we discuss some recent ideas about the boundary layer under combinations of surface waves and steady currents, and in section 2.5 other complicating factors are briefly discussed; namely, stratification of the water column due to suspended sediment, the effect of bed load on bottom roughness, the influence of acceleration of the flow on boundary layer characteristics, and the limitations imposed by the intrinsic intermittency of the stress. Finally, in section 2.6 we outline some of the techniques which can be used to estimate sea bed stress in a practical situation.

2.2 Types of Boundary Layer: the basic theoretical background

The forces which enter into the equations of motion for a fluid are: pressure gradients, acceleration forces, buoyancy forces (if the water is density-stratified), the Coriolis force due to the rotation of the earth, friction and the accelereation due to gravity. Let us consider first the simplest case, the steady flow of unstratified water, with negligible horizontal variations. For this flow the acceleration and buoyancy forces are set to zero. Close to the seabed ("close" to be defined below) the Coriolis force can be ignored also. Thus we have a region nearest to the seafloor where the basic dynamical balance for horizontal currents is between pressure gradient forces and friction. It is not difficult to show (e.g. Tritton 1977) that this balance leads to a layer close to the bed in which the frictional stress is essentially constant and equal to the bed stress τ_b. A related parameter which is frequently used is the **friction velocity**, u_*, which is given by

$$u_* = (\tau_b/\rho)^{1/2}$$

where ρ is the fluid density.

There are two contributions to the stress. The molecular viscosity of the fluid, denoted by ν, creates a stress which is proportional to the vertical rate of change of horizontal velocity. Turbulent motion of the fluid in the boundary layer also creates a stress by exchanging water between regions of rapid flow and regions of slower flow (see Section 2.6.4). The relative contributions of these two to the total stress in the constant stress layer varies with distance above the bed. If the boundary is smooth enough, there is a region immediately adjacent to the seabed where the molecular stress dominates, resulting in a VISCOUS SUBLAYER.

The horizontal velocity, u, in the viscous sublayer increases linearly with distance above the bed, z:

$$u = u_*^2 z/\nu \qquad (1)$$

Thus the slope of the velocity profile in this region depends only upon the bed stress.

Whether a viscous sublayer can exist or not depends upon the roughness of the sea bed. If a typical dimension of a roughness element on the sea bed is denoted by d (d might be a characteristic grain diameter for example), then the existence of a viscous sublayer requires

$$d < 3 \nu / u_*$$

If this is the case the flow is said to be "hydrodynamically smooth".

Figure 5-02 shows, from some laboratory measurements of hydrodynamically smooth flow, how the molecular and turbulent contributions to the constant stress layer vary as we move away from the bed. Clearly above a viscous sublayer there is a layer

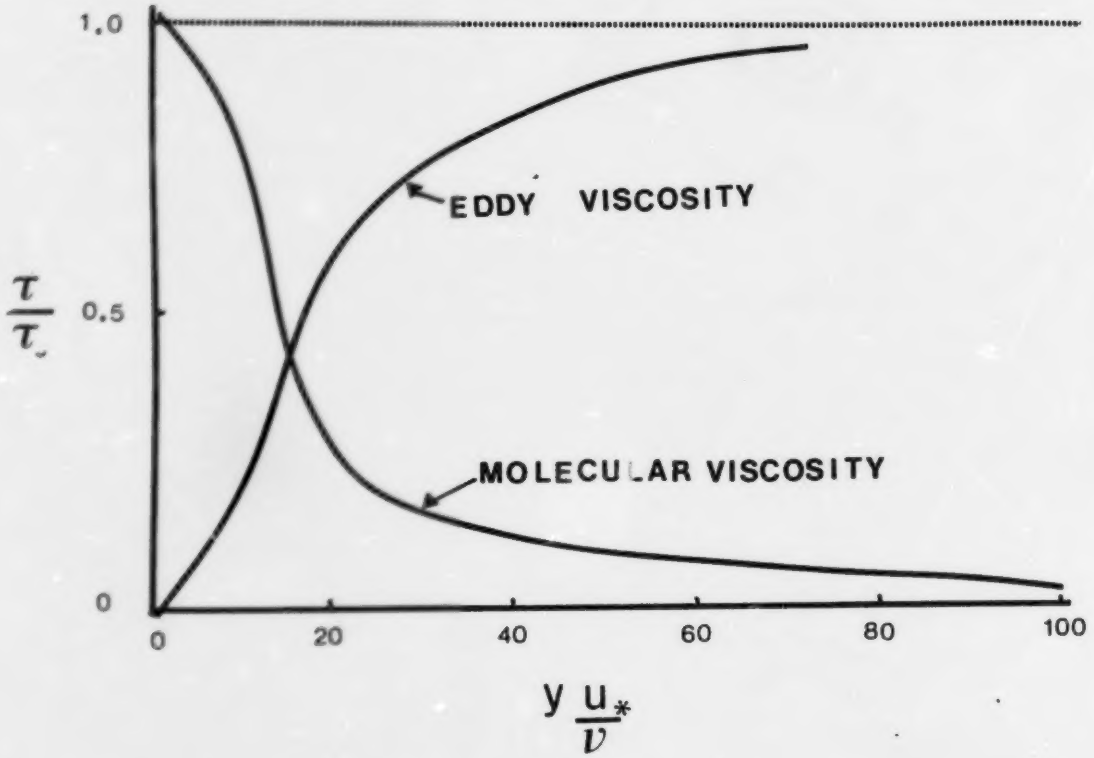

Figure 5-02 Schematic of the relative size of molecular and turbulent (eddy) stresses close to a hydrodynamically smooth boundary (from Tritton, 1977).

within which the stress is dominated by turbulence. In this layer, known as the INERTIAL SUBLAYER, molecular viscosity is no longer a relevant parameter to the velocity gradient. By similarity the velocity gradient can only take the simple form

$$du/dz = u_* / kz$$

where k is a constant. Integrating this gives the well known **logarithmic profile**

$$u = (u_*/k) \ln (z/z_0) \qquad (2)$$

where the constant k is known as Von Karman's constant and takes the value 0.4 (see sections 2.4 and 2.5 for some comments about this value). z_0 is known as the **roughness length.** For smooth flows its value depends upon matching the logarithmic profile to the linear profile in the viscous sublayer, and is given approximately by

$$z_0 = 0.1 \ \nu / u_* \qquad (3)$$

For rough flow

$$z_0 = d /30 \qquad (4)$$

According to Smith (1977), most flows on the continental shelf are in the transitional zone between smooth and rough flows. Figure 5-03 shows the appropriate form of z_0 to use in this zone (note that in this figure $z_f = z_0$ and $k_s = d!$). In the presence of bedforms, of course, the choice of an appropriate d is far from obvious, and, in fact, z_0 is found to vary with height above the bed. This problem will be discussed at some length in section 2.3.

Implicit in this development of the logarithmic profile is the result that the **eddy viscosity,** K, (the apparent viscosity of

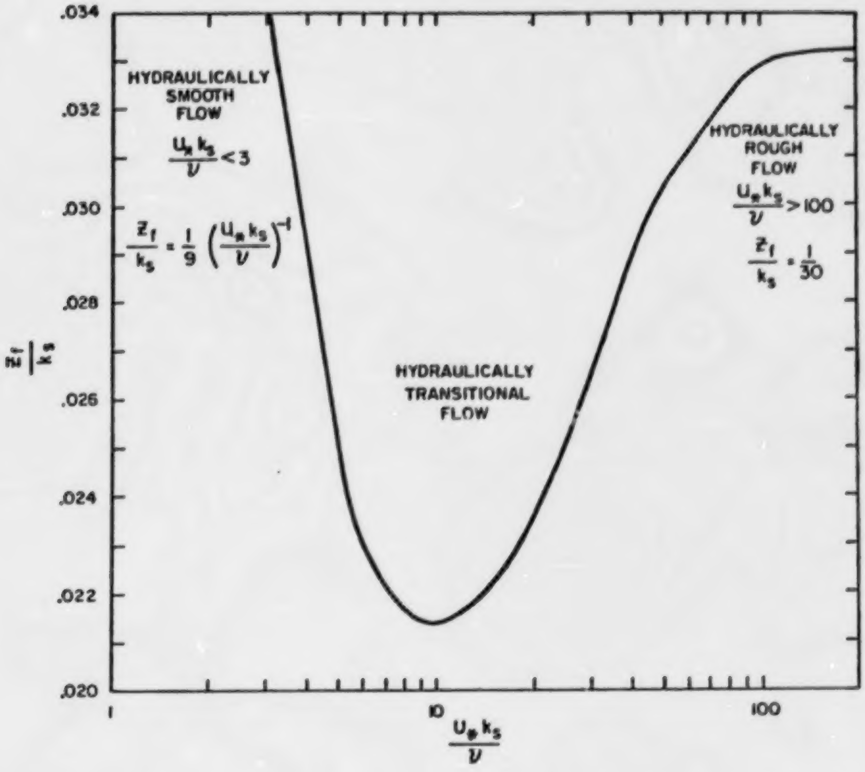

For $u_* k_s / v < 3$, the flow is called hydraulically smooth and $z_f = 0.11 v / u_*$; whereas for $u_* k_s / v > 100$, the flow is called hydraulically rough and $z_f = 0.033 k_s$. In many, if not most, interesting sediment transport situations, the flow is hydraulically transitional and a figure such as this one must be used to compute the roughness parameter z_f in the logarithmic velocity profile equation.

Figure 5-03 Relationship between z_f/k_s and $u_* k_s/\nu$ for hydraulically transitional flow, according to the data of Nikuradse (from Schlichting, 1960, p. 523).

the fluid due to the turbulent motion rather than the molecular motion) varies linearly with distance above the bed.

$$K = k\ u_*\ z \tag{5}$$

Another parameter of some interest is the thickness of the viscous boundary layer. Although Figure 5.02 shows that there is a buffer region, between the viscous sublayer and the logarithmic layer, where both molecular viscosity and turbulence are significant, the thickness of the viscous sublayer is usually defined from lab or field data as the height at which a best fit straight line in the viscous sublayer crosses a best fit log line in the log layer. Usually the sublayer thickness, δ, so defined is found to be

$$\delta = 12 \ \nu / u_* \qquad (6)$$

However, recent measurements on the Oregon shelf have given values ranging from 8 to 20 for the numerical constant in equation 6. This is important because it also implies a variable numerical constant in the equation for z_0 in smooth flow, and hence can potentially lead to inaccurate estimation of bottom stress (see section 2.6).

Above the logarithmic layer the Coriolis force becomes important. The Coriolis force progressively balances the bottom stress with increasing distance above the bed until, at about the **Ekman height**, L_E, the stress has become negligible and the velocity is a result of a balance between the Coriolis force and a pressure gradient (geostrophic flow). The thickness of the EKMAN LAYER is given approximately by

$$L_E = 0.4 \ u_* \ / \ f \qquad (7)$$

where $f = 2\Omega \sin \phi$, known as the Coriolis parameter, Ω is the rate of angular rotation of the earth and ϕ is the latitude. Figure 5-04 shows schematically the form of the velocity in the bottom Ekman layer. An important characteristic is the anticlockwise rotation of the velocity vector as the bottom is approached.

In the lower part of the Ekman layer, within about 0.1 L_E, the direction of the velocity is approximately constant and its magnitude increases according to the logarithmic profile.

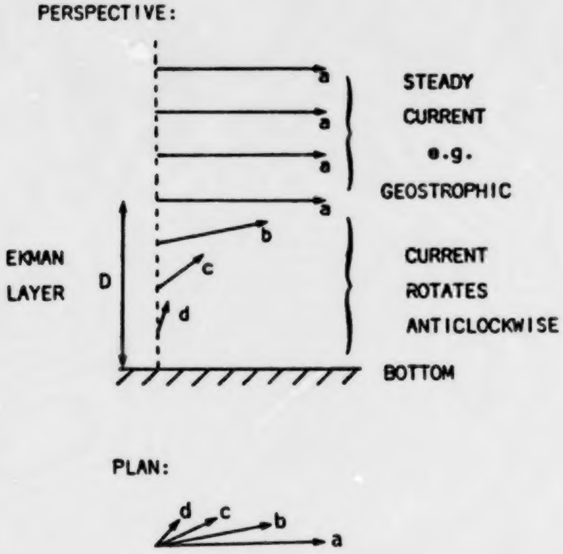
PERSPECTIVE:
a
a
a
a
STEADY
CURRENT
e.g.
GEOSTROPHIC
EKMAN
LAYER
D
b
c
d
CURRENT
ROTATES
ANTICLOCKWISE
BOTTOM
PLAN:
d
c
b
a

Figure 5-04 Frictional effects on a geostrophic current near the bottom of the ocean (northern hemisphere).

However, Ekman's original theory assumed an eddy viscosity which is independant of the height, and this is incompatible with the assumptions implicit in the logarithmic profile (equation 5). Various attempts have been made to derive a velocity profile which patches between a logarithmic profile below and an Ekman spiral above. Csanady (1967) obtains a relationship between u_*, z_0 and the free geostrophic velocity above the boundary layer, u_0, and Weatherly (1972) has discussed Csanady's theory in relation to measurements in the turbulent Ekman layer beneath the Florida current. Csanady's relationship, which allows us to estimate the friction velocity if we know the velocity above the boundary layer and can choose an appropriate roughness length is

$$[\,(u_0/u_*)^2 - A]^{1/2} = (1/k)\ \ln(u_*/fz_0) + B \qquad (8)$$

There are insufficient measurements to pin down the values of the constants A and B with any confidence; Weatherley favoured

$$A = 20 \qquad \text{and} \qquad B = -3$$

It is worth remarking in passing that the logarithmic layer seems to extend well above the height at which the constant stress assumption is valid. Wimbush and Munk (1970) suggest that the thickness of the layer, δ_{ln} can be an order of magnitude larger than expected. For a geostropic flow, above the boundary layer, of u_0 they suggest

$$\delta_{ln} = 2\ u_*^2/\ (f\ u_0)$$

Figure 5-05 shows the subdivisions of a benthic boundary layer for steady, unstratified flow, and Table 5-II gives some typical values for the deep sea and the continental shelf.

If we now drop the assumption that the flow is steady, and consider oscillatory currents whose frequency, ω , is large compared to the Coriolis parameter, i.e. $\omega >> f$, then a very different kind of boundary layer is found. One major difference is that the boundary layer is much thinner than for steady flows. Physically we can imagine this to be because the boundary layer velocity defect (or momentum defect, or vorticity!) does not have time to diffuse away from the boundary very far in one half wave period before the flow reduces to zero; on reversal of the flow during the next half wave period the boundary layer again develops from the seabed. Figure 5-06 (from Teleki, 1972) shows this happening for several theoretical models. Teleki reviews

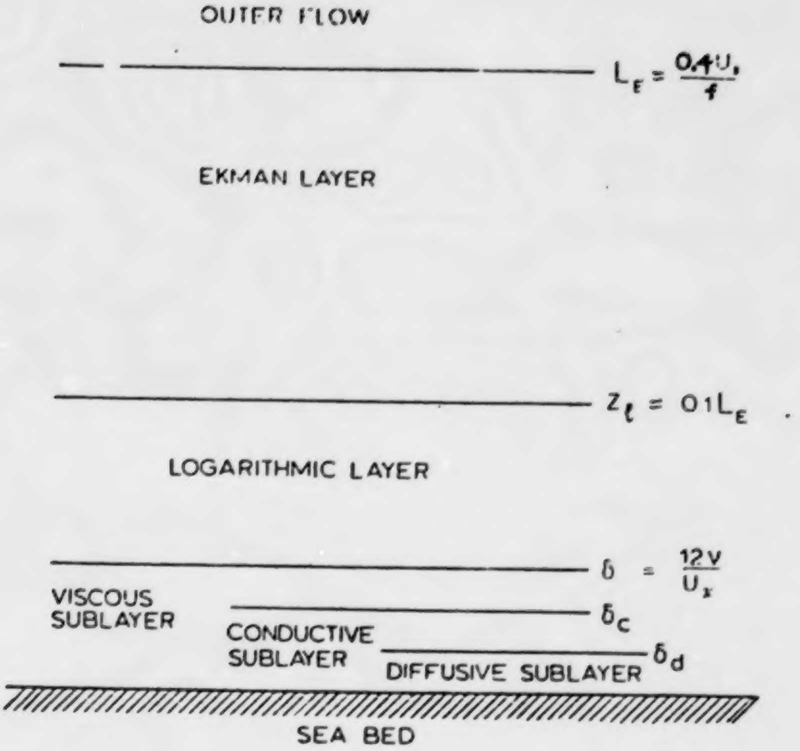
OUTER FLOW
$L_E = \frac{0.4U_*}{f}$
EKMAN LAYER
$z_l = 0.1L_E$
LOGARITHMIC LAYER
$\delta = \frac{12\nu}{U_*}$
VISCOUS SUBLAYER
δ_c
CONDUCTIVE SUBLAYER
δ_d
DIFFUSIVE SUBLAYER
SEA BED

Figure 5-05 Subdivisions of the benthic boundary layer (not to scale).

Table 5-II

Typical values of boundary layer parameters

Parameter	Symbol	Deep sea	Continental shelf
Velocity	U	4 cm s^{-1}	40 cm s^{-1}
Friction velocity	U_*	0.2 cm s^{-1}	2 cm s^{-1}
Ekman layer thickness	L_E	10 m	100 m
Logarithmic layer thickness	z_l	1 m	10 m
Viscous sublayer thickness	δ	1 cm	0.1 cm

the well known theories for LAMINAR OSCILLATORY BOUNDARY LAYERS (which begin with Stokes in 1851). The laminar boundary layer thickness is given by

$$\delta_{wL} = (2\nu / \omega)^{1/2} \tag{10}$$

Smith (1977) and Grant and Madsen (1979) give a theory for TURBULENT, OSCILLATORY BOUNDARY LAYERS based on similar assumptions to those leading to the logarithmic layer for steady flow. Figure 5-07 shows typical velocity profiles during half a wave period, in this case for 4-second waves. For a turbulent boundary layer the boundary layer thickness is given by

$$\delta_w = u_* / \omega \tag{11}$$

where u_* is now the amplitude of the oscillatory friction velocity, which can be estimated, for a given frequency, wave velocity and bed roughness, using graphs given by Smith (1977). Smith gives

$$u_* = k\, F^2\, u_0 \tag{12}$$

where F is the "amplitude" function given in Figure 5-08. The variable ξ_0 in this graph is given by

$$\xi_0 = 2\, (\omega z_0/u_0)^{1/2} (u_0/K_0)^{1/2} \tag{13}$$

and K_0/u_0 is found, for a given ω, z_0 and u_0, from Figure 5-09 (note that the amplitude of particle excursion in the wave motion near the seabed is equal to u_0/ω. The vertical axis in Figure 5-09 is therefore simply the ratio of boundary roughness to particle excursion). It should be said that this rather complicated procedure has not been well tested against field data. In fact, it is possible to formulate Smith's theory into the well known quadratic power law form (about which much more

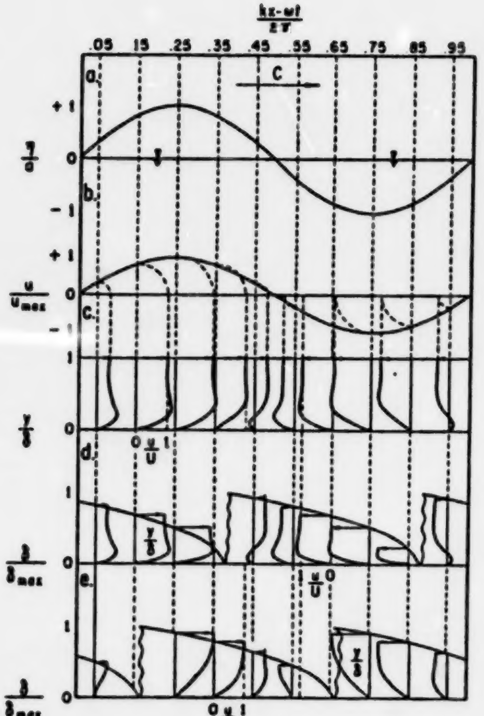

(a) is the elevation of free surface propagating with the phase velocity C,

(b) is the amplitude of the velocity in the boundary layer,

(c) is the velocity profile for the shear wave solution, unseparated flow,

(d) is the velocity profile for the shear wave solution with separation, and

(e) is the velocity profile for the Karman-Polhausen solution with separation.

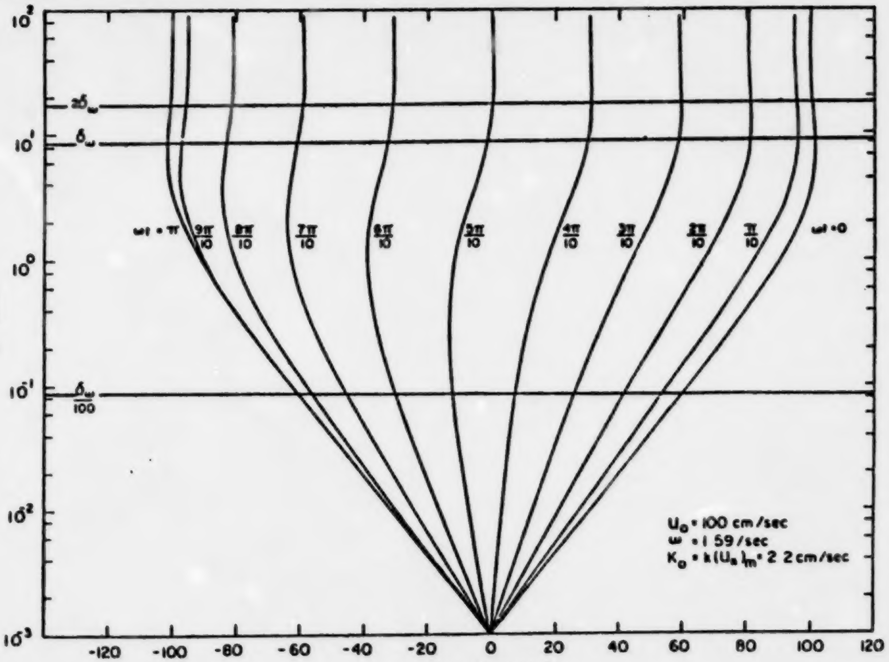

The scale thickness for the boundary layer, given as $\delta_\omega = (u_*)_m/\omega$, is shown on the left side of the diagram. Note that by $2\delta_\omega$ the velocity field is essentially that of the inviscid interior flow and that below $\delta_\omega/100$ the velocity profiles are logarithmic; moreover, at the times of maximum flow they are logarithmic to $\delta_\omega/10$.

Figure 5-06 Characteristic velocity profiles in the oscillatory boundary layer for a wave cycle.

Figure 5-07 Typical velocity field of the oscillatory turbulent boundary layer under a wind wave.

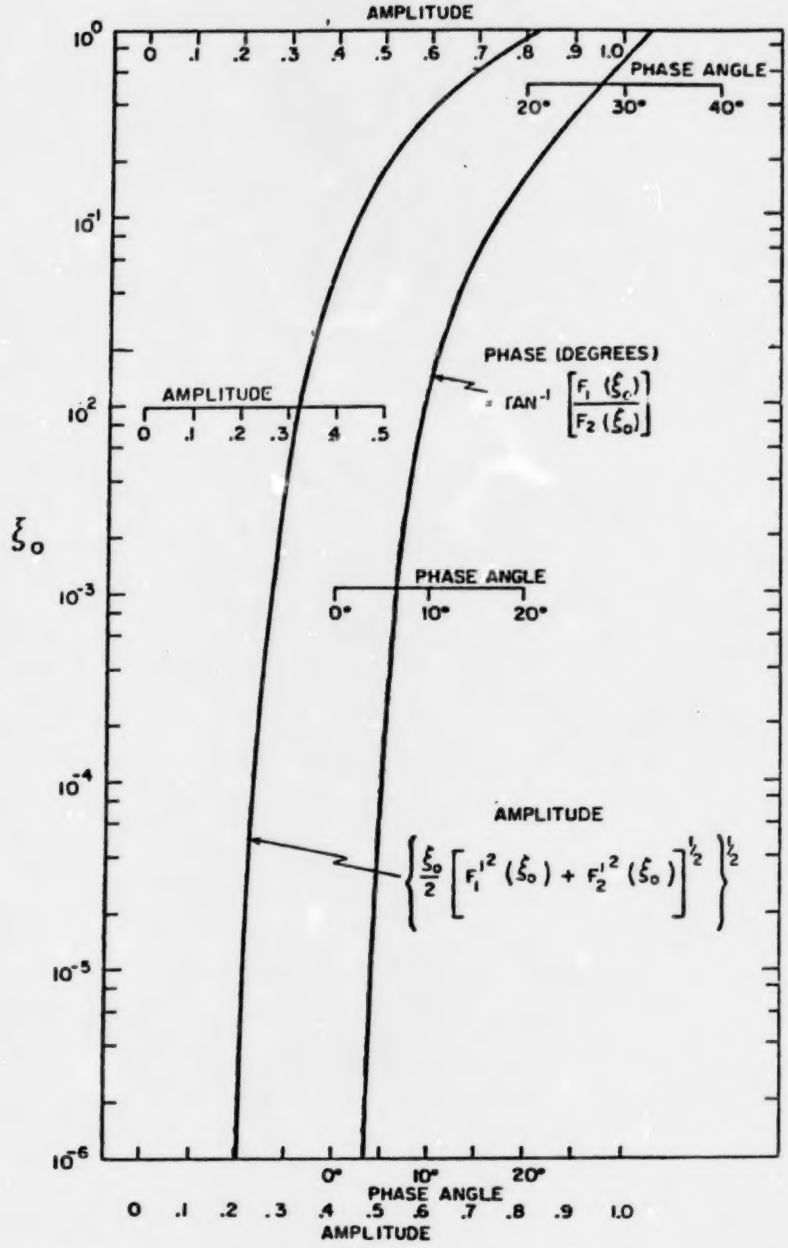

Figure 5-08 The "amplitude function" F (see equation 12) vs. ξ_o (from Smith, 1977). (The phase angle plot is not relevant to the present discussion).

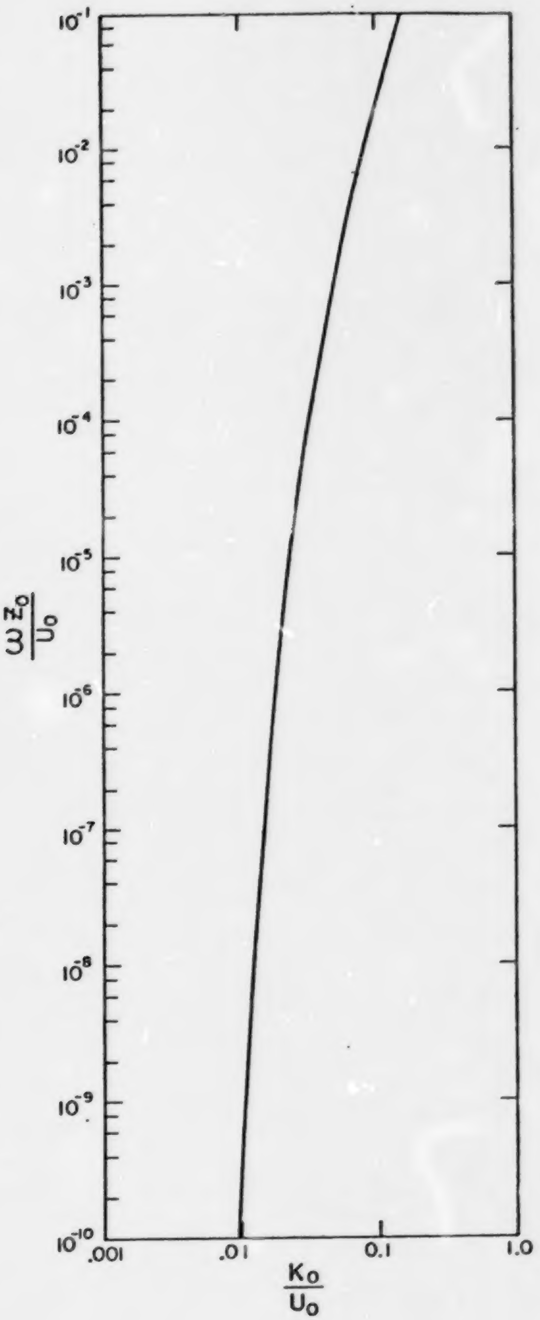

This allows calculation of ζ_o from equation 13, when ω, Z_o and U_o are known.

Figure 5-09 Plot of K_o/U_o vs. $\omega Z_o/u_o$, where u_o is the orbital velocity above the boundary layer (from Smith, 1977).

will be said in sections 2.4 and 2.6), where the bottom stress is given by

$$\tau_b = \rho(f/2)\ u_0^2 \tag{14}$$

and f is the wave friction factor. The equivalent friction factors, also given by Grant and Madsen (1979), are in excellent agreement with lab observations by Jonsson and Carlsen (1976).

A typical boundary layer thickness under waves on the shelf is a few cm. Since bottom shear stress in turbulent flow depends upon the boundary layer thickness relative to bottom roughness it is not surprising that shear stress associated with wind waves are considerably larger than those associated with steady flows. In fact, for the same current strength above the boundary layer, the wave stress can be 10 times larger than the steady flow stress. Waves therefore play an important role in sediment transport on the shelf. Although the oscillatory flow itself produces no net sediment transport, it can put sediment into motion, and hence make it available for transportation by weaker steady currents.

An added complication of wave motion is that the non-linear effects, outside the boundary layer but especially inside the boundary layer. produce wave-driven steady currents. Beginning with Longuet-Higgins (1953), a number of attempts have been made to model these currents theoretically. However, the few measurements that exist suggest that the theoretical results are generally not in good agreement with observations in turbulent boundary layers, and the flows and sediment transport when ripples are present on the sea bed are at present impossible to predict with any confidence (see for example Bijker et al., 1975).

Finally in this outline of theoretical ideas about boundary layers, mention should be made of the numerical modelling of boundary layers. These are primarily in use to study the effects of density stratification and bottom slope on boundary layers beneath geostrophic flows (e.g. Adams and Weatherly, 1981, Weatherly and Martin, 1978). However, there are some attempts to model the velocity profiles in tidal currents on the shelf (Tee 1972). These models are somewhat crude at present but, as work proceeds, could become more important in the future.

2.3 The Form Drag Problem

Bedforms commonly occur in sediment transporting flows on the continental shelf. These bed features create an internal boundary layer in the flow within which there is an acceleration in the water flow over the crest of the bedform and a deceleration near the trough. If the flow in this internal boundary layer is spatially averaged over a bedform, at fixed heights above the bed, the velocity profile is logarithmic, with a slope related to the boundary shear stress and a roughness length related to the grain roughness of the bed (equation 2). At a distance greater than about one tenth of a bedform wavelength away from the boundary, the spatial variability of the internal boundary layer has become smoothed out, the flow is uniform and the velocity profile is once again logarithmic.

However, in this upper region the slope of the logarithmic profile is determined by the average bed shear stress plus the force due to form drag on the bedform. In other words, the bedforms appear as roughness elements to the flow in the upper region. In the presence of several scales of bedforms, Smith and Mclean (1977) find evidence for multiple log layer velocity profiles, each corresponding to a particular bedform scale.

The form drag is the average of the horizontal components of the normal pressure distribution over the bedform, and it therefore does not contribute to sediment transport. Thus it is vital to be able to remove the form drag component from any measurement of bottom stress if we are to be able to estimate sediment motion. It is clear from the literature that the importance of this problem has been underestimated until very recently, and many of the standard assumptions about sediment transport may have to be modified in the light of recent results. Numerical models of flow over ripples, such as those of Smith (1969) and Taylor et al. (1976), suggest that for sinusoidal waveforms typically 25-33% of the total drag is due to form drag. However this percentage is sensitive to the asymmetry of the bedform and whether or not separation occurs. Field experiments suggest a much higher proportion for form drag. Smith (1977) found a ratio of total shear stress to skin friction of 5.7:1 for non-separating flows and 4:1 for separating flows over sand waves in Columbia River. Chriss and Caldwell (1982), measuring directly the stress in the viscous boundary layer and comparing it with stresses inferred from log profiles above. found ratios of total stress to skin friction ranging from 3.8 to as high as 10.6 on the Oregon shelf. Although there are too few field measurements to be sure that these ratios are characteristic of conditions on the shelf, it is clear that form drag can be a dominant part of the stress except very close to the bed. Some estimates suggest that. to be within the log layer related to true skin friction, measurements have to be within a tenth of a bedform wavelength (Gorsline and Swift, 1977); others suggest within two or three bedform heights (Krugermeyer and Grunwald, 1978).

The traditional way to treat this problem, exemplified by Einstein (1964), is to assume that the bedforms are formed by the ambient flow conditions and are in equilibrium with those conditions. In this way the magnitude of the form drag is assumed to be a unique function of the flow. Figure 5-10 shows Einstein's plot of friction velocity associated with form drag u''_* as a function of a hydraulic parameter which is the inverse of the Shields parameter (defined in section 3.2 below). This form drag, or "bar resistance" as it was called by Einstein, is based primarily on data from rivers and laboratory flumes, and, to my knowledge. it has not been tested in marine environments. Graf (1971) discusses some other estimates of form drag, including some interesting data from Raudkivi (1967) which show that, as might be expected, the form drag component of total stress is greatest for intermediate friction velocities. falling

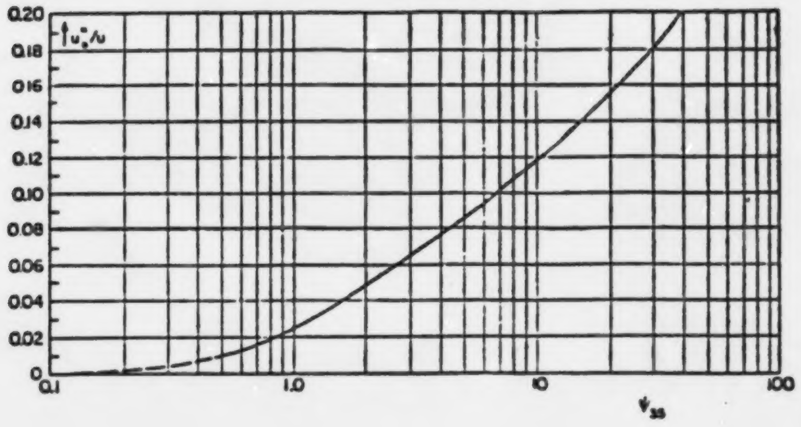

u_*'' is the form drag component of friction velocity
u is the velocity about the boundary layer
and ψ_{35} is essentially equal to the (Shield's parameter)$^{-1}$

Figure 5-10 Einstein's 1964 plot of u_*''/u vs. ψ_{35}.

off at low speeds, where bedload transport is weak or nonexistent, and at high speeds, where sheet flow flattens down the bedforms.

Generally on the continental shelf, where the flow regime can change more rapidly than the bedforms, the assumption of equilibrium bedforms is unlikely to be valid. We are therefore faced with having to estimate the form drag based on what might be rather scanty data on the size and geometry of bedforms in a region. Smith (1977) presents a scheme which can be used when only a single scale of bedform is present. His scheme depends upon matching the velocity at the height where the lower log layer meets the upper log layer. There are two parameters which must be estimated in order to calculate the ratio of skin friction to total stress; z_*, the height at which the two log layers are matched, and z_t, the apparent roughness length in the upper layer. Following Arya (1975), z_* is taken to be the average height that the internal boundary layer diffuses up to, from one roughness element to the next; an equation from air flow over a warm runway is used to calculate this diffusion distance. Clearly this estimate of z_* is best when the roughness elements are relatively widely spaced. Again following Arya's measurements of air flow over Arctic pressure ridges, Smith estimates z_t using a drag coefficient which, with the height and wave length of the bedforms, provides an independent estimate of the form drag. Other estimates of z_t are also available; for example Lettau (1969) proposes the relation

$$z_t = 0.5\ hs/S \qquad (15)$$

where h is the effective obstacle height, and s is the cross-sectional area seen by the flow per unit horizontal area. For two-dimensional ripples s/S approximates to the steepness, (height/wavelength), which is typically about 0.1. For a ripple of 3 cm height z_t would be about 0.15 cm. With these estimates Smith provides an equation, algebraically messy but straightforward to use, for the ratio of skin friction to total stress.

The input parameters for this scheme are the height and wavelength of the bedforms, and the drag coefficient, which is presumably dependent on bedform shape. Unfortunately, there are insufficient measurements at present to provide accurate values for the drag coefficient. Smith's own measurements give the drag coefficient, C_D, as 0.15 for separation and 0.70 for no separation over his river sand waves. Chriss and Caldwell (1982) invert the procedure to estimate the bedform size which could have been responsible for their measured form drag; their results, using a variety of drag coefficients, show that, for a constant form drag, doubling the drag coefficient halves the estimated bedform height.

Smith and Mclean (1977) extend Smith's procedure to allow for multiple log layers, the effect of suspended sediment load on the velocity profile, and the effect of bedload transport on roughness length. The result is a complex iterative scheme allowing skin friction to be found from a knowledge of bedform geometry and velocity profile in one of the upper layers. Their theory appears consistent with their field observations, though there are several very poorly known constants involved which make the scheme hard to use with confidence.

Clearly, there is a place for further theoretical and experimental work on this problem. Taylor et al. (1976) and Taylor and Dyer (1977) discuss some aspects of modelling the turbulent boundary layer over a wavy surface (which has obvious connections with the theory of the wind generation of surface waves). As with all turbulence problems, the major difficulty is in specifying the turbulence, but there is hope that increasingly realistic models can be developed soon. The rapidly increasing number of field programmes should also soon begin to provide the data against which to assess the theoretical models.

Finally, Dyer (1980) gives an interesting demonstration of the influence of form drag in tidal currents. Since the ripples on the seabed change as the tidal current strength changes, he finds that the upper layer apparent bed roughness and total stress change systemmatically with the stage of the tide. There is even a hysteresis effect between flood and ebb tides due to different ripple sizes.

2.4 Combined Wave and Current Effects

A combination of wind wave currents and mean flows is the most common environment on the continental shelf, particularly during important storms. Field observations (e.g. Butman et al. 1979) show that sediment movement by wave can occur right out to the edge of the shelf. We might expect waves of period 5-15 s. to start 'feeling' the seabed in about 20-180 m. water depth. It is therefore somewhat surprising to find that wave and current boundary layers have received very little attention, at least until relatively recently. Initial investigations centered around trying to find a formula for a combined wave and current friction factor which gave the correct form in the opposite limits of no wave or no currents (see for example Jonsson 1966). Other investigations have simply assumed that wave and current effects can be superimposed. Recently two rather similar theoretical studies of wave/current boundary layers have appeared Smith, (1977) and Grant and Madsen, (1979), and we will briefly discuss these theories in this section.

As we have seen, the wave boundary layer is much thinner than the boundary layer for steady flow. We can therefore distinguish two separate regions in the wave/current boundary layer; a region close to the bed in which both oscillatory and steady friction are important, and a region above that in which only the steady flow friction is locally important. It is important to realize, however, that the flow in the upper layer is modified appreciably by the presence of the wave boundary layer; in effect the flow in the upper layer feels an increased boundary resistance due to the presence of the wave-induced turbulence in the lower layer.

Smith (1977) and Grant and Madsen (1979) independently choose to approach the problem by assuming an eddy viscosity which varies linearly with distance above the bed, as in equation 5, but they differ in the form that they take for u_*. Smith simply assumes that, within the wave and current boundary layer, u_* is the sum of a $u_{*\,wave}$ (computed from his oscillatory, turbulent boundary layer model) and the steady flow u_*, u_{*s}. In the current boundary layer above, the wave component of the eddy viscosity is taken to be constant

(= $k\ u_{*\,wave}, \delta_w$

where δ_w is the thickness of the wave boundary layer).

As expected, both mean and oscillatory flows exhibit modified logarithmic layers. For mean flows

$$u = (u_{*s}/k)[1+(u_{*wave}/u_{*s})]^{-1}\ln(z/z_0) \qquad (16)$$

in the inner layer, and

$$u = (u_{*s}/k)\ \ln[(z+\delta_w \gamma)/z_1) \qquad (17)$$

where $z_1 = (1+\gamma)\ \delta_w\ (z_0/\delta_w)^{1/(1+\gamma)}$

and $\gamma = u_{*\,wave}/u_{*s}$,

in the current boundary layer above. The oscillatory flow in the wave/current boundary layer is identical in form to that for standing waves alone (Figure 5-07) but with the friction velocity replaced by the total wave + current friction velocity.

Equation 16 shows that the presence of waves has the apparent effect of increasing von Karman's constant and lowering the ratio of u/u_* for a given z/z_0. Thus for a given velocity at a fixed level from the seabed and a given roughness, a higher mean boundary shear stress results. This effect is significant even for small waves; if $u_{*\,wave}/u_{*s} = 1/4$ the boundary shear stress is increased by 56%. This enhanced bed stress is very important for sediment transprt, particularly as bedload.

Grant and Madsen compute appropriate values of friction velocity in the inner and outer layers by considering the form of the quadratic stress law for a combination of waves and currents. They consider the general case in which wave direction and steady current direction are at an angle to each other. They also treat the **mean** flow magnitude and direction in the quadratic stress law as an unknown, since, they argue, the bed shear stress and the relative magnitude of the wave and mean flows are inter-related in a complex non-linear manner so that it is not clear what the appropriate mean current is in the quadratic stress law. Their final scheme for computing the bed stress and velocity profiles, when the wave orbital velocity (outside the wave boundary layer) and the mean flow speed and direction at some given height are known, therefore involves an iterative procedure. Various values of mean flow are tried in the quadratic stress law until the resulting mean flow profile matches the given flow speed and direction at the given height above the bed.

As with Smith's theory (equation 17), they find that the profile of mean flow in the outer region has a modified apparent bottom roughness which can become much larger than z_0 as the wave amplitude increases relative to mean flow. Figure 5-11 shows their computed ratio of apparent bottom roughness to true bottom roughness, as a function of both the steady current to wave current ratio (U_a/U_b) and also the ratio of bed roughness to amplitude of wave particle motion (k_b/A_b). This prediction of enormously enhanced apparent bottom roughness in the presence of large waves has some support from observation on the shelf. Grant and Madsen quote results of Forristall et al. (1977) in

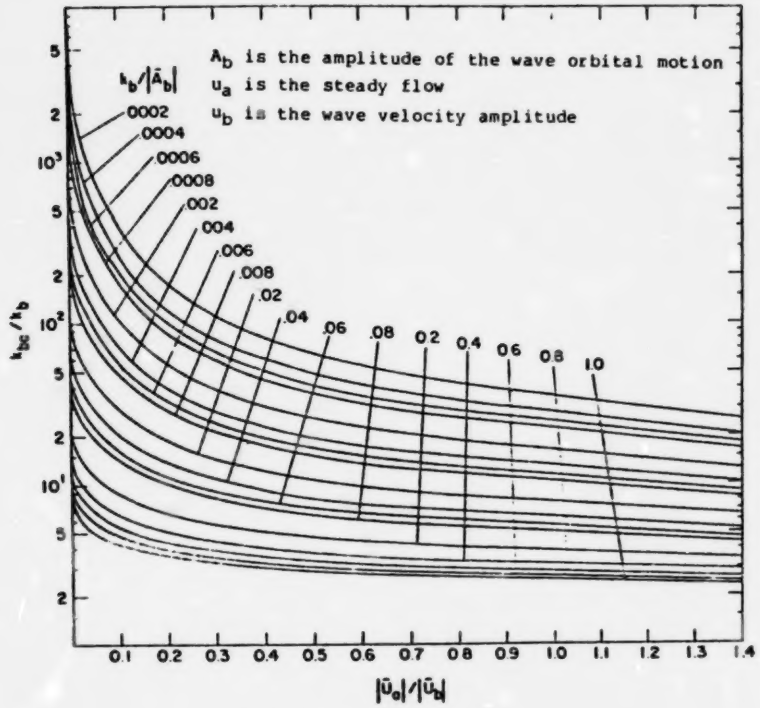

Figure 5-11 Ratio of apparent bed roughness, k_c, to true bed roughness, k_b, for waves and currents in the same direction (from Grant and Madsen, 1979).

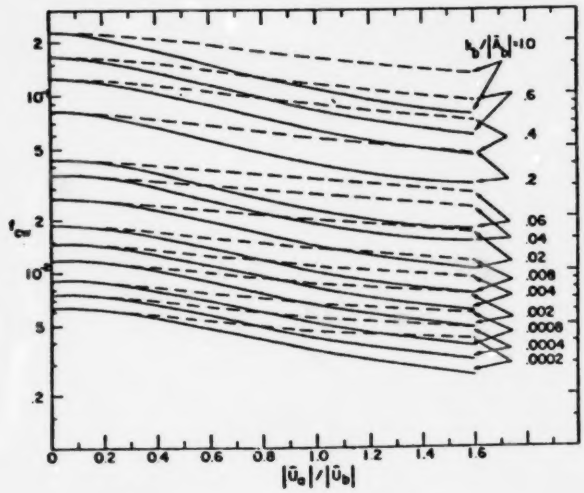

Figure 5-12 Wave current friction factors for codirectional (solid lines) and transdirectional 90° flow (dashed lines) (from Grant and Madsen, 1979).

which bottom roughness as high as 6 m. were determined over a mud bottom!

Grant and Madsen also calculate wave/current friction factors, which are reproduced in Figure 5-12. Note however that the steady flow u_a shown on this graph is the iteratively determined value and is not the value at any particular height above the bed; it is not clear how useful these friction factors are if a mean flow is simply guessed on the basis of observations.

Grant and Madsen claim that their method is most appropriate for wave/current interaction in a wave-dominated environment, while Smith's approach is most appropriate at the opposite extreme of current dominated flows. However, whatever the regime, the real need is for field data to test (and hopefully improve) these theories.

2.5 **Other complications**

2.5.1 Stratification due to sediment load

When sediment goes into suspension it changes the effective density of the water and leads to an apparent density stratification of the water column. This stratification, if stable (i.e. heavier water below), tends to suppress the turbulence, since it is harder to mix the water vertically. This in turn affects the velocity profile and the seabed stress. This phenomenon therefore represents a feedback between the fluid dynamics and the sediment dynamics which is difficult to model.

There is evidence that the effect can be very important locally on the continental shelf, particularly where fine sands and muds are in suspension. Einstein and Chien (1955) made some of the earliest laboratory measurements of this effect, and they described their results in terms of an effective reduction in von Karman's constant and an increase in effective roughness length. McCave (1973) found similar effects in velocity profiles over a sand bank in the North Sea, and he gave a procedure for modifying von Karman's constant based on his data. Gust (1976) found even more startling results for clay suspensions. Using samples of sediment and sea water from the North Sea in laboratory experiments, he found that the viscous sub-layer increased in thickness by a factor of 5, and the friction velocity in the log layer above decreased by 40% for a clay suspension. These anomalous results appear to be due to the elastic deformation of large aggregates of clay particles in the boundary layer.

The theory of stratified boundary layers was developed for the atmospheric boundary layer. It is not difficult to show that, in general, the effect of stratification increases with distance from the boundary. The appropriate distance at which stratification becomes important is usually given as the Monin-Obukhov length

$$L_M = u_*^3 / gkB \qquad (18)$$

where B is the buoyancy flux in the boundary layer (analogous with the turbulent stress, which can be considered as a **momentum** flux (see 2.6.4)). Physically L_M is the height at which the rate of generation of turbulent kinetic energy is balanced by the rate of loss to the potential energy by the mixing. Thus the layer will be mixed by turbulence up to L_M but at that height a density interface will tend to form. Using this parameter, the velocity in the logarithmic layer is modified

$$u = (u_*/k)\ [\ln(z/z_0) + az/L_M] \qquad (19)$$

where the constant a is found experimentally to be about 5. Figure 5-13 shows schematically the form of the velocity profile. The rate of increase of velocity with distance from the boundary is significantly reduced close to the boundary in the stratified case, resulting in reduced bed shear stresses.

Taylor and Dyer (1977) use the diffusion/advection model of suspended sediment profile (see section 3.4) to get explicit forms for velocity profile and sediment profile in a coupled sediment/water system (apparently previously derived by Russian workers). Figure 5-14 shows some examples of the results for a representative range of conditions; only in case 2 does a modified von Karman constant fit the profile well. Smith and Mclean (1977) take a more general non-linear form for the diffusion/advection equation for suspended sediment profile, but otherwise proceed as Taylor and Dyer. Their results, however, involve finding solutions, by iteration, to equations involving integrals. Since their non-linear form reduces to Taylor and Dyer's linear form in the limit of small sediment concentrations, it is obviously easier to use the latter's analytic solution unless sediment concentrations are high.

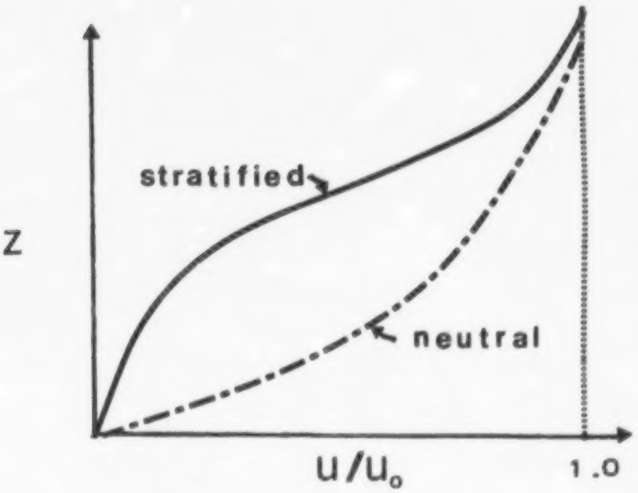

Figure 5-13 Schematic comparison of velocity profiles in stably stratified and neutral boundary layers.

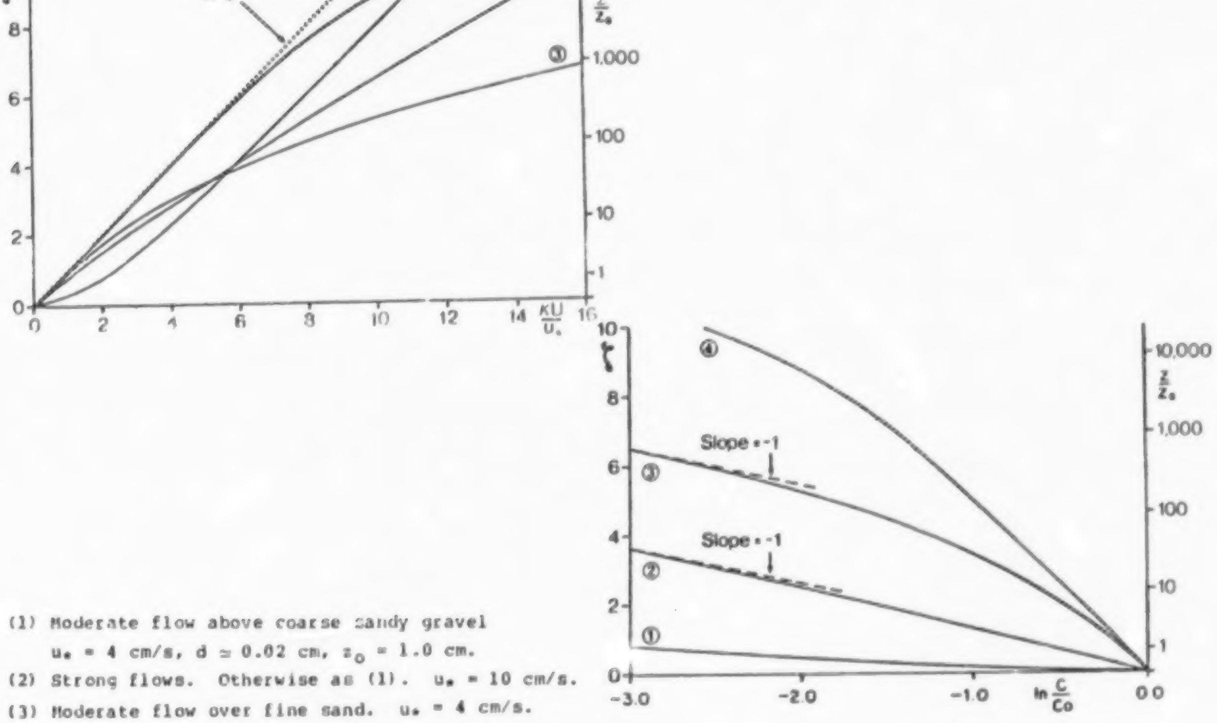

(1) Moderate flow above coarse sandy gravel
$u_* = 4$ cm/s, $d \simeq 0.02$ cm, $z_o = 1.0$ cm.

(2) Strong flows. Otherwise as (1). $u_* = 10$ cm/s.

(3) Moderate flow over fine sand. $u_* = 4$ cm/s.
$d \simeq 0.006$ cm., $z_o = 0.1$ cm.

(4) As case 3 but with $z_o = 0.001$ cm, i.e. nearly hydraulically smooth flow.

Figure 5-14 Velocity and sediment concentration profiles for four cases of stratified flow (from Taylor and Dyer, 1977) $\zeta = \ln[z/z_o]$.

The effect of stratification on the Ekman boundary layer above the log layer has been extensively studied in relation to the atmospheric boundary layer. The most common approach theoretically is to use numerical models to predict profiles and stresses. Results indicate that the stratification, as well as reducing bed stress, also increases the veering angle of the Ekman spiral, and reduces the thickness of the boundary layer. Weatherly and Martin (1978) and Adams and Weatherly (1981) are representative of the modelling schemes applied to the oceanic boundary layer (these models include the effects of a sloping bottom). Weatherly and Martin (1978) predict a modified Ekman layer thickness given by

$$L_E = 1.3u_*/f[1+(N^2/f^2]^{1/4}$$

where N is the Brunt-Vasaila frequency associated with the stratification (see Pond and Pickard (1978) for details of the Brunt-Vaisala frequency). Weatherly and Van Leer (1977) show data from the Florida shelf which tends to support this.

2.5.2 Bedload effect on apparent roughness length

Intense bedload movement of sediment is found to produce high values of z_0. Smith and McLean (1977), on the basis of their river boundary layer measurements, suggest that the modified roughness length, z_0, is proportional to the excess shear stress (equation 20) (the shear stress minus the critical stress, τ_c, required for bedload motion; see sections 3.2 and 3.3).

$$z_0' = 26.4(\tau_b - \tau_c)/(\rho_s - \rho)g + z_0 \qquad (20)$$

2.5.3 Flow acceleration

The effects of flow acceleration and deceleration are, in principle, embodied in the theory of oscillatory boundary layers, but for irregularly varying flows this may not be the most convenient way to describe them.

Nevertheless, the most important effects can be seen in Figure 5-07. During the deceleration of positive velocity from its maximum at t=0, the velocity profile curves so that the velocity in the lower part of the boundary layer is less than would be expected for a steady flow logarithmic layer (in this figure a steady flow log layer can be thought of as a straight line, from the zero current point to the free velocity at the height of the wave boundary layer); this can be seen most clearly in the curve labelled $4\pi/10$. During the acceleration of the negative velocity, on the other hand, the curvature in the upper part of the boundary layer is such that the velocity close to the boundary increases **faster** than the equivalent steady profile. In fact, at times of high acceleration (6 and $7\pi/10$) a boundary layer "jet" is formed, in which the flow is more rapid than in the frictionless region above the boundary layer. Thus u_* near the seabed is **reduced** during decelerations and **increased** during accelerations.

In dealing with irregular velocity changes in tidal flows, Soulsby and Dyer (1981) draw attention to the similarity between the shape of the velocity profile in decelerating flows and in stably stratified water (Figure 5-13), and suggest an "acceleration length" similar to the Monin-Obukhov length scale to describe this effect; in accelerating flows the acceleration length simply changes sign, becoming analogous to unstably stratified flows. They therefore model the velocity with a log-linear profile exactly like equation 19, but with L_M as an acceleration length scale given by

$$L_M = u_* |u_*| / u_*'$$

where $|u|$ implies the magnitude of u, and u_*' is the time rate of change of u_*. The appropriate value of the constant a in equation 19 was found using measurements of velocity profile and stress in tidal flow in 14 m. depth; a value of 20 appeared to fit the observations reasonably well. It must be said that, although this may be a useful way of predicting the velocity profile, the similarity between this and stratified flow modifications will not help in separating these effects in field data.

Another more subtle effect of flow changes on sediment transport is the fact that, despite the assumption usually made, sediment will not in general be able to respond to rapid changes in velocity. Hence there may be enhanced sediment transport during deceleration of the flow, for example. This can potentially be particularly important when an oscillatory flow is asymmetric, as is frequently the case for tides. Allen (1973) discusses some of the implications.

2.5.4 Stress intermittency

The velocity shear in the benthic boundary layer is intrinsically unstable and, except for a viscous layer adjacent to the bed over smooth sea floors, is turbulent. The dimensional arguments and scaling used above in relation to turbulent boundary layers are obviously poor substitutes for a proper physical understanding of the nature of the turbulence. Recent laboratory research has returned to a more descriptive study of the precise form of turbulent motion, using flow visualization techniques and very detailed velocity measurements. The results are revealing organized structures in flow in turbulent boundary layers, a particularly important form being "bursts" of low velocity fluid ejected from close to the boundary, and of high velocity fluid penetrating down into the boundary layer in a sweeping motion (see Cantwell 1981 for a comprehensive review).

The significance of all this to continental shelf boundary layers is that the bed stress is found to be strongly related to these intermittent "burst" phenomena. High frequency measurements of stress by the eddy correlation method (see next section) show that the short, intermittant bursts give very high values of stress, and stress is negligible between bursts. Heathershaw (1974), for example, found that 57% of the stress occurred in 7% of the time associated with bursts; peak values of stress reached as high as 30 times the mean stress. Thus the stress used in the formulae above is the mean of a highly irregular distribution of stress events. There are fairly well tested scaling laws to determine the average time interval between these bursts of high stress; typically they will be a few tens of seconds apart, but for some flows the interval can reach several minutes. Clearly, the implication of this is that an accurate measurement of the true average stress in the turbulent boundary layer requires measurements which span a long time interval, so that the average can be made over many stress events.

Heathershaw and Simpson (1978) find a variability of an estimated 50% in the stress measured over 600s. Interestingly, they argue that, in changing tidal currents, there is not the option of extending the averaging time to reduce this variability significantly since the flow cannot be considered steady for longer periods. There therefore appears to be an intrinsic uncertainty in the mean stress during a tidal cycle.

It seems reasonable to assume (on physical grounds) that this variability measured in the turbulent boundary is reflected in the stress experienced by the seabed. If this is the case then all estimates of bed stress are likely to be subject to the same uncertainty. Heathershaw and Simpson suggest that the experimental scatter in measured drag coefficients (see the next section and Figure 5-16) may result from this uncertainty (though there are several other possible explanations).

2.6 The practical estimation of bed stress

Enough has been said in the previous sections to show that we cannot, at present, estimate the true bed stress on continental shelves with any confidence. Nevertheless, there are many occasions when some sort of estimate has to be made, most commonly as part of estimating sediment transport rates. In this final section on boundary layer dynamics we briefly outline some of the techniques that are available for making such estimates.

The techniques are discussed below in increasing order of instrumental complexity. This increasing complexity also corresponds to increasing confidence in the accuracy of the results.

2.6.1 Quadratic stress law

On dimensional grounds, confirmed by measurements, the stress in the turbulent boundary layer for a steady flow u_z at a distance z above the bed is proportional to the square of that velocity, that is:

$$\tau = C_D \rho u_z^2 \qquad (21)$$

where the constant of proportionality, C_D, is known as the **drag coefficient**, and ρ is the density of the fluid.

The drag coefficient obviously varies depending on the height z at which the velocity is measured. In oceanographic work the usual standard distance is 1 m. (100 cm) above the bed, so the associated drag coefficient is denoted C_{100}.

Figure 5-15 shows the values of drag coefficient measured by Sternberg (1968) for a variety of bed types in tidal channels of Puget Sound. For hydrodynamically rough flows the drag coefficient is essentially constant, independent of the Reynolds number, Re; this occurs for Re greater than about 15×10^4, corresponding to $u_{100} > 15$ cm.s^{-1}. There does, however, seem to be a systematic difference in drag coefficient depending on the type of sea bed (almost certainly due to bedforms, since these measurements relate to the total stress, including form drag).

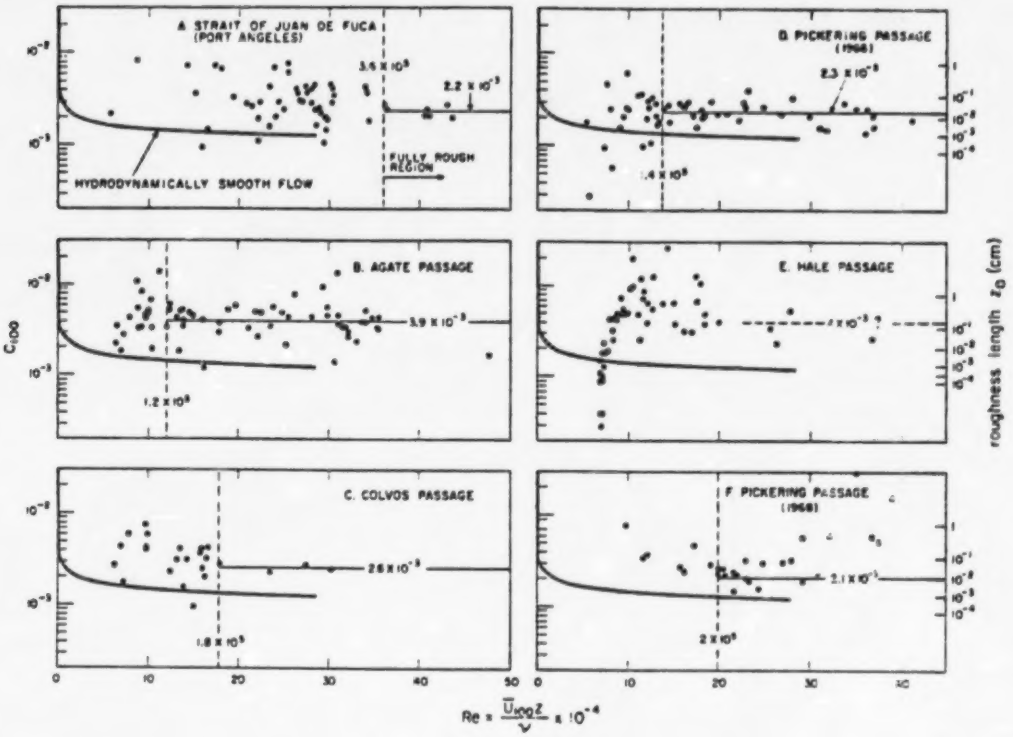

Figure 5-15 Drag coefficient (C_{100}) as related to the Reynolds number (from Sternberg, 1968).

Here $\overline{U}_{100}$ is the mean velocity one meter from the bed, z is 100 cm. and ν is the kinematic viscosity. Mean values of C_{100} and the boundary between regions of relatively large and small dispersion are also included. The open circles in F refer to measurements made during periods of significant suspended sediment motion. Equivalent values of roughness length (z_0) can be determined by using the right hand vertical axis.

The bed configurations in Figure 5-15 are classified as rocky (A), gravelly (B), rippled sand (D, F), and indistinctly roughened sand (E,C). However, Sternberg chooses to lump all estimates of C_D together, since variations over a single bed type are similar in magnitude to variations between bed types. The results are given in Figure 5-16 and Table 5-III. Sternberg comments that these results are probably representative except perhaps for large-scale ripples, dunes, or sand waves (> 5 cm. in height). Thus the best estimate for an overall drag coefficient is

$$C_D = 3 \times 10^{-3}$$

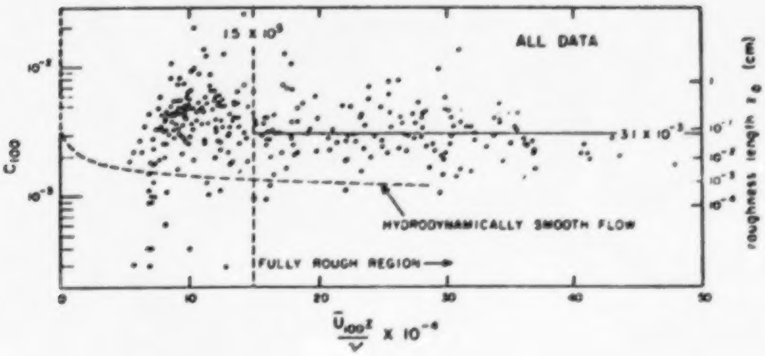

Here $\overline{U}_{100}$ is the mean velocity one metre from the bed, z equals 100 cm. r is the kinematic viscosity. Equivalent values of roughness length (z_0) can be determined by using the right-hand vertical axis.

Figure 5-16 Drag coefficient (C_{100}) as related to the Reynolds number for all data combined (from Sternberg, 1968).

Table 5-III

Mean C_{100} and 95% confidence limits for all boundary-layer data. regardless of bed configuration

	All data	Re<1.5 x 10^5	Re>1.5 x 10^5
C_{100}	3.1 x 10^{-3}	3.2 x 10^{-3}	3.0 x 10^{-3}
Upper limit	1.1 x 10^{-2}	1.6 x 10^{-2}	7.8 x 10^{-3}
Lower limit	8.7 x 10^{-4}	6.6 x 10^{-4}	1.1 x 10^{-3}

[a]After Sternberg, 1968.

Although a variety of other values have been used by other workers (indeed the drag coefficient is generally an adjustable "fudge factor" in many numerical models of flow over the shelf!), this value is probably as good as any.

Notice, incidently, that this drag coefficient is equivalent to the relation

$$u_* = 5.5 \times 10^{-2} u_{100}$$

This method obviously allows an estimate of stress to be made from a measurement of velocity at a single height. If such a velocity is not measured at the standard 100 cm. off the bottom it is often possible to use the logarithmic profile equation (2) to estimate u_{100}, though this involves an additional degree of uncertainty.

2.6.2 The Velocity Profile method

Converting from ln to $\log_{10}$ in equation 2 and assuming $k=0.4$ gives, for the velocity in the logarithmic layer

$$u = 5.75\, u_* \log (z/z_0) \qquad (22)$$

If we could assume a value of z_0, of course, it would be possible to use a single measurment of velocity in the log layer to estimate u_*. However such an estimate is very sensitive to the value of z_0 chosen, and z_0 is generally not at all well known.

With measurements of velocity at two heights in the log layer, u_1 at z_1 and u_2 at z_2, z_0 can be eliminated. The stress will then be estimated by

$$\tau = \rho\,[(u_2-u_1)/5.75(\log z_2-\log z_1)]^2 \qquad (23)$$

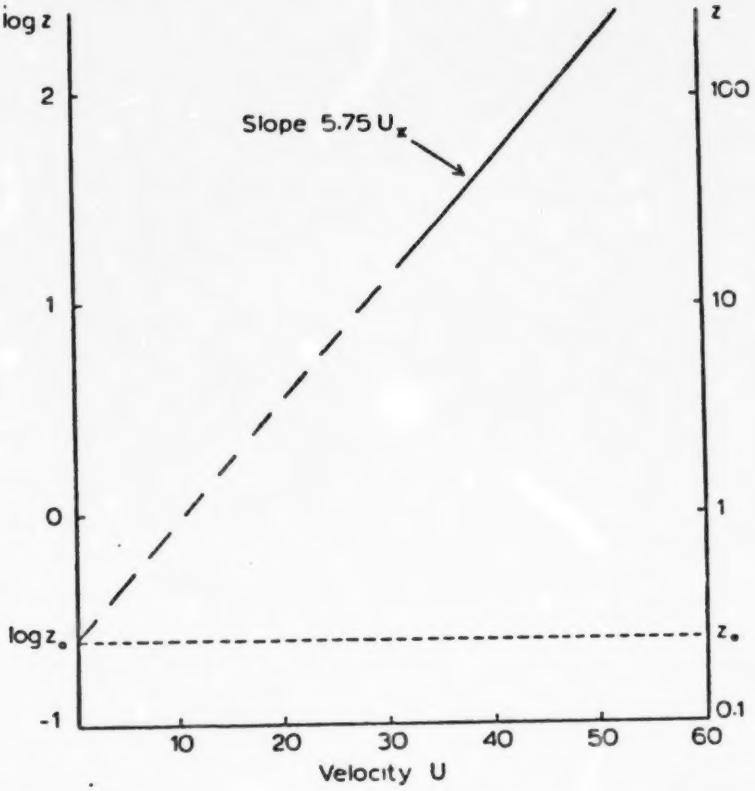

Figure 5-17 Determination of the friction velocity u_* and the roughness length z_0 from a logarithmic velocity profile.

In fact, to be sure that measurements are being made in the logarithmic layer, at least three current meters, placed within about 1.5 m. of the seabed, are required, and thus a considerable degree of instrumentation is involved in the application of this technique. With several measurements, the usual technique for estimating u_* involves plotting u against log z; the slope of the graph is then 5.75 u_* (see Figure 5-17).

The intermittency problem discussed in the previous paragraph means that the time over which the velocity measurements are made is an important parameter. Bowden (1978) reviews some of the measurements that have been made of current profile; he concludes that 10 minutes should be considered a lower limit for the averaging process.

One of the difficulties in using the profile technique is that a logarithmic profile is not always easy to identify in measured profiles (see for example Bowden 1962). Sternberg (1968), using a rather generous criterion for identifying a logarithmic layer (that at least 4 of his 6 measurements within 1.5 m of the bed fell within 10% of a linear relationship between u and log z), found that his measurements in Puget Sound yielded logarithmic profiles from 62% to 100% of the time, with an average of 85%. Nevertheless the uncertainties will generally be less than those involved in using drag coefficient.

2.6.3 The eddy correlation method

As we saw in section 2.2 above, turbulence is responsible for the stress above the viscous sublayer. A direct measurement of turbulent velocities can therefore be used to measure stress in the turbulent boundary layer.

Osborne Reynolds, in his fundamental work on turbulence, showed that, if we consider a horizontal plane of unit area above the bed in the turbulent boundary layer, then the turbulent shear stress in the horizontal direction which the water above the area imposes on the water below the area is given by

$$\tau = -\rho\,\overline{u'w'}$$

where u' and w' are the instantaneous turbulent velocities in the horizontal and vertical directions respectively, and the overbar implies a time average of their product. This stress is known as

the Reynolds stress.

The rationale leading to this form of the Reynolds stress can be seen as follows. By Newton's second law, a force is equivalent to a time rate of change of momentum (momentum = mass x velocity). Thus a stress is the rate of change of momentum per unit area. The instantaneous horizontal momentum per unit volume due to the turbulence is $\rho u'$ and this is being added to the water below the horizontal area at a rate determined by the instantaneous downward velocity $-w'$, so the instantaneous increase in momentum of the fluid below the area is just $\rho u'w'$, and this is also the instantaneous force. The Reynolds stress is then just the time average of this force; see Figure 5-18).

Measurement of turbulent velocities requires current meters capable of responding to the rapid fluctuations. Bowden and Fairbairn (1956) made some of the earliest measurements, using an electromagnetic flowmeter, and more recently a number of instruments have been developed which are capable of sensing

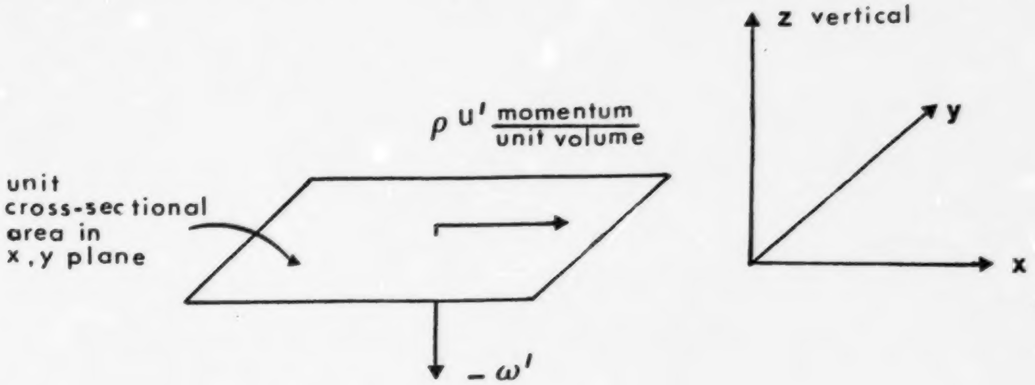
z vertical
y
x
$\rho u' \frac{\text{momentum}}{\text{unit volume}}$
unit cross-sectional area in x,y plane
$-\omega'$

Figure 5-18 Schematic diagram showing the motion of horizontal turbulent momentum $\rho u'$ through a horizontal plane by vertical turbulent velocity ω'.

turbulence. A full review of these techniques and their results is not relevant here; a short review, with emphasis on the oceanic boundary layer. is given by Bowden (1978). Suffice it to say that the work of Heathershaw (1976), Soulsby (1980) and others have shown that the technique is a very useful, if rather difficult, way of measuring stress, and provides a great deal of useful information on the spatial and temporal scales of the turbulence. Heathershaw for example, finds an equivalent drag coefficient $C_{100}=1.73 \times 10^{-3}$, with an uncertainty of 0.18×10^{-3}.

There apparently are, as yet, no simultaneous measurements in the benthic boundary layer of stress by all three of the above methods. The closest seems to be a series of measurements by McPhee and Smith (1976), in the boundary layer below a sheet of pack ice being driven by the wind. They found reasonable agreement between u_* values measured by the profile method and the eddy correlation method.

2.6.4 Viscous sublayer method

The methods outlined above are all used within the turbulent boundary layer, and generally measure a stress which includes a form drag component. While some measurements of velocity profile, using ducted impellors, have apparently come sufficiently close to the bed to eliminate form drag (e.g Smith and McLean 1977), an element of uncertainty remains. On the other hand, measurements taken close enough to include the viscous sublayer will essentially eliminate the possibility of form drag being important to the measured stress.

In a remarkable series of measurements on the Oregon shelf, Caldwell and Chriss (1979) have been able to measure velocity profiles right into the viscous sublayer where the velocity changes linearly with distance off the seabed (equation 1). This was made possible by using heated thermistors to measure current speed, and by moving the thermistors up and down from the seabed to a few centimetres or tens of centimetres above the bed on a motor-driven profiling arm. Figure 5-19 shows an example of their results.

The importance of these measurements lies in the fact that the stress can be estimated in the viscous sub-layer simply by multiplying the measured gradient of velocity by the accurately known molecular viscosity; no scaling or dimensional arguments required for the logarithmic profile are involved. As might be expected, the drag coefficient measured by Caldwell and Chriss in this way, $C_{100} = 1.1 \times 10^{-3}$, was significantly lower than the mean value found by Sternberg (Figure 5-16), though it was well within the speed of Sternberg's values.

Unfortunately, the heated thermistors are not easy to use in the marine environment, so it is unlikely that this technique will ever become routine. Nevertheless, it holds out considerable hope for providing accurate bottom stresses which can be compared with estimates made by the other techniques. This should lead to substantial improvements in both the theory and the practice of estimating the true stress experienced by sediment particles on the seabed.

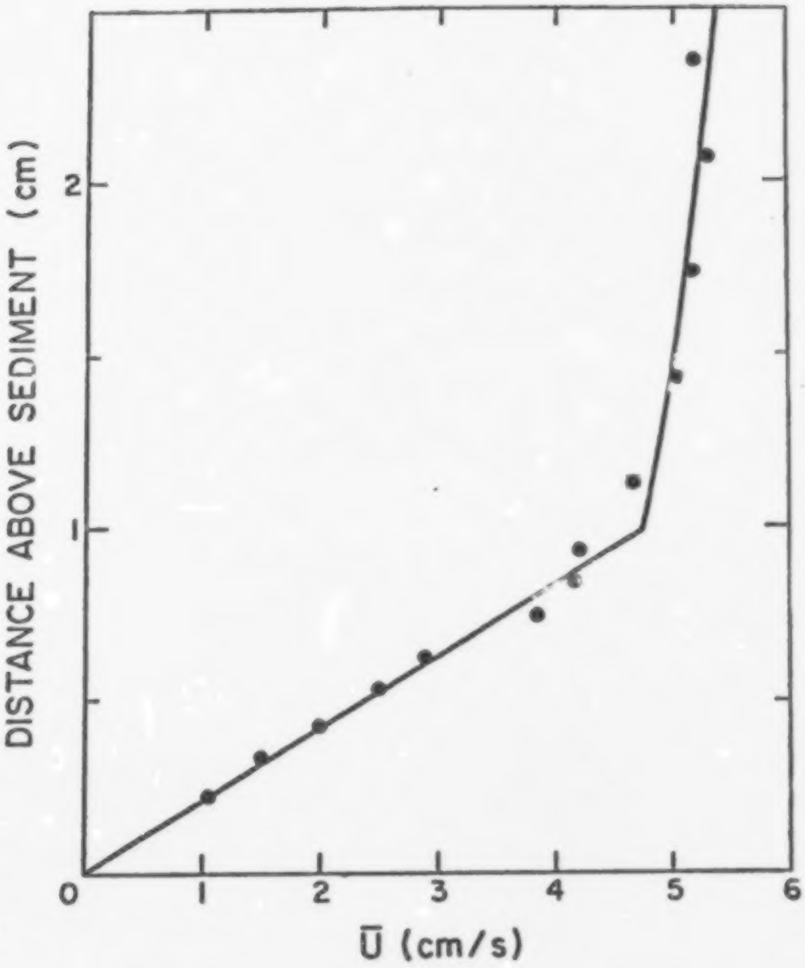

Figure 5-19 A linear velocity profile in the laminar sublayer within 1 cm of the bed. The region above 1 cm is the bottom of the logarithmic layer (from Caldwell and Chriss, 1979).

3. NON-COHESIVE SEDIMENT DYNAMICS

3.1 Introduction

So far we have dealt only with hydrodynamics. We now turn to some of the ideas dealing with sediment-water interaction. It must be admitted at the outset that both theory and measurement of this interaction are extremely difficult, and although some rather sophisticated ideas have been brought to bear on the problem, accurate estimation of sediment parameters on the shelf are still not possible. At best our estimates will be within a factor of two; most often they will be much worse than this.

There are two basic questions to be answered:

i) Under what circumstances will sediment move? This leads us to look at THRESHOLDS for sediment motion, often known as COMPETANCY.

ii) Once sediment is in motion, how much will move across unit length of the seafloor in unit time? This is the problem of sediment TRANSPORT.

These important questions have been much studied in relation to river flow and coastlines, but have only relatively recently been considered for continental shelves, and then primarily for geological reasons (Swift, et al. 1972). For steady unstratified flows Yalin (1972) found that the relevant parameters for threshold and transport should be flow depth, velocity outside the boundary layer. fluid viscosity and density, sediment size and density and the acceleration due to gravity. Shear stress or friction velocity could be substituted for fluid velocity, and sediment fall velocity could replace grain size. In fact, since we generally are dealing with water and with sediment whose properties do not differ significantly from those of quartz, the fluid and sediment parameters can generally be considered constants. Fluid viscosity can generally also be assumed constant. As a result there should be only three relevant variables: grain size, flow depth and fluid velocity. Southard (Middleton and Southard 1977) has in fact shown that several sediment flow parameters can be determined in terms of these parameters and occasionally only two are needed (see e.g. the Shields diagram below, Figure 5-20).

Despite this apparent simplification, prediction of sediment transport is complicated by several factors. Most important is the observation that sediment movement takes place by two distinct mechanisms (though there is obviously overlap between them):

a) Bedload transport, where grain/grain interactions are paramount. Bowden (1978) described two forms of bedload transport; rolling, in which a grain moves along the bed while remaining in contact with it, and saltation, in which a grain is lifted off the bed by an upward impulse and then falls back under gravity with some forward movement. Probably in water, rolling is much more important than saltation.

b) Suspended load transport, in which grains are supported by upward impulses due to fluid turbulence and move forward essentially at the speed of the fluid.

These two methods of transport are generally treated separately and have their own predictive equations.

As flow increases BEDFORMS appear in the sediment and, as discussed in the previous section, these have a profound effect on the flow. which in turn affects sediment threshold and transport. We generally therefore need independent measurements of bedforms, and even then there are. as yet. no accepted methods for modifying sediment parameters depending on bedform size and shape.

Another general difficulty for the practical estimation of sediment transport on continental shelves is the observation, fully supported by theory. that most sediment transport occurs during violent storm events. Based on measurement on the continental shelf off Oregon and Washington. Smith and Hopkins (1972) estimated that significant sediment transport occurs only during storms and that a severe storm occuring only every few years will have more significance than a number of less severe storms. Petrie and Bowen (1979) find similar results for the Scotian shelf.

With these general caveats in mind we will now consider specific models for sediment threshold and transport on shelves.

3.2 Threshold of Sediment Motion

The threshold at which sediment particles are just disturbed and set into motion is defined by a critical value of the stress τ_c which the water exerts on the bed. COMPETANCY CURVES, relating this stress (or some parameter related to stress) to sediment grain diameter have been produced by a number of authors. These curves are based on laboratory measurements under steady flow conditions and have generally not been well verified for the flow conditions and sediment mixtures of different marine environments. The most generally used competancy curves are those given by Shields (1936). At the critical stress the frictional and gravitational forces on the sediment are just balanced by the fluid forces. Shields therefore argued that the appropriate non-dimensional form for the critical stress is the ratio

$$\theta_t = \frac{\tau}{(\rho_s - \rho) g D} \qquad (24)$$

where D is the grain diameter and θ_t is known as the Shields parameter. Figure 5-20 shows the Shields diagram as modified by Vanoni (1964); a Shields curve of quartz grains in water is also shown in Figure 5-21, where the Shields parameter has been replaced by the friction velocity u_*. As an example, 0.5 mm sand is predicted to have a critical $u_* = 2$ cm/s, U_{100}=35 cm/s and $\theta_t = 0.05$.

Application of the Shields curve is really only valid for a flat bed and for uniform sediment size. The assumption of a flat bed is probably the most serious deficiency for its application to continental shelf environments. Inman (1963) shows a modified Shields curve with a branch towards higher threshold stresses for rippled beds. However, as Middleton and Southard (1977) point out, the critical bed stress over a rippled bed is actually less than over a flat bed once form drag has been removed because flow separation over the ripple crests produces locally high stresses which can put sediment into motion. Nevertheless measurements by

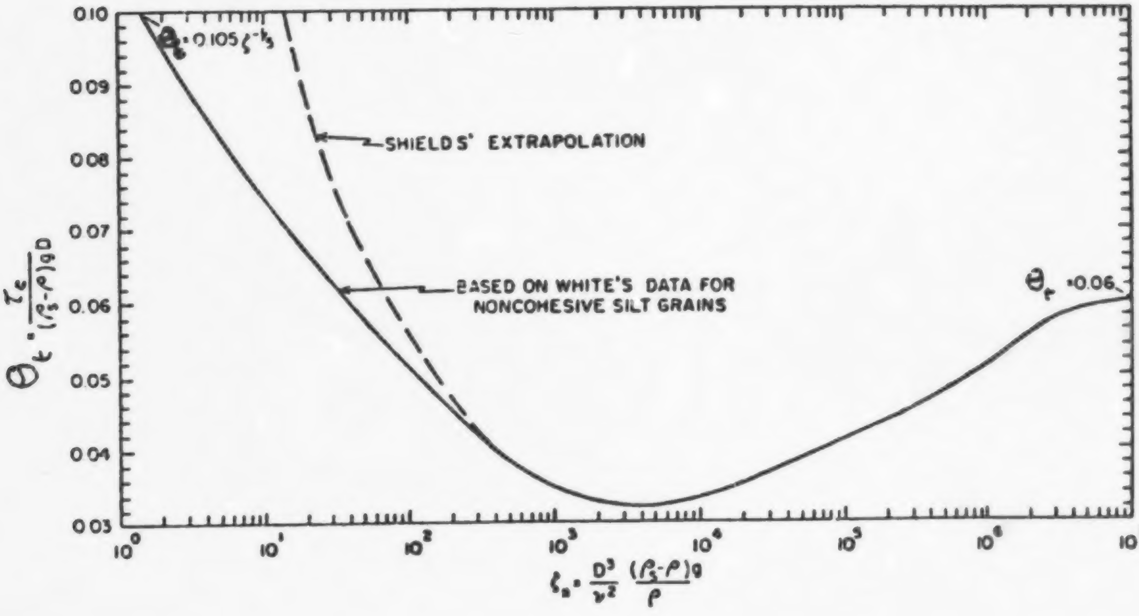

The dashed curve and the solid one to the right side of the branch are from the Shield's diagram as modified by Vanoni (1964) and usually plotted in terms of $(u_*)_c D/\nu = (\zeta_*\theta_t)^{1/2}$. The solid line to the left of the branch is based on data of White (1970) for noncohesive material of silt size. For large ζ_*, $\theta_t = 0.06$, and for small ζ_*, White's expression yields an asymptotic value of $\theta_t = 0.105\zeta_*^{-1/5}$. Strictly speaking, Shield's diagram and curves derived from it such as the one presented here apply only to geometrically smooth beds of well-sorted sedimentary material for which $D = k_s$.

Figure 5-20 Non-dimensional boundary shear stress required to initiate sediment transport, as a function of the non-dimensional number representing fluid and sediment properties.

Table 5-IV

Various size grade scales in common use

GRAIN SIZE SCALES FOR SEDIMENTS

U. S. Standard Sieve Mesh #		Millimeters	Microns	Phi (ø)	Wentworth Size Class	
		4096		-12		GRAVEL
		1024		-10	Boulder (-8 to -12ø)	
Use		256		- 8		
wire		64		- 6	Cobble (-6 to -8ø)	
squares		16		- 4	Pebble (-2 to -6ø)	
5		4		- 2		
6		3.36		-1.75		
7		2.83		-1.5	Granule	
8		2.38		-1.25		
10		2.00		-1.0		
12		1.68		-0.75		SAND
14		1.41		-0.5	Very coarse sand	
16		1.19		-0.25		
18		1.00		0.0		
20		0.84		0.25		
25		0.71		0.5	Coarse sand	
30		0.59		0.75		
35	1/2	0.50	500	1.0		
40		0.42	420	1.25		
45		0.35	350	1.5	Medium sand	
50		0.30	300	1.75		
60	1/4	0.25	250	2.0		
70		0.210	210	2.25		
80		0.177	177	2.5	Fine sand	
100		0.149	149	2.75		
120	1/8	0.125	125	3.0		
140		0.105	105	3.25		
170		0.088	88	3.5	Very fine sand	
200		0.074	74	3.75		
230	1/16	0.0625	62.5	4.0		
270		0.053	53	4.25		MUD
325		0.044	44	4.5	Coarse silt	
		0.037	37	4.75		
	1/32	0.031	31	5.0		
	1/64	0.0156	15.6	6.0	Medium silt	
Analyzed	1/128	0.0078	7.8	7.0		
	1/256	0.0039	3.9	8.0	Very fine silt	
by		0.0020	2.0	9.0		
		0.00098	0.98	10.0		
Pipette or		0.00049	0.49	11.0	Clay	
		0.00024	0.24	12.0		
Hydrometer		0.00012	0.12	13.0		
		0.00006	0.06	14.0		

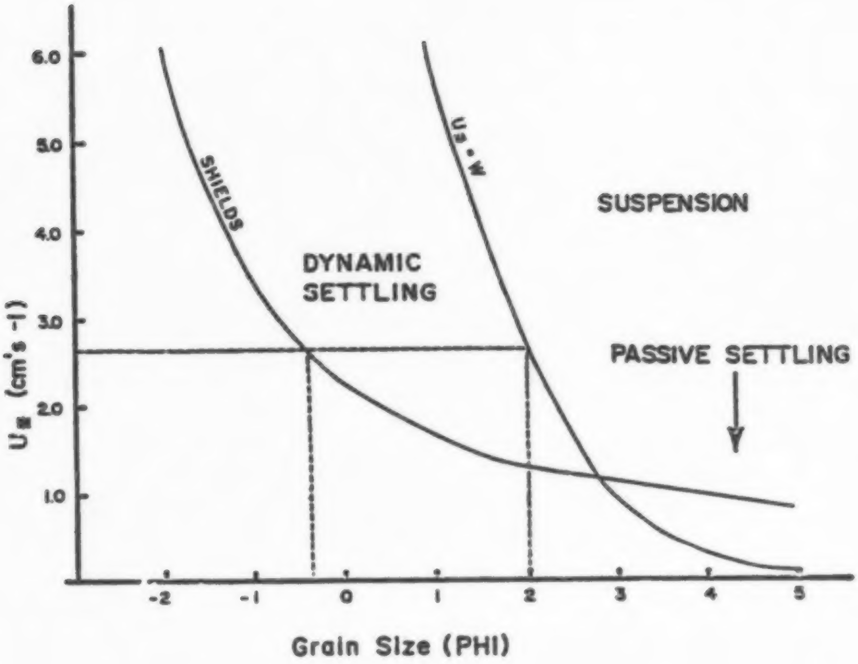

Also shown is the curve of $u_* = W$. Above the cross-over at PHI just below 3, grains will go straight into suspension once the stress reaches their threshold.

Figure 5-21 The Shield's curve for quartz grains in water.

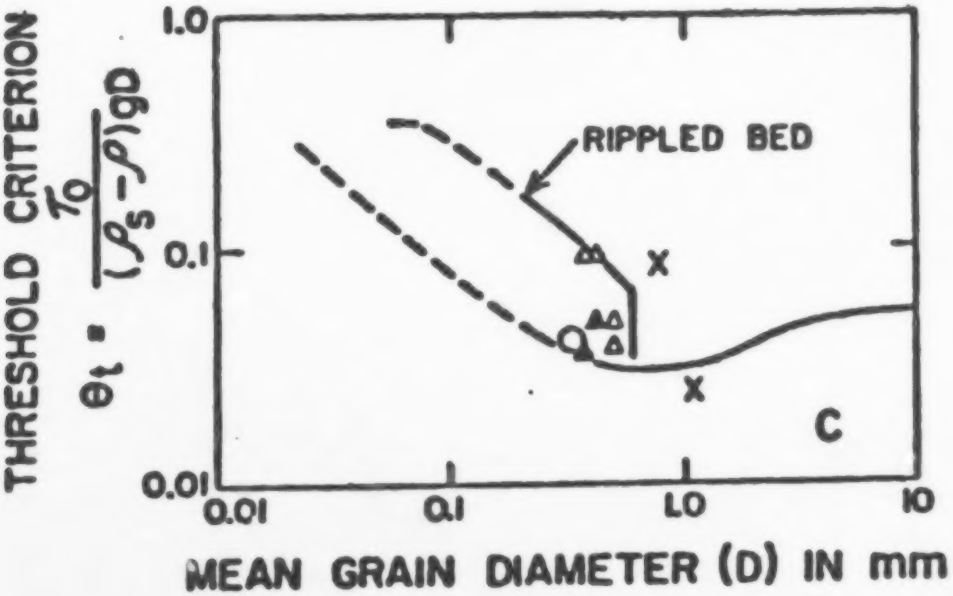

Figure 5-22 The modified Shield's curve for a rippled bed (Inman, 1963, from Sternberg, 1971).

Sternberg (1971) in tidal channels in Puget Sound suggest that the modified Shields curve predicts sediment threshold over rippled beds quite well if the total stress (including form drag) is used (Figure 5-22). His data also show surprisingly good agreement for thresholds for the sand fraction even when it is incorporated in a poorly sorted sediment mix including much larger sized particles. This indicates that the Shields curve is not critically dependent on the requirement of uniform sediment.

For oscillatory flow, Madsen and Grant (1975) show that the Shields curve applies equally well, provided the stress under the flow is correctly calculated. Komar and Miller (1975), on the other hand, by-pass calculation of stress by using empirical equations which give directly the threshold orbital velocity as a function of grain diameter, density and the orbital diameter of the wave motion at the seabed (Figure 5-23).

Clearly, the concept of a threshold stress is not precise, since local fluctuations of turbulent stress can initiate sediment motion when the average stress is well below the average threshold. In addition, under wave conditions, the spectral nature of wave motion will make instantaneous velocities and stresses impossible to predict. Laboratory observations by Grass (1970) demonstrate very clearly the stochastic nature of the threshold. In steady flow, he found that fluctuations in shear stress in the viscous sublayer due to turbulence in the flow above had a standard deviation of 40% of the mean, but that, in addition, there was a 30% variation in the stress at which

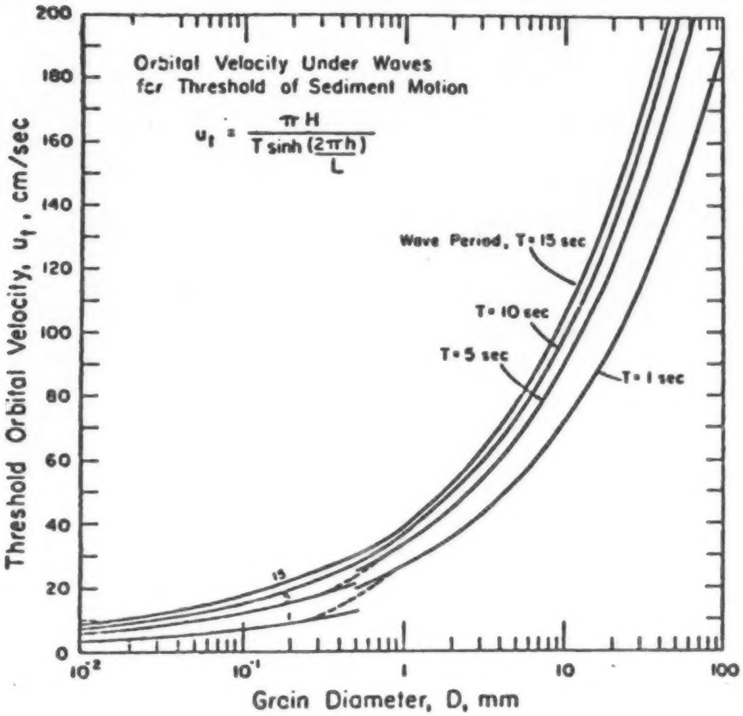

The nearbottom velocity and wave height can be related using the formula shown.

Figure 5-23 Threshold orbital velocity required to initiate motion of grains of quartz, as a function of grain diameter and wave period (from Komar, 1976).

individual particles moved, presumably due to variations in local packing and the exposure of grains. Davies and Wilkinson (1979) find a similar spread of threshold conditions in observations of sediment thresholds under waves in the field.

Various authors have studied the behaviour of sediment as the stress increases beyond the threshold. Neill and Yalin (1969) suggest that the number of grains in motion, above unit area of bed in a unit time, n, is determined by the dimensionless parameter

$$N = n D^3 / u_*$$

and estimate $N = 10^{-6}$. Fredsoe and Englund (1975) find a steady increase in grain velocity, u_G, as the stress increases beyond the threshold with

$$u_G/u_* = 10 \ (1-0.7 \ u_{*c}/u_*)$$

where u_{*c} is the critical friction velocity.

As we discuss below, sediment goes into suspension approximately when $u_* = w$, the settling velocity (see Table 5-V).

Table 5-V Fall Velocities for Quartz Grains in Water

Diameter D (mm)	10^{-3}	10^{-2}	10^{-1}	1	10
Velocity w in cm s^{-1}	10^{-4}	10^{-2}	0.8	12	45

By comparing this criterion with the Shields threshold criterion, Blatt et al. (1980) show that particles below a certain size go straight into suspension once set into motion, while heavier particles move by bedload motion at low stresses and only go into suspension, if at all, at much higher stresses. Figure 5-21 shows the appropriate curves for quartz grains in water at 20°C and suggests that grains smaller than about 0.10 mm will go straight into suspension. Middleton (1976) also uses this kind of plot to explain the trimodal sand size distribution frequently observed. He argues that for a given stress, there are modes associated with the onset of sediment motion, with the onset of suspended transport, and a main mode corresponding to intermittent suspension in between. Hill and Bowen (1982) use this idea with some success to describe sediment size distributions in the shelf-slope region off Nova Scotia.

3.3 Bedload transport

Of the many equations which have been proposed for bedload transport in rivers only three have been generally applied to the oceans:

i) the Bagnold (1966) formula
ii) Einstein's (1964) bedload function
iii) Yalin's (1963) bedload equation

All three of these techniques are semi-empirical and field studies have shown that errors in excess of 100% are common. We will briefly review each of the techniques below. For a more complete review see Graf (1971).

Table 5-VI

Bagnold's bedload transport model

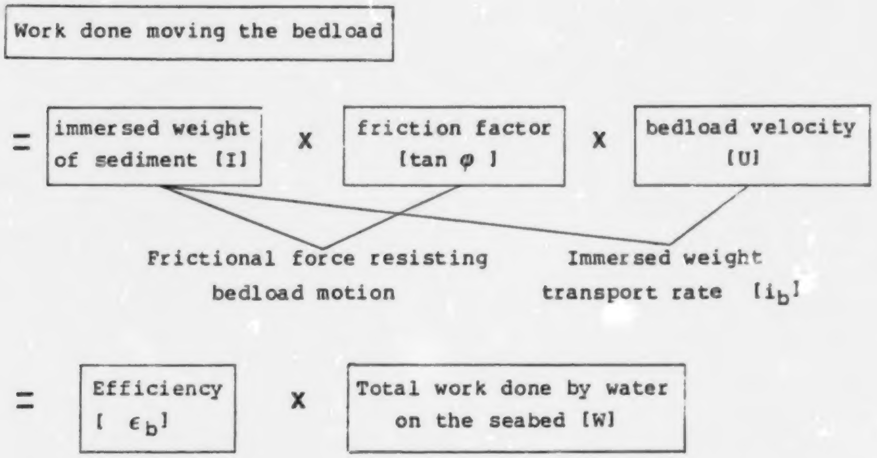
Work done moving the bedload
=
immersed weight of sediment [I]
x
friction factor [tan φ]
x
bedload velocity [U]
Frictional force resisting bedload motion
Immersed weight transport rate [i_b]
=
Efficiency [ϵ_b]
x
Total work done by water on the seabed [W]

where $I = gm_b (\rho_s - \rho) / \rho_s$ and m_b is the mass of bedload sediment above unit area of seabed.

3.3.1 The Bagnold formula

Bagnold's approach is based on a consideration of the overall energetics of the bedload transport. As such it is more satisfying from a physical point of view than the other methods, which depend upon very simplified models of forces acting on individual sediment grains. The basic ideas are shown schematically in table 5-VI. When a bedload moves down an inclined plane of slope β the frictional force must be combined with the downslope gravitational force $I\sin\beta$ and the immersed weight perpendicular to the seabed becomes $I\cos\beta$.

The bedload transport equation then becomes

$$i_b = \varepsilon_b W/(\tan\phi - \tan\beta) = K_b W \qquad (25)$$

Various expressions have been used for the work done by the fluid, W. Bagnold used the product of the shear stress and the fluid velocity. Assuming a quadratic stress law, this gives

$$W = C_D \rho U^3$$

Inman et al. (1966) on the other hand used stress multiplied by the friction velocity u_*, so that

$$W = \rho U_*^3$$

The difficulty with the Bagnold equation is the choice of efficiency parameter ε_b, or K. Bagnold (1963) finds evidence from flume and river data that K depends only on the ratio h/D where h is the water depth and D is the mean grain diameter. Kachel and Sternberg (1971), however, found that their field measurements did not agree with the Bagnold model for constant K. Sternberg (1972) combined his field data with flume data and deducted empirical curves for K as a function of the excess shear stress ($\tau - \tau_c/\tau_c$) and the sediment size. His diagrams are reproduced as Figure 5-24 . He also provides a nomogram for calculating the bedload transport once a value for K and a value for u_* are chosen

(Figure 5-25; here $j=[\rho_s/(\rho_s - \rho)g]i_b$)

Unfortunately, the Sternberg method fails to take into account the separation of total stress into a form drag and bed stress. The method, which uses the total stress, is therefore strictly only applicable in circumstances where the ratio of form drag to bed stress is the same as it was for the rippled bed where

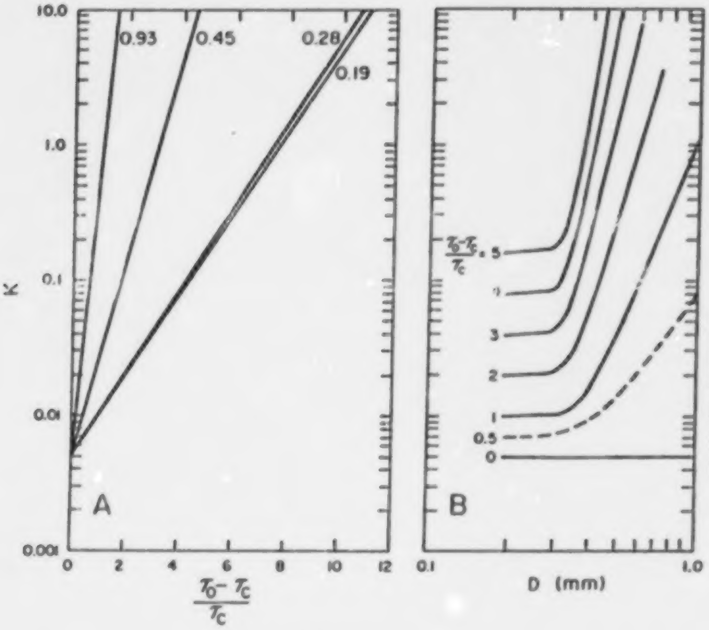

A. Relationship between excess shear stress $(\tau_o-\tau_c)/\tau_c$ and the coefficient K for various sediment sizes.

B. Relationship between sediment diameter D and the coefficient K for various values of excess shear stress $(\tau_o-\tau_c)/\tau_c$.

Figure 5-24 Relationships between the coefficient K, the excess shear stress and the sediment diameter.

By connecting any two known variables with a straight edge, the magnitude of the third variable can be read directly from the point of intersection on the scale.

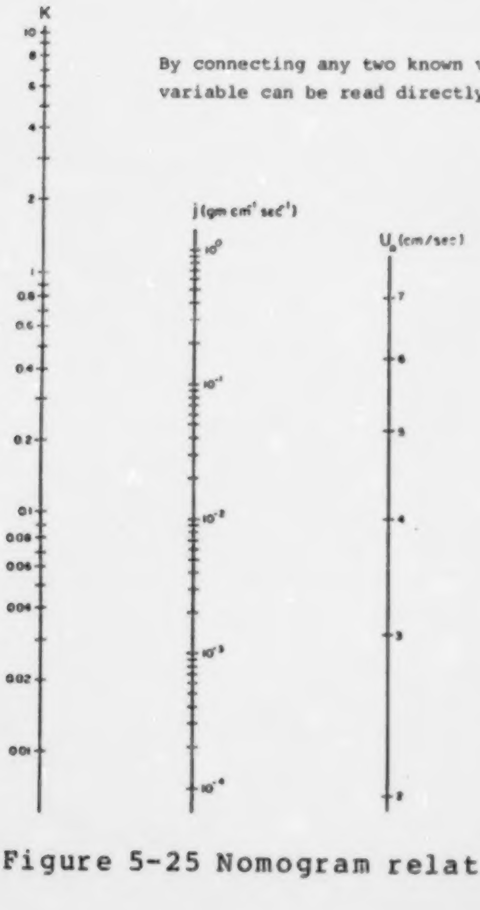

Figure 5-25 Nomogram relating U_*, j and K.

Sternberg made his measurements. Nevertheless the problem of choosing the relevant bed stress for rippled beds is common to all methods (at least if separation takes place). The Sternberg method is probably as good as any other if a properly averaged total stress is used.

3.3.2 Einstein's bedload function

Unlike Bagnold's model, for which grain-grain interactions are very important, Einstein's approach looks at the detailed force balance on an individual particle and neglects collisions between grains. The differential particle velocity around a particle on the sea bed creates a lift force on the particle through the Bernoulli effect. Once off the bed, however, this lift force reduces drastically and the particle falls back to the bed in a free fall trajectory. For bedload movement the average height of this motion is a few grain diameters and the distance travelled is about 100 grain diameters. Einstein also assumed that the probability of grain movement was related to a Gaussian distribution of the lift force about a mean.

Einstein incorporated these ideas into an empirical relationship between a hydraulic parameter and a bedload transport parameter. The details will not be given here but can be found most conveniently in Einstein (1964). Although the physical background to this approach suggests that it should be more applicable to low concentration flows, in fact the method involves the use of a number of empirically adjusted coefficients which make it more widely applicable (whilst also clouding the physics implied by the technique).

The shear stress for the Einstein method should be the flat bed stress (although there is some question about whether the laboratory measurements on which the equations are based were really made over flat beds). In principle, therefore, measured stress should be corrected for form drag before being used in the model; there are no provisions for separation-induced motion.

Brown (1950) suggested a useful simplification of Einstein's bedload function which fits the data well except at very low transport rates. His empirical equation is

$$\phi = 40\ \theta^3 \tag{26}$$

where $\phi = j/\rho\omega d$

and θ is the Shield's parameter.

3.3.3 Yalin's bedload equation

Yalin's approach is very similar to that of Einstein, dealing with a mechanistic model of individual grain motion. It differs in explicitly involving the critical stress given by the Shield's diagram. Again, although starting as an attempt to solve equations for the motion of grains, its final form involves empirical coefficients based on flume experiments. Smith (1977) gives the bedload equation in terms of the volume flux of sediment per unit flow width, Q_s $(=j/\rho)$ as

$$Q_s = a_1\ u_*S\ D(1-[\ln(1 + a_2\ S)/a_2\ S]) \tag{27}$$

where $a_1 = 0.635$

$$a_2 = 2.45\ (\rho/\rho_s)^{0.4}[\tau_c/(\rho_s-\rho)gD]^{0.5}$$

$$S = (\tau - \tau_c) / \tau_c$$

When $a_2S << 1$ this reduces to

$$Q_s = a_1 a_2 D u_* S^2 / 2 \qquad (28)$$

and for quartz sand in seawater this expression can be used for bed stresses less than 30% above the critical stress.

Again the appropriate stress for this equation is the actual seabed stress. Smith (1977) considers the Yalin equation to be the best method of estimating bedload if used in conjunction with his method of estimating bed stress from total boundary stress.

All of these currently available approaches are semi-empirical, and the failure of any to predict observed transport rates very closely suggests that their physical basis is still incomplete or inadequate. An apparently universal characteristic of bedload transport in a viscous sublayer is an along-stream streakiness or lineation of moving grains caused by organized flow structures in and near the sublayer. At least in low-concentration flows over flat beds this organization produces a shifting, irregular pattern of along-stream ridges and furrows at a scale of between 10 and 100 grain diameters. Jackson (1976) discusses some of the implications of this for the formation of bedforms and the initiation of bedload transport.

3.3.4 Bedload transport in oscillatory flows

So far we have only considered bedload transport under steady flows. There is no agreement at present on appropriate equations when oscillatory motion forms an appreciable component of the flow. Bagnold (1963) and Inman and Bagnold (1963) argued that the orbital motion of the waves, back and forth with no net transport, acts on the seabed to put sediment into motion where it can be readily moved by any net current superimposed on the wave motion. If the mean amplitude of the sediment's oscillatory velocity is U_0 then the mean oscillatory immersed weight transport of sediment is I x U_0 (I is the immersed weight of sediment in motion). By Bagnold's equation for i_b this is equal to KW. The net transport of sediment, i_m, on the other hand, will be IxU_m, where U_m is the steady flow. Thus

$$i_m = IU_m = KWU_m/U_0 \tag{29}$$

This equation forms the basis for a sediment transport equation for longshore currents in the surf zone. It is important to note, however, that it applies not only to bedload transport but encompasses suspended transport too since an equation analogous to Bagnold's bedload equation can be formulated for suspended load transport, differing only in the meaning of K.

Madsen and Grant (1977) have investigated the possibility of using the Einstein bedload function, in its modified form (Brown 1950), to estimate the total oscillating bedload transport in oscillatory flows. They find that, as with the threshold, the function works well when stress is calcuated using the wave friction factors of Jonsson (1966). They discuss possible net sediment transport which can arise when there is a sloping bottom, wave asymmetry, wave induced mean flow or a superimposed mean flow.

3.4 Suspended load transport

There is still substantial uncertainty about the relative importance of bedload and suspended load transport on continental shelves. Nevertheless, Smith and Hopkins (1972) and Smith (1977) consider bedload transport to be relatively inefficient, and suspended transport to be of primary concern.

The most complete technique for estimating suspended transport is to multiply a velocity profile by a profile of suspended sediment concentration and integrate the result over the water depth. Suspension depends upon a balance between the falling of grains under gravity and the upward diffusion of grains by turbulent diffusion in a concentration gradient. By neglecting the effect of sediment on turbulence, Rouse (1937) solved the resulting vertical advection-diffusion equation for the log layer to obtain, for sediment concentration C,

$$C/C_a = [(h-y)\; a \;/\; (h-a)\; y)]^p \tag{30}$$

where C_a is the concentration at some reference level a, usually taken as the top of the bedload layer, h is the water depth and $p=w/ku_*$ where k is von Karman's constant. Example plots of sediment concentration profiles are given in Figure 5-26. A slightly different expression is obtained by Smith and Hopkins (1972), based on a different form for the diffusion coefficient

$$C/(1-C) = [C_a/(1 - C_a)]\; [a/z]^p \tag{31}$$

The more recent coupled sediment turbulence models of Taylor and Dyer (1977) and Smith and McLean (1977) discussed in section 2.5.1 should provide more realistic profiles.

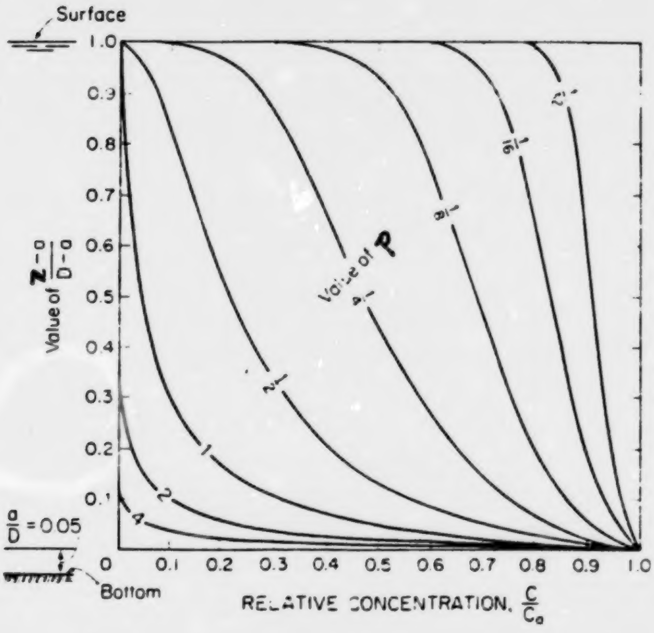

Figure 5-26 Variation in relative concentration of suspended sediment with relative depth above a datum, $z = a$ where
$a = 0.05D$ and D is total water depth.
$P = W/kU_*$ where W is fall velocity.

Figure 5-14 (from Taylor and Dyer) shows sediment profiles for a number of cases.

Note that all of these equations require a value for C_a, the concentration at the bottom of the suspended load region.

Einstein forms the product of the concentration given by equation 30 with a modified logarithmic velocity profile and integrates over the depth to obtain the total suspended sediment transport. He gives graphs of the relevant integral functions (Einstein (1964)). C_a is given by his bedload function and the reference distance is taken as a=2D. In fact, since C_a so determined is proportional to the bedload transport rate, bedload and suspended load are generally considered together in a single equation when applying Einstein's method.

Smith (1977) proceeds in a similar manner with his form of concentration profile and provides an equation (his equation 48) from which volume flux of suspended sediment "can be calculated easily on a digital computer or a programmable calculator for the particular p and C_a of concern". He also discusses a modification of the equation for the case when the sediment extends beyond the log layer. Rather than use a value of C_a from a bedload model, Smith, following Yalin (1963), uses a form which depends on the normalized excess shear stress S

$$C_a = C_0 \gamma_s S / (1 + \gamma_s S)$$

where C_0 is the volume concentration of sediment in the bed, and τ_s is a constant which was found to be =0.0112 for medium sand Smith and McLean (1977). Smith (1977, p. 565) comments that the inability to compute C_a with any degree of confidence is one of the most fundamental difficulties at present in marine sediment transport.

An alternative approach has been to use empirical equations. devised for river flow, to estimate the average concentration of suspended sediment. and to multiply this by a representative fluid velocity and water depth. Smith and Hopkins (1972) used expressions of the form

$$C_{av} = (D/h)^{7/6} S F$$

where F is either a function of u_*/w (given by Lausen 1958), or a function of D and gD/u_*^2 (given by Bogardi 1965). They multiplied the resulting values of C_{av} by velocities measured by moored current meters 3 m above the bed. The resulting estimates of transport were typically 6m^3 hr^{-1} per metre of shelf length

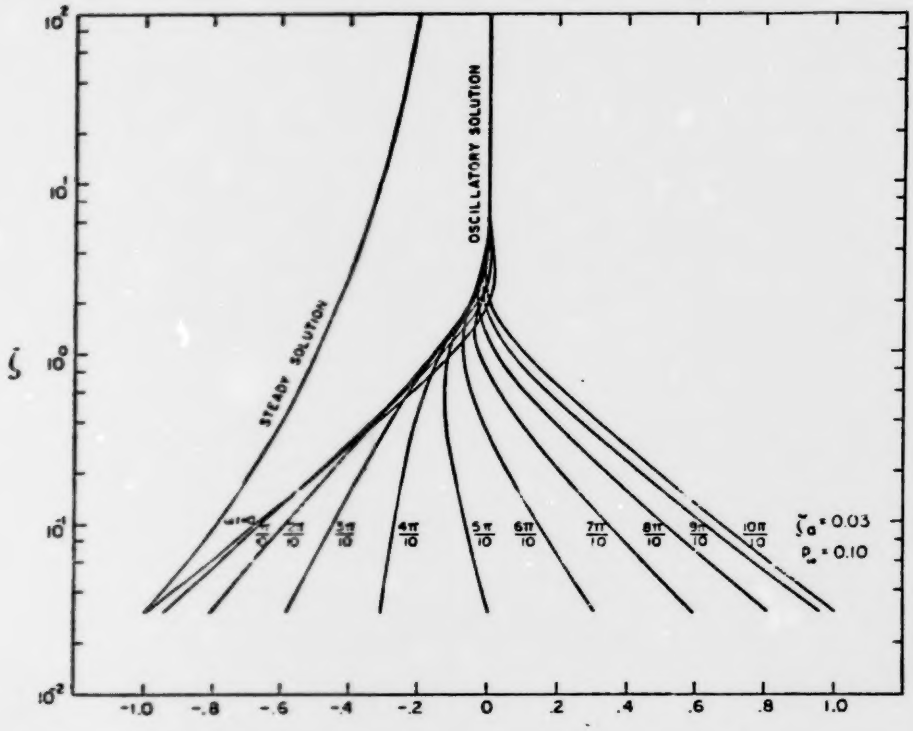

Figure 5-27 Typical shapes of suspended sediment concentration in an oscillatory boundary layer (from Smith, 1977). $\zeta = 2(wz/K_o)^{1/2}$ (see Fig. 5-09 for calculation of K_o).

when the current was 60 cm s^{-1}.

Although the crude approach used by Smith and Hopkins perhaps represents the best that can be done to estimate suspended sediment transport when very little information is available, it is clear that it can only give a rough estimate (Smith and Hopkins suggest they are within a factor of 2 or 3, but this is probably optimistic). There is general agreement that inferring suspended transport from a small number of measurements at discrete heights provides very unreliable results.

Very little quantitative information is available for predicting suspended sediment transport under combinations of waves and mean flows. Apart from the problem of predicting flow and sediment concentration profiles under oscillatory flow, the presence of ripples on the seabed immensely complicates the situation, as the laboratory experiments of Inman and Bowen (1963) and Kennedy and Locher (1972), for example, show.

Smith (1977) calculates sediment profiles under waves, assuming sinusoidal variations in concentration at each level (Figure 5-27). The implication is that this could be used along with steady flow profiles, perhaps calculated by taking into account the wave/mean flow stresses calculated by Grant and Madsen (see Section 2), to estimate net sediment transport. Bagnold's equation for wave/current environments, which was discussed above as a bedload equation is also perhaps equally applicable to suspended load transport, though it appears to have been tested against field data only in the very nearshore region.

Bowen (1980) has recently applied Bagnold's equations for both bedload and suspended transport to the wave dominated nearshore region assuming that the instantaneous response under time-varying flow can be modelled with the steady flow equations (the same assumption was made by Madsen and Grant when applying Einstein's theory to bedload transport under waves). Initial comparisons with field data are encouraging, but more data is needed to establish the viability of the method.

As with boundary layers dynamics, the major limitation for all theories of sediment transport on continental shelves is the great paucity of data from the field against which to test theories or even concepts. The problem of obtaining suitable data is magnified by the realization that most sediment transport takes place during storm conditions. There is no question that theoretical mdeas are signifmcantly outstripping the fata at present. Sucstantial efforts are being mafe to make relevant field measurements on the continental shelves, particularly around the Nosth American continent, using tripods of bottom mounted sensors (current meters, suspendef sediment sensoss, cameras, acoustic sediment profilers, and a host of other sensors), usually with highly sophisticated data logging packages, to record data remotely for long periods. It is to be hoped that these efforts, particularly the HEBBLE (High Energy Benthic Boundary Layer Experiment) project, the various projects involving members of the SANDS group, as well as the more modest programmes being funded in Canada, and elsewhere, will provide data of the right kind in the near future.

Number/
Numéro

6

Chapter 6. SEDIMENT TRANSPORT IN THE MARINE ENVIRONMENT

Alan W. Niederoda

1. INTRODUCTION

It must be stated at the outset that the scientific and engineering community's knowledge of sediment transport in the marine environment is quite limited. One needs only to reflect on the great range of environments (e.g. abyssal plain, continental rise, slope and shelf, the shoreface, beaches, estuaries, etc.), the variety of transporting agents (currents, waves, ice, gravity, etc.) and the range of sediment types, in order to appreciate the diversity and inherent complexity of this subject. Sediment transport has been studied since ancient times and rigorous physics has been applied for more than 100 years. The purpose of this chapter is to define the scope of the marine sediment transport problem, and to discuss the present state of the art of our analytic capabilities for dealing with this subject. The chapter is prepared for scientists and engineers with a good basic foundation in fluid mechanics and physics, but with a need for an overview of the mechanics of marine sediment transport. Consequently, the material will be presented selectively with the emphasis on a concise and comprehensible treatment at the expense of an exhaustive approach.

In order to provide a unified background for discussing marine sediment erosion and transport, several basics concerning the marine environment and marine sediments are reviewed. This is followed by a brief discussion of the different modes of sediment transport. After reviewing these basics, the principles of granular sediment transport theory are developed. This is followed by a development of the principles of suspended sediment transport. After the factors governing sediment transport have been established, the factors determining erosion, transport and deposition are reviewed for both bedload and suspended sediment transport.

2. BASICS OF MARINE SEDIMENTS

Before proceeding with a discussion of the analytic techniques which are available for studying and, in limited cases, predicting erosion and transport of marine sediments, it is well to establish a common background on the general subject of marine sediments. Points established in this section will then be utilized in later sections of this chapter.

2.1 Sediment Types

Sediments in the marine environment come from three major sources. Close to the continents, the major sediments result from the weathering and erosion of rocks and soils on the continent. Over geologic time periods sea level is not constant. As a consequence. many areas that are presently parts of the continental shelf have been subject to this type of erosion in the relatively recent geologic past. Another source of marine sediments is from biological production in the ocean. The volumetrically most significant source of these sediments are locally important, such as corals and algae in coral reef environments. Finally, a very small portion of marine sediments is derived chemically from the ocean. In certain restricted environments, calcium carbonate is directly deposited. In many cases, the chemical deposition of calcium carbonate surrounds a very small nucleus and produces an extremely spherical calcium carbonate sand grain. Volumetrically, the contintental source of marine sediments is the most important.

The total composition of marine sediments is extremely variable. Most marine sediments consist of grains of individual minerals. Seafloor deposits may be heterogeneous or homogeneous in collections of mineral types: the occurrence of multimineralic sediment grains also occurs, although it is uncommon. The composition of the minerals which make up marine sediments is extremely varied. There are more than 2.000 different minerals known, all of which occur in varying concentrations in the marine environment. A comprehensive discussion of the full range of minerals found in the marine environment is beyond the scope of this chapter. For the purpose of discussing marine sediment dynamics, it suffices to point out that there is only a small number of minerals which are important, and that they have many common mechanical properties. Perhaps fortunately, the chemical composition of the earth's crust and various chemical laws conspire to make more than 90% of earth surface materials out of a mere 8 minerals. For the purposes of discussing sediment transport in the marine environment this list is even more abbreviated by the relative chemical and physical instability of some of these minerals. Although rarer minerals will not be discussed, it is good to bear in mind that minerals such as garnet, diamond, rutile and gold, among others, are valuable economic resources in marine sedimentary environments. It is the very scarcity of these minerals that makes them valuable.

For engineering problems, the primary minerals which make up marine sediments are quartz, the feldspar group, calcite and the clay mineral group. Quartz. feldspar and calcite generally form blocky grains which may be angular or rounded. The crystal chemistry of these minerals is relatively simple and stable. There is relatively low chemical activity at the grain surfaces and strong chemical bonds within the mineral grains. This results in producing grains which, when reduced to sand size, resist further abrasion. Furthermore, deposits of these grains exhibit little cohesion due to electrostatic interaction of their grain surfaces.

The clay mineral group is a very important constituent of marine sediments. This group of minerals actually consists of several dozen individual minerals. Each clay mineral has a distinct crystal chemistry and structure, but to add to the complexity the chemical composition and crystal structure often varies, within limits. This chapter must ignore their complexities and focus on the properties of the clay mineral group which affect their mechanical behaviour. Clay minerals form near the earth's surface through the alteration of other minerals. They tend to have very small size, as well as a distinctly platey shape. An ordinary sheet of mica belongs to the same general mineral group and exhibits the same platey shape on a large scale which characterizes fine clay minerals. The crystal chemistry of the clay mineral group is complex. This results in producing rather large areas of the grain surfaces which do not have molecular electroneutrality. Put another way, various areas of the fine clay particle mineral surfaces are charged with negative or positive imbalances. The fine size of clay particles appears to be caused by the complexity of the crystal chemistry leading to mechanical stresses in the grain which do not permit formation of mineral grains above microscopic size. Therefore a deposit of clay is made up of a tremendous number of individual grains which are very small, and the total deposit has a very large total surface area. The imbalanced electrostatic charges at the grain boundaries interact and form a prime reason for the cohesive behaviour of clay deposits. We will point out later that changes in this cohesive behaviour can be brought about by changes in the chemical, as well as biological and mechanical environment of the clay deposit.

2.2 Sediment Size

Marine sediments range in size from house-size to colloidal-size particles. The overwhelming majority of these sediments can be classed as gravel, sand, silt or clay. Gravel generally consists of rock fragments. As rock fragments, each particle is made up of numerous mineral grains which are cemented together. Weathering and disaggregation of rock material leads to sand, silt and clay. A very large amount of the mineral grains in primary rocks are sand-sized. As these rocks weather and disaggregate, they release these mineral grains as sediments. Experiments conducted by P.H. Kuenen indicated that sand-sized particles undergo only minor abrasion as they are transported in river and ocean environments. The abrasion is primarily characterized by the rounding of angular edges as the grains collide during transport. After rounding has occurred, very little further abrasion develops. Kuenen felt that the reason for this lack of significant abrasion during transport of quartz and feldspar sand grains is that the impact developed by grain-to-grain collisions in water is small compared to the strength of these minerals. Therefore, sand-size material is quite stable and resistant to mechanical wear. The fragments broken from angular grains, as well as resulting from the rare splitting of larger sand grains, produce silt deposits. While sands range in diameter from 2 mm to .0625mm, silts range in size from .0625 mm to .0039 mm. Although mechanical abrasion of rocks and minerals can prodce grains smaller than silt, the main constituents of this finer population are clay minerals. This fine size range is called clay. Therefore, clay is both a mineralogical term and a size term. It is often easy to confuse the two usages of this word. Clay minerals result primarily from chemical weathering of the parent rocks. Minerals such as feldspars, micas, amphibole and pyroxenes have crystal structures and chemical compositions which can lend themselves to alteration and formation of clay minerals. As pointed out earlier, the atomic lattice of clay minerals is complex, and subject to both mechanical stress and electrical charge inequalities. This results in causing clay minerals to be characterized by very fine grains.

Several ways have been devised to measure and describe the size classes of sediments. These are shown in Table 6-I. A common method for making this division is to divide sediment sizes into classes defined by a geometric progression based on the factor 1/2. Therefore, coarse sand ranges in size between 2 and 1/2 mm in diameter, medium sand ranges down to 1/4 mm in

Table 6-I

Grain size scale for sediments

U. S. Standard Sieve Mesh #		Millimeters	Microns	Phi (ø)	Wentworth Size Class	
		4096		-12		GRAVEL
		1024		-10	Boulder (-8 to -12ø)	
Use		256		- 8	Cobble (-6 to -8ø)	
wire		64		- 6		
squares		16		- 4	Pebble (-2 to -6ø)	
5		4		- 2		
6		3.36		-1.75		
7		2.83		-1.5	Granule	
8		2.38		-1.25		
10		2.00		-1.0		
12		1.68		-0.75		SAND
14		1.41		-0.5	Very coarse sand	
16		1.19		-0.25		
18		1.00		0.0		
20		0.84		0.25		
25		0.71		0.5	Coarse sand	
30		0.59		0.75		
35	1/2	0.50	500	1.0		
40		0.42	420	1.25		
45		0.35	350	1.5	Medium sand	
50		0.30	300	1.75		
60	1/4	0.25	250	2.0		
70		0.210	210	2.25		
80		0.177	177	2.5	Fine sand	
100		0.149	149	2.75		
120	1/8	0.125	125	3.0		
140		0.105	105	3.25		
170		0.088	88	3.5	Very fine sand	
200		0.074	74	3.75		
230	1/16	0.0625	62.5	4.0		
270		0.053	53	4.25		MUD
325		0.044	44	4.5	Coarse silt	
		0.037	37	4.75		
	1/32	0.031	31	5.0		
	1/64	0.0156	15.6	6.0	Medium silt	
Analyzed	1/128	0.0078	7.8	7.0		
	1/256	0.0039	3.9	8.0	Very fine silt	
by		0.0020	2.0	9.0		
		0.00098	0.98	10.0		
Pipette or		0.00049	0.49	11.0	Clay	
		0.00024	0.24	12.0		
Hydrometer		0.00012	0.12	13.0		
		0.00006	0.06	14.0		

diameter, fine sand ranges down to 1/8 mm in diameter and so forth. Geologists frequently use a 'phi' scale devised by Krumbein. This scale is also shown on Table 6-I.

For our purposes, it is sufficient to know that sand, which makes up a major component of marine sediments, ranges in sizes from 2 mm to 1/16 mm. As a result, the finest sand grain corresponds in size to about the smallest dot which can be seen by the unaided eye. Silt ranges from 1/16 mm to 1/256 mm. This roughly corresponds to a size range from the smallest dot which can be seen with the unaided eye to the size at which a sediment deposit feels smooth rather than gritty. Clay sizes range from 1/256 mm to particles so small as to be considered colloidal in size.

Even relatively pure deposits of one type of marine sediment are not characterized by a single size for all grains. A great wealth of literature has been devoted to this subject. In general, the size of particles in sedimentary deposits tends to follow a Gaussian distribution. The second, third and fourth moment measures of these distributions (standard deviation, skewness and kurtosis) can be quite variable. Furthermore. sedimentary deposits are often mixtures of more fundamental size distributions. The overall use and complexity of data concerning sediment grain size distributions is beyond the scope of this text. It is merely pointed out that the simplifying assumptions which are made later in this chapter must be carefully applied to real situations.

2.3 Sediment Shapes

As there can be considerable variability in the mean grain size, standard deviation, skewness and kurtosis of marine sedimentary deposits there are also considerable variations in the shape of characteristic sedimentary grains from different deposits. Common quartz and feldspars most frequently produce blocky grains. They range in shape from angular irregular grains through various ellipsoidal shapes, although they can be abraded to nearly spherical shapes. Typical ranges in these shapes and roundnesses of sand grains was developed by Powers (1953), and is shown in Fig. 6-01.

Clay particles tend to be platey in shape. As pointed out earlier, the irregular platey outline of ordinary mica is a good model for the shape of fine clay grains. This shape may have some relevance in considering erosion, deposition and transport of marine sediments, but it is important to recognize that the high electrostatic charge imbalances of clay mineral grain surfaces generally results in clays being transported in sedimentary grains made up of a large number of individual clay mineral particles. Such grains are called flocculates. The shapes of these flocculates can be varied, but tends toward blocky to spherical shapes. Because such grains are made of a large number of individual clay mineral particles which are loosely adhering to one another, the overall density of flocculate grains is very low.

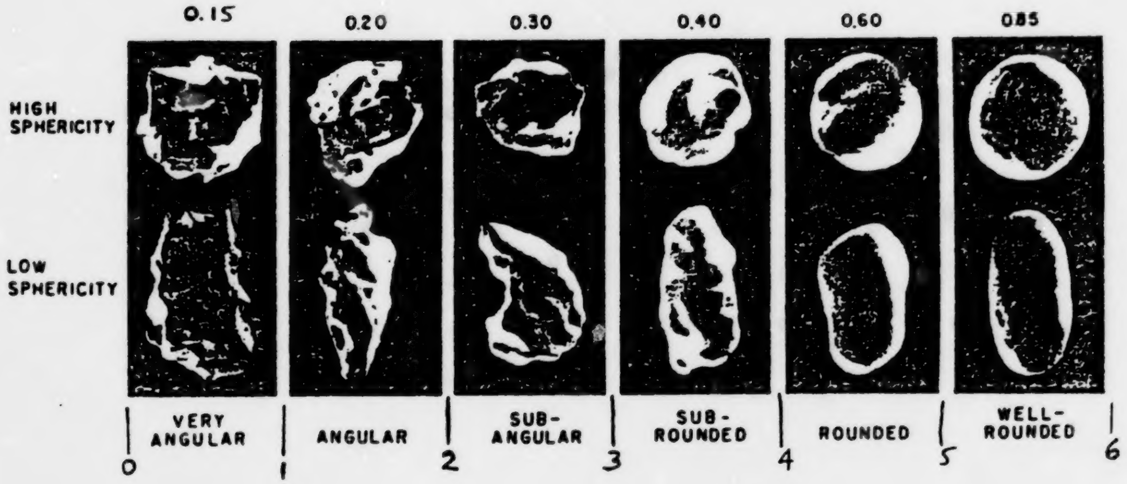
0.15
0.20
0.30
0.40
0.60
0.85
HIGH SPHERICITY
LOW SPHERICITY
VERY ANGULAR
ANGULAR
SUB-ANGULAR
SUB-ROUNDED
ROUNDED
WELL-ROUNDED
0
1
2
3
4
5
6

Figure 6-01 Qualitative roundness and sphericity illustrations for sand grains (from Powers, 1953).

3. CHARACTERISTICS OF MARINE FLOWS AND SEDIMENT TRANSPORT

In the first section of this course, we discussed a wide variety of flow types which characterize continental shelf environments. In Chapter 5, we reviewed the dynamics of marine boundary layers. At this point, we wish to link these two discussions so as to begin to establish the relationship between flow dynamics and sediment transport dynamics. Given the wide range of length scales and time scales which are required to characterize continental shelf water motions and boundary layers, it is clear that we will need to be highly selective in our approach. We must apply this selectivity so as to generate a list of flow kinematics which can be related to the basic principles of sediment dynamics. It must be stressed that this is an area of active research. In most cases, we will ignore vexing difficulties which are the subjects of current research, and stress engineering approaches which provide methods for forming understanding of the basic processes involved and, in certain cases, provides a methodology for estimating rates of sediment transport, erosion and deposition.

3.1 Modes of Marine Sediment Transport

Sediment is moved in almost all marine environments. The actual modes in which the sediment is transported are difficult to separate in nature, because there are frequently strong interactions between various modes. However, in order to provide a simplified starting point, it is common to describe sediment transport modes in terms of suspended transport, bedload transport, and mass movement.

Suspended transport develops as a result of the interaction of turbulent eddy motions in the flow and settling due to gravitational forces acting on sediment particles. This subject will be discussed in much greater detail later in this chapter. At this time, we wish only to discuss this mode of transport in a most generalized way.

Picture a very simple situation, where a fluid undergoing turbulent flow has suspended within it a given concentration of very small, and thus slowly settling, sediment particles. Let us imagine that the turbulence parameters are uniformly distributed throughout the depth of the fluid. Such a condition can be contrived through the use of a turbulence jar as shown in Fig. 6-02. A stack of coarse screen meshes is oscillated up and down to produce the uniform turbulence in such a jar. If the initial condition is such that the sediment particles are uniformly distributed throughout the depth of the flow, we can see that two factors influence their settling. Because the sediment has a higher density than water, the gravitational forces override the buoyancy forces and cause the particles to settle. The rate at which they move downward through the fluid is governed by a balance between the gravitational force and fluid drag acting to inhibit the downward motion of the particles. Superimposed on this is the isotropic turbulent motion of the fluid. We envision this as a series of roiling eddies. As the initial condition, the eddies have little net effect on the distribution of particles in the fluid. Since there is no vertical sediment

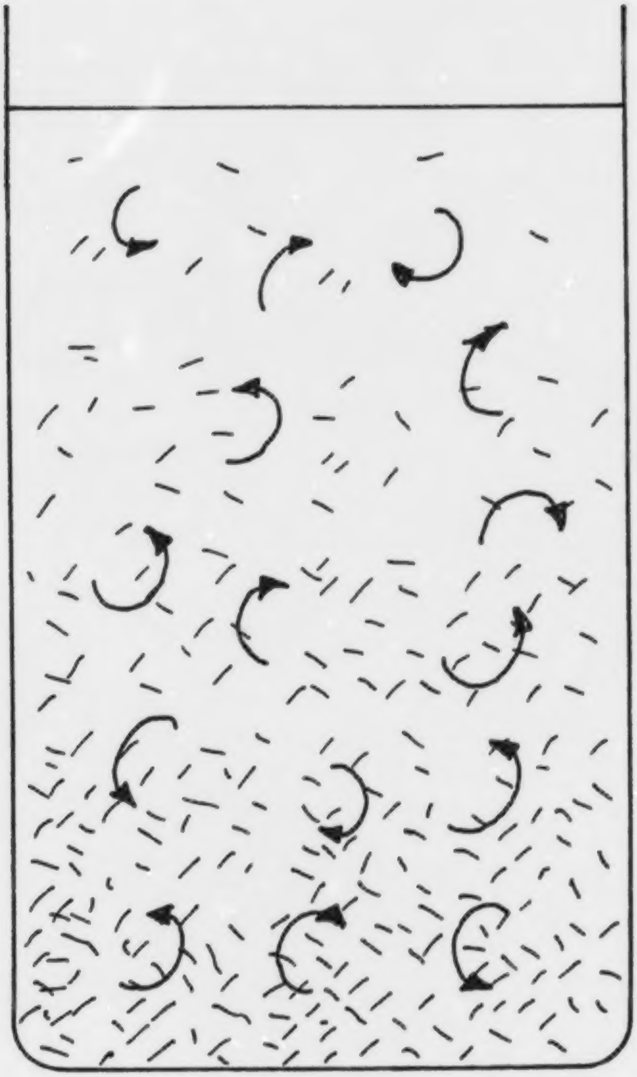

Figure 6-02 Schematic illustration of particle settling in isotropic turbulence.

concentration gradient at this time, the downward moving eddies and upward moving eddies displace volumes containing roughly equal amounts of the particles. However, there is a net downward motion of the particles relative to the fluid due to their settling. Thus, after some time, a concentration gradient develops, with lower concentration of suspended sediment toward the top of the fluid and higher concentration of sediment toward its bottom. In the presence of this concentration gradient, the situation is changed. Figure 6-03 shows an imaginary horizontal plane superimposed on this fluid; the turbulent eddies can move either upward or downward. On the average, the upward and downward motions will balance in simple isotropic turbulence. However, the downward-moving eddies will advect volumes of water containing fewer sediment grains than the upward-moving eddies, owing to the average increase in sediment concentration with depth. This process tends to move fine sediments upward in the fluid in a process very similar to diffusion of any material property in a turbulent fluid. It should then be easy to envision a balance between the upward turbulent diffusion of sediment concentrations due to the eddy motions, versus the net downward motion of the sediment particles due to gravitational settling. When such conditions are met, a given concentration of sediment, on the average, can be supported within the flow. This concentration is set by the average settling behaviour of the particles and the average behaviour of the turbulent eddies. If the turbulence is created as the result of fluid shear stresses developed in a moving water mass, then the suspended sediment is

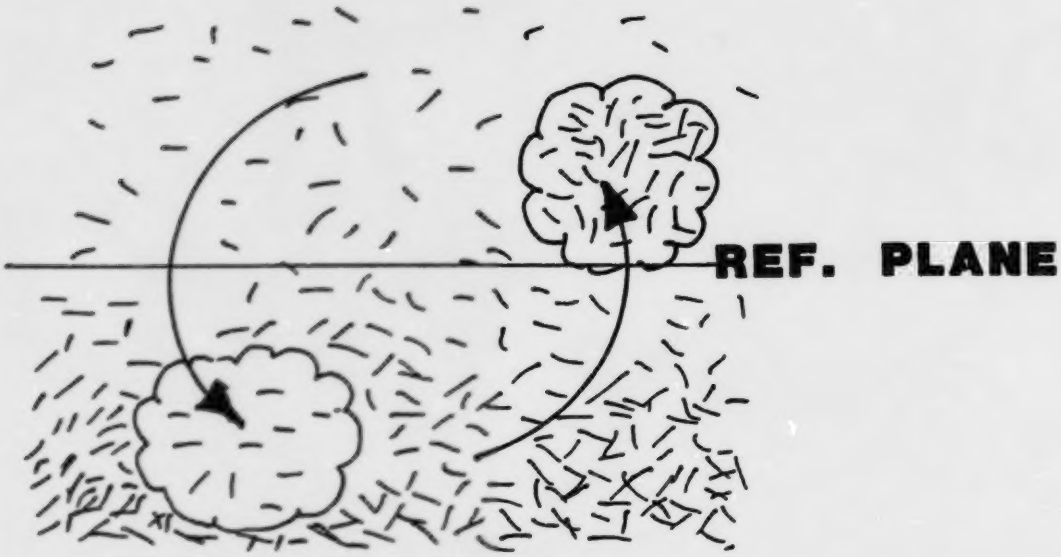

Figure 6-03 Schematic diagram of upward and downward advection of suspended particles.

transported. Thus, the distribution of turbulent shear stresses within the fluid is an important consideration in studying suspended sediment transport.

Bedload transport constitutes a different mode of sediment movement. Figure 6-04 shows a schematic of the bedload transport mode. Sediment particles may slide, roll or bounce along the sediment water interface. The general forces which cause this mode of sediment motion are shown in Figure 6-05. These forces consist of drag forces and pressure forces. They can be resisted by gravitational forces or cohesive effects. In the following, more detailed discussion of bedload sediment transport, we will show that it is presently not possible to analyze bedload transport by completely defining these forces. This is caused by the great variation in these forces, depending upon the exact

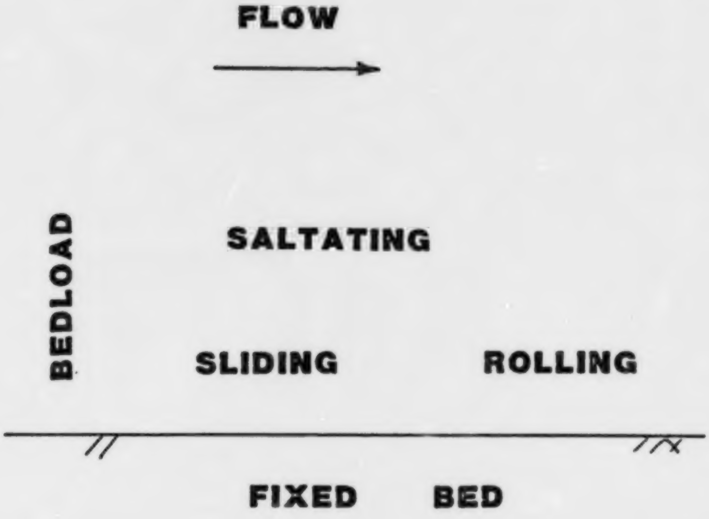
FLOW
BEDLOAD
SALTATING
SLIDING
ROLLING
FIXED BED

Figure 6-04 Schematic diagram of bedload transport.

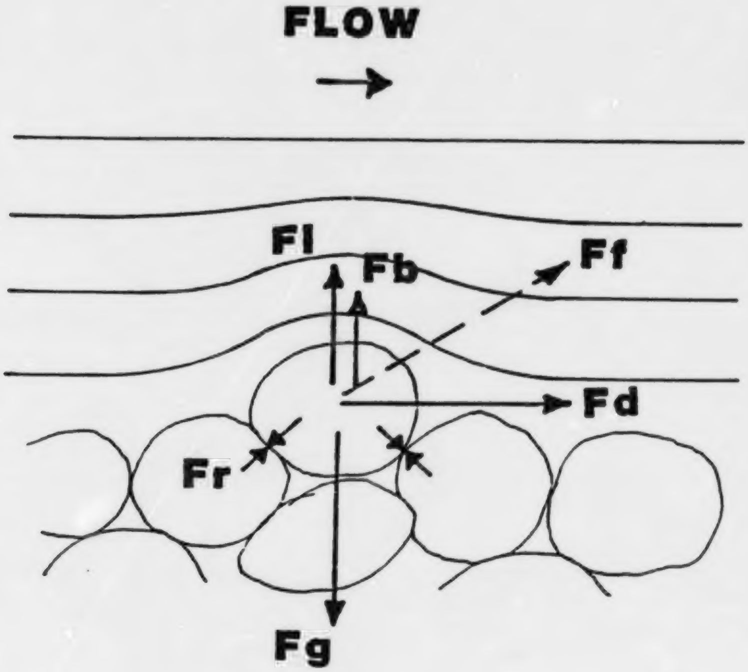
FLOW
Fl
Fb
Ff
Fd
Fr
Fg

Figure 6-05 Schematic diagram of forces causing bedload transport.

nature of the flow conditions and the exact type of sediment. Progress in defining bedload sediment transport results from generalizing the nature of a flow-sediment interaction, to relate the average level of fluid shear stress acting on the sediment bed to the magnitude of the forces tending to stabilize particles within the bed. Thus, the flow boundary layer shear stress acting on the bottom is a critical parameter in these studies.

Sediment mass movements generally result from an internal instability within the sediment mass. Briefly, the movement occurs as a result of exceeding the shear strength of the sedimentary deposit by the shear stresses produced primarily by gravitational effects. We will show later that pressure forces developed from wave motions can provide a trigger mechanism for such instabilities.

3.2 Benthic Boundary Layer Components

In a typical marine environment there are many boundary layers, and these frequently interact with one another. Wind stress acting on the sea surface creates a boundary layer at the air-water interface. Internal boundary layers can develop from opposed flow across pyncnoclines (density interfaces) in stratified flow conditions. Upwelling and downwelling can develop in areas of convergence and divergence over the mid-shelf and in the coastal boundary layer. Such up- or downwelling conditions produce boundary layers between surface and near-bottom flow zones. Of course, any flow impinging on the sediment-water interface results in producing a boundary layer.

The general boundary layer at the sediment-water interface is commonly referred to as the benthic boundary layer.

The benthic boundary layer can have many components. Slowly varying wind-driven or thermohaline currents can produce benthic boundary layers which interact with more rapidly varying tidal flows. One of the highest frequency flows affecting the sediment-water interface results from wave orbital velocities. Because of the rapidly reversing nature of this flow, the boundary layer is always thin. Recent work by Madsen and Grant (1976), Jonsson (1966) and others indicates that various boundary layers cannot be treated in isolation. A strong, nonlinear interaction develops between boundary layers related to flows of different frequencies. However, for the purposes of simplifying our discussions, we will begin by looking at idealized components of these flows. Fundamental division is made between wave orbital boundary layers and slowly varying benthic boundary layers. In subsequent discussions, we will occasionally treat both these as isolated occurrences. It is good to keep in mind that they are seldom really found in this condition.

Furthermore, we will frequently treat the slowly varying benthic boundary layer as though it were characterized by a relatively consistent turbulent behaviour. There is no a priori reason to expect this. In fact, one might expect that the vertical distribution of horizontal shear stresses, and thus the nature of the turbulence, should vary in the benthic boundary layer depending upon the mode of origin of the flow. However, successive field measurements indicate that a constant stress layer with a logarithmic mean velocity profile often characterizes the bottom 1 to 3 metres of benthic flows. Certainly, exceptions must exist, but there are not enough field measurements at this time to describe these conditions fully.

3.3 **Cohesive and Non-Cohesive Sediment Erosion**

From the above discussions, we see that suspended sediment transport is governed by the distribution of internal Reynolds stresses in a turbulent boundary layer, as well as the distribution of fluid shear stresses at the sediment-water interface. Bedload transport is controlled primarily by the distribution of the fluid shear stress at the sediment-water interface. The forces tending to stabilize sedimentary deposits are also important. Sands, gravels and many silts are made of sediment particles which generally have small intergranular electrochemical interactions resulting from regions of electrostatic charges on the grain surfaces. These forces are generally so small when compared to the gravitational forces that they are neglected. Such sediments are referred to as non-cohesive granular sediments.

On the other hand, clay particles frequently are bound together in sedimentary deposits. This binding has many origins, but appears primarily to result from electrostatic interactions between individual fine grains. Such binding is further enhanced by the effect of bottom organisms which burrow through mud deposits and cement particles together with organic mucous. Because of the small size, and thus low weight, of individual clay particles, as well as the relative strength of these intergranular bonds, such clay deposits are not primarily stabilized by gravitational effects. Thus when studying erosion of such deposits, it is necessary to understand the nature of the intergranular cohesive forces.

For the purpose of discussing the principles of sediment transport, erosion and deposition theory, we will divide our considerations into a discussion of non-cohesive sediment transport, and a discussion of cohesive sediment transport.

4. PRINCIPLES OF MARINE BEDLOAD DYNAMICS

4.1 Introduction

Now that the background has been established with respect to the overall nature of marine sediments and the very general nature of sediment transport in the marine environment, we turn our attention to a more rigorous treatment of the subject of marine bedload dynamics. It is good to stress that this is an area of active research, which means that many of the existing analytic formulations are merely approximations of the actual natural processes. The general aim of this section is twofold. On one hand, the existing theories and analytic approaches to this subject will be systematically developed. On the other hand, the areas where critical simplifying assumptions are made, and especially where these simplifying assumptions limit the applicability of the theory, will be pointed out. The point is not to confound the reader; it is to show clearly the balance between the strengths and weaknesses of present solutions.

The question of marine bedload transport must be broken down into sub-components to formulate an understanding. First, a description is given of bedload sediment transport to illustrate all of the phenomena involved. Once this has been established, a development of the analytic treatments of bedload transport dynamics will be given. Throughout these discussions, we will start with relatively simple conditions as yielded in steady uniform flow. This condition is met in some tidal estuaries and in some deep areas of the continental shelf during calm weather conditions. However, it is not until we can treat both unsteady and non-uniform flow that we can form an appropriate understanding of the dynamics of marine bedload transport in its full extent.

4.2 Description of Bedload Transport

A synthesis of the observations from a number of researchers (Bagnold, 1966; Einstein, 1942; Everts, 1973; Martin, 1963(b); Meland and Norrman, 1969; White, 1940) who have used flumes to observe bedload transport, yields the following general description. Envision a flat bed of relatively uniformly-sized granular sediment exposed to a steady uniform flow of sufficient intensity to cause bedload transport. Under these conditions, the sediment is transported in three principal modes. Some grains simply roll across the surface of the bed (Fig. 6-06), others slide over the surface (Fig. 6-06). Finally, many of the grains are momentarily lifted above the bed, carried downstream by the flow as they fall back toward the bed, and either bounce upward again or become lodged among the other grains (Fig. 6-07). The relative proportion of grains undergoing transport in each of these three modes is constantly changing. Furthermore, an individual grain may lift from the bed and bounce downstream for two or three hops before it comes to rest. Its next movement may take place by rolling or sliding. If the flow velocity is dramatically increased, these processes will occur more vigorously. and with an increased frequency. Under these conditions, it will appear as though there is a zone of sediment

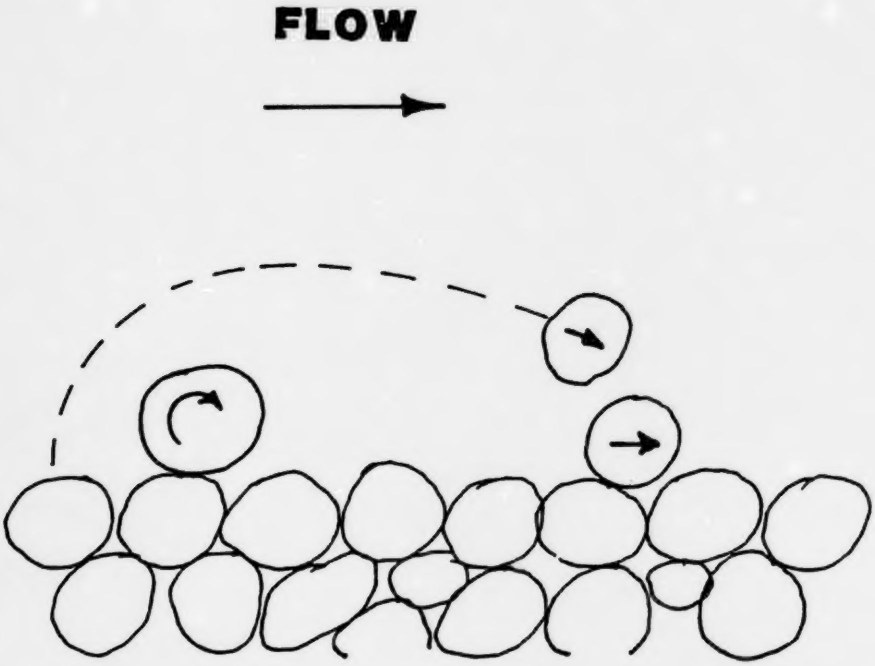

Figure 6-06 Representation of the rolling, sliding and saltating modes of bedload transport.

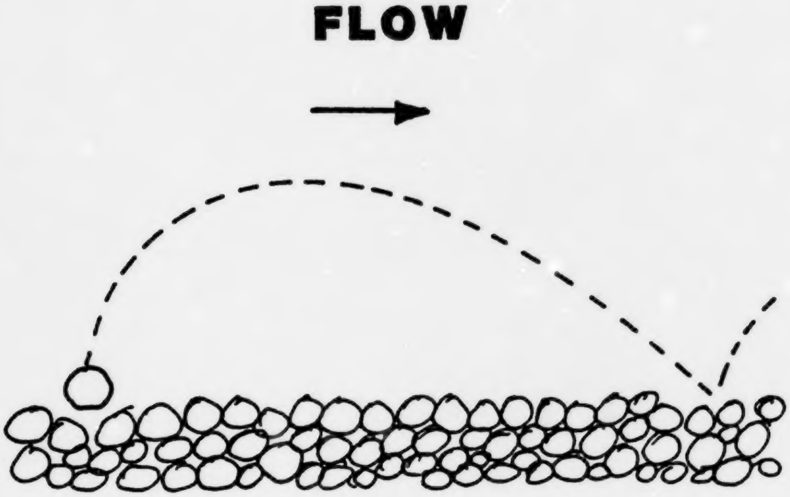

Figure 6-07 Trajectory of saltating bedload grain.

in transport extending from the upper limit of particle trajectories in the flow down to several grain diameters below the previous level of the undisturbed bed. Some researchers have likened the appearance of this zone to a fluidized layer being moved rapidly downstream.

Because of the complexity of modes of movement of bedload, it is difficult to ascribe particular importance to one mode over another. However, various sediment transport theories have departed over this point. For example, Einstein (1950) has described the results of flume experiments on the stochastic nature of sediment transport. He focuses particularly on the trajectory of saltating (bouncing) grains. Detailed photographic measurements (Middleton and Southard, 1977) indicate that the first motion of a saltating grain is vertically upward. This may be caused by a lift force generated by the flow over the partially exposed upper grain surface. As soon as the grain lifts more than a few grain diameters above the bed, this lift force vanishes. The particle appears to take on a nearly ballistic trajectory from this point. Einstein's work indicates that the average path length of this trajectory is independent of flow conditions. His experiments show that the average particle excursion length is in the order of 100 grain diameters.

Due to the difficulty in observing very small grains moving very rapidly there is little information concerning the nature of the time history of movement of individual grains. A synthesis of observations indicates that individual grains may move via any of the bedload transport modes for distances ranging from several to several hundred particle diameters. However, their motion is generally eventually arrested, and they come to rest within the bed material. Therefore, the history of motion is an interspersal of rapid motion events with episodes of burial and rest. Not only is the movement of individual grains somewhat episodic, but the general movement of bedload can be episodic as well. The turbulence of natural flows appears to produce variations in the intensity flow near the bed. Therefore, areas of the bed may momentarily witness more vigorous flow and transport than surrounding areas.

If the mean grain size of the sediment bed is less than approximately 0.6 mm, the movement of grains tends to produce semi-regularly spaced deposits which develop into ripple marks. Under most flow conditions, these ripple marks slowly migrate downstream via erosion of their upstream slope and deposition on the downstream side of the crest (see Figure 6-08).

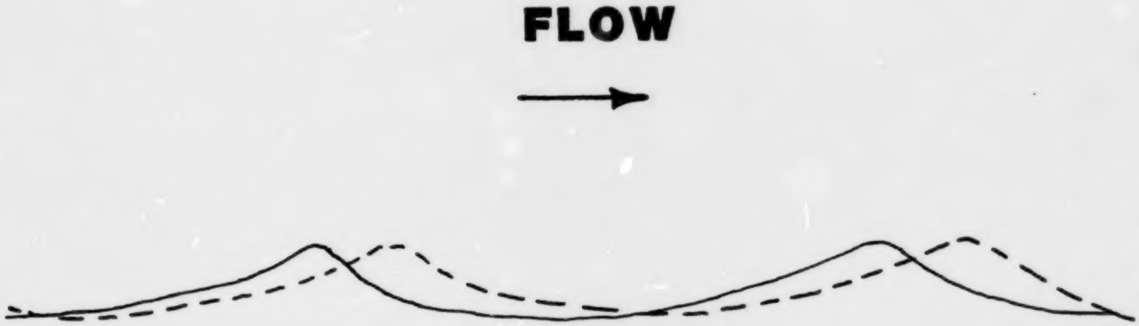

Figure 6-08 Schematic representation of ripple mark migration.

Thus, the individual grains may be transported rapidly from their site of erosion to the next site of deposition. They are then buried within the migrating ripple mark until they can be exposed again on the eroding upstream face. Thus, the rate of bedload transport in these conditions is more fundamentally controlled by the rate of ripple mark migration than by the rate of individual bedload particle motion.

The dynamics of ripple marks and other bed formations are ecovered in a later chapter. At this point, we merely point out that it is possible to have a hierarchy of migrating features on the seafloor. Individual ripple marks may form on the upstream side of larger features called sand waves. The bedload transport processes in areas characterized by such sand waves are mainly controlled by erosion on the upstream side of the sand wave with corresponding deposition on the downstream side. Here again, the overall rate of bedload transport is a function of the rate of migration of the large sand wave rather than that of the individual ripple marks or the individual grains.

The situation is made even more complex when the effects of poor sorting and irregular particle shape are taken into account. Everts (1973) showed that if a sediment bed, composed of nearly uniform sand grains, is exposed to a flow whose intensity is not quite strong enough to initiate bedload transport, and a sediment bedload of differing grain size distribution is introduced, this latter grain size distribution will overpass the pre-existing bed. Larger particles tend to roll and slide over the quiescent bed. Over-passing populations of grains which are smaller than the bed appear to move primarily through saltation. Middleton and Southard (1977) point out that the movement of bedload is strongly affected by the average particle shape. Particles whose shapes are that of prolate ellipsoids or rounded disks tend to roll more easily than others. Relatively platey or flattened particles tend to imbricate. (The imbrication has the appearance of a shingled roof; each flattened grain tends to tuck in behind the next). The resulting deposit is harder to erode and transport than a corresponding one made of spherical grains.

Nearly all of the field and flume observations which have been made concerning bedload sediment transport arrive at the conclusion that a certain intensity of flow is required before the sediment begins to move. As with the above described bedload transport condition, the initiation of bedload movement is made more complex by consideration of whether the bed is flat or in a rippled condition. If the flat bed condition is considered, then an experiment can be envisioned. A flat bed of nearly uniform sand is exposed to a weak flow. As the flow intensity is increased, a few of the grains, perhaps those resting in particularly unstable places, will roll or topple over. As the flow is increased, individual grains will periodically travel over the bed for short distances before coming to rest. With further increase in flow intensity, the majority of the grains will begin to undergo semi-continuous motion. Meland and Norrman (1969) distinguish three stages of grain motion. The first stage is stop-and-go motion, the second stage consists of continuous motion in contact with the bed, and the third stage consists of grains being lifted over the bed in long jumps.

The many variations in the way that bedload transport is initiated, as well as in the modes in which it occurs, have caused many difficulties in communicating the results of various experiments. The general body of information has grown up somewhat haphazardly, owing to lack of agreement in the exact nature of the transport processes. Thus, some researchers have explored the conditions necessary to initiate bedload transport with high-speed photography, and have counted the point of transport initiation as the first movement of grains. Others have used the onset of the phase of vigorous bedload transport for the same parameter. In order to progress in light of these ambiguities, we will need to take an engineering approach which glosses over many of the details and difficulties.

4.3 Dynamics of Bedload Transport in Steady Uniform Flow

The previous section of this chapter has described in some detail the complexity of bedload transport. In this section, the various analytic approaches to analyze bedload transport are developed. Before developing these approaches, it is necessary to digress from the main direction of development to discuss the factors controlling settling velocity of sediment grains in water. This information is necessary later in our discussion of the Einstein-Brown bedload transport formulation. After developing the section on particle settling velocities, the major theories concerning the dynamics of bedload sediment transport in steady uniform flow are developed.

4.3.1 Settling Velocity of Sediments

A brief digression is made here to explore the question of settling velocity of sediment particles. The information developed in this section will be used both in later developments on bedload transport and in a subsequent section on suspended sediment transport. The actual factors governing the settling of sediments in the marine environment are quite complex. It is best to initiate this discussion with the simplest possible case. Figure 6-09 shows a diagram of a spherical particle slowly settling through a still liquid. If the settling velocity is very small, then the flow around the particle will be laminar and close to the ideal potential flow solution. The particle is driven downward by its immersed weight which is the resultant of its dry weight minus the effect of buoyancy. The distribution of shear and pressure forces developed by the settling of the particle through the fluid are also shown in Figure 6-09. As small particles settle slowly through water, it is easily seen that a particle starting from rest will acceslerate to its terminal velocity in a short distance. At this terminal velocity, it is moving with a uniform speed, and the immersed weight force is exactly offset by the drag force.

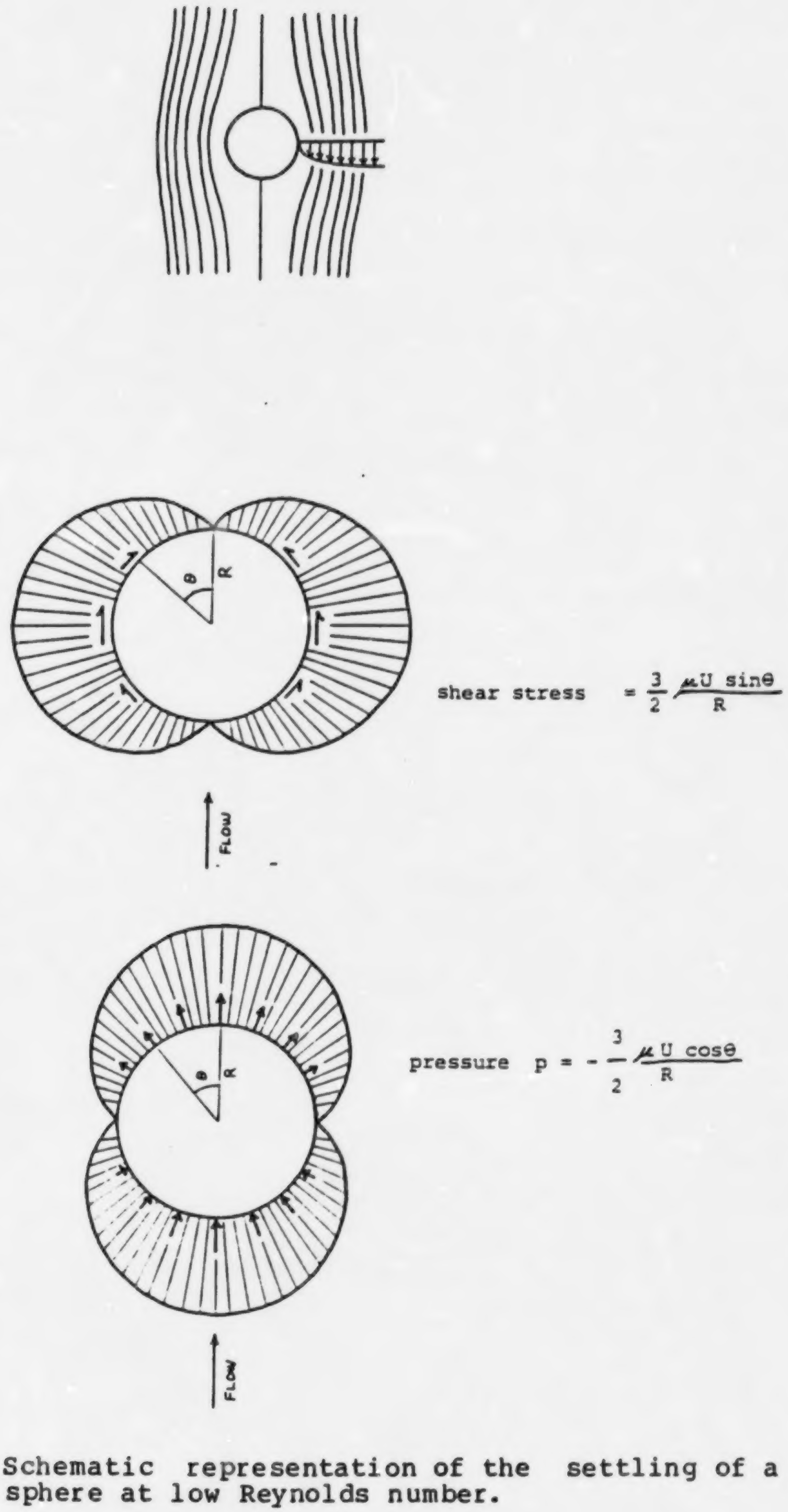

shear stress $= \frac{3}{2}\frac{\mu U \sin\theta}{R}$

pressure $p = -\frac{3}{2}\frac{\mu U \cos\theta}{R}$

Figure 6-09 Schematic representation of the settling of a small sphere at low Reynolds number.

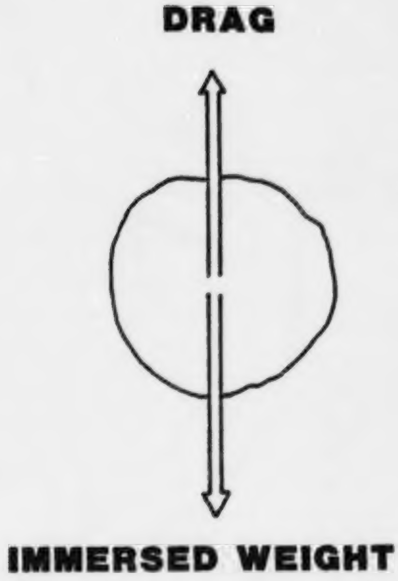

Figure 6-10 Definition sketch for force equilibrium of a settling sphere.

Figure 6-10 provides a simple definition sketch. If we assume that the grain has a spherical shape, then its immersed weight is given by:

$$\text{immersed weight} = g(\rho_s - \rho_f)\,\frac{\pi d^3}{6} \qquad (1)$$

where g = earth's gravitational acceleration constant.

ρ_s = density of the sediment particle,

ρ_f = density of the fluid, and

d = diameter of the grain.

The drag force is difficult to evaluate from fundamental principles. In light of this difficulty, a wealth of experimental data has shown that the fluid drag force can generally be determined from a quadratic stress law. A wide range of experimental data has shown that the fluid drag force. per unit area, is proportional to the product of the fluid density and the relative fluid velocity squared. The constant of proportionality is called the drag coefficient (C_D). Therefore, in the example of a spherical grain settling through a fluid, the total drag force acting on the grain is the product of the surface area of that grain with the drag coefficient multiplied by the fluid density and the fall velocity squared. Owing to a peculiarity in the definition of the drag coefficient, this relationship is often written as:

$$\text{drag} = \frac{C_D}{8} (\pi d^2)\ \rho_f W^2 \qquad (2)$$

At terminal velocity, the immersed weight force and the fluid drag acting on the grain are equal and opposite. Thus, Equation 1 can be set to Equation 2, and the resultant expression can be solved for the fall velocity. This yields an expression known as the Impact Law for particle settling, given by:

$$W^2 = \frac{4}{3}\ \frac{(\rho_s - \rho_f)}{\rho_f}\ \frac{gd}{C_D}\,. \qquad (3)$$

Experiments have shown that at low Reynolds numbers, the drag coefficient is inversely proportional to the Reynold's number. This expression is commonly written as:

$$C_D = \frac{24}{R_e} \qquad (4)$$

where R_e = Reynold's number

The Reynold's number is defined as

$$R_e = \frac{\rho W d}{\mu} \qquad (5)$$

where μ = viscosity of the fluid.

Substituting Equations 4 and 5 into Equation 3, and solving for the particle fall velocity yields Stokes' settling law, given as

$$W = \frac{g(\rho_s - \rho_p)}{18} \frac{d^2}{\mu} \tag{6}$$

The above discussion illustrates that an experimentally-determined drag coefficient must be used when applying the Impact Law. Middleton and Southard (1977) point out that the normal upper limit for Reynolds number for which Stokes' settling law can be used is in the range of 0.5 to 1. For a Reynolds number equal to 1, the actual settling velocity is about 12% lower than predicted by Stokes' law. At higher Reynolds number, the drag coefficient must be determined from experimental data.

Middleton and Southard (1977) show that if the problem is worked backwards, then Stokes' law is relatively valid for particle diameters smaller than 0.10 mm. Reference to Table 6-II shows that this corresponds to the size of very fine sand grains. Analysis of the settling velocity of larger grains is restricted to the use of the Impact Law.

One significance of the above is that larger particles settle with a velocity which is proportional to the square root of their diameter. Particles smaller than 0.1 mm settle with a velocity which is proportional to the square of their diameter. From this, it is clear that very fine clay particles settle very, very slowly.

The application of either Stokes' settling law or the impact settling law is severely limited by the simple situation which is used to develop them. It was assumed that these laws were developed for the settling of an individual spherical grain in still water. In reality, sediments are transported in large numbers, do not have ideal spherical shapes, and are subject to turbulence in natural flow conditions. Several processes develop when many grains are settling in the same body of water. Large grains tend to settle faster than small grains. Small grains can be swept into the wake of the larger grains and carried downward at a faster rate through a phenomenon known as "slipstreaming". Conversely, other small grains can be advected upwards by the eddies in the wake of larger grains. At high concentrations, the entire mixture of sediment and water may settle through surrounding clear water as a density current. The bulk density of the suspension of sediment particles and water has a higher weight per unit of volume than the surrounding clear water. This results in a tongue of the dense sediment water mixture settling as a unit. The shape of the settling grains also modifies their settling behaviour. Disk-shaped grains can either settle more rapidly or more slowly than equivalent spherical grains. If the disk-shaped grain achieves a stable position while falling, wherein its maximum surface area is exposed to the flow. it will settle slowly. On the other hand, if the disk-shaped particle develops a falling leaf pattern of sways and dips during its fall, it can settle more rapidly. In natural flows, the effect of upward and downward directed turbulent eddies also influences this behaviour.

In light of the differences between the idealized conditions under which the Impact settling law and Stokes' settling law have been developed and the complexity of the actual natural conditions, it is seen that both of these laws should be applied cautiously.

4.3.2 Fluid Forces Acting on Individual Grains

In the previous parts of this section, we have discussed many of the complexities associated with bedload sediment transport. There are different types of sediments which are affected by different types of flows and can move in different modes of transport. Various procedures have been developed to isolate the most important elements of the transport phenomenon and produce a unified theory. The foregoing analysis of settling velocity suggests that the analysis of forces acting on individual grains can lend insight into these processes. Unfortunately. very little progress has been made in the field of sediment dynamics via this route. A serious attempt was made by Eagleson, Dean and Peralta (1958), but this procedure failed to develop a significant following. Nevertheless, it is instructive to initiate the discussion of bedload sediment dynamics by considering the general forces acting on individual discrete sediment particles. Figure 6-11 shows the forces which are developed on a discrete sediment grain in the presence of steady uniform flow. We envision that the streamlines indicated in this

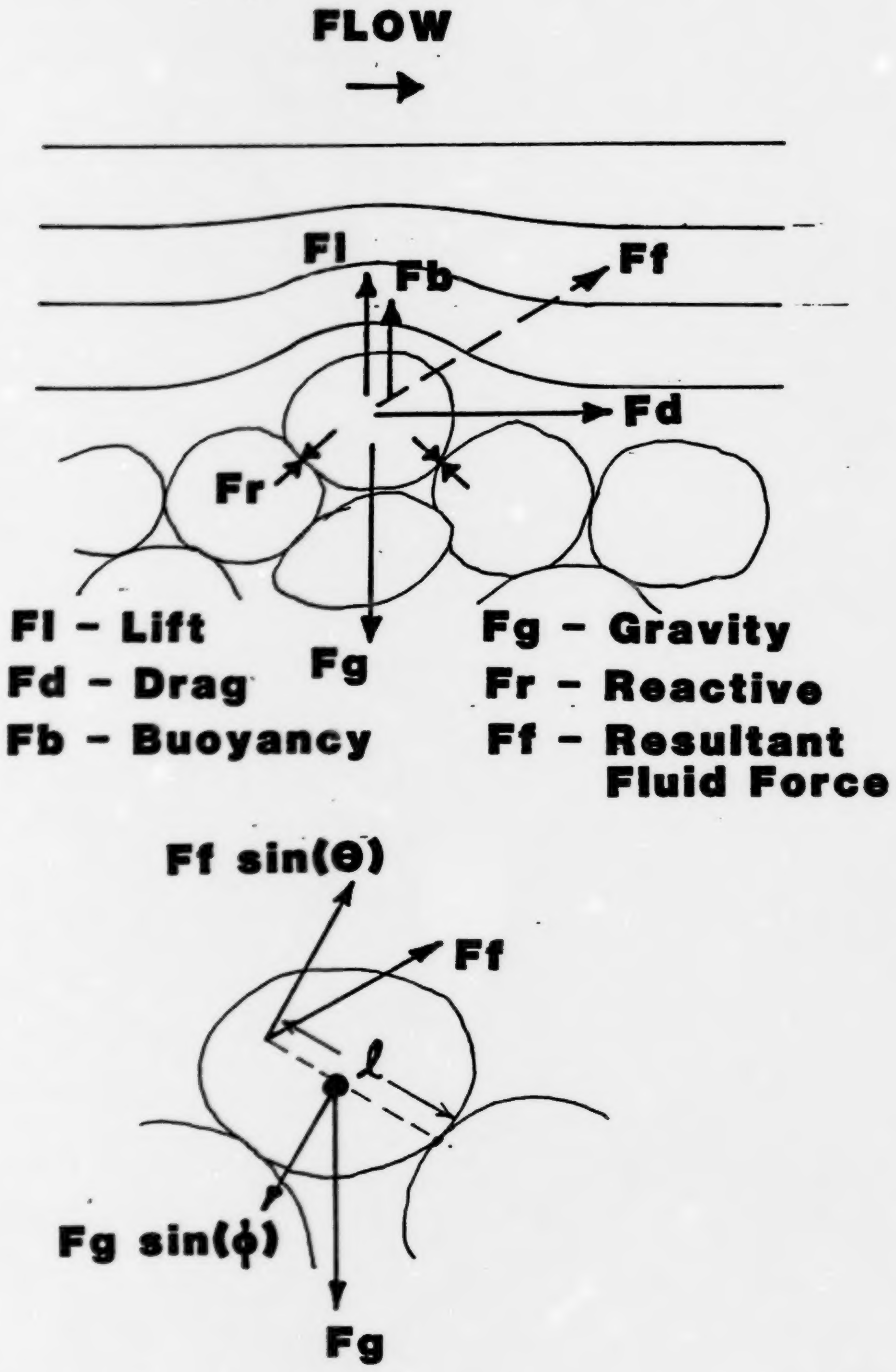
FLOW
Fl
Fb
Ff
Fd
Fr
Fg
Fl - Lift
Fd - Drag
Fb - Buoyancy
Fg - Gravity
Fr - Reactive
Ff - Resultant Fluid Force
Ff sin(Θ)
Ff
ℓ
Fg sin(ϕ)
Fg

Figure 6-11 Definition sketch for forces acting on a discrete grain in the bedload.

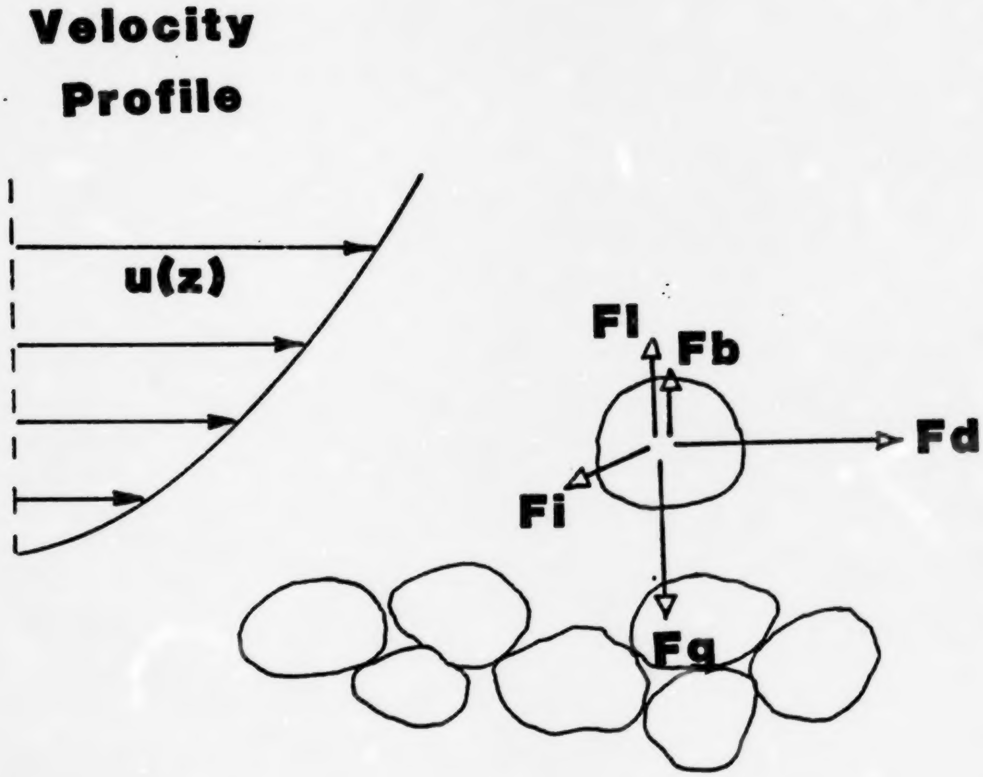
Velocity
Profile
u(z)
Fl
Fb
Fd
Fi
Fg

Figure 6-12 Schematic representation of resultant forces acting on a saltating grain.

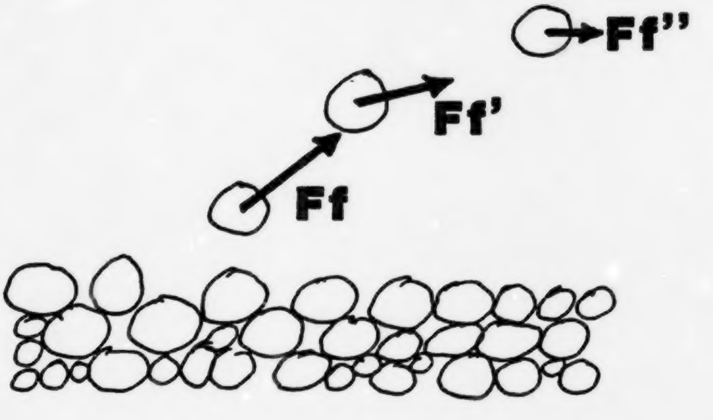

Figure 6-13 Schematic representation of the changes in resultant fluid forces acting on a saltating grain.

figure are part of the laminar sublayer of the overall boundary layer. The stream lines are deflected over the grain and induce both pressure forces and drag forces. The grain is also acted on by static forces caused by the combined effect of its own weight and buoyancy. As the grain rests on other sediment particles, there are reactive forces at the grain-to-grain contact points. The deflection of streamlines above the grain causes a lowering of fluid pressure in this area, and results in a vertical upward lift force. In addition, the motion of the fluid over the grain surface causes a drag force in the direction to which the water is flowing. The bottom part of Figure 6-11 shows a diagram of the force moments. Motion is initiated when the moment of fluid force is equal to the moment of gravitational force.

Figure 6-12 shows the instantaneous distribution of forces as the grain lifts off the bed. Because of the strong vertical gradient of horizontal velocity in the fluid boundary layer, the lift force continues to operate within a few grain diameters of the bottom. A force due to the inertia of the grain also comes into play. The inertial force resists acceleration caused by the drag and lift forces, and the lift force diminishes rapidly as the grain lifts higher off the bed. Figure 6-13 shows the resultant fluid forces acting on the grain as it begins the first part of its trajectory. As the lift force decreases with distance above the bed, the resultant fluid force becomes almost entirely a drag and pressure coefficient acting in the downstream direction.

It is immediately apparent that the distribution of forces acting on individual grains and the way they change as the grain moves is quite complex. At this point. we have not discussed the effect of a falling grain as it impacts the bed. These collisions can be nearly elastic, so that the grain is forced to rebound with very little loss of energy. On the other hand, should the grain collision with the bed occur in an appropriate space between other grains, it can either come to rest with its energy dissipated as heat. or it can trigger the release of other grains from the bed. When one considers that many thousands or millions of grains are involved in these processes for even a relatively small area of bedload transport, one quickly sees that a deterministic approach to the question of sediment bedload transport will be extremely complex.

4.3.3 Initiation of Bedload Transport

In light of all of the complexities related to the distribution of forces on the grains at different times in their movement, as well as the possibility of different sediments in different types of flow, it is necessary to develop our understanding carefully. Therefore, we will start with a simple case of examining the conditions necessary to initiate bedload transport on a flat, horizontal bed of nearly uniform-sized spherical grains.

Figure 6-14 shows a very simplified diagram with a single grain resting on two others. This grain, resting in a small hollow between the other two grains, is stabilized in its position by the net gravitational force resulting from the sum of buoyancy and gravity operating on the grain. This force should be proportional to the submerged weight of the grain times its volume. This can be represented as

$$F_s \propto (\rho_s - \rho_f) g \frac{\pi}{6} d^3 \propto (\rho_s - \rho_f) g d^3 \qquad (7)$$

where F_s = stabilizing force

Movement of the grain will occur when entraining forces overcome this stabilizing force. We have seen from our previous discussion that the exact nature of these entraining forces can be quite complex. However, numerous researchers have used empirical data to show that the sum of all entraining forces is proportional to the average fluid shear stress acting on a unit area of the bed. For an individual grain, then, the average fluid shear stress acting upon it is the fluid shear stress per unit area of the bed times some portion of the grain surface exposed to the flow. This can be represented as

$$F_e \propto \tau_o \pi d^2 \propto \tau_o d^2 \qquad (8)$$

where F_e = entraining force acting on an average grain.

τ_o = average fluid shear stress acting on a unit area of the bed

The condition for incipient transport of a grain is given when the entraining forces equal or exceed the stabilizing forces. This can be represented by the ratio

$$\psi = \frac{F_e}{F_s} = \frac{\tau_o \cancel{d^2}}{(\rho_s - \rho_f) g d^{\cancel{3}}} = \frac{\text{Entraining Forces}}{\text{Stabilizing Forces}} \qquad (9)$$

where ψ = the Shields parameter.

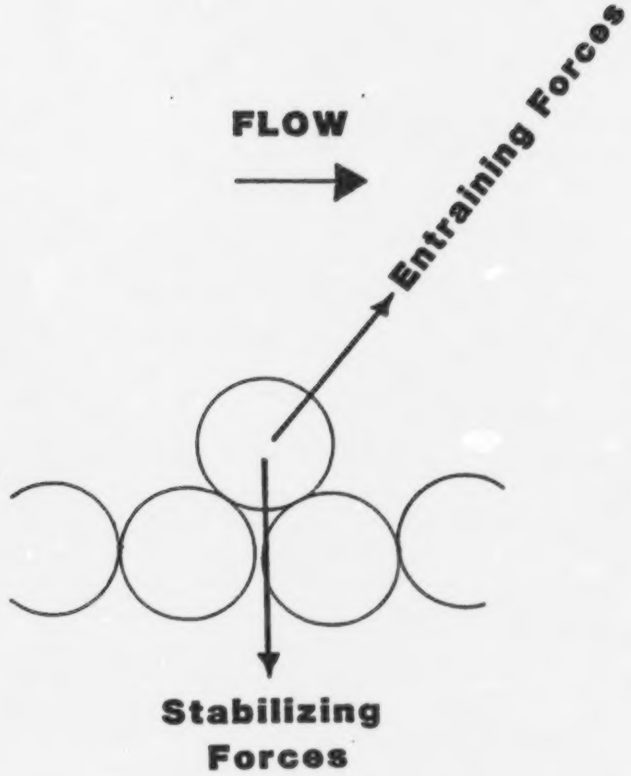

Figure 6-14 Schematic representation of forces considered in developing the Shield's parameter.

Notice that the constants of proportionality are not required in developing the ratio which is defined by the symbol ψ. In fact, these proportionality constants are incorporated into the value of ψ through the use of empirical experiments. These experiments show that ψ is not constant for all flow conditions. An evaluation of the behaviour of this parameter was first carried out by Shields (1936). He used tilting flumes 80 and 40 cm wide, with beds composed of carefully levelled fragments of granite, coal, amber, and barite. He computed the average shear stress per unit area of the bed from the discharge of the flume. The shear stress level was increased in increments for each experimental run. In fact, he determined the threshold criteria for the initiation of grain movement by back-extrapolating his sediment discharge curves to where they correspond to a zero value. Thus, he generalized the effects of weak grain movement and the influence of ripple marks which developed during his experiments.

These experiments showed that the critical value of ψ (the Shields parameter) varied monotonically with the boundary layer Reynolds number defined as

$$R_* = \frac{u_* d}{\nu} \tag{10}$$

where R_* = the boundary layer Reynolds number,

ν = the kinematic viscosity of a fluid defined as

$$\nu = \frac{\mu}{\rho_f} \tag{11}$$

where μ = the molecular viscosity of the fluid, and

$$u_* = \sqrt{\frac{\tau_o}{\rho_f}} \tag{12}$$

The parameter u_* is called the friction velocity. This terminology is somewhat misleading, as it is defined to be the square root of the bottom shear stress divided by the fluid density. This quantity has dimensions of velocity and thus has been termed the friction velocity.

The significance of the boundary layer Reynolds number can be shown by noting an expression given in Madsen and Grant (1976) for the thickness of the laminar sublayer of the fluid boundary layer. This expression is

$$\zeta_L = 5 \frac{\nu}{u_*} \tag{13}$$

where ζ_L = thickness of the laminar sublayer.
Substituting Equation 13 into Equation 10 yields

$$R_* = 5 \frac{d}{\zeta_L} \tag{14}$$

This shows that the boundary layer Reynolds number used by Shields is the ratio of the mean grain diameter of the bedload to the thickness of the laminar sublayer of the fluid boundary layer.

A plot of the critical value of the Shields parameter against the boundary layer Reynolds number is shown in Figure 6-15. This figure is called a Shields Diagram. The curve shown on this diagram indicates the value of the Shields parameter which must be matched or exceeded for bedload transport to be initiated againt different values of the boundary Reynolds number (R_*).

It may be noted that the quantity u_* contains the fluid shear stress acting on the bottom in its definition. Therefore, this parameter occurs in both axes of the Shields diagram. Furthermore, this parameter can be extremely difficult to evaluate in many flow conditions. Madsen and Grant (1976) have introduced a modification to the Shields diagram by replotting the data with respect to a new parameter, S_*, defined as

$$S_* = \frac{d}{4\nu} \left[\frac{(\rho_s - \rho_f)}{\rho_f} gd\right]^{\frac{1}{2}} \tag{15}$$

Madsen and Grant (1976) state that Prof. A.T. Ippen at MIT gave the non-dimensional parameter S_* physical significance by expressing it in terms of a non-dimensional fall velocity. Their modified Shields diagram is shown on Figure 6-16.

The modified Shields diagram permits evaluation of the critical Shields parameter from knowledge of the mean grain size of the sediments, the sediment and fluid densities, and the fluid viscosity. Thus, for a given sediment and fluid, the critical shear stress necessary to initiate bedload transport can be determined directly from the modified Shields diagram.

The Shields diagram or modified Shields diagram is used widely in studying bedload sediment transport. The limitations of its use must be considered. In developing the Shields diagram, the inertial effects of grain motions are ignored. Furthermore. the experiments used in developing this curve used carefully screened bedload material so that the range of bedload size was small. In addition, only grains of equal density were used in any particular experiment. Thus, for mixed deposits of grains with different densities and poor size sorting, there can be significant departures between the behaviour of actual sediment and that predicted from the application of the Shields criteria. More recent experiments by McQuivey and Keefer (1969) and Everts (1973) have addressed some of these questions. However, much more research is needed before a more complete formulation is developed. At the present time. it is common practice to use the Shields diagram and simply accept the many probable sources of error inherent in its use.

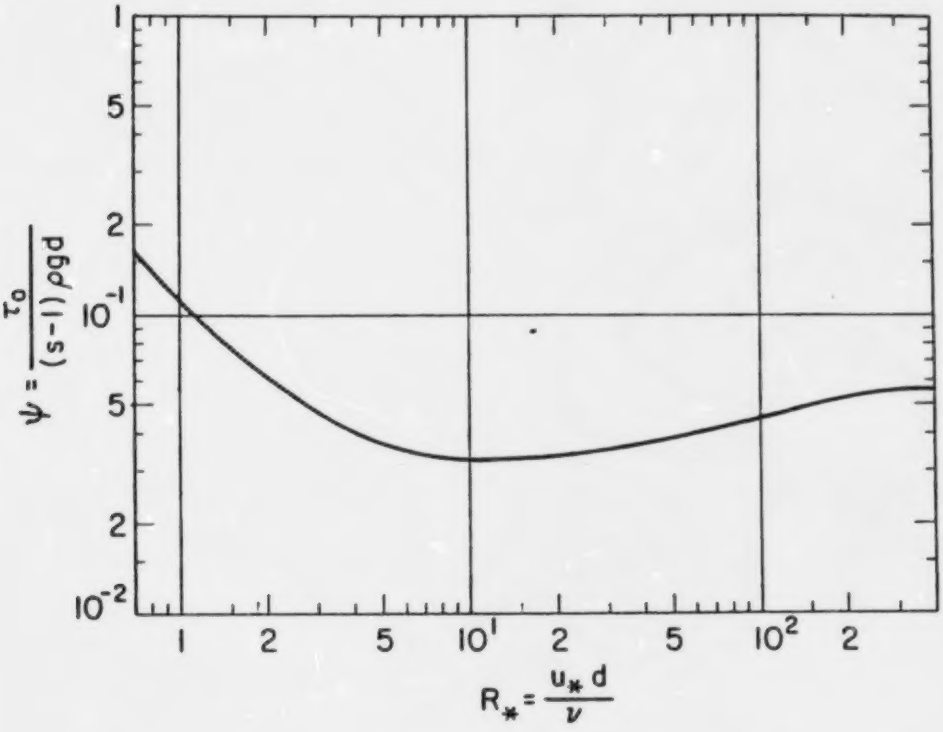

Figure 6-15 The Shield's diagram (from Madsen and Grant, 1976).

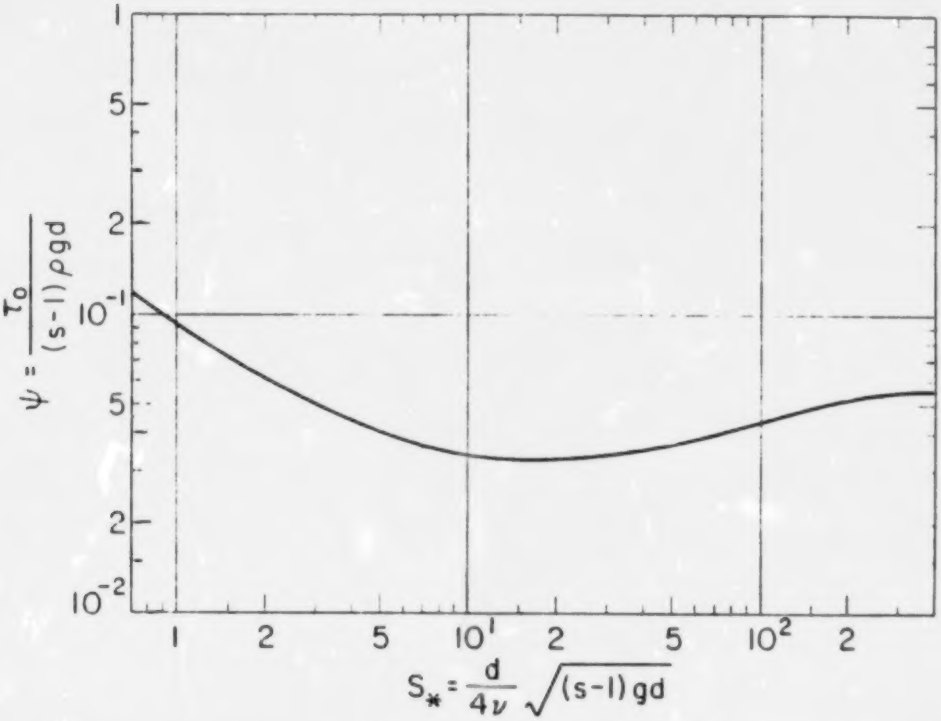

Figure 6-16 The modified Shield's diagram (from Madsen and Grant, 1976).

4.3.4 Bedload Transport in Steady Uniform Flow

Over the past 100 years, many researchers have contributed to the study of bedload transport in steady uniform flow. Much of this work results from a combination of analytic studies with river and flume experiments. There are enough similarities between marine and fluvial environments to permit the use of river and flume studies to provide the foundations of marine bedload transport studies. Of the many expressions developed, the two which are the most widely applied in marine studies originate from R.A. Bagnold and H.A. Einstein and his co-workers.

The development of Bagnold's sediment transport theory can be found in several references (Bagnold, 1963, 1966; Rouse. 1961; Raudkivi, 1967; Vanoni, 1977). The following development represents a synthesis of these papers as applied to the general case of bedload sediment transport in the marine environment.

Bagnold's underlying assumption is that work is required to move bedload sediment. The work required to move bedload sediment comes from a decrement in the power of the driving flow. In his view, the host of details related to the actual processes of grain movement in bedload transport can be encapsulated in a general concept which involves the transport of a semi-fluidized layer of granular material close to the bed (see Figure 6-17). Bagnold envisions this layer as a dilated zone where grain movement extracts energy from the flow and maintains a given concentration of grains in a dilated state through grain-to-grain collisions. This roughly corresponds to the condition of intense bedload transport. He argues that the mass flux of bedload

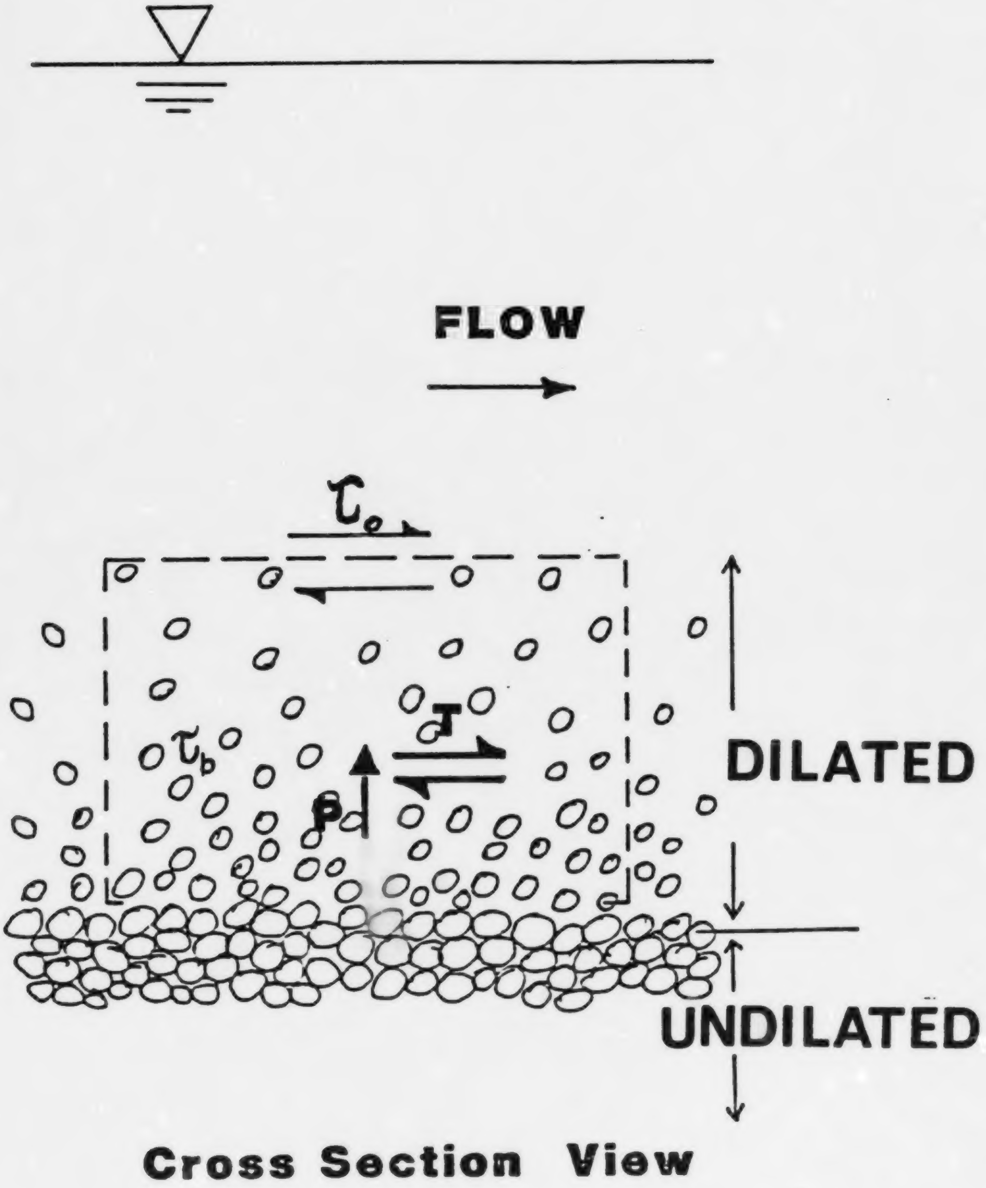
FLOW
τ_o
τ_b
T
P
DILATED
UNDILATED
Cross Section View

Figure 6-17 Definition sketch for Bagnold's sediment transport theory.

transport can be simply determined as the product of the immersed mass of dilated sediment per unit area of the bed and a given fraction of the depth mean velocity of the flow adjacent to the bed. There is a considerable difficulty in determining exactly where this velocity should be measured or what the proportionality constant between the flow measurement and the average sediment transport velocity should be. At this point, we will sidestep this difficulty.

Bagnold initiates his development by introducing the ordinary definition of the friction angle for a granular deposit as

$$\tan \phi = \frac{T}{P} \qquad (16)$$

where T is the shear stress within the granular deposit and P is the normal stress. The parameter φ is the friction angle. Thus, the normal stress necessary to support the dilated portion of the sediment bed can be related to the general shear stress applied to the bedload sediments by the fluid. The shear stress within the dilated bed is written as

$$T = P \tan \phi \qquad (17)$$

This shear stress within the dilated bed, due to intergranular collisions, is augmented by a small shear stress due to the differential movement of water within this dilated zone. These two shear stresses are taken to be proportional to the shear stress applied by the moving fluid, which can be written as

$$\tau_o \propto T + \tau_b = P \tan \phi + \tau_b \qquad (18)$$

for a horizontal bed. The parameter τ_b represents a small contribution to the overall shear stress balance due to shearing of the fluid between the grains in the dilated layer. This is considered small when compared to the shear stresses arising within the dilated layer from intergranular collisions. The normal stress within the dilated layer must be equal to the immersed weight per unit area of the dilated sediment. This can be written as

$$P = \frac{\rho_s - \rho_f}{\rho_s} gm' \qquad (19)$$

where m' is the mass of dilated grains over a unit area of the bed. When Equation 19 is substituted in Equation 18 and the parameter τ_b is taken to be negligible, the mass of sediment per unit area which is dilated can be taken as proportional to the applied fluid shear stress.

$$\tau_o \propto \frac{\rho_s - \rho_f}{\rho_s} gm' \tan \phi \qquad (20)$$

If we introduce a constant of proportionality. this relationship can be written as an equation:

$$\tau_o = K_1 \frac{\rho_s - \rho_f}{\rho_s} gm' \tan \phi \qquad (21)$$

This equation can be rewritten in terms of the mass of sediment in the dilatd layer per unit area of the bed.

$$m' = \frac{\rho_s \tau_o}{K_1 (\rho_s - \rho_f) g \tan \phi} \quad \text{for } \tau_o > \tau_{cr} \qquad (22)$$

where τ_{cr} is the critical shear stress necessary to entrain the bedload particle.

If we assume that the mass of dilated sediment is moved in the direction of flow with the velocity which is proportional to an index velocity taken at some point near the top of the moving dilated layer, then the following expression can be written for the mass flux.

$$q_m = Kum' = K\frac{\rho_s \tau_o u}{(\rho_s - \rho_f) g \tan\phi} \text{ for } \tau_o > \tau_{cr} \qquad (23)$$

In this relationship, the constant of proportionality, K, incorporates both the constant relating applied fluid shear stress to the average level of shear stress within a dilated bed, and the constant relating index measure of the fluid velocity to the measure of the average horizontal velocity of the dilated sediment layer. The fluid shear stress per unit area of the bed is difficult to evaluate. One frequently used empirical relationship is the quadratic stress law, given as

$$\tau_o = C_D \rho_f u^2 \qquad (24)$$

where C_D = drag coefficient

u = measure of the flow at some undefined level in the boundary layer.

If the u selected for this quadratic stress law is the same selected for use in Equation 23, then the mass flux can be written as

$$q_m = KC_D \frac{\rho_f \rho_s u^3}{(\rho_s - \rho_f) g \tan\phi} \text{ for } \tau_o > \tau_{cr} \qquad (25)$$

In this derivation. we have limited our consideration to a horizontal sea floor. Should there be a local or general slope in the area of interest. then a correction can be readily introduced into our definition of the friction angle relationship

$$\tan \phi = (\tan \phi - \tan \beta) \qquad (26)$$

where β is the angle of slope of the sea floor pointed in the direction of flow. This yields the following relations

$$T = P\ (\tan \phi - \tan \beta)$$

$$P = \frac{\rho_s - \rho_f}{\rho_s}\, gm \cos \beta \qquad (27)$$

which can be incorporated into the above derivation.

It is important to note that equations 23 and 25 rely on an unspecified constant proportionality. This constant arises from the need to relate the average speed of movement of the dilated bedload to an index velocity measured in the overlying fluid flow. Bagnold and other workers have introduced a series of relationships aimed at specifying the level of this index velocity, or a method for computing it from other flow parameters. Unfortunately, each of these methods is rather specific to the particular flow situation (e.g. river channel, flume, etc.). As a result, the methods applicable for determining bedload transport in rivers or flumes is different from those which may be applicable to the ocean environment. There is no standardized body of experimental data which permits the application of Bagnold's sediment transport theory to the unsteady and non-uniform flow of the ocean environment, owing to the unspecified nature of this constant of proportionality.

It is instructive to note that the mass flux of bedload sediment transport is generally proportional to the third power of an index velocity of the flow. This is consistent with Bagnold's starting point that the mass flux of bedload transport should be related to the decrement of fluid power.

Einstein's bedload transport theory is significantly different from that developed by Bagnold. The development of this theory can be found in many references, including Einstein, (1942 and 1950); Rouse, (1961); Raudkivi, (1967); and Vanoni. (1977). Unfortunately, many of the explanations of Einstein's sediment transport theory are obtuse and even confusing. The best original source appears to be his 1942 paper, q.v.

The basic assumptions of Einstein's sediment transport theory are:

1. There is no single "critical" boundary shear stress where all of the grains of the same size simultaneously begin to move.

2. Movement of grains should be expressed via a probability, related to variations in the local conditions of the bed and fluctuations in the behaviour of boundary layer turbulence.

3. The formulation of his theory is restricted to relatively uniform bedload size distributions.

4. Bedload movement is taken to consist of relatively quick steps interspersed with relatively long periods of rest.

5. The average step length for a given diameter grain is the same in all intensities of flow.

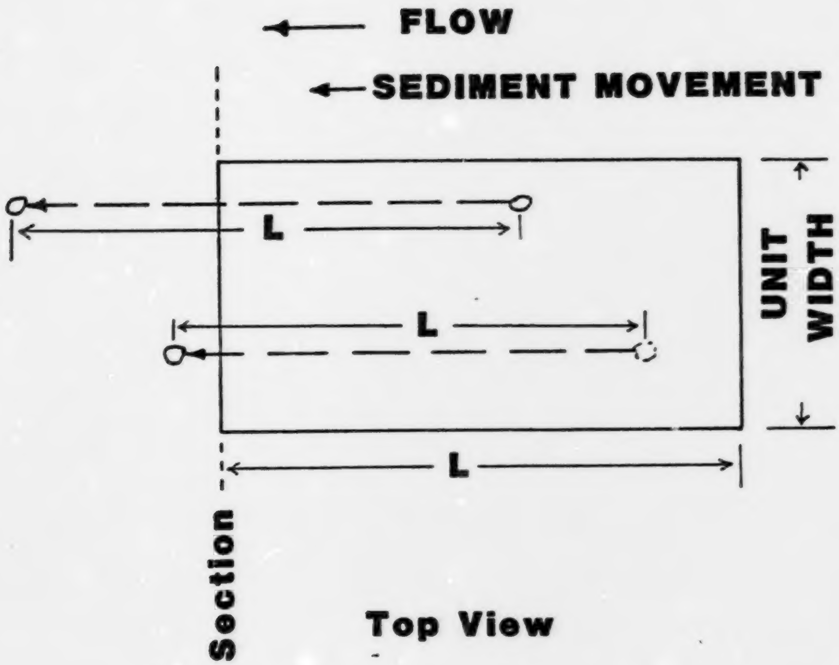

Figure 6-18 Definition sketch for Einstein's bedload transport theory.

6. Different rates of transport are produced by a change in the average time between two successive steps of a particle and by a change in the thickness of the moving bedload layer.

Figure 6-18 shows a definition sketch for the development of Einstein's bedload transport theory. This figure consists of a top view of a unit width of a bed undergoing uniform bedload transport. The volume discharge of sediments through a vertical section of unit width is equal to the number of particles which are lifted from the bed upstream of this section in a second.

The volume discharge of bedload sediment or bedload volume flux (q_v) is given as

$$q_v = \frac{q_s}{(\rho_s - \rho_f)g} \tag{28}$$

where q_s = weight flux of bedload transport.

The basic formulation of this problem can be assembled from the definition sketch given in Figure 6-18, and the following definitions:

$A_2 d^3$ = the volume of individual particles (for spheres $A_2 = \frac{\pi}{6}$)

$A_1 d^2$ = the horizontal projected area of each sediment grain

P_s = the probability that a particle will start moving in a given second (29)

Einstein uses many observations of bedload transport in a flume to come to the conclusion that the average trajectory length of a saltating grain is proportional to its diameter. This is written as

$$L = \lambda_o d \tag{30}$$

With this definition of the length of the source bed feeding grains through the unit width discharge section, the total number of grains in the source bed can be determined by the relationship

$$N = \frac{L x 1 \text{ (unit width)}}{A_1 d^2} = \frac{\text{total area of the "source bed"}}{\text{total area of the grain}} \tag{31}$$

The volume flux of bedload passing through the control section is equal to the number of grains in the source bed times the probability that the grains will be transported by the flow times the volume of the individual sediment grains.

This is expressed mathematically as:

$$q_v = N \times p_s \times (A_2 d^3) \tag{32}$$

Using Equations 30 and 31, Equation 32 can be rewritten as:

$$q_v = \lambda_o \frac{A_2}{A_1} p_s d^2 \tag{33}$$

which can be algebraically rewritten

$$p_s = \frac{A_1}{A_2} \frac{q_v}{\lambda_o d^2} \tag{34}$$

The problem can be reduced to determining the nature of the probability p_s. Note that both sides of Equation 34 have the dimensions of T^{-1}. To make this relationship non-dimensional. Einstein selects a time which represents the time required for a grain to fall its own diameter at terminal velocity in the fluid. He remarks that this selection is arbitrary. However, as it is to be used to make the probability, p_s, non-dimensional. it may not be an unreasonable choice. Multiplication of probability p_s by this time should yield dimensionless probability that a given grain will move at any instant. Clearly, the maximum value of this dimensionless probability should have the value of 1 if the flow is such that surface bedload transport is at its maximum. Therefore, this nondimensional time is probably a good estimator of the shortest time that a grain can take to come in contact with an area of the bed equal to the projected area of the grain, and then be re-entrained in the flow.

The product of the time required for a grain to fall its own diameter at terminal velocity in the fluid and the specific probability p_s is defined to be this dimensionless probability (p). "...p is dimensionless and gives the number of steps that start from any given place during the time it takes to remove one particle. The maximum value of p is 1, and indicates that at all times and at all points, particle by particle starts to move. The minimum value of p is zero, therefore, p expresses the probability that a step is about to begin at a given place. These steps start everywhere on the bed. Therefore, p can be interpreted as the probable part of the bed area in which steps are starting. A step is started only at a point where the hydraulic lift of the water is able to overcome the weight of the particle. Therefore, p expresses the probability that the hydraulic lift on any particle along the bed is about to overcome the weight of the particle". (Einstein, 1942 p. 564).

Considerable algebra is used to rewrite the above equations in a form which becomes

$$p = A\left[\frac{q_v}{wd^2}\right] = f\left[B\left[\frac{(\rho_s - \rho_f)gd}{\tau_o}\right]\right] \tag{35}$$

where

$$A = \frac{A_1 A_3}{A_2 \lambda_o} \text{ and } B = \frac{A_2}{A_4}$$

where f = unknown function

This relationship can be further simplified by making the following definitions:

$$\phi = \frac{q_v}{wd^2};\ \psi' = \frac{(\rho_s - \rho_f)gd}{\tau_o} \tag{36}$$

Using Equation 36 in Equation 35, these results can be simplified to:

$$p = A = f(B \psi') \qquad (37)$$

Note that Equation 37 incorporates the constants A_1, A_2, A_3 and λ_o, which represent unknown functions throughout this derivation. Given the uncertainties in making determinations for all of these coefficients, Einstein felt it was better to evaluate the functional form of the equation given in Equation 37. Using data from experiments conducted by G.K. Gilbert, E. Meyer-Peter and White, (personal communication), he found that the best expression was

$$0.465 = e^{-0.391} \qquad (38)$$

which implies that the values of the coefficients and function in Equation 37 are

$$A = 0.465 \quad ; \quad B = 0.391 \quad ; \quad f(x) = e^{-x} \qquad (39)$$

Einstein went on to develop a nonlinear relationship based on the assumption that particles do not necessarily make a single leap when saltating. The development of this more elaborate expression adds little to the basic definition of his concepts. and therefore is not developed here. Data supporting the generation of Equation 38 is given in Figure 6-19.

Some years later, Brown (1950) re-examined Einstein's data and came to the conclusion that a relatively simple expression would provide a better fit of the data than that given by Equation 38. Brown offered the following expression:

$$\phi = 40 \left(\frac{1}{\psi}\right)^3 \qquad (40)$$

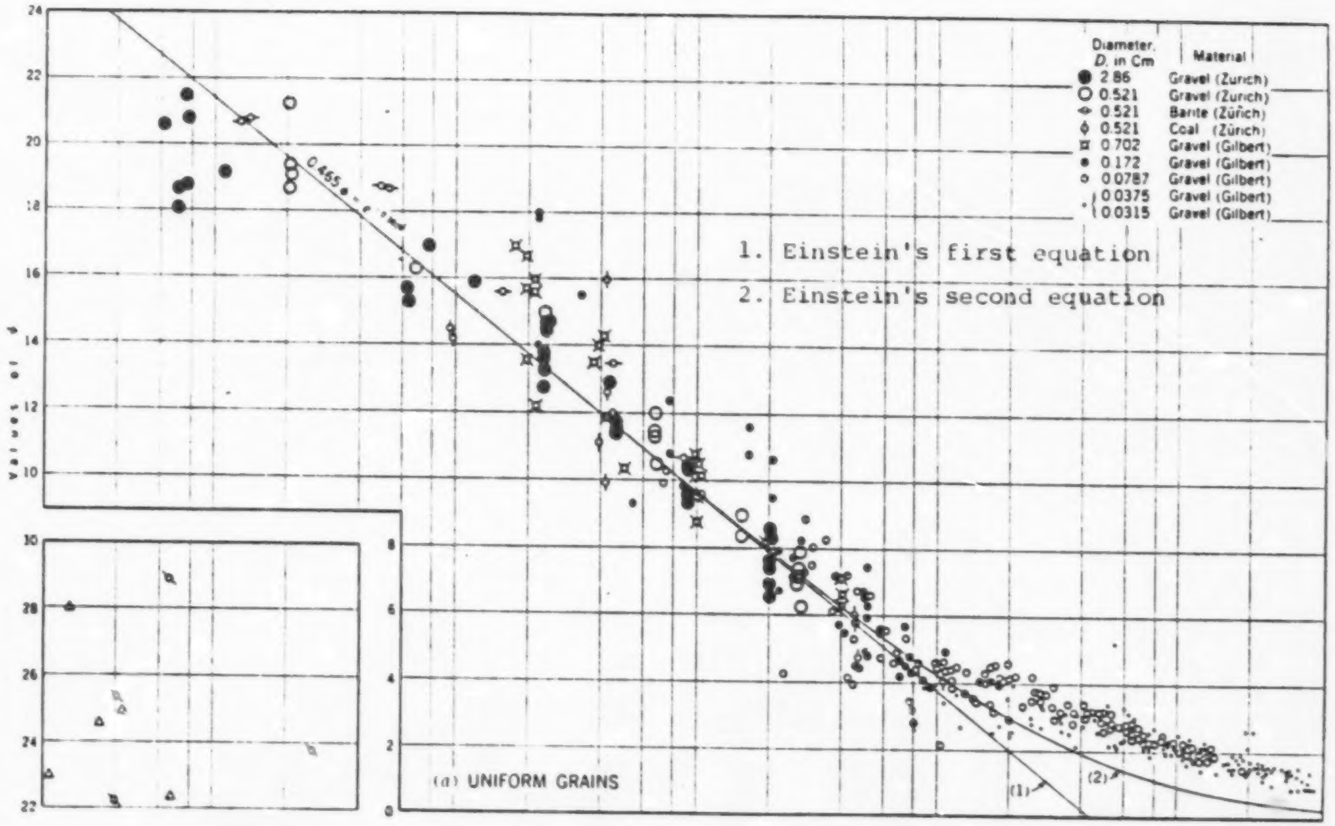

Figure 6-19 Comparison of Einstein's bedload relationship with experimental data (from Einstein, 1942).

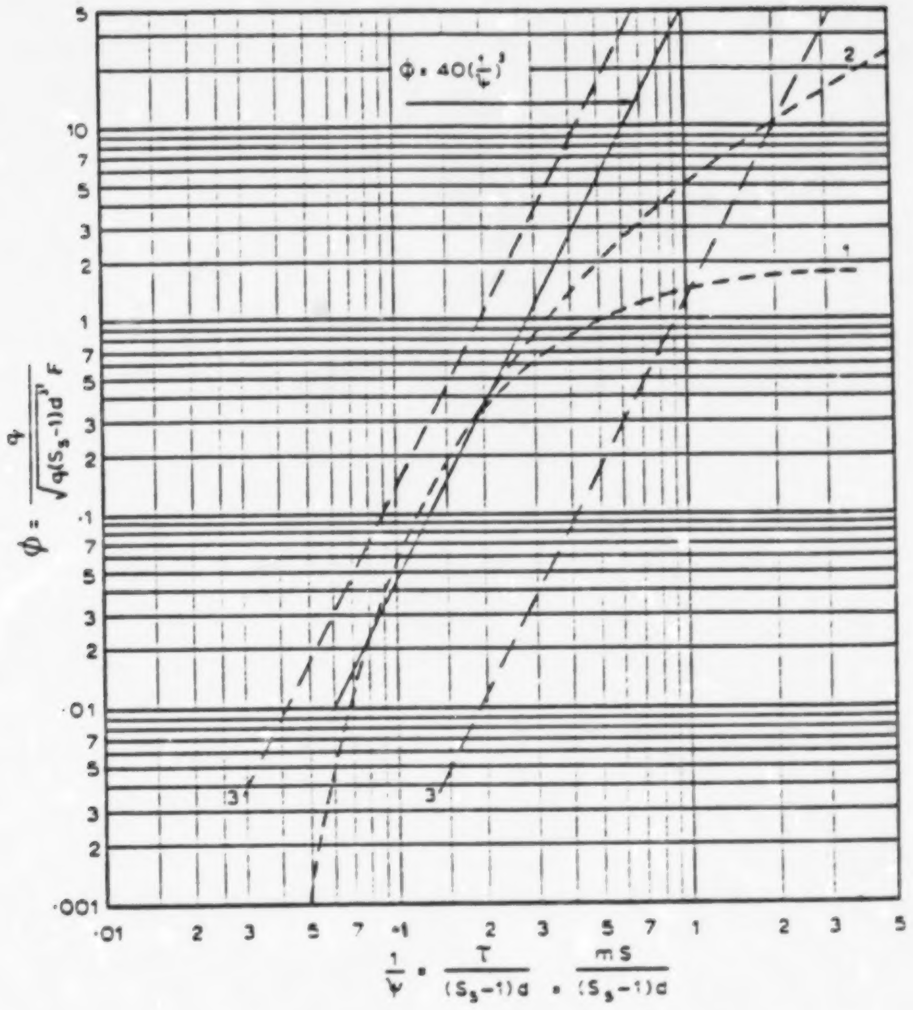

1. Einstein's equation
2. Deviation between Einstein's equation and measured data
3. Approximate limits of available data

Figure 6-20 Comparison of the Einstein-Brown bedload transport relationship with measured data (from Vanoni, Ed., 1977).

The justification for this relationship is shown in Figure 6-20. It is interesting to note that the definition of the parameter ϕ in Einstein's approach is the inverse of the ordinary Shields parameter, or

$$\phi = \frac{1}{\psi'} \qquad (41)$$

Thus, Einstein's relationship given by Equation 37 can be rewritten using the approach of Brown, using the ordinary Shields parameter in the simple form of:

$$\phi = 40 \, \psi^3 \qquad (42)$$

Equation 42 can be rewritten in terms of the volume flux of bedload discharge as:

$$q_v = 40 \, wd \, \psi^3 \qquad (43)$$

Equations 42 and 43 are frequently used expressions when computing marine bedload transport. They are referred to as the Einstein-Brown relationship.

Numerous other workers, such as Schoklitsch, Meyer-Peter, Muller and others, have examined the phenomenon of bedload transport in alluvial channels and produced semi-empirical relationships between flow parameters and sediment discharge. However, none of these approaches has gained acceptance in marine environment applications. Therefore, we will end our discussion of the principles of bedload sediment transport in steady uniform flow with these brief discussions of the work of Bagnold, Einstein and Brown.

4.4 Dynamics of Bedload Transport in Oscillating Flows

Transport of bedload sediment in the marine environment generally results from the effect of wave orbital velocities acting on the bottom. This transport can develop purely from the wave motion, or from a combined effect of a mean flow with the wave orbital velocities acting on the bottom. These combined effects serve to further complicate bedload dynamics. In this section, we will consider the question of determining the conditions necessary to initiate bedload particle movement in oscillating flows, the dynamics of bedload transport due to wave orbital velocities and, finally, examine the question of the dynamics of bedload sediment transport due to the combined effect of waves and currents.

4.4.1. Initiation of Particle Movement by Oscillating Flows

Oscillating flows, such as those associated with near-bottom wave orbital velocities, have many properties which differ significantly from steady flows. The boundary layer between the irrotational portion of the wave velocity flow and the seafloor is necessarily thin, owing to the relatively short period of time available for its development before the orbital velocity stops and reverses direction. Natural scale waves can develop boundary layers which are laminar. transitional and fully turbulent. Nevertheless, even in their most fully developed form they are very thin (generally less than 5 cm). Another effect of wave orbital velocities acting near the bottom is to produce high-frequency current direction variations. Thus, there is a question whether the response time of the sediment due to inertial effects is significant in influencing the threshold conditions for entraining sediment and the conditions for transporting sediment.

Many authors have explored this question with both laboratory and field measurements. Nakato et al (1977) used a long tank and an optical sediment concentration sensor to measure the conditions necessary to support bedload grains in the wave orbital boundary layer. They showed that entrainment and sediment suspension conditions varied, both in time over a wave cycle. and in position over the ripple marks. However, they offered no useful relationship for computing the threshold of sediment motion under wave orbital boundary layers.

Sternberg and Larsen (1975) used field measurements of waves, currents and photographs of the seafloor on the Washington continental shelf at a depth of 167 metres to determine a relationship for the onset of bedload motion under waves. They offer the following relationship:

$$\frac{\rho_f \, u_{1/10}^2}{(\rho_s - \rho_f) g d} = 0.13 \left[\frac{A_b}{d}\right]^{\frac{1}{2}} \qquad (44)$$

where $u_{1/10}$ = the maximum near-bottom wave orbital velocity related to the highest 1/10 of the waves

A_b = the water particle excursion length for the same waves

Notice that the left-hand side of this equation looks similar to the Shields parameter, except for the absence of a drag coefficient in the numerator.

Komar and Miller (1974, 1975) offer the following two relationships for the threshold of bedload transport under oscillating currents, from a re-analysis of data provided by Bagnold (1946), Carstens et al (1969), Manohar (1955) and Rance and Warren (1968).

$$\theta_t' = \frac{u_m^2 \rho_f}{(\rho_s - \rho_f) gd} = 0.21 \left[\frac{A_b}{d}\right]^{\frac{1}{2}} \text{ for } d < 0.5 \text{ mm}$$

$$\theta_t' = \frac{u_m^2 \rho_f}{(\rho_s - \rho_f) gd} = 0.463 \left[\frac{A_b}{d}\right]^{\frac{1}{4}} \text{ for } d > 0.5 \text{ mm} \tag{45}$$

These equations are very similar to those given by Sternberg and Larsen, except that u_m is the maximum near-bottom horizontal wave orbital velocity developed in the various wave tank experiments.

There have recently been a number of significant advances in understanding the entrainment and transport of bedload sediment by waves, as well as the combined effect of waves and currents. due to studies published by Ole Madsen of MIT and William Grant of Woods Hole (1974, 1976, 1977). In order to explain these developents, it is necessary to establish a few pieces of common groundwork. Madsen and Grant's work draws heavily upon earlier work by Ivar Jonsson (1966) of the Technical University of Denmark. Jonsson studies the frictional losses of wave energy as they propagated over granular seabeds. In a study published in 1966. he re-analyzed the data from both field and laboratory experiments of numerous other workers. He showed that most of the data could be brought into agreement by considering the state of the wave orbital bottom boundary layer. Because of the relatively rapidly changing magnitude and direction of bottom wave orbital velocities, the thin boundary layer can either be laminar, smooth turbulent, or rough turbulent. The state of this boundary layer can be described in terms of two parameters. One is a wave orbital boundary layer Reynolds number defined as

$$Re_w = \frac{u_b A_b}{\nu} \tag{46}$$

where the parameter u_b is the maximum near-bottom horizontal wave orbital velocity developed over the wave cycle. This velocity is determined at a point immediately above the wave orbital boundary layer. For practicl purposes, the thickness of the wave orbital boundary layer is generally ignored in computing this value. The other parameter used in Jonsson's evaluation is $\frac{A_b}{d_s}$. (47)

This parameter represents the ratio of the maximum near-bottom water particle excursion length (A_b), due to the orbital movement, to the mean diameter of the sediment grains (d_s). Using these two parameters, the value of a wave orbital velocity friction coefficient (f_w) was evaluated via analogy to the Darcy-Weisbach friction factor. This evaluation is shown in Figure 6-21. Figure 6-21 can be used to determine the value of the wave orbital velocity friction factor and this, in turn, can be used to determine the instantaneous fluid shear stress acting on the bottom sediments due to the wave orbital boundary layer through the relationship

$$\tau_{om} = \frac{1}{2} f_w \rho_f u_b^2 \ . \tag{48}$$

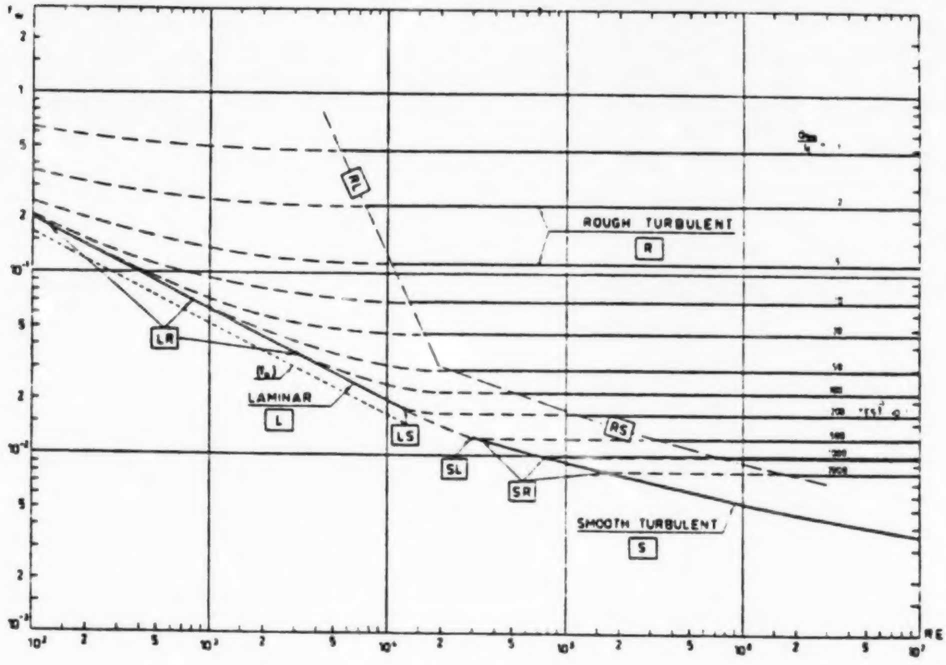

Figure 6-21 The Jonsson wave friction coefficient diagram (from Jonsson, 1966).

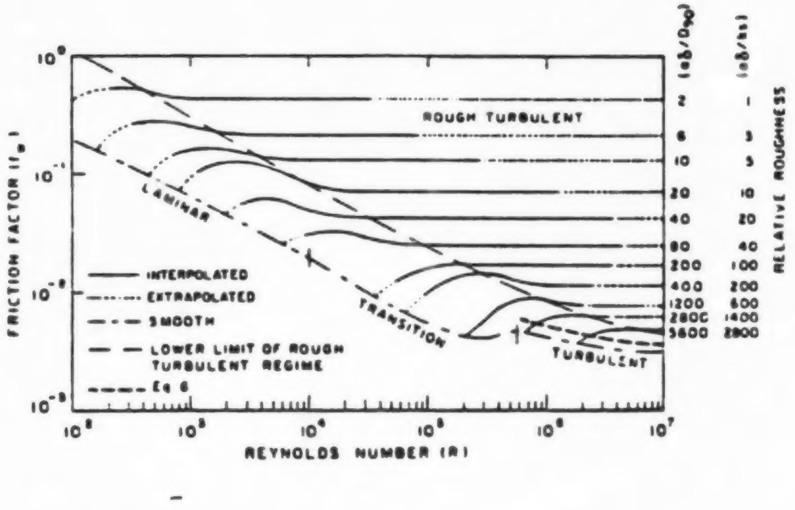

Figure 6-22 The Kamphius wave friction coefficient diagram (from Kamphius, 1975).

Kamphius (1975) conducted a number of careful laboratory wave tank experiments to improve the data base for the wave friction factor developed by Jonsson. The results of this research are shown in Figure 6-22.

Madsen and Grant used the relationships developed by Jonsson to evaluate the use of the Shields parameter for predicting the initiation of bedload movement under oscillating unsteady flow. They re-analyzed data from Rance and Warren (1968) developed through the use of an oscillating water tunnel, from Vincent, (1958) and Horikawa and Watanabe, (1967) developed from a laboratory wave tank , and data from Bagnold (1946) and Manohar (1955), whose data was produced by a laboratory device which consisted of a horizontal tray on which the sediment lay, and which could be oscillated back and forth beneath still water. The re-analysis of this data shows good agreement between predicted and measured conditions for the onset of bedload transport in oscillating unsteady flow. This implies that the response time of sediments is small compared to the normal range of frequencies of both laboratory and ocean waves.

It should be noted that all of the studies which provide analytic expressions for predicting the onset of bedload transport under the unsteady oscillating flow conditions utilized two parameters which closely resemble the Shields parameter and the ratio of a near-bottom horizontal excursion amplitude of the orbital motion to the mean diameter of the bottom sediment. The agreement in the general form of Equations 44 and 45 is satisfying. Considering the great difficulties in determining the onset of bedload transport under oscillating conditions in either field or laboratory environments, the variation in the parameters of these equations is relatively small. The application of the work of Jonnson (1966), as well as Madsen and Grant (1974), is relatively straightforward. In all cases, it is interesting to note that the problem of establishing the proper level from which to measure the index horizontal velocity, which plagues bedload entrainment and transport analyses under steady flow conditions, is relatively readily specified for wave orbital flows. Thus, a quadratic stress law is easy to apply for these conditions.

4.4.2 Bedload Transport in Oscillating Flows

One of the more significant advances in developing a predicted capability for computing bedload sediment transport in the presence of wave orbital velocities comes from the work of Madsen and Grant (1976). In this study, they carefully reanalyzed data developed by Kalkanis (1964) and Abou-Seida (1965) from experiments using an oscillating sediment tray. at the laboratory facilities of the University of California at Berkeley, under the direction of H.A. Einstein. The oscillating tray containing the sediment had a trough in its center which acted as a sediment trap. As the tray oscillated in a horizontal direction, sediment was moved into this trap on both the forward and backward sweeps of motion. After a known number of sweeps, the apparatus was stopped and the dry weight of sediment collected in the trap was measured. Madsen and Grant (1976) used Jonsson's formulation to

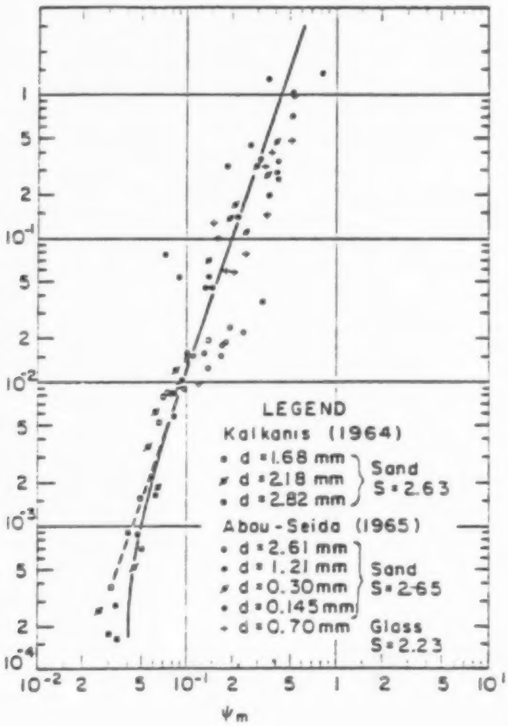

Figure 6-23 Comparison of measured values of sediment entrainment with that predicted by Madsen and Grant's application of the Shield's parameter to oscillating flow (from Madsen and Grant, 1976).

calculate the fluid shear stresses acting on the sediment for each experimental run. They also utilized the Shields parameter to limit their calculations to those times in the wave cycle when bedload sediment was subject to transport. This analysis showed that the Einstein-Brown relationship, given in Equations 42 and 43. produced remarkably reliable predictions of the observed transport rates (Figure 6-23).

The Kalkanis and Abou-Seida experiments utilized a sinusoidal motion of the sediment tray. In natural conditions, wave orbital velocities rarely exhibit such a purely sinusoidal motion. Gravity waves at sea tend to have higher and more peaked crests with broader and flatter troughs than that exhibited by a sine wave. As a result, the horizontal orbital velocity acting on the bottom attains a greater magnitude under the crest of the wave than under the trough of the wave. Conversely, the duration of the horizontal velocity under the crest of the wave is briefer than under the trough of the waves. Depending upon the type of wave theory used to represent these current distributions, one can estimate the motions as resulting in zero net transport despite the asymmetry in magnitudes and durations in the different phases of the flow, or as containing a small net flow as a residual after each wave cycle. In either case, the waves are capable of producing unidirectional transport of the bedload sediment. Madsen and Grant (1976) also examined this phenomenon. They re-analyzed data published by Manohar (1955). Manohar used an oscillating sediment tray in a water tank. Unlike the work of Kalkanis and Abou-Seida, Manohar's equipment made it possible to oscillate the tray so that it had a fast and brief forward motion with a slower but longer return motion. Ripple marks formed on the tray in some of his experiments, but not all of them. Madsen and Grant utilized a quasi-steady application of the Einstein-Brown relationship to analyze these data. The results are shown in Figure 6-24. They also noted that the appropriate fit between computed and measured data was developed when the bottom friction

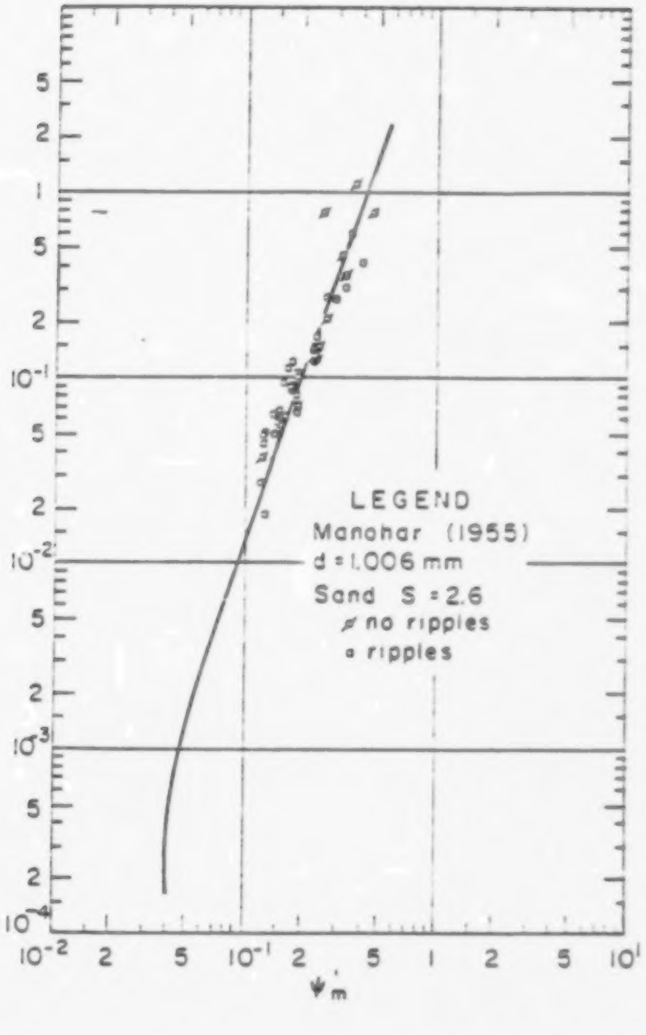

Figure 6-24 Comparison of measured data from Manohar's 1955 data on sediment transport due to waves with that predicted by Madsen and Grant through the application of the Einstein-Brown bedload transport formula to oscillating flows (from Madsen and Grant, 1976).

element was considered to be the mean grain size of the sediment rather than the height of the ripple marks which formed on the tray during some experiments.

4.4.3 Dynamics of Bedload Transport Due to the Combined Effects of Waves and Currents

In previous discussions, we have indicated that a primary difficulty in computing bedload discharge as a result of transport arising from a steady mean current, comes from the difficulty in evaluating the fluid shear stress acting on the bed. In laboratory flumes and many alluvial channels, the average fluid shear stress can be computed from the slope of the energy line. In marine flows, this is seldom possible. The slowly varying currents affecting continetnal shelf areas may be driven by surface shear stresses due to the wind, internal pressure fields due to slopes of the sea surface or slopes of the interface between water masses of different densities, or from tidal action. All of these driving forces can produce different forms of turbulent behaviour in the benthic boundary layer. As a result, the attempt to establish a specific reference level from which a single current measurement can be taken to permit the evaluation of bottom shear stress have been frustrated.

They have shown in the above discussion that the fluid shear stress acting on the seafloor due to oscillating wave orbital currents can be approximated by relatively simple calculations. In real situations where the bedload is influenced by the combined effect of both oscillating wave orbital currents and slowly varying mean currents, there is a significant problem in determining the value of the fluid shear stress acting on the bottom. This fluid shear stress is a rapidly varying vector quantity. The presence of the thin wave orbital boundary layer changes the behaviour of the thicker mean current boundary layer. The net result is actually to produce a better friction coupling between the water mass and the sediments.

Jonsson (1966) performed an analytic study coupled with limited laboratory data to provide a method for estimating the fluid shear stress due to the combined effect of wave orbital velocities and a steady current. His experiments were limited by the wave tank facility to the condition where the two flows operate along the same axis. His formulation consists in using two independent friction factors. The friction factor for the pure current (f_c) was obtained from a Moody diagram, and used to estimate the fluid shear stress acting on the bed from evaluation of the depth mean current in the bottom boundary layer. The friction factor for pure wave motion (f_w) was obtained as described above. The friction factor for the combined effect of both waves and currents was estimated from the relationship

$$f_{cw} = \frac{|\vec{U}|\, f_c + |\vec{u}_w(t)|\, f_w}{|\vec{U}| + |\vec{u}_w(t)|} \qquad (49)$$

where $\vec{u}$ = the depth mean horizontal velocity of the steady current boundary layer

$\vec{u}_w(t)$ = the instantaneous horizontal velocity of the wave orbital motion just above the wave orbital boundary layer.

With this combined wave current friction factor, a form of the quadratic stress law can be used to compute the fluid shear stress acting at any instant on the sediment bed, using the relationship

$$\vec{\tau}_o(t) = \frac{\rho_f f_{cw}}{2} \left|\vec{u}(t)\right|^2 \frac{\bar{u}(t)}{\left|\bar{u}(t)\right|} \tag{50}$$

where $\vec{u}(t) = (\vec{u}_w(t) + \vec{U})$

Two publications deal with the problem of the interaction of a wave orbital boundary layer with a slowly varying boundary layer and its relationship to bedload transport in continental shelf environments. Smith (1977) develops an analytic approach for determining the skin friction component of the overall fluid stress applied to the bed for the case of codirectional mean currents and wave orbital velocities. His approach is limited to current dominated environments. Grant and Madsen (1979) have developed a similar analytic approach for the case of a wave-dominated environment. They emphasize the non-linear coupling between the slowly varying boundary layer and the thin wave orbital boundary layer. Their approach defines characteristic shear velocities in both boundary layers. The details of time varying boundary layer and turbulent behaviour are averaged through the use of a time invariant turbulent eddy viscosity model which increases linearly with height above the bed. Governing equations are developed for combined flow within the wave orbital boundary layer and above this boundary layer. These solutions involve relatively complex notations which must be solved either through computer-based iterative techniques or through nomographs presented in the paper.

The results indicate that when the magnitude of the wave orbital flow in the wave boundary layer is large with respect to that of the magnitude of the slowly varying current component, both the magnitude and the direction of the mean shear stress acting on the bed changes. The magnitude is enhanced, which is represented in their formulation by an enhanced apparent bottom roughness and an increase in the combined wave current friction factor. The direction of the mean stress within the wave orbital boundary layer tends to be turned in the direction of wave propagation so that it is not parallel with the direction of the mean or slowly varying flow.

The principal bottom roughness length utilized in this approach is the height of bottom ripple marks. The enhancement in the frictional coupling between the slowly varying boundary layer and the bottom sediments owing to the presence of the wave orbital boundary layer is represented by an increase in the apparent roughness length over that given by the ripple mark height. The result is a significant reduction in the speed of the slowly varying current boundary layer flow. Grant and Madsen point out that in computing bedload sediment transport fluxes, the fundamental roughness scale used in determining the skin friction component of the total shear stress acting on the bed is still the mean grain size of the sediment. However, the wave current boundary layer interaction must be considered in determining the strength of the mean current in the wave boundary layer, and thus the value of the mean current friction factor (which is combined into the joint wave current friction factor for calculating bedload sediment fluxes).

Grant and Madsen (1982) examine the question of the significant roughness length affecting the wave orbital boundary layer in continental shelf environments, with more detail than they had in their previous analysis. They show that the apparent roughness can be divided into two parts. When ripple marks with steepnesses (i.e. ripple height divided by ripple length) of greater than 0.1 are developed, their height and lengths form a parameter which defines the predominant roughness length for the problem. When ripple marks are not present and vigorous bedload transport is occurring, the significant roughness length affecting the wave orbital boundary layer is given by a factor relating the average grain size of the moving sediment and the thickness of the moving sediment layer. They show that analyses which do not consider these factors underpredict the scale of bottom friction by a factor of 5 to 10.

4.4.4. Erosion and Deposition of Bedload in the Marine Environment

In the previous sections of this chapter we have discussed the mechanics of bedload transport in steady uniform flows, in oscillating flows and in flows that have both components. It is seen that a principal difficulty in computing bedload transport comes from the determination of the skin friction component of the overall bottom stress, which is used in the sediment transport theories as a principal flow parameter controlling bedload transport rates. To a degree, this problem is actually overcome in considering bedload transport purely induced by asymmetrical wave orbital velocities or produced via the combined interaction of wave orbital and mean current flows. Owing in part to our ability to predict the gross nature of wave orbital velocity distributions throughout the water column, the work of Grant and Madsen (1979a) also provides an adequate representation of the total skin friction component of bottom stress resulting from both waves and currents.

The general subject of erosion and deposition in the marine environment is quite complex. It can be approached simply in formulating the governing relationship. However the application of this governing relationship requires considerable specific information concerning sediments and flow in the particular region of interest. These complexities will not be considered in this chapter.

The problem of erosion and deposition of marine bedload can be represented mathematically through the sediment continuity equation, given as

$$\frac{\partial q_x}{\partial x} + \frac{\partial q_y}{\partial y} = - \frac{\partial D}{\partial t} (1-E) \qquad (51)$$

where x = a horizontal coordinate direction (say north);

y = a horizontal coordinate direction (say east);

q_x = the bedload sediment transport, per unit width, in the x-direction;

q_y = the bedload sediment transport, per unit width, in the y-direction;

D = the local water depth;

t = time;

E = porosity of the sediment bed.

This equation shows that if there is no convergence or divergence in the local bedload transport rate, the level of the seafloor will remain the same. Therefore, large volumes of bedload can be moved past a given area without eroding or building up the seafloor. If divergences are present in the rate of bedload sediment transport. then local erosion must occur. The rate of local erosion is linearly related to the magnitude of this divergence. Conversely, convergences in the bedload transport rate lead to deposition.

5. SUSPENDED SEDIMENT DYNAMICS

The kinematics and dynamics of suspended sediment transport deposition and erosion are considerably more complex than those of bedload transport. Transport of suspended sediment is accomplished through supporting the sediment grains within the fluid by the turbulent fluctuations of the flow. Turbulence in the marine environment is only now beginning to witness significant research. Therefore, the flow situations illustrated in this section will be limited to extremely simple cases which may not represent the majority of the marine cases particularly well. In addition to the complexity arising from our lack of adequate knowledge of the general turbulent behaviour of continental shelf flows, the problem of suspended sediment dynamics is further complicated by interactions which develop between the particles suspended in the flow. Changes in salinity affect the electrolytic behaviour of seawater. This, in turn, causes changes in the settling behaviour of the suspended sediment. Generally, fine clay particles are carried in a relatively dispersed state in rivers and nearshore portions of marine flows which have very low salinities. As these flows discharge into the ocean, the increased salinity enhances the electrolytic behaviour of the transporting fluid and induces flocculation of the finely dispersed clay grains. Flocculation seems to result primarily from the random collisionm of particles due to turbulence, and the adhesion of particles through electrochemical affinities due to imbalanced surface charges on the individual clay grains. This agglomeration of individual clay particles into larger and less dense particles generally increases the settling velocity of particles. However, the exact behaviour is complex and influenced by many chemical parameters within seawater other than simply the salinity, and by the clay minerals involved. That is, different clay minerals flocculate at different rates and in different ways.

The eroding of fine sediments which may eventually be carried in a suspended mode is also a complex phenomena. The conditions of suspended sediment concentration in the flow, changes in the boundary layer. and history of the underlying seafloor must be considered when studying this erosion.

In light of these complexities, the presentation of this section of the chapter will be limited to relatively general statements.

5.1 Dynamics of Suspended Sediment Transport

As previously stated, the transport of suspended sediment can be treated as being independent of the transport of bedload. Suspended sediment is supported within the water by the turbulence of the flow.

In order to illustrate the principles of suspended sediment transport, a simple situation is envisioned. This condition consists of a given concentration of fine sediments which do not change their flocculated state, and are being transported by a shear flow. Our analysis closely follows that given in Middleton and Southard (1977). The settling rate per unit volume of the sediment in this flow can be given as

$$\text{(Settling rate per unit volume)} = -WC \tag{52}$$

where W = the settling velocity of the particles

C = the concentration of sediment

and the negative sign appears because the vertical coordinate axis is taken to be positive upward from the seafloor.

At the same time that the fine particles are settling, they are influenced by the turbulent oscillations which exist in the shear flow. This results in causing a diffusion (thought to be uniform in all directions) of momentum of any particles carried by the flow. The rate of turbulent diffusion per unit volume is given by

$$\text{(rate of turbulent diffusion per unit volume)} = \varepsilon' \frac{dc}{dz} \tag{53}$$

where ε' = the sediment diffusion coefficient.

In equilibrium, the settling of the particles downward must be offset by an upward diffusion of particles due to the turbulence. Therefore, if a vertical concentration gradient exists such that there is a higher concentration of the suspended sediment at greater depth, there will be a net upward diffusion of the sediment particles due to the turbulence. The balance of this upward diffusion of sediment particles with their settling can be written as

$$WC + \varepsilon' \left(\frac{dc}{dz}\right) = 0 \tag{54}$$

It has been shown in an earlier chapter that the distribution of turbulent shear stresses within the flow can be given by

$$\tau = \rho \varepsilon \left(\frac{dU}{dz}\right) \tag{55}$$

where $\tau(z)$ = the turbulent shear stress within the flow

$U(z)$ = the mean current velocity at height z above the seafloor

ε = the eddy viscosity

z = a vertical coordinate axis directed positive upward from the seafloor.

It is commonly assumed that the sediment diffusion coefficient is proportional to the eddy viscosity. This can be represented as

$$\varepsilon' = A\,\varepsilon \tag{56}$$

where ε' = sediment diffusion coefficient

A = a proportionality constant taken to be close to 1.0

In a shear flow, the distribution of turbulent shear stresses within the fluid can be written as

$$\tau = \tau_o\left(1-\frac{z}{D}\right) \tag{57}$$

where D = the total flow depth

Combining equations 56 and 57 yields

$$\tau = \frac{\varepsilon'\rho_f}{A}\left(\frac{dU}{dz}\right) . \tag{58}$$

Combining Equations 57 and 58 yields

$$\varepsilon' = A\,\frac{\tau_o}{\rho_f}\;\frac{\left(1-\frac{z}{D}\right)}{\left(\frac{dU}{dz}\right)} . \tag{59}$$

Recall the definition of the friction velocity given earlier in this chapter.

$$u_* = \sqrt{\frac{\tau}{\rho}} .$$

Using this definition of the friction velocity, Equation 59 can be written as

$$\varepsilon' = Au_*^2 \frac{(1-\frac{z}{D})}{(\frac{dU}{dz})} . \tag{61}$$

In an earlier chapter, the following relationship between the vertical velocity gradient of the flow and the friction velocity was developed from the Law of the Wall,

$$\frac{dU}{dz} = \frac{u_*}{Kz} \tag{62}$$

where K = Von Karman's Constant

This relationship can be substituted for the differential in Equation 61 to yield

$$\varepsilon' = Au_* \ (1-\frac{2}{D})Kz. \tag{63}$$

The above equation represents a relationship between the sediment diffusion coefficient and the distribution of shear stresses in the turbulent flow. This equation can be used with the equilibrium transport condition given by Equation 54 to yield an equation which defines the vertical concentration gradient in equilibrium transport. The combination of Equation 63 and 54 yields

$$\frac{dc}{C} = \frac{-W \ dz}{AKu_* \ (1-\frac{z}{d})z} . \tag{64}$$

The vertical distribution of suspended sediment concentration can be determined through the integration of Equation 64. This equation must be integrated from an aribtrary level. usually taken to be very close to the bottom, to the upper limit of the shear flow. The integration yields

$$\ln C = \frac{W}{AKu_*} \int_a^D \frac{dz}{(1 - \frac{z}{D})z} \tag{65}$$

$$\frac{C}{C_a} = \left[\frac{D-z}{z}\,\frac{a}{D-a}\right]^B \tag{66}$$

where $B = \dfrac{W}{AKu_*}$.

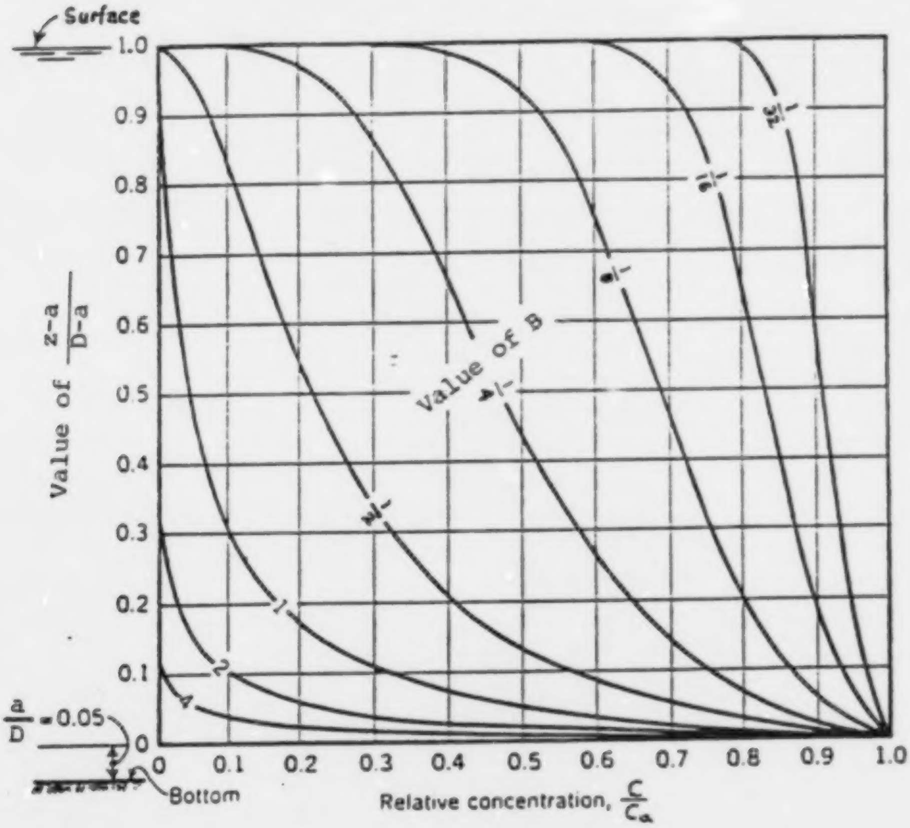

Figure 6-25 Figure showing the vertical distribution of relative concentration of suspended sediment against depth for different values of the parameter beta (from Middleton and Southard, 1978).

Equation 66 gives the concentration of suspended sediment in the shear flow for different levels (z) provided the near-bottom index concentration (C_a) is known.

Graphs of Equation 66 are shown in Figure 6-25 for different values of the parameter B (called the Rouse number). Note that when the settling velocity is large relative to the intensity of the turbulent shear stresses, the highest concentration of sediment is found very close to the bottom, with the concentration diminishing to zero a short distance up into the flow. Concentrations such as those illustrated in Figure 6-25 have been measured in a few river environments. It is significant to point out that in the marine environment, complications in the settling properties of the suspended sediment, as well as significant changes in the distribution of turbulence parameters from those associated with simple shear flow, generally lead to sediment concentration distributions with depth which differ significantly from those given in Figure 6-25. Because of the wide range of factors influencing the behaviour of turbulence in ocean flows, it is not possible to give a full description of these variations in the context of this course. The variations from the above derivation which arise as a result of a more complete representation of the settling behaviour of most suspended sediments in the ocean is illustrated in the following section on deposition of suspended sediment.

5.2 Suspended Sediment Deposition

In the previous section, an idealized case for equilibrium transport of suspended sediment in a turbulent shear flow has been covered. The discussion of more complex situations than those therein described have been deferred to this section. This is because an examination of the settling behaviour of suspended material is best addressed in the context of suspended sediment deposition.

In the previous section, we pointed out the difficulties involved in predicting the distribution of turbulent shear stresses and the nature of suspended sediment flocculation in the marine environment. These difficulties have greatly retarded the progress of research on the subject.

As noted in the introduction to this chapter, the source of the clay minerals which make up most of the suspended sediment in the ocean is ultimately the weathering and erosion of rock material on land. Rivers transport these clay minerals to estuaries. In estuaries, a number of complex interactions develop which lead to the deposition of some clay minerals and the bypassing of others to the open ocean. The major focus of this chapter has been to look at sediment transport in continental shelf environments. Therefore, the wealth of literature and studies on suspended sediment transport and deposition in estuaries will not be covered. The reason for this is that most of the processes related to suspended sediment deposition in estuaries are intimately tied to the rapidly changing salinity and electrochemical environment of water masses in estuaries. On continental shelves, these conditions tend to be much more homogeneous.

A major difficulty with the simple equilibrium of the suspended sediment transport model presented in the previous section of this chapter is that the settling behaviour of suspended clay minerals tends to change with their position in a flow. Most of the research into this phenomenon has been carried out by groups at the University of California at Berkeley and the University of Florida at Gainesville, and has mainly been accomplished by R.B. Krone; R. Ariathurai; E. Parthenaides; A. Mehta; R. MacArthur and M. Jonsson. Krone (1963) and Ariathurai et al (1977) have provided data which shows that the aggregation or flocculation of clay minerals progresses in a hierarchy of floccule sizes. In fresh water, clay minerals tend to be in their most dispersed state, owing to the poor electrolytic property of fresh water. Even under this condition, individual fine clay particles are transported in a flocculated state where each floccule consists of many hundreds to thousands of individual clay particles. These are often referred to as 'zero order flocculates', or 'zero order aggregates'. When zero order aggregates enter the marine environment, they tend to come together to form larger and less dense aggregates. The combination of a number (tens to hundreds) of zero order aggregates produces a 'first order aggregate'. These aggregates can go on to clump together into successivly higher order aggregates. Obviously, the process is not clear-cut. The possibility of producing higher order aggregates through a mixture of several lower order aggregates exists. Nevertheless, this does illustrate a general trend.

Each higher order of flocculate or aggregate is characterized by a lower bulk density and a lower shear strength. Higher order aggregates are larger, and settle faster in spite of their lower density. Table 7-II from Ariathurai et al. (1977), illustrates for five samples the changes in bulk density and shear strength associated with a different order of suspended sediment aggregates.

The tendency for lower order aggregates or flocculates to collide and grow to higher orders in turbulent flows is offset by the reduction in the shear strength of the aggregates with increased order. Krone and the other researchers of this group state that a balance exists between the Reynolds stresses in the turbulent flow and the shear strength of the flocculated suspended sediment. For a given intensity of turbulence, as measured by the local value for the Reynolds stress, the flocculates can only grow to a certain order before they are torn apart by the turbulence.

The above concepts introduce a complexity to the simple model for suspended sediment transport given in the previous section of this chapter. The Reynolds stresses in natural flows tend to increase with distance above the bed. As a consequence, larger and more rapidly settling aggregates are stable in the lower portion of turbulent boundary layers. Therefore, a correction should be made in Equation 54 to express the settling velocity as a function of height above the bed.

The above-described method of looking at flocculation of suspended sediment in turbulent flows contains within it the statement that the sea bed represents an area where aggregates of suspended sediment come to rest at one order of aggregation higher than that of the near-bottom suspended material. The newly deposited sediments on the seafloor are weaker than the largest aggregate in the suspended flow. This permits ready exchange of suspended sediment between the bottom and that moving in the flow.

According to this concept of suspended sediment transport. the deposition occurs when the Reynolds stresses in the fluid are reduced. Reducing the Reynolds stresses causes higher order aggregates to form. These aggregates settle more rapidly than can be supported by the level of turbulence in the flow, and thus deposition results.

It must be pointed out that the above description of suspended particle aggregation, as well as the intimate relationship between particle size, settling velocity, and turbulent parameters of the flow represents an idealized case. Because of the rapid changes in flow conditions and water masses on the continental shelf, there are many instances where this idealized equilibrium does not develop. Furthermore, many of the deposits of fine cohesive sediments on the seafloor are not in adjustment with the suspended sediment load at any particular instant. These seafloor deposits may have aged hours, days, or many years from the time that they were originally deposited. The aging process largely consists of a slow dewatering of the clay deposits resulting in compaction and marked increases in the strength of interparticle cohesion. Such a deposit may require significantly higher levels of turbulence to re-entrain than could have been accomplished shortly after it was deposited.

5.3 **Erosion of Suspended Sediments**

In environments where the flow is uniform and steady, it has been shown that the transport of sediment is controlled by shear stresses within and at the boundaries of the transporting fluid. The rate of sediment transport has been shown to be proportional to the fluid shear stress acting on the bottom area. Erosion develops when there are temporal or spatial gradients in the distribution of the fluid shear stress. When the bottom sediments are granular (that is, of sand size or larger), the rates of transport and erosion can be related to the size and density of the sediment. However, when the bottom sediment has a significant content of clay, the relationship between transport, erosion and fluid shear stresses is much more complex. The complexity arises from the small size and platey nature of the clay minerals, the relatively high intensity of electrochemical forces acting betwen individual particles in proportion to gravitational and fluid forces, complex interactions between individual clay particles of different mineralogy, and binding by organic substances. These complexities have caused research on the transport and erosion of cohesive sediments to lag significantly behind similar research on granular sediments. The difficulty is to discover the fundamental parameters which control the cohesion of clay-size particles.

Intuition suggests that the shear stress needed to erode and scour cohesive sediments should be related to the general strength of the sediment. Dunn (1959) used a water jet directed against a submerged clay sample to determine a qualitative relationship between the vane shear strength, plasticity index and grain size. Smerdon and Beasley (1959) repeated Dunn's experiments and produced data which suggested that the critical shear stress necessary to initiate suspension of the bottom sediment was related to the plasticity index and Middleton's disperson ratio. A series of experiments were conducted in the early 1960's using both the water jet equipment and a specialized cylindrical shear stress generating apparatus to study the relationship between the erosion of cohesive sediments and various soil parameters.

Espey (1963), Rektorik and Smerdon (1964), Masch and Espey (1965), as well as Masch, Espey and Moore (1965) all conducted experiments which indicated a relationship between the critical stress necessary to initiate the erosion of cohesive sediment and the vane shear strength and moisture content measurements. However, only a limited number of samples were tested. Figure 6-26 shows the general characteristics of these experimental results. When the erosion rate is plotted against the applied fluid shear stress, a disjointed curve commonly results. The intersection of this curve with the shear stress axis indicates the shear stress value necessary to initiate particle-by-particle erosion of the sample. The erosion of the sediment continues to

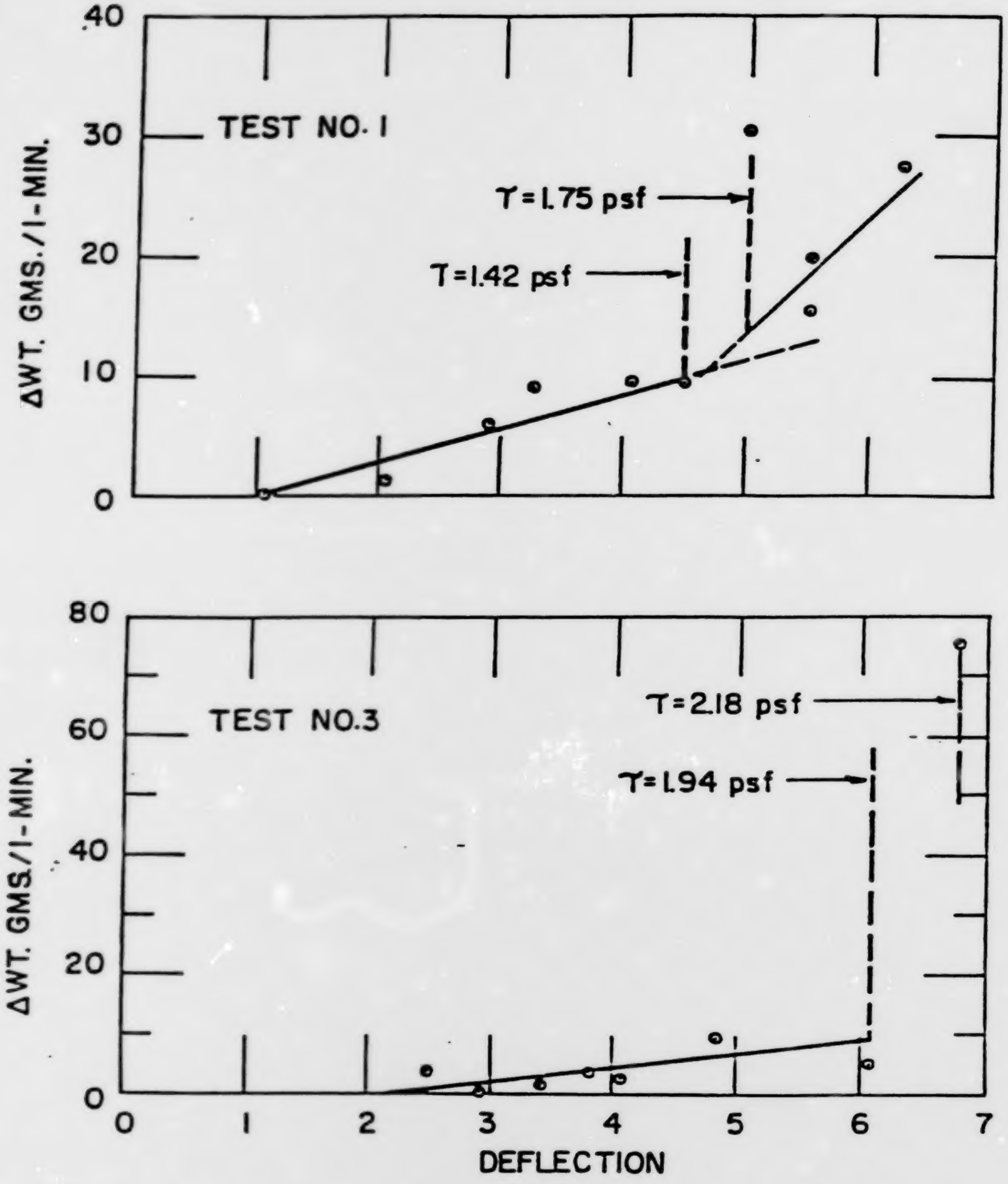

Figure 6-26 Weight loss per one minute versus deflection (from Masch, Espey and Moore, 1964).

increase linearly with increased shear stress until a particular value is reached. At this point, the rate of erosion increases sharply, and appears to result from mass erosion of chunks of the cohesive sediments. In Figure 6-26, this critical shear stress corresponds to a value of approximately 1.5 lb/ft^2 (kg/metre^2). Note that this value of shear stress does not represent the true point where the initial particle-by-particle erosion began. This illustrates an important aspect of published results from a variety of experiments. Most investigators report the point where mass erosion begins as the point corresponding to the critical shear stress necessary to entrain the bottom sediments. However, several investigators, particularly those using flume tests to achieve their data, report the critical shear stress as the value necessary to initiate particle-by-particle erosion. Unfortunately, it is generally impossible to reconcile these two different methods of reporting with results of experiments. The results shown in Fig. 26 represent values for the Taylor Marl. This is a calcareous silty marl which has many of the properties of cohesive sediments, but is atypical in the sense that its cohesion is developed by carbonate mineral grains rather than clay mineral grains.

Figure 6-27 shows data from a paper by Masch and Espey (1965) relating the vane shear strength values to the critical erosive shear stress for the Taylor Marl. Figure 6-28 is also adapted from this paper and shows a linear relationship between values of moisture content and the critical erosive shear stress. In viewing both Figure 6-27 and 6-28, one should note the limited

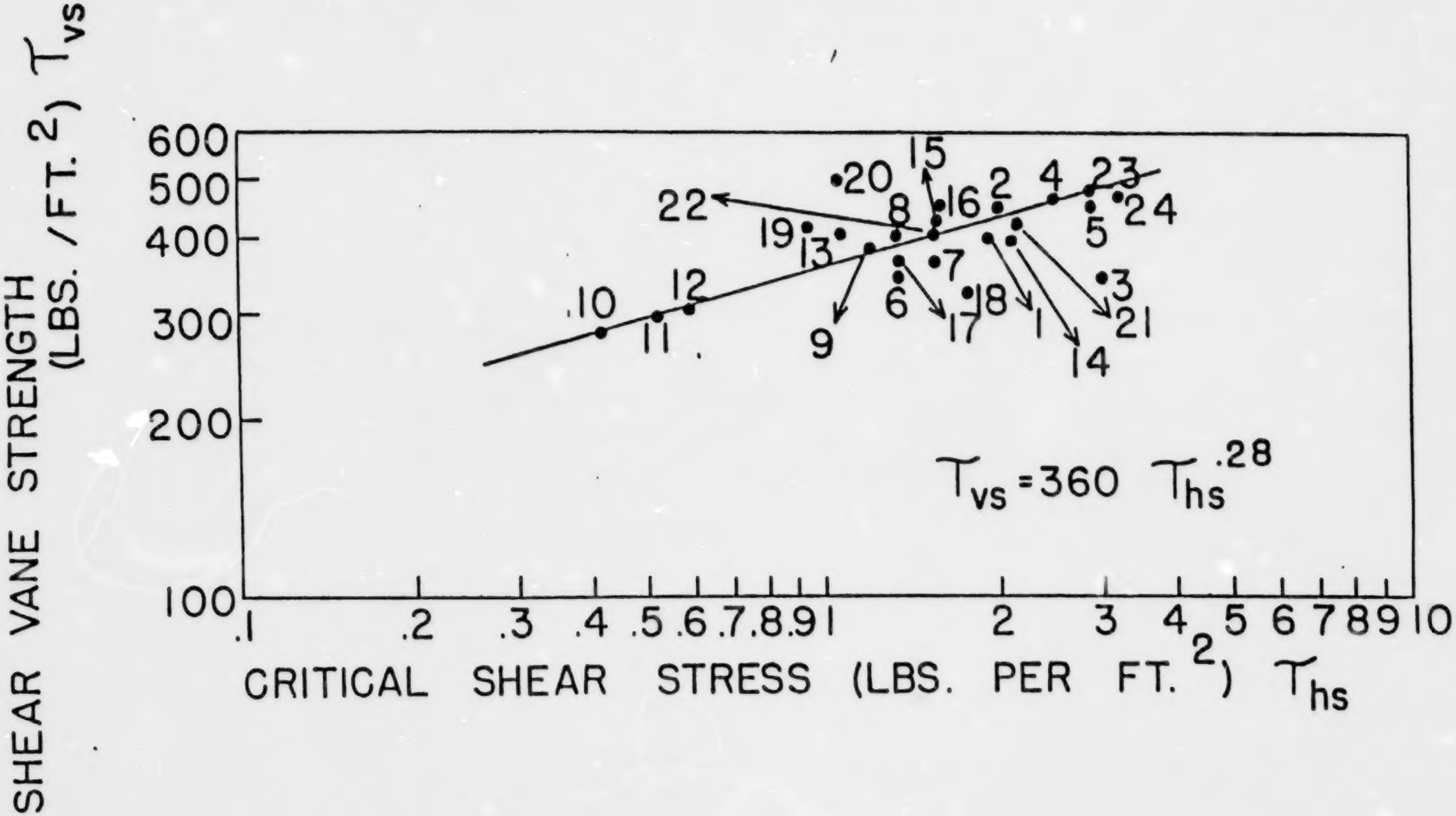

Figure 6-27 Shear vane strength versus critical shear stress for the Taylor Marl (from Masch and Espey, 1965).

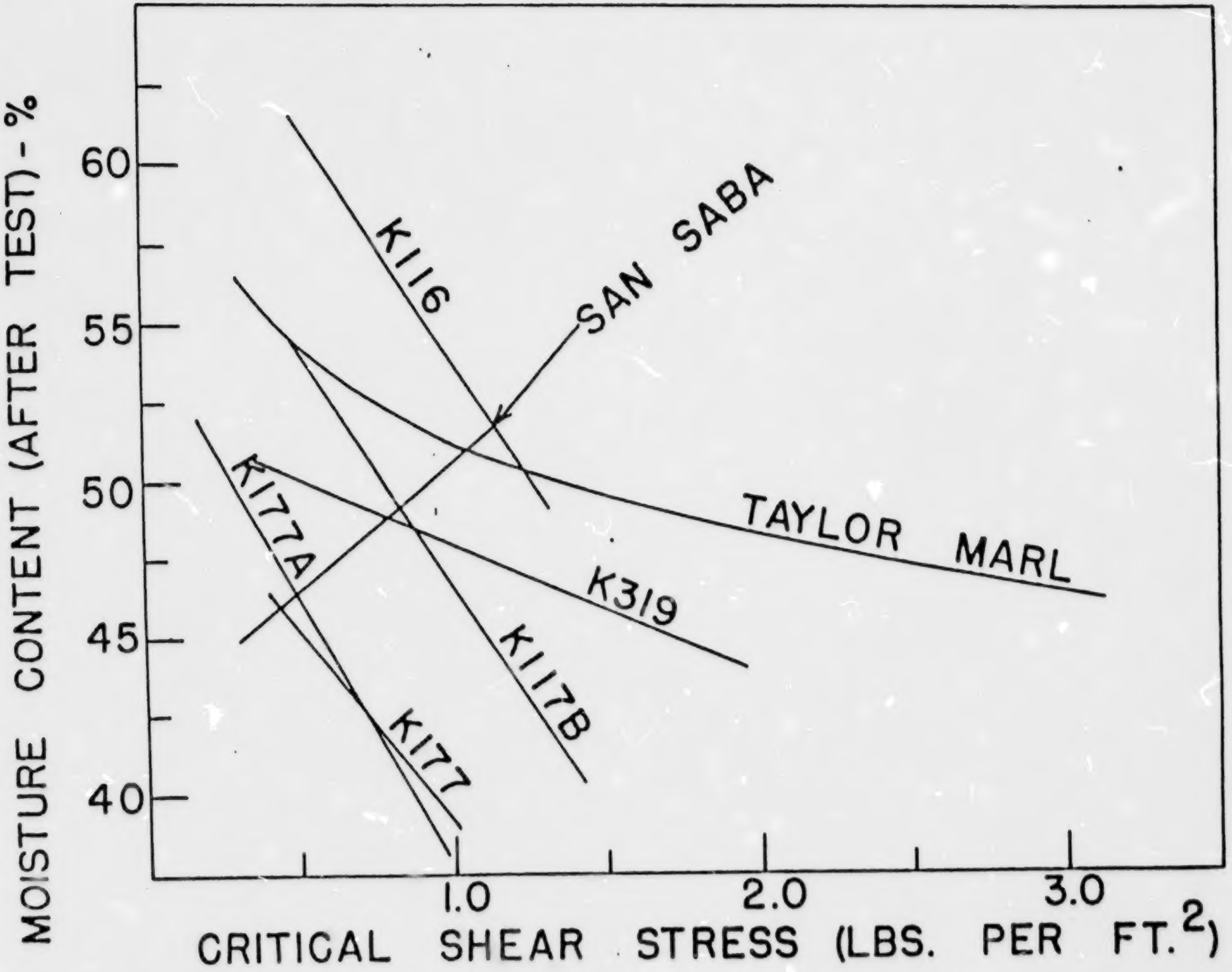

Figure 6-28 Critical shear stress versus moisture content (from Masch and Espey, 1965).

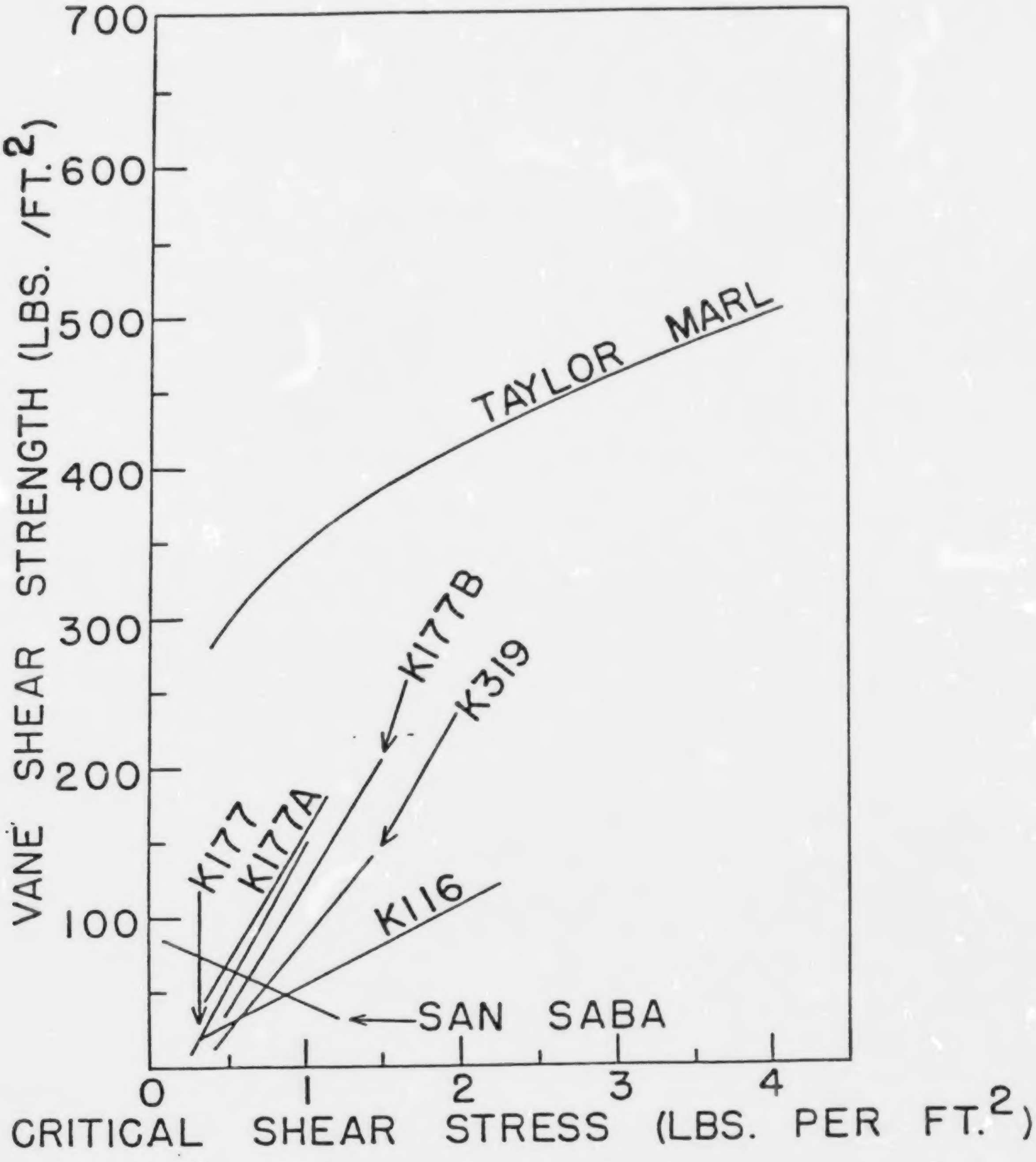

Figure 6-29 Vane shear strength versus critical shear strength (from Masch and Espey, 1965).

range of vane shear strengths and moisture contents used in the experimental samples.

Figure 6-29 is also adapted from the paper by Masch and Espey (1965). This figure shows a number of curves relating the values of vane shear strength to the critical erosive shear stress. The different curves correspond to different samples of cohesive sediments including the Taylor Marl and Houston Clays. It is clear from this figure that there is no simple relationship between vane shear strength values and the critical erosive shear stress as each sample demonstrates a unique line. However, a general tendency for increased critical shear stress values corresponding to increased vane shear strength values can be seen. No attempts were made by the authors of these data to evaluate the effect of other parameters in producing the scatter of their results.

Figure 6-30, adapted from a paper by Smerdon and Beasley (1959), shows a linear relationship between the plasticity index and the critical shear stress from a few experiments. Figure 6-31 shows a similar linear relationship. In all cases, the scatter about the linear relationship is rather large and the number of experimental points is small.

At about the same time, other investigators attempted to determine the role of additional parameters which would help to account for the observed scatter in previous experimental data. Grissinger and Asmussen (1963) showed that the moisture content of the sample appeared to be the primary controlling parameter of the critical shear stress necessary to erode. The latter authors

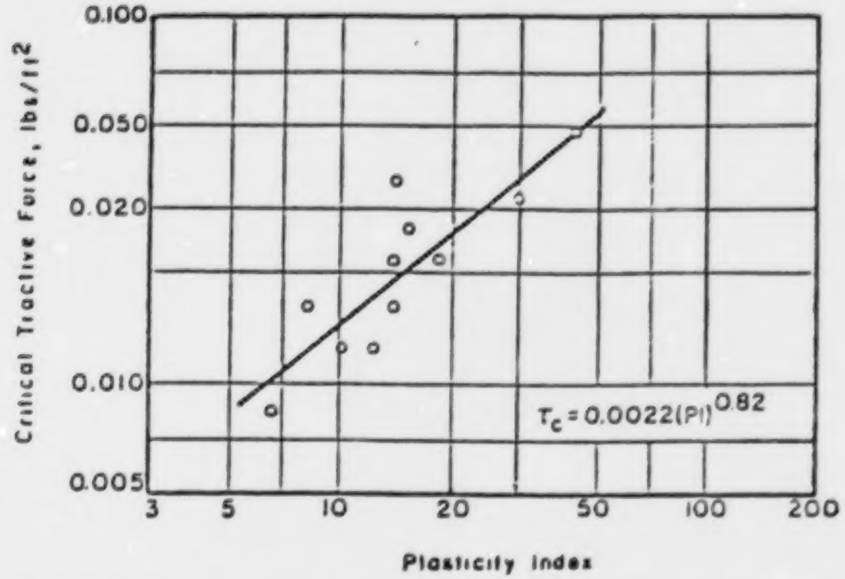

Figure 6-30 Critical tractive force determined from velocity profile versus plasticity index (U.S. Committee on Sedimentation, 1968).

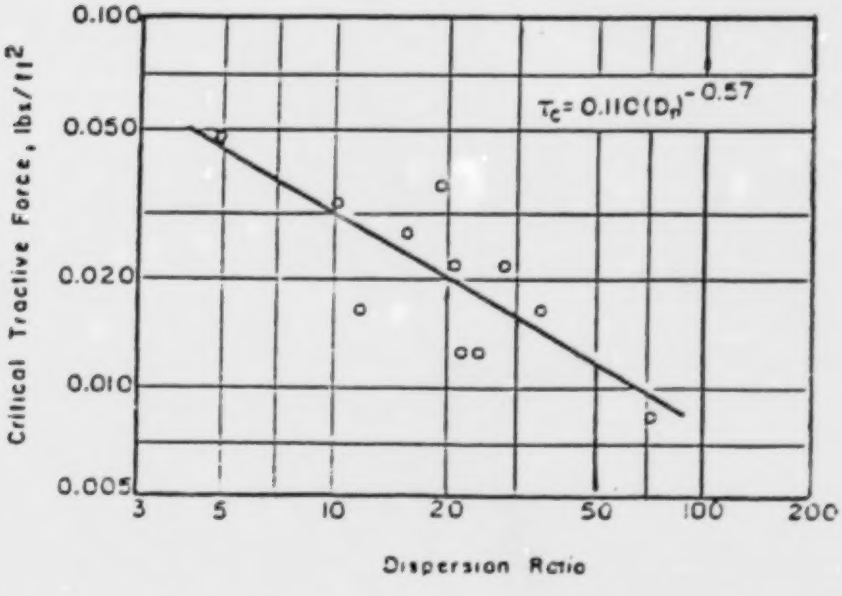

Figure 6-31 Critical tractive force determined from velocity profile versus dispersion ratio (U.S. Committee on Sedimentation, 1968).

also pointed out that the amount of time that the sample had been at a particular level of saturation also affected the values of critical fluid shear stress. Grissinger (1966) further points out the effect of different mineralogies, as well as the imbrication or orientation of platey minerals, on controlling the erosion processes.

Parthenaides and Paaswell (1970) reviewed the previous literature and conducted experiments of their own. They conclude that an appraisal of previous experiments indicates that attempts to correlate the critical erosion fluid shear stress values to vane shear strength values, moisture content. and Atterberg limit value show very inconsistent results. They also point out that the use of different types of apparatus such as rotating cylinders, various types of flumes, and water jets to evaluate the erosive fluid shear stresses acting on cohesive sediments have produced such scattered results that little can be learned from comparison of different experiments.

More recent studies have tended to concentate on various other parameters related to the erosion resistance of cohesive sediments, and generally to turn away from basic soil test parameters. Sargunam et al., (1973) conducted a series of rotating flume experiments to evaluate the critical shear stres and rate of erosion of San Francisco Bay Muds under different concentrations of sodium chloride. The results are shown in Figure 6-32. There is a clear indication that the critical shear stress necessary to entrain, and the erosion rate, differ considerably for different sodium chloride concentrations

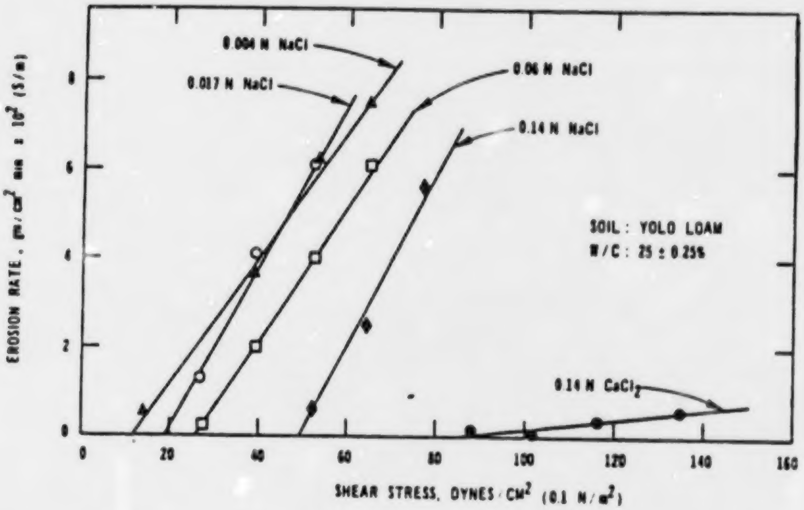

Figure 6-32 Specimen erosion rate versus shear stress (from Sargunam et al. 1973).

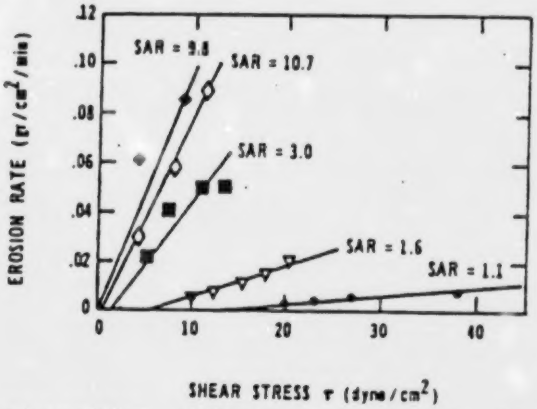

Figure 6-33 Relationship between erosion and shear stress for differential SAR for the Yolo loam, concentration 0.005 N-w/c = 23% (from Arulanandan et al., 1975).

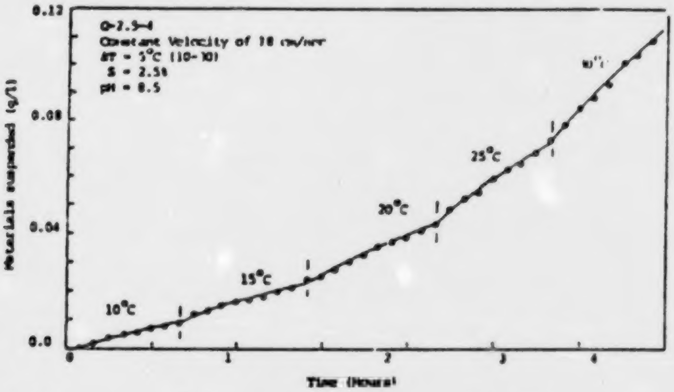

Figure 6-34 Variation of suspended sediment concentration with time and temperature (from Kelly et al., 1979).

(essentially different salinities). This direction of work was followed by Arulandan, Loganathan and Krone (1975). They conducted similar tests using a measure of exchangeable cations in the pore and eroding fluid known as the sodium adsorption ration (SAR). Their results are shown in Figure 6-33, and these also indicate considerable variation in critical shear stresses and erosion rates based on different values of the SAR. Kelly, Gularte and Nacci (1979) have studied the effect of temperature on the erosion rate of cohesive sediments. Their data are shown in Figure 6-34.

The best source of information on the erosion of cohesive sediments is found in Ariathurai, MacArthur and Krone (1977) (e.g. Table 6-II). A review of this study shows that most recent research is directed at understanding the nature of the physiochemical and biochemical bonds between individual clay minerals in cohesive sediments as they affect the erodibility of these deposits. This study points out the important effect on its erodibility of such factors as cation exchange capacity, sodium absorption ratio, and order of the original aggregates which formed the cohesive deposit.

The foregoing brief review of research literature indicates that early results suggested relatively straightforward relationships between primary soil parameters and the erodibility of cohesive sediments. However, these early results were based on a small number of experiments conducted on only a few types of cohesive sediments. As research continued, more and more variability resulted. At present, there does not appear to be a

Table 6-II

Properties of sediment aggregates

Sediment Sample	Order of Aggregation	Density g/cu cm	Shear Strength dynes/sq cm
Wilmington District	0	1.250	21
	1	1.132	9.4
	2	1.093	2.6
	3	1.074	1.2
Brunswick Harbor	0	1.164	34
	1	1.090	4.1
	2	1.067	1.2
	3	1.056	0.62
Gulfport Channel	0	1.205	46
	1	1.106	6.9
	2	1.078	4.7
	3	1.065	1.8
San Francisco Bay	0	1.269	22
	1	1.179	3.9
	2	1.167	1.4
	3	1.113	1.4
	4	1.098	0.82
	5	1.087	0.36
	6	1.079	0.20
White River (salt)	0	1.212	49
	1	1.109	6.8
	2	1.079	4.7
	3	1.065	1.9

From - Ariathurai, R., MacArthur, R.C., & R. B. Krone, 1977,
Mathematical Model of Estuarial Sediment Transport
U. S. Army Engr. Contr. No. DACW39-75-C-0080 Rep't., 70pp.

Table 6-III

Parameters potentially related to the critical fluid shear stress to erode cohesive sediments

Ordinary Soil Parameters

- grain size - mean and range
- mineralogy
- plasticity index
- moisture content
- vane shear strength
- Atterberg limit
- dispersion ratio
- bulk density

Special Sedimentary Parameters

- order of primary aggregates
- orientation of platey minerals
- degree of compaction and duration in this state
- roughness of bed surface

Chemical Parameters

- surface charge density of the mineral grains
- salt concentration of the surrounding water
- valency of the cations in solution
- temperature
- pH of the surrounding fluid
- kind of anions in solution
- cation exchange capacity
- sodium adsorption ratio

Biological Parameters

- amount of organic mucous binding
- concentration of bacteria
- concentration of detritavour infauna

unique set of fundamental parameters which permits the accurate prediction of erodibility for cohesive sediments. Table 6-III lists many of the parameters which have been investigated in the hope of discovering this relationship. It serves to emphasize the complexity of the factors which control the erodibility of cohesive sediment, but does little to answer the fundamental problem. Therefore, accurate predictions of the erodibility of cohesive sediments require direct laboratory measures of the critical shear stress necessary to initiate erosion and the relationship between erosion rate and fluid bed shear. Only with these direct laboratory measurements can accurate predictions be made.

Number/
Numéro

7

Chapter 7 BEDFORMS ON CONTINENTAL SHELVES - THEIR GENESIS AND MOBILITY

Carl L. Amos

1 INTRODUCTION

The advent of high resolution sidescan sonar, seabed photography and the development of submersible technology have shown that continental shelves, even to a depth of 200 m, are actively changing due to modern day physical and biological processes. Although the gross features of continental shelves are determined by bedrock geology and their geological evolution (Curray et al., 1977), recent processes such as seismic activity, ice dynamics, wave and current forces, degassing or dewatering of sediment and slumping are all major elements in the character of continental shelf sediment (Bouma, 1981). Continental shelves can be generally classified into the following types on the basis of process:

1. Tidal shelves, such as the North Sea
2. Wave dominant shelves, such as those of the western USA
3. Storm current shelves, such as those of S.E. America and eastern USA
4. Ice dominant shelves such as the Beaufort Sea and the Labrador Sea shelf.

Swift et al., (1971) have subdivided the main physical processes influencing continental shelves. This summary is shown in Figure 7-01 and is composed of:

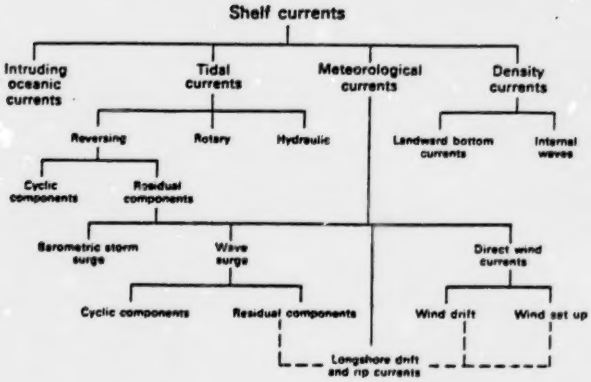
Shelf currents
Intruding oceanic currents
Tidal currents
Meteorological currents
Density currents
Reversing
Rotary
Hydraulic
Landward bottom currents
Internal waves
Cyclic components
Residual components
Barometric storm surge
Wave surge
Direct wind currents
Cyclic components
Residual components
Wind drift
Wind set up
Longshore drift and rip currents

Figure 7-01 A summary of the main physical processes influencing continental shelf sediments (from Swift et al., 1971).

1. Intruding Oceanic Currents
2. Tidal Currents
3. Meteorological Currents
4. Density Currents

Superimposed on these processes are flow from waves and wind drift. The distribution of the active processes across the continental shelf is shown in Figure 7-02. Wave dominance and shore normal processes are important on the inner shelf; geostrophic and storm driven flows, parallel to the shelf strike. are important on the outer shelf.

The process on each of these shelf types produces its own suite of characteristic bedforms, from which the history of near recent events can be interpreted. The suite of bedforms generated depend upon the nature of the substrate and can generally be defined as (1) unconsolidated (2) consolidated and (3) cohesive or (4) non-cohesive.

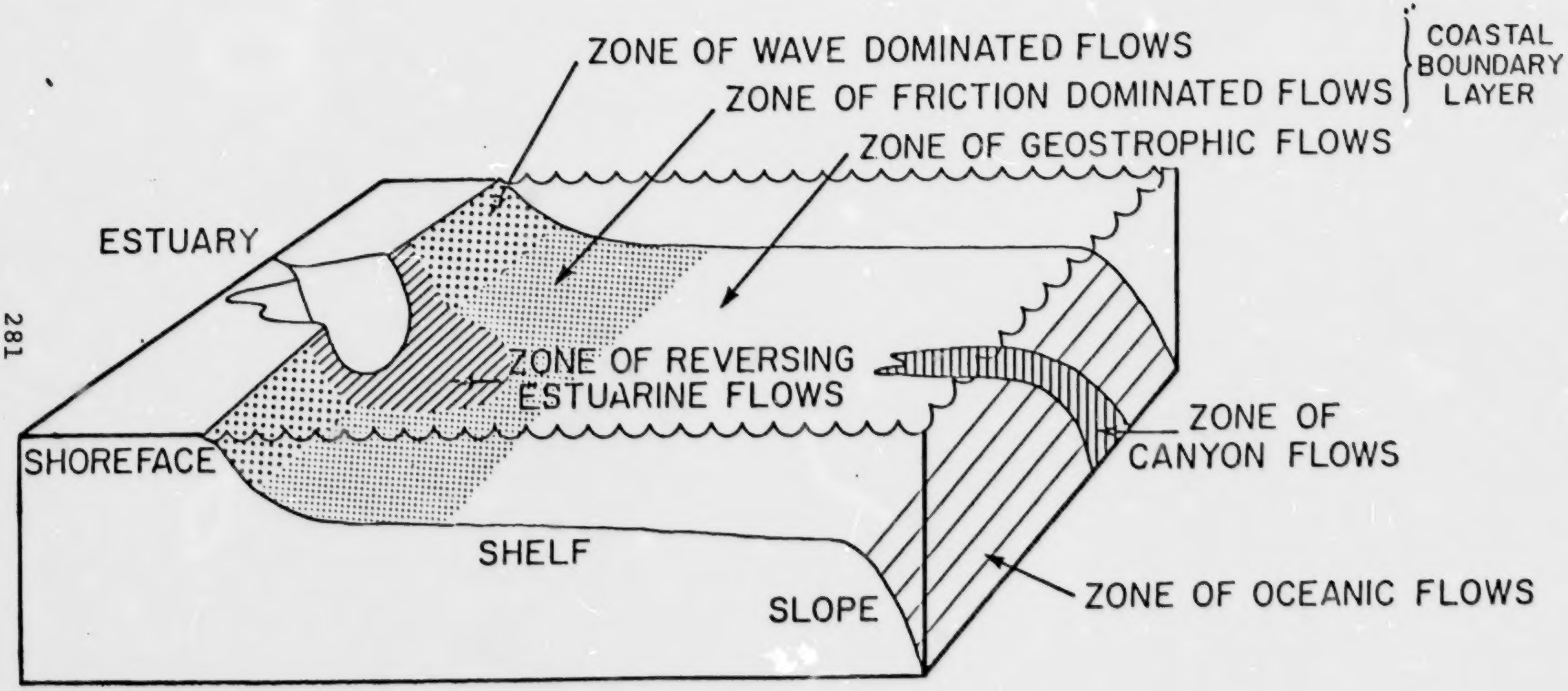
ZONE OF WAVE DOMINATED FLOWS
ZONE OF FRICTION DOMINATED FLOWS
COASTAL BOUNDARY LAYER
ZONE OF GEOSTROPHIC FLOWS
ESTUARY
ZONE OF REVERSING ESTUARINE FLOWS
ZONE OF CANYON FLOWS
SHOREFACE
SHELF
SLOPE
ZONE OF OCEANIC FLOWS

On the inner shelf, waves are dominant, together with the shore normal tidal and storm driven currents. This zone is termed the coastal boundary zone. On the outer shelf, contour parallel geostrophic currents predominate, with the occurrence of infrequent storm generated events.

Figure 7-02 The distribution of processes on the continental shelf.

Sediment instabilities result from :

1. sediment erosion, transport and deposition by waves and currents
2. slumping and sliding (shelf edge and basinal)
3. turbidity currents (basinal)
4. liquefication and plastic deformation
5. seismic activity
6. permafrost heaving
7. gas or ground water seepage.

The tell-tale sedimentary structure by which the originating process can be interpreted will develop provided (i) an adequate surficial sediment cover exists and (ii) the presevation potential is high.

Figure 7-03, taken from Reading (1979), shows a hypothetical reconstruction of a shelf depositional environment. The example, based on geological reconstruction (A), and on a modern analogy (B), illustrates the potential use of sedimentary structures in the interpretation of depositional environment. Furthermore, such structures are preserved geologically and are excellent indicators of the regional processes. Knowledge of these is vital to engineers designing structures expected to withstand such processes.

The sedimentary structures may represent the record of a series of events dating back to glacial times. The engineer should not overlook such "records", given that the monitoring of these processes has perhaps only been taking place for a few years.

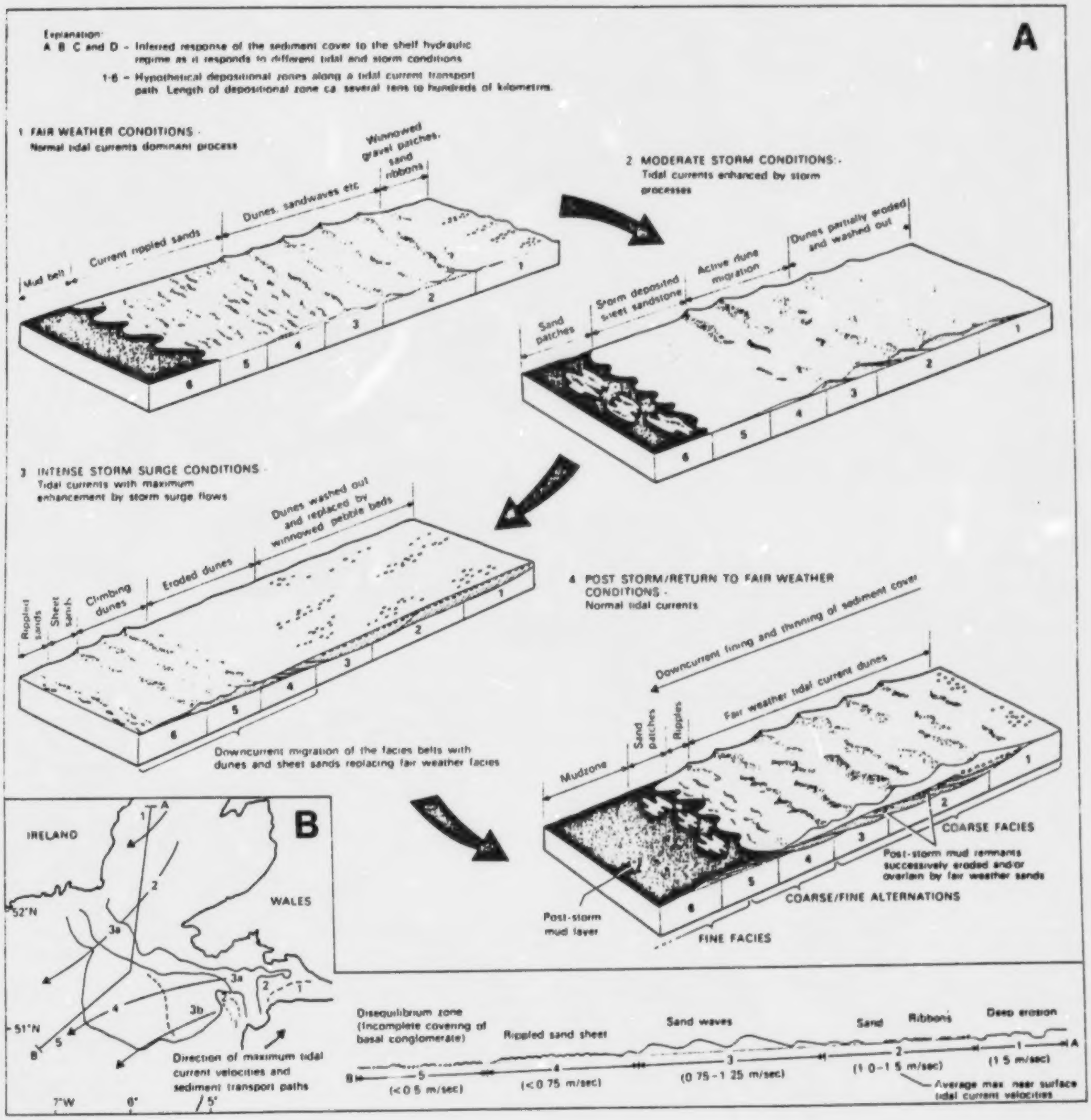
A
Explanation:
A B C and D - Inferred response of the sediment cover to the shelf hydraulic regime as it responds to different tidal and storm conditions
1-6 - Hypothetical depositional zones along a tidal current transport path. Length of depositional zone ca. several tens to hundreds of kilometres.
1 FAIR WEATHER CONDITIONS -
Normal tidal currents dominant process
Mud belt
Current rippled sands
Dunes, sandwaves etc.
Winnowed gravel patches, sand ribbons
2 MODERATE STORM CONDITIONS:-
Tidal currents enhanced by storm processes
Sand patches
Storm deposited sheet sandstone
Active dune migration
Dunes partially eroded and washed out
3 INTENSE STORM SURGE CONDITIONS -
Tidal currents with maximum enhancement by storm surge flows
Rippled sands
Sheet sands
Climbing dunes
Eroded dunes
Dunes washed out and replaced by winnowed pebble beds
Downcurrent migration of the facies belts with dunes and sheet sands replacing fair weather facies
4 POST STORM/RETURN TO FAIR WEATHER CONDITIONS -
Normal tidal currents
Downcurrent fining and thinning of sediment cover
Mudzone
Sand patches
Ripples
Fair weather tidal current dunes
COARSE FACIES
Post-storm mud remnants successively eroded and/or overlain by fair weather sands
COARSE/FINE ALTERNATIONS
Post-storm mud layer
FINE FACIES
1
2
3
4
5
6
B
IRELAND
WALES
52°N
51°N
7°W
6°
5°
3a
3b
Direction of maximum tidal current velocities and sediment transport paths
Disequilibrium zone (Incomplete covering of basal conglomerate)
Rippled sand sheet
Sand waves
Sand
Ribbons
Deep erosion
5 (<0.5 m/sec)
4 (<0.75 m/sec)
3 (0.75-1.25 m/sec)
2 (1.0-1.5 m/sec)
1 (1.5 m/sec)
Average max. near surface tidal current velocities

Figure 7-03 A hypothetical reconstruction of a sandy shelf (from Reading, 1979).

Figure (A) shows the sequence of anticipated bed forms across the shelf under (1) fair weather conditions (2) moderate storm conditions (3) intense storm surge conditions and (4) post storm recovery.

Figure (B) shows the sequence of bedforms developed in the Celtic sea (after Belderson and Stride, 1966). The general transport direction is from north to south with decreasing current conditions. The bedforms generated are scours - sand ribbons - plane bed - sand waves (megaripples?) - ripples.

The purpose of this section is to give a brief overview of the genesis of the major sedimentary bedforms and to describe the key features by which such bedforms can be recognized. Sedimentary structures are universal in that, given the same processes and equivalent sediment grain size, the same structures will be generated, irrespective of location. Indeed sand waves have been recognized on Mars, and scouring (wind?) on the moon. As a result, I have not attempted to restrict this discussion to those features observed on Canadian continental shelves only, but rather to highlight the bedforms which would be expected given the known processes and sediment distribution.

Clearly, one of the most significant features of Canadian shelves is ice and ice scouring. I have omitted this process as it will be dealt with elsewhere in Chapter 4.

2 THE GENESIS OF BEDFORMS

The origin and nature of continental shelf bedforms in the natural marine environment are poorly understood, due to the complex interaction of a variety of processes. The dominant processes are (i) the constructional effects of oscillatory fluid motions under waves superimposed on the prevailing unidirectional tidal or storm driven currents, and (ii) the destructive effects of bioturbation, liquefaction or slumping. Further complications in the development and morphology of bedforms are the complex inhomogeneities of bottom sediments, seabed slopes and the time history of the interaction of the above processes.

2.1 Non-cohesive Bedforms

In order to understand the mode of bedform generation we must first examine the effects of simple, single, time-constant processes as revealed by flume tank experimentation. Such study has been underway since the 19th Century, and involved the work of Sorby, (1859) and Gilbert, (1914). In more recent years a considerable amount of similar work has been carried out, yet the principle of spontaneous bedform generation remains a mystery. Why do bedforms generate at all, and what significance do they hold in the interpretation of shelf sediment stability?

Perhaps the most universal of all bedforms are the constructive, rhythmic "ripple-like" features. Such features occur in a variety of sizes, from centimetres to kilometres in wavelength and up to tens of metres in height. How do such bedforms generate and under what prevailing conditions are they preserved?

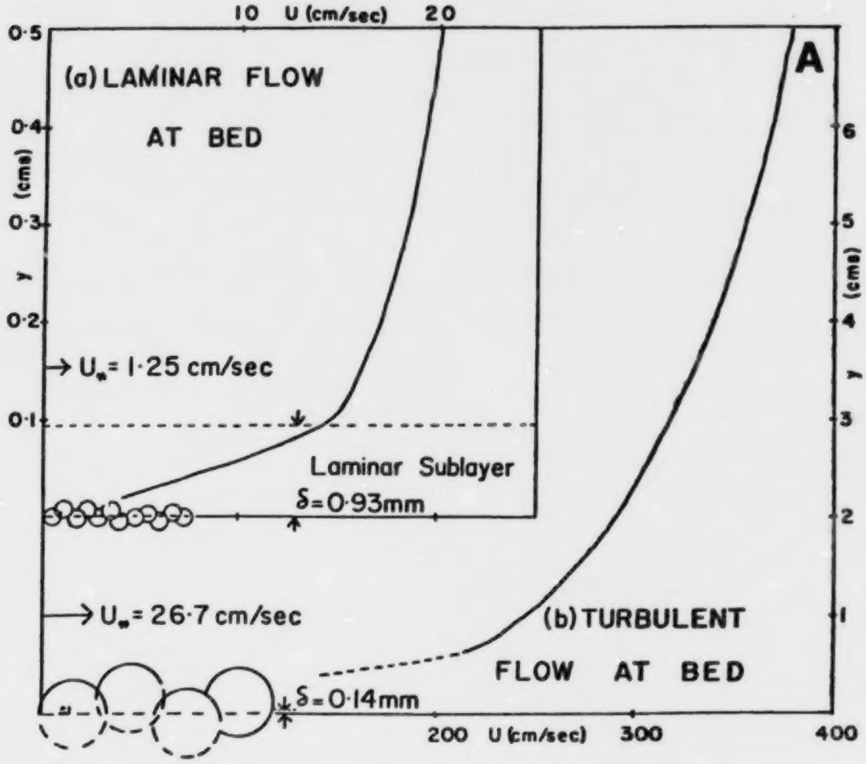

At lower flows (U_{40} = 13 cm/s), the laminar sublayer is much thicker than the sediment grains. Turbulence is suppressed, bedforms cannot generate and transport occurs at higher velocities.

Figure 7-04 (A) The relationship of grain size to boundary layer flow close to the bed.

The work of Simons et al. (1965) and more recently that of Costello and Southard (1981) indicate that bedforms initially are the result of current parallel fluid stress variations at the seabed, related to bottom roughness elements. This results in flow separation (either laminar or turbulent) from the bed. This view, initially postulated by Raudkivi (1963), also requires a downstream reattachment point to produce a local change in sediment transport rate and direction which leads to bedform generation. At the point of separation the bottom stress is

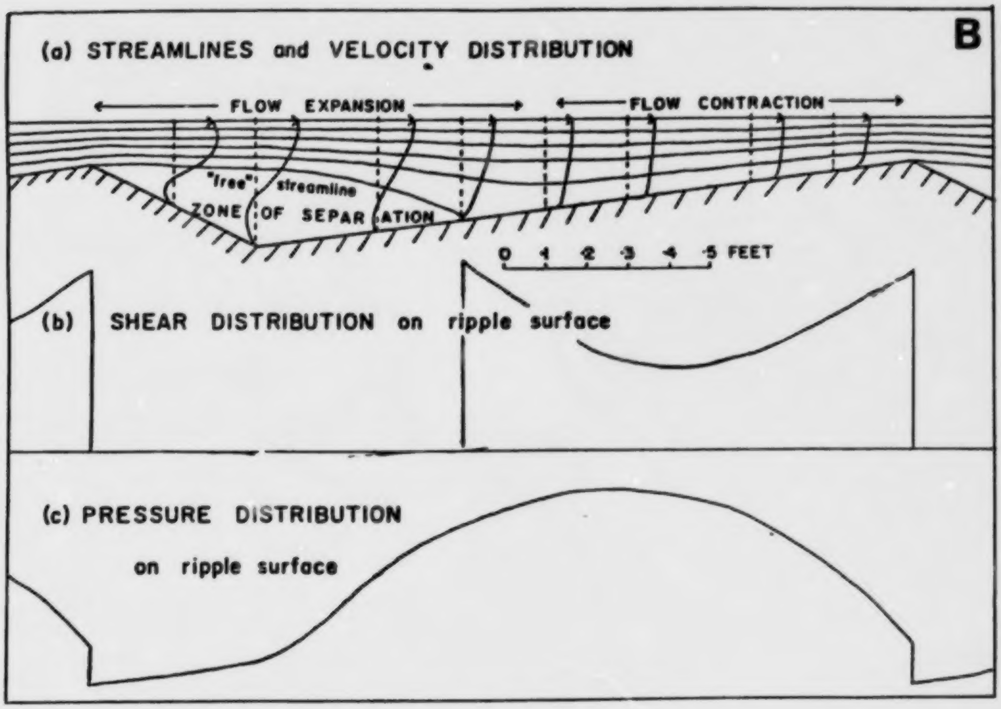
B
(a) STREAMLINES and VELOCITY DISTRIBUTION
FLOW EXPANSION
FLOW CONTRACTION
"free" streamline
ZONE OF SEPARATION
0 ·1 ·2 ·3 ·4 ·5 FEET
(b) SHEAR DISTRIBUTION on ripple surface
(c) PRESSURE DISTRIBUTION on ripple surface

Flow separation takes place at the crest, with the point of reattachment downstream of the trough. Maximum stresses occur at the crest of the bed form and at the point of reattachment. The maximum pressure is on the middle of the stoss face and the minimum in the trough.

Figure 7-04 (B) The pattern of flow streamlines over ripple bedforms.

zero. Just downstream of the point of reattachment, the stress is maximum. This concept is indicated in Figure 7-04(B). The differential in sediment transport rate leads to the development of a sediment mound immediately up-current of the point of minimum stress. In practice, the sediment mound quickly develops a downstream slip face at the angle of repose of the composite grains, onto which is avalanched layer upon layer of grains as transport continues. These grains, caught in the "zone of separation" accumulate on the slip face, where they become incorporated into the advancing bedform. This leads to a downcurrent depletion of sediment. The ripple trough develops in the zone of separation due to this depletion of sediment and due to reverse flows. The combination of (i) the upstream mound, (ii) the developing slip face, and (iii) the downstream trough produce the classic "ripple type" bedform profile.

The creation of these bedforms (over a previously flat surface) takes place in a downstream direction and results from the change in bottom stress at the point of reattachment. This is emphasized by the "first" ripple. Turbulence and wake eddies produced by the developing bed feature impinge upon the bed at the point of reattachment, resulting in maximum local bottom stresses (Raudkivi, 1967). The sediment transport at this point is greatest and takes place in a downstream direction. Downstream of this point the bottom stresses decrease due to the stabilization of the flow and the suppression of turbulence. The result is a net build up of bottom sediment, creating a second mound, which begins the cycle of bedform generation anew. This principle appears to apply to all ripple forms and pre-supposes that flow conditions are above the critical stress for sediment motion. The terminology applied to ripple-type bedforms is shown in Figure 7-05(A).

We now arrive at an important point in the curve. Non-cohesive bedforms are generated in response to variations in bottom stresses, exerted by fluid flow and within definable limits. The lower limit is the critical stress for the initiation of sediment movement, the upper limit is based on criteria such as Reynolds number, Froude number and grain diameter of the

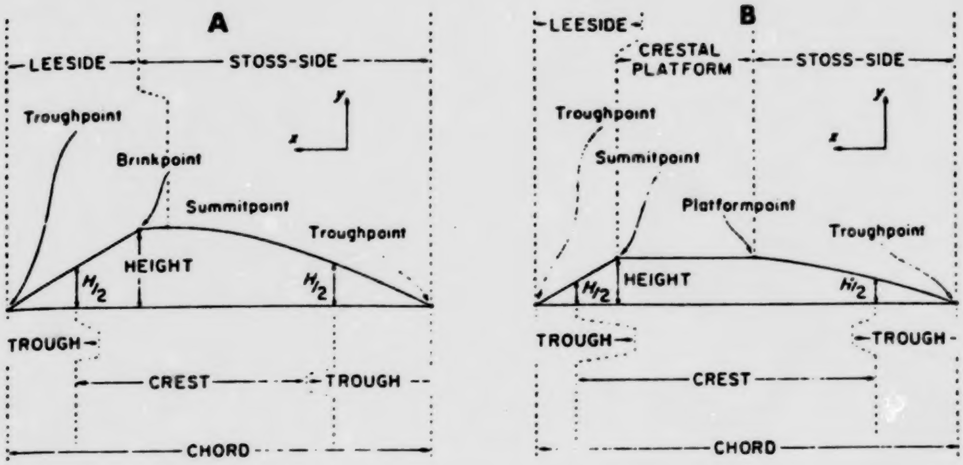
A
LEESIDE
STOSS-SIDE
y
x
Troughpoint
Brinkpoint
Summitpoint
Troughpoint
HEIGHT
H/2
H/2
TROUGH
CREST
TROUGH
CHORD
B
LEESIDE
CRESTAL PLATFORM
STOSS-SIDE
y
x
Troughpoint
Summitpoint
Platformpoint
Troughpoint
HEIGHT
H/2
H/2
TROUGH
TROUGH
CREST
CHORD

Figure 7-05 (A & B) The terminology used to define the morphology of rhythmic bedforms in non-cohesive material.

(A) refers to megaripple type bedforms with a low ripple index (see figure 7-22(E)).
(B) refers to ripple or sand wave type bedforms with a high ripple index and a flat crest.

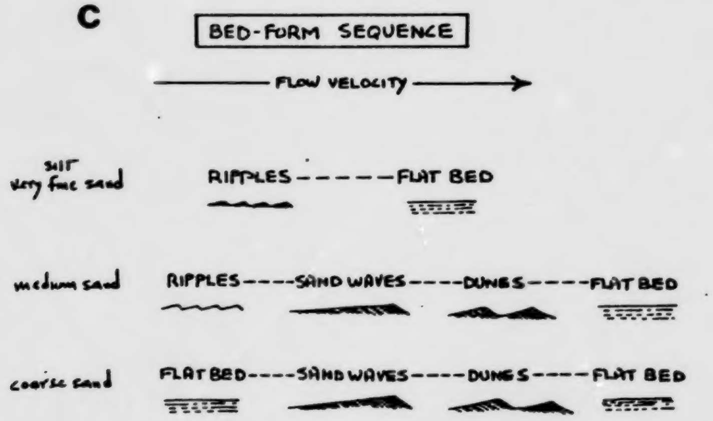
C
BED-FORM SEQUENCE
FLOW VELOCITY
silt very fine sand
RIPPLES - - - - - FLAT BED
medium sand
RIPPLES - - - - SAND WAVES - - - - DUNES - - - - FLAT BED
coarse sand
FLAT BED - - - - SAND WAVES - - - - DUNES - - - - FLAT BED

Figure 7-05 (C) The progression of bedforms resulting from an increase in unidirectional flow over silt and very fine sand, medium sand and coarse sand (from Middleton and Southard, 1977).

In silt and very fine sand the progression of bedforms is from small ripples to upper flat bed; in medium sand, ripples develop, followed by sand waves, 2-dimensional megaripples (dunes), 3-dimensional megaripples and upper flat bed. In coarse sand, no ripples develop, sand waves form from lower plane bed followed by 2-dimensional megaripples, 3-dimensional megaripples and finally upper flat bed. The gradation from one type to the next is gradual with a large degree of overlap in types. Several bedforms can coexist because of local differences in elevation and grain size.

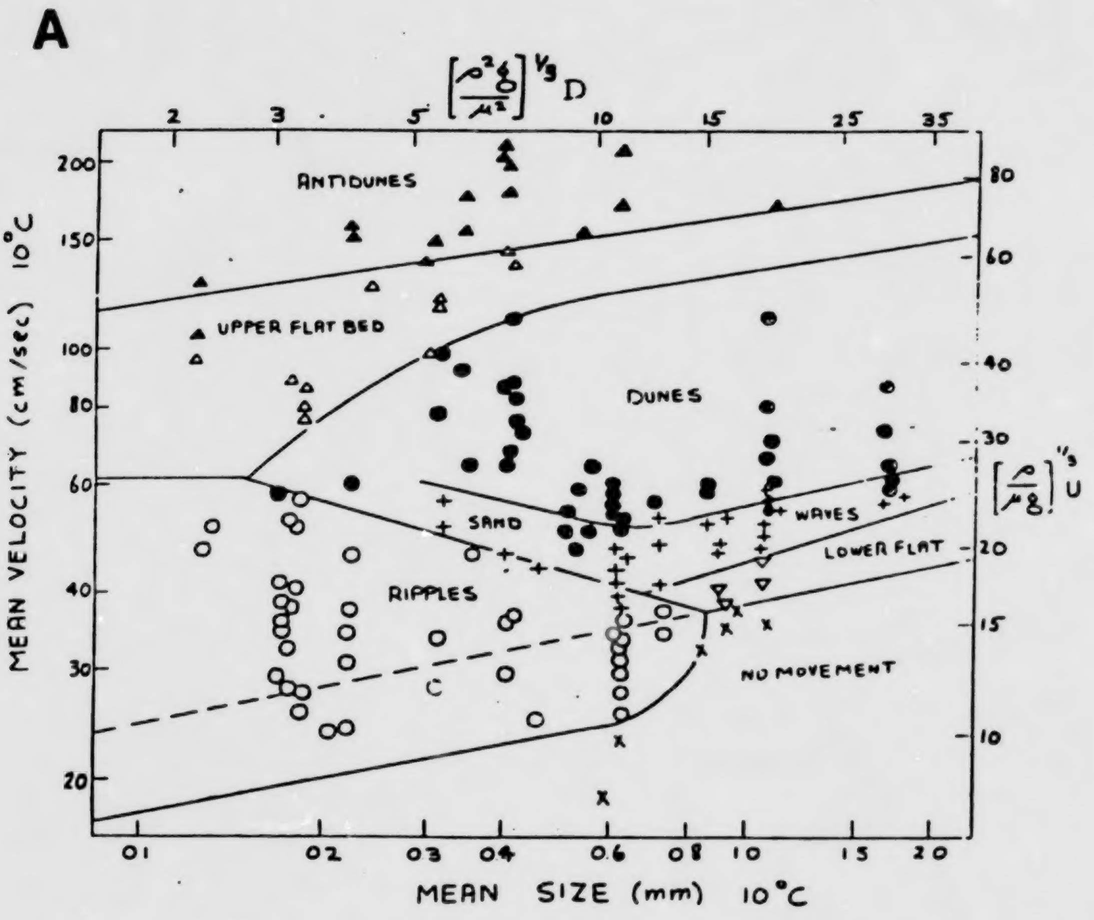

Figure 7-06 (A) The phase relationship between bedform type, mean flow velocity (over a flow depth of 40 cm) and grain size (mm).

The normalization to temperature (10°C) is related to grain transport mechanics and fluid stress which is a function of fluid density. The dimensionless equivalents of diameter and flow velocity are also shown. The term "dunes" refers to megaripples as defined herein. No subdivision is made between 2-dimensional and 3-dimensional megaripples, nor combined fields such as sand waves with superimposed megaripples.

bed material. Observation has shown that there is an orderly and repeatable sequence of bedforms which generate in response to increasing current strength and hence bottom shear stress. In sediments composed of silt and very fine sands, ripples will generate immediately. when the sediment begins to move. As the sediment transport increases bedforms degrade producing a flat bed characterized by parting lineations and current lineations. In medium sand, ripples are generated 'initially', but become displaced by sand waves, followed by megaripples (dunes) and thereafter by a flat bed phase as the current flow increases. In coarse sand, no ripples generate at all. Despite sediment motion, the bed remains flat. At higher flows sand waves generate. followed by megaripples (dunes) and thereafter by a flat bed phase (see Figure 7-05(B)).

Let us first examine the lower bound for bedform (ripple) generation under unidirectional flow. Figure 7-06(A) is a scatter diagram of bottom current velocity versus grain diameter (mm), and shows the occurrences of differing types of bedforms (after Middleton and Southard, 1977). For particles of diameter less than about 0.7 mm (i.e. coarse sand), ripples form directly upon the initiation of sediment motion. As seen in previous chapters, this stress can be defined using the Shield's criterion as follows:

$$= 0.06\ (\rho_s - \rho)g.d.; \quad R_e > 100 \qquad (1)$$

$$= 0.04\ (\rho_s - \rho)g.d.; \quad 10 < R_e < 100 \qquad (2)$$

For particle diameters larger than 0.7 mm no ripples generate at all, and sediment transport occurs as flat bed (lower).

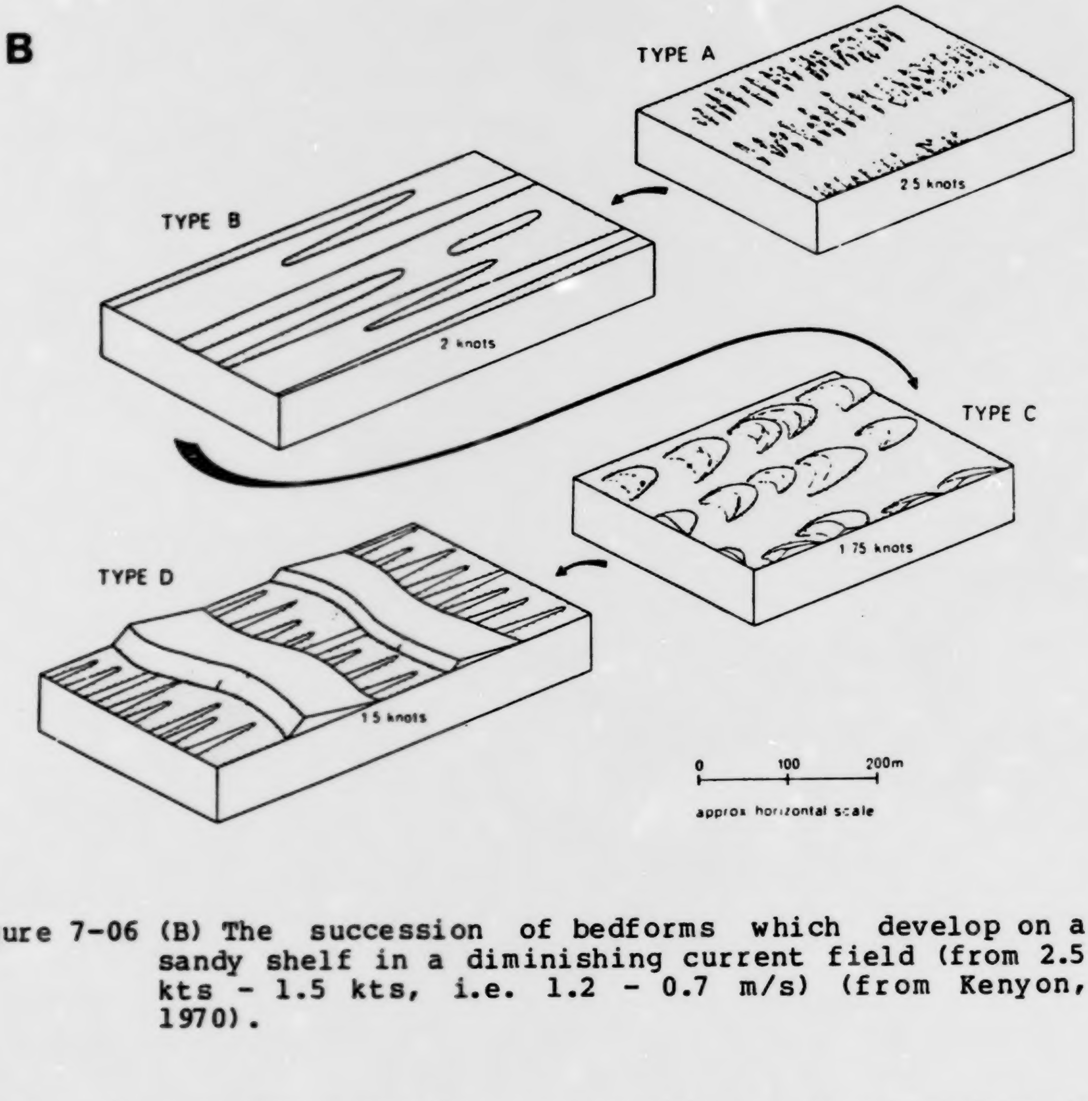
B
TYPE A
2.5 knots
TYPE B
2 knots
TYPE C
1.75 knots
TYPE D
1.5 knots
0
100
200m
approx horizontal scale

Figure 7-06 (B) The succession of bedforms which develop on a sandy shelf in a diminishing current field (from 2.5 kts - 1.5 kts, i.e. 1.2 - 0.7 m/s) (from Kenyon, 1970).

At 2.5 kts a disaggregated ribbon pattern develops with the majority of sediment in suspension. As the velocity drops to 2 kts. well developed sand ribbons form showing bifurcation patterns. As the velocity drops further, 3-dimensional megaripples form on the sand ribbons, which give way, as the flow drops further, to 2-dimensional megaripples and sand waves. The flow in the diagram is from right to left and is typical of bed forms developed during spin down of a storm event.

The upper bound for ripple generation is less clearly defined, but appears to occur at progressively decreasing bottom stresses (or mean current velocity) with increasing grain diameter. In terms of mean velocity (40 cm above the bed), the upper bound for ripple generation decreases from about 60 cm/s to 35 cm/s, while the lower bound (over the same size range of 0.1 - 0.7 mm) increases from about 13 cm/s to 25 cm/s. Table 7-I summarises the approximate mean velocities bounding each bedform type for fine, medium, coarse and very coarse sand. This data is derived from flume tank experimentation of a number of workers and exhibits a reasonable coherency to field results. The calculated upper and lower bounds of bedform generation, interpreted as the iniation of grain motion and onset of grain suspension respectively, are shown in Table 7-II. The initiation of bed motion (U_{40}) varies from 13.3 cm/s to 21.7 cm/s over the sand size range. Under turbulent conditions, suspension of sand will take place at mean current velocities (U_{40}) varying from 15.6 cm/s (fine sand) to 83.0 cm/s (coarse sand). This indicates that the bedload phase in fine sand is limited to a narrow range of current speeds and that suspension quickly ensues. The criterion for suspension, given as $U_* \approx w$, (where U_* is the friction velocity ($\sqrt{\frac{\tau}{\rho}}$) and w is the grain settling velocity in still water) is parallel to, but lower than the stress separating the sand wave and megaripple phases (Figure 7-09 (B) p.302). Costello and Southard (1981) have shed light on the generation of megaripples showing that sediment transport over these bedforms is as bedload. The concept of suspension representing the upper

Table 7-I

The approximate mean current velocities (40 cm above the bed) bounding to the various types of constructional. non-cohesive bedforms for fine, medium, coarse and very coarse sand

		Sand			
BEDFORM	BOUNDS	FINE	MEDIUM	COARSE	V. COARSE
Ripples	Upper	60 cm/s	50 cm/s	35 cm/s	No
	Lower	13 cm/s	20 cm/s	25 cm/s	Ripples
Flat Bed (lower)	Upper	No flat	No flat	45 cm/s	50 cm/s
	Lower	bed	bed	40 cm/s	45 cm/s
Sandwaves	Upper	No sandwaves	60 cm/s	50 cm/s	60 cm/s
	Lower		50 cm/s	40 cm/s	50 cm/s
2-D Megaripples	Upper	No 2-D	70 cm/s	70 cm/s	70 cm/s
	Lower	Megaripples	60 cm/s	50 cm/s	60 cm/s
3-D Megaripples	Upper	No 3-D	100 cm/s	110 cm/s	120 cm/s
	Lower	Megaripples	70 cm/s	70 cm/s	70 cm/s
Flat Bed (upper)	Upper	120 cm/s	120 cm/s	130 cm/s	140 cm/s
	Lower	60 cm/s	100 cm/s	110 cm/s	120 cm/s

Table 7-II

The approximate entrainment stresses and velocities for the initiation of grain motion and for grain dispersion of sand size sediment

	Sand			
	Fine (0.2 mm)	Medium (0.4 mm)	Coarse (0.7 mm)	V. Coarse (1.5 mm)
A) BED MOTION				
(i) stress	1.94 dynes/cm^2	3.88 dynes/cm^2	6.80 dynes/cm^2	14.57 dynes/cm^2
(ii) current velocity	13.3 cm/s	15.3 cm/s	17.5 cm/s	21.7 cm/s
(iii) friction velocity	1.39 cm/s	1.97 cm/s	2.61 cm/s	3.82 cm/s
B) SUSPENSION				
(i) stress	4.20 dynes/cm^2	30.03 dynes/cm^2	109.41 dynes/cm^2	463.11 dynes/cm^2
(ii) current velocity	15.6 cm/s	27.5 cm/s	44.7 cm/s	83.0 cm/s
(iii) friction velocity	2.05 cm/s	5.48 cm/s	10.41 cm/s	21.52 cm/s

The stress is expressed in dynes/cm^2 and assumes a water density of 1.00. The relation between friction velocity and mean current is derived using equation 4 and is expressed in cm/s. The current velocity is referenced to a height of 40 cm above the bed and has units of cm/s.

bedform phase is thought reasonable. However, the relation $U_* \approx W$ which represents the criterion for suspension is low. A value of $U_* \approx 2W_s$ is a closer representation of the onset of suspension. The above principles are considered representative of shelf environments, with perhaps one exception. Notice that in Figure 7-06, which shows the bedform types as a function of grain size (mm) and current speed (cm/s), both an upper flat bed phase and an antidune phase occur in fine sand. This is probably the result of flume tank conditions, where the water depth is limited (usually around 40 cm). This leads to lower Reynolds numbers for the same current speed than would be expected on the shelf. Indeed, antidunes result entirely from the bed response to stationary surface waves, which generate in phase with these waves at a Froude number of 1.0. Antidunes on the shelf are, therefore, extremely unlikely due to the depth of water. It is theoretically possible, however, to develop such features from internal stationary waves moving along a near bottom thermocline.

The determination of the upper limit for bedform generation (i.e. suspension) is based on the assumption that the critical friction velocity for suspension (U_*) bears some relationship to the terminal settling velocity (w) of the seabed sediment particles. Gibbs et al. (1971) have formulated a relationship between settling rate and grain diameter for silica spheres. This relationship has proved applicable to most types of sediment with the exception of heavy minerals or mica flakes. The equation he derived is:

$$W_s = \frac{4}{3}\left[g\rho(\rho_s-\rho)r^3 + g\mu^2 + 3\mu\right]^{\frac{1}{2}} \rho r \qquad (3)$$

where r = grain radius (cm)

μ = viscosity (poises)

g = gravity

ρ = fluid density

ρ_s = sediment density

For sediments which do not settle in a Newtonian manner, the settling rates can be determined by experimentation using standard settling tubes (see Amos et al., 1981). It should be noted here that sands do not settle as a simple function of grain diameter, due to the complex interrelationship of grain Reynold's number and coefficient of drag.

Observations (from high resolution, side scan sonar records and bottom photographs) from the Canadian continental shelves, show the whole suite of constructive, non-cohesive bedforms, with the exception of antidunes. Figure 6 (B) shows the sequence of these bedforms as interpreted from such records (Kenyon, 1970). Notice that only the large scale features are defined. Undoubtedly, the small scale feature are below the limits of detection of the system. At stresses for suspension increase, sand ribbons will generate, the sediment swept laterally in response to current parallel vortices. The appropriate velocities for the development of such features are shown in Table 7-II.

The generation of bedforms on the continental shelf, in water depths up to 150 m, is due to the virtual interdependency

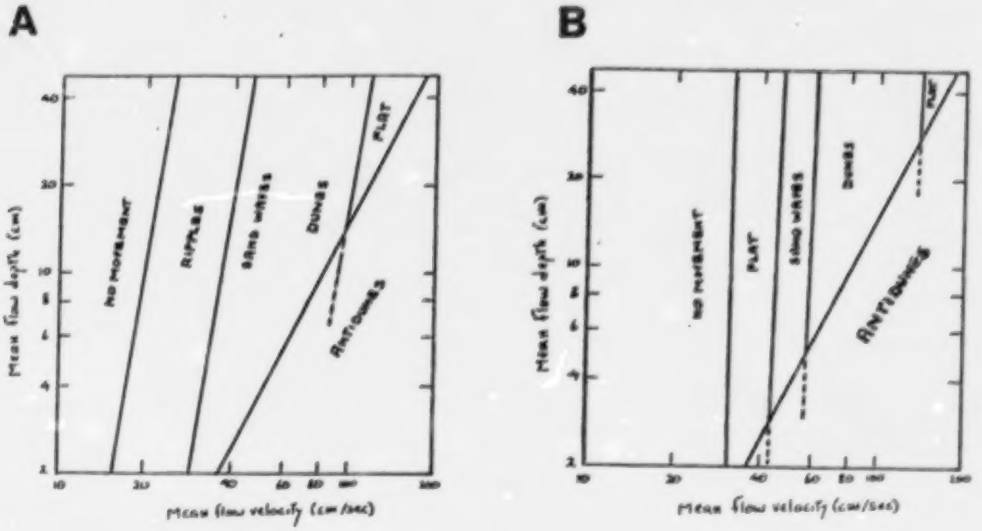

Figure 7-07 (A and B) The phase relationship between mean flow depth, mean flow velocity and bedform type for medium sand substrates (A) and coarse sand substrates (B) (from Middleton and Southard, 1977).

The results show only a slight variation with water depth. The medium sand substrate shows the greatest sensitivity to depth changes with a 10 cm/s increase in the critical velocity. This effect is negligible in depths typical of Canadian shelves.

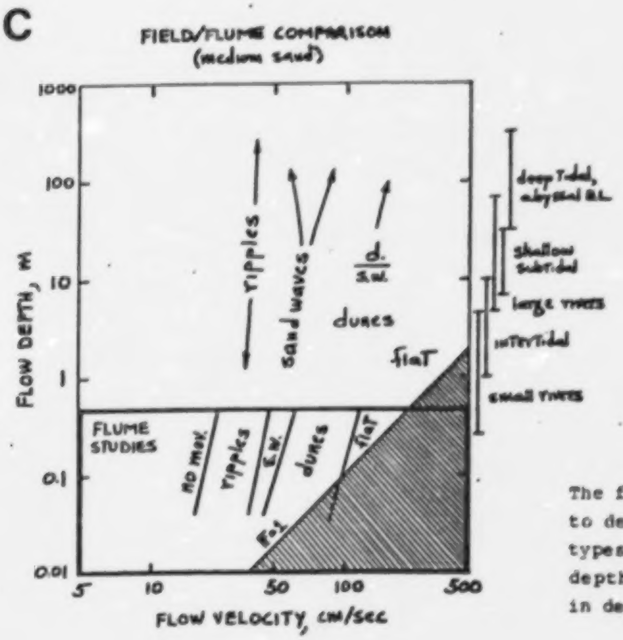

The figure shows that the use of critical flow criteria to determine flow conditions on the basis of bedform types is valid and can be applied irrespective of water depth. The figure shows the elimination of antidunes in depths greater than 1 metre.

Figure 7-07 (C) The extrapolation of flume tank data to field conditions for medium sand substrates.

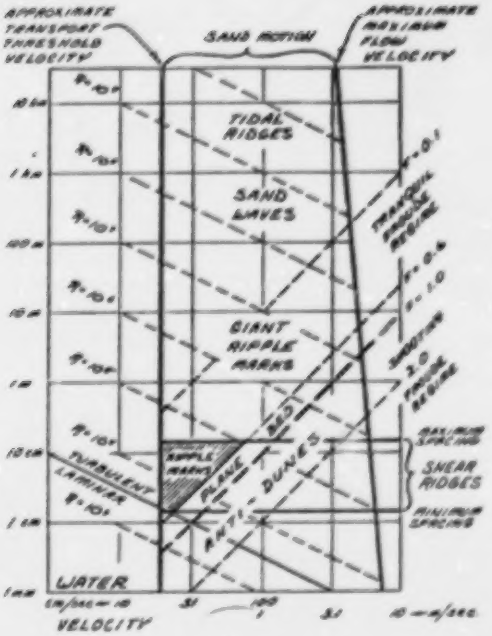
APPROXIMATE TRANSPORT THRESHOLD VELOCITY
SAND MOTION
APPROXIMATE MAXIMUM FLOW VELOCITY
TIDAL RIDGES
SAND WAVES
GIANT RIPPLE MARKS
RIPPLE MARKS
PLANE BED
ANTI-DUNES
MAXIMUM SPACING
SHEAR RIDGES
MINIMUM SPACING
TURBULENT
LAMINAR
F = 0.1
F = 0.6
F = 1.0
2.0
WATER
10 km
1 km
100 m
10 m
1 m
10 cm
1 cm
1 mm
cm/sec → 10
31
100
1
31
10 → m/sec
VELOCITY

All constructive, non-cohesive bedforms are generated in turbulent, subcritical flows (i.e. above Re:3 x 10^3 and below $F_v \approx 0.6$). The relationship applies only to unidirectional flow.

Figure 7-08 (A) The phase relationship between Reynolds number (Re), Froude number (Fr) and bedform types (from Middleton and Southard, 1977).

Flows can be defined as (1) laminar/subcritical (2) laminar supercritical (3) turbulent/subcritical or (4) turbulent/supercritical. Most flows on the shelf are turbulent/subcritical or laminar/subcritical.

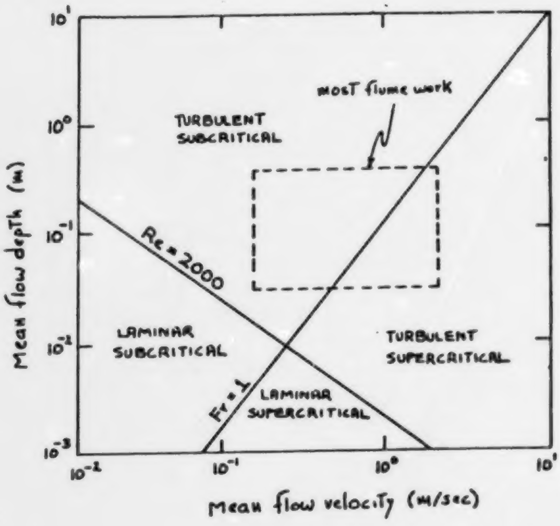

Figure 7-08 (B) The phase relationship between flow velocity, flow depth, Reynolds number and Froude number.

between the critical mean flow for bedform generation and flow depth. Figures 7-07(A and B) clearly demonstrate this fact. Although the two figures cover a range to a depth of only 40 cm, general observations indicate it to be valid in depths typical of continental shelves (see Figure 7-07(C)). Note that antidunes do not show this interdependency. In fact, such bedforms are only found in depths usually less than 1 m (i.e. those flows capable of exceeding a Froude number of 1.0). Although the velocities at which the various bedforms are generated remain independent of depth, the absolute size and wave-length of these bedforms increase with depth up to a limiting size (defined in section 3).

Note that due to the logarithmic decrease in velocity with depth in the boundary layer, mean velocity, without reference to a depth, is virtually meaningless. For this reason many workers relate bedform genesis to bottom shear stress (τ), friction velocity (U_*) or stream power ($\tau . u$) which are depth independent. For hydrodynamically rough flows the "law of the wall" equation relating U/U_* and y/K_s (where y is height above the bed and K_s is the boundary roughness height) can be applied to relate mean flow at one depth to that of another:

$$U/U_* = 5.75 \log_{10} (y/K_s) + 8.5 \qquad (4)$$

Figures 7-08(A and B) illustrate the use of mean flow velocity without reference to depth. Notwithstanding this limitation, the two figures illustrate the significance of the relative and absolute magnitude of Reynolds number and Froude number on the generation of bedforms. Figure 7-08(A) illustrates that ripples form only at Froude numbers less than 0.6 and only in turbulent flows between Reynolds numbers of about 5×10^3 to 10^5. Megaripples, as defined herein (referred to in the figure as giant ripple marks) generate at Froude numbers less than 0.6 and at Reynolds numbers between 10^6 to 10^7. Sand waves and tidal ridges generate at progressively higher Reynolds numbers and lower Froude numbers. The flow conditions for the generation of these bedforms are turbulent and sub-critical (see Figure 7-08(B)).

Figure 7-09 (A and B) show the various phases for bedform generation as a function of grain diameter (D), stream power ($\tau.u$) and shear velocity (U_*). In Figure 7-09(A) the term "dunes" refers to both sand waves and megaripples. These figures are of value in that, given the grain size of the bottom sediment and the type of bedform, one could use this diagram to hindcast the range of stream powers which must have occurred on the shelf to produce that bedform. This application can be extremely useful to the interpretation of shelf processes where current information is limited or unavailable.

Megaripples are somewhat larger features than ripples and differ from the generation of ripples in that they appear to develop (in the short crested case) from kinematic shock waves generated by subtle irregularities in bed relief. There are two types of megaripples: long crested and short crested. The former are termed 2 - dimensional megaripples (2-D) the latter features are termed 3 - dimensional megaripples (3-D) (see page 356 for detailed description). The wavelength of successive 2-D megaripples are often irregular, with smaller forms overtaking

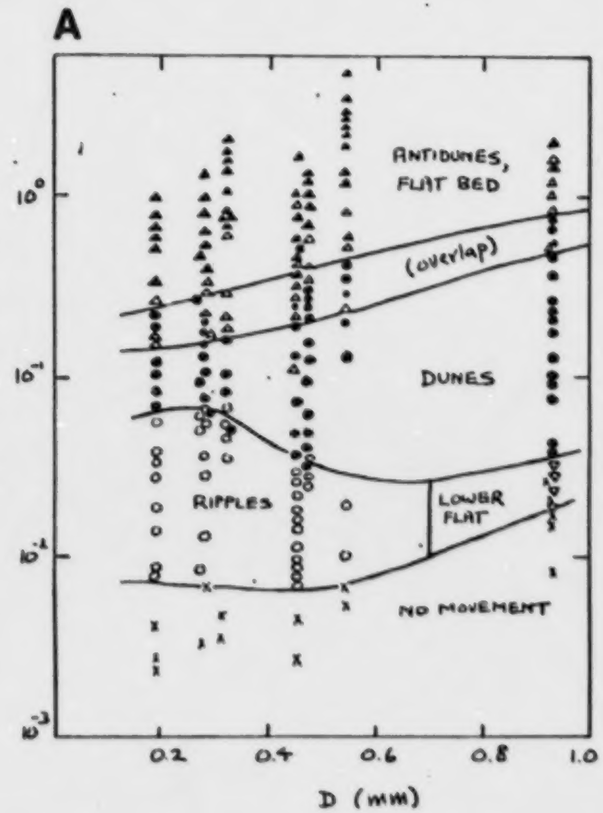

A. Ripples occur immediately upon the initiation of sediment motion, and at grain sizes less than 0.7 mm. The figure does not differentiate between sand waves, 2-dimensional megaripples and 3-dimensional megaripples, referring to them collectively as "dunes".

B. The figure is more easily interpreted than 7-09(A) in that the mean current flow can be derived directly from U_*. The figure differentiates between sand waves and megaripples (dunes) and further differentiates flows developing sand waves with ripples and sand waves with megaripples.

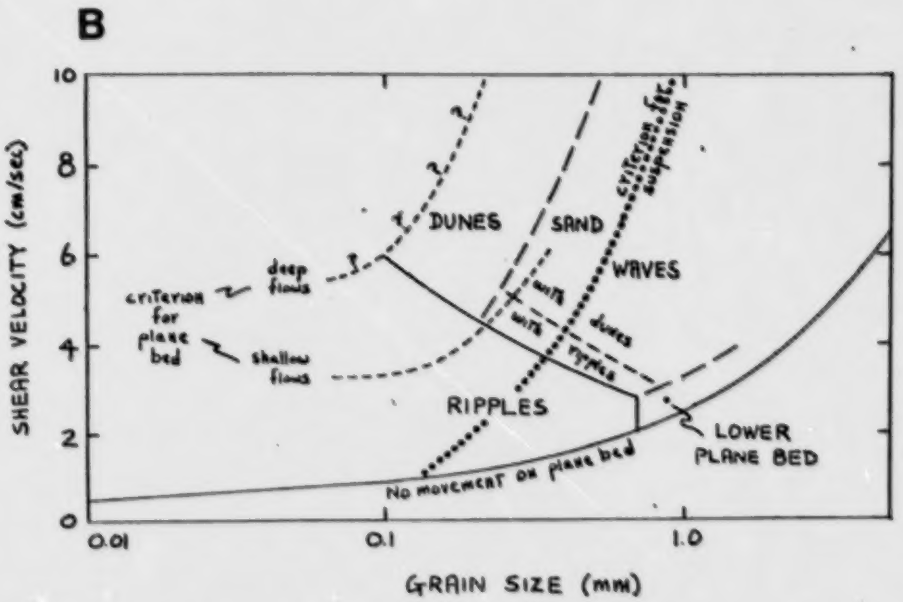

Figure 7-09 (A) The phase relationship between stream power (τ_oU) grain diameter (D) and bedform type for non-cohesive, sand-sized sediments.
(B) The phase relationship between shear velocity (U_*), grain diameter (D) and bedform type.

and merging with larger forms. A single bedform migrates no more than a few wavelengths before being overlapped by other forms. Such bedforms develop slip faces, presumably due to flow separation. In the case of 3-D megaripples, the wavelength and rate of migration are more regular due to an increasing control of the shock wave on the bedform geometry. Both bedforms are asymmetric waves. Short crested types exhibit blowouts and scours due to turbulences in the shock wave pattern across the current. There is no separation of the boundary layer and the troughs are scoured zones. The shear velocity (U_*) separating the 3-D megaripples and 2-D megaripples has been shown by Dalrymple et al., (1978) to be independent of depth and equal to 4.4 cm/s. This is equivalent to a U_{40} of 23.7 cm/s. Dalrymple et al., (1978) from work carried out in the Bay of Fundy, were able to differentiate combined bed phases which were hydraulically unique. They found that megarippled sand waves were often present and overlapped with 3-D megaripples, forming at higher velocities than 2-D megaripples. The generation of the appropriate bedform type is determined by the sediment grain size. Sand waves occur only in sediments coarser than about 0.31 mm (medium sand) and may require a minimum thickness of sediment before they form. Megaripples, on the other hand, can coexist with sand waves though they occur alone at finer grain sizes. Ripples and sand waves can also coexist, though they overlap considerably with 2-D megaripples in terms of grain size and flow velocity.

Briggs and Middleton (1965, p. 14) state "In order to understand the formation of sedimentary structures it is important to be able to understand the factors governing not only the initiation of grain movement, but also the rate of bed-load movement". Both of these parameters rely on a roughness expression relating flow velocity to bottom stress. The common roughness expressions are Manning's "n", Chezy's "c" and the Darcy-Weisbach friction factor "f". They are necessarily derived by direct measurement or by inference from similar known areas. The coefficient of drag (C_D) which varies as a function of the roughness terms (or more appropriately, the Reynolds number) is equally unpredictable. A considerable scatter exists in the data which leads to a consequent uncertainty in the critical velocity for the genesis of bedforms.

Exner (Leliavsky, 1966) attempted to model the formation of ripples (in profile) with the formulation:

$$h = A_o + A_1 \cos\left(\frac{2\pi}{\lambda} \cdot x\right) \tag{5}$$

where h is the elevation in reference to some datum, A_o and A_1 are constants, λ = wavelength and x is distance downstream. In the case of megaripples, Exner extended his formulation as follows:

$$h = A_o + A_1 \cos \frac{2\pi}{\lambda} \left[x - \frac{\varepsilon Q}{b} \cdot \frac{t}{(z - h)^2} \right] \tag{6}$$

where ε is an erosion coefficient, Q is the discharge, b is a unit width, t is time, and (z-h) is the depth of flow. According to Exner (in Leliavsky, 1966), the propagation rate of a bedform is equal to $[(Q/b)/(z-h)^2]$. The formulation expresses a gradual asymmetric moulding of a seabed "mound" in a downstream direction.

The rate of bedform generation and migration depends on the number of grains in transport or the sediment discharge rate. A considerable body of information exists on sediment transport under unidirectional flow; a large portion of this is reviewed by A.S.C.E. (1977). Rates vary one order of magnitude. For marine environments, the theory of Engelund and Hansen (1972) is generally accepted as giving the best results, and has been built into a general model for shelf sediment transport by Madsen and Grant. (1976, a and b). The details of the method and the theory of shelf sediment transport are reviewed in previous sections of the course.

On continental shelves, oscillatory flow resulting from wave motion is often the prevailing process generating bed features. Draper (1967) has shown that ripples in northwest European shelves can be generated in water depths of 200 m. Under such flows, oscillatory ripple marks and subsequently flat bed are the only bed forms which generate. Komar, (1974) and Miller and Komar. (1980) have shown that the wavelenth of such ripples is dependent on the orbital diameter (d_o) and the absolute magnitude of the oscillatory flow (U_{max}) being shorter than (d_o):

$$x = 0.65\ (d_o) \tag{7}$$

The determination of orbital diamter (d_o) is based on linear wave theory and assumes a monochromatic wave train. The obvious limitation of this application is that waves over the shelf occur as a spectrum of wavelengths and propagate in a number of differing directions. However, due to the hyperbolic decrease in oscillatory velocity with depth, only the longest period waves "feel" bottom and contribute to sediment movement. In fact, only waves of period greater than 10 s will induce motion at the seabed at the shelf edge. Figure 7-10(A) shows the nature of oscillatory flow to bed morphology in sand (in Allen, 1970). This relation is only valid for orbital diameters less than about 70 cm. This is equivalent to a wave period of 10 s, in 80 m of water and for a 10 m high wave.

The relative combination of wave height to wave length upon which the linear wave theory applies lies in the range:

$$H/L < 0.142 \tanh (2 \pi H/C) \quad (8)$$

Figure 7-24, p. 72, illustrates the relationship between orbital diameter (d_o) and ripple wave length (λ) as a function of grain size for mean diameters of 0.125 mm, 250 mm and 0.5 mm. The ripple wavelength reaches a maximum value and then decreases with further increasing orbital diameter. The maximum wavelength increases with increasing grain size.

The orientation of ripple crests is normal to the propagation direction of the wave. The crests develop in response to flow separation at the end strokes of the forward and return phases of the motion. The development of a crest, as in the case of unidirectional flows, depends on local bottom roughnesses. Separation from the bed will take place at the crest of the irregularity. Once separation has initiated, sand accumulates immediately beyond the point of separation in a zone of low stress. This leads to a positive feedback in crest

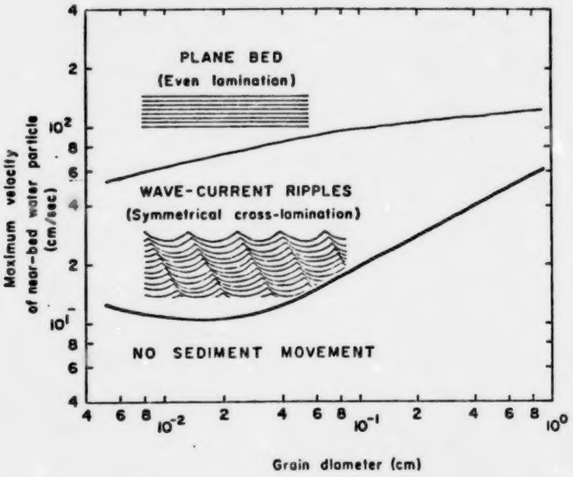

Figure 7-10 (A) The phase relationship between maximum orbital velocity under waves (U_{max}) and grain diameter (from Allen, 1970).

Ripples and plane (flat) bed are the only phases of bedforms generated under waves. Ripples form at Umax of 10-20 cm/s while plane bed occurs at Umax of 60-100 cm/s. The phase relationship is dependent of grain size of the bottom sediment.

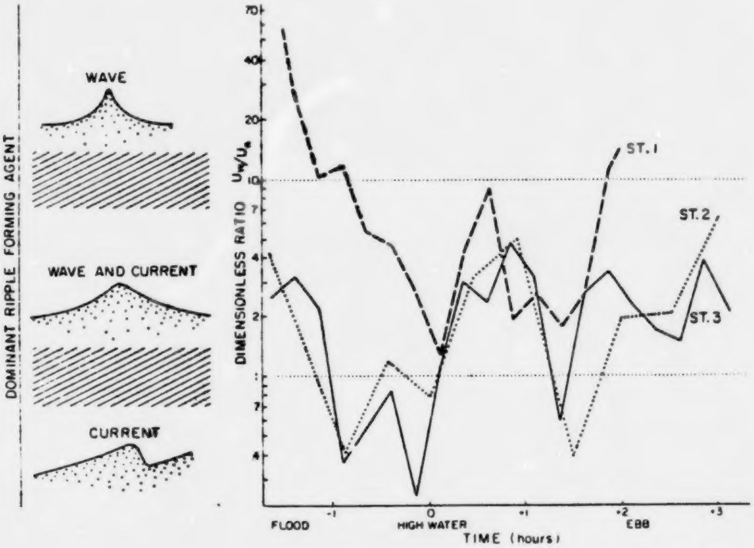

Figure 7-10 (B) The relationship between the combined ratio of the maximum wave oscillatory velocity (U_w) and the unidirectional friction velocity (U_*), based on results from The Wash, E. England (from Amos and Collins, 1979).

Above a ratio of 10 ripples became symmetrical and are purely wave formed, below a ratio of 1, ripples are fully asymmetric and are purely current formed: at intermediate ratios both processes are active producing an intermediate ripple.

Table 7-III

The range in threshold velocities for the generation of wave formed ripples and flat (plane) beds

Grain Diameter (mm)	* Ripples (bedload)	Flat Bed	Settling Velocity (at 20° C) (W)	Suspension Velocity (40 cm)
0.2 (fine sand)	10	60	2.36	15.13
0.4 (medium sand)	16	70	5.91	25.11
0.6 (medium/coarse sand)	16	80	9.29	34.61
0.8 (coarse sand)	15	80	12.43	43.44
1.0 (coarse sand)	20	90	15.34	51.62
1.5 (very coarse sand)	25	100	21.83	69.86

*The critical velocity was determined using the equations of Komar, 1974.

generation, which is further enforced by separation on the down current face of the mound during the return pulse. This type of flow separation (deflected upwards) leads to a concave up profile with a sharp, straight crest. Once formed, the development of further crests (in both directions) is governed by the approximate orbital diameter of the flow as previously discussed.

The generation of wave formed ripples will only take place above the threshold of sediment motion under waves. The range in U_{max} values for incipient motion is given in Table 7-III. The value is minimum (10 cm/s) in the fine sand-size range and increases for both finer and coarser material. The reason for the increase with progressively finer material is due to the size of the roughness elements (grain size) in comparison to the wave boundary layer. In very fine sand the grains do not "poke" through the laminar sub-layer.

Wave-formed ripples do not exist above an approximate (U_{max}) velocity of 90 cm/s. At such velocities sediment oscillates back and forth in a flat (plane) bed phase. This occurs with the grains in suspension in the wave boundary layer (according to the criterion of Bagnold, 1963).

The wave conditions can be hindcast from the bedform wavelength, sediment grain size and water depth (Komar, 1974), notwithstanding the previously described limitations. The method requires working backwards through Airy theory.

When combined flows occur (wave and current) a modified ripple type is formed (see Amos and Collins, 1979). Wave dominance occurs below a ratio of (U_{max}/U_*) $\approx$ 10 and current dominance occurs below a ratio of $(U_{max}/U_{*}) \approx 1$. The orientation of the crest in intermediate forms is normal to the unidirectional current (see Figure 7-10 (B)).

2.2 Cohesive Bedforms

The effect of cohesion on sediment is significant below grain sizes of 2 microns (clays) and results in a much greater resistance of the sediment to superimposed flows. Cohesive materials do not normally behave as individual particles, but deform plastically or fail catastrophically. Bed features formed in cohesive material tend, therefore, to be deformational or destructional. Bedforms developed in cohesive sediments develop by: (i) particle-by-particle (or aggregate-by-aggregate) erosion, (ii) plastic deformation and (iii) catastrophic failure. The nature of cohesive soils depends largely on the water content, grain size. compaction and depositional history. The sedimentation phases of cohesive materials differ greatly from noncohesive materials in having no bedload transport phase. Figures 7-11(A and B) show the various phases of sedimentation for non-cohesive and cohesive sediments respectively (after Amos and Greenberg, 1980) for particle-by-particle process. There are two critical stresses apparent in the particle erosion of cohesive soils. The first (τ_3) separates the phase of sediment deposition from sediment transport with no erosion. The second (τ_4) separates the phase of sediment transport with no erosion from sediment erosion.

The rate of sediment deposition, which is a key parameter in the shear strength of the sediment, and in the development of dewatering structures, is predictable and determined as follows:

$$\text{deposition rate (x)} = c.w_s(1-\tau/\tau_3)\,\rho \qquad (9)$$

where τ is the prevailing bottom shear stress, ρ is the

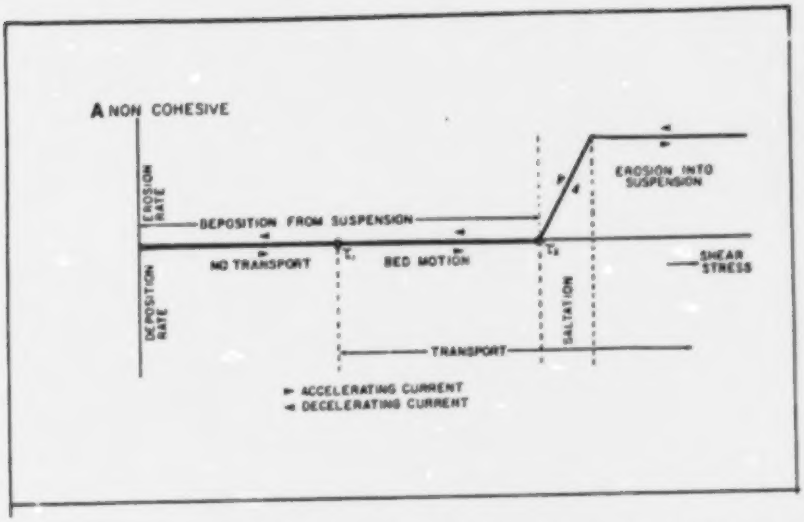
A NON COHESIVE
EROSION RATE
DEPOSITION RATE
DEPOSITION FROM SUSPENSION
NO TRANSPORT
τ_1
BED MOTION
τ_2
EROSION INTO SUSPENSION
SHEAR STRESS
SALTATION
TRANSPORT
► ACCELERATING CURRENT
◄ DECELERATING CURRENT

Figure 7-11 (A) A schematic of the sediment transport phases for non-cohesive material as a function of bottom stress.

τ_1 represents the critical stress for transport, at which point ripples begin to develop. τ_2 represents the critical stress for suspension (saltation) at which point megaripples develop. Erosion into suspension takes place over a flat bed.

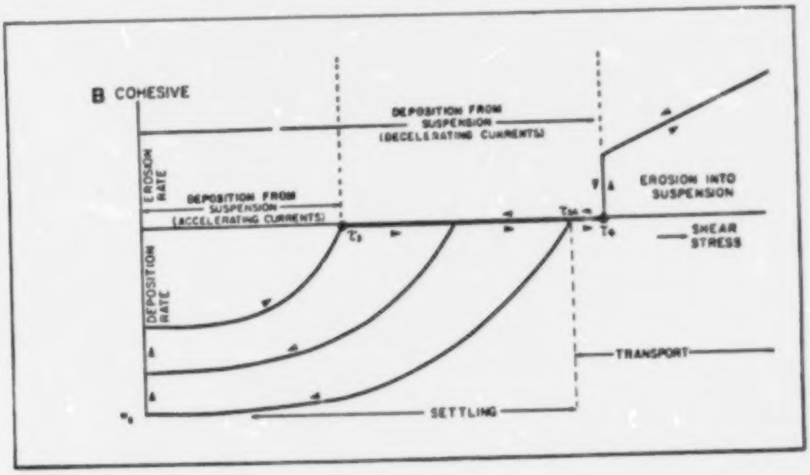
B COHESIVE
DEPOSITION FROM SUSPENSION (DECELERATING CURRENTS)
EROSION RATE
DEPOSITION FROM SUSPENSION (ACCELERATING CURRENTS)
τ_3
τ_{3A}
τ_4
EROSION INTO SUSPENSION
SHEAR STRESS
DEPOSITION RATE
TRANSPORT
SETTLING
w_s

Figure 7-11 (B) A schematic of the sediment transport phases for cohesive material as a function of bottom stress.

τ_3 represents the critical stress separating deposition from suspension from transport with no deposition. Most deltas developing slump and slide structures are found in zones exhibiting similar stresses. τ_4 represents the critical stress for erosion. Megaflutes and scours develop under flows of similar or greater stresses. τ_{3A} represents a modified critical stress for deposition developed under turbid environments, such as turbidity currents or turbid delta plumes.

Table 7-IV

The critical stress for erosion of cohesive sediments, based on flume tank and in-situ measurments

Critical stress (dynes/cm^2)	U_{40}(cm/s)	Soil Type
0.16 - 0.24	14.5 - 15.8	newly deposited calcareous oozes
0.50 - 0.90	19.1 - 22.7	10 hours after deposition of calcareous oozes
0.21	15.4	in-situ estuarine muds
0.11 - 0.72	13.4 - 21.2	in-situ estuarine muds
0.27 - 1.43	16.3 - 26.4	bioturbated, laboratory muds
0.71 - 1.71	21.1 - 28.1	flat bedded, laboratory muds
0.44	18.4	unconsolidated silts
0.13	13.9	pitted, laboratory muds
0.16	14.5	flat, laboratory muds
3.7	37.3	laboratory muds with 37% sand
4.52	40.3	laboratory muds with 37% sand
0.65	20.6	laboratory muds with 7% sand
0.83	22.1	laboratory muds with 2% sand
1.25	25.3	San Francisco Bay mud
0.49	10.2	after Einstein and Krone (1962)

probability of grain resuspension and $(1 - \tau/\tau_3)$ is the probability of grain deposition (Krone, 1962).

The critical stress for erosion of cohesive sediment varies considerably, depending on the sediment depositional history and character. Critical stresses vary from 0.11 dynes/cm^2(13.4 cm/s at 40 cm above the bed) to 4.52 dynes/cm^2 (40 cm/s above the bed). For compacted, ancient sediments this stress is likely to be considerably higher. Table 7-IV summarizes these critical stress values recorded in the literature.

The rate of erosion of bottom sediment varies in proportion with the applied stress. Parthenaides (1971) has found that the erosion rate is proportional to the excess shear stress.

$$\text{erosion rate } (x) = k(\tau - \tau_4) \qquad (10)$$

The relationship within the limits of flume tank experimentation appears linear with a K value of about 2. In closed systems, where the concentration in suspension increases steadily, the net erosion decreases and will eventually cease. Under such circumstances, the downward particle flux is in dynamic equilibrium with upward particle erosion. In marine environments the system is considered open and the above principle does not apply. A typical erosion rate is mm's/hour.

The cohesive force of a sediment has experimentally been related to standard soil tests with limited success. Sunborg (1956), formulated the following relationship for evaluating the critical shear stress for sediment erosion (τ_4).

$$\tau_4 = \frac{C_1 A_1}{C_2 A_2} (\rho_s - \rho)\, g.d_{50} \tan \Theta + C_3 S \qquad (11)$$

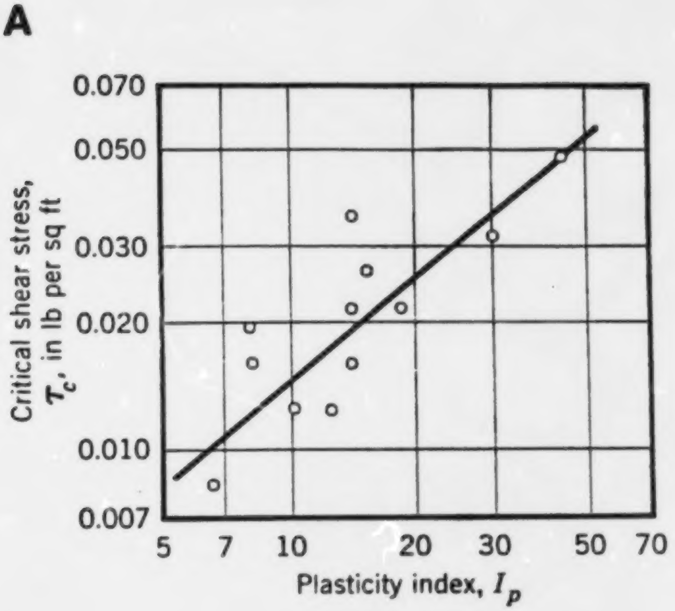

Figure 7-12 (A) The correlation between plasticity index and critical shear stress for erosion for a numberof terrestrial soils (from Smerdon and Beasley, 1961).

There appears to be a good correlation between the two parameters: The resistance to erosion increases in proportion to increases in plasticity index.

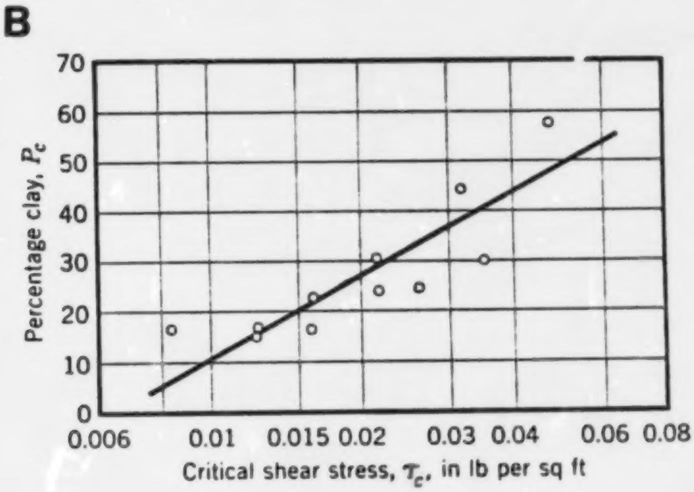

Figure 7-12 (B) The correlation between critical shear stress and percentage clay, based on the analysis of a number of terrestrial samples (from Smerdon and Beasley, 1961).

There is good correlation between the two parameters, the resistance to erosion increasing in relation to increase in clay content. There appears to be good evidence to suggest that the above relationships are applicable to marine soils (Meyerhoff, pers. comm.).

Table 7-V

Data on critical shear stress of sediments

Geometric mean grain sized d_g, millimetres	Geometric standard deviation σ_g	Percentage of silt and clay	Plasticity Index, I_p	Vane Shear Strength of Sediment S_v in pounds per square foot Min	Max	Observed Critical Shear stress τ_c, in pounds per square foot Min	Max
0.022	6.08	69.0	11.1	77	167	0.48	0.49
0.072	6.00	35.0	0.0	268	520	0.18	0.33
0.328	-	12.5	-	96	138	0.057	0.063
0.319	-	18.0	-	96	118	0.057	0.083
0.308	-	26.0	-	110	110	0.11	0.12
0.250	-	44.0	-	128	140	0.14	0.15
0.078	3.25	41.0	0.0	75	233	0.19	0.28
0.081	2.79	31.0	0.0	102	243	0.11	0.15
0.038	3.25	46.0	2.5	173	242	0.30	0.33
0.016	4.83	78.0	8.8	105	250	0.30	0.45
0.015	4.66	81.0	13.3	137	263	0.40	0.41
0.026	3.48	56.0	3.5	100	300	0.19	0.32
0.014	3.48	88.0	11.2	144	187	0.43	0.48
0.014	3.05	95.0	15.6	137	143	0.48	0.49
0.139	1.57	10.0	0.0	43	155	0.053	0.053
0.173	1.29	5.0	0.0	95	110	0.043	0.033

where s is the shear strength of the sediment, θ is the angle of repose of the sediment in water, and a_1 and a_2 are length measurements of grain size (A.S.C.E., 1977, p. 108). Some measurements of the critical stress for erosion are presented in Table 7-05 from Dunn (1959) based upon laboratory analyses. His results show a relationship between plasticity index (Ip) and the shear strength (S) defined by

$$\tau_4 = 0.001 (S + 180) \tan (30 + 1.73 Ip)s \qquad (12)$$

(units in lbs/ft^2)

Further work on the critical shear stress carried out by Smerdon and Beasley (1961) is shown in Figure 7-12 (A and B) in relation to the plasticity index and the percentage clay respectively. Karasev (1964) expresses the aggregate-by-aggregate erosion of cohesive sediments in terms of the mean critical velocity $(U)_{cr}$:

$$(U)_{cr} = 0.142 c \quad 2d \frac{(\rho_s - \rho)}{\rho . g} g + 30m \left(1.2 + 8 \frac{D}{D_a}\right) \qquad (13)$$

where c is the Chezy coefficient, m is sediment cohesion, D_a is atmospheric pressure and D is ambient pressure.

Hjulstrom, (1935) developed a phase diagram relating the erosion, transport and sedimentation of material from clay size to gravel. His results show that clay erodes at a mean velocity of about 250 cm/s and silts at between 20-100 cm/s (see Figure 7-13).

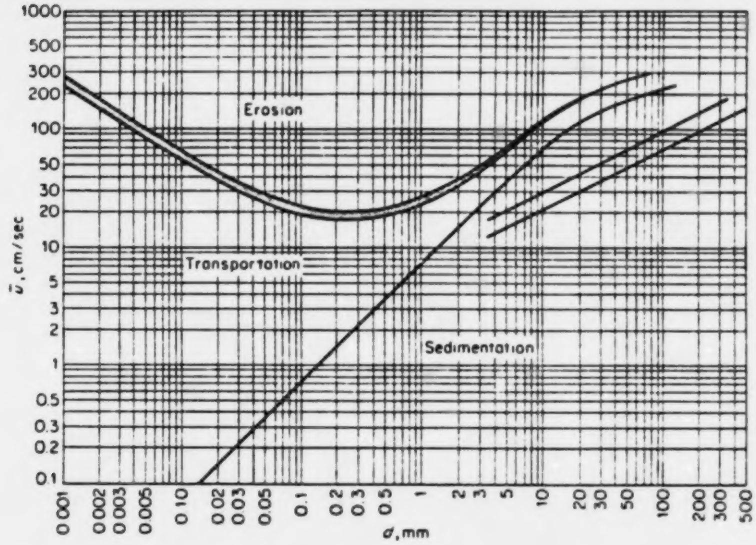

The flow is not related to any depth and therefore the relationship is approximate only. It is, however, of practical use for in-field, general interpretation.

Figure 7-13 The relationship between average flow velocity ($\bar{\mu}$) grain diameter (d) and sedimentation phase (from Hjulstrom, 1935).

Allen (1969) has performed some of the only work on cohesive bedform generation. His results show that with increasing flow the bed generates: (1) longitudinal, rectilinear grooves, (2) longitudinal meandering grooves, (3) flute marks and (4) transverse erosional markings. The development of these successive bed features is the result of increases in the distortion of the laminar sublayer. Scours and flute marks are erosive features, created in cohesive sediments when the flow is greater than the critical shear stress for erosion. These features are generated by the development of flow turbulence behind an obstruction, or by irregularities in the nature of the bottom material. The shape of a scour reflects the geometry of

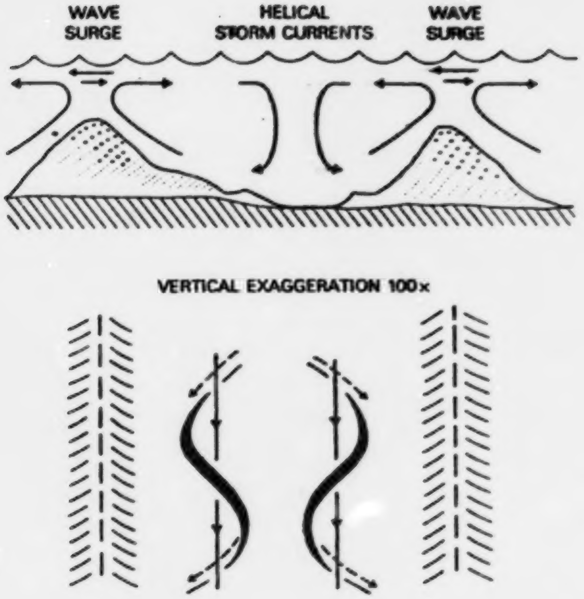

Figure 7-14 (A) Spiral vortices on the shelf inferred to create sand ridges (from Reading, 1978).

fluid turbulence. In the case of flute marks, the greatest stress and highest turbulence occurs immediately downstream of the irregularity, thus producing the deepest scouring. The depth of scouring decreases downstream as turbulence dissipates. This is manifested by a decrease in the equilibrium scour depth, which occurs with a widening of the flute due to lateral dispersion of the turbulent effect. Such flutes vary in size from cm to km. The latter features, termed megaflutes, were observed in Placentia Bay, Newfoundland by King, (1979).

The formation of rectilinear and meandering grooves results from the development of cross current flows, such as those shown in Figure 7-14. Sets of these vortices develop across the flow

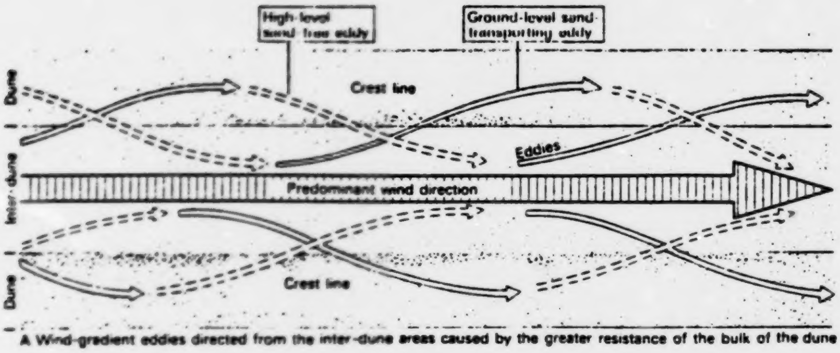
High-level sand-free eddy
Ground-level sand-transporting eddy
Crest line
Eddies
Predominant wind direction
Dune
Inter-dune
Dune
Crest line

A Wind-gradient eddies directed from the inter-dune areas caused by the greater resistance of the bulk of the dune

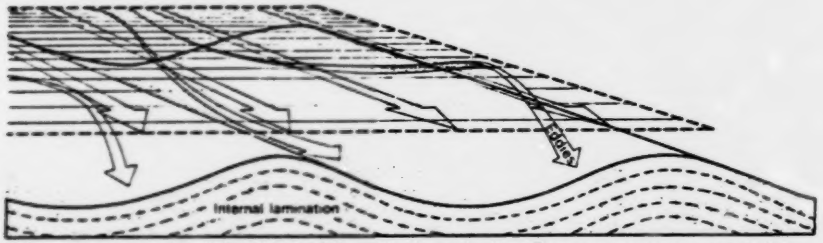
Eddies
Internal lamination

B Schematic representation of the spiral path followed by the wind eddies. They may give rise to crestal slip faces. A deviation of the wind from the predominant direction will accentuate the development of slip faces on one side of the dune

The principle is equally applicable to the development of sand ribbons on continental shelves. The vortices converge at the sand ribbon crest and diverge in the troughs. The flow is "highlevel" over the crests and near bottom in the troughs.

Figure 7-14 (B) A schematic representation of spiral vortices originally used to explain linear features in deserts (from Reading, 1978).

leading to current parallel zones of divergence (low stress) and convergence (high stress). The mechanisms leading to the silting of such features is poorly understood; however, it is considered to be related to bed roughness. The grooves develop in the zones of convergence. As flow increases these vortices become unstable and meander down current.

2.2.1 Gravity Flows

Perhaps the most significant of the cohesive bedforms are those produced by sediment gravity flows. Such flows can take place on slopes of about 1^o and can occur on the slopes of shelf basins, the heads of submarine canyons and in shelf valleys.

Middleton and Hampton (1976) have classified sediment gravity flows, distinguishing four main types:

1. turbidity current
2. fluidized sediment flow
3. grain flow
4. debris flow

The classification of these flows and the ensuing deposit types is shown schematically in Figure 7-15(A), with the hypothetical interrelationship of the differing processes involved in any one event shown in Figure 7-15(B) and (C). Turbidity currents can be triggered by (1) mass sedimentation, (2) cyclic wave loading or (3) seismic activity. The majority of these features occur in submarine canyons and are more a slope feature than a shelf process. They move over the seabed as a dense cloud of suspended sediment, maintained in suspension by turbulence and capable of deeply eroding the substrate over which they pass. Fluidized sediment flows are typically coarser grained than turbidity currents. The sediment is supported by the upward flow of water displaced by the settling particles. Grain flows represent a more dense flow, in which the grains are supported by intergranular contact rather than by fluid turbulence. Debris flows are the most viscous of the gravity flows. The larger grains are

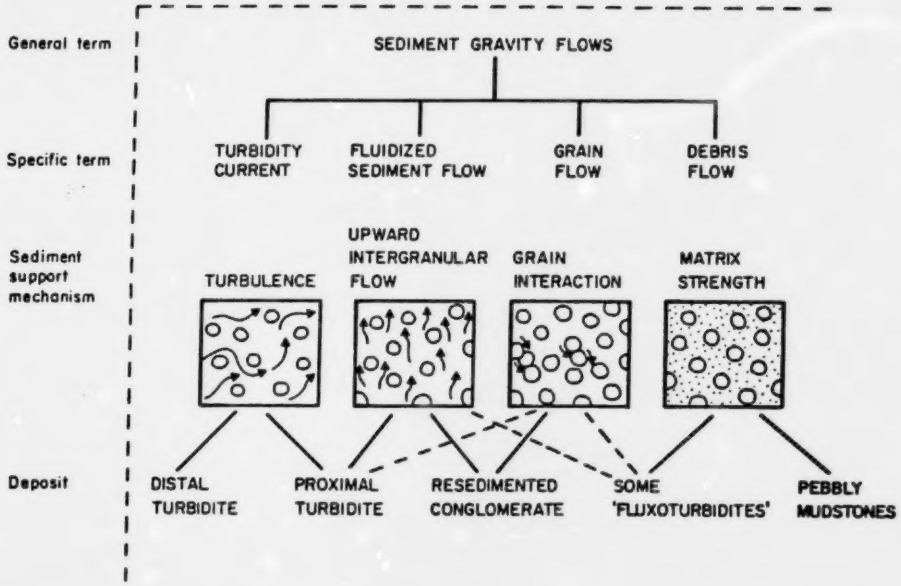
General term
SEDIMENT GRAVITY FLOWS
Specific term
TURBIDITY CURRENT
FLUIDIZED SEDIMENT FLOW
GRAIN FLOW
DEBRIS FLOW
Sediment support mechanism
TURBULENCE
UPWARD INTERGRANULAR FLOW
GRAIN INTERACTION
MATRIX STRENGTH
Deposit
DISTAL TURBIDITE
PROXIMAL TURBIDITE
RESEDIMENTED CONGLOMERATE
SOME 'FLUXOTURBIDITES'
PEBBLY MUDSTONES

Such flows usually originate from a slump or slide, triggered by an event such as an earthquake or wave loading. The slump causes liquefaction and turbulence which evolves into one of the four flows defined in Figure 7-15(A). These phenomena are short lived (up to several hours) but can cover extremely large areas (up to 400 km).

Figure 7-15 (A) The classification of sediment gravity flows.

supported by a matrix of finer material which deforms plastically.

2.2.2 Slides and Slumps

Slides and slumps are also catastrophic features leading to definable sedimentary structures. Slides differ from sediment gravity flows in that the deformation is minimal, with movement taking place along a plane of rupture (slide plane or shear

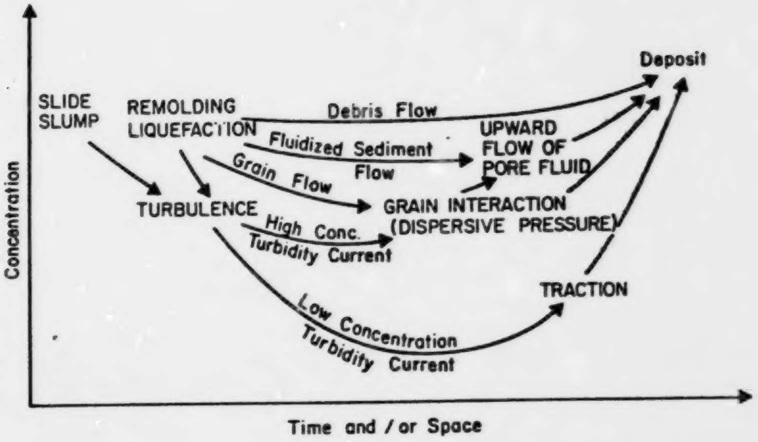
Deposit
SLIDE
SLUMP
REMOLDING
LIQUEFACTION
Debris Flow
Fluidized Sediment Flow
UPWARD FLOW OF PORE FLUID
Grain Flow
TURBULENCE
GRAIN INTERACTION (DISPERSIVE PRESSURE)
High Conc. Turbidity Current
TRACTION
Low Concentration Turbidity Current
Concentration
Time and / or Space

Four main types of flow are identified (1) turbidity currents (2) fluidized sediment flow (3) grain flow and (4) debris flow. Turbidity currents are generated by flow turbulence maintaining grain suspension, with very little drag between the flow and the seabed. Fluidized sediment flows are maintained by an upward intergranular flow. Grain flows usually occur in sandy sediments and the grains in transport are in contact. A debris flow occurs in poorly sorted sediment with coarse clasts and a fine matrix. The flow is maintained by deformation of the matrix.

Figure 7-15 (B) An hypothetical evolution of a single flow.

plane). The mass remains in contact with the slope throughout the movement. Slides can be triggered in two distinct ways: (1) when the imposed stress exceeds the shearing resistance of the sediment (by wave or seismic loading) and (2) reduction of the shear strength (by removal of overburden). Submarine slides can result from underconsolidation due to high pore water pressures in regions of high sedimentation rates.

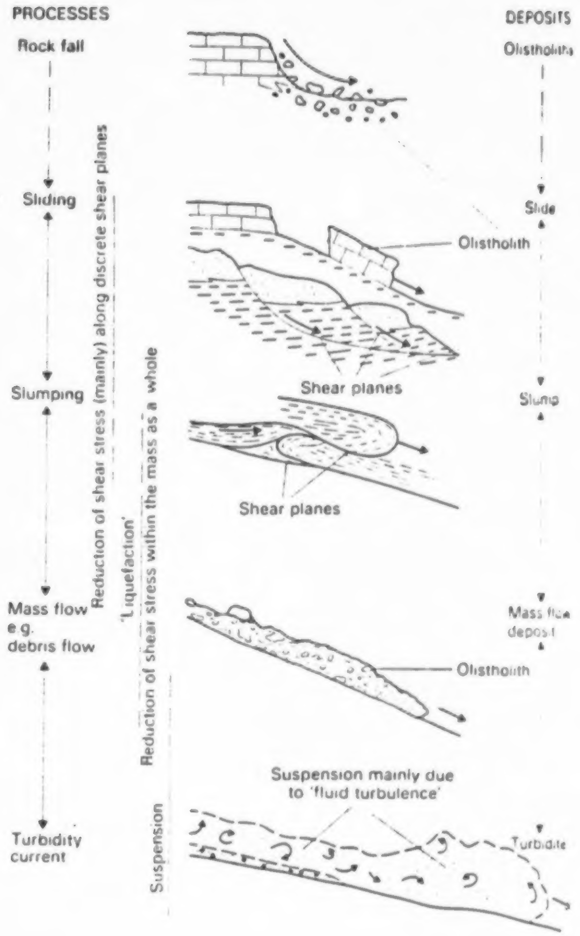
PROCESSES
Rock fall
Sliding
Slumping
Mass flow
e.g.
debris flow
Turbidity
current
Reduction of shear stress (mainly) along discrete shear planes
'Liquefaction'
Reduction of shear stress within the mass as a whole
Suspension
DEPOSITS
Olistholiths
Slide
Olistholith
Shear planes
Slump
Shear planes
Mass flow
deposit
Olistholith
Suspension mainly due
to 'fluid turbulence'
Turbidite

Figure 7-15 (C) The internal structures of sediment gravity flows.

Slumping represents an intermediate stage between slides and sediment gravity flows where-by the internal structure of the sediment is moderately disturbed. Slumping occurs in regions of high sedimentation and is seldom seen on the open shelf.

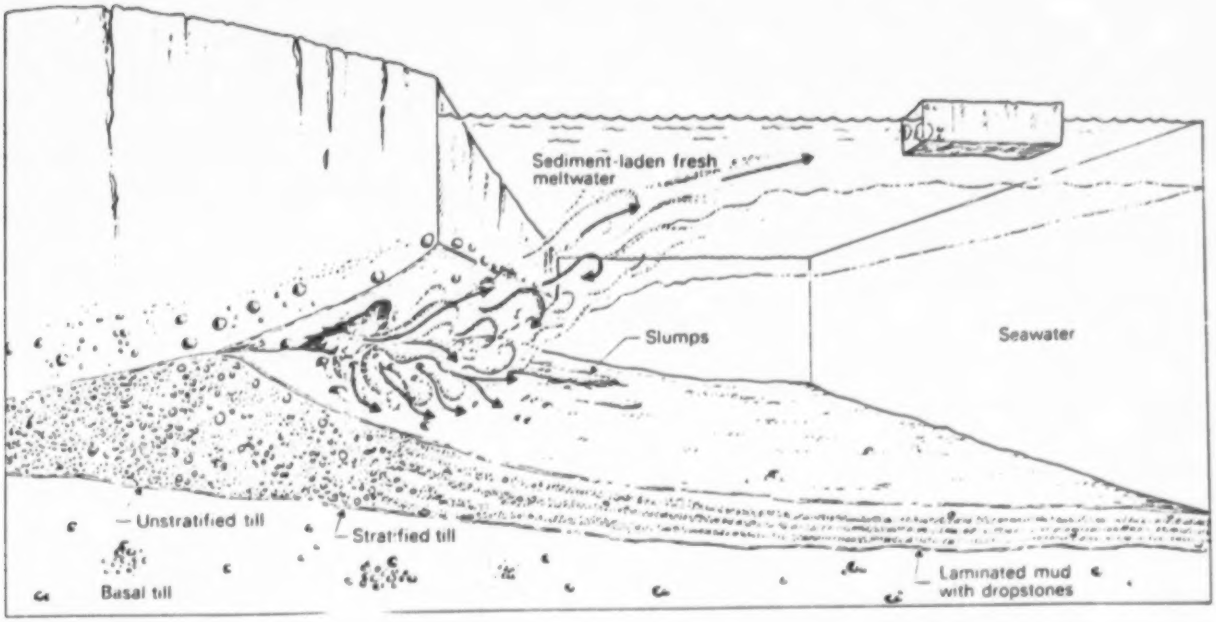
Sediment-laden fresh meltwater
Slumps
Seawater
Unstratified till
Stratified till
Basal till
Laminated mud with dropstones

Slumping is local only and will take place preferentially in regions where the seabed is sloping and composed of soft, fine grained material.

Figure 7-15 (D) Slumping generated at the edge of a grounded ice floe, or at the margin of a scouring iceberg.

Localized, progressive slumping can occur on the shelf, whereby a small slide can override a sediment pile leading to localized increases in pore water pressure, thus inducing failure. Slumping can be initiated locally by the effects of ice grounding or ice tectonics (see Figure 7-15 (D)). Ice push at the edge of an ice sheet, or in an ice scour can lead to local sediment instabilities.

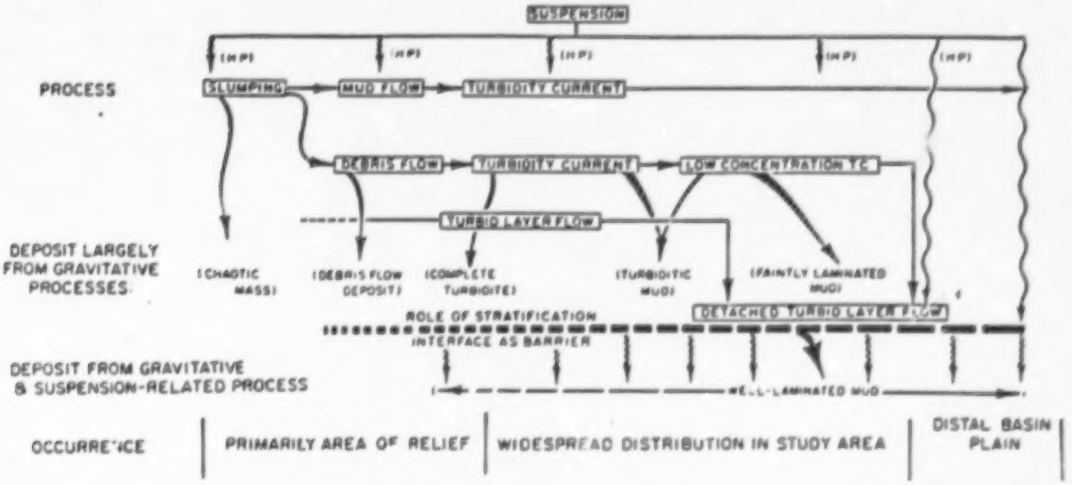
SUSPENSION
(HP)
(HP)
(HP)
(HP)
(HP)
PROCESS
SLUMPING
MUD FLOW
TURBIDITY CURRENT
DEBRIS FLOW
TURBIDITY CURRENT
LOW CONCENTRATION TC
TURBID LAYER FLOW
DEPOSIT LARGELY FROM GRAVITATIVE PROCESSES
(CHAOTIC MASS)
(DEBRIS FLOW DEPOSIT)
(COMPLETE TURBIDITE)
(TURBIDITIC MUD)
(FAINTLY LAMINATED MUD)
DETACHED TURBID LAYER FLOW
ROLE OF STRATIFICATION
INTERFACE AS BARRIER
DEPOSIT FROM GRAVITATIVE & SUSPENSION-RELATED PROCESS
WELL-LAMINATED MUD
OCCURRENCE
PRIMARILY AREA OF RELIEF
WIDESPREAD DISTRIBUTION IN STUDY AREA
DISTAL BASIN PLAIN

Figure 7-16 (A) A fine-grained depositional model for continental margins under well stratified water masses (from Stanley and Maldonaldo, 1981).

Deposition takes place across the entire shelf, from suspension. Slumping on the shelf edge or basinal margins leads to mud flows and possibly turbidity currents, or debris flows, turbidity currents and low concentration turbidity currents. The role of stratification is to detach the turbidity layer from the seabed. The result is well laminated mud over the distal portion of the flow.

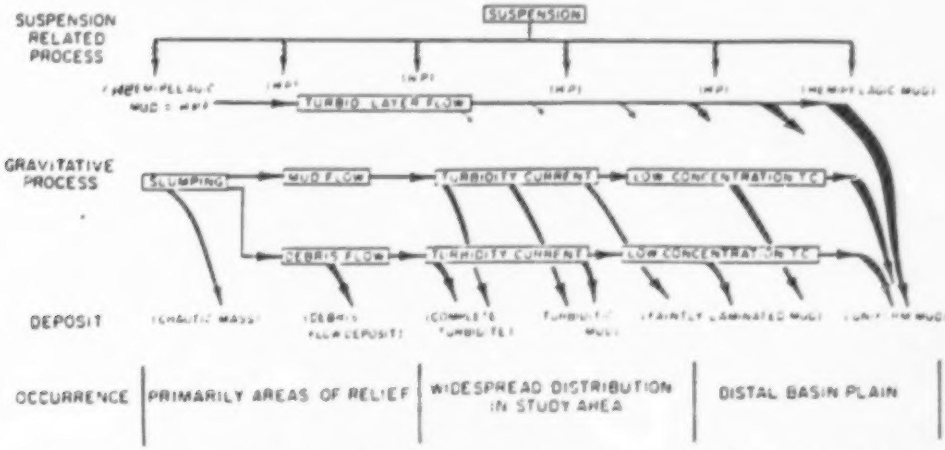
SUSPENSION RELATED PROCESS
SUSPENSION
(HEMIPELAGIC MUD = HP)
(HP)
(HP)
(HP)
(HP)
(HEMIPELAGIC MUD)
TURBID LAYER FLOW
GRAVITATIVE PROCESS
SLUMPING
MUD FLOW
TURBIDITY CURRENT
LOW CONCENTRATION TC
DEBRIS FLOW
TURBIDITY CURRENT
LOW CONCENTRATION TC
DEPOSIT
(CHAOTIC MASS)
(DEBRIS FLOW DEPOSIT)
(COMPLETE TURBIDITE)
TURBIDITIC MUD
(FAINTLY LAMINATED MUD)
(UNIFORM MUD)
OCCURRENCE
PRIMARILY AREAS OF RELIEF
WIDESPREAD DISTRIBUTION IN STUDY AREA
DISTAL BASIN PLAIN

Figure 7-16 (B) A fine-grained depositional model for continental margins under well stratified water masses (from Stanley and Maldonaldo, 1981).

The model involves the transport of suspended sediment across the shelf in turbid layers, deposited in ever increasing amounts hemi-pelagically, across the shelf. They envisage slumping on the inner shelf, mudflow and debris flows in shelf areas of relief, turbidity currents on the slope and low concentration flows in the deep ocean. The deposits formed by those processes grade from chaotic - debris flow deposit - turbidity sequence - faintly laminated - uniform mud. The model was developed for an observation in the Mediterranean where wave conditions are minimal.

Stanley and Maldonado (1981) working in the western Hellenic trench, have evolved a classification of deposit types differentiating between suspension related processes and gravitative processes in either highly stratified water masses (Figure 7-16(A)) or minimally stratified water masses (Figure 7-16(B)). They found that the gravitative processes produced the largest sedimentary section, and that the most common sequence of events was dense slump - debris flow turbidity current - low density turbidity currents. The statified model in Figure 7-16(A) involves sediment being trapped at the pycncline and being deposited pelagically over large distances.

Many of the processes described can occur on "muddy" shelves such as the North Puerto Rico Shelf (Pilkey et al., 1978). Such shelves show active sediment transport of mud. Particles move by "hopping" across the shelf during successive storms (Figure 7-17(A)). McCave (1979) shows that the Outer Oregon Shelf is also predominantly muddy at depths greater than about 100 m. The process of fine grained transport is somewhat different though from the "hopping" theory of Pilkey et al., (1978).

Stow and Bowen (1980), postulate that the sedimentation history of the Scotian Shelf has lead to the presence of fine-grained turbidity currents in the region (see Figure 7-18). They believe that turbidity currents on the Scotian Slope can be up to 1000 m thick, derived from fine grained sediments slumped from the shelf break. The resulting deposits, they argue, are laminated due to segregation of particles in the sub-boundary layer.

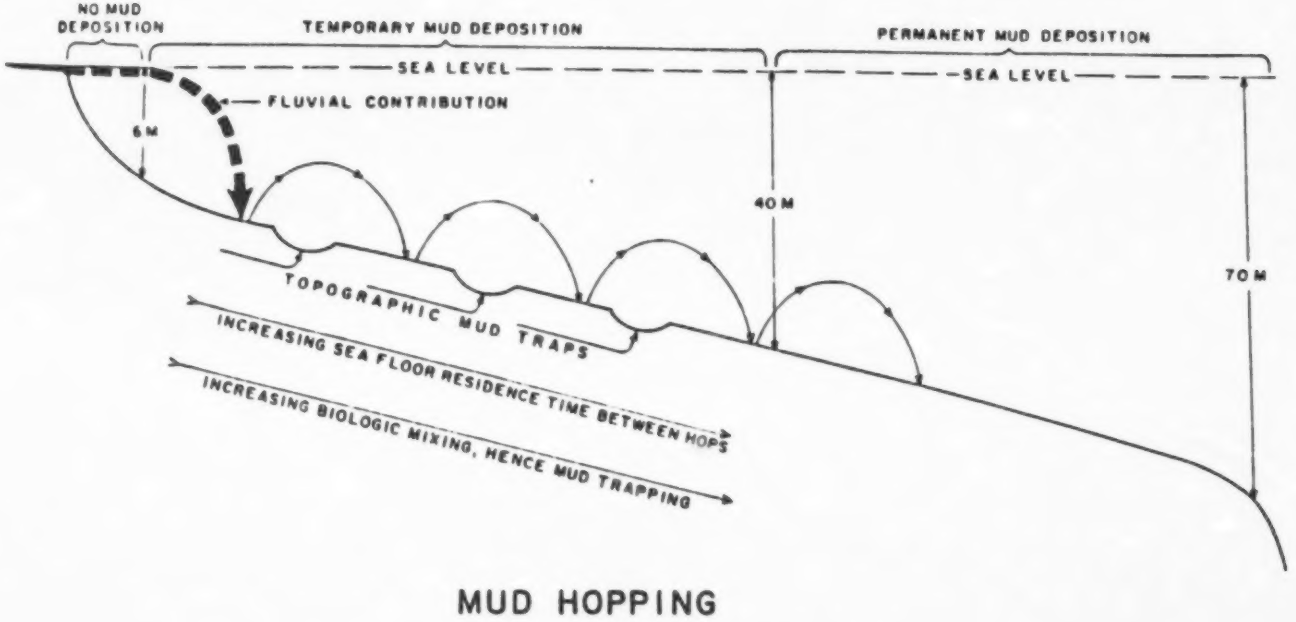
NO MUD DEPOSITION
TEMPORARY MUD DEPOSITION
PERMANENT MUD DEPOSITION
SEA LEVEL
SEA LEVEL
FLUVIAL CONTRIBUTION
6 M
40 M
70 M
TOPOGRAPHIC MUD TRAPS
INCREASING SEA FLOOR RESIDENCE TIME BETWEEN HOPS
INCREASING BIOLOGIC MIXING, HENCE MUD TRAPPING
MUD HOPPING

Figure 7-17 (A) A proposed mechanism for transporting cohesive material across the continental shelf based on observation on the North Puerto Rico Shelf.

Mud is introduced, typically from rivers, and is bypassed through the nearshore zone to an approximate isobath of 6 m. Between depths of 6 - 40 m mud is deposited temporarily only, except in topographic lows termed "mud traps". Between depths of 40 - 70m mud deposition is quasi-permanent. The mud is transported seawards in a series of "hops": The residence time between each "hop" increases with distance seawards. The rate of hopping, the depth of each zone and the distance of each hop will vary from shelf to shelf, depending on the wave climate. On Grand Banks, for example, there is no mud accumulation, partly due to the high wave energy and partly due to the low sediment input. On the Scotian Shelf, mud accumulates in the topographic lows such as Emerald Basin.

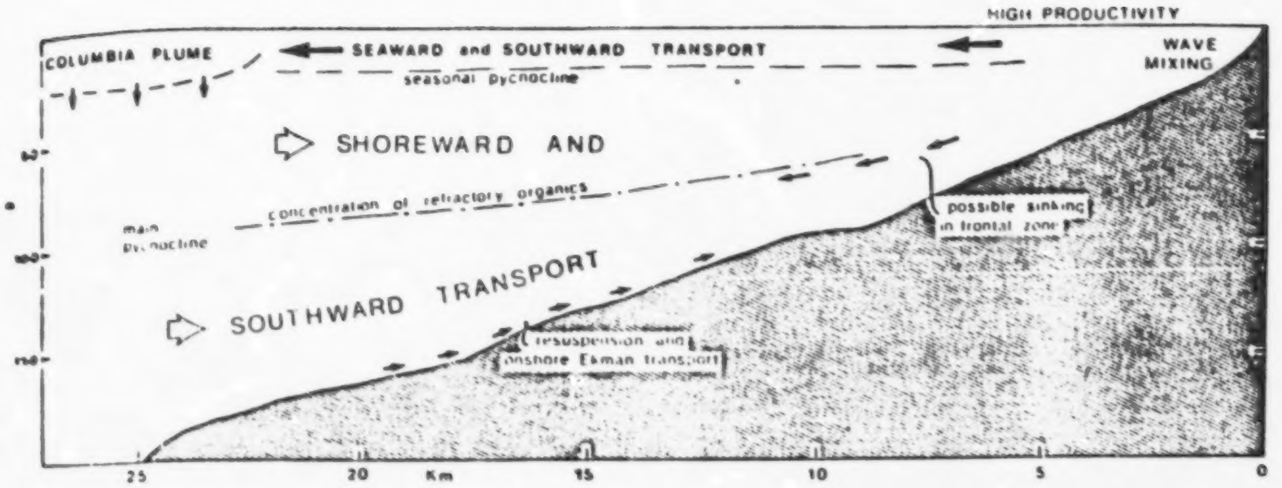
HIGH PRODUCTIVITY
COLUMBIA PLUME
SEAWARD and SOUTHWARD TRANSPORT
seasonal pycnocline
WAVE MIXING
SHOREWARD AND
concentration of refractory organics
main pycnocline
SOUTHWARD TRANSPORT
possible sinking in frontal zone
resuspension and onshore Ekman transport
25
20
Km
15
10
5
0

Figure 7-17 (B) A proposed model for the transport of suspended sediment across the continental shelf, based on measurements made on the Oregon shelf (from McCave, 1979).

The model proposes a seaward transport of fluvially derived sediment in the near surface waters to the edge of the shelf, whereupon material settles to the lower waters. Within the lower water the sediment is transported landward due to Ekman transport. McCave also proposes a mid-level seaward transport of fines along the main pycnocline.

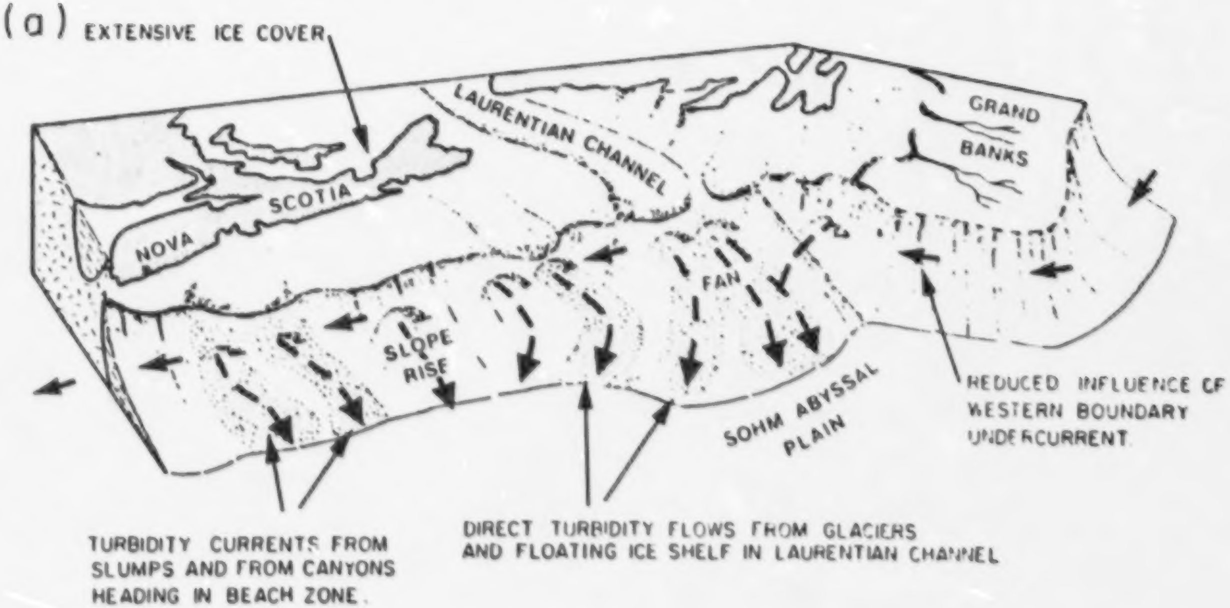

(a)
EXTENSIVE ICE COVER
NOVA
SCOTIA
LAURENTIAN CHANNEL
GRAND
BANKS
FAN
SLOPE
RISE
SOHM ABYSSAL
PLAIN
REDUCED INFLUENCE OF
WESTERN BOUNDARY
UNDERCURRENT
TURBIDITY CURRENTS FROM
SLUMPS AND FROM CANYONS
HEADING IN BEACH ZONE.
DIRECT TURBIDITY FLOWS FROM GLACIERS
AND FLOATING ICE SHELF IN LAURENTIAN CHANNEL

Figure 7-18 A summary of sedimentation patterns on the Nova Scotian continental shelf leading to slumping at the shelf edge and the development of turbidity currents (from Stow and Bowen, 1980).

Figure 7-18(A) shows the shelf during late glacial times. Sea level was 100m lower than today, with the beach zone at the shelf edge. Slumps and turbidity currents were generated directly from glacial action and deposition in the canyons heading in the beach zone.

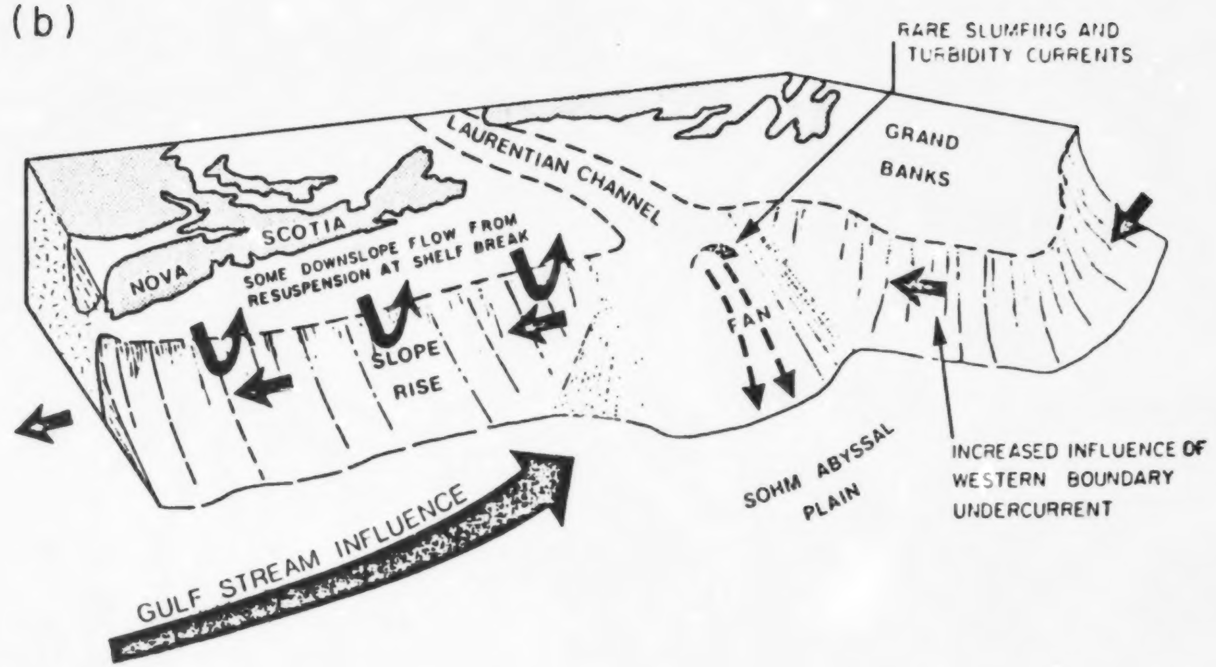
(b)
RARE SLUMPING AND TURBIDITY CURRENTS
GRAND BANKS
LAURENTIAN CHANNEL
SCOTIA
NOVA
SOME DOWNSLOPE FLOW FROM RESUSPENSION AT SHELF BREAK
SLOPE
RISE
FAN
SOHM ABYSSAL PLAIN
INCREASED INFLUENCE OF WESTERN BOUNDARY UNDERCURRENT
GULF STREAM INFLUENCE

Figure 7-18(B) shows the present day processes with resuspension at the shelf break and downslope transport of material hemipelagically. Slumping results from the thick accumulations of sediment at the shelf break which trigger turbidity current zones. As sea level rose, these became modified increasingly by the western boundary undercurrent.

Table 7-VI

A review of terminology used to describe constructive non-cohesive bedforms by various authors

Dalrymple et al, 1978	Costello and Southard, 1981	Harms and Fahnestock, 1970	Reineck and Singh, 1975
Ripples	Ripples	Ripples	Small scale ripples
Sand Waves	Sandwaves	Dunes	Giant current ripples
Type 1 megaripples	2-D Dunes	Dunes	Mega-current ripples
Type 2 megaripples	3-D Dunes	Transition	Mega-current ripples
Antidunes	Antidunes	Antidunes	Antidunes

3 THE MORPHOLOGY AND DISTRIBUTION OF SHELF BEDFORMS

3.1 Non-Cohesive Bedforms

These types of bedforms, which include ripples, are perhaps the best known of all sedimentary structures, and have been studied in great detail by fluvial and marine hydrologists. The genesis and internal sedimentary structures are a clear indication of the flow type and intensity during the time of their formation. The significance of these bedforms is that they occur in any environment given the appropriate flow conditions, flow depth, and grain size, and can be used to hindcast depositional flow conditions.

Unfortunately, there is a considerable variation in the terminology used to describe the suite of non-cohesive bedforms. Table 7-VI shows some of the terms used by different workers to describe these bedforms (modified from Middleton and Southard, 1977).

In this report, we chose the classification of Dalrymple et al., (1978) which can be cross-referenced to other authors' terminology in Table 7-VI. The size parameters used to identify each of the bedform types is based on data from Reineck and Singh (1975) (see Table 7-VII), and from Dalrymple et al., (1978).

3.1.1 Current-formed Ripples

These bedforms are less than 60 cm in wavelength and vary in height from 0.6 cm to 6 cm. They are uniform in width, and are sharp crested, exhibiting an asymmetry in the down current direction. Figure 7-5(A and B) p. 11, show the nomenclature used to

Table 7-VII

Size parameters used to identify bedform types

a) Current ripples (transverse)

Name	Nature of Crest	Size Parameters	Ripple Index L/H
Small-current ripples	Straight Undulatory Lingoid Rhomboid	L = 4-60 cm H = up to 6 cm	>5 Mostly 8 - 15
Megacurrent ripples	Straight Undulatory Lunate Lingoid	L = 0.6-30 m H = 0.06-1.5 m	Mostly 15
Giant-current ripples	Straight Undulatory Bifurcating	L = 30-1000 m H = 1.5-15 m	Mostly >30 Up to about 100
Antidunes	Straight	L = 0.01-6 m H = 0.01-0.45 m	

b) Wave Ripples

Name	Nature of Crest	Size Parameters	Ripple Index L/H
Symmetrical wave ripples	Straight, partly bifurcating	L = 0.9-200 cm H = 0.3-19.5 cm	4-13 Mostly 6-7
Asymmetrical wave ripples	Straight, partly bifurcating	L = 1.5-105 cm H = 0.3-19.5 cm	5-16 Mostly 6-8

c) Isolated (incomplete) ripples

Name	Nature of Crest	Size Parameters
Isolated small-current ripples	Like small-current ripples	Like small-current ripples but lesser in height
Isolated mega-current ripples	Straight Curved Sickel-shaped	Like megacurrent ripples, but lesser in height
Isolated giant-current ripples	Like current ripples	Similar to giant-current ripples
Isolated wave ripples	Straight Curved	Like wave ripples, but lesser in height

Table 7-VII cont'd

d) Combined current/wave ripples

Name	Name of Crest	Size Parameters
Longtitudinal current/wave ripples (direction of wave propagation at right angles to current direction)	Straight, unbranched crests parallel to the current direction; also known to occur in mud	L = 2.6-5 cm
Transverse current rent/wave small ripples (wave direction parallel to current direction)	Mostly rounded crests, transverse to current direction	

e) Wind Ripples

Name	Nature of Crest	Size Parameters	Ripple Index L/H
Wind sand ripples	Straight, partly bifurcating	L = 2.5-25 cm H = 0.5-1.0 cm	10-70 and more
Wind granule ripples	Straight, cuspate, barchan-like	L = 25 cm-20 m H = 2.5-60 cm	12-20

define the morphology of sharp and flat crested bedforms. The lee face of the ripple is the slip face, in the zone of flow separation. The stoss face is the erosional face. The lee face is oriented in the direction of bedform migration. Ripples can form in any flow depth, provided the flow is above the critical velocity for sediment motion. They develop only in coarse silts and sands between grain sizes of about 0.03 mm to 0.6 mm. Allen (1968) has classified ripple trains into a variety of differing types, indicative of slightly different depositional environments:

straight transverse
straight swept
transverse sinuous - in phase
transverse sinuous - out of phase
transverse catenary - in phase
transverse catenary - out of phase
catenary swept
linguoid
cuspate
lunate (see Figure 7-19(A)).

Each ripple train type is indicative of differing flow conditions.

The significance of these forms in terms of either flow velocity or depth changes can be seen in Figure 7-19(B). As currents increase (or water depth decreases below a depth equivalent to the height of the bedforms) there is a progression of bedforms from straight crested to sinuous to linguoid or

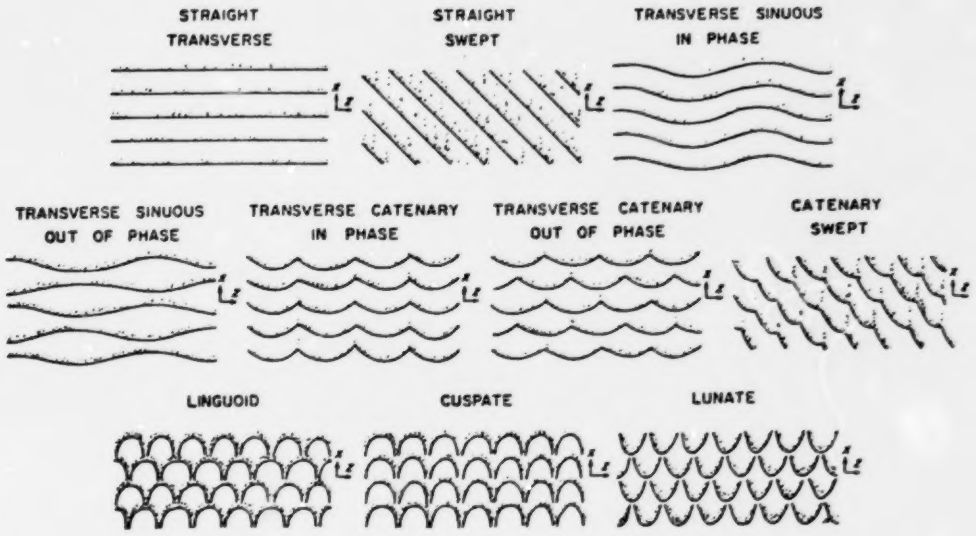
STRAIGHT TRANSVERSE
STRAIGHT SWEPT
TRANSVERSE SINUOUS IN PHASE
TRANSVERSE SINUOUS OUT OF PHASE
TRANSVERSE CATENARY IN PHASE
TRANSVERSE CATENARY OUT OF PHASE
CATENARY SWEPT
LINGUOID
CUSPATE
LUNATE

The current flow is in the x-direction, stippling indicates the lee face. Straight, straight swept and transverse sinuous (in phase) form at lower current speeds (15-20 cm/s). The catenary bedforms generate at intermediate current speeds (20-30 cm/s) and the linquoid and cuspate forms generate at higher current speeds (> 30 cm/s). The lunate bedforms are not ripples in a generic sense, but refer to 3-D megaripple morphology.

Figure 7-19 (A) A classification of ripple train crest patterns based on observation and flume tank experimentation (from Allen, 1968).

lunate. In reality, the lunate ripples are 3-D megaripples and are therefore generated in a different manner from ripples. Linguoid ripples, also called "high energy" ripples develop prior to flat bed and are characterized by "blowouts" through the crests of undulating ripples.

B

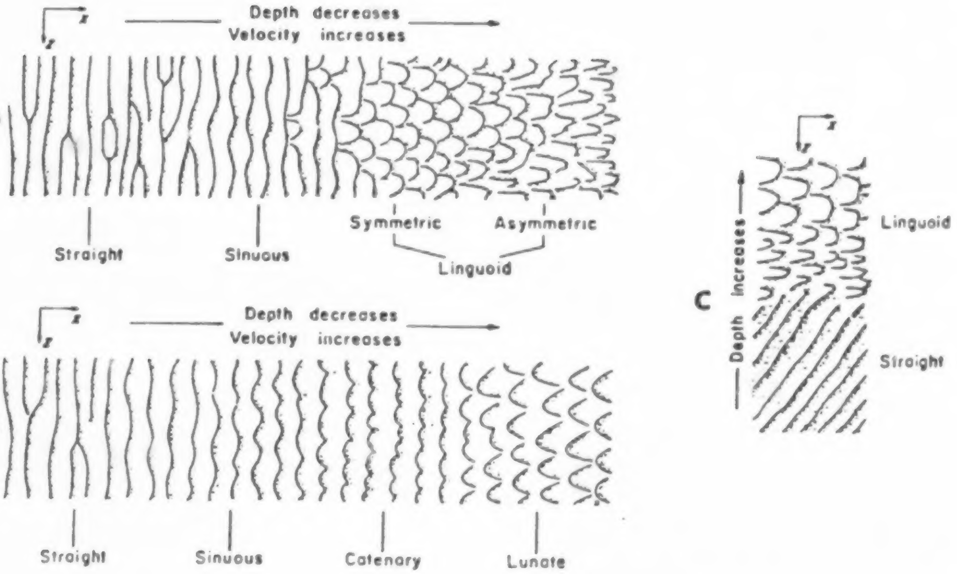
z
y
Depth decreases
Velocity increases
A
Straight
Sinuous
Symmetric
Asymmetric
Linguoid
B
Depth decreases
Velocity increases
Straight
Sinuous
Catenary
Lunate
C
Depth increases
Linguoid
Straight

Over the continental shelf, the progression is independent of depth, and is only affected by depth in flows less than 50 cm deep. The straight anastomosing (bifurcating) types are wave formed: The sinuous types are current formed. As the current increases, so the degree of asymmetry increases and the crest length decreases. The lunate forms generate as a megaripple phase, progressing from 2-D (Sinuous) megaripples into short crested 3-D megaripples as the flow velocity increases. This development results only if the grain sizes are greater than 0.7 mm. Wave formed ripples can form in material coarser than current ripples.

Figure 7-19 (B) The sequence of ripple train crest patterns which will develop under varying unidirectional flows (from Allen, 1968).

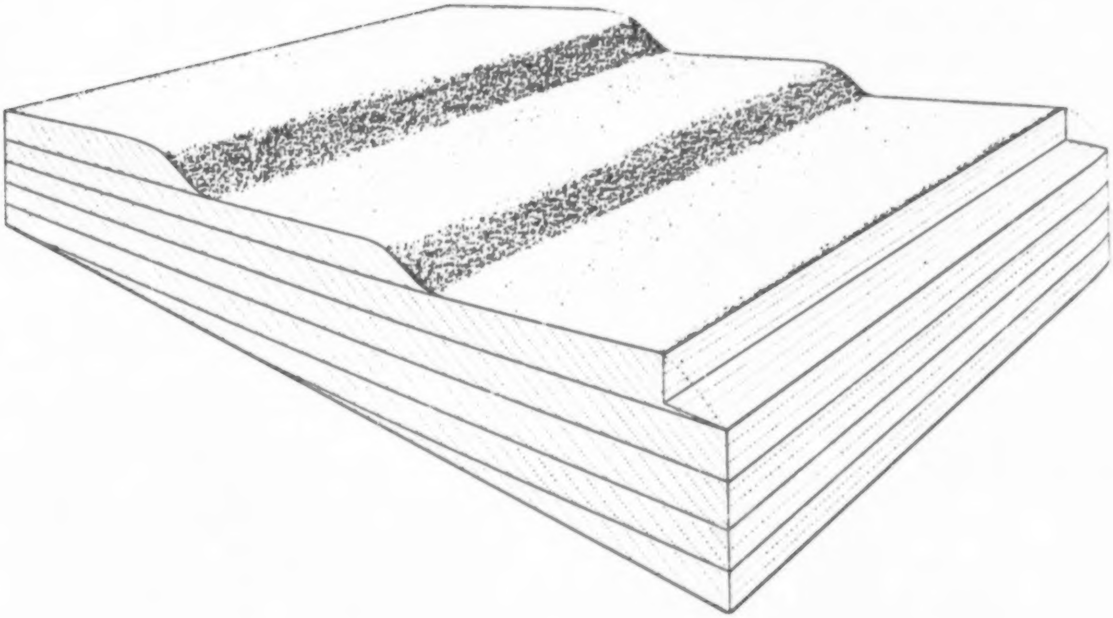

Cross laminae are tabular and oblique to the flat lower bounding surface.

Figure 7-20 (A) A block diagram showing the internal structure and morphology of straight crested, current formed ripples (from Reineck and Singh, 1975).

A detailed sketch of straight crested and sinuous ripples is shown in Figure 7-20(A and B). Figure 7-20(A) shows climbing ripples (which result from an abundant supply of sediment). The internal structures by which these bedforms can be identified, are the tabular (or planar) cross laminae, which are the preserved slip faces of earlier ripples.

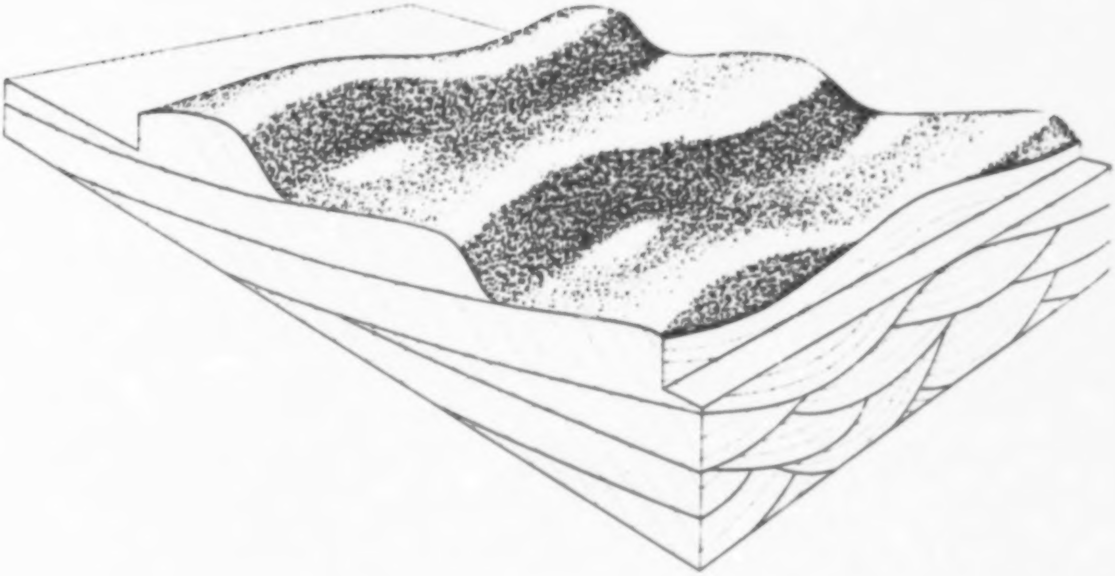

The cross laminae are weakly festoon shaped in the crest parallel section and are slightly tangential in the crest normal section. The lower bound is curved and truncated.

Figure 7-20 (B) A block diagram showing the internal structure and morphology of undulatory, current formed ripples (from Reineck and Singh, 1975).

Figure 7-20(B) shows the internal structure of climbing, sinuous ripples. The cross laminae are tangential with the bottom set in ripple section, and appear festoon like in the crest-parallel section.

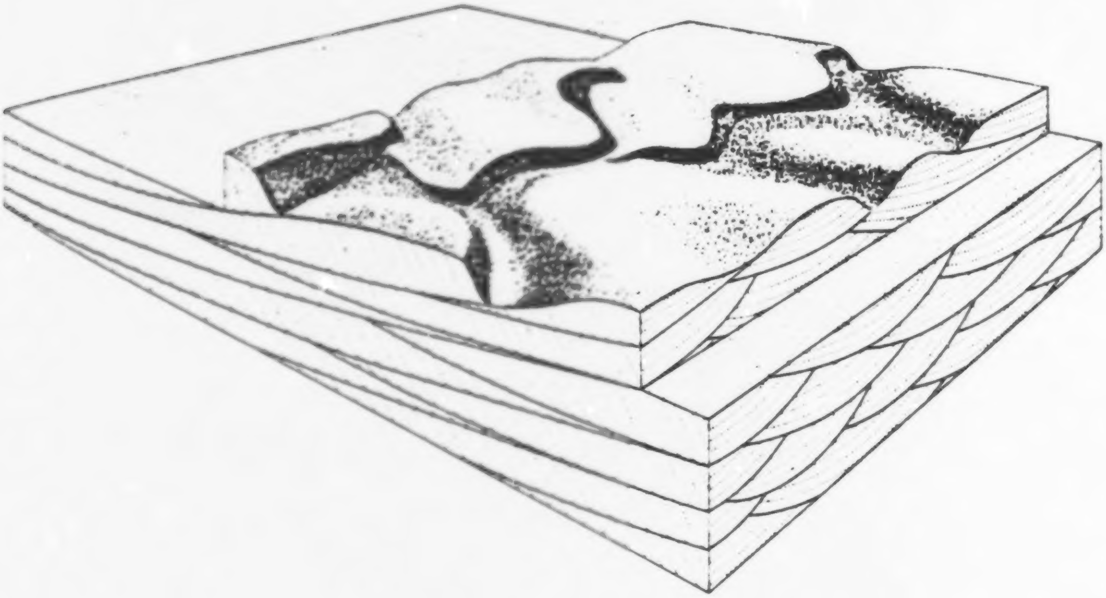

The cross lamination is strongly festoon shaped in the crest parallel section and tangential in the crest normal section. The lower bound is concave up and highly truncated in both sections.

Figure 7-21 (A) A block diagram showing the internal structure and morphology of linguoid ripples (from Reineck and Singh, 1975).

Figure 7-21(A) shows the morphology and internal structure of linguoid (or tongue-like) ripples. The slip face indicates the direction of migration of the bedform. These features fall into the same size as "low energy" ripples, though their crest length is restrictd to the approximate wavelength of the ripple. The cross laminae are tangential to the bottom set in ripple section and show strong festoon bedding in the crest parallel section.

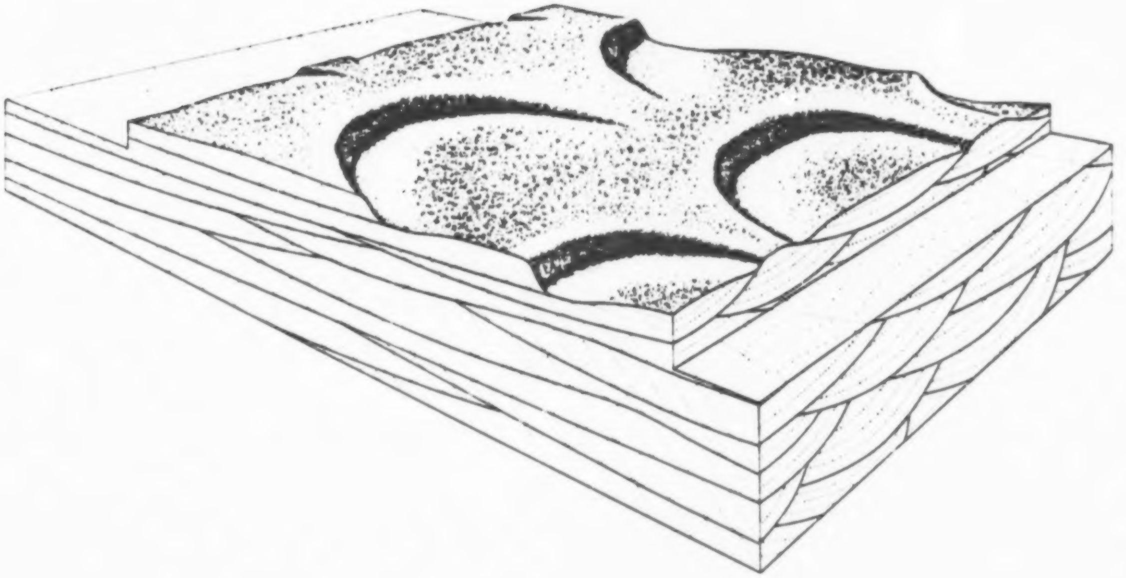

The cross lamination is strongly festoon shaped in the crest parallel section and strongly tangental in the crest normal section. The cross sets are larger than those produced by ripples (up to 150 cm).

Figure 7-21 (B) A block diagram showing the internal structure and morphology of lunate (3-D) megaripples (from Reineck and Singh, 1975).

Linguoid cross sets are discontinuous and wedge in and out between other sets producing a complex internal structure.

A number of dimensionless indices have been devised to describe the morphology of ripples in such a way that their origin and nature can be easily expressed by a few simple measurements (Tanner, 1967). The following are the most

important: Ripple Index
Ripple Symmetry index
Parallelism index
Straightness index
Continuity index

The definition of these indices is shown in Figure 7-22(E). By use of several of these indices, a differentiation can be made between wave and current dominant ripples. Figure 7-22(C) shows the values of these indices at which this discrimination can be made. For example, ripples with symmetry indices below 2.5 are wave formed, but are current formed above 3.0 The ripple index is less conclusive, with a wide transitional zone beween 4 and 15.

3.1.2 Wave Formed Ripples

There are a number of significant differences between wave and current formed ripples. The most significant difference is that wave formed ripples are quasi-symmetrical in section and tend to be sharp crested. These ripples have a greater height to length ratio, and they show a well developed bifurcation pattern (see Figure 7-22(D)). Such bifurcation patterns can be used to distinguish wave formed ripples in seabed photographs, where no other information is available. Current ripples do not bifurcate in this fashion. Wave formed ripples vary in length from 9-200 cm, and in height from 0.3 - 23 cm. The most common ripple index is between 6 and 7.

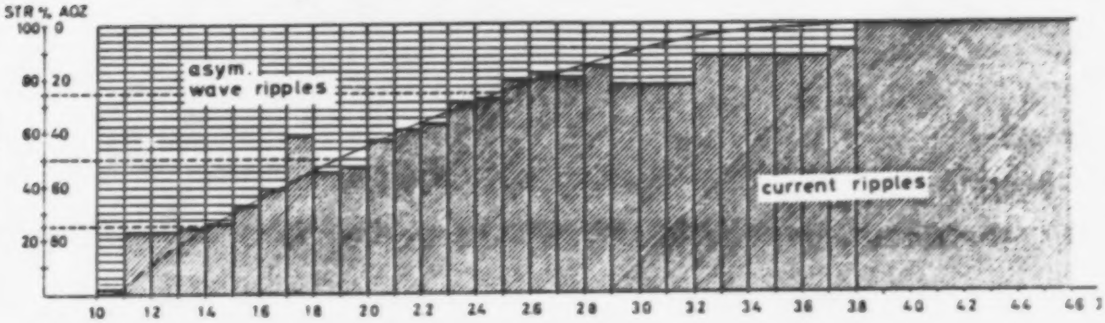

At R.S.I. greater than 3.8 only current ripples are present.

Figure 7-22 (A) The frequency of occurrence of asymmetric ripples versus current ripples as a function of wave ripple symmetry index (from Reineck and Wunderlich, 1968).

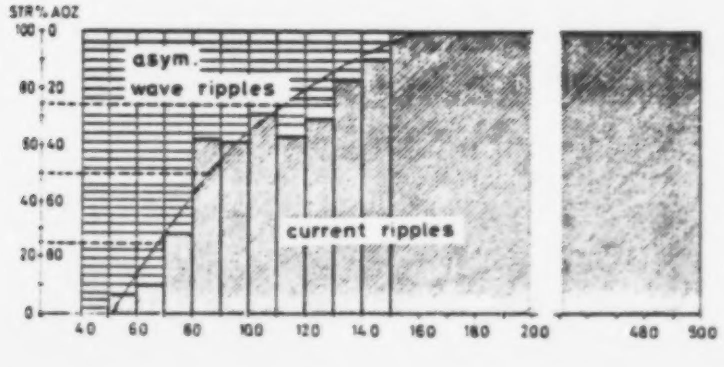

At R.I. greater than 15, only current ripples exist. The diagram shows the problems related to interpretation of process (wave or current) between intermediate R.S.I. and R.I. values.

Figure 7-22 (B) The frequency of occurrence of asymmetric wave ripples versus current ripples as a function of ripple index (from Reineck and Wunderlich, 1968).

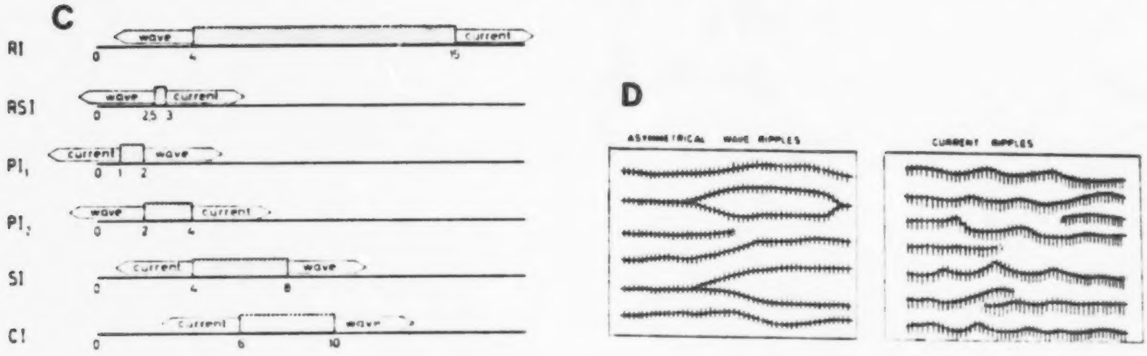
C
RI
wave
current
0
4
15
RSI
wave
current
0
2.5
3
PI₁
current
wave
0
1
2
PI₂
wave
current
0
2
4
SI
current
wave
0
4
8
CI
current
wave
0
6
10
D
ASYMMETRICAL WAVE RIPPLES
CURRENT RIPPLES

E

RI — Ripple index

$$= \frac{\text{ripple length}}{\text{ripple height}}$$

RSI — Ripple symmetry index =

$$= \frac{\text{length of horizontal projection of stoss side}}{\text{length of horizontal projection of lee side}}$$

PI₁ — Parallelism index =

$$= \frac{\text{length of curved part of crestline} \cdot \text{min. ripple length}}{\text{mean ripple length} \cdot \text{max. ripple length}}$$

PI₂ — Parallelism index =

$$= \frac{\text{max. ripple length} - \text{min. ripple length}}{\text{mean ripple length}}$$

SI — Straightness index =

$$\frac{\text{length of curved part of crestline}}{\text{departure of curvature from straight (crest) line}}$$

CI — Continuity index =

$$\frac{\text{crest length between bifurcations}}{\text{mean ripple length}}$$

Figure 7-22 (C) The values of various ripple indices at which waves or currents predominate in the generation of bedforms, and the intermediate zones where interpretation is difficult.
(D) A plan view of two sets of ripple train crests. The first is wave formed and exhibits bifurcation of the crests. Current ripples do not show this bifurcation.
(E) The definition of the various ripple indices used to define ripple types.

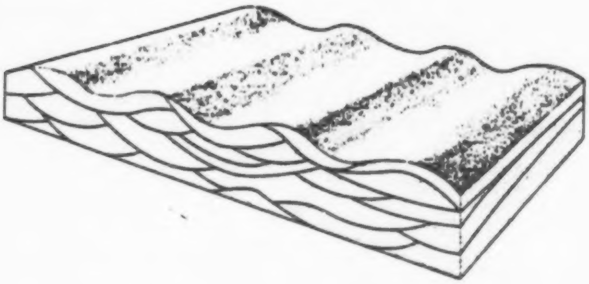

Such ripples tend to have rounded crests, an irregular lower bounding surface, interfingering of lenses, the presence of both lee and stoss face cross lamination and the presence of trough lamination.

Figure 7-23 (A) Wave ripple cross-lamination and morphology of symmetric wave ripples.

Figure 7-23(A) shows a block diagram of the morphology of asymmetric wave formed ripples and their internal lamination. The internal lamination shows festoon development at right angles to the ripple crest (not to be confused with festoon bedding of linguoid ripples which produce these structures in section parallel to the ripple crest). Asymmetrical wave ripples develop under shoaling waves or in the presence of a weak unidirectional current. Such features exhibit an irregular lower bounding surface, interfingering lenses, cross lamination in both lee and stoss directions and the predominance of trough lamination and foreset drapes (Reading, 1979).

In many cases, interference patterns can develop resulting from the superposition of one ripple set onto another. Figure 7-23(B) demonstrates the example of linguoid ripples, produced by

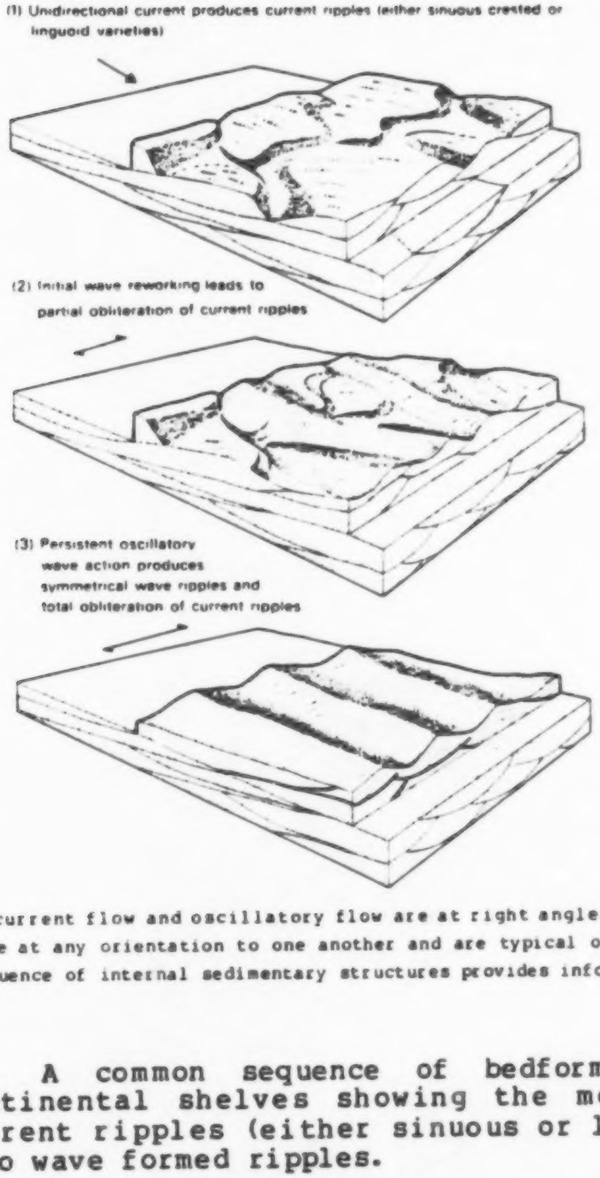
(1) Unidirectional current produces current ripples (either sinuous crested or linguoid varieties)
(2) Initial wave reworking leads to partial obliteration of current ripples
(3) Persistent oscillatory wave action produces symmetrical wave ripples and total obliteration of current ripples

In the case shown the current flow and oscillatory flow are at right angles. In reality, the two processes can take place at any orientation to one another and are typical of seabed recovery after a storm event. The sequence of internal sedimentary structures provides information on the sequence of events.

Figure 7-23 (B) A common sequence of bedforms generated on continental shelves showing the modification of current ripples (either sinuous or linguoid types) into wave formed ripples.

unidirectional currents overlapped by wave formed ripples. Often an intermediate stage of development is preserved making interpretation difficult. In such cases, an examination of the internal sedimentary structure can shed light on the history of the event.

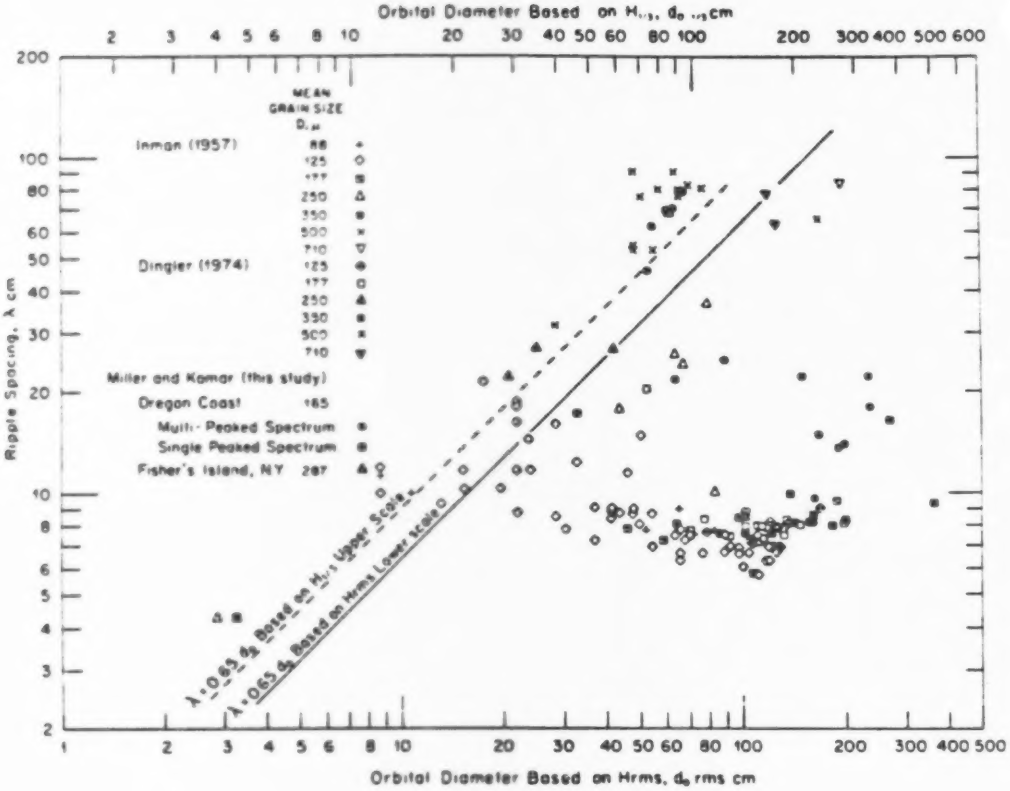

Figure 7-24 A composite diagram of ripple spacing (λ) versus orbital diameter (d_o) compiled by Miller and Komar (1980) from data by others.

The relationship $\lambda = 0.65\ (d_o)$ is the best fit although a considerable scatter in the results exist. Some caution should be exercised in attempting to deduce wave conditions on the basis of ripple spacing. It is thought that the straight line relationship results from a monochromatic wave train, while longer wave lengths (for a constant d_o) result from a complex wave spectrum.

Dingler (1974) has found that wave formed ripple steepness is related to the Shield's parameter (θ) and that flat bed phase ensues at a value of 240 (where $\theta = \rho Um^2/(\rho_s - \rho)$ g.d, and U_m is the maximum wave orbital velocity).

Miller and Komar, (1980) have recently reviewed the data on ripple wavelength to orbital diameter (d_o). Their results are shown in Figure 7-24. It appears that wave length is a function of grain size. The larger the grain size, the longer the wave length. Furthermore. for one grain size two equilibrium wave lengths can occur. Data from the Oregon shelf (d_{50} = 0.165 mm) shows that ripple spacings of 9 cm and 20 cm occurred in the same sediment type. The former spacing results from a monochromatic wave train, while the longer wave length results from a polymodal wave spectrum.

In considering wave formed ripples, it has been assumed that the waves are progressive. In the nearshore, standing waves can be generated which can generate an entirely new suite of bedforms, which include such features as banks, crescentic bars, cusps, longshore bars etc. The effect of such features on the development of sand ridges will be discussed in a later section.

3.1.3 Sand Waves

The term "sand wave" has been used in the past as a collective term, denoting any rhythmic seabed feature of sand, or as a generic term for a specific type of bedform. The present use of the term refers to its generic application, whereby these features are unique to a specific flow strength and grain size, and quite distinct from either megaripples (dunes) or ripples. Sand waves are approximately equivalent to the giant-current ripples of Reineck and Singh, (1975) and are current transverse features. They are characterized by their straight crests, a distinct asymmetry and usually heights ranging from 1.5 - 3 m. They form in sediments coarser than 0.31 mm, under unidirectional currents (U_{40}) in excess of 40 cm/s and in water depths greater than 2 m. They form in hours, the process of construction being faster than the process of destruction. They have been observed over a great many regions of the world at a great many depths. On the Canadian east coast shelf, they have been recognized in the Bay of Fundy, on the Grand Banks of Newfoundland (Amos and Barrie, 1980) and on the Scotian shelf (Stanley, 1969).

Dalrymple et al (1978) have measured the morphology of sand waves in the Bay of Fundy and have found that these features are formed of bundles of megaripple cross-sets and that sand waves are usually associated with megaripples or ripples. The smaller forms climb the backs of the larger. Megarippled sand waves range in wavelength from 10-215 m and in height, from 0.15 - 3.4 m. Rippled sandwaves range in wavelength from 5-25 m and in height, from 0.15 - 0.75 m. On the Grand Banks, sand waves have been observed ranging in wavelength up to about 1000 m, but have heights less than 1 m, with no definable slip face (Fader and King, 1981). These bed features (which occur in 70 m water depths) are thought to differ from those in the Bay of Fundy in that they occur on a thin layer of sand and are possibly "starved" and may move only intermittently (perhaps every 10-20

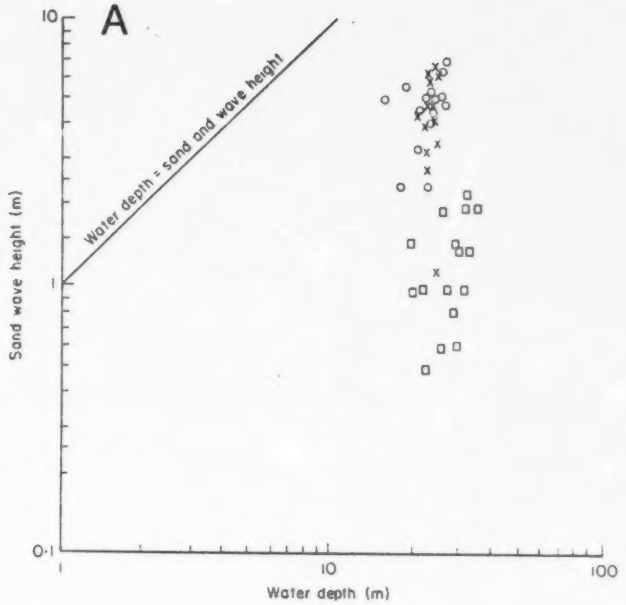

The figure shows the lack of correlation between the two variables, and shows that most sand waves range in height from 0.5 - 8 metres. Sand waves tend to be lower on shelf banks, due to higher wave effect, and higher in deeper water. The height of sand waves is thought to be related to the thickness of the boundary layer in which they form.

Figure 7-25 (A) The relationship between water depth and sand wave height for selected Atlantic shelf sand wave fields (from Swift, Freeland and Young, 1978).

years). The relationship of sand wave height and water depth is shown in Figure 7-25(A) and shows the apparent independence between the two variables. The relationship between sand waves height and wavelength is shown in Figure 7-25(B) and shows a wide range in ratios. Dalrymple et al. (1978) have demonstrated that water depth is not a controlling factor in the generation of sand waves. Sand waves generate under prevailing unidirectional currents such as tidal currents or storm driven currents. On the

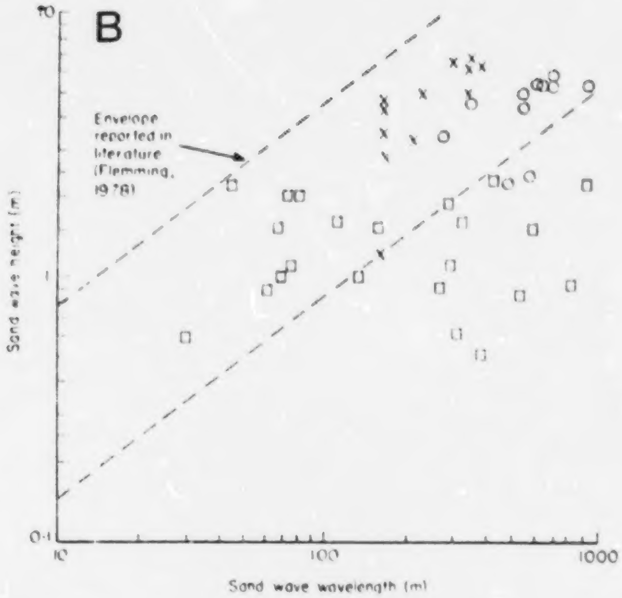

Sand waves vary in length from 30-1000 metres and are considered solitary features (the spacing of the downcurrent sand wave is not controlled by boundary layer distortions of the upcurrent sand wave). They fall generally within the envelop reported by Flemming (1978), i.e., no obvious relationship of the two variables, suggesting both that sand wave spacing and sand wave wavelength are not necessarily the same, and that many may be degraded or generated intermittently.

Figure 7-25 (B) The relationship between sand wave height and sand wave wavelength for selected Atlantic shelf sand wave fields (from Swift, Freeland and Young, 1978).

outer shelf, the latter is the most important process, though ocean currents which at times impinge on the shelf edge may in some cases be responsible. For example, Fleming (1978) has recognized sand waves on the shelf edge of Southeast Africa, generated by the Agulhas Current. Sand waves are an indication of sediment dispersal or transport. The direction of transport is in the direction of asymmetry (i.e. eroded from the stoss

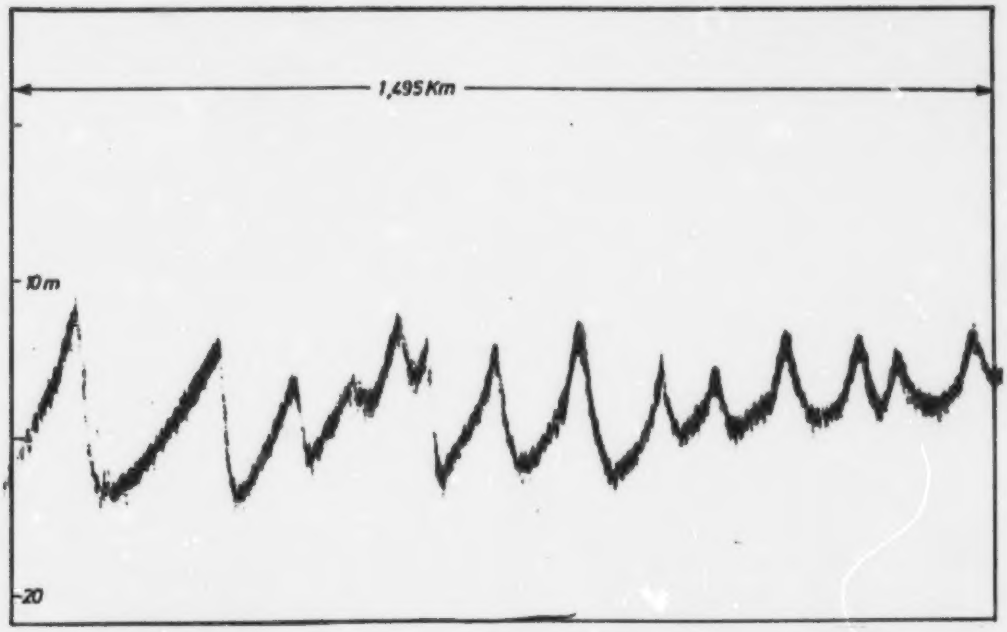

The pattern is typically "saw-tooth" with well developed stoss and lee faces. The direction of migration of these features is from left to right. The spacing is irregular, due to the solitary nature of sand waves. The height of the sand waves varies from crest to crest from 2 - 10 m. Also composite sand waves occur, whereby one feature exhibits 3 or more crests. The mean wave-length of these sand waves is about 100 m.

Figure 7-26 (A) An echogram through a sand wave field in the North Sea (from Reineck and Singh, 1975).

slope and deposited on the lee slope). Sand waves tend to occur in fields or patches and can be distinguished by their saw tooth profiles on echo grams see Figure 7-26(A)). Sand waves do not exhibit scour pits in their troughs. Sand wave migration rates are a function of the sediment transport rate, but are in the order of metres/day (figure 7-26(C)). Megaripples on the other hand, move 10-15 times faster (Boothroyd and Hubbard, 1975) and therefore climb up the back of sand waves when they occur

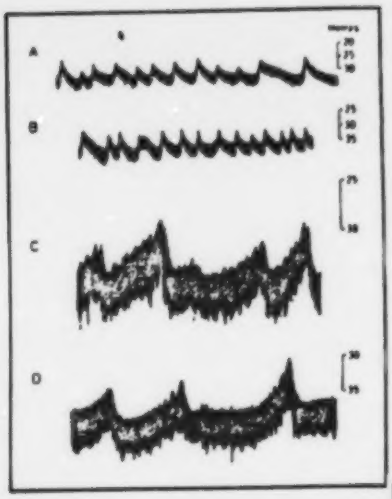

B

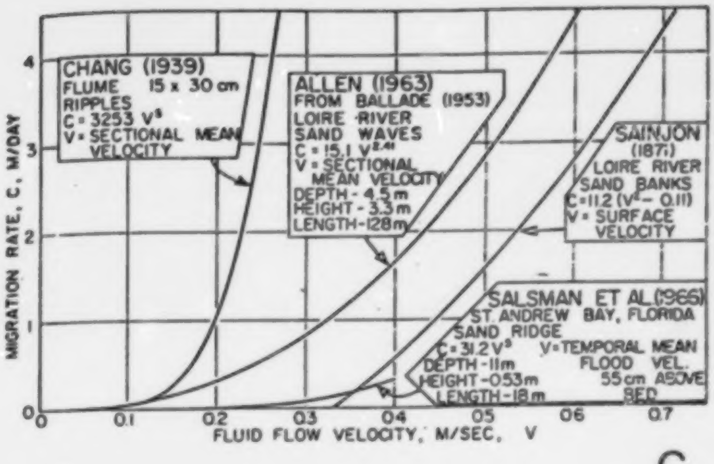

C

Figure 7-26 (B) Various profiles of sand waves from the southern bight of the North Sea (from McCave, 1971).

The lengths of the sections are 3 800 m (A), 2 800 m (B), 900 m (C) and 1220 m (D).

Figure 7-26 (C) The migration rate of various types of bedforms as a function of current velocity, taken from a variety of locations worldwide.

Ripples and megaripples migrate fastest at rates of over 4 m/day, and at flow velocities of 30 cm/s. Sand waves migrate at rates of about 1 - 4 m/day. Sand bars migrate only above velocities of 35 cm/s and at rates lower than sand waves, while sand ridges show the slowest rate of migration (cm/day).

together providing sediment to the slip face of the sand wave. Sand waves are composite bedforms, showing form discordant cross-laminae, reactivation surfaces, erosional phases and previous depositional events. Boersma and Terwindt, (1981) show the internal structure of two sand waves from the North Sea. (Figure 7-27 B and C). Clearly, much of the history of sand wave development can be determined from an examination of the internal structure.

Low Activity Sandwave Station

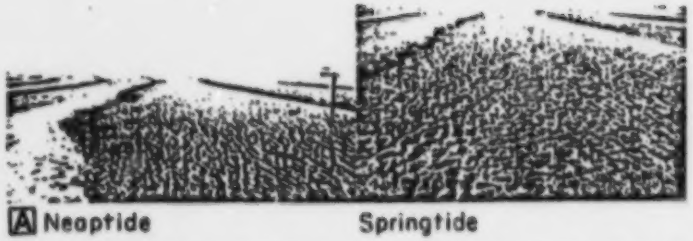
A
Neaptide
Springtide

(A) photographs of the sand waves, exposed during low tide in the Jade estuary.

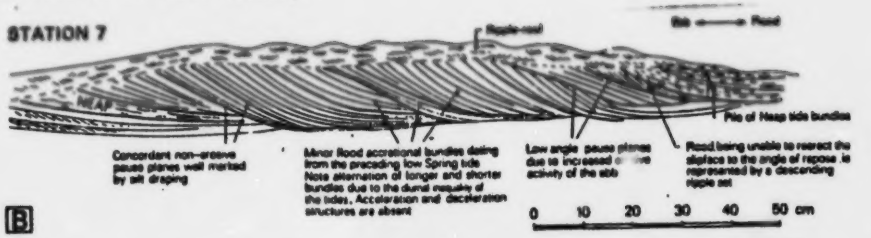
STATION 7
Ripple-nod
Ebb ⟷ Flood
NEAP
Pile of Neap tide bundles
Concordant non-erosive pause planes well marked by silt draping
Minor flood accretional bundles dating from the preceding low Spring tide Note alternation of longer and shorter bundles due to the diurnal inequality of the tides. Acceleration and deceleration structures are absent
Low angle pause planes due to increased activity of the ebb
Flood being unable to reerect the slipface to the angle of repose is represented by a descending ripple set
0 10 20 30 40 50 cm
B

(B) The internal structure of a sand wave showing the composite structure of cross-laminae. The internal structure is composed of concordant, festoon bedding with an irregular lower bounding surface.

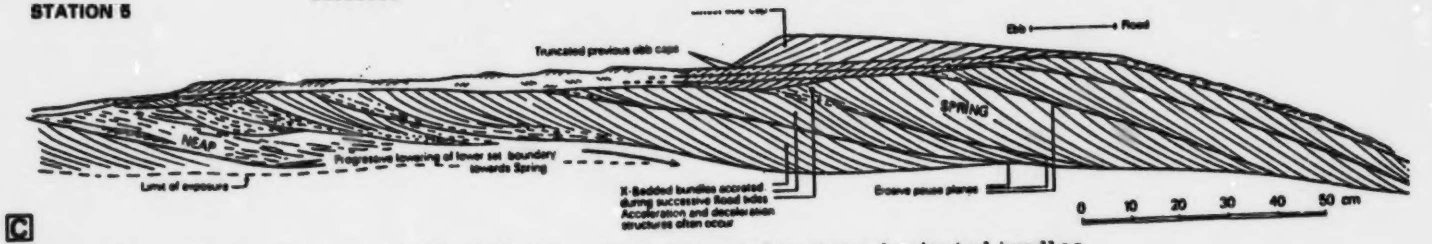
STATION 5
Truncated previous ebb caps
Ebb ⟷ Flood
SPRING
NEAP
Progressive lowering of lower set boundary towards Spring
Limit of exposure
X-Bedded bundles accreted during successive flood tides Acceleration and deceleration structures often occur
Erosive pause planes
0 10 20 30 40 50 cm
C

(C) The internal structure of a spring tide sand wave, showing composite cross-laminated bundles interpreted to have developed during successive spring tides. There is a reactivation surface near the top, separating flooding cross laminae from ebbing cross laminae, the latter developing during the ebb preceding exposure. The sand wave represents a composite feature, formed by a number of events. Such internal structures can be of value on the shelf in determining the sequences of events in the development and transport of sand waves.

Figure 7-27 Sand waves from the North Sea (from Boersma and Terwindt, 1981).

Swift and Freeland, (1978) have recognized sand waves on the U.S. east coast shelf. They conclude that these bedforms are persistant for many years but are reactivated during periods of intense storms, and are therefore in equilibrium with the modern hydraulic regime. They interpret these features not to be "relict".

Sand waves can occur in association with sand ribbons. In such cases the sand waves are barchan-like with a convex stoss face and concave lee face. The shape is a function of the rate of sediment transport. The greatest transport occurs at the edge of the ribbons. These edges produce the spurs associated with the barchan shape.

Examples of sand waves seen on sidescan sonar records are shown in Figures 7-28 and 7-29 (taken from Swift, Freeland and Young, 1979). These examples are from the Middle Atlantic Bight and are common on the inner shelf of North Carolina, Virginia, and on shelf edge shoals such as in the vicinity of Wilmington canyon.

3.1.4 Megaripples

Megaripples (or dunes) form at higher current speeds than ripples or sand waves. Two types of megaripples exist, 2-D and 3-D types. Two-dimensional (type I) megaripples are straight, long crested asymmetric features with wavelengths from 0.1 - 25 m and wave heights from 5 - 50 cm. Crests tend to be smoother and oftentimes sinuous. They occur in sands coarser than 0.18 mm and

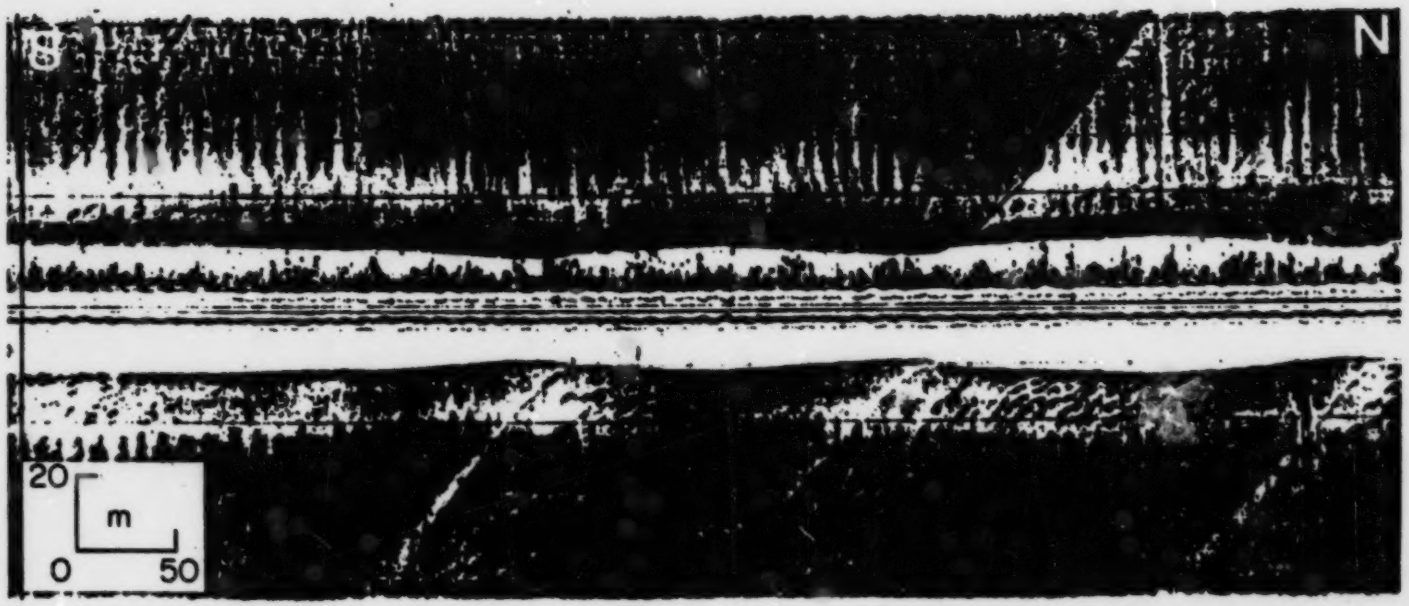

The sand wave crests are oriented obliquely across the record and are migrating from left to right. They have a wavelength of about 120 m and have well developed slip faces indicating recent transport. The megaripple crests are parallel to the sand wave crests and occur predominantly in the troughs of these features. Smaller scale (2m wavelength) megaripples occur on the crest of the sand waves. It is considered that this is the response to a change in grain size of the bottom sediment, the crests are composed of finer material than the troughs. The megaripples also show well developed slip faces and are migrating from left to right in the frame. The cross track band stripping in the image is probably due to sidescan fish motion, resulting from wave activity.

Figure 7-28 A sidescan sonar record of sand waves with superimposed 2-D megaripples, from the Atlantic shelf near Cape Hatteras (from Swift, Freeland and Young, 1979).

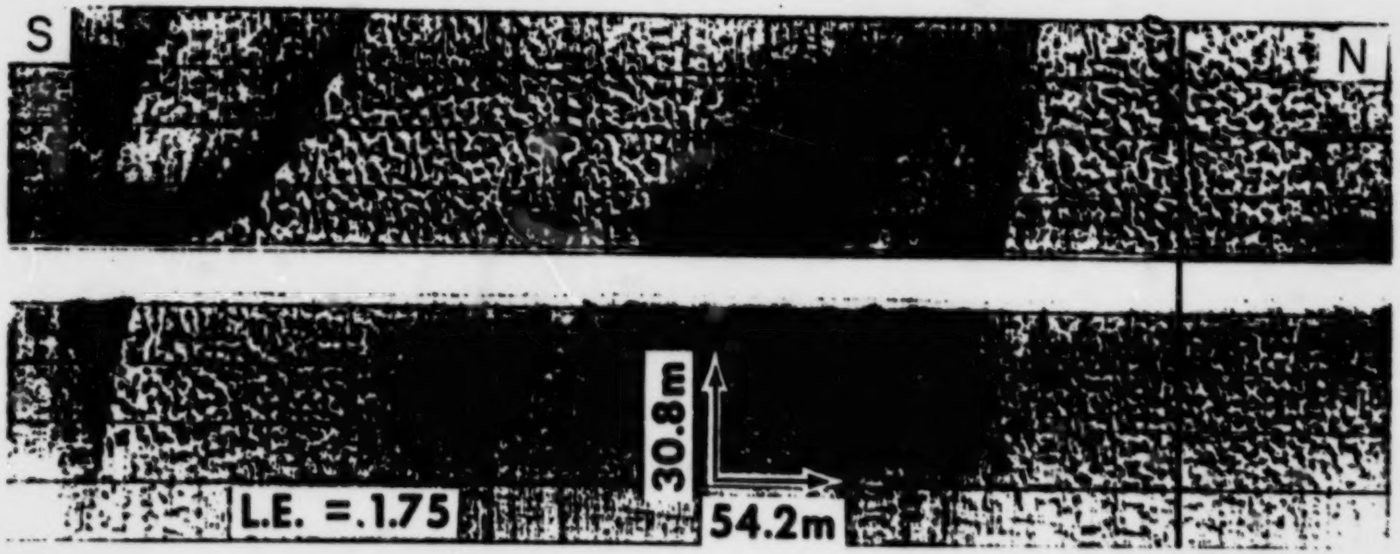

The crest of the sand waves are from top to bottom in the frame. The dark zones represent the troughs of the sand waves, composed of pebbley, shelly coarse sand. The sand waves are migrating from right to left in the frame. The lee slope is represented by the sharp change in reflectivity, the stoss slope by the gradual change in reflectivity. The 3-D megaripples are short crested and difficult to interpret orientation from. They appear to show a crest trend normal to the sand waves. The cusps of the megaripples indicate a migration direction running from the bottom to the top of the frame. The megaripples occur preferentially on the crest of the sand waves, the material in the trough is too coarse to maintain this type of bedform.

Figure 7-29 A sidescan sonar record of low amplitude sand waves with superimposed 3-D megaripples from the Long Island inner shelf (from Swift, Freeland and Young, 1979).

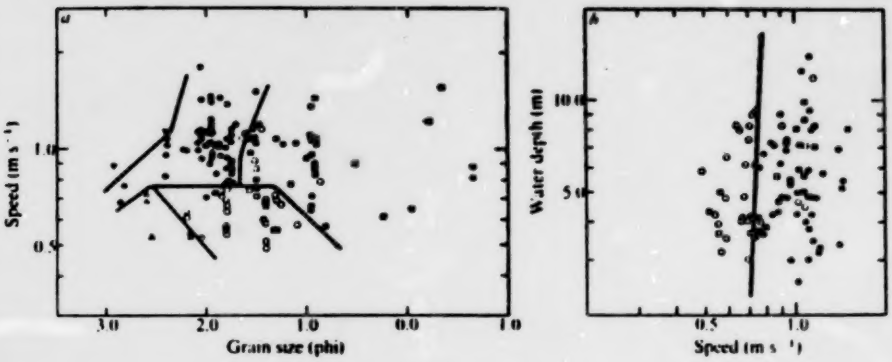

Notice bedform type is independent of water depth.

Triangles refer to ripples, open circles to 2-D megaripples, blocked circles to 3-D megaripples, open squares to rippled sand waves, blocked squares to megarippled sand waves and upside down triangles to upper plain bed.

Figure 7-30 (A) A phase diagram relating current speed (depth averaged), grain size (in phi units) and bedform types for the Minas Basin, Bay of Fundy (from Dalrymple et al., 1978).

Figure 7-30 (B) A phase chart relating water depth, current speed and bedform type for the Minas Basin (from Dalrymple et al., 1978).

Mean values of sediment and flow parameters characterising the occurrence of the various bedform types

Bedform type	Mean grain size (mm)	Average-maximum mean speed (m s⁻¹)	Mean water depth (m)	Average-maximum shear velocity (m s⁻¹)	Average-maximum stream power (kg s⁻¹ m⁻¹)
Ripples	0.184 (2.44ϕ)	0.603	5.37	0.035	0.739
Type 1 Megaripples	0.328 (1.61ϕ)	0.687	5.57	0.044	1.800
Type 2 Megaripples	0.272 (1.88ϕ)	1.052	6.00	0.082	7.628
Megarippled sandwaves	0.507 (0.98ϕ)	0.955	6.45	0.065	4.748
Rippled sandwaves	0.369 (1.44ϕ)	0.701	4.50	0.045	1.750

Figure 7-30 (C) The flow characteristics and sediment type for the generation of bedforms in Minas Basin (from Dalrymple et al., 1978).

at mean flows comparable to those producing ripples. These features are formed at flow strengths between 50-70 cm/s and are independent of the water depth. Two dimensional megaripples are often associated with sand waves (see Figure 28). The combined types occur at approximately 70 cm/s, which is higher current flow than produces 2 - D megaripples, yet is lower than that producing 3 - D megaripples. Figures 7-30 (A and B), taken from Dalrymple et al., (1978) show the relationship between 2-D and 3-D megaripples.

An excellent example of 2-D megaripples is given in Reinson (1977), taken in the Gulf of St. Lawrence (see Figure 31). These features have also been recognized by Newton and Werner, (1972) in the Baltic Sea, although they termed these features "transitional-size ripples".

Three-dimensional megaripples are complex in appearance. They are characterized by being sinuous or discontinuous, and produce a lunate morphology (see Figure 21(B)) p. 69. They are short crested and exhibit scour pits in their troughs, separated by well developed spurs. The bedform height varies considerably along the crest line. These features have steep profiles and are higher and shorter than 2-D megaripples. They form in finer sands than 2-D megaripples, though there is considerable overlap in the grain size range. Such features can coexist with megarippled sand waves, one type grading into the other as a result of changes in grain size only. Figure 7-29 shows the co-existence of sand waves and 3-dimensional megaripples from the Long Island; inner shelf (Swift et al., 1979).

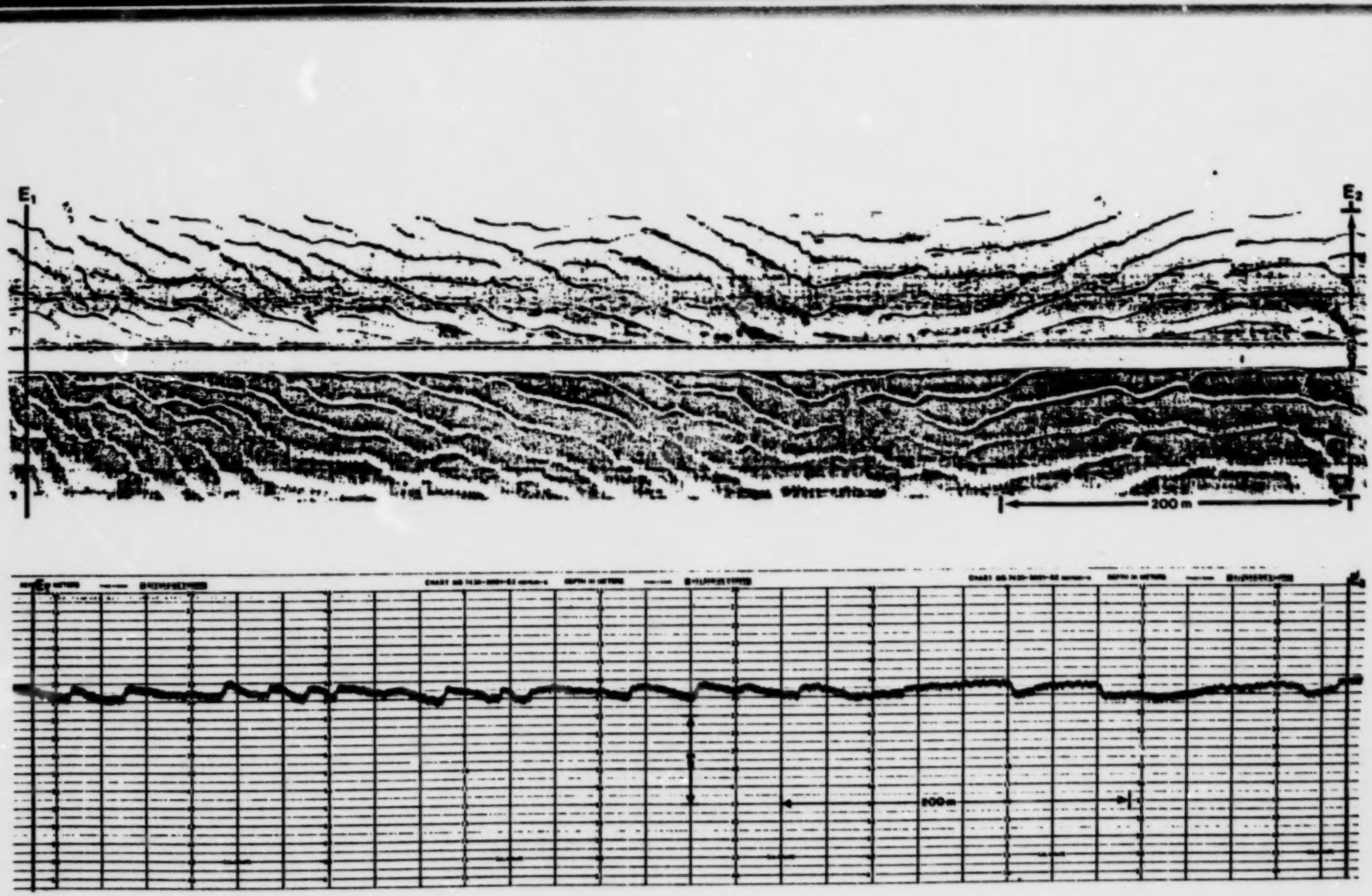

The features show a radial divergence of material, with transport from the top to the bottom of the frame. These megaripples show well-developed lee faces and a marked asymmetry of form. They are about 1 m in height and 20 m in wave-length. They show evidence of onlap, with one crest being cut by another, representing differing migration rates.

Figure 7-31 A sidescan sonar and echo sounding record of planar 2-D megaripples from the Miramichi estuary, Gulf of St. Lawrence (from Reinson, 1977).

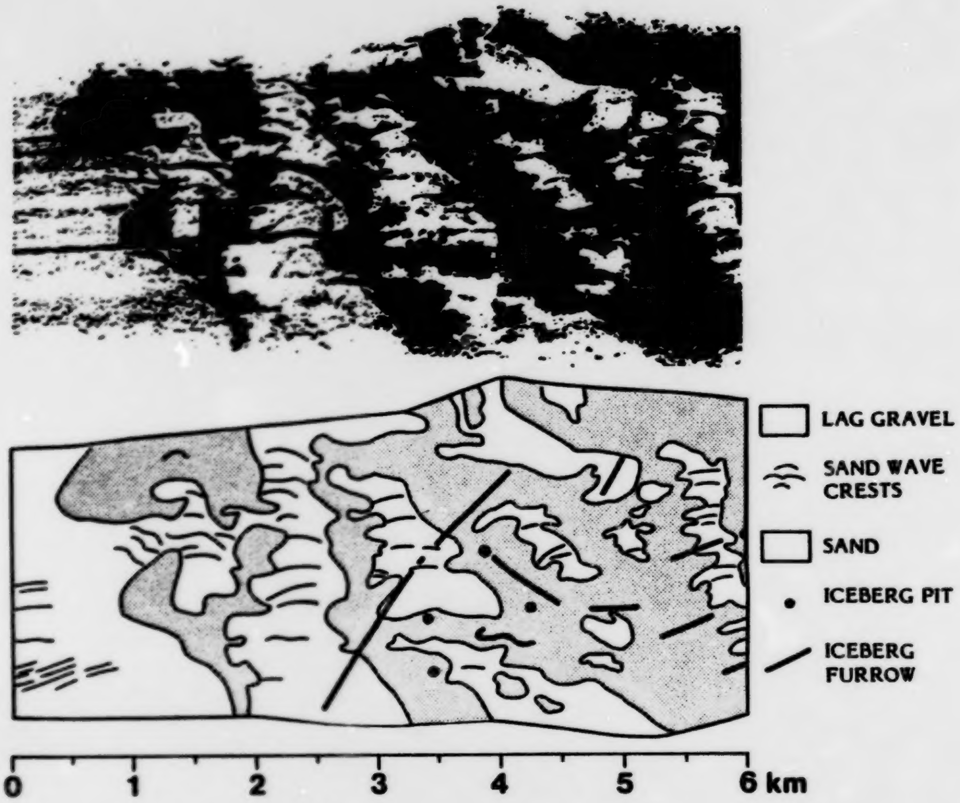
LAG GRAVEL
SAND WAVE CRESTS
SAND
ICEBERG PIT
ICEBERG FURROW
0
1
2
3
4
5
6 km

The records show sinuous, poorly developed sand ribbons running from the top to the bottom of the frame (N to S). Superimposed on these ribbons are arcuate sand waves showing a N to S migration. Those features are thought to be poorly developed due to a poor supply of sediment and the intermittent nature of transport. The features generate during severe storms, when bottom currents exceed 1.25 m/s. No currents greater than 0.3 m/s have been measured in the region.

Figure 7-32 A sidescan sonar mosaic of the Hibernia region, Grand Banks of Newfoundland (from Fader & King, 1981).

3.1.5 Sand Ribbons

Sand ribbons are elongate "ribbons" of sand which are formed parallel to the dominant current. They were first observed by Kenyon, (1970) in the North Sea. They form under intense unidirectional currents above those required to form 3-D megaripples, and at velocities between 100-125 cm/s. Helical flows sweep the sand laterally to create these ribbons, which form at the line of convergence of two adjacent helixes. Newton and Werner, (1972) observed them in the Baltic Sea resulting from the transport of a thin (30 cm) sediment cover over Pleistocene deposits. These authors also note similar features from the West Africa continental shelf. Such features have also been observed at the Hibernia Site on the Grand Banks of Newfoundland (Fader and King, 1981) (see Figure 7-32) and are approximately 1 km wide and extend over 30 km in length. The orientation of the Grand Banks features is N/S, which is parallel to the local contour pattern. Asymmetric and symmetric sand ribbons have been observed on the Spanish Sahara shelf. The degree of asymmetry varies according to the supply of sediment (Newton et al, 1973).

Sand ribbons represent an intermediate form of longitudinal bedforms which begin at the microscale with parting lineations (size scale in the order of mm) and end at the macroscale with sand ridges. They can form in sand or gravel and can have spacing ranging from metres to hundreds of metres (Allen, 1968). They have length-to-width ratios greater than 40 and occur in regions comprised of a coarse substrate. Sand ribbons can be rectilinear and sinuous and often bifurcate into a complex pattern of bands.

Sand ribbons often have bedforms superimposed on them. In the Hibernia region, for example, sand waves are found in the centre of sand ribbons. with 2-D megaripples, while at the edges of the ribbons, 3-D megaripples are found often grading into upper flat bed. A similar association of features occurs on the Middle Atlantic Bight (Swift and Freeland, 1978). An example of degrading sand ribbons, with superimposed transverse sand waves is seen in Figure 7-32 (Fader and King, 1981).

3.1.6 Sand Ridges

Sand ridges are large scale, linear bedforms, less asymmetric than sand waves. The origin of such features is somewhat speculative. often exhibiting orientations related to the transgressive history of the shelf rather than the dominating current direction. There appear to be two types of sand ridges:

i) linear "tidal-type" ridges, such as those of the North Sea (Houbolt, 1968) and

ii) nearshore. "oblique" ridges in regions of shoreline recession (e.g. the Maryland coast, Swift and Freeland, 1978).

The "tidal type" sand ridges are a natural progression from sand ribbons, being parallel to the dominating unidirectional current. They form in regions of abundant sediment supply and where the hydrodynamic process is relatively stable through time. They are typically 10-40 m high. 1-2 km wide and up to 60 km long. They often occur in "swarms", having crest spacings of 4 to 12 km. Such features are usually asymmetric, with the steep

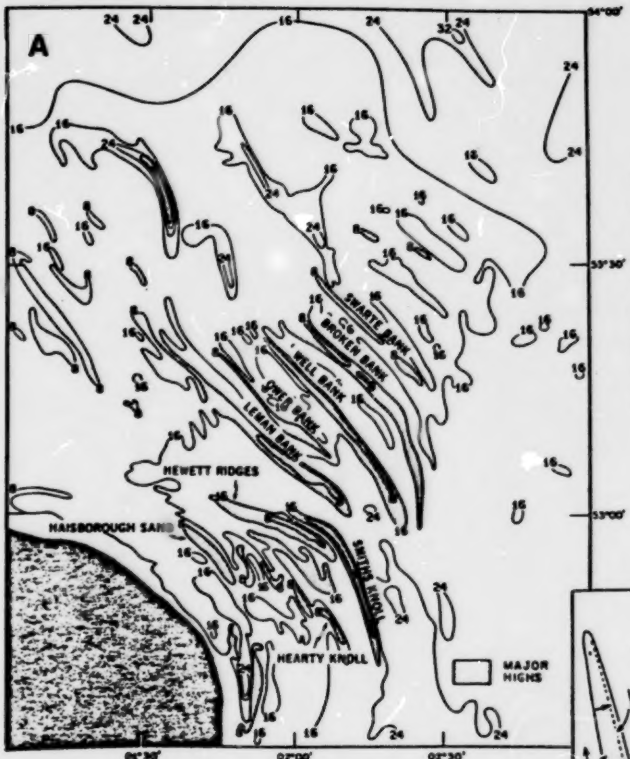
A
54°00'
53°30'
53°00'
01°30'
02°00'
02°30'
SWARTE BANK
BROKEN BANK
WELL BANK
OWER BANK
LEMAN BANK
HEWETT RIDGES
HAISBOROUGH SAND
SMITHS KNOLL
HEARTY KNOLL
MAJOR HIGHS

These ridges are low, asymmetric features usually parallel to the principal tidal flow direction or the relict "grain" of the shelf. They form only in regions of relatively strong tidal currents (i.e. above the critical threshold for sand transport) and are not a feature of storm dominant shelves. They are about 10 - 50m high, 2 - 3 km across and 10 km long.

Sediment is swept towards the crest from both sides, with usually one side dominating. The ridges migrate in the direction of dominant sediment transport. Ridges usually form between two opposite and mutually evasive flows. Such flows can produce arcuate and sinuous ridges as shown in the figure.

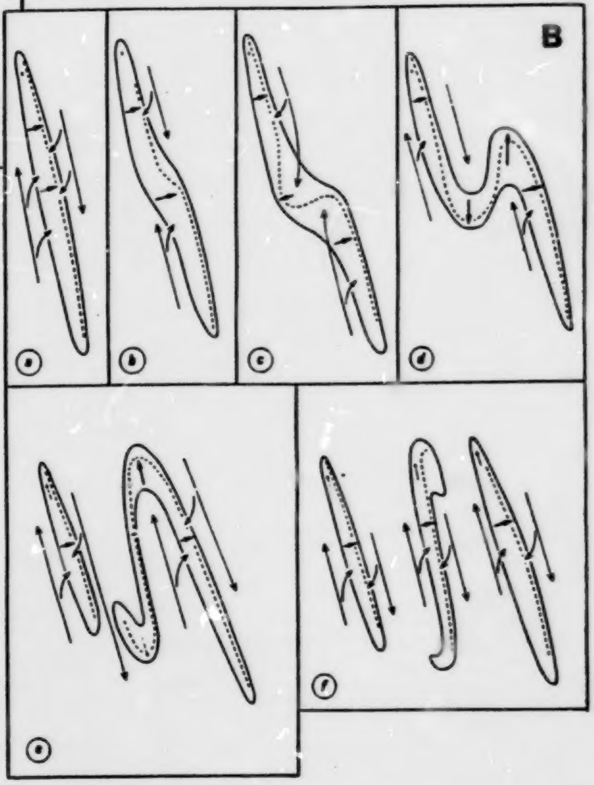

Figure 7-33 (A) The distribution of tidal sand ridges in the southern North Sea.

(B) The process of formation and modification of tidal sand ridges.

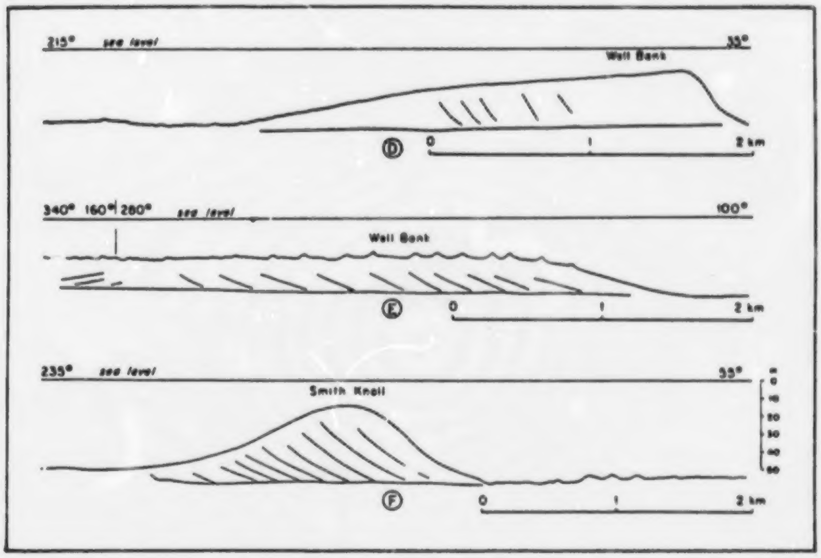
215°
sea level
35°
Well Bank
Ⓓ
0
1
2 km
340°
160°
280°
sea level
100°
Well Bank
Ⓔ
0
1
2 km
235°
sea level
35°
m
0
10
20
30
40
50
Smith Knoll
Ⓕ
0
1
2 km

The asymmetry of the ridges can be clearly seen together with the cross bedding produced by migration of the ridge. These ridges are often covered with sand waves and megaripples, indicating the local sediment transport direction.

Figure 7-33 (C) Interpretation of three sparker profiles through tidal sand ridges of the southern North Sea (from Houbolt, 1968).

oriented shoreward and at an angle of 4 to 7°. Internal bedding planes indicate these features move in the direction of the steep face (see Figure 7-33(C)). The tidal ridges of the North Sea are presumed in equilibrium with the tidal currents which flow obliquely across these features (see Figure 33(B)). Sand waves are often associated with these ridges and occur on both flanks of the ridge. The orientation of these sand waves shows a transport of sediment to the crest of the feature from both sides, with the stoss side dominating.

The nearshore "oblique" sand ridges are shoreface ridges which have become inundated during the late Holocene marine transgression. They have been forming for perhaps 2000 years, becoming detached from the shoreline through time and modified by the dominating modern current regime. As the sea level continued to rise these ridges became "offshore sand ridges" (Swift and Field, 1981); storm driven flows often modified their morphology further. Such ridges are often "comma" shaped and are shorter, relative to width, than the nearshore "oblique ridges". Such ridges are asymmetric and exhibit transverse bedforms. They have a well developed lee face, which is coarser in grain size than either the crest on the stoss face. Although the above features have been principally observed on the U.S. eastern shelf (Swift, 1976), results from the Argentinian Shelf show a similar pattern of development (Parker et al., 1982).

3.1.7 Grain Flows

Grain flows, as defined by Lowe (1976), refer to sediment gravity flows of cohesionless solids, maintained in suspension by intergranular pressures. Such flows are usually less than 30 cm thick and flow at speeds less than 100 cm/s. Lowe's calculations indicated that flows in coarse sand are less than 4 cm thick, in medium sand less than 2.5 cm thick and in fine sand about 1.5 cm thick. They are therefore surficial features. These features have been identified in the geologic record by reverse grading and cyclic stratigraphy.

Grain flows are envisaged to have two components:

1) an upper turbidity current-type flow, and

2) a lower, faster moving grain supported flow.

Shepherd, (1961) has observed such features in the upper parts of submarine canyons on the Californian shelf. Such features have been thought to cause sand spill-over from Sable Island Bank, Scotian shelf (Stanley et al., 1971).

Figure 7-34 shows the evolution of Sable Island Bank leading up to the development of grain flows.

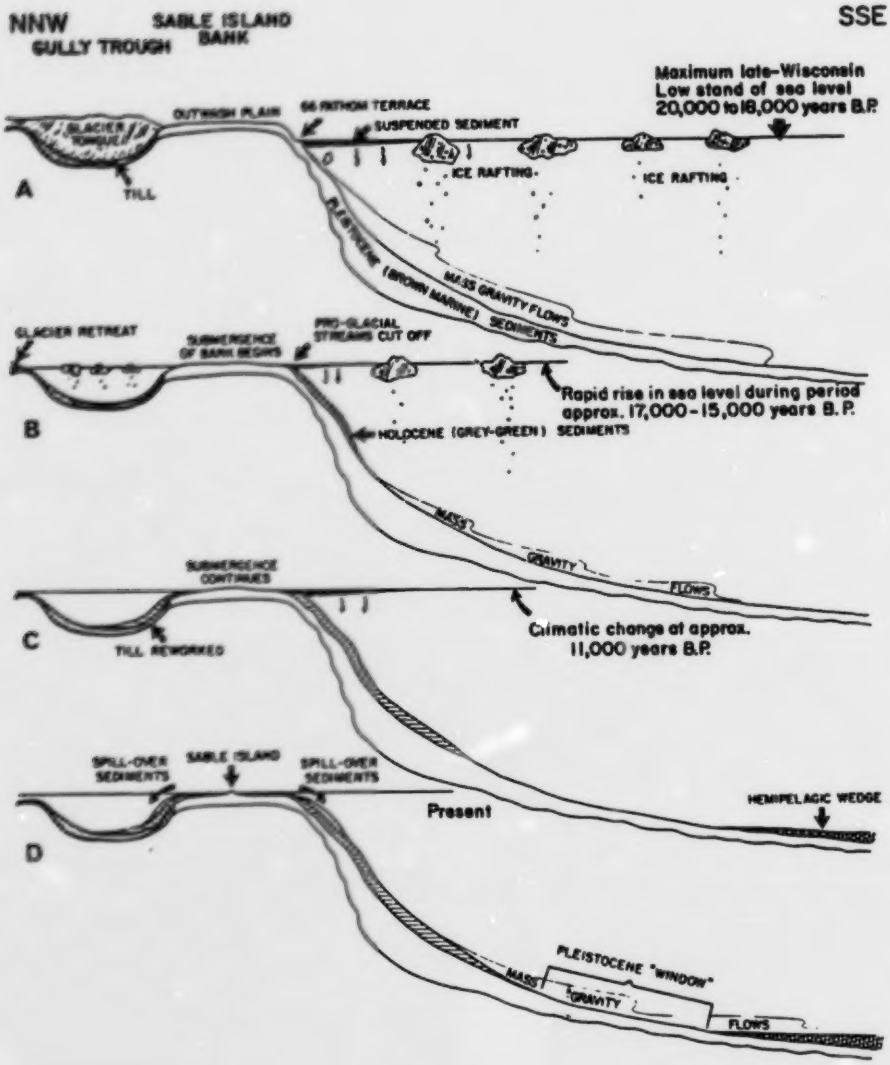
NNW
SABLE ISLAND BANK
GULLY TROUGH
SSE
Maximum late-Wisconsin Low stand of sea level 20,000 to 18,000 years B.P.
GLACIER TONGUE
OUTWASH PLAIN
66 FATHOM TERRACE
SUSPENDED SEDIMENT
ICE RAFTING
ICE RAFTING
A
TILL
PLEISTOCENE (BROWN MARINE) SEDIMENTS
MASS GRAVITY FLOWS
GLACIER RETREAT
SUBMERGENCE OF BANK BEGINS
PRO-GLACIAL STREAMS CUT OFF
Rapid rise in sea level during period approx. 17,000-15,000 years B.P.
B
HOLOCENE (GREY-GREEN) SEDIMENTS
MASS
GRAVITY
FLOWS
SUBMERGENCE CONTINUES
C
TILL REWORKED
Climatic change at approx. 11,000 years B.P.
SPILL-OVER SEDIMENTS
SABLE ISLAND
SPILL-OVER SEDIMENTS
Present
HEMIPELAGIC WEDGE
D
PLEISTOCENE "WINDOW"
MASS
GRAVITY
FLOWS

Figure 7-34 The evolution of the surficial sediments on the Sable Island Bank and Scotian slope. Figures A-D show the development through time of the various recognized deposits (from Stanley, 1969).

(A) At lower stands of sealevel sediment was transported directly to the shelf edge depositing thick accummulations of slumped and contorted sediments on the slope.

(B) As the sealevel rose, sediment accumulated at the shelf edge while sediment gravity flows took place in the shelf troughs and slopes.

(C) Reworking of glacial till took place with continued development of the shelf edge sediments.

(D) Wave reworking of till continued, winnowing the fines from the banks and depositing them on the slope and troughs. Spill-over of sediment takes place during storms, entering the submarine canyons, cut during lower stands of sea level. Mass gravity flows continue through to the present.

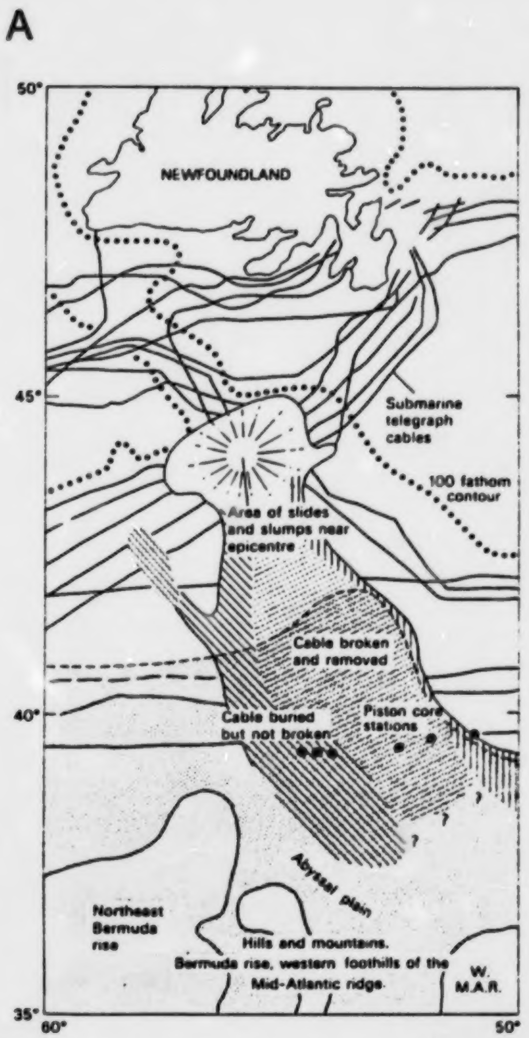
A
50°
NEWFOUNDLAND
45°
Submarine telegraph cables
100 fathom contour
Area of slides and slumps near epicentre
Cable broken and removed
40°
Cable buried but not broken
Piston core stations
?
?
Abyssal plain
Northeast Bermuda rise
Hills and mountains.
Bermuda rise, western foothills of the Mid-Atlantic ridge
W. M.A.R.
35°
60°
50°

Figure 7-35 (A) The location and nature of the famous Grand Banks slump and turbidity current which took place during 1929 (from Heezen and Hollister, 1971).

The slump was generated by a strong earthquake (7.4 magnitude) and took place in a thick sequence of shelf edge sediments, deposited during late glacial times. The slump originated at the north of the Laurentian channel. A turbidity current was generated from the slump which severed 13 trans-Atlantic cables on its 400 km path to the Sohm Abyssal plain. An estimated total of 100 km^3 of sediment was moved and dispersed over an area of 100,000 km^2.

3.2 Cohesive Bedforms

The classification of cohesive bedforms can be subdivided into two components 1) features produced by particle-by-particle erosion of the seabed in a systematic manner and (2) by a catastrophic sediment failure producing a sediment gravity flow, slump or slide. The former features are produced by the fluid drag on the sediment surface resulting in plastic deformation or erosion. They are usually restricted to the sediment surface. The catastrophic events tend to be larger scale than the erosive features, and demonstrate both surface expressions as well as internal deformations. Such features are characterized by:

1) an erosional event
2) a transport phase, and
3) a depositional event.

3.2.1 Sediment Gravity Flows

A. Turbidity Currents

Although turbidity currents, per se, are slope features, they usually originate at the shelf edge and are therefore partially a shelf feature. Perhaps the best documented turbidity current occurred on the Southern Grand Banks of Newfoundland. Set off during 1929 by an earthquake of magnitude 7.4, a thick sequence of late Pleistocene sediments slid down the front of the Laurentian Channel. The slump measured 100 km in length and was 400 m thick and initiated a turbidity current that travelled several hundred kms into the Sohm Abyssal Plain. Figure 7-35(A) shows the site of the slump and the ensuing turbidity current

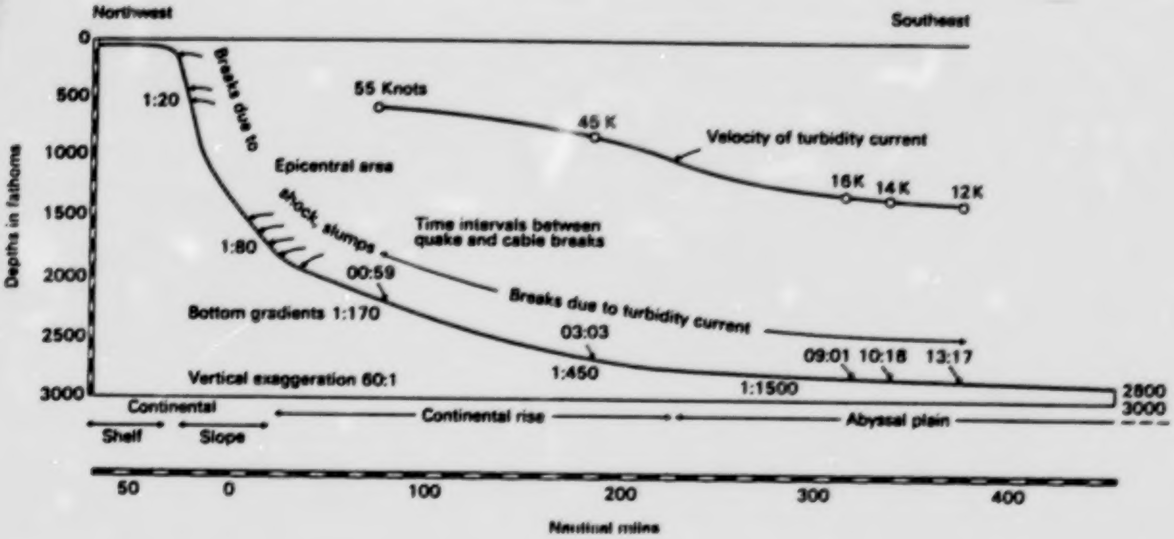
Northwest
Southeast
Depths in fathoms
0
500
1000
1500
2000
2500
3000
1:20
Breaks due to
Epicentral area
shock, slumps
55 Knots
45 K
Velocity of turbidity current
16K
14K
12K
Time intervals between quake and cable breaks
1:80
00:59
Breaks due to turbidity current
Bottom gradients 1:170
03:03
09:01
10:18
13:17
1:450
1:1500
Vertical exaggeration 60:1
2800
3000
Continental
Shelf
Slope
Continental rise
Abyssal plain
50
0
100
200
300
400
Nautical miles

The current travelled at a maximum speed of 70 km/hour and took 13 hours to reach the distal point on the Sohm Abyssal plain.

Figure 7-35 (B) The velocity of the 1929 turbidity current and the profile of its path.

swath (from Reading, 1979, after Heezen and Hollister, 1971). The current broke 13 trans-Atlantic cables, over a distance of 400 nautical miles. The maximum velocity of the current was about 70 km/hour (see Figure 7-35(B)). Diagnostic features associated with turbidity currents are sole markings, the presence of terrigenous and bioclastic material and graded bedding. Stanley and Maldonado, (1981) have identified sediment gravity flows in the western Hellenic Trench on the basis of such structures.

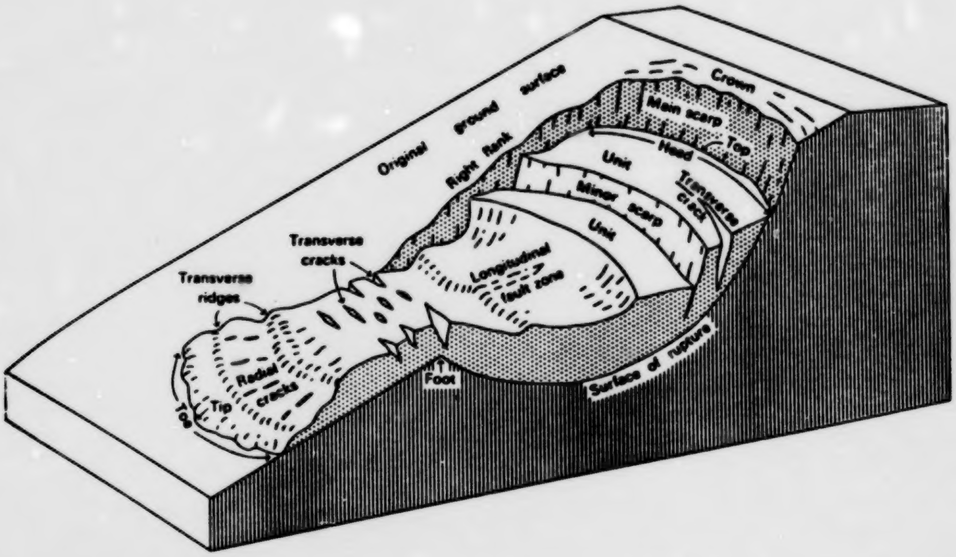
Crown
Main scarp
Top
Head
Unit
Transverse crack
Minor scarp
Unit
Original ground surface
Right flank
Transverse cracks
Longitudinal fault zone
Transverse ridges
Radial cracks
Tip
Toe
Foot
Surface of rupture

The morphology of such features is based on the Mississippi Delta surveys, where such features are common. They are classified morphologically into a head, the slump and a toe, narrowing at the foot to produce the bottleneck. Transverse cracks develop due to tension above the head, while radial cracks develop at the toe due to pressure buildup. Slumps usually have a well developed slip plane (surface of rupture) with deformation and folding of associated sediment beds.

Figure 7-36 A "bottle-neck" slump structure, typical of regions of high sedimentation rates and low shear strengths.

B. Slumps and Slides

Slumps are medium sized (60-200 m) sediment gravity flows, initiated by cyclic loading of the sediment causing local increases in the porewater pressure, or by high sedimentation rates. Slumps occur typically in muddy areas associated with high sedimentation rates, such as the Mississippi delta where they occur on slopes of 0.1 - 0.4°. They have a distinct morphology comprised of a broad head, a narrow slump zone and a lobate toe. On the Mississippi delta they are referred to as Bottleneck Slides (Figure 7-36). The head is characterized by circular tensional cracks (crown cracks) which may be stepped into a hummocky block surface. Coleman and Prior, (1981) have recognized three types of slumps and slides in the Mississippi delta region:

1) collapse depressions and bottleneck slides
2) peripheral rotational slides
3) mudflow gullies and lobes

High resolution seismic records from the upper Bay of Fundy show evidence of slumping similar to that observed in the Mississippi delta. The slumps exhibit distorted bedding in the toe. These features have no surface expression, making them impossible to recognize on sidescan sonar. Basinal slumping may be important on the Scotian and Labrador shelves where fine grained deposition is taking place, or on any shelf region where fine grain deposition is taking place on seabed slopes of more than about 1°.

3.2.2 Flute Marks and Megaflutes

These features are produced by particle-by-particle erosion of the seabed by a fast moving, unidirectional flow of water or sediment slurry. The most common scour is the flute mark, formed by flow separation behind an obstruction. Flute marks come in all shapes and sizes, ranging from deep bulbous forms to shallow, pointed forms. There are four major types of flute marks 1) linguiform, 2) triangular or conical, 3) elongate-symmetrical and 4) bulbous. Flutes may be isolated or arranged in groups.

The apex of the flute points in the upcurrent direction and is often the site of an obstruction which causes the necessary flow turbulence generating the features. The orientation of flutes around seabed irregularities or dropstones can often indicate the direction of the prevailing shelf current, and is extremely useful in highlighting the rare event (e.g. storm driven current). The largest of flutes are the megaflutes recognized by King (1979) from Placentia Bay, Newfoundland. Whereas regular flutes range in size from a few centimetres to decimetres in length, and up to a few cm in depth, megaflutes can be 100-200 m long, 50-150 m wide and up to 5 m deep. These megaflutes are erosional, eroding the relatively soft La Have clay, leaving a gravel lag in their troughs. Downcurrent of the troughs, sand waves (moulded in the residual material) have been formed. The scouring process appears to be active still, though the rate of scouring is unknown. These megaflutes indicate periodic high velocity flow moving southward along the east side of Placentia Bay.

3.2.3 Transverse Scour Marks

These features are formed by unidirectional currents and are asymmetric and transverse to the flow. They vary in size from cm to decimetres. The largest forms have been observed on the Nicaraguan Shelf and are thought to represent the troughs of kinematic mud waves. Their origin and character is still unclear.

3.2.4 Longitudinal Furrows

Longitudinal furrows are erosional features which develop parallel to the current flow. They range in size from a few mm to 3 m wide. These features are fixed in position and are formed during periods of rapid erosion followed by long periods of deposition. Flood, (1981) has examined longitudinal furrows from Southampton water and indicates that they have analogies on the continental shelf. These furrows often occur in clusters and are usually evenly spaced (5-10 m). They often join in the down current direction to produce a "tuning fork" pattern. They are often associated with sand waves and look suspiciously similar to ice scours. They differ from ice scours in that they tend to be rhythmic and anastomose.

Shells on the sea bed can often initiate the development of these features. On the southern Grand Banks, shallow depressions between sand banks are filled with bivalves. These bivalves, it is postulated, reworked the seabed material in a similar fashion thus creating circular depressions over time.

3.2.5 Pockmarks

Pockmarks are cone-shaped depressions left in unconsolidated mud by degassing or dewatering of these sediments some time in the past (Josenhans, et al., 1979). These features are known to occur on many differing shelves. They have an average diameter of 85 m, are about 6 m deep and, on the Scotian shelf, have a density of 23 pockmarks/km^2 (King, 1979). The cones develop by suspension and removal of material during the process of

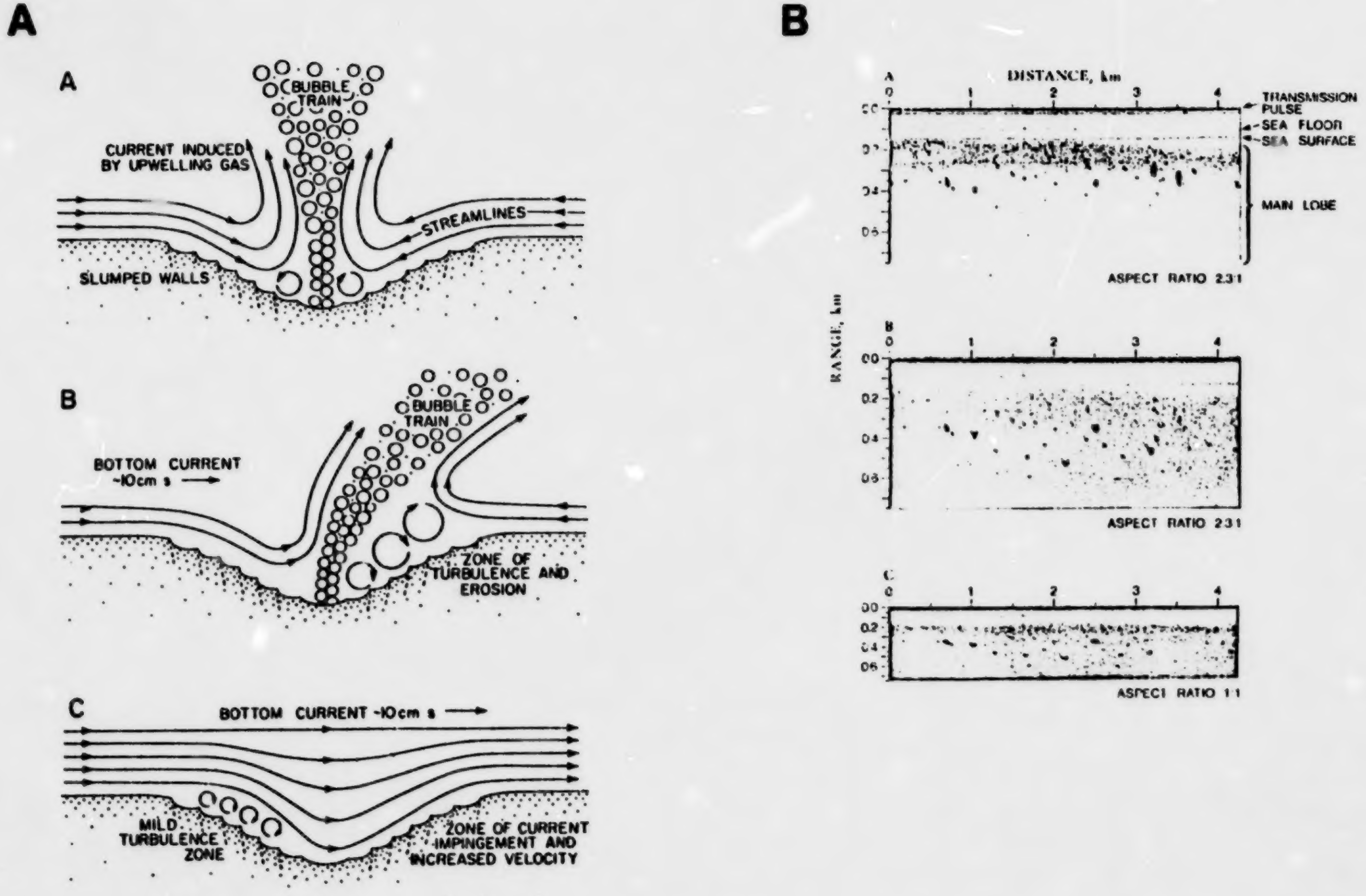
A
A
BUBBLE TRAIN
CURRENT INDUCED BY UPWELLING GAS
STREAMLINES
SLUMPED WALLS
B
BUBBLE TRAIN
BOTTOM CURRENT ~10cm s
ZONE OF TURBULENCE AND EROSION
C
BOTTOM CURRENT ~10cm s
MILD TURBULENCE ZONE
ZONE OF CURRENT IMPINGEMENT AND INCREASED VELOCITY
B
A
DISTANCE, km
0
1
2
3
4
TRANSMISSION PULSE
SEA FLOOR
SEA SURFACE
MAIN LOBE
ASPECT RATIO 2.3:1
RANGE, km
B
ASPECT RATIO 2.3:1
C
ASPECT RATIO 1:1

Figure 7-37 The development of pockmarks on the Scotian Shelf, the effect of degassing (or dewatering) of the seabed (from Josenhans et al., 1979)..

degassing (or dewatering). Many of these features are elongated. The interpretation is that the direction of elongation is parallel to the prevailing current direction at the time of formation. Figure 7-37 (after Josenhans et al., 1979) shows a section through a pockmark, and the mode of origin of these features.

3.2.6 Pingos

Pingos are conical, ice core hills, typical of areas subject to permafrost (MacKay, 1973). There are about 1500 pingos in the Western Arctic coastal plain; more are being discovered offshore. There are generally two types of pingos: (1) open types, and (2) closed types. Pingos are blister-like features that attain a height of up to 60 m. They develop by frost heave and are often associated with drained lakes. Pingos generally form in areas of permafrost of thicknesses greater than 350 m. They tend to be restricted, therefore, to the MacKenzie delta region where the sediment thickness can accommodate such a development of permafrost. Measurements of these features show that pingos can grow, and may expand at any time of the year. Through time, pingos appear to pulsate in size, in response to the build-up of free water lenses beneath the pingo, and the periodic escape of water by peripheral dyking (MacKay, 1977). The source of the water is expelled pore water from beneath aggrading permafrost in saturated, porous lake bottoms. The artesian pressure of the freezing lens overcomes geostatic pressure in creating the pingo. Mackay relates the development of these features to the principle of freezing milk inside a narrow-neck milk bottle. The "neck" of the pingo "bottle" is the zone of relatively thin permafrost beneath lakes. The size diameter of the pingo is considered therefore to be related to the dimension of the previously existing lake. On drainage of a lake, freezing of the lake bottom soil will take place, leading to frost heave and sediment expansion.

Pingos can grow at a rate of 40 cm/year (MacKay, 1973) during lake drainage. About 5 pingos have commenced growth since 1935 (i.e. earliest photographic coverage). It is thought that the pingos on the Beaufort Sea shelf are relict, and developed during sub-aerial exposure of the shelf. Ryckborst (1975) contests the freezing milk bottle theory on the basis of the geotechnical properties of the arctic soil. He contests that the soil strength is greater than the stresses exerted by frost heave.

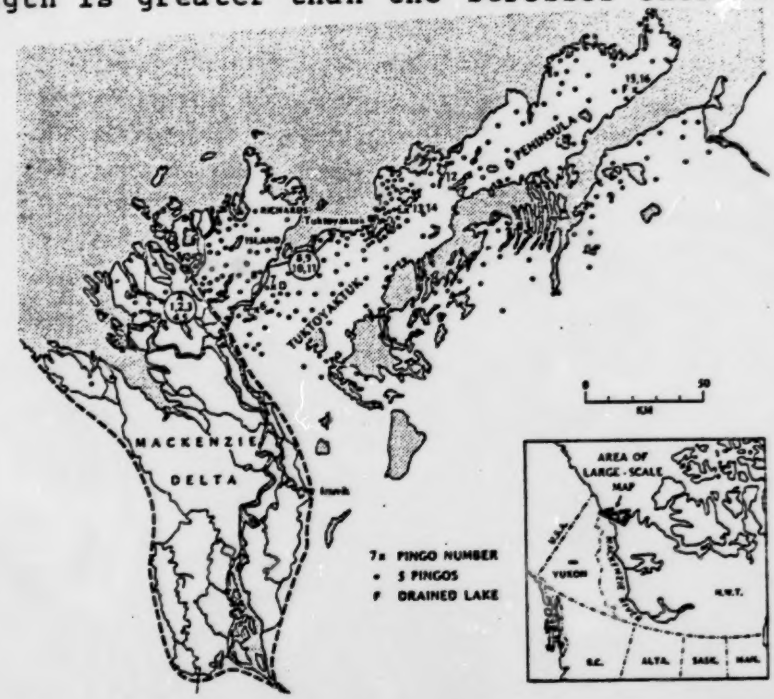
PENINSULA
RICHARDS
ISLAND
Tuktoyaktuk
TUKTOYAKTUK
MACKENZIE
DELTA
Inuvik
0
50
KM
7x PINGO NUMBER
• 5 PINGOS
DRAINED LAKE
AREA OF LARGE-SCALE MAP
YUKON
N.W.T.
B.C.
ALTA.
SASK.
MAN.

Figure 7-38 (A) The distribution of pingos on the MacKenzie delta (from Mackay, 1973).

Figure 7-38(A) shows the distribution of pingos in the subaerial MacKenzie delta area. They are also known to extend offshore. Figure 7-38(B) shows conceptually the method of formation of these features (After MacKay, 1973) Figure 7-38(C) illustrates the detailed stratigraphy through one such feature in the Beaufort Sea (After MacKay, 1978).

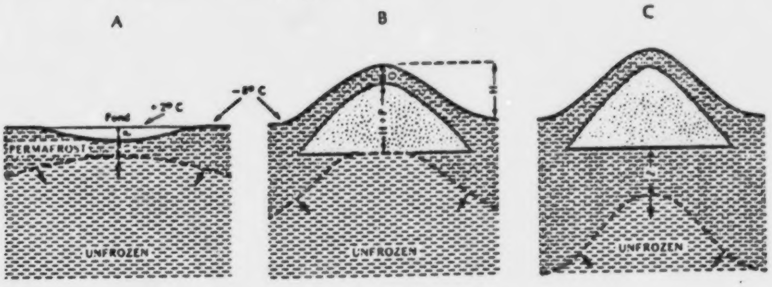
A
B
C
Pond
PERMAFROST
UNFROZEN
UNFROZEN
UNFROZEN

Figure 7-38 (B) The formation of pingos in the Beaufort Sea (from Mackay, 1973).

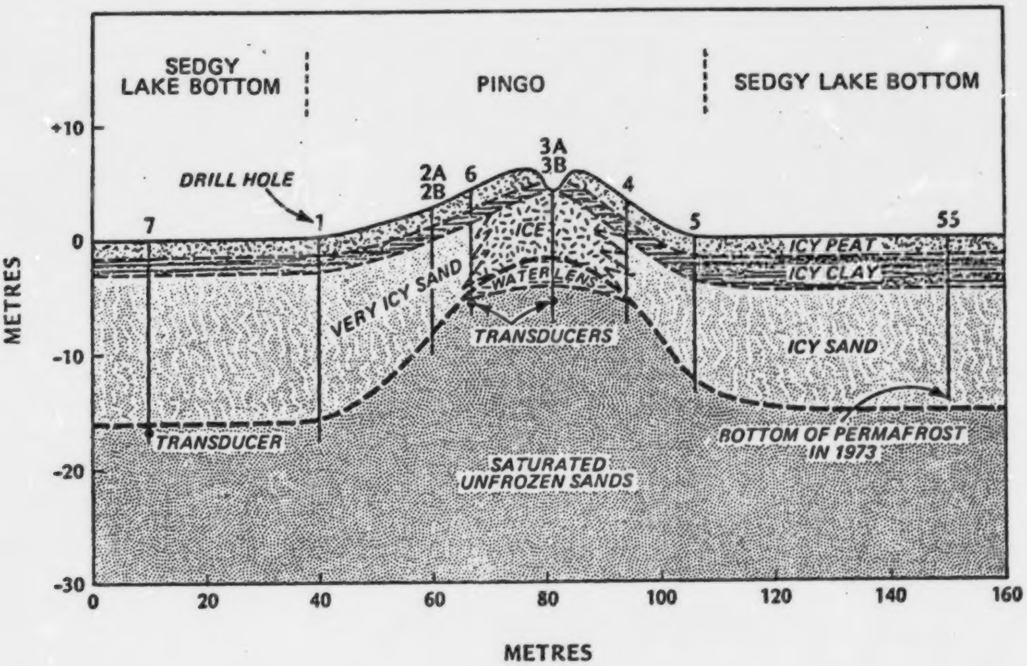
SEDGY LAKE BOTTOM
PINGO
SEDGY LAKE BOTTOM
+10
0
-10
-20
-30
METRES
DRILL HOLE
7
1
2A
2B
6
3A
3B
4
5
55
ICE
ICY PEAT
ICY CLAY
VERY ICY SAND
WATER LENS
TRANSDUCERS
ICY SAND
TRANSDUCER
BOTTOM OF PERMAFROST IN 1973
SATURATED UNFROZEN SANDS
0
20
40
60
80
100
120
140
160
METRES

Figure 7-38 (C) The stratigraphy on a specific pingo in the Beaufort Sea (from Mackay, 1973).

Number/
Numéro

8

Chapter 8. SEABED SCOUR ABOUT DISCRETE STRUCTURES

Alan Niedoroda and Charles Dalton

1 INTRODUCTION

The purpose of this chapter is to examine the scour processes from the viewpoint of fluid and sediment dynamics, to describe the formation of scour holes about discreet structures in the marine environment. The results are aimed at guiding an offshore engineer through the dynamics of the marine scour problem, so that he can use the existing literature to evaluate scour potential. To this end, the fluid mechanics of marine scour are examined first. This is followed by an examination of the sediment mechanics of the problem. These two areas are then combined to examine the mechanics of scour under steady currents, pure waves, and the combined action of waves and currents in the marine environment.

2 FLUID MECHANICS OF THE SCOUR PROBLEM

Scour is caused by the fluid flow characteristic of the marine environment and the particular geometry of a structure resting on the seafloor. The flow/structure interaction produces changes in the primary flow field, as well as significant secondary flow caused by interaction of a boundary layer or shear flow with the obstruction. In reality, all of these perturbations interact. However, for the purpose of clarity, the individual components of the interaction of a flow with the seafloor and ocean structure are examined separately.

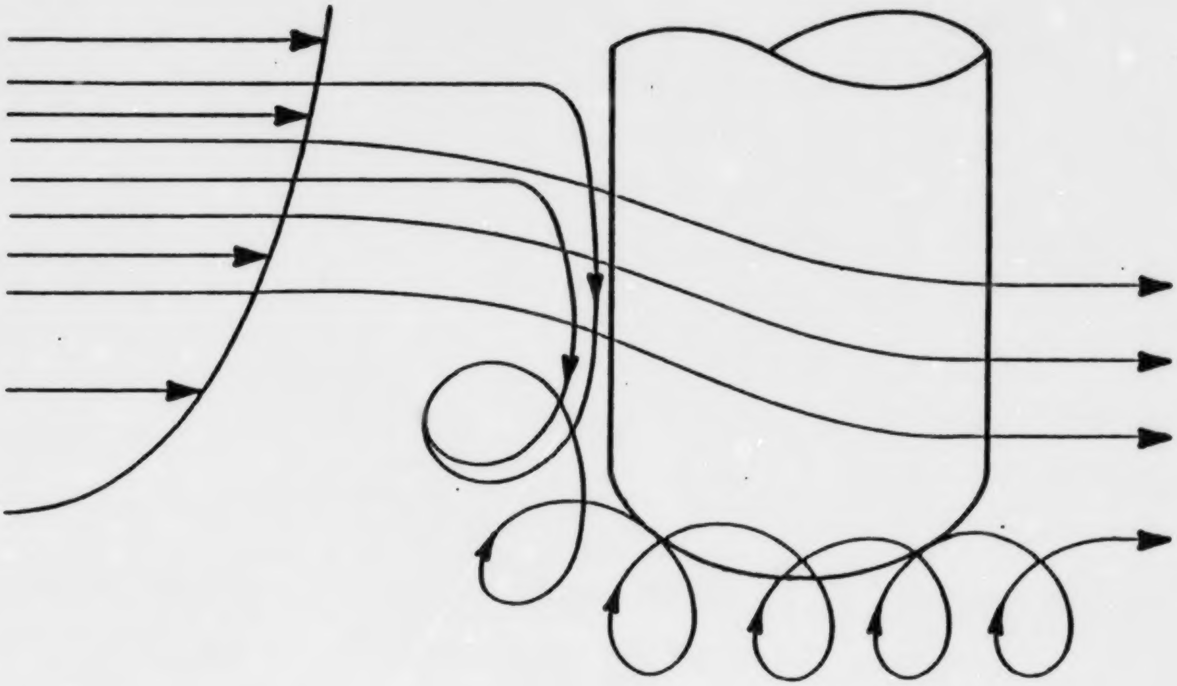

Figure 8-01 Sketch of flow around a cylindrical obstruction.

2.1 Secondary Flow

The principal flow feature, responsible for scour whenever a slowly-varying boundary layer current is present, results from secondary flow. This situation is most simply described when considering a circular cylinder mounted normal to a plane surface. The passage of a steady flow boundary layer along the surface past the cylinder causes a stagnation pressure gradient. Because the stagnation pressure gradient decreases toward the plane surface, i.e. toward the decreasing velocity, a secondary flow is generated toward the surface. This secondary flow has two effects on the shear or boundary layer flow. The main effect is the formation of a vortex, or rollup, of the flow at the midplane of the intersection of the cylinder and the surface. This horseshoe vortex wraps itself around the cylinder and trails off downstream, as shown in Figure 8.01. Scour occurs from an intensification of bottom fluid shear stresses, resulting as this secondary flow and the accompanying horseshoe vortex interact with bottom sediments.

Previous analyses have failed to produce a complete mathematical description of the complex flow associated with the horseshoe vortex. However, considerable laboratory data is available from scale model experiments, although most are directed at examinations of the horseshoe vortex in river environments. Though these results provide insight into the basic mechanism of the generation of the horseshoe vortex and its characteristics of flow, it is not possible to apply the results of river models directly to problems related to large scale structures in the marine environment. A major deficiency is the lack of appropriate dynamic and kinematic scaling laws. Work by Shen et al. (1966) and others has shown that changes in the scale and intensity of the horseshoe vortex can, in part, be related to a Reynolds number based on the use of the diameter of the cylindrical obstruction as a characteristic length. However, a second kinematic dimensionless parameter is clearly needed to scale the effects of velocity profiles. It is not presently possible to apply results from cylindrical obstructions to any of the other possible shapes for which this type of analysis may be necessary. This problem is further complicated by the fact that the bottom boundary layer of ocean currents generally does not extend upward to the surface, as it generally does in rivers and flumes.

Experimental work by Peake and Galway (1965), and Shen et al. (1966) suggests that for cylinders whose height exceeds the thickness of the bottom boundary layer, the region affected by the horseshoe vortex extends approximately one cylinder diameter upstream of the obstruction. No information is available for cylinders whose height does not extend across the entire bottom boundary layer, or for other shaped obstruction geometries. The velocity distribution within the horseshoe vortex is not well understood. Data from Shen et al. (1966) indicates that the downward flowing portion of the vortex in the stagnation plane has a maximum velocity which is nearly equal to the velocity of the undisturbed flow at the edge of the boundary layer.

Data from Hjorth (1975) and Schwind (1962) indicate that the fluid shear stresses impinging on the bottom beneath the horseshoe vortex are amplified eleven- and twelve-fold, respectively, above the values associated with the undisturbed freestream flow. These values result from two specific laboratory experiments, and it is not possible to determine the validity of generalizing the results.

The increased bottom shear stresses associated with a horseshoe vortex cause bottom sediments to be scoured. This, in turn, changes the shape of the bottom. As the shape of the bottom is altered, the flow in the horseshoe vortex also changes. Experimental data on these changes is extremely limited. Some discussion of this phenomenon is given in a later section of this chapter.

Another effect of the secondary flow about a cylindrical obstruction is the downward deflection of the external flow streamlines around the cylinder. This convective effect has little influence on the horseshoe vortex, except for a slight enhancement of the vortex due to the rotation caused by the streamline deflection. The horseshoe vortex shown in Figure 1 is indicated by the spiral curve extending around the cylinder base. The secondary flow is shown at the stagnation line, and the downward deflection of the external streamlines is indicated.

2.2 Convective Accelerations of the Flow

A circular cylinder causes a blockage in the approach flow which results in a convective acceleration in the direction of the azimuthal coordinate of the cylinder. This acceleration generates an increase in bottom shear stress by a factor of up to four over the bottom shear stress in the undisturbed approach flow. This amplification decreases approximately inversely with the square of distance from the cylinder.

2.3 Flow in the Obstruction's Wake

Flow patterns in the wake of the cylinder also influence the scour problem. There is a net downward flow in the wake of a cylinder resting on a plane surface. This can be explained by the fact that the wake region is a low-pressure region. A first-order representation of the flow field momentarily disregards the influence of the horseshoe vortex. This leads to a two-dimensional analysis of the problem. The wake in the high-velocity region is at a higher pressure than the wake in the low-velocity region (near the bottom), owing to the velocity gradient in the boundary layer. This difference in wake pressure causes a flow to occur in the wake, downwards toward the bottom. When the effects of the horseshoe vortex are included, the downward wake flow is enhanced by the direction of rotation of the trailing vortices.

At Reynolds numbers which characterize almost all flows in the marine environment, flow separation will develop in the cylinder. As natural flows tend to occur at relatively high Reynolds numbers, the structure of this separated flow is irregular and turbulent. The effect of this elevated turbulence in the wake of a cylindrical obstruction on the scour of bottom sediments is discussed later in this chapter.

2.4 Flow Disturbances in Oscillating Flows

The relative scales and magnitudes of the flow disturbances caused by a cylinder mounted on a horizontal flat plate and discussed above, differ depending upon whether the flow is fundamentally steady or oscillatory. In the case of scour developed by waves only, the mechanism for erosion is different from that associated with the steady flow. The steady current is thought of as having persisted over a great distance so that the boundary layer (region of velocity gradient flow) is relatively thick, possibly as much as six meters. In contrast, the distance of the fluid particle travel for an oscillatory flow, whose scale is typical of that associated with ocean waves, is not great enough for a substantial boundary layer height to develop. Therefore, the horseshoe vortex which might develop in the thin boundary layer characteristic of oscillatory flow is significantly smaller and weaker than for the case of the steady current flow. Sediment scour in oscillatory flow appears to be caused by acceleration of the primary flow past the obstruction, as well as the small- and large-scale flow patterns in the wake. Even when a wave-produced scour hole is fully developed, the orbital current boundary layer remains thin, and does not contribute to the formation of the horseshoe vortex.

2.5 Flow Disturbances Due to the Combined Effect of Waves and Currents

Scour of sea bottom sediments almost invariably results from the combined effect of wave orbital velocities and slowly-varying boundary layer flows. The combination of waves and currents produces an interplay between the factors discussed for each of the two types of flow alone. Two different situations are considered and, in this discussion, the concept of large and small is qualitative. For whatever situation considered, it should be remembered that the pressure gradient developed between two points on the stagnation line along the flow obstruction is proportional to the difference in the square of the instantaneous approach flow velocity at those two points. The implication is that, given an increased velocity due to both waves and currents, the secondary flow will be stronger due to the increased magnitude of velocity. Hence, the stronger the secondary flow, the stronger the horseshoe vortex system.

First, consider the case of a large current and a small wave velocity, which could be thought of as a deep water situation. When the wave motion is in the same direction as the current, the velocity field and secondary flow are enhanced, as well as the resulting horseshoe vortex. When the wave motion reverses, the first order effect is that the current velocity is decreased, which lessens the secondary flow on the upstream (with respect to the current) side of the cylinder. The horseshoe vortex also loses some strength as a result of the wave reversal. However, the overall effect is similar to the case of the flow developed by the steady boundary current alone, in that the horseshoe vortex will always be present, although pulsating in strength.

Second, the case of small current and large wave velocity is considered. The presence of the current makes this case different from the case of waves only. In this situation, the horseshoe vortex will form (although it could be small in strength) only when the current and wave orbital velocity are acting in the same direction. When the strong wave orbital velocity opposes the weak current, the bottom boundary layer will be very thin, thus suppressing the development of a horseshoe vortex.

The case of comparable values of current and wave velocities presents difficulty in analyzing the flow behavior. When the combined velocities are in the same direction, the horseshoe vortex is intensified. When the flows are opposed, the first-order result is a cancellation of the effects of each. However, this first-order approximation for opposed flow is physically lacking because of the presence of the wake generated in the previous half-cycle of the steady current. When the velocities are comparable, the current effects will not be completely overcome by the wave effects. The opposed-flow case is at present not sufficiently understood to pursue further. However, the situation for the two flows in the same direction can be pursued further. This case results in a "pumping" of the secondary flow, i.e. horseshoe vortex, on the upstream-current side of the obstruction.

3 SEDIMENT MECHANICS OF THE SCOUR PROBLEM

3.1 Sediment Types

The movement of bottom sediment involves entrainment. transport, and erosion or deposition. There is a large range of bottom sediment types and sizes in the natural environment, and many classifications exist to describe these elements. For the purpose of defining the major physical differences in the dynamics of marine sediment scour, bottom sediments fall into two major groups. Non-cohesive sediments are those whose principal stabilizing force is gravity, and whose individual particles act as discrete masses (i.e. clean, well-sorted gravels, sands and silts). Cohesive sediments are those which are stabilized in their position on the seabed by electrostatic forces between adjacent grain surfaces or by mucous binding and pelletization of the sediments by organisms living in and on the seafloor.

3.2 Entrainment Criteria

Entrainment of bottom sediments results when the fluid forces overcome the stabilizing forces. Because of the complexity of the fluid forces involved in moving bottom sediments, the standard practice is to assume that the net effect of all entraining forces is proportional to the fluid shear stress acting at the sediment-water interface. For noncohesive sediment, the magnitude of the fluid shear stress needed to initiate grain movement can be determined from the Shields Parameter (Madsen and Grant, 1976). For cohesive sediments.

there is no generally accepted relationship to define the level of fluid shear stress necessary to initiate grain movement. Only careful flume tests are capable of establishing the critical fluid shear stress needed to entrain each particular sediment type.

The ranges of critical bottom shear stress needed to entrain noncohesive sandsize sediment is from 2 dyn/cm^2 (0.004 lb/ft^2) to 12 dyn/cm^2 (0.026 lb/ft^2). The corresponding range for cohesive clays is much greater and more poorly known. It extends at least from 0.5 dyn/cm^2 (0.001 lb/ft^2) for very soft bay muds to above 250 dyn/cm^2 (0.5 lb/ft^2) for overconsolidated Gulf of Mexico clays. The relative level of fluid shear stress needed to initiate movement of bottom sediment is often used to describe the erodibility of the sediment.

Evaluation of the near-bottom current velocities required to develop these levels of fluid shear stresses depends on the type of flow, the characteristics of the boundary layer, bottom roughness, and the nature of the flow turbulence. If a representative steady boundary layer flow case is used to establish a rough idea of these current velocities, it can be shown that the corresponding values are: 20 cm/sec (0.4 kts) to 50 cm/sec (1 kt) for noncohesive sand; and 10 cm/sec (0.2 kts) to 220 cm/sec (4.4 kts) for cohesive clays. These current values are well within those which are commonly encountered in the marine environment. Therefore, entrainment and transport of sediment commonly occurs and can be particularly common due to the intensified flows around seafloor obstructions.

3.3 Transport, Erosion and Deposition

Transport of sediment develops when the fluid shear stresses acting on the bottom exceed the values needed to initiate entrainment of the sediments. Granular sediments tend to move on or close to the seafloor (bedload transport). Fine clay and silt-size particles tend to be suspended and transported within the flow by turbulence (suspended transport). Various modern theories, developed to compute bedload sediment transport fluxes, relate the flux of bedload to the excess fluid shear stress (above the value necessary to entrain the sediment particles).

The transport of fine sediments is difficult to evaluate. The suspended transport depends on a concentration gradient of the suspended particles. The high concentrations at and near the sediment/water interface supply upmoving turbulent eddies with more sediment particles than are carried downward by downmoving eddies. Therefore, the flow turbulence and sediment concentration profiles interact to promote transport. In most natural deposits, a higher level of fluid shear stresses is required to erode fine cohesive sediments than is necessary to transport them. Therefore, in analyzing the development of scour features, it is generally not necessary to consider suspended sediment transport rates.

Erosion and deposition of bedload sediment results from spatial gradients in the transport rates. If the spatial gradient of the bedload transport rate is zero, then no net erosion or deposition will occur even when large volumes of sediment are in transport. Positive spatial gradients in the sediment transport fluxes result in erosion. Negative spatial gradients in the sediment transport flux result in deposition.

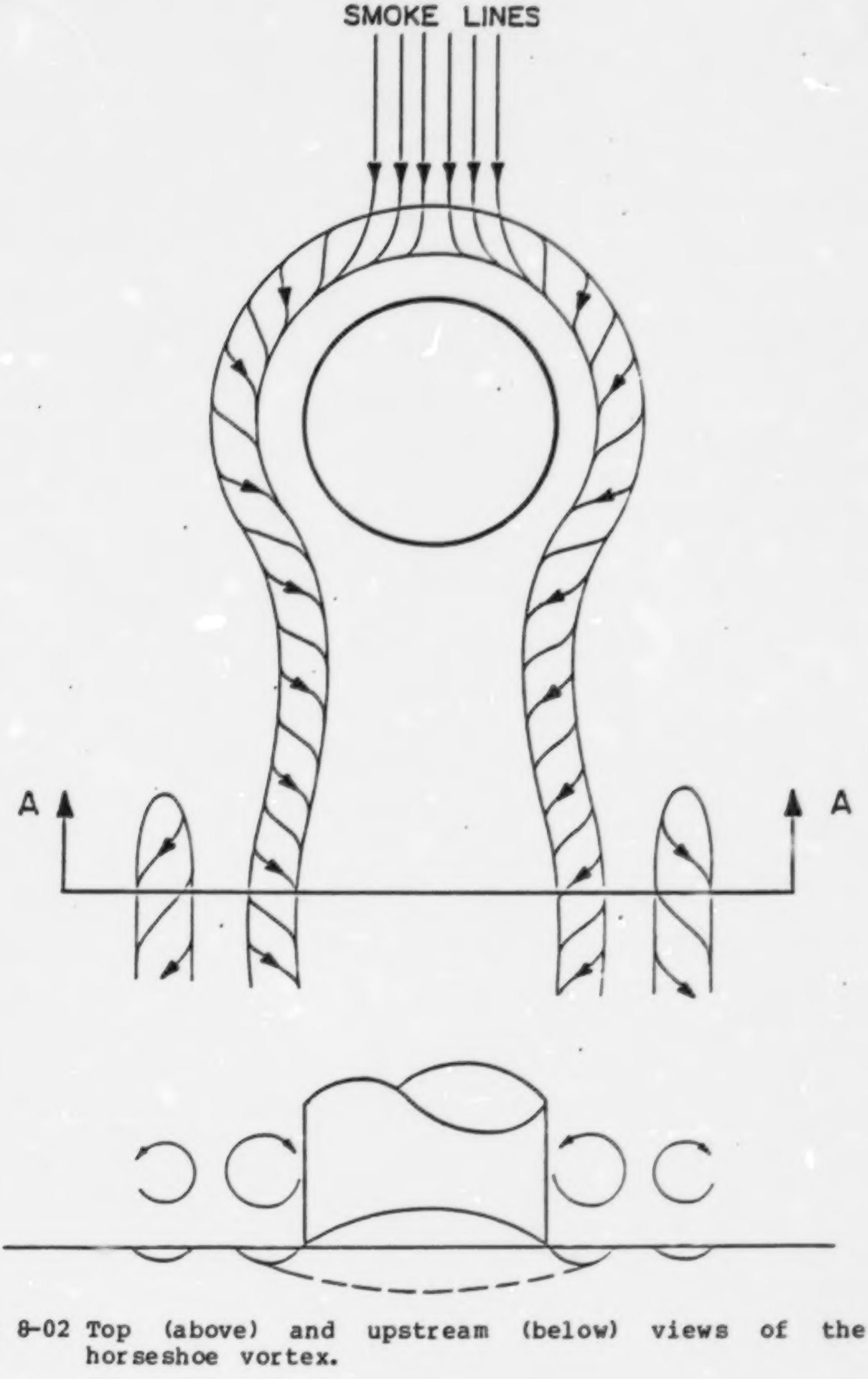
SMOKE LINES
A
A

Figure 8-02 Top (above) and upstream (below) views of the horseshoe vortex.

4 THE MECHANICS OF SCOUR IN STEADY CURRENTS

The flow disturbances caused by a cylindrical obstruction resting on a flat bed in a steady boundary layer flow have been discussed earlier. Baker (1978) has examined the horseshoe vortex problem thoroughly for both laminar and turbulent flows. Baker's studies were done using flow visualization and showed both steady and unsteady vortex systems existing for different flow parameters. The unsteady case had a complex oscillatory behavior. Whichever case exists, the horseshoe vortex represents a complicated flow field for which there is presently no analytical solution.

Repeated observations show that the scale and shape of the scour hole closely matches the scale and shape of the horseshoe vortex. The portion of the scour hole distributed around the upstream half of the cylinder is that of a half-frustrum of an inverted cone. The rear half of the shape consists of two parallel troughs extending downstream (see Figure 8.02 from Gregory and Walker, 1951). In noncohesive sediments, the upstream face of the scour hole is at the angle of repose of the sediment, and therefore, the depth of scour controls the size of the hole. In cohesive sediments, the upstream face can be nearly vertical and the size and depth of the hole are controlled by the scale of the horseshoe vortex. Some deposition of sediment may occur in the wake of the cylinder.

Shen et al. (1966) have shown that for moderate flow conditions, the depth of the scour hole, and therefore its size, is limited by the flow conditions. They show that under these flow conditions, the depth of the scour hole is a function of the cylinder-diameter Reynolds number. Above a Reynolds number of 10^5 this relationship was found not to hold. Results of model experiments indicate that under these stronger flow conditions, the ratio of the depth of scour to cylinder diameter is between 1.3 to 1.75 (Breusers, 1972). Sediment size, erodibility, and transport rate do not appear significantly to affect the size of the scour hole in strong flows (Shen et al, 1966; Breusers, 1972; Chitale, 1962).

The scour is caused by the strong bottom fluid shear stress gradients beneath the horseshoe vortex. As described earlier, the initial horseshoe vortex, before scour begins, exerts bottom fluid shear stresses that are approximately one order of magnitude greater than that in the surrounding undisturbed flow. Therefore, scour can develop even when sediment is not eroded and transported in adjoining areas. If general bedload transport is occurring, then the elevated bottom fluid shear stresses beneath the horseshoe vortex produce more rapid transport, positive sediment trasport gradients, and erosion.

As erosion of bottom sediments proceeds, the intensity of the horseshoe vortex decreases as it expands into the scour cavity. The decrease in intensity of the horseshoe vortex decreases the fluid shear stresses acting on the bottom sediments in the scour cavity. At equilibrium, the fluid shear stress acting upstream at the bottom of the scour cavity is equal to the fluid sheer stress acting downstream on the undisturbed portions of the seabed. The fluid shear stress acting on the upstream

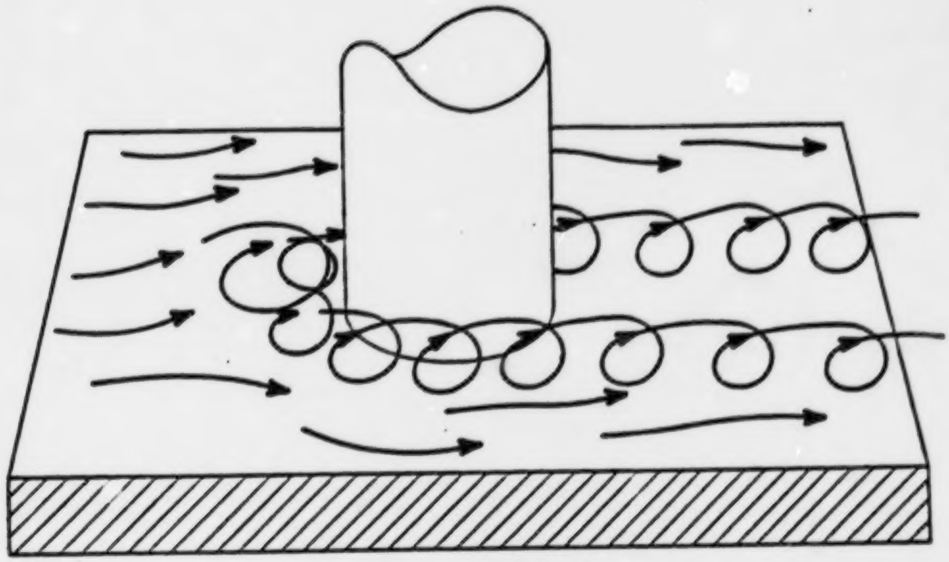

INITIAL STAGE

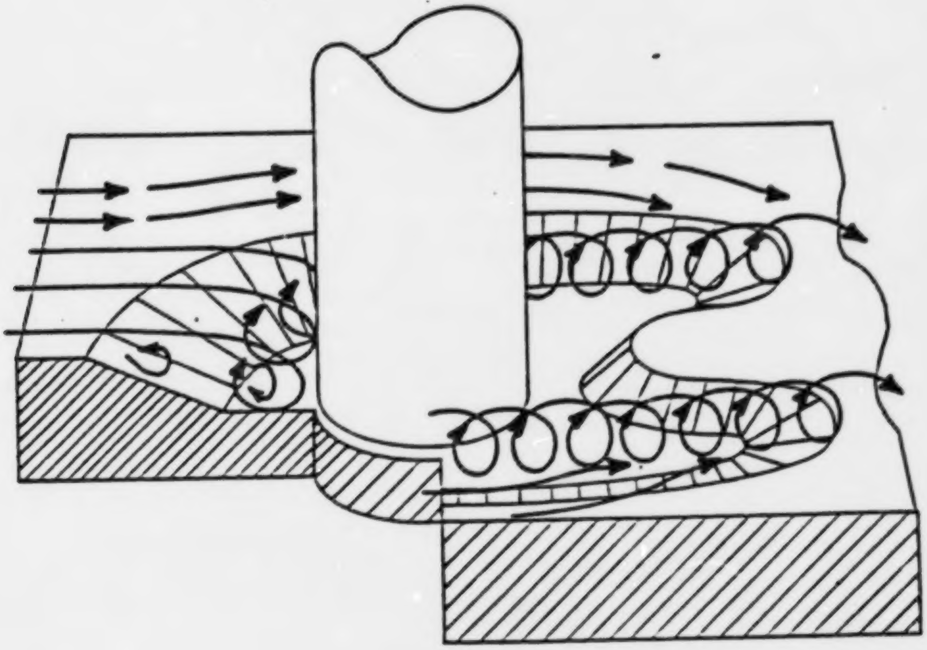

EQUILIBRIUM STAGE

Figure 8-03 Flow and scour produced by a steady boundary layer flow.

face of the scour cavity is equal to the fluid shear stress acting on the undisturbed portion of the seafloor, plus an increment approximately equal to the fluid shear stress necessary to entrain the sediment. When this distribution of fluid shear stresses from the weakened horseshoe vortex has been achieved, the scour hole is at its equilibrium size and shape (see Figure 8.03). The rate of transport of sediment from the scour hole is equal to the rate of supply.

5 THE MECHANICS OF SCOUR IN OSCILLATING FLOW

Close to the seabed, wave orbital velocities are simple oscillating flows parallel to the seafloor. If higher order effects, such as orbital asymmetry and mass transport, are ignored, the flow can be described as a simple sinusoidal oscillation at the wave period. This flow is capable of developing scour around seafloor obstructions.

Observations of scour development from oscillating flows are given by Das (1970) and Palmer (1969). The exact sequence of scour hole development depends upon the cylinder diameter, intensity of the oscillating flow, and the sediment transport on the surrounding seafloor. However, the following generalized description of the sequence of scour hole development is instructive.

Both Das and Palmer note that the scour hole initiates at the sides of the cylinder and, in many cases, some deposition is noted against the upstream and downstream sides of the cylinder. As the scour hole continues to develop, these deposits are removed, and the locus of deposition shifts to a rim outside the scour hole. When fully developed, the scour hole is a radially symmetric frustrum of an inverted cone with sideslopes at the angle of repose of the sediment. Palmer's data shows that the ratio of the depth of the equilibrium scour hole to the cylinder diameter is between 0.5 and 0.75. This generalized description shows that unlike the steady current case, an important transition occurs between the initial scour hole shape and its final shape.

The nature of oscillating flow past a cylindrical obstruction has been discussed earlier. It was pointed out that the horseshoe vortex is insignificant because the orbital boundary layer is very thin. Therefore, scour initiates from the concentration of bottom fluid shear stress produced by the acceleration of the primary flow by the obstruction. This results from a bottom fluid shear stress gradient which is positive from upstream of the cylinder to the point of maximum velocity, and negative from that point to the downstream limit of disturbed flow (Figure 8.04). If the maximum bottom fluid shear stresses are above the sediment entrainment threshold, then erosion will occur from upstream of the cylinder to the point of maximum velocity. Deposition will occur downtream from this point.

The nature of the zone of separation in the cylinder wake depends upon the Keulegan-Carpenter number (Keulegan and Carpenter, 1958). For large Keulegan-Carpenter numbers, even sand-size sediment can be suspended in the flow and convected away from the cylinder. Thus, deposits will form on the up- and downstream sides of the cylinder in the early stages of scour hole formation only if the value of the Keulegan-Carpenter number is small. This is generally supported by data given by Das (1970).

In order for the equilibrium oscillating flow scour hole to develop with radial symmetry from the initial hole geometry, another flow condition must develop. The initial scour hole produces bottom slopes close to the cylinder which must

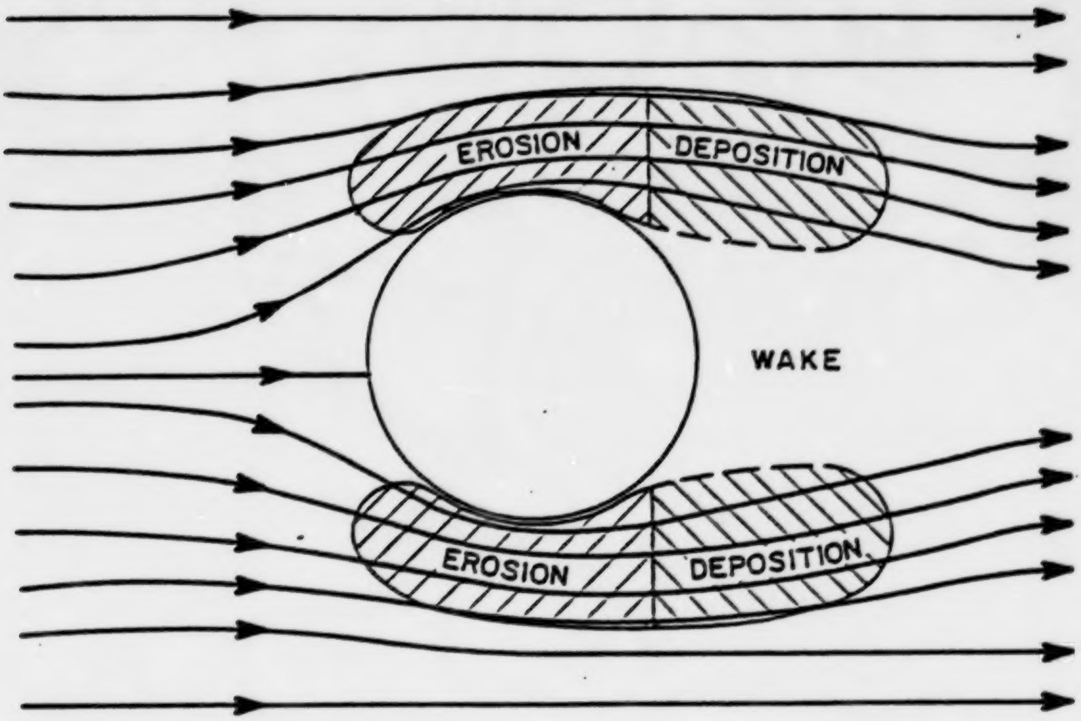
EROSION
DEPOSITION
WAKE
EROSION
DEPOSITION

SEPARATED FLOW

Figure 8-04 Instantaneous flow and scour due to oscillating flow.

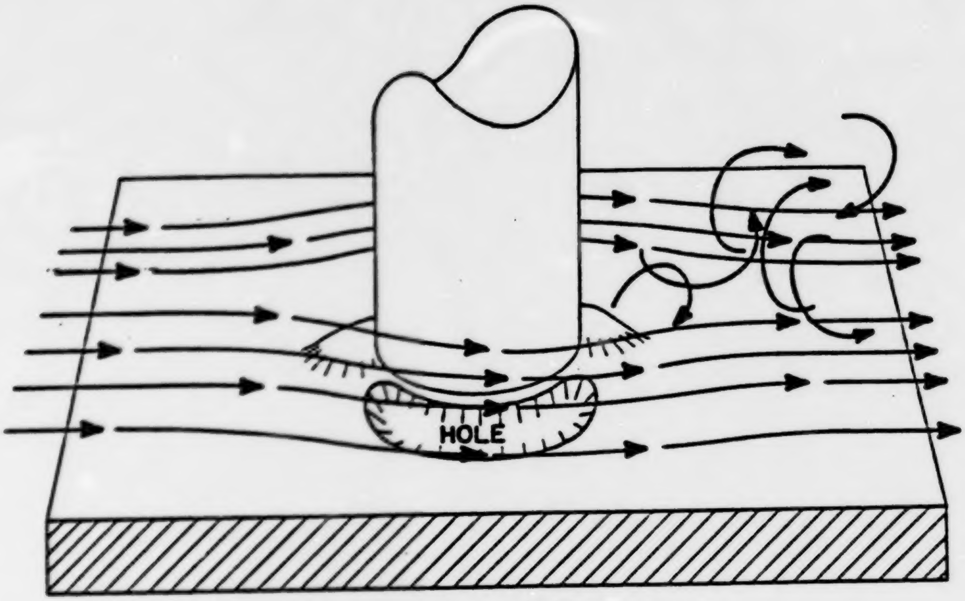

INITIAL STAGE

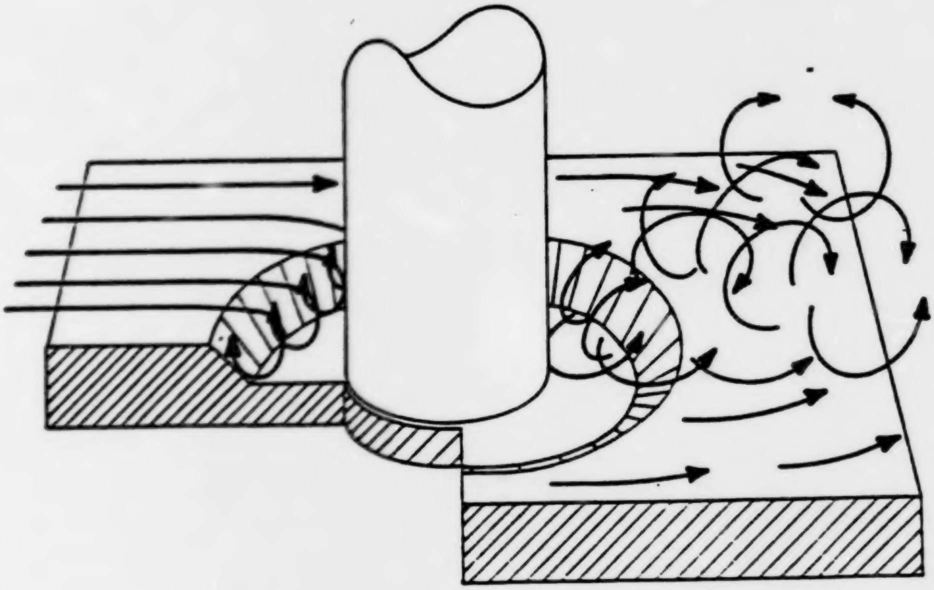

EQUILIBRIUM STAGE

Figure 8-05 Stages of wave-induced scour hole formation.

eventually trigger flow separation of the thin orbital boundary layer. Reverse eddies in the separated flow erode the initial sideslopes to the angle of repose of the sediment. This steepening of the sideslopes quickly spreads the zone of separated bottom boundary layer flow around the obstruction, and leads to the final equilibrium shape of the scour hole (Figure 8.05). Thus, the equilibrium size and shape of the scour hole is related to the nature of boundary layer separation, rather than to the nature of secondary flow as in the case of scour due to a steady boundary layer flow.

The information available from the literature on scour caused by purely oscillating flow only pertains to cylinders whose diameters are small compared to the maximum excursion length of the fluid oscillation. When the converse is true, the resulting flow disturbance is limited by the duratin of each half cycle. This must result in greatly reducing the rate and magnitude at which scour can develop.

6 MECHANICS OF SCOUR DUE TO WAVES AND CURRENTS

In almost all marine environments, scour develops through the combined effect of waves and currents. Ninomiya et al. (1972) have demonstrated in scale model experiments that the shape of the scour hole produced by the combined effects of waves and currents is similar to the shape developed by a steady current without waves. They note that the rate of scour hole development is considerably faster in the case of combined wave and current action. Wilson and Abel (1973), Breusers (1972) and Ninomiya, et al., (1972), all note that the maximum depth of the scour hole developed by waves and currents is equal to or less than the maximum depth developed by steady currents alone.

The general nature of flow around a bottom obstruction resulting from the combined effects of an oscillating wave orbital flow and a steady boundary layer flow have been discussed earlier. It was brought out that if the steady flow velocity is stronger than the oscillating flow velocities, a horseshoe vortex will form around a cylindrical obstruction as it does in the steady flow case. The intensity of this vortex will vary according to the differences in the square of the combined steady and oscillating flow velocities. The bottom fluid shear stresses in the scour hole should vary as well. The equilibrium scour hole size and shape should not be expected to be as great as that developed from a steady current whose mean velocity is equal to the combined velocities of the wave orbital and mean current condition. This is caused by the fact that the combined velocities will result in a flatter velocity profile than that achieved in simple steady boundary layer flow. On the other hand, the equilibrium scour hole should be deeper than that associated with a steady boundary layer current with no waves superimposed, because the stagnation pressure gradient acting on the upstream cylinder wall is proportional to the difference of the square of velocities at two different heights. These predictions are reasonably close to the results given by Breusers (1972) and Ninomiya. et al. (1972).

When the maximum velocity of the oscillating current is greater than the velocity of the steady boundary layer flow, significant changes can be expected in the equilibrium geometry of the resulting scour hole. When the oscillating velocity and steady flow are in the same direction, the horseshoe vortex will develop in the downstream direction. However, when these two flow components are opposed, the horseshoe vortex collapses. Therefore, with each wave cycle, the horseshoe vortex must reform. As an unsteady horseshoe vortex requries time to obtain maximum intensification and the period of gravity waves is short, the horseshoe vortex will not realize its maximum intensity about anything but the smallest ocean structures. Therefore, the scale of the resulting scour hole will be similar to that developed by a steady current of much lower speed. The rate of scour hole formation under the combined effects of waves and steady currents is greater than the rate of formation due to steady currents alone. The oscillating flow provides an excess fluid shear stress which serves to entrain the sediments. Little net sediment motion results from the oscillating flow. However, the horseshoe vortex formed from the steady portion of the flow can more readily transport the wave-agitated sediment, thus increasing the rate of scour hole formation.

When the magnitude of the wave orbital flow and the steady current is nearly the same. the situation is difficult to evaluate. The scour hole shape and size will generally be controlled by the horseshoe vortex related to the steady current component. Erosion will progress rapidly due to the waves. However, it is not possible to generalize whether the scale and intensity of the pulsing horseshoe vortex will be larger of smaller than the corresponding steady current case.

The size and depth of the scour hole, produced by the combined effect of both waves and currents acting on a flow obstruction which is large with respect to the oscillation amplitude (Keulegan-Carpenter number is small), will be considerably smaller than that predicted from a small cylinder, except when the steady current is larger than the maximum wave orbital velocity. This is caused by the fact that due to the steady current, the horseshoe vortex will not wrap completely around the obstruction before the flow reverses.

When the maximum velocity of the oscillating current is greater than the velocity of the steady boundary layer flow, significant changes can be expected in the equilibrium geomtry of the resulting scour hole. When the oscillating velocity and steady flow are in the same direction, the horseshoe vortex will develop in the downstream direction. However, when these two flow components are opposed, the horseshoe vortex collapses.

Therefore, with each wave cycle, the horseshoe vortex must reform. As an unsteady horseshoe vortex requires time to obtain maximum intensification and the period of gravity waves is short, the horseshoe vortex will not realize its maximum intensity about anything but the smallest ocean structures. Therefore, the scale of the resulting scour hole will be similar to that developed by a steady current of much lower speed. The rate of scour hole formation under the combined effects of waves and steady currents is greater than the rate of formation due to steady currents alone. The oscillating flow provides an excess fluid shear stress which serves to entrain the sediments. Little net sediment motion results from the oscillating flow. However, the horsehshoe vortex formed from the steady portion of the flow can more readily transport the wave-agitated sediment, thus increasing the rate of scour hole formation.

When the magnitude of the wave orbital flow and the steady current is nearly the same, the situation is difficult to evaluate. The scour hole shape and size will generally be controlled by the horseshoe vortex related to the steady current component. Erosion will progress rapidly due to the waves. However, it is not possible to generalize whether the scale and intensity of the pulsing horseshoe vortex will be larger or smaller than the corresponding steady current case.

The size and depth of the scour hole produced by the combined effect of both waves and currents acting on a flow obstruction which is large with respect to the oscillation amplitude (Keulegan-Carpenter number is small) will be considerably smaller than that predicted from a small cylinder, except when the steady current is larger than the maximum wave orbital velocity. This is caused by the fact that due to the steady current, the horseshoe vortex will not wrap completely around the obstruction before the flow reverses.

7 CONCLUSIONS

1. The mechanisms of scour around discrete ocean structures include the generation of the horseshoe vortex due to the stagnation pressure gradient associated with the relatively thick boundary layer of steady or slowly varying ocean currents, convective accelerations of the main flow in both steady and oscillating flow, wake turbulence, and bottom boundary layer separation associated with waves.

2. The mechanisms for scour hole development due solely to waves are substantially different from the mechanisms for scour hole development due to steady or slowly varying currents.

3. The mechanisms for scour hole development due to the combined effects of both waves and currents are complex. In the case of a strong current and weak wave orbital flow, the development of the scour hole will be dominated by a horseshoe vortex with a pulsing intensity. The scour hole will develop faster than in a corresponding steady current case, due to the excess bottom fluid shear stress developed by the wave orbital boundary layer.

In the case of a weak current and a strong wave orbital flow, the scour hole will have a shape similar to that developed by a steady current. This feature will develop more rapidly than it would in the presence of a steady current alone, due to the additional bottom fluid stresses developed by the orbital boundary layer. However, the equilibrium depth of the scour hole can be less than that associated with a steady current whose magnitude is equal to the sum of the weak current and the maximum orbital velocity.

When the magnitude of the wave orbital flow and the steady current is nearly the same, the situation is difficult to evaluate. The scour hole shape and size will generally be controlled by the horseshoe vortex related to the steady current component. Erosion will progress rapidly due to the waves. However, it is not possible to generalize whether the scale and intensity of the pulsing horseshoe vortex will be larger or smaller than the corresponding steady current case.

4. The size and depth of the scour hole produced by the combined effect of both waves and currents acting on a flow obstruction which is large with respect to the oscillation amplitude (Keulegan-Carpenter number is small) will be considerably smaller than that predicted from a small cylinder, except when the steady current is larger than the maximum wave orbital velocity. This is caused by the fact that the horseshoe vortex will not wrap completely around the obstruction before the flow reverses due to the wave orbital velocity.

Number/
Numéro

9

CHAPTER 9 DISCUSSIONS

1. BEAUFORT SEA EXPERIENCES

Chaired by: S.M Blasco

Question: V. Barrie

Steve, have they done any bottom current meter work at all in the Beaufort?

Answer: S. Blasco

During the Beaufort Sea project years 1974 and 1975, Stan Hoget and others did some work and there has been some work done by Dome. Unfortunately, two of their units have been consumed by ice last year, and even some of their upper looking sonar equipment to look at ice keels, have been damaged. But there is a data base that exists, the quality of that data base is not very clear. We have a joint project with APOA to look at the sediment dynamic issues in the Beaufort Sea and try and synthesize the data base that exists and evaluate their ability to give some information on the dynamics and processes.

Question: A. Ruffman

Did Kate Krank get out and look at flocculation last summer?

Answer: S. Blasco

Yes, she took some samples last year and is working on them.

Question: J. deJong

Has the technique that has been used to identify gas gaps on oil reservoirs been successful at all on identifying seismically the presence of hydrate gas or shallow gas.

Answer: S. Blasco

The presence of shallow gas on analog records can be detected. It can sometimes be confused with shallow permafrost. They in fact have a similar response. But if you get a phase change and you have some borehole control or some other bits of information you can, in the analog data, in the first 100 m, get a good idea of the presence of gas. We are not really certain how much gas. What happens in an acoustic record is that the amount of gas from 0 to 10% significantly affects the record, but above 10% it does not change that record, you simply get voids and white-outs and you don't see what is happening. When you get into multi-channel data, when in fact you are in areas where you don't have permafrost, you can detect those events from fading.

When you get deeper into multi-channel data, when in fact you are in areas where you are going to have permafrost, you can detect those events from phase changes, but when you get into permafrost and hydrate areas you get such rapid lateral and vertical variations of velocity your records don't stack well, and you end up with a very difficult data base to work with, and as a consequence your geometry is not very well defined and neither is your gas. The whole issue about hydrates is that nobody really understands the fundamental properties to even determine what in fact may be an acoustic response to the presence of a hydrate. Some work done by Allan Judge, who is working with fundamental properties, suggests that in fact hydrates have a very high acoustic absorption, much higher than permafrost, and you might be able to identify it by in fact a relative degree of absorption of signal with depth. The problem in using things like sonic logs and resistivity is that the response is very similar between permafrost and hydrates, so the actual identification at this point in time is really coming from borehole data and correlation with that with resistivity, sonics and other information. I think one of the most definitive properties is really the thermoconductivity, but we don't have a thermoconductivity tool yet.

Question: Speaker unknown

What were the results like of the CIP used in the Alaskan Beaufort?

Answer: S. Blasco

It worked quite well I understand.

Question: A. Niedoroda

What does the CIP stand for?

Answer: S. Blasco

Actually. I think it is a marriage of both EM techniques and induced polarization techniques, where you simply send out a pulse and you record the return and the decay. The rate of the return of the decay is basically a product of what soils the signal is going through and which soils are in permafrost. It responds quite positively so in fact the rate of decay is quite effective. From that you may in fact, if it is calibrated, have an effective tool. Unfortunately, electrical methods in the offshore have problems.

Question: A. Hay

Getting back to your comments about the hydrates, are you saying that there is no real knowledge of the elastic constants of the hydrates?

Answer: S. Blasco

I think that there is some knowledge of it. The problem is they probably exist for pure hydrates. How do those elastic constants apply to the case here, where we may in fact have a hydrated sand or clay (more than likely a sand)? How does that apply to the real world and what is your real world response?

Statement: N. Morgenstern

Steve, we can manufacture hydrates quite easily in our lab. We can provide some control.

Statement: S. Blasco

I believe that your hydrates are in a sand matrix, aren't they? So that is a closer approximation to what the real event may be, as opposed to manufacturing a pure hydrate which is needed to get fundamental properties of hydrates. Then you can start to marry them with properties of soil.

2 EASTERN CANADIAN SHELF EXPERIENCES

Chaired by: C.F.M. Lewis

Question R. Hiscott

It seems to me that if you are interested in putting some objects or installations on the seafloor you don't necessarily want to know what icebergs hit the seafloor but how many come within, say 10 metres of the seafloor. Are you able to generate any numbers from your methods of analysis to depth of keels or perhaps depths of scour. If the scour depths are normally distributed, how many would come within a certain distance?

Answer: M. Lewis

It could be crudely derived, but there is no real data base on iceberg draft distributions. I guess in all there is something like 400 icebergs that have been measured to date, but not very many of these are in the public domain as yet, and those measurements have all been made far to the north. So the actual draft distribution we should apply to the Grand Bank icebergs is very much a matter of interpretation, in my view.

Question: V. Barrie

I have a question for the people presenting the sediment dynamics sections of the course. One of the problems as far as a geotechnical subsea system, if you go for a floating system, is that the wellhead and flowlines have to be protected from icebergs by burial. Your wellhead will be in a glory hole and therefore you have to keep the hole open. Do we have any way of measuring sediment transport rates or fill-in rates if someone tells you what size your hole is to be?

Answer: A. Niedoroda

This is the problem of calibration that I mentioned to you all yesterday. There aren't any real calibrations around for sediment transport rates in shelf environments. There have been field calibrations done along the shoreline for research though. We just happen to have a group with us that has some data along these lines from off San Francisco and we have written up the abstract for the ASCE Conference in South Africa and now we have got to do the work on this.

Question: V. Barrie

Do we have any idea of the actual migration of bedforms, how much volume goes with each bedform, or is that still a very difficult question to answer?

Answer: C. Amos

I would say "no" until you get some good calibration data; and the results I wouldn't trust as far as you could throw them because of the inherent fluid dynamic problems out there. Secondly, you don't know what realistic time sequence is. You could probably select a design criteria that you could sort of test it against, perhaps.

Question: J. deJong

Looking at the material that is there, you first stated that there is a mantle of one to perhaps three metres of glaciated material of various gradations of fine sand to a lot of gravel and so forth. At that water depth you are not dealing with a high current environment. There seems to be very little evidence of anything like sandwaves or anything, and it doesn't seem to be an area where sediment stability is a major concern.

Question: C. Amos

Which area are you talking of?

Answer: J. deJong

The Hibernia. Grand Banks area.

Statement: V. Barrie

We should emphasize that there are large areas that we have sidescan mosaiced in the Hibernia site that display a series of megaripples and sand waves.

Question: A. Ruffman

But relatively thin?

Answer: M. Lewis

Yes, relatively thin, there may be a small volume of sediment in storage at any one time.

Statement: A. Hay

You could take your calibration of iceberg scour rate one step further and get a bedform migration rate, knowing the thickness of the sand. This will enable you to get an infill rate for some sort of hole.

Statement: C. Amos

You don't have the bedform migration rates though, which is the problem.

Statement: A. Hay

I guess you have to have it crossing two scours.

Statement: C. Amos

There is another problem which comes into this in terms of the sediment dynamics as far as the processes are concerned. You cannot discount the fact that these bedforms may not be storm induced phenomena at all. Somebody put forward the idea of the breaking internal waves and certainly they are known in Davis Straits and Labrador Sea. You can't discount this idea even though it may be improbable. Fundamentally, the whole thing that drives these bedforms is in somewhat of an arbitrary state right now.

Question: N. Morgenstern

Would you see it as a serious engineering problem? I have had lots of experience in controlling sand wave problems in the North Sea and seems if you want to protect some hole or pipeline you heap up a bunch of gravel around it and the sand waves move around it, given good construction materials.

Statement: A. Neidoroda

They are expensive though.

Statement: V. Barrie

If you produce your oil by a floating system your wellheads are in a glory hole. My question is, how fast would that pit fill, and if that pit fills, is that an operational problem?

Answer: N. Morgenstern

There is a great deal of jetting technology available.

Question: C. Amos

Can anybody tell me what the effects of pressure transmittal is from an iceberg grounding? In the case of an infilled glory hole and an iceberg which happens to impinge on the seabed, would the pressure transmitted by the iceberg grounding likely damage the wellhead facility, even though it is buried under 8 metres of granular fill?

Answer: N. Morgenstern

It is theoretically possible. it depends on the nature of the loading.

Answer: S. Haider

In the model test that we conducted on the iceberg, we realized that the pressure was transmitted beyond the scour track, into the soil. I am talking about a 2 cm wide model in which we could feel the pressure into the bottom, beyond the track, up to about 1 metre beyond it.

Question: A. Ruffman

What width was the model?

Answer: S. Haider

The model width was about 52 cm. Dr. Chari has conducted similar tests.

Statement: T. Chari

I think it will depend more on the depth of the scour than on the width of the model itself. The development depends on how deep the scouring is and what will result is burial depth at least one and a half time the maximum depth of scour. That is in terms of the sediment movement. Now if one is talking about the pressures due to grounding icebergs, it depends on the particular situation. Theoretically it is possible that the energy under 8 metres of filling will be felt. It depends on how much weight comes from that filling.

Question: C. Amos

I have another question in relation to this. If for example one could conceive some sort of fairly wide glory hole, of one in five slope, is it conceivably possible that an iceberg which might otherwise bypass any kind of wellhead facility, could it be effectively focussed or direction changed? In particular is it possible to take the path of least resistance and therefore tend to go towards the deeper central portion of a glory hole. The glory hole sucks the iceberg to it, so to speak.

Statement: A. Ruffman

On Mike Lewis' famous slide that has been shown a number of times at the Montebello workshop, it shows a scour going through a topographic low and you notice the scour has changed a bit but the berg drives his tail across the bottom and straightens up a bit as it goes through. A berg willl continue following in the same direction through a glory hole and then tilts a little bit more and drags its tail. It is almost certain a lot of bergs are dragging their tails and are tilted in the direction of travel with the driving force, be it pack ice or currents or currents and wind, probably just ignore the wellhead, do its damage and continue on.

Statement: C. Amos

If it follows the path of least resistance it has the choice of going into deeper water, as it doesn't have to scour.

Statement: R. Hiscott

It has a lot of momentum.

Statement: A. Ruffman

Once it gets up on the top of the flat shelf I think there is certainly going to be a selection over the 140 m water depth. Once it has been pushed or has got up on the top shelf then it is in fact the driving forces that are going to determine the direction and I have not very often seen two iceberg scours come together and then continue on, they cross one another. If you dredge your glory hole north south you would tend to catch them more than east west bound.

Statement: V. Barrie

The impression we get is that the iceberg scour design criteria in the Beaufort Sea situation is the same as the East Coast. We need to find the maximum probable depths of penetration of an iceberg keel over the life of the well. This is your basic criteria for your design. Correct me if I am wrong.

Answer: A. Ruffman

It is wrong, I think, because you are assuming that a berg is not going to straighten up and get any deeper in the glory hole and that is what you are aiming for as depth to dredge or trench a glory hole. If the bergs only just scour and go across a low and don't go any deeper, then that is all you have to find out, but if in fact bergs will straighten up a bit and the keel will reach a little deeper into the bottom of a topographic low, and there is lots of evidence they do, then that is not a good enough criteria.

Statement: S. Haider

Generally, the depth that they are talking about is 40 ft or more in the Beaufort Sea.

Statement: N. Morgenstern

It depends on the water depth.

Statement: A. Ruffman

Vertical silos seem to be quite possible to put into the Beaufort Sea but they spent an immense amount of money into an unsuccessful attempt to drill a vertical silo type glory hole on the Grand Banks. They haven't come back to that experiment as yet and were instead looking at a drag line type of linear feature that you could sink your wellheads in.

Question: S. Haider

We are talking of glory holes on a ground which already has some established scour depths for design. I don't see that some new iceberg can come and scour that much deeper, do you think it would?

Answer: A. Ruffman

I am not sure the amount of what I call over-scouring you could get, but you could certainly get 12 to 15 m demonstratively on the Labrador shelf. where a berg has scoured uphill and then downhill. I think it can be much more, as a matter of fact. It can be worked out in the physics of icebergs and stability of bergs.

Question: S. Haider

You are talking of metastable situations?

Answer: A. Ruffman

Most icebergs coming down over Hibernia are not stable. They are near the end of their lives, they are at various stages of stability, melting all the time and finding new positions and eventually disappearing. The question is are any modern bergs deep enough to scour, passing over the Hibernia area? How many of those are there?

Question: J. deJong

That frequency of 8 scouring bergs that was mentioned, was that for a 2 km square area Mike, did I understand that correctly?

Answer: M. Lewis

No, those grounding frequencies were per square km. Four hundred icebergs pass south of 48° N on average every year.

Question: A. Hay

Is it possible to determine what force is necessary to scour a trough of a given depth?

Answer: T. Chari

Yes.

Question: A. Hay

Then it should be possible to calculate the mass of a berg to scour a 2 m trough. Is that not true?

Answer: T. Chari

Yes, you can calculate it but with what accuracy?

Question: A. Hay

But if you know what the mass of the berg is and how much force it is exerting on the bottom then if the bottom is suddenly removed you should be able to find out how much deeper it is going to sink. Is that not true?

Answer: A. Neidoroda

Well, the berg is supported in part by the bottom and mainly by buoyancy, so then it is an unknown fraction of the berg's mass that's being supported by the bottom.

Statement: C. Woodworth-Lynas

It is going to vary according to the sediment type as well.

Question: A. Hay

Well you know what the sediment type is?

Answer: C. Woodworth-Lynas

Well you do and you don't. If you see the mosaics from Hibernia you have sand, gravels and mixture of sands and gravels and if the berg traverses across there it will create all kinds of problems in calculations.

Statement: T. Chari

The answer to the question is that there are too many variables that we do not have a good handle on. We can make theoretical calculations if we know the shape of the iceberg above and below water, shape of the scour and the amount it lifts up. If you know all these things then you can make the necessary calculations.

3 GEOTECHNICAL PERSPECTIVE

Chaired by: T.R. Chari

Question: D. Huntley

You commented relative to the continental slope at the beginning, and I got the impression that was because the continental slope had a slope and the continental shelf is flat.

Answer: T. Chari

No, in terms of the geotechnical problem the stability of any slope is a major geotechnical problem, in terms of analysis and the stability aspect.

Question: D. Huntley

The comment I was going to make was that the continental shelf is not in fact flat. The Scotian Shelf for example is very undular. Are the slopes there relevant to the phenomenon that you would study?

Answer: T. Chari

Sure, if one feels that there is a susceptibility of slope failure either in terms of cyclic loading or wave effect.

Question: D. Huntley

So what slope do you start getting interested in?

Answer: T. Chari

Maybe Dr. Morgenstern will have some comments on that.

Answer: N. Morgenstern

Massive earthquakes have induced slides in sands on slopes as flat as a couple of degrees.

Statement: S. Haider

Slopes of 1^{o} on the eastern shelf of the U.S.A. have been documented to become unstable.

Statement: T. Chari

That depends on the type of the sediment.

Question: M. Lewis

I was just interested in this question of liquefaction, as many of the sands which we have on the Grand Banks Shelf are in that medium or fine sand grain size category. Can you visualize any processes which might lead to liquefaction and instability of these sands?

Answer: T. Chari

In terms of the material, yes, it's an ideal material for getting liquefied because it's uniform size and fine size. Now I know one can hypothesize so many situations where it can get liquefied. You can imagine wave action while there'll be cyclic action or you can imagine earthquake conditions where it will be liquefied.

Question: M. Lewis

So it might be that in severe waves a pressure gradient is set up within the sand and induce flow and then reduce the effect of the wave on the grains. Would that extend to a significant depth like a metre or is there any feeling for that ?

Answer: A. Neidoroda

I tried a calculation on that a few months ago and I used pretty rough and dirty approximations on the flow velocities, the porosities and permeabilities, and this can develop within the surf zone where the depths are very shallow with typical values of the liquefied layer in the order of a few cm's to maybe a foot or so. But the pressure disturbance is like the orbital velocity, it drops off very rapidly with depth and I wasn't very encouraged to look further into this mechanism as a method.

Statement: N. Morgenstern

But there is another mechanism which is due to the differential loading of the wave effect and the porous material, depending on the rate of loading. That is the amplitude wave length and velocity of the waves will feel transience in the stresses. This transience in the stresses will create a collapsing mechanism which can generate pore pressures on its own. A limiting extreme example, it is not related to sands as it happens in parts of the Gulf, is where the large waves will actually move the sediments back and forth because there is a layer of almost zero shear strength, in some incidents about 50 ft below the mud line.

Statement: A. Neidoroda

That's usually a very under-consolidated clay material.

Answer: N. Morgenstern

Yes, but in the case of the sand, if the waves are moving fast enough that the pore pressure is generated by stress changes that do not dissipate, then you can accumulate pore pressure changes leading to collapse. It isn't just the Darcy flow.

Statement: A. Neidoroda

There have been a couple of outflows that have floated up as a result of this. You start with a loosely compacted soil and trigger it.

Statement: A. Ruffman

Phillips Petroleum has a pipeline that runs across the Frisian Islands, top of Holland, and out to a gas field. The pipeline is regularly unburying itself because of the large waves from the North Sea that are coming down. I don't know if the effect is just simply the change in loading. They feel that the reduced pressure possibly in the troughs is letting sediment get moved from on top of this pipeline. There is one company that has a regular job once every six months, surveying to see if it is still buried.

Statement: N. Morgenstern

Another trigger mechanism would be, having created a mass of this meta-stable sand, to have a rather rapid influx of sediment due to some storm effect suddenly loading it, and it will then behave in a different way.

Question: M. Lewis

What if we brought in an iceberg and it just touched bottom at that time when we had stresses built up?

Answer: N. Morgenstern

It depends on how the iceberg touches it, it could lead to a liquefication failure. As Dr. Chari said, lots of things.

Question: A. Ruffman

Can a large ship set up vibrations, especially in quiet conditions, that cause things to become meta-stable?

Answer: N. Morgenstern

In principle, yes, but in practice the accumulative low level vibrations have in past led to a consolidation of the sediment.

4 OPEN DISCUSSION

Chaired by: J.V. Barrie

Question: S. Haider

I have a little concern. Alan was talking of scouring by currents and Mike Lewis was talking of scouring by icebergs, so we seem to have a problem with terminology.

Answer: M. Lewis

It was brought up at the workshop on ice scouring at Montebello in February, and the general feeling was that we would retain the term "ice scouring" for the general description of the process of ice/seabed interaction. Now the American participants would disagree.

Question: S. Haider

Regarding the current scour, Alan, I would call it erosion, were those experiments you conducted in relation to your presentation of current scour around a cylindrical structure?

Answer: A. Neidoroda

What I was doing was for illustrative purposes. I took the simplest possible case, from the results of a fairly large number of experiments that have been conducted in modelling facilities, to serve as sort of a basis of a computer model that we're developing. This attempts to essentially simulate some of the flow conditions, and also simulate some of the scouring conditions.

Question: S. Haider

My question was then, have you tried a horizontal obstruction for investigating pipeline problems?

Answer: A. Niedoroda

We do have some experimental data that has been looked at, but we just simply haven't worked it into this scheme yet. The problem is conceptually very similar, in the sense that the obstruction generates a vortex, it's a different orientation and slightly different shaped, but it is this vortex that creates the intensifying shear stress and therefore the gradients that are necessary in producing erosion. As erosion progresses it interacts with the flow in such a way as to reduce this intensification, and eventually give you an equilbrium condition. It is also complicated by the fact that in the ocean you are dealing with a combined oscillating and mean flow, so you wind up with a situation that has to take into account both of these components.

Question: A. Hay

One of the things that I don't think has been brought up is the most probable origin and most probable fate of sediments on the Grand Banks, specifically in the Hibernia Area? How do they get there, where do they go, are they still being transported there by ice rafting? What is the probable lifetime of a sand deposit in that area?

Answer: M. Lewis

Well if we take your word probable, I think that the general feeling is that surface sediments on the Grand Banks are relict sediments. They result from deposition under glacial conditions. The outer Grand Banks, obviously, have not been glaciated in the last glaciation, but they may have been glaciated in earlier glaciations. Another source is reworking of the underlying Tertiary sediments, because there is an erosion unconformity bounding their upper surface, so sometime in the past that's been eroded and perhaps the results of that erosion have given rise to the sediments that we see on the surface.

Question: A. Ruffman

If these sand waves are moving, are they going over the edge and dumping into deeper water?

Answer: M. Lewis

Let's just get the source first. The other source of course would be ice rafting, there is obviously ice rafted boulders and perhaps sand size material too.

Statement: C. Amos

Also, Mike, you mentioned a biogenic source, that many organisms push sediment up through the gravel lag.

Statement: M. Lewis

Then the shell hash itself becomes a sedimentary component in the sediments.

Statement: V. Barrie

One thing pointed out earlier, that should be re-emphasized, is that most of the bedform sequence we see on the Grand Banks is showing a flow parallel to the bathymetric contours essentially north to south, following the slope.

Question: A. Hay

Let's get to the second component. If you talk about the fate of sediments and their migrating along the edge of the shelf, what happens when they get to the submarine canyon?

Answer: M. Lewis

If they intersect the canyon, they must certainly be gone from Shelf environment.

Statement: C. Amos

Examples from the west coast are good in that Shepard has recorded grain flows in the upper heads of the canyons, that come up on the California shelf. I think he actually measured these active flows, and has got figures on volumes, and there's an astronomic amount that actually disappears and get transported off the shelf.

Statement: A. Ruffman

It's not all canyons. Bill Ryan gave a talk at Dalhousie University about two months ago with large-scale sidescan mosaics of the whole continental slope. showing massive slumps in great detail. Some of these current forms we are seeing are being recorded as well. He switched from one picture of a sidescan mosaic showing downslope massive movement, to avalanches of snow, to draw comparisons between the two different sorts of features. The sidescan mosaics were covering water depths from 200 metres to 3,000 metres.

Question: V. Barrie

Where were those mosaics from?

Answer: A. Ruffman

Those mosaics were essentially off Cape Cod area. if I'm not mistaken, or Baltimore Canyon. He is coming out next spring (1983) with BIO to the Grand Banks slope area and the Laurentian fan earthquake area.

Question: M. Lewis

Did he say those slumps from the top of the slope related to the sediment pileup?

Answer: A. Ruffman

I don't think he really gave us the source. He ignored your question as to where the trail is coming from. The real question is can you go and do surveys that show evidence of pile up and say there's an area that's prone. He showed cracks along the top of some of these slumps and just above that in depth. The pieces didn't quite get moving. He also showed the same sort of thing in avalanches. There are a couple of areas of the Continental Slope off northeast Newfoundland and Labrador where you do see some linear notches as much as 20 m deep that run right along the contours that sure resemble some sort of small slide plane. You see evidence downslope of what we think is mass movement but we only have echosounders to verify that.

Question: A. Hay

Carrying it one step further, it would seem to me then that the canyons are likely to be reasonably active if the transport rates are at all significant.

Answer: M. Lewis

Yes, I think that's true. They are most likely to be active during glacial periods when we have the possibility of glaciers bringing sediment out on to the shelf or at least remobilizing and flushing sediment out on to the shelf.

Statement: V. Barrie

I think that is a good point that Alex has brought up. We haven't done much research in this area and we know that future hydrocarbon exploration will take place along the continental slope. As far as the Canadian slope and shelf edge area, we know very little, especially in the northern areas of Labrador and the northeastern Grand Banks.

Statement: M. Lewis

It may be an excellent place to look, because if there is any movement from the present day, from the shelf onto the slope, it is likely going to be funnelled through canyons, so that is perhaps the place to go to find out if there is substantial volume of sediment undergoing that process.

Number/
Numéro

10

List of Authors

C.L. Amos
Geological Survey of Canada
Atlantic Geoscience Centre
Bedford Institute of Oceanography
Box 1006
Dartmouth, Nova Scotia
B2Y 4A2

J.V. Barrie
C-CORE
Memorial University
St. John's, Newfoundland
A1B 3X5

C. Dalton
Dean of Engineering
University of Houston
Houston, TX

D.A. Huntley
Dept. of Oceanography
Dalhousie University
Halifax, Nova Scotia
B3H 4J1

N. Morgenstern - Oral Paper
Professor, Civil Engineering
University of Alberta
Edmonton, Alberta
T6G 2G7

A.W. Niederoda
Ocean Services Division
Woodward-Clyde Consultants
7330 Westview Drive
Houston, TX 77055

C.P.G. Pereira
C-CORE
Memorial University
St. John's, Newfoundland
A1B 3X5

C. Woodworth-Lynas
C-CORE
Memorial University
St. John's, Newfoundland
A1B 3X5

Discussion Papers

S.M. Blasco
Geological Survey of Canada
Atlantic Geoscience Centre
Bedford Institute of Oceanography
Box 1006
Dartmouth, Nova Scotia
B2Y 4A2

T.R. Chari
Associate Dean
Faculty of Engineering
Memorial University
St. John's, Newfoundland
A1B 3X5

C.F.M. Lewis
Geological Survey of Canada
Atlantic Geoscience Centre
Bedford Institute of Oceanography
Box 1006
Dartmouth, Nova Scotia
B2Y 4A2

List of Participants

C. Brown
Geomarine Associates
Box 41, Station M
Halifax, Nova Scotia
B3J 2L4

K.S. Chang
C-CORE
(Now at Faculty of Medicine
Memorial University
St. John's, Newfoundland
A1B 3V6)

W. Collins
C-CORE
Memorial University
St. John's, Newfoundland
A1B 3X5

T. Chriss
Department of Oceanography
Dalhousie University
Halifax, Nova Scotia
B3H 4J3

R. Dawe
Department of Engineering
Memorial University
St. John's, Newfoundland
A1B 3X5

J. DeJong
CanOcean Engineering Limited
Box 2535
926-5th Avenue, S.W.
Calgary. Alberta
T2P 0N7

P. Ferris
Department of Indian Affairs
and Northern Development
Ottawa. Ontario
K1A 0H4

S.H.C. Foo
Mobil Research & Development Corp.
P.O. Box 900 (FRL)
Offshore Engineering
Dallas, Texas 75221

G. Fortin
Geoterrex Limited
2060 Walkley Road
Ottawa. Ontario
K1G 3P5

Q. Gall
Department of Geology
Memorial University
St. John's, Newfoundland
A1B 3X5

R.R. Good
McElhanney Surveying and
Engineering Limited
999-8th Street, W.
Calgary. Alberta
T2R 1J5

P. Green
Department of Engineering
Memorial University
St. John's, Newfoundland
A1B 3X5

S. Haider
Hudson's Bay Oil & Gas Limited
700-2nd Street, S.W.
Calgary. Alberta
T2P 0X5

A. Hay
Department of Physics
Memorial University
St. John's, Newfoundland
A1B 3X7

R. Hiscott
Department of Geology
Memorial University
St. John's, Newfoundland
A1B 3X5

E. King
Huntec ('70) Ltd.
P.O. Box 851
Dartmouth, Nova Scotia
B2Y 3Z5

List of Participants Cont'd

L. Lazic
Petro Canada
P.O. Box 2844
Calgary. Alberta
T2P 2M7

K. Minhas
Canada Oil & Gas Lands
Administration
Dept. Energy. Mines & Resources
580 Booth Street
Ottawa. Ontario
K1A 1E4

A. Pushpanathan
C-CORE
(Now at NORDCO Limited
P.O. Box 8833
St. John's, Newfoundland
A1B 3T2)

A. Ruffman
Geomarine Associates
Box 41, Station M
Halifax, Nova Scotia
B3J 2L4

P. Sabbatini
Petro-Canada
840-7th Avenue. S.W.
Calgary, Alberta

D. Vetrici
McElhanney Surveying and
Engineering Limited
999-8th Street. S.W.
Calgary, Alberta

H. Westergard
Canterra Energy Limited
P.O. Box 1051
Calgary, Alberta
T2P 2K7

W.L. White
Newfoundland Geosciences Limited
P.O. Box 2367
St. John's, Newfoundland

REFERENCES

Abdel-Rahman, N.M.

1963 "The effect of flowing water on cohesive beds", **Mitte Vawe**, Swiss Fed. Inst. Tech., Zurich. #56.

Abou-Seida. M.M.

1965 "Bedload function due to wave action", **Univ. Calif., Berkeley, Hydraul. Eng. Lab. Tech. rep.** HEL 2-11, 78 pp.

Adams, C.E. Jr. and Weatherby. G.L.

1981 Some effects of suspended sediment stratifications on an Oceanic Bottom Boundary Layer. **J. Geophys. Res.** V.86, 4161-4172.

Alishahi, M.R. and Krone. R.B.

1964 "Suspension of cohesive sediments by wind generated waves", **Univ. Calif., Berkeley, Hydraul. Eng. Lab. Tech. rep.** HEL 2-9, 24 pp.

Allen, J.R.L.

1963a "Asymmetrical ripple marks and the origin of water-laid cosets of cross-strata". **Liverpool and Manchester Geol. J.,** V. 3. 187-236.

1963b "The classification of cross-stratified units. with notes on their origin". **Sedimentology,** V. 2, 93-114.

1965 "Sedimentation to the lee of small underwater sand waves: An experimental study." **J. Geol.** V. 73(1), 95-116.

1966 "On bedforms and paleocurrents". **Sedimentology** V. 6. 153-190.

1968 "**Current Ripples**", Amsterdam: North-Holland Publishing. 433 pp.

1969 "Erosional current marks of weakly cohesive mud beds", **J. Sediment. Petrol.** V. 39(2), 607-623.

1970 "**Physical processes of sedimentation; an introduction**", London: Unwin University books, 248 pp.

1973 "Phase differences between bed configuration and flow in natural environments, and their geological relevance." **Sedimentology**. V. 20. 323-329.

1980 "Large transverse bedforms and the character of boundary-layers in shallow water environments", **Sedimentology**. V. 27, 317-323.

Allen, J.R.L. and Leeder. M.R.
1980 "Criteria for the instability of upper-stage plane beds", **Sedimentology** V. 27, 209-217.

Amos, C.L.
1978 "The post-glacial evolution of the Minas Basin, N.S.; a sedimentological interpretation. **J. Sediment. Petrol.** V. 48, 965-982.

Amos, C.L., Asprey, K.W. and Rodgers, N.A.
1981 "Bedford Institute sedimentation tube", **B.I.O., Report, Series BI-R,** No. 81-4, 60 pp.

Amos, C.L. and Barrie. J.V.
1980 "Hibernia and Ben Nevis seabed study - Polaris V, June 1980" **C-CORE Data Rep.,** #80-17. 40 pp.

Amos, C.L. and Collins, M.B.
1979 "The combined effects of waves and currents on the morphology of intertidal ripple marks - The Wash." **J. Sediment. Petrol.** V. 48 (3), 849-856.

Amos, C.L. and Greenberg, D.A.
1980 "The simulation of suspended particulate matter in the Minas Basin, Bay of Fundy - a region of potential tidal power development". in Proc. **Canadian Coastal Conference.** Burlington, Ontario, 1980; N.R.C. publ., 460 pp, 2-20.

Andrews, J.T.
1963 "End moraines and late-glacial chronology in the northern Nain-Okak section of the Labrador coast" **Geogr. Ann.**, V. 45, 158-170.

d'Apollonia, S.J. and Lewis, C.F.M.
1981 "Ice Scour Database - user's manual". **Can. Geol. Surv.** unpublished MS. 45 pp.

Ariathurai. R. and Krone. R.B.
1976 "Finite element model for cohesive sediment transport", **ASCE J. Hydraul. Div.** V. 102, No. HY3, Proc. Pap. 11987, p. 323-338.

Ariathurai. R., MacArthur. R.C. and Krone. R.B.
1977 "Mathematical model of estuarial sediment transport", **U.S. Army Eng., Waterw. Exp. St., Tech. Rep.** D-77-12, 149 pp.

Arulandan, K., Loganathan, P. and Krone. R.B.
1975 "Pore and eroding fluid influences on surface erosion of soil", ASCE **J. Geotech. Eng. Div.**, V. 101, No. GT1. Proc. Pap. 11078, 51-66.

Arya, S.P.S.
1975 "A drag partition theory for determining the large scale roughness parameter and wind stress on the Arctic pack ice." **J. Geophys. Res.** V. 80, 3447-3454.

Bagnold, R.A.
1946 "Motions of waves in shallow water; interaction between waves and sand bottoms", **Royal Soc. London, Proc. Ser. A,** V. 187, 1-18.

1956 "The flow of cohesionless grains in fluids", **Royal Soc. London Phil. Trans., Ser. A,** V. 249, 235-297.

1963 "Beach and Nearshore Processes, Part I: Mechanics of Marine Sedimentation"; in **The Sea, V. 3**, M.N. Hill, (Ed.), N.Y., Wiley Interscience, 507-528.

1966 "An approach to the sediment transport problem from general physics", **U.S. Geol. Surv., Prof. Pap.** 422-I, 37 pp.

Baker, J.B.
1978 "Vortex flow around the bases of obstructions", **Ph.D. Dissertation, Univ. of Cambridge,** 123 pp.

Baker, R.S., and Friedman, G.M.
1973 "Sedimentation in an Arctic marine environment: Baffin Bay between Greenland and the Canadian Archipelago" in **Earth Science Symposium on Offshore Eastern Canada**, P.J. Hood; (Ed.) Can., Geol. Surv., Pap. 71-23, 471-498.

Barnes, P.W., McDowell, D., and Reimnitz, E.
1978 "Ice gouging characteristics: their changing patterns from 1975-1977, Beaufort Sea Alaska." **U.S. Geol. Surv. open file report,** #78-730.

Barnes, P.W., and Reimnitz, E.
1979 "Ice gouge obliteration and sediment redistribution event; 1977-1978, Beaufort Sea, Alaska." **U.S. Geol. Surv. open file report**, #79-848.

Barrie, J.V.
1980 "Iceberg/Seabed interaction, northern Labrador Sea". **Ann. Glaciology**, V.1, 71-76.

1983 "Sedimentary processes and the preservation of iceberg scours on the eastern Canadian continental shelf." in **Proc. 7th Int. Conf. on Port and Ocean Eng. under Arctic Conditions**, (POAC 1983), Helsinki, Finland; Tech. Res. Centre. Lab. Struct. Eng., V. 3.

Barrie, J.V. and Snyder, H.L.
1981 "Seabed investigations on the Canadian Atlantic Continental Shelf." in **Can. Pet. Assoc. Colloquium III: Petroleum Mapping and Surveys in the 80's**, Banff. Alberta. October, 1981, 273-289.

Barrie, J.V., Woodworth-Lynas, C.M.T., and Pereira, C.P.G.
1982 "Data report of the Hekja Wellsite Marine Survey undertaken during CSS Hudson Cruise No. HU81-045, October. 1981" **C-CORE Data Report.** #82-2, 50 pp.

Belderson, R.H. and Stride, A.H.
1966 "Tidal current fashioning of a basal bed.", **Mar. Geol.** V. 4, 237-257.

Berjker. D. and Ladd, C.C.
1974 "Erosion of cohesive soils", In **Research on the Physical Properties of Marine Soils**, ONR Contract Nonr-1841(29), Research Report. R64-1. Dept. of Civil Eng., M.I.T., Cambridge, Mass., 35 pp.

Berkson, J.M. and Clay, C.S.
1973 "Microphysiography and possible iceberg grooves on the floor of western Lake Superior". **Geol. Soc. Am. Bull.**, V.84, 1315-1328.

Bijker, E.W., Kalkwijk, J.P. and Pieters, T.
1975 "Mass transport in gravity waves on a sloping bottom" **Proc. 14th Conf. Coastal Eng.** Copenhagen, 1975, ASCE 447-465.

Blake, W., Jr. and Lewis, C.F.M.
1975 "Marine surficial geology: observations in the High Arctic, 1974"; in **Report of Activities, Part A;** Can. Geol. Surv. Pap. 75-1A, 383-387.

Blatt, H., Middleton, G.V. and Murray, R.C.
1980 **"Origin of Sedimentary Rocks".** New Jersey: Prentice-Hall, 782 pp.

Boersma, J.R.
1969 "Internal structure of some tidal megaripples on a shoal on the Westerschelde Estuary of Netherlands". **Geol. Mijnb.** V. 48, 409-414.

Boersma, J.R. and Terwindt, J.H.L.
1981 "Neap-spring tide sequences of intertidal shoal deposits in a mesotidal estuary". **Sedimentology** V. 28, 151-170.

Bojardi, J.L.
1965 "European concepts of sediment transportation." **Proc. ASCE J. Hydraul. Div.**, V. 91 (HYI), 29-54.

Boothroyd, J.C. and Hubbard, D.K.
1975 "Genesis of bedforms in meso-tidal estuaries". in **Estuarine Research, V. 2, Geology and Engineering** Cronin, L.E. (Ed.), N.Y., Academic press, 217-235.

Bornhold, B.D.,

1982 "Surficial sediments on the Continental Shelf, west central Vancouver Island;" **Can. Geol. Surv. Pacific Geoscience Centre**. map. O.F. 827.

Bornhold, B.D., Finlayson, N.M., and Monahan, D.

1976 "Submerged drainage patterns in Barrow Strait, Canadian Arctic;" **Can. J Earth Sci.**, V. 13, 305-311.

Bouma, A.H.

1964a "Sampling and treatment of unconsolidated sediments for study of internal structures." **J. Sediment. Petrol.**, V. 34, 349-354.

1964b "Notes on X-ray interpretation of marine sediments," **Mar. Geol.**, V. 2, 278-307.

1968 "Distribution of minor structures in Gulf of Mexico sediments". **Trans. Gulf Coast Assoc. Geol. Soc.**, V. 28, 26-33.

1981 "Introduction to offshore geologic hazards" in **Offshore Geologic Hazards**, A.A.P.G., Education Course Note Series #18, 1.1-1.72.

Bowden, K.F.

1962 "Turbulence." in **The Sea V.1**, M.N. Hill (Ed.), N.Y.; Wiley-Interscience, 802-825.

1978 "Physical problems of the benthic boundary layer." **Geophys. Surv.**, V. 3, 255-296.

Bowden, K.F. and Fairbairn L.A.

1956 "Measurements of turbulent fluctuations and Reynolds stresses in a tidal current." **Proc. R. Soc. London**, Series A 237; #1210. 422-438.

Bowen, A.J.

1980 "Simple models of nearshore sedimentation; beach profiles and longshore bars". in **The Coastline of Canada.** S.B. McGann (Ed.). Can. Geol. Surv., 1-11.

Breusers, H.N.C.

1972 "Local scour near offshore structures", **Delft Hydraulics Lab. Rep't.** # 105, 7 pp.

Briggs, L.I. and Middleton, G.V.

1965 "The hydromechanics of sediment formation" in **Primary sedimentary structures and their hydrodynamic interpretation.** Middleton, G.V. (Ed.), S.E.P.M., spec. publ. #12, 5-16.

Brown, C.B.

1950 "Sediment Transportation", in: **Engineering Hydraulics**, Rouse, H. (Ed.), N.Y.; John Wiley and Sons, Inc., 1039 pp.

Bucher, W.H.

1919 "On ripples and related sedimentary surface forms and their palaeogeographic interpretation." **Am. J. Sci.**, V. 47, 149-210. and 241-269.

Buckley, D.E.

1971 "Recent marine sediments of Lancaster Sound, District of Franklin", **Marit. Sediments**, V. 7(3), 96-117.

Butman, B., Noble. M. and Folger. D.W.

1979 "Long-term observations of bottom current and bottom sediment movement on the mid-Atlantic continental shelf". **J. Geophys. Res.**, V. 84, 1187-1205.

Caldwell. D.R. and Chriss, T.M.

1979 "The viscous sublayer at the seafloor". **Science** # 205, 1131-1132.

Calvert, S.E., and Veevers, J.J.
1962 "Minor structures of unconsolidated marine sediments revealed by x-radiography." **Sedimentology** V. 1, 287-295.

Cantwell, B.J.
1981 "Organized motion in turbulent flow". **Ann. Rev. Fluid Mech.** V.13, 457-515.

Carstens, M.R., Neilson, F.M. and Altinbilek, H.D.
1969 "Bedforms generated in the laboratory under an oscillatory flow: analytical and experimental study", **U.S. Army Coastal Eng. Res. Cen.**, Tech. Memo #28, 39 pp.

Carter, L.
1972 "Surficial sediments of Barkley sound and the adjacent continental shelf, west coast Vancouver Island"; **Can. J. Earth Sci.**, V. 10, #4, 441-459.

Carter, L., and Murray, J.W.
1969 "Topography and bottom sediments in Barkley Sound, and the adjacent continental shelf, southwestern British Columbia" **Can. Geol. Surv. Report of Activities**, Part A, Pap. 69-1, 12-14.

Chari, T.R.
1978 "Model studies of iceberg scouring". **Proc. 4th Intl. Conf. on Port and Ocean Eng. under Artic Conditions**, (POAC, 1977) St. John's, Nfld., Fac. Eng., Memorial Univ., V. 1., 775-783.

Chari, T.R. and Peters, G.R.
1981 "Estimates of iceberg scour depths". Proc. **Symposium on Production and Transportation Systems for the Hibernia Discovery**, St. John's, Nfld., 1981. Petrol. Directorate, Govt. Nfld. and Labrador, 178-206.

Chase, R.L., Tiffen, D.L. and Murray, J.W.
1975 "The western Canadian continental margins", in **Canada's continental margins and offshore petroleum exploration,** C.J. Yorath. E.R. Parker and D.J. Glass (Eds.) Can. Soc. Pet. Geol., Memoir #4, 701-722.

Chitale, S.V.
1962 "Discussion of Scour at Bridge Crossings", **ASCE Trans.,** V. 127, pt. 1, 191-196.

Chriss, T.M. and Caldwell. D.R.
1982 "Evidence for the influence of form drag on bottom boundary layer flow". **J. Geophys. Res.,** V. 87, 4148-4154.

Claque, J.J.
1976 "Pleistocene sediments in the northern Strait of Georgia. British Columbia"; in **Report of Activities, Part B; Can. Geol. Surv.** Pap. 76-1B, 157-160.

Cloet, R.L.
1954 "Sandwaves in the southern North Sea and in the Persian Gulf". **J. Inst. Navig.** V. 7, 272-279.

Coleman, J.M. and Prior. D.B.
1981 "Subaqueous sediment instabilities in the offshore Mississippi River Delta". in **Offshore Geologic Hazards,** A.A.P.G. Education Course Note Series, #18, 5.1 - 5.53.

Costello, W.R., and Southard, J.B.
1981 "Flume experiments on lower flow regime bedforms in coarse sand". **J. Sediment Petrol.** V. 51(3), 849-864.

Craig, B.G. and Fyles, J.G.
1960 "Pleistocene geology of Arctic Canada;' **Can. Geol. Surv.,** Pap. 60-10, 21 pp.

Creutzberg, F. and Postma, H.

1979 "An experimental approach to the distribution of mud in the southern North Sea". **Netherlands J. Sea Res.** V. 13(1), 99-116.

Csanady, G.T.

1976 "Mean circulation in shallow seas". **J. Geophys. Res.** 81, 5389-5399.

1967 "On the 'resistance law' of a turbulent Ekman layer". **J. Atmos. Sci.** 24, 467-471.

Curray, J.R., Dickinson, W.R., Dow, W.G., Emery, K.O., Seely, D.R., Vail, P.R. and Yarborough, H.

1977 "Geology of continental margins", **A.A.P.G. Education Course Note Series #5.** Catalog #879, 122 pp.

Dalrymple, R.W., Knight, R.J., and Lambiase, J.J.

1978 "Bedforms and their hydraulic stability relationships in a tidal environment, Bay of Fundy, Canada". **Nature**, V. 275 (5676), 100-104.

Das

1970 "A literature review on bed-load transport due to wave action and localized scour in noncohesive sediments"; in Einstein, H.A., and R.L. Weigle, **A Literature Review on Erosion and Deposition of Sediments near Structures in the Ocean**, Contract Rep't. N62399-69-C-0007, U.S. Navy Civil Eng. Lab., Pt. Hueneme.

Davies, A.G. and Wilkinson, R.H.

1979 "Sediment motion caused by surface water waves". **Proc. 16th Conf. Coastal Eng.**, Hamburg, Germany, (1978); ASCE, V. 2, 1577-1595.

Denton, G.H. and Hughs, T.
1981 **"The last great ice sheets".** N.Y.: John Wiley and Sons, 484 pp.

Dingler, J.R.
1975 "Wave formed ripples in nearshore sands", Abstract of Dissertation for Ph.D., Univ. Calif.

Dinsmore. R.P.
1972 "Ice and its drift into the North Atlantic ocean". **Int. Commission for the Northwest Atlantic Fisheries,** Special Publication #8, 89-127.

Dionne, J.-C.
1972 "Ribbed grooves and tracks in mud tidal flats of cold regions". **J. Sediment. Petrol.** V. 42, 848-851.

Dodd, R.T., Salisbury, J.W. and Smalley, V.G.
1963 "Crater frequency and the interpretation of lunar history". **Icarus,** V.2, 466-480.

Drake, D.E., Totman, C.E. and Winberg, P.L.
1979 "Sediment transport during the winter on the Yukon Prodelta North Sound, Alaska", **J. Sediment. Petrol.** V. 49 (4), 1171-1180.

Draper, L.
1967 "Wave activity at the seabed around northwestern Europe". **Marine Geol.** V. 5, 133-140.

Dunn, I.S.
1959 "Tractive resistance of cohesive channels", **ASCE, J. Soil Mech. Found. Div.,** V. 85, (SM3), Proc. Pap. 2062, 1-24.

Dyer, K.R.
1980 "Velocity profiles over a rippled bed, and the threshold of movement of sand". **Estuarine and Coastal Mar. Sci.** V.10, 181-199.

Eagleson, P.S., Dean, R.G. and Peralta, P.
1958 "The mechanics of the motion of discrete spherical bottom sediment particles due to shoaling waves", **U.S. Army Beach Erosion Board, Tech. Mem.** #104, 41 pp.

Einstein, H.A.
1942 "Formulas for the transport of bed load", **ASCE Trans.**, V. 107, 561-597.

1950 "Bed-load function for sediment transport in open channel flow", **U.S. Dept. Agric., Tech. Bull.** # 1026, 71 pp.

1964 "River sedimentation". in **Handbook of Applied Hydrol.** V. Te Chow (Ed.) N.Y.; McGraw-Hill, Section 17-II, 35-67.

Einstein, H.A. and Chien, N.
1955 "Effects of heavy sediment concentration near the bed on velocity and sediment distribution". **U.S. Army Corps of Engineers, Missouri River Division.** Sediment Series #8, 76 pp.

Einstein, H.A. and Krone, R.B.
1962 "Experiments to determine modes of cohesive sediment transport in salt water". **J. Geophys. Res.**, V. 67, 1451-1461.

Emery, K.O.
1938 "Rapid method of mechanical analysis of sands", **J. Sediment. Petrol.** V. 8, 105-111.

1977 "Stratigraphy and structure of pull-apart margins", in **Geology of Continental Margins**; A.A.P.G. Education Course Note Series #5, Catalog #879, 122 pp.

Engelund, F. and Hansen, E.
1972 **"A monograph on sediment transport in alluvial streams".** Copenhagen; Technical University of Denmark. 62 pp.

Espey. W.H. Jr.
1963 "A new test to measure the scour of cohesive sediments", **Tex. Univ. Hydraul. Eng. Lab. Tech. Rep.**, # Hyd 01-6301, 42 pp.

Evans, O.F.
1941 "The classification of wave formed ripple marks". **J. Sediment. Petrol.**, Vol. 11, p. 37-41.

Evans-Hamilton, Inc.
1973 "A Grand Banks wind, wave and visibility persistance study". **Contract report to Mobil Oil Canada.** 151 p.

Everts, C.H.
1973 "Particle overpassing on flat granular boundaries", **ASCE Proc., J. Waterways, Harbors and Coastal Eng.**, V. 99 (WW4), 425-438.

Fader. G.B., King, L.H. and Josenhans. H.J.
In press "Surficial geology of the Grand Banks, of the Laurentian Channel and western Grand Banks of Newfoundland". Marine Sci. Branch, **Can. Dept. Energy, Mines and Resources.**

Fader. G.B. and King, L.H.
1981 "A reconnaissance study of the surficial geology of the Grand Banks of Newfoundland", **Can. Geol. Surv. Pap.** 81-1A, 45-81.

Falconer, R.K.H.
1977 "Marine geophysical and geological research in Baffin Bay and the Labrador Sea, CSS Hudson, 1976"; Report of Activities, Part B; **Can. Geol. Surv. Pap.** 77-1B, 255-260.

Field, M.E.
1980 "Sand Bodies on coastal plain shelves. Holocene record of the U.S. Atlantic inner shelf off Maryland". **J. Sediment. Petrol.**, V. 50(2), 505-528.

Fillon, R.H.
1975 "Deglaciation of the Labrador Shelf", **Nature**. 253. 429-431.

1976 "Hamilton Bank, Labrador Shelf: Postglacial sediment dynamics and paleo-oceanography", **Marine Geol.**, V. 20, 7-25.

1980 "High resolution sub-bottom profiles across the northern Labrador Shelf: Do they provide evidence of glaciation?" **Program with Abstracts**, Geol. Assoc. Can., May 1980, Halifax, N.S., p. 53.

Fillon, R.H., Ferguson, C. and Thomas, F.
1978 "Cenozoic provenance and sediment cycling: Hamilton Bank, Labrador Shelf" **J. Sediment. Petrol.** 48, 253-268.

Fillon, R.H., Folinsbee, R.A. and Palmer, R.
1978 "Deep shelf and slope terraces off northern Labrador". **Nature**, 273, 743-746.

Fillon, R.H. and Harmes, R.A.
1982 "Northern Labrador shelf glaciation: chronology and limits", **Can. J. Earth Sci.**, V.19, 162-192.

Flaxman, E.M.

1962 "A method of determining the erosion potential of cohesive soils,", **Int. Assoc. Sci. Hydrol., Commission of Land Erosion**, Publ. #59, 114-123.

Flemming, B.W.

1978 "Underwater sand dunes along the southeast African continental margin: observations and implications". **Marine Geol.**, V. 26. 177-198.

Flood, R.D.

1981 "Distribution, morphology and origin of sedimentary furrows in cohesive sediments, Southampton Water", **Sedimentology**. V. 28(4), 511-530.

Forristall, G.Z., Hamilton, R.C. and Cardone, V.T.

1977 "Continental shelf currents in tropical storm Delia: Observations and theory". **J. Phys. Oceanogr.** 7 (4), 532-546.

Fortier, Y.O. and Morley, L.W.

1956 "Geological unity of the Arctic Islands"; **Trans. Royal Soc. Can.**, Series 3, 3-12.

Fredsoe, J.

1978 "Natural backfilling of pipeline trenches", **Proc. 10th Offshore Tech. Conf. (OTC 1978)**, 1223-1230.

Fredsoe, J. and Engelund, F.

1975 "Bed configurations in open and closed alluvial channels". **Tech. Univ. Denmark., Inst. Hydrodyn. and Hydraul. Eng. Series**, Pap. 8, 39 pp.

Gadd, P.E., Lavelle, J.W., and Swift, D.J.P.
1978 "Estimates of sand transport on the New York shelf using near-bottom current meter observations". **J. Sediment. Petrol.** V. 48(1), 239-252.

Geldof, H.J. and Slot, R.E.
1979 "Settling tube analysis of sand". **Univ. of Tech., Delft, lab. of fluid mech.** Internal Rep. # 4-79, 31 pp.

Gibbs, R.J.
1977 "Clay mineral segregation in the marine environment". J. **Sediment. Petrol.** V. 47(1), 237-243.

Gibbs, R.J., Matthews, M.D., and Link, D.A.
1971 "The relationship between sphere size and settling velocity". **J. Sediment. Petrol.** V. 41(1), 7-18.

Gilbert, G.K.
1914 "The transportation of debris by running water", **U.S. Geol. Surv., Prof. pap. #** 86, 236 pp.

Gilbert. G.R. and Barrie. J.V.
1983 "Surficial geology of two ice-scoured banks on the Labrador Shelf" **C-CORE, unpublished MS.**

Gilbert, R.
1982a "The Broughton Trough on the continental shelf of eastern Baffin Island, Northwest Territories"; **Can. J. Earth Sci.**, V. 19, 1599-1607.

1982b "Contemporary sedimentary environments on Baffin Island, N.W.T., Canada: glacimarine processes in fiords of eastern Cumberland Peninsula"; **Arctic and Alpine Res.**, V. 14, 1-12.

Gordon, C.M.
1975 "Sediment entrainment and suspension in a turbulent tidal flow", **Marine Geol.**, V. 18, m57-m64.

Gorsline, D.S. and Swift, D.J.P. (Eds.)
1977 "Continental shelf sediment dynamics: A national overview", **proc. workshop held in Vail, Colorado (1976),** (sponsored by National Science Foundation (IODE), and others), 134 pp.

Graf, W.H.
1971 **"Hydraulics of sediment transport".** N.Y.; McGraw-Hill, 513 pp.

Graf, W.H., and Acaroglu, E.R.
1966 "Settling velocities of natural grains". **Bull. Intl. Ass. Sc. Hydrol.** V. 16, 27-43.

Grandstein, F.M. and Srivastava, S.P.
1980 "Aspects of Cenozoic stratigraphy and paleo-oceanography of the Labrador Sea and Baffin Bay: **Palaeogeography, Palaeoclimatology, Palaeoecology,** V. 30, 261-295.

Grant, A.C.
1965 "Distributional trends in the recent marine sediments of Northern Baffin Bay"; **BIO Unpublish. MS., Rept. #65-9,** 74 pp. (M.Sc. Thesis, Univ. New Brunswick).

1966 "A continuous seismic profile on the continental margin off N.E. Labrador"; **Can. J. Earth Sci.,** V. 3, 725-730.

1970 "Recent crustal movements on the Labrador shelf"; **Can. J. Earth Sci.,** V. 7, 571-575.

1971 "Distributional trends in the recent marine sediments of northern Baffin Bay" **Maritime Sediments,** V. 7 (2) 41-63.

1972 "The continental margin off Labrador and Eastern Newfoundland - morphology and geology" **Can. J. Earth Sci.**, V. 9, 1394-1430.

1975 "Geophysical results from the continental margin off southern Baffin Island" In **Canada's continental margins and offshore petroleum exploration**, C.J. Yorath. E.R. Parker, and D.J. Glass (Eds.). Can. Soc. Petrol. Geol., Memoir # 4, 411-431.

Grant, W.D. and Madsen, O.S.

1979a "Combined wave and current interaction with a rough bottom". **J. Geophys. Res.** V. 84, #C4, 1797-1808.

1979b "Bottom friction under waves in the presence of a weak current", **NOAA Tech. Rep.**, ERL-MESA, NOAA 150 pp.

1982 "Moveable bed roughness in unsteady oscillatory flow", **J. Geophys. Res.**, V. 87, #C1, 469-481.

Grass, A.J.

1970 "Initial instability of fine bed sand". **ASCE., J. Hydraul. Div.**, V. 96 (HY3), 619-632.

Greene, B.A.

1974 "An outline of the geology of Labrador", **Mineral Dev. Div.**, Newfoundland Dept. of Mines and Energy, 64 pp.

Gregory, N. and Walker. W.S.

1951 "The effect of transition of isolated surface excrescences in the boundary layer", R & M 2779, ARC, London.

Grissinger, E.H.

1966 "Resistance of selected clay systems to erosion by water", **Water Resources Res.** V. 2, # 1, 131-138.

Grissinger, E.H. and Asmussen, L.E.
1963 "Discussion of Channel stability in undisturbed cohesive soils, by E.M. Flaxman", **ASCE., J. Hydraul. Div.**, V. 89 (HY6), Proc. Pap. 3708, 259-264.

Gust, G.
1976 "Observations on turbulent drag reduction in a dilute suspension of clay in sea-water". **J. Fluid Mech.** 75, 29-47.

Gust, G. and Walger. E.
1976 "The influence of suspended cohesive sediments on boundary layer structure, and erosive activity of turbulent seawater flow", **Marine Geol.**, V. 22, 189-206.

Gustajtis, K.A.
1979 "Iceberg scouring on the Labrador shelf. Saglek Bank", **C-CORE Tech. Rep.** #79-13, 89 pp.

Guy.H.P., Simons, D.B., and Richardson. E.V.
1966 "Summary of alluvial channel data from flume experiments, 1956-61". **U.S. Geol. Surv. prof. pap. #.** 462-I, 96 pp.

Haaf, E.T.
1959 "Properties and occurrence of turbidities". **Geol. Mijnb.** (N.W. Ser.) 21e Jaargang, 217-222.

Harms, J.C.
1969 "Hydraulic significance of some sand ripples". **Geol. Soc. Am. Bull.** V. 80, 363-396.

Harms, J.C. and Fahnestock, R.K.
1965 "Stratification, bedforms and flow phenomena (with an example from the Rio Grande)", in **S.E.P.M. Spec. Publ., #** 12, 84-115. (see Middleton. G.V., 1965).

Harms, J.C., Southard, J.B., Spearing, D.R. and Walker, R.G.
1975 "Depositional environments as interpreted from primary sedimentary structures and stratification sequences". **S.E.P.M. Short Course # 2**, Lecture notes, 161 pp.

Harris, I.McK.
1974 "Iceberg marks on the Labrador Shelf. **Can. Geol. Surv. Res. Pap.** 74-30, 97-101.

Harris, I.McK. and Jollymore. P.G.
1974 "Iceberg furrow marks on the Continental shelf northeast of Belle Isle. Newfoundland". **Can. J. Earth Sci.**, 11, 43-52.

Hartmann. W.K.
1977a "Cratering in the solar system". **Sci. Am.**, Jan. 1977. 84-99.

1977b "Relative crater prodution rates on planets". **Icarus**, 31. 260-276.

Hawley, N.
1981 "Flume experiments on the origin of Faser bedding". **Sedimentology** V. 28, 699-712.

Heathershaw. A.D.
1974 " 'Bursting' phenomena in the sea". **Nature**. 248, 394-395.

1976 "Measurements of turbulence in the Irish Sea benthic boundary layer". in **The Benthic Boundary Layer**. I.N. McCave (Ed.), N.Y. and London; Plenum Press. 323 pp., 11-31.

Heathershaw, A.D. and J.H. Simpson.
1978 "The sampling variability of the Reynolds stress, and its relation to boundary shear stress and drag coefficient measurements". **Estuarine and Coastal Mar. Sci.**, V. 6, 263-274.

Heezen. B.C. and Hollister. C.D.
1971 **"The face of the Deep"**, N.Y., Oxford Univ. press, 659 pp.

Heffler, D.E.
1979 "Ralph - A sediment dynamics monitor." in **Proc. Workshop on instrumentation for currents and sediments in the nearshore zone.** Oct. 1979, Ottawa. N.R.C., 163-173.

Henderson, P.J.
1971 "Textural study of sediments of Barrow Strait, District of Franklin" **Maritime Sediments**, V. 7, #3, 126-137.

Henderson, G., Schiener. E.J., Rissum, J.B., and Croxton, C.A.,
1981 "The west Greenland basin" In **Geology of the Atlantic Border lands and basins**, J.W. Kerr and A.J. Fergusson (Eds.), Can. Soc. Petrol. Geol., Memoir #7.

Herzer, R.H.
1978 "Submarine canyons and slumps on the continental slope off southern Vancouver Island" in **Can. Geol. Surv. Curr. Res., Pt. A**; Pap. 78-1A, 357-360.

Heywood, H.
1938 "Measurement of the fineness of powdered materials". **Inst. of Mech. Eng. Proc.**, V. 140, 257-308.

Hill. P.R. and Bowen, A.J.
In Press "Modern sediment dynamics at the shelf-slope boundary layer off Nova Scotia".

Hill, H.M., Srinivasan, V.S. and Neunny, T.E.
1969 "Instability of flat bed in alluvial channels", **ASCE J. Hydraul. Div.**, V. 95 (HY5), Proc. Pap. 6770, 1545-1558.

Hjorth, P.
1975 "Studies on the Nature of Local Scour", **Lund. Inst. Techn. Bull.** Ser. A, # 46, Univ. Lund., Sweden.

Hjulstrom, F.
1935 "Studies of the morphological activities of rivers, as illustrated by the River Fyris". **Bull. Geol. Inst. Uppsala.** V. 25. 221-527.

Hnatiuk, J. and Brown, K.D.
1977 "Sea bottom scouring in the Canadian Beaufort Sea". **9th Annual Offshore Tech. Conf.**, (OTC, 1977). V. 3, 519-527.

Holtedahl, H.
1956 "Some remarks on geomorphology of continental shelves off Norway, Labrador and Southeast Alaska", **J. Geol.**, V. 66, 461-471.

Holtedahl, O.
1929 "On the geology and physiography of some Antartic and sub-Antarctic Islands - with notes on the character and origin of fjords and strandlines of some northern lands" **Norwegian Antarctic Research 1928-1929, Vol. 3.** Pub. by Det Norske Videnskaps Akademi i Oslo.

1950 "Supposed marginal fault lines in the shelf area off some high northern lands" **Geol. Soc. Am. Bull.**, V. 61. 493-500.

1970 "On the morphology of the west Greenland Shelf with general remarks on the 'marginal channel' problem" **Mar. Geol.**, V. 8, 155-172.

Horikawa, K. and Watanabe, A.
1967 **Coastal Eng. Japan**, V. 10, 39-57.

Horn, D.R.
1963 "Marine geology of Peary Channel, district of Franklin" **Can. Geol. Surv. Pap.** 63-11, 33 pp.

Houbolt, J.J.H.C.
1968 "Recent sediments in the southern Bight of the North Sea". **Geol. Mijnb.** V. 47, 245-273.

Hunting, Geology and Geophysics Ltd.
1971 "Investigation of seabed scouring in the Beaufort Sea". For **A.P.O.A.** by Hunting, Geology and Geophysics Ltd. Boreham Wood, Herts, U.K., 29 pp.

Inman, D.L.
1957 "Wave generated ripples in nearshore sands". **U.S. Dept. of Army, Beach Erosion Board** Tech. Memo #100. 42 pp.

1963 "Sediments: Physical properties and mechanics of sedimentation" in **Submarine Geology** F.P. Shepard, (Ed.), N.Y.; Harper & Row, 2nd Ed., 101-151.

Inman, D.L., Ewing, G.C., and Corliss, J.B.
1966 "Coastal sand dunes of Guerrero Negro, Baja California, Mexico". **Geol. Soc. Am. Bull.** V. 77, 787-802.

Inman, D.L. and Bagnold, R.A.
1963 "Beach and nearshore processes; Part 2, Littoral Processes", in **The Sea, Vol. 3**, Hill, M.N. (Ed.), N.Y.; Wiley-Interscience. 529-553.

Inman, D.L. and Bowen, A.J.

1963 "Flume experiments on sand transport by waves and currents". **Proc. 8th Conf. Coastal Eng.**, Mexico City, ASCE. 137-150.

Ives, J.D.

1978 "The maximum extent of the Laurentide ice sheet along the east coast of North America during the last glaciation", **Arctic**, 31. 24-53.

Jackson, R.G. II.

1976 "Sedimentological and fluid-dynamic implications of the turbulent bursting phenomenon in geophysical flows". **J. Fluid Mech.**, V. 77. 531-560.

James, N.P. and Stanley, D.J.

1968 "Sable Island Bank off Nova Scotia: Sediment Dispersal and Recent History", **Am. Assoc. Pet. Geol. Bull.**, V. 52, 2208-2230.

Johnson, G.L., McMillan, N.J. and Egloff. J.

1975 "East Greenland Continental Margin", in **Canada's Continental Margins and Offshore Petroleum Exploration**, C.J. Yorath, E.R. Parker and D.J. Glass, (Eds.) Can. Soc. Petrol. Geol., Memoir 4, 205-224.

Johnson, R.F.

1967 "The distribution and significance of frosted sand grains on core samples from Ungava Bay and Hudson Strait, northern Canada"; Unpublished **B.Sc. Thesis, M.I.T.**, 37 pp.

Johnston, W.A.

1921 "Sedimentation of the Fraser River delta", **Can. Geol. Surv. Memoir** 125, 46 pp.

Jonsson, I.G.
1966 "Wave boundary layers and friction factors". In **Proc. 10th Conf. Coastal Eng.**, Tokyo, 1965, ASCE, V. 1, 127-148.

Jonsson, I.G. and Carlsen, N.A.
1976 "Experimental and theoretical investigations in an oscillatory turbulent boundary layer". **J. Hydraul. Res.** V. 14 (1), 45-60.

Jopling, A.V.
1963 "Hydraulic studies on the origin of bedding". **Sedimentology** V. 2, 115-121.

Josenhans, H.W.
1983 "Evidence of pre-late Wisconsinan glaciations on the Labrador Shelf - Cartwright Saddle region". **Can. J. Earth Sci.**, V. 20, 225 - 235.

Josenhans, H.W. and Barrie, J.V.
1982 "Preliminary results of submersible observations on the Labrador Shelf." **Can. Geol. Surv. Current Res.**, Part B, 269-276.

Josenhans, H.W., King, L.H. and Fader. G.B.
1979 "A sidescan sonar mosaic of pockmarks on the Scotian Shelf. **Can. J. Earth Sci.**, V. 15, 831-840.

Kachel, N.B. and Sternberg, R.W.
1971 "Transport of bedloads as ripples during an ebb current". **Mar. Geol.** V. 19, 229-244.

Kalkanis, G.
1964 "Transport of bed material due to wave action", **U.S. Army Corps of Eng.**, Tech. Memo # CERC 2, 38 pp.

Kamphuis, J.W.
1975 "Friction Factor Under Oscillatory Waves", **ASCE, J. Waterways, Harbors and Coastal Eng.**, V. 101 (WW2), Pap. #11292, 135-144.

Karasev, I.F.
1964 "The regimes of eroding channels in cohesive materials", **Sov. Hydrol. Sel. Pap.** (Am. Geophys. Union) V. 6.

Keen, C.E., Keen, M.J., Ross, D.I. and Lack, M.
1974 "Baffin Bay: small ocean basin formed by sea-floor spreading", **AAPG Bull.**, V. 58, 1089-1108.

Kelly, W.E., Gularte, R.C. and Nacci, V.A.,
1976 "Erosion of Cohesive Sediments as Rate Process", **ASCE J. Geotech. Eng. Div.**, Tech. Notes, V. 105, (GT5), 673-676.

Kennedy, J.F.
1964 "The formation of sediment ripples in closed rectangular conduits and in the desert". **J. Geophys. Res.**, V. 69, 1517-1524.

1969 "The formation of sediment ripples, dunes and antidunes", **Annu. Rev. Fluid. Mech.** W.R. Sears (Ed.) V. 1. 147-168.

Kennedy, J.F. and Locher. F.A.
1972 "Sediment suspension by water waves". in **Waves on Beaches and Resulting Sediment Transport**, R.E. Meyer (ed.). N.Y., Academic Press, 249-295.

Kenyon, N.H.
1970 "Sand ribbons of European tidal seas", **Mar. Geol.** V. 9, 25-39.

Keulegan, G.H. and Carpenter, L.H.

1958 "Forces on cylinders and plates in an oscillating fluid", **J. Res. Nat. Bur. Stand.** (U.S.), V. 60, #5, 423-440.

King, L.H.

1969 "Submarine end marines and associated deposits on the Scotian Shelf". **Geol. Soc. Am. Bull.** V. 80, 83-96.

1970 "Surficial Geology of the Halifax-Sable Island Map Area", Dep. EMR, Ottawa, **Mar. Sci. Branch** Pap. 1, 16 pp.

1976 "Relict iceberg furrows on the Laurentian Channel and Western Grand Banks", **Can. J. Earth Sci.**, V. 13, 1082-1092.

1979 "Aspects of regional surficial geology related to site investigation requirements - Eastern Canadian Shelf" in **Offshore Site Investigation**, Ardus, D.A. (Ed.) London; Graham and Trotman, 37-60.

King, L.H. and Fader, G.B.

1980 "Seabed conditions east of the Avalon Peninsula to the Virgin Rocks - their relationship to the feasibility of a pipeline from the Hibernia P-15 wellhead area to Newfoundland", **Can. Geol. Sur.** Open File Report 723.

King, L.H. and MacLean, B.

1970 "Pockmarks on the Scotian Shelf". **Geol. Soc. Am. Bull.**, V. 81, 3141-3148.

Klein, G. de V.

1977 "Sedimentary processes, and processes of detrital sedimentation", **S.E.P.M., Reprint series**, # 4, 236 pp.

Komar, P.D.
1971 "Nearshore cell circulation and the formation of giant cusps". **Geol. Soc. Am. Bull**, V. 82, 2643-2650.

1973 "An occurrence of 'brick pattern' oscillatory ripple marks at Mono Lake, California", **J. Sediment. Petrol.** V. 43(4), 1111-1113.

1974 "Oscillatory ripple marks and the evaluation of ancient wave conditions and environments". **J. Sediment. Petrol.** V. 44(1), 169-180.

Komar, P.D. and Miller, M.C.
1973 "The threshold of sediment movement under oscillatory water waves". **J. Sediment. Petrol.**, V. 43, # 4, 1101-1110.

1975 "On the comparison between the threshold of sediment motion under waves and unidirectional currents, with a discussion of the practical evaluation of the threshold". **J. Sediment. Petrol.**, V. 45, 362-367.

Komar. P.D. and Reimers, C.E.
1978 "Grain shape effects on settling rates". **J. Geol.** V. 86, 193-209.

Kovacs, A. and Mellor. M.
1974 "Sea ice morphology and ice as a geologic agent in the southern Beaufort Sea", in **The Coast and Shelf of the Beaufort Sea**. Reed, J.C. and Sater. J.E., (Eds.), Arctic Inst. N. Am., Arlington, Va., 113-161.

Kranck, K.
1966 "Sediments of Exeter Bay. Baffin Island, District of Franklin" **Can. Geol. Surv.** Pap. 66-8, 60 pp.

Krone, R.B.

1962 Flume Studies of the Transport of Sediment in Estuarial Shoaling Processes". **Univ. Calif., Berkeley, Hydraul. Eng. Lab.**, Final rep. to U.S. Army Corps of Eng. Contract No. DA-04-203, 110 pp.

1963 "A study of rheological properties of Estuarial sediments", U.S. Army Corps of Eng., **Committee on Tidal Hydraul.**, Tech. Bull. #7, 91 pp.

Krugermeyer, L. and M. Grunwald

1978 "The influence of sea waves on the wind profile. **Boundary Layer Meteorol.** V. 10, 403-414.

Krumbein, W.C. and Pettijohn, F.J.

1938 **"Manual of Sedimentary Petrography"** N.Y.; Appleton - Century - Crofts, 549 pp.

Kulm, L.D., Rousch R.C., Harlett, J.C., Neudeck, R.H., Chambers, D.M. and Runge, E.J.

1975 "Oregon continental shelf sedimentation: Interrelationships of facies distribution and sedimentary processes". **J. Geol.**, V. 83, 145-176.

Kurtz, D.D. and Anderson, J.B

1979 "Recognition and sedimentological description of recent flow deposits from the Ross and Weddell Seas, Antarctica". **J. Sediment. Petrol.**, V. 49 (4), 1159 - 1170.

Laursen, E.M.

1958 "The total sediment load of streams". **ASCE J. Hydraul. Div.**, V. 84 (HYI), Pap. 1530.

Leliavsky, S.

1966 **"An Introduction to Fluvial Hydraulics"**. Dover Publishing Inc., 257 pp.

Lerand, M.
1973 "Beaufort Sea"; in **Future Petroleum Provinces of Canada**, R.G. McCrossan (Ed.); Can. Soc. Petrol. Geol., Memoir 1, 315-386.

Lettau, H.
1969 "Note on aerodynamic roughness - parameter estimation on the basis of roughness element description." **J. Appl. Meteorol.**, V. 8, 828-832.

Lewis, C.F.M.
1978 "The frequency and magnitude of drift-ice groundings from ice-scour tracks in the Canadian Beaufort Sea". **Proc. 4th Intl. Conf. on Port and Ocean Eng. Under Arctic Conditions**, (POAC, 1977), St. John's, Nfld., Fac. Eng., Memorial Univ., V. 1. 568-579.

1981 "**CSS Baffin** 81-012 Cruise Report". **B.I.O. Cruise Report 81-012.**

Lewis, C.F.M. and Barrie. J.V.
1980 "Ice scour studies on the Labrador Shelf". **Workshop on Research in the Labrador Coastal and Offshore Region**, Goose Bay. Labrador; Memorial Univ. of Newfoundland; 264-265.

1981 "Geological evidence of iceberg groundings and related seafloor processes in the Hibernia Discovery area of Grand Bank, Newfoundland" in **Symposium on Production and Transportation Systems for the Hibernia Discovery**, St. John's, Nfld., Feb. 1981. C-CORE Report 81-8, 146-177.

Lewis, C.F.M., Blasco, S.M., Bornhold, B.D., Hunter, J.A.M., Judge, A.S., Kerr, W.J., McLaren, P. and Pelletier, B.R.
1977 "Marine geological and geophysical activities in Lancaster Sound and adjacent fiords"; in **Can. Geol. Sur. Rep. of Activities, Part A,** Pap. 77-1A, 495-506.

Lewis, C.F.M., MacLean. B. and Falconer, R.K.M.
1979 "Iceberg scour abundance in Labrador Sea and Baffin Bay: A reconnaissance of regional variability". in **Proc. 1st Can. Conf. Mar. Geotech. Eng.,** Calgary, Alberta; Can. Geotech. Soc., Montreal; 79-94.

Lewis, J. and Benedict, C.P.
1981 "Icebergs on the Grand Banks: oil and gas considerations", **World Oil,** January 1981.

van der Linden, W.J.M., Fillon R.H. and Monahan, D.
1976 "Hamilton Bank, Labrador Margin: Origin and evolution of a glaciated shelf". **Can. Geol. Sur. Pap.** 75-40.

Loken, O.H. and Hodgson, D.A.
1971 "On the submarine geomorphology along the east coast of Baffin Island"; **Can. J. Earth Sci.,** V. 8, 185-195.

Longuet-Higgins, M.S.
1953 "Mass transport in water waves". **Phil. Trans. Roy. Soc. London.** Ser. A, #245, 535-581.

Lowe, D.R.
1976 "Grain Flows and Grain Flow Deposits". **J. Sediment. Petrol.** V. 46 (1), 188 - 199.

Ludwick, J.C.
1974 "Tidal currents and zig-zag sand shoals in a wide estuary entrance". **Geol. Soc. Am. Bull.,** V. 85, #5, 717-726.

1972 "Migration of Tidal Sand Waves in Chesapeake Bay Entrance", in **Shelf Sediment Transport.** Swift, D.J.P., Duane. D.B., and Pilkey. O.H (Eds.), Stroudsberg, Pa., Dowden, Hutchinson and Ross Inc., 377-410.

Luternauer. J.L.
1977 "Fraser delta sedimentation" in **Rep. of Activities, Part A; Can. Geol. Surv.,** Pap. 77-1A, 65-72.

Luternauer, J.L., and Murray. J.W.
1969 "Sediments of Queen Charlotte Sound, British Columbia"; in **Rep. of Activities, Part A, Can. Geol. Surv.** Pap. 69-1, 9-12.

Luternauer, J.L. and Swan. D.
1978 "Kitimat submarine slump deposits: a preliminary report" in **Report of Activities, Part A; Can. Geol. Surv.** Pap. 78-1A, 327-332.

MacKay, J.R.
1973 "The growth of Pingos, Western Arctic Coast, Canada". **Can. J. Earth Sci.,** V. 10, 979-1004.

1977 "Pulsating Pingos, Tuktoyaktuk Peninsula. N.W.T.", **Can. J. Earth Sci.,** V. 14, 209-222.

1978 "Sub-Pingo water lenses, Tuktoyaktuk Peninsula, N.W.T.", **Can. J. Earth Sci.,** V. 15, 1219-1227.

MacLean, B.
1979 "Geological/Geophysical studies in Baffin Bay and Scott Inlet - Buchan Bay and Cape Dyer - Cumberland Sound areas of the Baffin Island Shelf", **Can. Geol. Sur.,** Current Res., Part B: Paper 79-1B, 231-244.

1982a "Cruise report HU82-034", **B.I.O., unpublished report.**

1982b "Investigations of Baffin Island shelf from surface ship and research submersible in 1981", **Can. Geol. Sur., Sci. Tech. notes** in Current Res., Part A. Pap. 82-1A. 445-447.

Maclean, B., Jansa, L.F., Falconer, R.K.H., and Srivastava, S.P.
1977 "Ordovician Strata on the southeastern Baffin Island Shelf revealed by shallow drilling", **Can. J. Earth Sci.**, 14, 1925-1939.

MacLean, B., Falconer. R.K.H., and Levy. E.M.
1981 "Geological, geophysical and chemical evidence for natural seepage of petroleum off the northeast coast of Baffin Island", **Bull. Can. Petrol. Geol.**, V. 29 (1) 75-95.

Madsen, O.S. and Grant. W.D.
1975 "The threshold of sediment movement under oscillatory water waves: A discussion". **J. Sediment. Petrol.** V. 45, 360-361.

1976 "Sediment transport in the coastal environment", **Ralph M. Parsons Lab. (MIT), Rep. #** 209, 105 pp.

1977 "Quantitative description of sediment transport by waves", **Proc. 15th Conf. Coastal Eng.**, Honohulu, Hawaii, ASCE, V. 2. 1093-1112.

Mann, R.G., and Swift, D.J.P.
"Size classes of flow-transverse bedforms in a subtidal environment, Nantucket Shoals, North American Atlantic Shelf". Unpublished MS., NOAA, Miami. Fla., 8 pp.

Manohar, M.
1955 "Mechanics of bottom sediment movement due to wave action", **U.S. Army Corps of Eng., Beach Erosion Board**, Tech. Memo No. 75, 121 pp.

Marlowe, J.I.

1965 "Sedimentology of the Prince Gustaf Adolf Sea area. District of Franklin", B.I.O. Unpublish. MS, Rep. #65-15, 140 pp.

1967 "The geology of part of the continental slope near Sable Island, Nova Scotia". **Can. Geol. Sur.** Pap. 65-38, 30 pp.

1968 "Unconsolidated marine sediments in Baffin Bay", **J. Sediment. Petrol.**, V. 38, 1065-1078.

Martin, C.S.

1963a "Transition of Oscillatory Boundary-Layer Flow", in **Tech. Rep. No. 3, Project No. A-628,** Georgia Institute of Technology. 1-11.

1963b "The effect of uplift on incipient motion of bed particles", **Georgia Institute of Technology,** Tech. Rep No. 3, Project No. A-628, 12-22.

Masch, F.D. and Espey, W.H., Jr.

1965 "Effects of some soil properties on the critical hydraulic shear stress of cohesive sediments", Univ. Tex., Dept. Civil Eng., Austin, TX, 26 pp.

Masch, F.D. and Espey, W.H., Jr. and Moore, W.L.

1965 "Measurements of the shear resistance of cohesive sediments", U.S. Dept. Agric., **Agric. Res. Serv., Misc. Publ.** # 970 p. 151-155.

McCave, I.N.

1973 "Some boundary layer characteristics of tidal currents bearing sand in suspension". **Mem. Soc. Roy. Sci.** Liege. 6th ser., # 6., 107-126.

1979 "Suspended material over the central Oregon continental shelf in May 1974; 1, Concentrations of organic and inorganic component". **J. Sediment. Petrol.** V. 49(4), 1181-1194.

McLaren, P.
1977 "The coasts of Eastern Melville and Western Byam Martin Islands: Coastal processes and related geology of a high Arctic environment". **Unpublished Ph.D. Thesis,** Univ. South Carolina, 304 pp.

1982 "The coastal geomorphology. sedimentology and processes of eastern Melville and western Byam Martin islands, Canadian arctic archipelago" **Can. Geol. Surv. Bull. #333.** 39 pp.

McKee, E.D., and Weir, C.W.
1953 "Terminology for Stratification and Cross-Stratification in Sedimentary Rocks". **Geol. Soc. Am. Bull.,** V. 64, 381-390.

McLeish, W., Swift. D.J.P., Ross, D. and Merrill. G.
1981 Seafloor bedforms recorded by radar, southern Bight of North Sea". unpublished MS. NOAA, Miami. Florida. 12 pp.

McMillan, N.J.
1973 "Shelves of Labrador Sea and Baffin Bay, Canada", in **Future Petroleum provinces of Canada,** R.G. McCrossan (Ed.), Can. Soc. Petrol. Geol. Memoir # 1, 473-518.

McPhee, M.G. and Smith, J.D.
1976 "Measurements of the turbulent boundary layer under pack ice". **J. Phys. Oceanogr.** V. 6, 696-711.

McQuivey. R.S. and Keefer. T.N.
1969 "The relation of turbulence to deposition of magnetite over ripples", **U.S. Geol. Surv. Prof. Pap.** 650-D, 244-247.

Mehta, A.J.
1977 "Sediment Movements", in **Hydraulic Behaviour of Estuaries** McDowell, D.M. and B.A. O'Connor (Eds.), N.Y.; Wiley.

Mehta, A.J. and Hayter, E.J.
1981, "Preliminary investigation of fine sediment dynamics in cumbarjua canal, Goa, India", **Coastal and Oceanogr. Eng. Dept., Univ. Fla.,** Rep. UFL/COEL-81/012, 67 pp.

Mehta, A.J. and Parthenaides, E.
1979 "Kaolinite resuspension properties", **ASCE J. Hydraul. Div.,** Tech. Notes V. 105, (HY4), 411-416.

Meland, N. and Norrman, J.O.
1969 "Transport velocities of individual size fractions in heterogeneous bed load" **Geog. Ann.,** Ser. A, V. 51, 127-144.

Merrifield, P.M. and Lamar, D.L.
1968 "Sand waves and early earth-moon history". **J. Geophys. Res.** V. 73 (14), 4767-4774.

Middleton, G.V.
1965 "Primary sedimentary structures and their hydrodynamic interpretation". **S.E.P.M. Spec. Pub.** 12.

1966 "Small scale models of turbidity currents, and the criterion for auto-suspension", **J. Sediment. Petrol.,** V. 36 (1), 202-208.

1976 "Hydraulic interpretation of sand size distributions". **J. Geol.,** V. 84, 405-426.

Middleton, G.V. and Hampton, M.A.
1976 "Subaqueous sediment transport and deposition by sediment gravity flows" in **Marine sediment transport and environmental management.** D.J. Stanley, and D.J.P. Swift. (Eds.) N.Y.; J. Wiley & Sons., 197-218.

Middleton, G.V. and Southard, J.B.
1977, "Mechanics of sediment movement" **S.E.P.M. Eastern Section, Short Course #** 3, Lecture notes, 246 pp.

Miller, M.C. and Komar, P.D.
1980 "A field investigation of the relationship between oscillation ripple-spacing and the near-bottom water orbital motions. **J. Sediment. Petrol.** V. 50(1), 183-191.

Milliman, J.D.
1976 "Sand and gravel deposits off southwestern Vancouver Island, British Columbia", **Can. Geol. Surv. Rep. of Activities**, Part A; Pap. 75-1A, 23-26.

Milliman, J.D. and Emery, K.O.
1968 "Sea levels during the past 35,000 years", **Science** 162, 1121-1123.

Mooers, C.N.K.
1976 "Introduction to the physical oceanography and fluid dynamics of continental margins". in **Marine Sediment transport and environmental management.** D.J. Stanley and D.J.P. Swift (Eds.), N.Y.: Wiley Inc., 7-21.

Moore. H.J., Boyce. J.M., and Hann. D.A.
1980 "Small impact craters in the lunar regolith - their morphologies, relative ages, and rates of formation". **The Moon and the Planets**, V. 23, 231-252.

Moore, W.L. and Masch, F.D., Jr.
1962 "Experiments on the Scour Resistance of Cohesive Sediments", **J. Geophys. Res.,** V. 67, #4, 1437-1446.

Murray, J.F.
1969 "The drift, deterioration and distribution of icebergs in the North Atlantic Ocean", **CIM Special** Vol.10, The Ice Seminar, 3-18.

Nakato, T., Locher, F.A., Glover, J.R. and Kennedy, J.F.
1977 "Wave Entrainment of sediment from Rippled Beds", **ASCE J. Waterways, Port, Coastal and Ocean Division,** V. 103 (WW1), Pap. #12736, 83-99.

National Research Council
1979 **"Continental margins: Geological and Geophysical Research Needs and Problems"**, Washington; Natl. Acad. Sci., 302pp.

Neill, C.B. and Yalin, M.S.
1969 "Quantitative definition of beginning of bed movement", ASCE J. Hydraul. Div. V. 95 (HYI) 585-588.

Nelsen, T.A.
1976 "An Automated Rapid Sediment Analysis, 'ARSA' " **Sedimentology,** V. 23, 867-872.

Newton, R.S.
1968 "Internal Structure of wave formed ripple marks in the near-shore zone". **Sedimentology** V. 11, 275-292.

Newton, R.S., Seibold, E., and Werner, F.
1973 "Facies distribution patterns on the Spanish Sahara continental shelf mapped with sidescan sonar". **Meteor Forschungsergebnisse,** Series C, V. 15, 55-77.

Newton, R.S. and Werner, F.
1972 "Transitional - size ripple marks in Kiel Bay". **Meyniana** 22, 89-94.

Ninomiya. K., Tagaya. K., and Murase. Y.
1972 "A study on suction and scouring of sit-on-bottom type offshore structures", 4th Annual **OTC 1605**, 1972, Vol.1, Pap #1605, 869-878.

Palmer, H.D.
1969 "Wave-induced scour on the sea floor", **Proc. Conf. Civil Eng. in the Ocean II**, Miami Beach; ASCE; 703-716.

Parker, G., Lanfredi, N.W. and Swift, D.J.P.
1982 "Substrate response to flow in a southern hemisphere sand ridge field: Argentine Inner Shelf". **Sedimentary Geology**, V. 33, 195-216.

Parrott, D.R., Dodds, D.J., King, L.H. and Simpkin, P.G.
1980 "Measurement and evaluation of the accoustic reflectivity of the seafloor." **Can. J. Earth Sci.**, 17. 722-737.

Parthenaides, E.
1965 "Erosion and deposition of cohesive soils", **ASCE Proc., J. Hydraul. Div.**, V. 91, (HY1), Proc. Pap. 4202, 105-139.

1971 "Results of recent investigations on erosion and deposition of cohesive sediments" in **River Mechanics**, H.W. Shen, (Ed.) Colo. State Univ., 25-1 to 25-91.

Parthenaides, E., Kennedy, J.F., Etter, R.J. and Hoyer, R.P.
1966 "Investigations of the depositional behaviour of fine cohesive sediments in an annual rotating channel", Contract No. AID/la-118 for Agency for International Development, U.S. State Dept., **M.I.T. Dept. Civil Eng.** Hydrodyn. Lab. Rep. # 96, R66-28, 81 pp.

Parthenaides, E. and Mehta, A.J.
1971 "Reposition of fine sediments in turbulent flows", US. EPA Water Poll. Control Res. Ser., #16050 ERS 08/71, 39 pp.

Parthenaides, E. and Paaswell, R.E.
1970 "Erodibility of channels with cohesive boundary", **ASCE J. Hydraul. Div.**, V. 96 (HY3), Proc. Paper 1156, 755-771.

Peake, D.J. and Galway, R.D.
1965 "The three-dimensional separation of a plane incompressible laminar boundary layer produced by a circular cylinder mounted normal to a flat plate", **Natl. Res. Coun. Can.**, Rep. LR-428, 16 pp.

Pelletier. B.R.
1964 "Development of submarine physiography in the Canadian Arctic and its relation to crustal movements" B.I.O. Unpublish. MS. Rept., # 64-16, 45 p.

1966 "Development of submarine physiography in the Canadian Arctic and its relation to crustal movements"; in **Symposium on continental Drift**, G.V. Garland, (ed.), Royal Society of Canada, Special Publ. # 9, 77-101.

1975 "Sediment dispersal in the southern Beaufort Sea" **Environment Can. Beaufort Sea Project**, Beaufort Sea Tech. Rep. No. 25a, 80 pp.

1979 "Review of surficial geology and engineering hazards in the Canadian offshore", **Marit. Sediments**, V. 15, # 2/3, 55-91.

Pelletier, B.R. and Shearer, J.M.
1972 "Sea bottom scouring in the Beaufort Sea of the Arctic Ocean," in **Proc. 24th Int Geol. Cong.**, Sect. 8, 'Mar. Geol. and Geophys.', 251-261.

Pelletier, B.R., Ross, D.I., Keen, C.E., and Keen , M.J.
1975 "Geology and geophysics of Baffin Bay;" **Can. Geol. Surv.,** Pap. 74-30, 247-258.

Pereira, C.P.G., and Gillespie. R.J.
"Southeast Baffin Island Continental Shelf sediments and iceberg scours study program: results," **C-CORE Tech. Rep.** (in prep).

Pereira. C.P.G., Woodworth-Lynas, C.M.T., and Barrie. J.V.
"Hekja wellsite iceberg scouring analysis;" **C-CORE Tech. Rep.** (in prep).

Perry, R.B.
1961 "A study of the marine sediments of the Canadian eastern Arctic Archipelago," **Can. Fish. Res. Board,** MS Rep. # 89, 89 pp.

Petrie, B. and Bowen, A.J.
1979 "Bottom currents near the shelf edge". (Abstract). **Atmosphere-Ocean** 17, 60.

Pettijohn, F.J., Potter, P.E. and Siever, R.
1972 **"Sand and Sandstone".** N.Y., Springer-verlag, 618 pp.

Pharo, C.H. and Barnes, W.C.
1976 "Distribution of surficial sediments of the central and southern Strait of Georgia, British Columbia;" **Can. J. Earth Sci.,** V. 13, # 5, 684-696.

Pilkey, O.H., Trumbull, J.V.A., and Bush, D.M.
1978 "Equilibrium shelf sedimentation, Rio de la Plata Shelf, Puerto Rico". **J. Sediment. Petrol.** V. 48 (2), 389-400.

Pilkington, G.R. and Marcellus, R.W.
1981 "Methods of determining pipeline trench depths in the Canadian Beaufort Sea." Proc. **6th Int. Conf. on Port and Ocean Eng. Under Arctic Conditions,** (POAC 1981), Quebec, Dep. de genie civil, Univ. Laval, V. 2, 674-687.

Piper, D.J.W.
1974 "A late Quaternary stratigraphic marker in the central basin of Baffin Bay;" **Marit. Sediments,** V. 9, 62-63.

Pond, S. and G.L. Pickard.
1978 **"Introductory Dynamic Oceanography"** London: Pergamon International Library. Pergamon Press.

Poole, D.M.
1957 "Size analysis of sand by a sedimentation technique", **J. Sediment. Petrol.** V. 27, (4), 460-468.

Poole, D.M., Butcher Q.Q. and Fisher, R.L.
1951 "The use and accuracy of the Emery settling tube for sand analysis". **U.S. Army Corps. of Eng., Beach Erosion Board** Tech. Memo # 23.

Powers, M.
1953 "A new roundness scale for sedimentary particles". **J. Sediment. Petrol.,** V. 23, 117-119.

Praeg, D.B.
1982 "Seafloor relief - Baffin Island shelf;" **Can. Geol. Surv., Open File Rep. # 862,** 5 pp, 4 maps.

Prest, U.K.
1970 "Quaternary geology;" In **Geology and Economic Minerals of Canada.** Can. Geol. Surv., Economic Geology Report 1, 675-764.

Prior, D.B. and Coleman, J.M.

1981 "Geologic mapping for offshore engineering, Mississippi delta". in **Proc. 13th Annu. Offshore Tech. Conf.**, Pap. 4119, 35-38.

Rance, P.J. and Warren, N.F.

1968 "The threshold of movement of coarse material in oscillatory flow", **ASCE Proc. 11th Conf. on Coastal Engineering**, London, 1968, 487-491.

Raudkivi, A.J.

1963 "Study of sediment ripple formation". **Proc. ASCE, J. Hydraul. Div.**, V. 89, pap. 1146, 15-33.

1967 **"Loose Boundary Hydraulics"**, Oxford, Pergamon Press. 331 pp.

Reading, H.G., (Ed.)

1979 **"Sedimentary Environments and Facies,"** New York, Elsevier, 557 pp.

Reimnitz, E. and Barnes, P.W.

1974 "Sea ice as a geological agent on the Beaufort Sea shelf of Alaska," in **'The Coast and Shelf of the Beaufort Sea'**, J.C. Reed and J.E. Sater (Eds.) Arctic Inst. of N. Am., 301-353.

Reimnitz, E., Barnes, P.W., Toimil, L.J. and Melchior. J.

1977 "Ice gouge recurrence and rates of sediment reworking, Beaufort Sea. Alaska". **Geology**, V. 5, 405-408.

Reineck, H.E. and Singh, I.B.

1967 "Primary sedimentary structures in the recent sediments of the Jade, North Sea". **Mar. Geol.**, V. 5, 227-235.

1975 **"Depositional Sedimentary Environments"**, Berlin, Springer - verlag, 439 pp.

Reineck, H.E., and Wunderlich, F.
1968 "Classification and origin of flaser and lenticular bedding". **Sedimentology** V. 11, 99-104.

Reinson, G.E.
1977 "Examination of bedforms in shallow water using sidescan sonar, Miramichi Estuary, N.B." **Can. Geol. Surv.**, Pap. 77-1B, 99-105.

Rektorik, R.J. and Smerdon, E.T.
1964 "Critical shear stress in cohesive soils, from rotating shear apparatus", ASAE trans., June, Pap. # 64-216.

Rouse, H.
1937 "Modern conceptions of the mechanics of turbulence". **A.S.C.E. Trans.**, V. 102, 436-505.

1939 "Experiments on the mechanics of sediment suspension:" in **Proc. 5th Intl. Cong. Applied Mech.**, Cambridge, Mass. 550-554.

1950 **"Engineering Hydraulics"** N.Y.; J. Wiley & Sons. 1039 pp.

1961 **"Fluid Mechanics for Hydraulic Engineers,"** N.Y., Dover, 422 pp.

Rubey, W.W.
1933 "Settling velocities of gravel, sand and silt particles" **Am. J. Sci.**, V. 25, 325-338.

Ruffman, A., Meagher, L. and Stewart, J.M.
1978 "Sable Island sand waves and related shore processes". **Marit. Sediments**, V. 14, 35.

Ryckborst, H.
1975 "On the origin of Pingos", **J. Hydrol.**, V. 26, 303-314.

Sanders, J.E.
1965 "Primary sedimentary structures formed by turbidity currents and related resedimentation mechanisms" in **Primary Sedimentary Structures and their Hydrodynamic Interpretation.** G.V. Middleton (Ed.), S.E.P.M. Spec. Publ. # 12, 265 pp, 192-219.

Schlichting, H.
1960 **"Boundary layer theory".** N.Y.: McGraw Hill 4th Ed. 647pp.

Schwind, R.G.
1962 "The three-dimensional boundary layer near a strut", **M.I.T. Gas Turbine Lab. Rep.**, # 67, 26 pp.

Selley, R.C.
1979 "Concepts and methods of subsurface facies analysis". **AAPG Continuing Ed. Course Note Series #9**. Dec. 1979.

Shearer, J.M.
1971 "Preliminary interpretation of shallow seismic reflection profiles from the west side of Mackenzie Bay, Beaufort Sea;" in **Can. Geol. Surv., Rep. of Activities**, Part B; Pap. 71-1B, 131-138.

Shearer, J.M. and Blasco, S.M.
1975 "Further observations of the scouring phenomena in the Beaufort Sea". **Can. Geol. Surv., Current Res. Part A**, 483-493.

Shen. H.W., Schneider, V.R., and Karaki, S.S.
1966 "Mechanics of Local Scour", **Colorado State Univ. Eng. Res. Cent.**, Rept. No. CER66HWS22, 55 pp.

Shepard, F.P.

1931 "St. Lawrence (Cabot Strait) submarine trough." **Geol. Soc. Am. Bull.**, 42, 853-864.

1961 "Deep-sea sands." **21st Int. Geol. Congr. Rep.**, pt. 23., 26-42.

Shields, A.

1936 "Anwendung der Ahnlichkeitsmechanik und der Turbulenzforschung auf die Geschiebebewegnung", **Mitteilungen der Preuss.** Versuchsanst. fur Wasser, Erd. und Schiffbau, Berlin, v. 26, 26 pp., (for translation see Middleton, G.V. and Southard, J.B. 1977.)

Simons, D.B., Richardson, E.V. and Nordin, C.F.

1965 "Sedimentary structures generated by flow in alluvial channels" in **Preliminary sedimentary structures and their hydrodynamic interpretation** Middleton. G.V.(Ed.) S.E.P.M. Special Pub., #12, 34-52.

Slatt, R.M.

1974 "Continental shelf sediments off eastern Newfoundland: a preliminary investigation." **Can. J. Earth Sci.**, V. 11, 362-368.

Slatt. R.M. and Lew, A.B.

1973 "Provenance of Quaternary sediments on the Labrador continental shelf and slope." **J. Sediment. Petrol.**, 43, 1054-1060.

Smerdon, E.T. and Beasley, R.P.

1959 "Tractive force theory applied to stability of open channels in cohesive soils", Research Bulletin # 715, **Univ. Missouri, Agric. Exp. St.**, Columbia, Mo.

1961 "Critical tractive forces in cohesive soils". **Agric. Eng.,** 26-29.

Smith, J.D.

1969 "Investigations of turbulent boundary layers and sediment transport phenomena as related to shallow marine environments. Part 2. Studies of non-uniform boundary layer flows". **Univ. of Washington, Dept. of Oceanogr.** Report A 69-7.

1970 "Stability of a sand bed subjected to a shear flow of low Froude number", **J. Geophys. Res.** V. 75, No. 30, 5928-5940.

1977 "Modelling of sediment transport on continental shelves", in **The Sea, Vol. 6,** E.D. Goldberg, I.N. McCave, J.J. O'Brien and Q.Q. Steele (Eds.), N.Y., Wiley-Interscience.

Smith, J.D. and Hopkins, T.S.

1972 "Sediment transport on the continental shelf off Washington and Oregon in light of recent current measurements" in **Shelf Sediment Transport.** D.J.P. Swift, D.B. Duane, and O.H. Pilkey, (Eds.) Stroudsberg, Penn., Dowden, Hutchinson and Ross, Inc., 143-180.

Smith, J.D. and McLean, S.R.

1977 "Spatially averaged flow over a wavy surface". **J. Geophys. Res.** V. 82, 1735-1746.

Smith, R.J.

"Working with sea floor sediments". Dept. Oceanography, Naval Postgrad. School. 20-25.

Sorby, H.C.

1859 "On the structures produced by the currents present during the deposition of stratified rocks". **Geologist** V. 2. 137-147.

Soulsby, R.L.
1980 "Selecting record length and digitization rate for near-bed turbulence measurements". **J. Phys. Oceanogr.**, V. 10, 208-219.

Soulsby, R.L. and Dyer, K.R.
1981 "The form of the near-bed velocity profile in a tidally accelerating flow". **J. Geophys. Res.**, V. 86, 8067-8074.

Southard, J.B.
1971 "Representation of bed configurations in depth-velocity-size diagrams". **J. Sediment. Petrol.** V. 1, 41, 903-915.

Srivastava, S.P.
1981 "Davis Strait: structure, origin and evolution", in **Proc. NATO Advanced Res. Inst. Symp.**, Bressanone, Italy, May 1981, 34 pp.

Srivastava, S.P., Baret, D.L., Keen, C.E., Manchester, K.S., Shih, K.G., Tiffen, D.L., and Lister, C.R.B.
1971 "Preliminary analysis of geophysical measurements north of Juan de Fuca Ridge", **Can. J. Earth Sci.**, V. 8, # 10, 1265-1281.

Stanley, D.J. (Ed.)
1969 "Outer shelf sedimentation; processes and products". in **The New Concepts of Continental Margin Sedimentation.** A.G.I. Short Course lecture notes. 400 pp.

Stanley, D.J. and Maldonado, A.
1981 "Depositional models for fine-grained sediment in the Western Hellenic trench, Eastern Mediterranean". **Sedimentology**, V. 28, 273-290.

Stanley, D.J., Swift, D.J.P., Silverberg, N., James, N.P. and Sutton, R.G.
1971 "Recent sand spill-over off Sable Island Bank, Scotian Shelf." **Can. Geol. Surv.**, pap. 71-23, 167-194.

Stanley, D.J. and Swift. D.J.P. (Eds.)
1976 **"Marine sediment transport and environmental management"**. N.Y.; John Wiley Inc., 602 pp.

Sternberg, R.W.
1968 "Friction factors in tidal channels with differing bed roughness". **Mar. Geol.**, V. 6, 243-260.

1970 "Field measurementns of hydrodynamic roughness in the deepsea boundary", **Deepsea Research**, Vol. 17, 413-420.

1971 "Measurements of incipient motion of sediment particles in the marine environment". **Mar. Geol.**, V. 10, 113-119.

1972 "Predicting initial motion and bed-load transport of sediment particles in the shallow marine environment", in **Shelf Sediment Transport**, D.J.P. Swift, D.B. Duane and O.H. Pilkey (Eds.), Stroudsburg, PA., Dowden, Hutchinson and Ross Inc., 61-82.

Sternberg, R.W. and Larson, L.H.
1975 "Threshold of sediment movement by open ocean waves: observations", **Deep Sea Res.**, V. 22, 299-309.

1976 "Frequency of sediment movement on the Washington continental shelf: a Note", **Mar. Geol.**, V. 21, m37-m47.

Stewart, H.B. and Jordan, G.F.
1964 "Underwater sand ridges on Georges Shoal", in **Papers in Marine Geology**, R.L. Miller (Ed.) N.Y., Macmillan, 102-114.

Stow, D.A.V.
1978 "Regional review of the Nova Scotia outer margin." **Marit. Sediments**, V. 14, 17-32.

Stow, D.A.V., and Bowen, A.J.
1980 "A Physical model for the transport and sorting of fine-grained sediment by turbidity currents", **Sedimentology**, V. 27, 31-46.

Stride. A.H., and Chesterman, W.D.
1973 "Sedimentation by non-tidal currents around northern Denmark". **Mar. Geol**, V. 15, m53-m58.

Strom, R.G.
1977 "Origin and relative ages of Lunar and Mercurain inter-crater plains". **Physics of the Earth and Planetary Interiors**, V. 15, 156-172.

Sundborg, A.
1956 "The river Klaralven, a study of fluvial processes", **Geograf. Ann.**, V. 38, 127-316.

Sutherland, A.J.
1967 "Proposed mechanism for sediment entrainment by turbulent flows", **J. Geophys. Res.**, V. 72, 6183-6194.

Swift, D.J.P.
1976 "Continental shelf sedimentation" in **Marine Sediment Transport and Environmental Management**, D.J. Stanley, and D.J.P. Swift. (Eds.) N.Y., J. Wiley and Sons, 311-350.

1981 "Storm built sand ridges on the Maryland inner shelf: a Preliminary Report", **Geo-Marine Letters, V. 1**, 33-37.

Swift. D.J.P., Duane. D.B. and Pilkey. O.H. (Eds.)
1972 "**Shelf Sediment Transport: Processes and Pattern**". Stroudsberg, PA.; Dowden. Hutchinson & Ross Inc.

Swift, D.J.P. and Field, M.E.
1981 "Evolution of a classic sand ridge fields, Maryland sector, N. American Inner Shelf" **Sedimentology**, V. 28(4), 461-482.

Swift, D.J.P. and Freeland, G.L.
1978 "Current lineations and sand waves on the inner shelf, middle Atlantic Bight of North America", **J. Sediment. Petrol.**, V. 48(4), 1257-1266.

Swift, D.J.P., Freeland, G.L. and Young, R.A.
1979 "Time and space distribution of megaripples and associated bedforms, Middle Atlantic bight, North American Atlantic Shelf", **Sedimentology**. V. 26 (3), 389-406.

Swift, D.J.P., Parker, G. and Figge, K.
1978 "Shoreface - connected sand ridges on American and European Shelves" A comparison". **Estuarine and coastal mar. sci.**, V. 7, 257-273.

Swift, D.J.P., Stanley, D.J., and Curray, J.R.
1971 "Relict Sediments on continental shelves: A reconsideration", **J. Geol.**, V. 79, 322-346.

Tanner, W.F.
1967 "Ripple mark indices and their uses", **Sedimentology**. V. 9, 89-104.

Taylor. P.A. and Dyer. K.R.
1977 "Theoretical models of flow near the bed and their implications for sediment transport". in **The Sea. Vol. 6**, E.D. Goldberg, I.N. McCave. J.J. O'Brien and Q.Q. Steele (Eds.). N.Y. , Wiley-Interscience, 579-601.

(Eds.). N.Y. , Wiley-Interscience, 579-601.

Taylor, P.A., Gent, P.R. and Keen, J.M.
1976 Some numerical solutions for turbulent boundary-layer flow above fixed, rough, wavy surfaces. **Geophys. J. Royal Astronom. Soc.**, V. 44, 177-201.

Tee, K.T.
1972 "The structure of three dimensional tide-generating currents: experimental verification of a theoretical model". **Estuarine, Coastal and Shelf Sci.**, V.14, 27-48.

Teleki, P.G.
1972 "Wave boundary layers and their relation to sediment tranpsort". in **Shelf Sediment Transport**, D.J.P. Swift, D.B. Duane and O.H. Pilkey (Eds.). Stroudsberg, Pa., Dowden, Hutchinson & Ross Inc., 21-54.

Terwindt, J.H.J. and Breusers, H.N.C.
1972 "Experiments on the origin of flaser, lenticular and sand-clay alternating bedding", **Sedimentology**, V. 19, 85-98.

Thacker, W.C. and Lavelle. J.W.
1978a "Stability of settling of suspended sediments", **Phys. fluids**, V. 21 (2), 291-292.

1978b "Effects of hindered settling on sediment concentration profiles", **J. Hydraul. Res.**, V. 16 (4), 527-535.

Thompson, W.O.
1937 "Original structures of beaches, bars and dunes, **Geol. Soc. Am. Bull**, V. 48, 723-752.

Thorsteinsson, R.
1958 "Cornwallis and Little Cornwallis Islands, District of Franklin, North West Territories", **Can. Geol. Surv. Memoir**

Tiffen, D.L.
1969 "Continuous seismic reflection profiling in the Strait of Georgie, British Columbia", **Univ. B.C., unpublished Ph.D. thesis,** Vancouver. Canada.

Tiffen. D.L., Bornhold, B.D., Yorath. C.J., Herzer, R.H., and Taylor, G.C.
1978 "Bottom sediments - vicinity of Juan de Fuca and Explorer Ridges, northwest Pacific Ocean", in **Can. Geol. Surv. Current Res., P. A**; Pap. 78-1A, 533-537.

Tiffen, D.L., Cameron, B.E.B., and Murray, J.W.
1972 "Tectonics and depositional history of the continental margin off Vancouver Island, B.C."; **Can. J. Earth Sci.**, V. 9, 280-295.

Trask, P.D.
1932 "The bathymetry and sediments of Davis Strait. chapter III"; in **The 'Marion' expedition to Davis Strait and Baffin Bay, 1928**; U.S. Coast Guard Bull. # 19, Part 1. 62-81.

1939 **"Recent Marine Sediments"**, New York, Dover Publ. Inc., 736 pp.

Trenhaile. A.S
1973 "Nearshore ripples; some hydraulic relationships". **J. Sediment. Petrol.**, V. 43(2), 558-568.

Tritton, D.J.
1977 **"Physical Fluid Dynamics".** London; Van Nostrand Reinhold.

U.S. Army Corps of Engineers
1973 **"Shore Protection Manual"**, Coastal Eng. Res. Cent., Washington, DC: U.S. Govt Printing Office, 3 vols., 1160 pp.

U.S. Hydraulic Laboratory
1941 "Measurement and analysis of sediment loads in streams", **Univ. Iowa Report #4**, 203 pp.

U.S. Sub-Committee on Sedimentation
1953 "Measurement and analysis of sediment load in streams". **Univ. Iowa, Report #** 10, Hydraulic Laboratory, 115 pp.

Vanoni, V.A.
1964 "Measurements of critical shear stress for entraining fine sediments in a boundary layer". **Calif. Inst. Tech., Keck Hydraul. Lab. Rept.** KH-R-7. 47 pp.

Vanoni, V.A. (ed.)
1977 **"Sedimentation Engineering"**, New York, ASCE hydraul. div., 745 pp.

Van Straaten, L.M.J.U.
1953 "Megaripples in the Dutch Wadden Sea", **Geol. Mijnb.**, 15, 1-11.

1959 "Minor structures of some recent littoral and neritic sediments", **Geol. Mijnb.**, 21st year, 197-216.

Van Veen, J.
1935 "Sand waves in the North Sea". **Hydrograph. Rev.**, V. 12, 21-29.

Vilks, G.
1980 "Postglacial basin sedimentation on Labrador Shelf. **Can. Geol. Surv.** Pap. 78-28, 28 pp.

Vilks, G. and Mudie. P.J.
1978 "Early deglaciation of the Labrador Shelf", **Science**, 202, 1181-1183.

Vilks, G., Wagner, F.J.E. and Pelletier, B.R.
1979 "The Holocene marine environment of the Beaufort Sea" **Can. Geol. Surv.** Bull. 303, 43 pp.

Vilks. G. and Wang, Y.
1981 "Surface texture of quartz grains and sedimentological processes on the southeastern Labrador Shelf". **Can. Geol. Surv.** Current Res., Pt. B, 55-62.

Vincent, C.E., Young, R.A. and Swift, D.J.P.
1982 "Bedload transport under waves and currents" **Marine Geology, V. 39,** 71-80.

Vincent, G.E.
1958 "Contribution to the study of sediment transport on a horizontal bed due to wave action" **Proc. 6th Conf. Coastal Eng.** ASCE. 326-354.

Visher, G.S. and Howard, J.D.
1974 "Dynamic relationship between hydraulics and sedimentation in the Altamaha Estuary". **J. Sediment. Petrol.,** V. 44, 502-521.

Wadhams, P.
1975 "Sea ice morphology in the Beaufort Sea", Can. Dept. of Environment, **Beaufort Sea Tech. Rep.** #36, Victoria, B.C., 66 pp.

Wahlgren, R.V.
1979 "Ice scour tracks in eastern MacKenzie Bay and north of Pullen Island, Beaufort Sea". **Can. Geol. Sur. Current Research, Pt. B,** 51-62.

Walker, R.G. (Ed.)
1979 "Facies Models", **Geoscience Canada, Reprint** Series 1. Can. Geol. Assoc., 211 pp.

Weatherly, G.L.
1972 "A study of the bottom boundary layer of the Florida Current". **J. Phys. Oceanogr.** 2, 54-72.

Weatherly, G.L. and Martin, P.J.
1978 "On the structure and dynamics of the oceanic bottom boundary layer". **J. Phys. Oceanogr.** 8, 557-570.

Weatherly, G.L. and Van Leer. J.
1977 "On the importance of stable stratification to the structure of the bottom boundary layer on the Western Florida shelf". in **Bottom Turbulence**. J. Nihoul (Ed.). N.Y.; Elsevier, 103-122.

Weber, J.N.
1958 "Recent grooving in lake bottom sediments at Great Slave Lake, Northwest Territories". **J. Sediment. Petrol.**, V. 28, 333-341.

Weeks, W.F., Barnes. P.W., Rearic, D. and Reimnitz. E.
1980 "Statistical aspects of ice gouging on the Alaskan shelf of the Beaufort Sea". **Unpub. MS.** available from U.S. Geol. Surv. Pacific - Arctic Branch of Mar. Geol., Menlo Park, California. 51 pp.

Weeks, W.F., Kovacs, A. and Hibler, W.D.
1971 "Pressure ridge characteristics in the Arctic coastal environment". **Proc. 1st Int. Conf. on Port and Ocean Eng. under Arctic Conditions** (POAC 1971), Trondheim. Norway. Tech. Univ. Norway; V. 1, 152-183.

Wetmiller. R.J. and Forsyth. D.A.
1978 "Seismicity of the Arctic, 1908 - 1975" in **Arctic Geophysical Review**; J.F. Sweeney (Ed.), Earth Physics Branch. Geol. Surv. Can., V. 45, #4, 15-24.

White, C.M.
1940 "The equilibrium of grains on the bed of a stream", **Royal Soc. London, Proc.**; Ser. A, V. 174, 322-358.

White, S.J.
1970 "Plane-bed thresholds for fine grained sediments". **Nature** 228, (5267), 152-153.

Wilson. N.D. and Abel. W.
1973 "Seafloor scour protection for a semi-submersible drilling rig on the Nova Scotian shelf", 5th Annual **OTC, paper #1891**, 631-639.

Wimbush, M. and Munk, W.
1970 "The benthic boundary layer". in **The Sea, Vol. 4, Pt. 1**, A.E. Maxwell (ed.) N.Y., Wiley-Interscience, 730-758.

Woodworth-Lynas. C.M.T.
1983 "The relative age of ice scours using cross-cutting relationships". **C-CORE Tech. Rep.** 83-3, 54 pp.

Yalin, M.S.
1963 "An expression for bed load transportation. ASCE. **J. Hydraul. Div.**, V. 89 (HY3), 221-250.

1972 **"Mechanics of Sediment Transport"**. Oxford, Pergamon Press, 290 pp.

Yorath, C.J., Currie. R.G., Tiffen, D.L., and Cameron. B.E.
1978 "Submersible operations on the Canadian Pacific continental margin. Report II", in Current Res., Pt. A: **Can. Geol. Surv.** Pap. 78-1A, 344-349.

Yorath, C.J., and Norris, D.K.
1975 "The tectonic development of the Southern Beaufort Sea and its relationship to the origin of the Arctic Ocean basin" in **Canada's Continental Margins and Offshore Petroleum Exploration**, C.J. Yorath, E.R. Parker and D.J. Glass (Eds.); Can. Soc. Petrol. Geol., Memoir 4, 589-612.

Young, I.F. and Chase, R.L.
1977 "Marine geological-geophysical study: southwestern Hecate Strait, British Columbia", in **Report of Activities**, Pt. A; **Can. Geol. Sur.** Pap. 77-1A, 315-318.

POOR

QUALITY

ORIGINAL